

Ripples in Communication

# Reconfigurable and Adaptive Wireless Communication Systems based on Wavelet Packet Modulators

PROEFSCHRIFT

ter verkrijging van de graad van doctor  
aan de Technische Universiteit Delft,  
op gezag van de Rector Magnificus prof. ir. K.C.A.M. Luyben,  
voorzitter van het College voor Promoties,  
in het openbaar te verdedigen op maandag 21 november 2011 om 12.30 uur  
door

Madan Kumar LAKSHMANAN

masteropleiding in de elektrotechnisch ingenieur  
geboren te Chennai, India.

Dit proefschrift is goedgekeurd door de promotor:

Prof. dr. ir. L.P. Ligthart

Samenstelling promotiecommissie:

Rector Magnificus	voorzitter
Prof. dr. ir. L.P. Ligthart	Technische Universiteit Delft, promotor
Dr. ir. H. Nikookar	Technische Universiteit Delft, copromotor
Prof. dr. R. Prasad	Aalborg Universitet, Denemarken
Prof. dr. A.J.v.d. Veen	Technische Universiteit Delft
Prof. dr. N. Baken	Technische Universiteit Delft
Prof. dr. E. Fledderus	Technische Universiteit Eindhoven
Prof. dr. K.C. Chen	National Taiwan University

Copyright © 2011 by M.K. Lakshmanan

All rights reserved. No part of the material protected by this copyright notice may be reproduced or utilized in any form or by any means, electronic or mechanical, including photocopying, recording or by any information storage and retrieval system, without the prior permission of the author.

ISBN 978-94-6186-004-0

*To our Sahana . . .*



*“Kattrathu Kaimann alavu. Kallaalathu Ulagalavu.”*

What we have learnt amounts to a handful of sand. What we are yet to learn is of global proportions..

Auvaiyar, Tamizh Poetess.

# *Acknowledgements*

At the outset I would like to express my deepest gratitude to my mentor Dr. H. Nikookar for his kind co-operation, guidance and support. Without his tireless and patient mentoring and boundless enthusiasm this research work would not have been undertaken.

I would also like to acknowledge the support and advice offered by Professor Ligthart. I greatly benefited from the many informative and enjoyable discussions I have had with him. He encourages his students to pursue their interests, both academic and non-academic, and this has been a primary factor in making my stay at IRCTR enjoyable.

I am most grateful to Professor Yarovy for his encouragement and advice.

My special thanks are due to Professor Nico Baken for facilitating this opportunity. I am deeply indebted to him for his help, stimulating suggestions and encouragement all through my PhD. He is a true visionary and an inspiration to many of us at the Wireless group.

I will fail in my duty if I don't express my deepest appreciation and gratitude to Professor Alle Jaan van der Veen for his extensive and valuable feedback on my thesis work.

I thank the Dutch Research Delta (DRD) for funding my research work. Without their generous grant we would never have ventured into this exciting field of research. Beyond the realm of financial support, DRD has also been an important nurturing ground for me to enhance and fine-tune my soft skills. How can I ever forget the many workshops and seminars organized under the aegis of DRD - I so thoroughly enjoyed and so immensely benefited from them.

I would also like to extend my thankfulness to the many fine members of DRD - Professor Eric Fledderus, Ms. Arjanna van der Plas, Ms. Christine Balch, Mr. Hamza Ouibrahim. Especially, I am obliged to Professor Fledderus for his ideas and suggestions which have helped me reposition my work to a larger audience. I also deeply cherish all the fantastic times I have had interacting with fellow DRD-ians - Edgar van Boven, Maurice Kwakkernaut, Yue Lu, Antonio Madureira, Javad Vazifehdan.

I am most grateful to the administrative team at IRCTR/MTS-R for their untiring efforts and ready co-operation. In this regard my heartiest thanks go to Ms. Stefanie van Gentevoort, Mrs. Mia van derVoort, Mr. Jefferey Ransun, Mr. Ad deRidder, Ms. Marjon Verkaik, Ms. Laura Bauman, Ms. Dominique Meijer and Ms. Wendy Murtinu.

Thanks also to all my peers and lab mates at the IRCTR - Xiaohua Lian, Hao Lu, Galina Babur, Venkat Roy, Shenario Ezhil, Ibrahim Budiarjo, Jamal Karamehmedovic, Berna Torun, Anurag Bajpai, Rahmat Mulyawan, Prastiyono Hari Mukti - for the many interesting discussions and the relaxed atmosphere in the office. Dyonosius Dony Ariananda needs particular mention as he has

been an inspiration and conversations with him have always been enlightening. Special thanks to Jose Wubbeling and Xiaohua Lian for their kind help in translating my thesis summary and propositions to Dutch.

Outside the realm of the TUD campus, I have found great comfort and support from many kind people. Krishna Kowgi, Murugaiyan, Vijay Venkat and Dr. Venkatesha Prasad stand out in that list. Krishna has been a caring friend and has always provided a different perspective on life. He is fast turning into my philosopher and guide. Krishna has also been instrumental in arousing my enthusiasm for science. A significant portion of my spare time has been spent on reading and collecting information on science.

Finally, I dedicate this work to my parents - Mr. Lakshmanan and Mrs. Lakshmi, wife - Vidya, sister-Sindhu and daughter-Sahana. Without their unwavering and unconditional love, affection, support and sacrifice, I would have never embarked on my doctoral study.

*Delft,  
November 2011*

*Madan Kumar Lakshmanan*

# Contents

<b>Acknowledgements</b>	<b>ii</b>
<b>I Introduction</b>	<b>1</b>
<b>1 Introduction</b>	<b>2</b>
1-1 Background . . . . .	2
Trends in wireless communication . . . . .	2
The need . . . . .	4
The means . . . . .	5
1-2 Wavelet transform as a tool for extending boundaries . . . . .	5
1-2-1 Wavelets and wavelet transform . . . . .	5
1-2-2 Advantages of wavelet transform for wireless communication . . . . .	6
a. Intelligent utilization of signal space . . . . .	6
b. Adaptability by customization of wavelet properties . . . . .	7
c. Flexibility with sub-carriers . . . . .	7
d. Enhanced multi-access transmission . . . . .	7
e. Reduced sensitivity to channel effects . . . . .	7
f. Generic and multi-purpose transceivers . . . . .	7
g. Optimal power utilization . . . . .	8
h. Reduced complexity of implementation . . . . .	8
1-2-3 Application of wavelets for wireless transmission . . . . .	8
1-3 Research goals, original contributions and challenges . . . . .	9
1-3-1 Wavelet packet based multi-carrier modulator (WPM) . . . . .	9
1-3-2 Aim and scope of the thesis work . . . . .	10
a. Demonstrable advantages . . . . .	11
b. Implementation challenges . . . . .	11
1-3-3 Specifics of the thesis work . . . . .	12
a. System implementation on computer platform . . . . .	13
b. Study of loss of synchronization (Chapter 4) . . . . .	13
c. Evaluation of Peak-to-Average-Power Ratio (PAPR) performance (Chapter 5) . . . . .	13
d. A spectrum estimator based on wavelet packets (WPSE) (Chapter 6) . . . . .	13
e. A wavelet packet transceiver for dynamic spectrum access (WPSE/WPM) (Chapter 7) . . . . .	13

f. A framework to design wavelets (Chapter 8)	14
g. Equalization of channel (Appendix C)	14
1-3-4 Original contributions of the thesis work	14
1-3-5 Research challenges	15
1-3-6 Research approach and feasibility	16
1-4 Organization of thesis work	16
<b>II Theoretical Background</b>	<b>19</b>
<b>2 Theory of wavelets</b>	<b>20</b>
2-1 Introduction	21
2-1-1 Representation of signals	21
2-1-2 Fourier analysis	22
2-1-3 Gabor transform	23
2-1-4 Wavelet analysis	23
2-2 Continuous wavelet transform	25
2-2-1 Orthonormal wavelets	27
2-2-2 Non-dyadic wavelets	27
2-3 Multi-resolution analysis	27
2-4 Discrete wavelet transform	30
2-5 Filter bank representation of DWT	31
2-5-1 Analysis filter bank	31
2-5-2 Synthesis filter bank	34
2-6 Wavelet packet transform	37
2-7 Wavelet types	40
2-7-1 Wavelet properties	40
i. Compact support	40
ii. Para-unitary Condition	40
iii. Regularity	41
iv. Symmetry	42
2-7-2 Popular wavelet families	42
a. Daubechies	42
b. Coiflet	42
c. Symlet	43
2-8 Summary	43
<b>3 Wavelet packet modulator</b>	<b>44</b>
3-1 Modulation techniques for wireless communication	45
3-1-1 Single carrier transmission	45
3-1-2 Multi-carrier transmission	46
3-1-3 Frequency division multiplexing	47
3-2 Orthogonal frequency division multiplexing	48
3-3 Filter bank multi-carrier methods	53
3-3-1 Filtered multi-tone (FMT)	53
3-3-2 Cosine modulated multi-tone (CMT)	54
3-3-3 Offset QAM/staggered multi-tone (SMT)	54

3-4	Wavelet and wavelet packet based multi-carrier modulators . . . . .	56
3-4-1	Wavelet packet modulator (WPM) . . . . .	56
3-4-2	Variants of wavelet packet modulator . . . . .	60
3-4-3	Interpolated tree orthogonal multiplexing (ITOM) . . . . .	62
3-5	Summary . . . . .	63
<b>III Implementation Challenges</b>		<b>64</b>
<b>4</b>	<b>Synchronization errors in wavelet packet modulation</b>	<b>65</b>
4-1	Introduction . . . . .	65
4-2	Frequency offset in multi-carrier modulation . . . . .	66
4-2-1	Modeling frequency offset errors . . . . .	67
4-2-2	Frequency offset in OFDM . . . . .	67
4-2-3	Frequency offset in WPM . . . . .	69
4-2-4	Numerical results for frequency offset errors . . . . .	69
	a. Performance under frequency offset error . . . . .	70
	b. Influence of number of sub-carriers . . . . .	73
	c. Influence of WPM frame size . . . . .	73
	d. Influence of wavelet filter length . . . . .	73
	e. Constellation plots . . . . .	73
	f. Dispersion of sub-carrier energy . . . . .	75
4-3	Phase noise in multi-carrier modulation . . . . .	76
4-3-1	Modeling the phase noise . . . . .	77
4-3-2	Phase noise in OFDM . . . . .	78
	1. Common phase error (CPE) - case when $k' = k$ . . . . .	79
	2. Inter carrier interference (ICI) - case when $k' \neq k$ . . . . .	80
4-3-3	Phase noise in WPM . . . . .	80
	1. Common phase error (CPE) - case when $k' = k$ and $u' = u$ . . . . .	81
	2. Inter symbol- inter carrier interference (IS-ICI) - case when $k' \neq k$ and/or $u \neq u'$ . . . . .	81
4-3-4	Numerical results for phase noise . . . . .	82
	a. Phase noise characteristics . . . . .	82
	b. Performance under frequency offset error . . . . .	83
	c. Influence of number of sub-carriers and WPM frame size . . . . .	84
	d. Influence of wavelet filter length . . . . .	84
	e. Constellation plots . . . . .	85
4-4	Performance under loss of time synchronization . . . . .	90
4-4-1	Modeling time offset errors . . . . .	90
4-4-2	Time offset in OFDM . . . . .	90
	a. Time offset away from the cyclic prefix . . . . .	91
	b. Time offset towards the cyclic prefix . . . . .	91
4-4-3	Time synchronization error in WPM . . . . .	93
4-4-4	Modulation scheme . . . . .	94
4-4-5	Numerical results for time offset . . . . .	95
	a. Performance of WPM without time errors . . . . .	95

b.	Performance when time offset is modeled as a discrete uniform distribution . . . . .	96
c.	Influence of number of sub-carriers . . . . .	97
d.	Influence of number of symbols/frame . . . . .	98
e.	Influence of different lengths of wavelet filters . . . . .	99
f.	Constellation plots . . . . .	100
g.	Dispersion of energy of the sub-carriers . . . . .	100
4-5	Summary . . . . .	103
<b>5</b>	<b>Peak-to-average power ratio performance</b>	<b>104</b>
5-1	Introduction . . . . .	104
5-2	Distribution of the PAPR . . . . .	105
5-2-1	OFDM . . . . .	105
5-2-2	WPM . . . . .	106
a.	WPM signal characteristics . . . . .	106
b.	Amplitude distribution . . . . .	107
c.	Power distribution . . . . .	107
d.	PAPR distribution . . . . .	108
5-3	Techniques to mitigate PAPR . . . . .	111
5-3-1	Signal scrambling techniques . . . . .	111
5-3-2	Signal distortion techniques . . . . .	111
5-3-3	Criteria for the selection of best PAPR mitigation strategy . . . . .	112
5-4	Selected mapping with phase modification . . . . .	113
5-4-1	Description of algorithm . . . . .	113
5-4-2	Numerical results . . . . .	115
a.	Performance of the PAPR mitigation technique . . . . .	115
b.	Influence of phase-sequence distribution . . . . .	116
c.	Impact of phase alphabet . . . . .	116
d.	Impact of wavelet families . . . . .	118
e.	Influence of the PAPR reduction technique on the BER performance . . . . .	118
5-5	Hill climbing optimization heuristics for minimization of PAPR in WPM transmission . . . . .	120
5-5-1	PAPR reduction as an optimization problem . . . . .	121
5-5-2	Hill climbing algorithm . . . . .	121
5-5-3	Mitigation of PAPR for WPM systems with hill climbing algorithm . . . . .	123
5-5-4	Numerical results . . . . .	125
a.	Performance of the algorithm to reduce PAPR . . . . .	125
b.	Convergence of the algorithm . . . . .	125
c.	Impact of the wavelet family . . . . .	126
d.	Computational complexity of the algorithm . . . . .	128
5-6	Summary . . . . .	129
<b>IV</b>	<b>Demonstration of Advantages</b>	<b>131</b>
<b>6</b>	<b>Wavelet packet spectrum estimation</b>	<b>132</b>
6-1	Introduction . . . . .	133
6-1-1	Periodogram . . . . .	134

6-1-2	Correlogram . . . . .	134
6-1-3	Other techniques . . . . .	134
6-2	Spectrum estimation as a filter bank analysis problem . . . . .	135
6-2-1	Filter bank interpretation of spectrum analysis . . . . .	136
6-2-2	Multi-taper spectral estimator (MTSE) . . . . .	137
6-2-3	Filter bank spectral estimator (FBSE) . . . . .	138
6-3	Wavelet packet spectrum estimator (WPSE) . . . . .	141
6-3-1	Wavelet packet representation . . . . .	141
6-3-2	Frequency ordering of wavelet packet coefficients . . . . .	142
6-3-3	Re-ordering of wavelet packet coefficients . . . . .	144
	A. Gray to binary code conversion . . . . .	144
6-3-4	Wavelet packet based spectrum estimation as a filter bank analysis problem . . . . .	145
	B. Modified wavelet packet tree structure . . . . .	146
6-3-5	Wavelet packet transform and energy conservation . . . . .	146
6-3-6	Calculating power spectrum density from wavelet packet coefficients . . . . .	148
6-4	Optimizations to wavelet packet implementation . . . . .	149
6-4-1	Enhanced WPSE to mitigate edge artifacts . . . . .	149
6-4-2	Enhanced WPSE with padding . . . . .	150
6-5	Experiment scenarios, sources and their characteristics . . . . .	151
6-6	Results and analysis . . . . .	153
6-6-1	Partial band source estimation . . . . .	153
	A. Comparison with Welch and Periodogram estimators . . . . .	153
	B. Comparison with windowed Periodogram and MTSE methods . . . . .	155
	C. Impact of wavelet families . . . . .	155
	D. Impact of wavelet lengths . . . . .	156
	E. Impact of decomposition levels . . . . .	156
6-6-2	Single-tone source estimation . . . . .	159
	A. Comparison with Welch and Periodogram methods . . . . .	159
	B. Comparison with windowed-Periodogram and MTSE techniques . . . . .	160
	C. Impact of wavelet families . . . . .	162
	D. Influence of filter length . . . . .	162
	E. Influence of decomposition level . . . . .	162
6-6-3	Multi-Tone Source Estimation . . . . .	165
	A. Comparison with Welch and Periodogram methods . . . . .	165
	B. Comparison with windowed-Periodogram and MTSE techniques . . . . .	165
	C. Impact of wavelet families . . . . .	167
	E. Impact of decomposition levels . . . . .	167
6-6-4	Swept-tone source estimation . . . . .	167
6-6-5	Estimation with limited number of samples . . . . .	169
	A. Partial band . . . . .	173
	B. Single tone . . . . .	177
	C. Multi-Tone . . . . .	177
6-6-6	Enhanced wavelet packet spectrum estimator (E-WPSE) . . . . .	177
	A. Estimation of partial band source . . . . .	177
	A.1. Comparison with Welch and periodogram techniques . . . . .	178
	A.2. Comparison with Windowed periodogram and MTSE . . . . .	180
	A.3. Influence of decomposition levels . . . . .	180

	B. Single tone source . . . . .	183
	B.1. Comparison with Welch and periodogram methods . . . . .	183
	B.2. Comparison with Windowed periodogram and MTSE techniques . . . . .	183
	B.3. Influence of decomposition levels . . . . .	184
6-6-7	Impact of padding on E-WPSE estimation . . . . .	184
6-7	Summary . . . . .	186
<b>7</b>	<b>A wavelet packet transceiver for spectral analysis and dynamic spectrum access</b>	<b>187</b>
7-1	Introduction . . . . .	188
7-2	Multi-carrier methods for Cognitive Radio . . . . .	189
	7-2-1 FFT based OFDM . . . . .	189
	7-2-2 Filter bank multi-carrier methods . . . . .	191
7-3	Wavelet packet transceiver for spectral analysis and dynamic spectrum access . . . . .	192
	7-3-1 Wavelet packet multi-carrier modulation (WPM) . . . . .	194
	7-3-2 Wavelet packet spectrum estimator (WPSE) . . . . .	194
	7-3-3 Identification of spectrum holes and waveform shaping . . . . .	195
7-4	Simulation setup . . . . .	196
	7-4-1 System parameters . . . . .	196
	7-4-2 Comparison with Periodogram/Welch-OFDM systems . . . . .	196
	7-4-3 Sources and their characteristics . . . . .	197
	7-4-4 Experiment scenarios . . . . .	198
7-5	Results and analysis . . . . .	199
	7-5-1 Characteristics of OFDM and WPM sub-channels . . . . .	199
	7-5-2 Comparison of efficiency of spectrum estimators . . . . .	200
	7-5-3 Evaluation of different sources . . . . .	202
	A. Partial band source . . . . .	202
	Carrier removal and reduction of interference . . . . .	204
	B. Multi-tone source . . . . .	206
	C. Single-tone source . . . . .	206
	D. Swept-tone source . . . . .	208
	7-5-4 Evaluation of efficiency of spectral utilization . . . . .	208
7-6	Summary . . . . .	218
<b>8</b>	<b>A unified framework to design orthonormal wavelet bases</b>	<b>220</b>
8-1	Introduction . . . . .	220
8-2	Criterion for design of wavelets . . . . .	221
	8-2-1 Design procedure . . . . .	221
	8-2-2 Filter bank implementation of WPM . . . . .	221
	8-2-3 Important wavelet properties . . . . .	222
	A. Wavelet existence and compact support . . . . .	223
	B. Para-unitary condition . . . . .	223
	C. Flatness/K-Regularity . . . . .	224
	8-2-4 Degrees of freedom to design . . . . .	225
8-3	Example 1 - Maximally frequency selective wavelets . . . . .	226
	8-3-1 Formulating the design problem . . . . .	227
	8-3-2 Transformation of problem from non-convex to convex . . . . .	228
	A. Compact support or admissibility constraint . . . . .	229

	B. Double shift orthogonality constraint . . . . .	230
	C. K-Regularity constraint . . . . .	230
	D. Stop-band constraint . . . . .	231
	E. Spectral factorization and discretization on stop band constraint . . . . .	232
8-3-3	Reformulation of optimization criterion in the $Q(\omega)$ function domain . . . . .	233
	A. Compact support . . . . .	234
	B. Double shift orthogonality . . . . .	234
	C. Spectral factorization . . . . .	235
	D. Stop band constraint . . . . .	235
8-3-4	Solving the convex optimization problem . . . . .	236
8-3-5	Results and analysis . . . . .	238
	A. Frequency and impulse responses of the newly designed filter . . . . .	238
	B. Evaluation of spectrum estimator performance . . . . .	242
	C. Evaluation of the receiver operating characteristics (ROC) . . . . .	244
	D. Other studies - filter characteristics and their influence . . . . .	244
8-4	Example 2 - Wavelets with low cross correlation error . . . . .	246
8-4-1	Time offset errors in WPM . . . . .	247
8-4-2	Formulation of the design problem . . . . .	248
	A. Design criterion . . . . .	248
	B. Wavelet-domain to filter bank-domain . . . . .	248
8-4-3	Transformation of the mathematical constraints from a non-convex problem to a convex/linear one . . . . .	249
8-4-4	Results and analysis . . . . .	251
	A. Frequency and impulse responses of the designed filter . . . . .	251
	B. Evaluation of the designed filter under a loss of time synchronization . . . . .	253
	C. Dispersion of sub-carrier energy . . . . .	255
8-5	Summary . . . . .	257
 <b>V Conclusion</b>		<b>259</b>
 <b>9 Conclusions and future research topics</b>		<b>260</b>
9-1	Introduction . . . . .	260
9-2	Summary of chapters and key conclusions . . . . .	262
	A. Study of WPM performance under loss of Synchronization (Chapter – 4) . . . . .	262
	B. PAPR performance studies (Chapter – 5) . . . . .	264
	C. Wavelet packet spectrum estimator(WPSE) (Chapter – 6) . . . . .	264
	D. WPSE/WPM for Dynamic Spectrum Access (Chapter – 7) . . . . .	266
	E. Design of Wavelets (Chapter – 8) . . . . .	266
9-3	Future research topics . . . . .	267
9-3-1	Enhancements to this PhD . . . . .	268
	A. Study of WPM performance under loss of Synchronization . . . . .	268
	B. PAPR performance studies . . . . .	268
	C. Wavelet packet spectrum estimator (WPSE) . . . . .	269
	D. WPSE-WPM for dynamic spectrum access . . . . .	270
	E. Design of wavelets . . . . .	270

F. Channel equalization . . . . .	271
9-3-2 Related studies . . . . .	271
9-3-3 Beyond this work . . . . .	272
A. Wavelet-Based modeling of time-variant wireless channels . . . . .	272
B. Multiple access communication . . . . .	273
C. Wavelet radio for green communication . . . . .	273
D. Wavelet based multiple-input multiple-output communications (MIMO) . . . . .	275
9-4 Concluding remarks . . . . .	275
<b>A Design of Wavelets . . . . .</b>	<b>276</b>
A-1 Semi-definite programming . . . . .	276
A-2 Spectral factorization . . . . .	277
A-3 Sum of squares of cross-correlation function . . . . .	278
A-4 Partitioning of energy . . . . .	278
<b>B Graphical User Interface . . . . .</b>	<b>281</b>
B-1 GUI for WPM testing . . . . .	281
B-2 GUI for wavelet design . . . . .	282
B-2-1 Details of the filter design program . . . . .	282
<b>C Channel Equalization in WPM by minimization of peak-distortion . . . . .</b>	<b>285</b>
C-1 Introduction . . . . .	285
C-2 Equalization by minimization of the peak-distortion . . . . .	286
C-2-1 Equalizer with Infinite Taps . . . . .	287
C-2-2 Equalizer with Finite Taps . . . . .	288
C-3 Simulation Setup . . . . .	289
C-4 Simulation Results . . . . .	291
C-4-1 Performance under Channel Condition-1 . . . . .	291
C-4-2 Performance under Channel Condition-2 . . . . .	294
C-4-3 Eye Diagrams . . . . .	298
C-5 Conclusion . . . . .	301
<b>Bibliography . . . . .</b>	<b>302</b>
<b>Summary . . . . .</b>	<b>316</b>
<b>Samenvatting . . . . .</b>	<b>317</b>
<b>Curriculum Vitae . . . . .</b>	<b>319</b>

# **Part I**

## **Introduction**

# Chapter 1

## Introduction

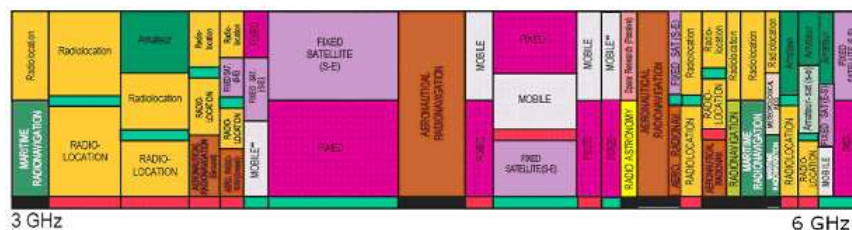
### 1-1 Background

#### **Trends in wireless communication**

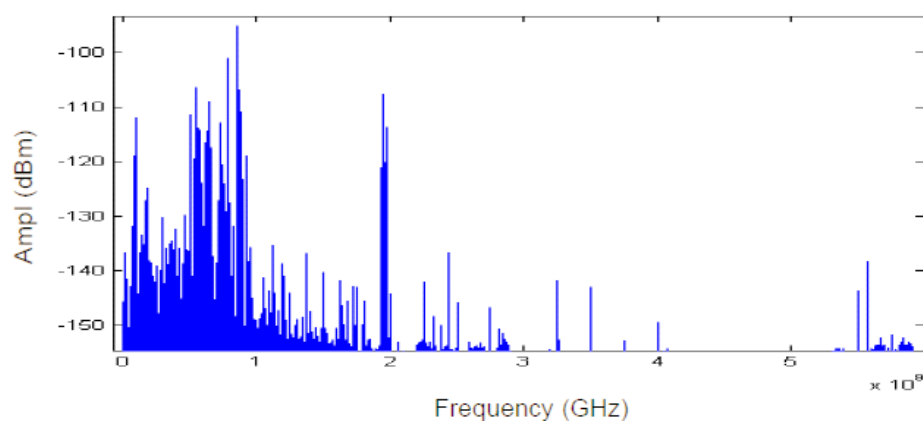
The advancements in the field of digital wireless communication have led to many exciting applications like mobile internet access, health care and medical monitoring services, smart homes, combat radios, disaster management, automated highways and factories. With each passing day novel and advanced services are being launched even while existing ones continue to flourish. While traditionally only voice and data communication were possible, wireless services have now found applicability in other sectors too including health care, transportation, security, logistics, education and finance. For example, tele-medicine can render emergent and easy-to-access health care at distance. Through rural connectivity, people living in remote places in developing/under-developed nations can be given access to good quality education via long distance learning programs. In the era of open course ware (OCW), this can prove to be a boundary breaker in spreading top quality educational content to students who hitherto might not have access to them. Demand for wireless services is thus expected to grow in the foreseeable future.

However, with increasing popularity of the wireless services the requirements on prime resources like battery power and radio spectrum are put to great test. For example, currently most spectrum has been allocated (see fig. 1.1(a)), and it is becoming increasingly difficult to find frequency bands that can be made available either for new services or to expand existing ones. Even as the available frequency spectrum appears to be fully occupied, a survey [1] conducted by the American regulatory body Federal Communications Commission (FCC) in 2002 revealed that much of the available spectrum is underused most of the time [1]. The study [1]

also showed that only 20% or less of the spectrum is used and that spectrum congestions are more due to the sub-optimal use of spectrum than to the lack of free spectrum (see fig. 1.1(b)).



(a)



(b)

FIGURE 1.1: Illustration of sub-optimal utilization of Spectrum. (a) Frequency Allocation in the region 3-6 GHz. (b) Actual spectral utilization in the same 3-6GHz band. Measurements taken in an urban area at mid-day with 20 KHz resolution over a time span of 50 microseconds with a 30 degree directional antenna [1].

Concomitant with the growth of wireless services is the increase in the volume of data-exchanged by a factor of about 10 every 5 years following Moore's law. For example, the average mobile broadband connection in the year 2009 generated a traffic of 1.3 gigabytes per month (equivalent to about 650 MP3 music files). This number is expected to grow to 7 gigabytes of traffic per month (roughly equivalent to about 3,500 MP3 music files) by 2014 (refer to fig. 1.2) [2, 3]. The ten-fold increase in data volume every 5 years corresponds to an increase of the associated energy consumption by about 20% annually. In fact, the current world-wide energy requirements of Information and Communication Technology (ICT) systems contributes to nearly 2% of the CO<sub>2</sub> emissions, a figure comparable with the total emissions due to global air travel or about one quarter of the emissions due to cars and trucks.

Another emerging trend is the demand for higher data rates as exemplified in fig. 1.3 where the growth of home bandwidth since the 1970s has been shown [4]. Today, UMTS is one of the fastest solutions on the market that can operate in dispersive environments at a rate of

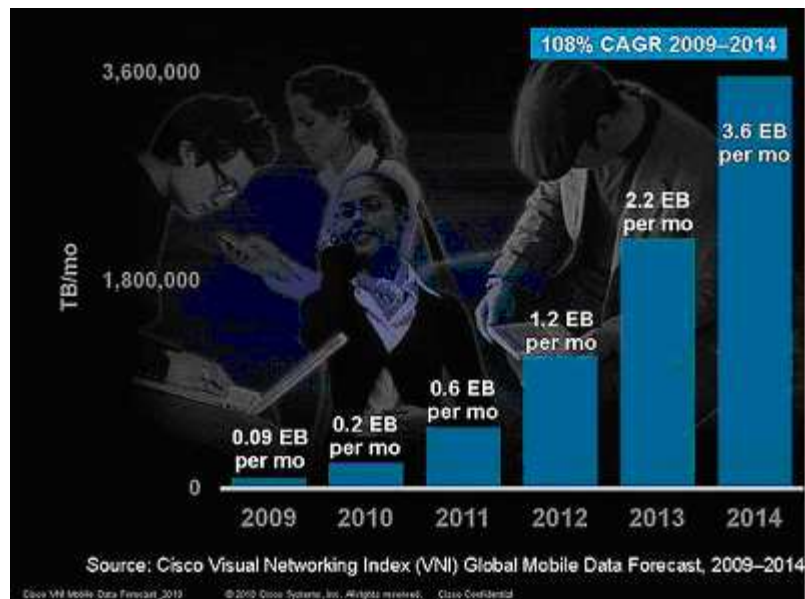


FIGURE 1.2: Global Mobile Data Traffic Growth (Mobile traffic will grow by 39 times from 2009 to 2014). Notations in the figure: EB: Exa-bytes ( $10^{18}$  bytes), mo: Month, TB: Terra-bytes ( $10^{12}$  bytes) [2].

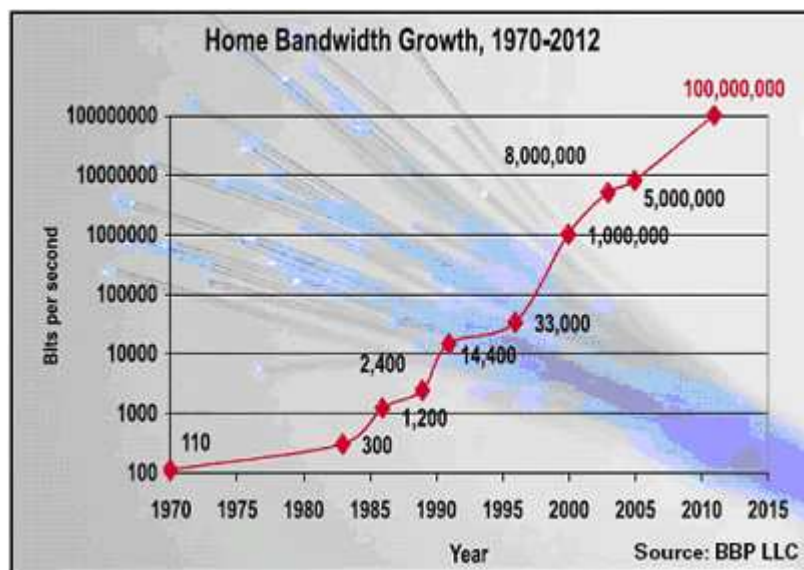


FIGURE 1.3: Growth of home bandwidth since the 1970s [3].

$3.84 \times 10^6$  chips but the rapid progress of telecommunication market has created a need for newer techniques that can accommodate data rates even higher than this.

### The need

There is therefore an emergent need for developing energy efficient, green technologies that optimize premium radio resources, such as power and spectrum, even while guaranteeing a desirable

quality of service. Of signal interest is in the development of a capable radio/PHY layer platform that facilitates optimum utilization of energy in addition to guaranteeing spectral efficiency, adequate coverage and good Quality of Service (QoS). Spatially, temporally and spectrally localized transmission strategies which minimize the energy spent to transmit information bearing symbols will be crucial towards achieving high energy efficiency. Moreover, wireless systems operate under dynamic conditions with frequent changes in the propagation environment and user requirements. Thus in a wireless environment the system requirements, network capacities and device capabilities have enormous variations giving rise to significant design challenges. All these trends point to an untapped niche available for flexible, reconfigurable systems that can adapt to its radio neighborhood.

### **The means**

Existing wireless systems are based on the mathematical precept of Fourier transform. In comparison to the Fourier transform the recently formulated theory of wavelets offers many advantages for the design of sophisticated wireless devices. The suitability of wavelets for these applications is in their ability to characterize signals with adaptive time-frequency resolution. By careful adaptation of the main system parameters according to the radio environment the operation of wavelet based radios can be optimized to save valuable radio resources.

## **1-2 Wavelet transform as a tool for extending boundaries**

### **1-2-1 Wavelets and wavelet transform**

A wavelet is a waveform of limited duration. As the name suggests, wavelets are small waveforms with a set of oscillatory structures that is non-zero for a limited period of time (or space). The wavelet transform is a multi-resolution analysis scheme where an input signal is decomposed into different frequency components with each component studied with resolutions matched to its time-scales. The Fourier transform also decomposes signals into elementary waveforms but the bases used are trigonometric functions. Thus, when one wants to analyze the local properties of the input signal, such as edges or transients, the Fourier transform is not an efficient analysis tool. By contrast the wavelet transforms which uses irregularly shaped wavelets offer better prospects of representing sharp changes and local features.

The wavelet transform is used in various applications and is finding tremendous popularity among technologists, engineers and mathematicians alike. In most of the applications, the power of the transform comes from the fact that the basis functions of the transform are localized in

time (or space) and frequency, and offer different resolutions in these domains. These resolutions often correspond to the natural behavior of the process one wants to analyze, hence the power of the transform. Such properties make wavelets and wavelet transforms natural choices in fields as diverse as image synthesis, data compression, computer graphics and animation, human vision, radar, optics, astronomy, acoustics, seismology, nuclear engineering, biomedical engineering, magnetic resonance imaging, music, fractals, turbulence, and pure math.

While the wavelet transform is the *de jure* standard<sup>1</sup> for many signal processing applications, especially, in the fields of image processing, speech analysis and data compression, the technique has not been extensively applied to the design of communication systems.

### 1-2-2 Advantages of wavelet transform for wireless communication

The motivation for pursuing wavelet based systems primarily lies in the freedom they provide to communication systems designers [5, 6]. Unlike the Fourier bases which are static sines/cosines, wavelet bases offer flexibility and adaptation that can be tailored to satisfy an engineering demand. This feature is attributable to the fact that the wavelet transform is implemented entirely using filter bank tree structures obtainable from paraunitary filters<sup>2</sup>. The freedom to alter the properties of the wavelet and the filter bank tree structure gives the opportunity to fine tune and optimize the modulated signal according to the application at hand.

The benefits of wavelet based radios for research and development of energy efficient communication are summarized in the following sections.

#### a. Intelligent utilization of signal space

The wavelet based systems are realized from tree structures obtained by cascading a fundamental Quadrature Mirror Filter (QMF) pair of low and high pass filters. The construction of this tree structure can be adjusted to come out with an optimum tree structure that caters to various requirements. The requirements could typically be:

- identification and isolation of time-frequency "atoms" affected by an interfering source and communicating around the source of interference [7],
- flexibility with time-frequency tiling of the carriers that can lead to multi-rate systems which can transmit with different rates in different bands [8]. Such a feature can be exploited in scenarios where the channel characteristics are not uniform.

---

<sup>1</sup>Examples include JPEG 2000, an image compression standard and MPEG-4 Part 14 or MP4, a multimedia container format standard.

<sup>2</sup>Paraunitary filters are a class of perfect-reconstruction filters which generates orthogonal bases

**b. Adaptability by customization of wavelet properties**

By careful selection of the fundamental filters which greatly influence the transmission characteristics, it is possible to optimize the system performance in terms of the bandwidth efficiency, localization of the transmitted signal in time and frequency, minimization of inter-symbol Interference (ISI), inter-carrier interference (ICI) or peak-to-average-power ratio (PAPR), robustness towards interference from competing sources. This can also aid in opportunistic communication (e.g. Cognitive Radio) where unused resources can be cleverly utilized.

**c. Flexibility with sub-carriers**

The derivation of wavelets is directly related to the iterative nature of the wavelet transform. The wavelet transform allows for a configurable transform size and hence a configurable number of carriers. This facility can be used, for instance, to reconfigure a transceiver according to a given communication protocol; the transform size could be selected according to the channel impulse response characteristics, computational complexity or link quality [7].

**d. Enhanced multi-access transmission**

Wavelets offer a new dimension of diversity called the "Waveform diversity" that can be exploited to enhance multiple access transmission [9]. The wavelet transform generates wavelet bases which are orthogonal to one another. By designating these bases to different users in adjacent cellular communication cells, the inter-cell interference can be minimized.

**e. Reduced sensitivity to channel effects**

The performance of communication systems is influenced by the kind of modulation scheme used. The modulation mode in turn is affected by the set of waveforms used. By cleverly altering the nature and characteristics of the waveforms used the sensitivity of the communication system to harmful channel effects can be reduced [10].

**f. Generic and multi-purpose transceivers**

Furthermore, a generic and parameterized wavelet based radio can help simplify the system architecture by doing away with multiple firmware, software, drivers which indirectly contributes to reduced power consumption and improved battery life. The radio can be designed merely by altering the parameters instead of adding/removing hardware components to the transceiver chain.

### **g. Optimal power utilization**

While there is no explicit relationship between power optimization and waveforms, the nature and characteristics of the waveform can be altered to suit a set of requirements which can indirectly contribute to a more efficient system resulting in lower requirements of power and energy. These criteria could typically be:

- minimization of ISI, ICI or PAPR,
- greater tolerance and robustness to time/frequency/phase offset errors,
- robustness towards interference from competing sources,
- possibilities for opportunistic communication (e.g. Cognitive Radio) where unused resources can be cleverly utilized.

### **h. Reduced complexity of implementation**

It has been proved [10] that the complexity of the Wavelet systems is by and large simpler than OFDM systems. A lower complexity also means lower power requirements in the execution of the signal processing algorithms. The implementation of Wavelet systems can be simplified even further if fast-wavelet transforms are employed.

## **1-2-3 Application of wavelets for wireless transmission**

The wavelet transform holds promise as a possible analysis scheme for the design of sophisticated digital wireless communication systems, with advantages such as flexibility of the transform, lower sensitivity to channel distortion and interference and better utilization of spectrum. Wavelets have found beneficial applicability in various aspects of wireless communication systems design including channel modelling, design of transceivers, data representation, data compression, source and channel coding, interference mitigation, signal de-noising, energy efficient networking. Fig. 1.4 gives a graphical representation of some of the facets of wireless communications where wavelets hold promise [6].

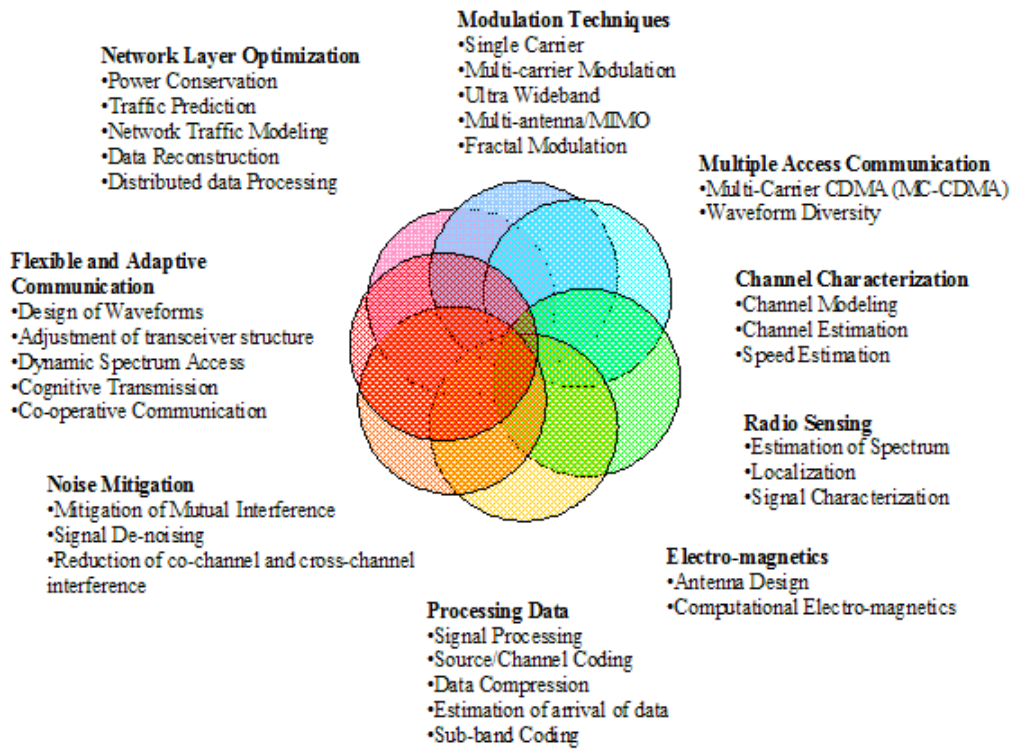


FIGURE 1.4: The spectrum of wavelet applications for wireless communication.

## 1-3 Research goals, original contributions and challenges

### 1-3-1 Wavelet packet based multi-carrier modulator (WPM)

The promise of wavelets for wireless systems design is exemplified in this research work with the realization of an orthogonal multi-carrier modulator (MCM) based on wavelet packets<sup>3</sup>. Orthogonal multi-carrier communication is a modulation format that places independent information carrying symbols on orthogonal signals. These orthogonal signals are typically equi-spaced sub-carriers which are modulated to occupy different center frequencies. In traditional implementations of MCM, such as the Orthogonal Frequency Division Multiplexing (OFDM), the sub-carriers are Fourier bases (complex exponential functions). Recently, the Wavelet Packet transform has emerged as an important signal processing tool. The basis functions in wavelet packet representation are obtained from a single function called the mother wavelet through scaling and translations. When the scales and translations are dyadic the resultant basis functions are orthogonal and span<sup>4</sup> embedded subspaces of  $L^2(\mathbb{R})$ <sup>5</sup> at different resolutions yielding a Multi Resolution Analysis. From the perspective of communication system design, this has important and interesting implications -finite energy signals in  $L^2(\mathbb{R})$  can be decomposed into orthogonal subspaces through a wavelet packet transform or conversely information can be combined into

<sup>3</sup>Wavelet packets are generalized form of wavelets and will be dealt in detail in Chapters 2 and 3.

<sup>4</sup>The span of  $\mathbb{S}$  may be defined as the collection of all (finite) linear combinations of the elements of  $\mathbb{S}$ .

<sup>5</sup>set of square-integrable functions in  $\mathbb{R}$

mutually orthogonal wavelet packet basis functions in a way that they do not interfere with one another. Since the basis functions and subspaces are orthogonal, such structures can be used for obtaining orthogonal waveforms leading to the idea of WPM.

The pioneering work on applying the theory of wavelets and wavelet packets for the design of multi-carrier modulators was carried out by Lindsay [11] who laid out the theoretical foundations to establish the link between wavelet packets and digital communication. He also showed that the entire WPM transceiver structure can be realized with a pair of conjugate quadrature mirror filters which satisfy a set of constraints. His idea has since then been taken forward by other researchers. In [12] and [10], respectively, the authors study few aspects of applying wavelet and wavelet packet filters for multi-carrier modulation. The decoding of WPM data with Maximum likelihood estimators has been addressed by Suzuki [13]. A preliminary study of an equalization scheme suited for WPM has been conducted by Gracias [14]. In [15, 16] an investigation on the performance of WPM systems in the presence of time offset is performed. In [17] its PAPR performances are analyzed. The advantages of the wavelet transform in terms of the flexibility they offer to customize and shape the characteristics of the waveforms have been demonstrated in [18–21]. Three use-cases where the waveforms are designed and applied to optimize the WPM system performance according to specific system demands are illustrated in [18–20]. In [21], the work of [18, 19] is extended to establish a unifying mathematical framework where the waveforms are designed according to a pre-defined criteria.

### 1-3-2 Aim and scope of the thesis work

In spite of the developments mentioned in the previous section, existing knowledge on wavelets for multi-carrier modulation is limited and the literature on the topic continues to remain sparse. This lacuna in available knowledge is a key motivation for this PhD work. Furthermore, in the effectuation of wavelet packet modulator for wireless systems two fundamental questions arise, namely (see fig. 1.5),

- a. What are the demonstrable advantages of WPM?
- b. What are the challenges in the implementation of WPM?

Answering these two questions form the basis of this thesis work. We confine ourself to the mathematical modeling and implementation of the Wavelet Packet Modulator (WPM) on a simulation platform. <sup>6</sup>

---

<sup>6</sup>A preliminary implementation of the WPM algorithms on a FPGA/DSP platform was also attempted.

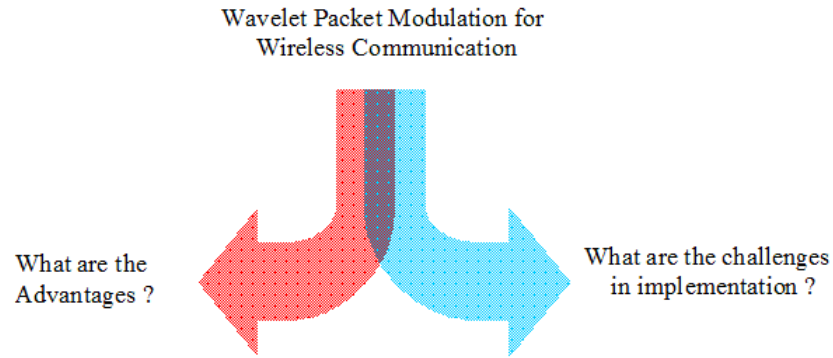


FIGURE 1.5: Primary questions handled in the thesis work.

### a. Demonstrable advantages

In this work we pursue two main advantages of the WPM system:

1. **Design of wavelets:** The time-frequency characteristics of the the wavelets can be altered according to a system specification. Hence, by careful selection of the wavelets it is possible to optimize WPM performance in terms of bandwidth efficiency, frequency selectivity of sub-carriers, sensitivity to synchronization errors, PAPR, etc. Furthermore, the WPM can be efficiently implemented with filter banks which make it convenient for applications related to digital communications.
2. **Frequency selectivity of the wavelets:** Another advantage of pursuing WPM systems is in the promise of better confinement of spectra and lower out-of-band energy spillage. This ability is due to the fact that WPM symbols overlap in time resulting in greater localization in frequency. The signal energy can hence be better confined without leaking into neighboring bands.

### b. Implementation challenges

We consider 2 challenges in the implementation of WPM, namely,

1. Performance under loss of synchronization.
2. Peak-to-average-Power (PAPR) ratio performance.

In fig. 1.6 these areas of research have been enlisted in the form of puzzle-pieces. Each piece in the puzzle represents a research challenge that has to be handled to aid the actualization of the WPM system. The challenges are ordered in 5 columns. The first two columns list the implementation challenges (*Items 1 to 10*). Column 3 enumerates important advantages of

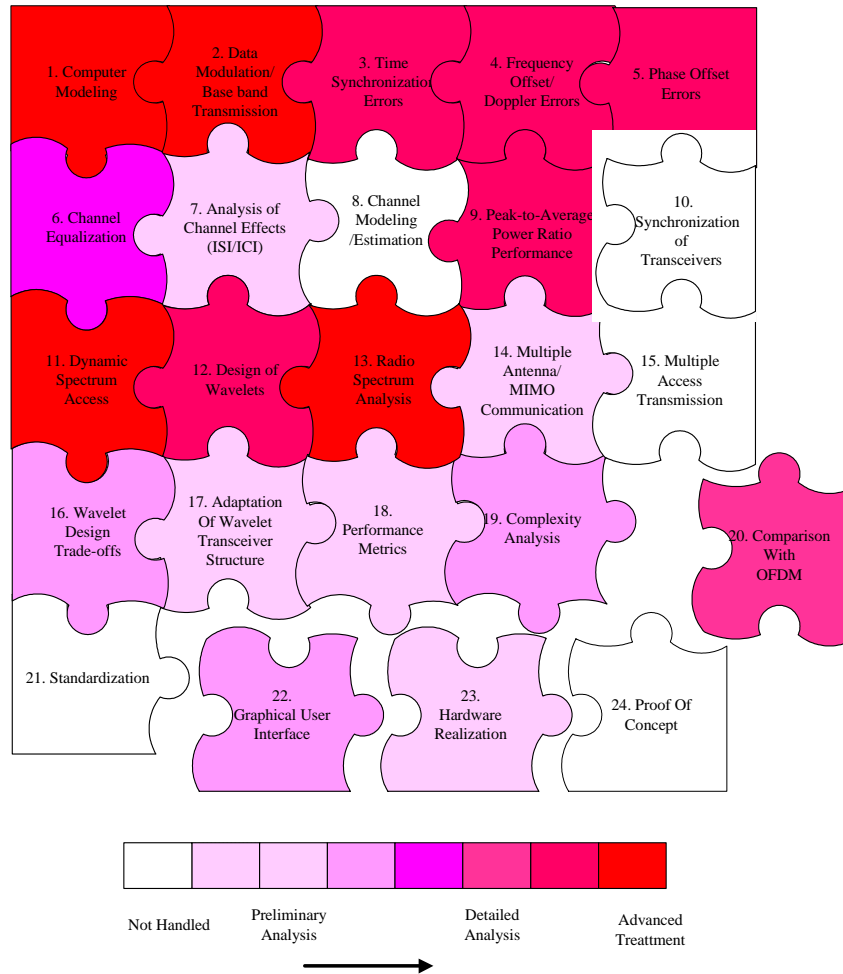


FIGURE 1.6: Pieces of the Puzzle - realizing the WPM system.

wavelets that have to be demonstrated (*Items 11 to 15*). Column 4 names some of the auxiliary issues (*Items 16 to 20*) that have to be taken into account. In column 5 the issues related to the practical realization and deployment of the WPM system (*Items 21 to 24*) are listed.

We would like to emphasize here that not all topics listed above have been covered in this thesis work. For example, channel modeling (*Item 8*), synchronization of transceivers (*Item 10*), multiple access communication (*Item 15*), standardization issues (*Item 21*) and Proof of Concept (*Item 24*) have not been taken up. Furthermore, some of the topics have been handled in detail while others have been treated only preliminarily. Various shades of red have been used in fig. 1.6 to indicate the degree to which the topic has been covered in this dissertation. Only the radio transmission (physical layer) challenges have been considered.

### 1-3-3 Specifics of the thesis work

In this section we explain in more detail the various activities carried out in the framework of the PhD (as depicted in fig. 1.6).

**a. System implementation on computer platform**

A simulation setup in MATLAB© for the implementation of the WPM transceivers was established. (*Items 1, 2, 18 and 19 in fig. 1.6*).

**b. Study of loss of synchronization (Chapter 4)**

The performance of the proposed WPM system under loss of time, frequency or phase synchronization was evaluated. The mathematical expressions for inter-carrier interference (ICI) and inter-symbol interference (ISI) in WPM transmission were derived. (*Items 3, 4, 5 and 7 in fig. 1.6*)

**c. Evaluation of Peak-to-Average-Power Ratio (PAPR) performance (Chapter 5)**

The PAPR performance of the WPM system was analysed. Two mechanisms to reduce the PAPR in WPM transmission were devised. (*Item 9 in fig. 1.6*)

**d. A spectrum estimator based on wavelet packets (WPSE) (Chapter 6)**

An investigation of wavelet packet transform as a viable spectral analysis tool was conducted. The main attraction for wavelet packets is the trade-offs they offer in terms of satisfying performance metrics such as frequency resolution, side lobe suppression and variance of the estimated power spectral density (PSD). The performance of the system was evaluated through simulation studies. The results of the experiments show that the wavelet based approach offers greater flexibility and adaptability apart from its performances which were found to be comparable and at times even better than Fourier based estimates. (*Item 13*).

**e. A wavelet packet transceiver for dynamic spectrum access (WPSE/WPM) (Chapter 7)**

A reconfigurable wavelet Packet transceiver for spectral analysis and dynamic spectrum access was tested. The transceiver consisted of a wavelet packet spectral estimator (WPSE) and a wavelet packet multi-carrier modulator (WPM). The WPSE senses the radio environment to identify spectrum holes and occupied bands. This information is then used to alter the time-frequency characteristics of the WPM transmission waveform such that the occupied bands are evaded. The WPSE uses the same filter bank structure as used for data modulation and hence does not add to the implementation costs. The performances were compared with architectures based on FFT/OFDM. The studies showed that WPSE/WPM performed better than FFT/OFDM

in regard to estimation of spectrum and spectral confinement of transmission waveforms. This in turn contributed to better bit-error-rate (BER) performance and bandwidth efficiency. (*Items 11, 13 and 17*)

#### **f. A framework to design wavelets (Chapter 8)**

A filter design framework that facilitated the development of new wavelet bases according to specific demands was established. The design constraints were expressed as mathematical constraints and suitable optimization tools (including convex optimization and semi-definite programming) were employed to solve the problem. The results were then tested for optimality. The procedure was illustrated with two examples:

1. maximally frequency selective wavelets which generated transmission waveforms with compact support in both time- and frequency-domains.
2. wavelets which reduced sensitivity of WPM systems to loss of time synchronization.

Through computer simulations the advantages of the newly designed filter were compared and contrasted with standard wavelets. (*Items 12, 16*)

#### **g. Equalization of channel (Appendix C)**

Channel equalization in WPM is unique because the symbols overlap in time leading to inter-symbol interference (ISI) and inter-symbols inter-carriers interference (ISCI). To mitigate the detrimental effect of the channel an algorithm to equalize the channel was implemented. (*Items 6 and 7 in fig. 1.6*).

### **1-3-4 Original contributions of the thesis work**

The main contributions of this work are:

1. A wavelet packet analyser for estimation of spectrum (Chapter 6).
2. A transceiver based on wavelet packets for dynamic spectrum access applications (Chapter 7).
3. A framework to design and test new wavelets (Chapter 8).

Other contributions include:

1. Evaluation of performance of WPM under time/frequency and phase offsets and comparison with OFDM (Chapter 4).
2. Analysis of PAPR performance of WPM and implementation of two PAPR reduction algorithms (Chapter 5).
3. Implementation of a basic equalizer to aid WPM transmission (Appendix-C).

Some of the related activities accomplished during the course of the thesis work include:

**a. Software tools and graphical user interface (GUI) (Appendix B)** – A user-friendly GUI ((Item 22 in fig. 1.6) was developed to test and run the simulation models for:

- design of wavelets,
- operation of WPM transceiver.

**b. Tutorial material** – Study materials on the topic of wavelets for wireless communication were created to promote and motivate more research on the topic [22–25]

### 1-3-5 Research challenges

A few of the challenges encountered and addressed during the course of the PhD work are summarized below:

- System realization and establishment of a simulation environment to test WPM operation.
- Evaluation of the inherent properties of the wavelet packet modulator (in time and frequency domains) and devise algorithms that they aid WPM transmission.<sup>7</sup>
- Creation of a generic framework/toolbox to design wavelets.
- Translate system specifications into mathematical expressions to aid design processes.
- Define suitable performance metrics to evaluate WPM system operation.

It must also be stated that since the theory of wavelets emerged from diverse fields, there are no clear guidelines that can be readily used to design and develop wavelet based communication systems. Moreover, the nomenclature in the literature on wavelets is diverse and inconsistent. Therefore, to aid the development of wavelet based radios the notations and conventions had to be made uniform.

---

<sup>7</sup>The WPM transmission is unique because the symbols overlap in both time and frequency. This means that existing algorithms used in systems like OFDM cannot be used for WPM. This problem is particularly acute with regard to maintaining time-synchronization between the transceivers and equalization of channel.

### 1-3-6 Research approach and feasibility

The research strategy was theoretical studies and numerical simulation of typical scenario on a MATLAB® platform. The tasks specified in the previous section (see fig. 1.6) will be handled individually and when necessary holistically. The feasibility of the research approach will be demonstrated through simulation studies. The results will also be corroborated with analytical expressions and formulas. Wherever possible, the performance of the proposed WPM system will be compared and contrasted with FFT based OFDM systems.

## 1-4 Organization of thesis work

The dissertation is organized in 9 chapters. The contents provided thus far constitute the first chapter. The rest of the material is categorized into 3 parts namely, theoretical background (Part II), implementation challenges (Part III) and demonstration of advantages (Part IV).

**Part II - Theoretical background (Chapters 2 and 3)** In this part we provide the theoretical background. In chapter 2, material on the theory of wavelets is provided. And in chapter 3 the wavelet packet modulator, which is the focus of this research work, is introduced.

**Part III - Implementation challenges (Chapters 4 and 5)** In this dissertation we take up three of the issues encountered in the implementation of WPM. Each of these challenges is handled in a separate chapter. In Chapter 4 the influence of loss of synchronization (time/frequency/phase) on the performance of the WPM system is analyzed. For each of these synchronization errors a model is presented and theoretical analysis is given for both WPM and OFDM. The Bit error rate (BER) performance under time offset, frequency offset and phase noise is investigated by means of simulations studies. The simulations are performed for WPM with different types of standard wavelets and compared to OFDM. In Chapter 5 the sensitivity of WPM to PAPR is explored.

**Part IV - Demonstration of advantages (Chapters 6,7 and 8)** In Part IV some of the benefits of pursuing wavelet based systems for wireless systems' design are demonstrated. Three examples are considered: In chapter 6, a spectrum estimator based on wavelet packets is explained. The proposed method is shown to be efficient in estimation of spectrum for various sources and the performances comparable with existing techniques.

In chapter 7, a wavelet packet transceiver for spectral analysis and dynamic spectrum access is presented. The transceiver consists of a Wavelet Packet Spectral Estimator (WPSE) and a Wavelet Packet Multi-carrier Modulator (WPM). The WPSE senses the radio environment to identify Licensed Users (LU) bands and spectrum holes. This information is then used to shape the time-frequency characteristics of the WPM transmission waveform

Chapter	Subject matter	Item in fig. 1.6
1	Introduction	-
2	Theory of wavelets	-
3	Theory of wavelet packet modulator (WPM)	1,2, 18, 19
4	Study of time, frequency and phase Offset errors	3,4,5, 7, 20
5	Peak-to-average power ratio studies	9, 20
6	Wavelet packet spectrum estimator	13
7	Dynamic spectrum analysis	11, 13, 17 and 20
8	Design of wavelets	12 and 16
9	Conclusion	-
Appendix-B	Graphical user interface	22
Appendix-C	Channel equalization and transceiver synchronization	6, 7 and 10

TABLE 1.1: Chapters and contents.

to evade the LU transmission zones. The shaping is done by vacating those sub-carriers which lie in and around the LU bands. The studies show that WPSE/WPM performs better than Fourier based OFDM in regard to bit-error-rate (BER), bandwidth efficiency and interference to the licensees.

In Chapter 8, a general, unified approach to design and develop orthogonal wavelet packet bases according to a requirement. To this end, the design criterion and the wavelet constraints are first listed. The problem which is originally non-linear and non-convex in nature is then converted into a tractable convex optimization problem and finally solved using suitable Semi Definite Programming (SDP) tools. The proposed mechanism is demonstrated through two toy examples where families of wavelets which are i) maximally frequency selective and ii) have the lowest cross correlation energy, respectively, are developed. The design procedure borrows from the studies conducted in earlier chapters. For e.g. the design of maximally frequency selective filters borrows from the studies of Chapters 6 and 7 while the construction of filters with low cross correlation uses the conclusions of chapter 4.

Finally, the dissertation concludes in Chapter 9 with the main conclusions of the work and recommendations for future research.

Fig. 1.7 depicts the chapters of the thesis work, their organization and the link between the chapters. Table 1.1 gives the details of the chapters and their relation to the items listed in fig. 1.6<sup>8</sup>.

<sup>8</sup>Items 8, 15, 21 and 24 have not been handled in this work.

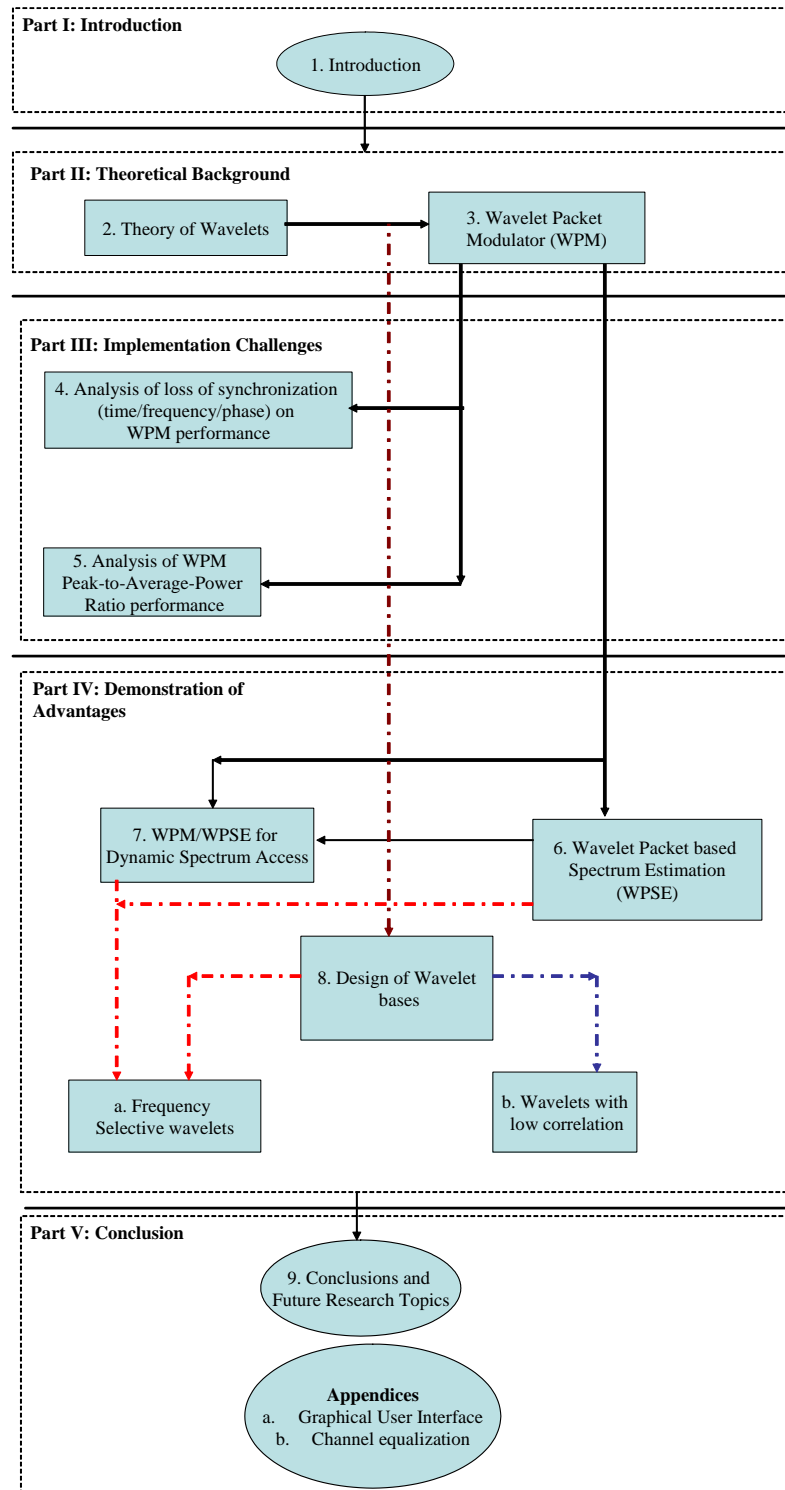


FIGURE 1.7: Organization of Chapters. The links between chapters have been indicated with arrows.

## **Part II**

# **Theoretical Background**

## Chapter 2

# Theory of wavelets

The Wavelet transform is a powerful new tool to analyze data. It can be used to represent known/unknown signals as a set of known functions, called wavelets, and gain insights on their characteristics. The tool is used in various applications and is becoming very popular amongst technologists, engineers and mathematicians alike. In most of the applications, the power of the transform comes from the fact that the basis functions of the transform have compact support in time (or space) and are localized in frequency. Furthermore, the technique allows analysis of signals at resolutions which correspond to the natural behavior of the process one wants to understand. These properties make wavelet transform a natural choice in fields as diverse as image synthesis, data compression, computer graphics and animation, human vision, radar, optics, astronomy, acoustics, seismology, nuclear engineering, biomedical engineering, magnetic resonance imaging, music, fractals, turbulence, and pure mathematics [5]. Recently wavelet transform has also been used in the design of sophisticated digital wireless communication systems including channel modeling, transceiver design, data representation and compression; source/channel coding, interference mitigation, signal de-noising and energy efficient networking [26].

In this chapter we provide an overview of the mathematical foundations of the wavelet theory. The material provided in this chapter will not only aid the understanding of later chapters but also serve to make the dissertation self-contained. A thorough study of the subject can be found in [5, 6, 8, 22, 26–39].

We start the chapter with a discussion on the representation of signals in Section 2-1. In this regard we trace the progression of the field of signal representation from classical Fourier analysis through Gabor transform to wavelet transform. The sections that follow Section 2-1 will elaborate further on the theory of wavelets. The two major branches of wavelet transform, namely Continuous Wavelet Transform (CWT) and Discrete Wavelet Transform (DWT) are explained in Section 2-2 and Section 2-4, respectively. Section 2-3 will detail an important facet

of the wavelet theory known as Multi-Resolution Analysis (MRA). This will be followed by a discussion on the filter bank implementation of DWT which includes material on analysis and synthesis of signals using filter banks in Section 2-5. An important variant of the wavelet transform known as Wavelet Packet Transform will be presented in Section 2-6. Finally, a review on a few popular wavelet families is given in Section 2-7.

### Notation

Throughout this dissertation, continuous variables are enclosed in curved brackets, e.g.  $f(x)$ ,  $g(t)$ , while discrete variables are denoted in square brackets, e.g.  $f[n]$ ,  $g[k]$ . Vectors are denoted in boldface, e.g.  $\mathbf{z} = z[n] = [z_0 \ z_1 \ z_2 \ \dots \ z_{N-1}]$ . The discrete index for time is represented with  $n$  while  $t$  is used to connote the continuous time variable. The corresponding indices in the frequency domain are denoted with  $f$  (continuous) and  $k$  (discrete). Finally, variables in time/space domain are given in small cases while their representation in transform domain (e.g. Fourier, Gabor, Wavelet) is expressed in upper case.

## 2-1 Introduction

### 2-1-1 Representation of signals

Mathematical representation of signals or transforms are a way to describe information or data a physical signal in terms of known mathematical functions. Through transformations valuable insights on the signal can be gained that can be exploited for various practical purposes. Burke [30] considers the transforms to be *mathematical prisms* that facilitate a better interpretation of signals just the way optical prisms split light into colors to enable a better understanding of light. The applications can be as diverse as processing audio/video/image data to modeling geological processes such as Tsunami or Earthquakes.

A mathematical transform is usually a linear expression where any given signal  $f(x)$  in space  $\mathbb{S}$  is expressed as a linear combination of a set of known signals  $\varphi_i; \forall i \in \mathbb{Z}$  as [28]:

$$f(x) = \sum_i \alpha_i \varphi_i \quad (2.1)$$

Here  $\alpha_i$  are the expansion coefficients or weights which tell how much of the component  $\varphi_i$  is available in the original signal  $f(x)$ . The space  $\mathbb{S}$  can be finite dimensional like the set of all real numbers  $\mathbb{R}^n$  or the set of all real integers  $\mathbb{Z}^n$ ; or infinite dimensional like the set of all square integrable functions  $L^2$  or the set of square sum able functions  $l^2$ .

The set is said to be complete for the space if there exists a dual set  $\tilde{\varphi}_i; \forall l \in \mathbb{Z}$  such that the expansion coefficients  $\alpha_i$  can be computed from them, i.e.

$$\alpha_i = \langle f(x), \tilde{\varphi}_i \rangle \quad (2.2)$$

Here, the operator  $\langle . \rangle$  represents the inner-product operation. The set  $\varphi_i; \forall l \in \mathbb{Z}$  is considered to be orthonormal and complete when  $\varphi_i = \tilde{\varphi}_i$  and

$$\langle \varphi_i, \varphi_j \rangle = \delta[i - j] \quad (2.3)$$

here  $\delta[.]$  is the dirac-delta function. On the other hand the set is said to be bi-orthogonal if it is complete and the vectors  $\varphi_i$  are linearly independent (but not orthonormal) and satisfy the relation:

$$\langle \varphi_i, \tilde{\varphi}_j \rangle = \delta[i - j] \quad (2.4)$$

The choice on the right set of basis functions depends on the type of signal to be represented and the application in hand.

### 2-1-2 Fourier analysis

The earliest recorded work on signal representation was conducted by Jean Baptiste Joseph Fourier in the early 19th century. He investigated problems of diffusion of heat and proved that periodic functions can be represented as a series of harmonically related sinusoids. This work, popularly known as the Fourier Series expansion, was published in the *Théorie Analytique de la Chaleur* (The Analytical Theory of Heat) in the year 1822 [30]. While Fourier series allows representation of periodic functions, a variant called Fourier Transform enabled decomposition of non-periodic functions of finite energy. Fourier Transform is an integral transform that expresses any complex-valued function of a real variable  $x(t)$  in terms of trigonometric basis functions:

$$X(f) = \int_{-\infty}^{\infty} x(t) \exp(-j2\pi ft) dt, f \in \mathbb{R}. \quad (2.5)$$

In signal processing applications  $x(t)$  exists in the time (or space) domain and the transform  $X(f)$  represents  $x(t)$  in the frequency domain. This is analogous to what music composers do when they represent musical chords in terms of the constituent notes. Through the reverse transform  $x(t)$  can be reconstructed from  $X(f)$  as follows:

$$x(t) = \int_{-\infty}^{\infty} X(f) \exp(j2\pi ft) df, t \in \mathbb{R}. \quad (2.6)$$

Since the Fourier transform analyses time-based signal to provide frequency information, the operation is regarded as frequency-amplitude decomposition.

The nice thing about the Fourier operations is that frequency information one obtains after the transforms often corresponds to the actual physical waves which constitute the signal [30].

### 2-1-3 Gabor transform

The Fourier Transform offers excellent frequency resolution but fails to provide any information on the temporal variations <sup>1</sup>. Furthermore, the sine/cosine functions which are the basis functions of these operations stretch to infinity in time. In order to have a representation that gives both time and frequency information of the signal studied, Dennis Gabor <sup>2</sup> adapted the Fourier transform to analyze only a small section of the signal at a time. In his adaptation, called the Short-Time Fourier Transform (STFT), the signal is windowed into small segments (taken to be stationary) which are then studied independently [8]. For a window function  $w(t)$  the STFT operation maps a signal or function  $f(t)$  into a two-dimensional function of time  $\tau$  and frequency  $f$  and can be defined as:

$$\mathbf{STFT}\{x(t)\} \equiv X(\tau, f) = \int_t [x(t)w(t - \tau)] \exp(-j2\pi ft) dt \quad (2.7)$$

The STFT is a compromise between time and frequency-based views of a signal [40]. A trade off between the time and frequency resolution is enabled in STFT by altering the dimensions of the window function. Smaller windows offer better time resolution but poorer frequency resolution. On the other hand if the size of the window is enlarged to allow better frequency resolution, the time resolution is compromised. Another drawback is that once a time window is chosen it remains the same for the analysis of all frequencies. Many signals require a more flexible approach, one where the window size can be varied to accurately determine both time and frequency. The solution - *Wavelet Analysis*.

### 2-1-4 Wavelet analysis

The wavelet transform is a multi-resolution analysis (MRA) mechanism where an input signal is decomposed into different frequency components; then each component is studied with resolutions matched to its time-scales. The Fourier transform also decomposes signals into elementary waveforms, but these bases are trigonometric functions (sines and cosines). Thus, when one wants to analyze the local properties of the input signal, such as edges or transients,

<sup>1</sup>The temporal data after a Fourier transform is not totally lost but encoded as phase information, which is usually inaccessible.

<sup>2</sup>He won the Nobel Prize in 1971 for his investigation and development of holography.

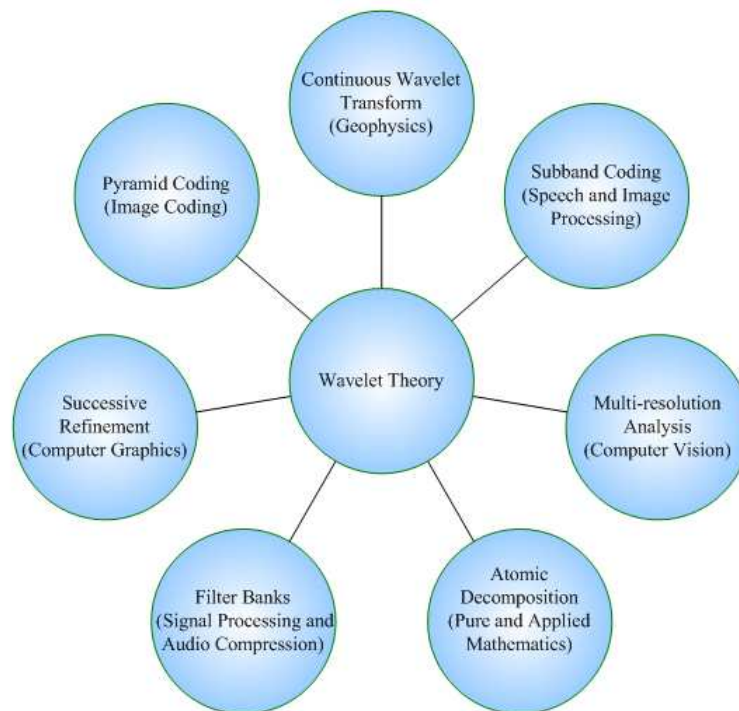


FIGURE 2.1: Wavelet Nomenclature: The figure depicts various terms associated with wavelet theory and the respective domains, enclosed within close brackets, from which the terminologies originated.

the Fourier transform is not an efficient analysis tool. By contrast the wavelet transforms which use irregularly shaped wavelets offer a better representation of sharp changes and local features. The wavelet transform gives good time resolution and poor frequency resolution at high frequencies and a good frequency resolution and poor time resolution at low frequencies. Such an approach is appropriate when the studied signal has high frequency components for short durations and low frequency components for long durations. Fortunately, the signals that are encountered in most applications are often of this type.

The theory of wavelets emerged from multiple backgrounds (refer fig. 2.1) - as Continuous wavelet transform (CWT) in Geo-Physics, as sub-band coding in speech and image processing, as filter Banks from the fields of signal processing and audio compression, as Multi-resolution Analysis from Computer Vision, as pyramid coding from Image Coding and as atomic decompositions in applied Mathematics. These topics had been studied independently under different names by different scientific communities and only recently did these ideas converge to facilitate a unified understanding of the subject. Even though the wavelet nomenclature is diverse, the wavelet theory can be interpreted broadly in terms of its continuous time and discrete time representations. We shall present these topics in the coming sections.

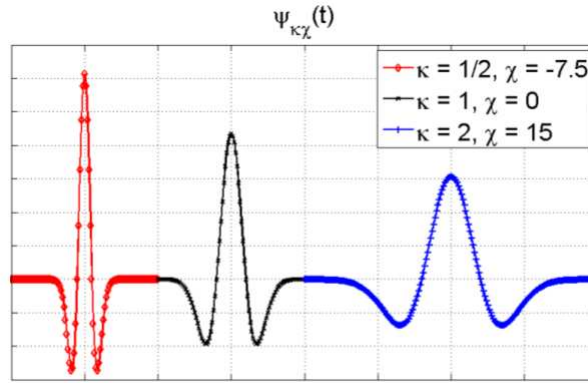


FIGURE 2.2: Mexican Hat Wavelet at different translations and scales.

## 2-2 Continuous wavelet transform

Wavelets for signal representation was introduced by Morlet and Grossmann [32] who showed that continuous-time functions  $f(t)$  in  $L^2(\mathbb{R})$  can be represented by a set of basis functions  $\{\psi_{\kappa, \chi}(t)\}$  obtained by scaling  $\kappa$  and shifting  $\chi$  primary functions known as mother wavelets  $\psi(t)$ . The continuous wavelet transform (CWT) of any continuous square-integrable function or signal  $f(t)$  in terms of wavelets  $\{\psi_{\kappa, \chi}(t)\}$  can be expressed as [29]:

$$\Upsilon_{\kappa, \chi} = \frac{1}{\sqrt{\kappa}} \int_{-\infty}^{\infty} f(t) \psi_{\kappa, \chi}^*(t) dt; \forall \kappa \in \mathbb{Z}^+, \chi \in \mathbb{Z}^+. \quad (2.8)$$

The expression (2.8) is a general form of CWT where  $\Upsilon_{\kappa, \chi}$  give the wavelet coefficients of the continuous signal  $f(t)$  as a function of the various scaled  $\kappa$  and the shifted  $\chi$  versions of the mother wavelet  $\psi(t)$ . The operator  $*$  stands for complex conjugation.

The mother wavelet  $\psi(t)$  is continuous in both time and frequency and the set of baby (or daughter) wavelets functions  $\psi_{\kappa, \chi}(t)$  are obtained by scaling  $\kappa$  and shifting  $\chi$  the mother wavelet  $\psi(t)$  [29]:

$$\psi_{\kappa, \chi}(t) = \frac{1}{\sqrt{\kappa}} \psi\left(\frac{t - \chi}{\kappa}\right); \forall \kappa \in \mathbb{Z}^+, \chi \in \mathbb{Z}^+. \quad (2.9)$$

The scaling parameter is similar to the frequency variable in Fourier Transform. It describes how a wavelet basis function is stretched or contracted. On the other hand, the shift variable, also known as translation parameter, represents the location of the wavelet in time. Both these parameters are continuous-real variables. An example of scaled and translated wavelet is illustrated in fig. 2.2, where a wavelet, popularly known as the Mexican Hat because of its shape, is shown for three different translation and scale factors. The wavelet shown at the origin represents the mother wavelet, which is neither shifted nor scaled.

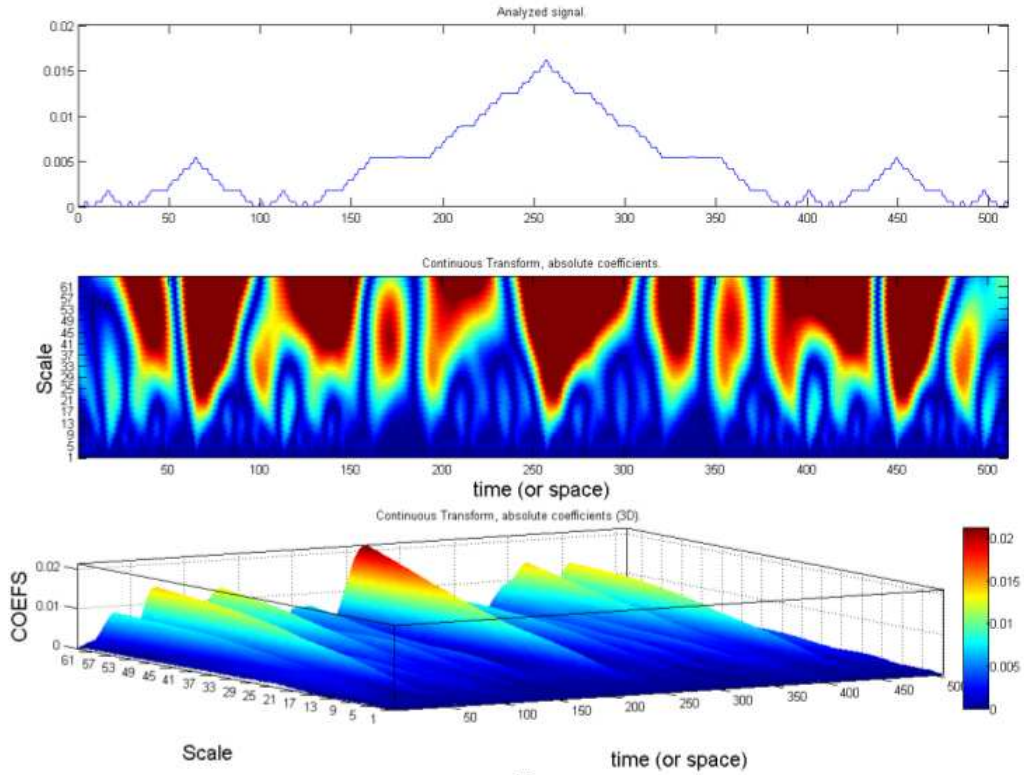


FIGURE 2.3: Translation-Scale Representation of a Signal.

The original signal  $f(t)$  can be reconstructed from wavelet coefficients through the inverse wavelet transform [41]:

$$f(t) = \frac{1}{c_\psi} \int_{\kappa} \int_{\chi} \Upsilon_{\kappa, \chi} \frac{1}{\kappa^2} \tilde{\psi} \left( \frac{t - \chi}{\kappa} \right) d\chi d\kappa, \quad (2.10)$$

where  $\tilde{\psi}(t)$  is the dual function of  $\psi(t)$  and must satisfy the condition [41],

$$\int_0^{\infty} \int_{-\infty}^{\infty} \psi \left( \frac{t_1 - \chi}{\kappa} \right) \tilde{\psi} \left( \frac{t - \chi}{\kappa} \right) \frac{d\chi d\kappa}{|\kappa|^3} = \delta(t - t_1) \quad (2.11)$$

For orthogonal expansion sets,  $\tilde{\psi}(t) = C_\psi^{-1} \psi(t)$  where [41],

$$c_\psi = \int_{\mathbb{R}} \frac{|\hat{\psi}(\omega)|^2}{|\omega|} d\omega. \quad (2.12)$$

Here,  $\hat{\psi}(\omega)$  represents the Fourier transform of  $\psi(t)$ .

An example of the CWT where a signal of finite support is expressed as a two-dimensional (2D) and three-dimensional (3D) time-scale array of coefficients is illustrated in fig. 2.3. The signal considered is a fractal developed by the Swedish Mathematician Helge von Koch. The large

amplitude in the figure corresponds to high frequency-correlation of the signal with the wavelet function of a particular scale at a certain time instance.

### 2-2-1 Orthonormal wavelets

In theory any function which has zero integral can be considered as the mother wavelet  $\psi(t)$ . Furthermore, the shift and scale parameters can be real continuous values ( $\kappa \in \mathbb{Z}^+$ ,  $\chi \in \mathbb{Z}^+$ ). Hence the CWT, as expressed in eq. (2.8), leads to a representation which is infinitely redundant in nature. Such an expression is unwieldy and difficult to implement. To get around this problem, a sparse representation which gives perfect reconstruction of the signal while avoiding redundancy is preferred. The answer is *orthogonal wavelets*.

Meyer [42] proved that there exist wavelets  $\psi(t)$  that provide an orthogonal expansion set of  $L^2(\mathbb{R})$  and is of the form:

$$\psi_{\alpha,\beta}(t) = \sqrt{2^\alpha} \psi(2^\alpha t - \beta); \forall \alpha, \beta \in \mathbb{Z}. \quad (2.13)$$

In eq. (2.13)  $\alpha$  and  $\alpha$  are the scaling and shift parameters which vary in discrete integer units, i.e.  $\alpha, \beta \in \mathbb{Z}$ . Meyer also showed that these wavelets are generalized form of the Haar function. The work of Meyer was carried forward by Daubechies [27, 43] who came out with a family of wavelets which in addition to being orthogonal also had compact support.

### 2-2-2 Non-dyadic wavelets

It is important to note that Orthonormal wavelets need not always be of the form eq. (2.13) nor do the scales have to be dyadic. In fact recent studies show that the scaling factor can be different from 2 and can take any rational value  $p/q > 1$  [43]. However, in these more general cases, it may be necessary to introduce more than one (but always a finite number) of mother wavelets.

We would like to mention here that through out this dissertation only orthonormal wavelets of the form eq. (2.13) will be used. This is because, not only is the theory of dyadic wavelets well established, the bases with factor-2 are also easy to implement for numerical computations.

## 2-3 Multi-resolution analysis

An important advancement in the field of wavelets was the Multi-resolution Analysis (MRA) framework developed by Mallat [44] and Meyer [42]. The MRA allows characterization of

$\psi(t) \in L^2(\mathbb{R})$  that result in an orthonormal basis. The starting point in the discussion on MRA is to consider the wavelet coefficients  $\langle f(t), \psi_{\alpha,\beta}(t) \rangle$  at any scale  $\alpha$ , which covers the difference in the approximations of  $f(t)$  at resolutions  $2^{\alpha+1}$  and  $2^\alpha$ , respectively. To characterize the successive vector spaces  $V_\alpha$  in which the function  $f(t)$  is approximated, a complementary function called the scaling function  $\varphi(t)$  is defined<sup>3</sup>. As in the case of wavelet functions  $\psi_{\alpha,\beta}(t)$ , there also exists an extended family of scaling functions  $\varphi_{\alpha,\beta}(t)$  which are obtained by time shifted version of the fundamental scaling function  $\varphi(t)$  [31]:

$$\varphi_{\alpha,\beta}(t) = 2^{\alpha/2} \varphi(2^\alpha t - \beta), \quad \forall \beta \in \mathbb{Z} \quad \varphi \in L^2 \quad (2.14)$$

The approximation subspaces  $V_\alpha$  spanned by the scaling functions  $\varphi_{\alpha,\beta}(t)$  over integers  $-\infty < \beta < \infty$  are defined by:

$$V_\alpha = \overline{\text{Span}_\beta \{\varphi_\beta(2^\alpha t)\}} = \overline{\text{Span}_\beta \{\varphi_{\alpha,\beta}(t)\}} \quad (2.15)$$

Low values of  $\alpha$  provide coarse representation of a signal while higher values of  $\alpha$  represent the finer details. MRA requires the spaces  $V_\alpha$  spanned by the scaling functions  $\varphi_{\alpha,\beta}(t)$  to have finite energy and ordered as a nested approximation space as [31]:

$$0 \cdots \subset V_{-2} \subset V_{-1} \subset V_0 \subset V_1 \subset V_2 \cdots \subset L^2 \quad (2.16)$$

i.e.:

$$V_\alpha \subset V_{\alpha+1} \quad \forall \alpha \in \mathbb{Z}$$

$$\begin{aligned} \bigcap_{\alpha \in \mathbb{Z}} V_\alpha &= \{0\} \\ \bigcup_{\alpha \in \mathbb{Z}} V_\alpha &= L^2(\mathbb{R}) \end{aligned} \quad (2.17)$$

Eq. (2.17) implies that the space that contains high resolution approximates of a signal will also contain information on its lower resolution representation. The nested vector spaces spanned by the scaling functions are illustrated in fig. 2.4.

The MRA imposes strict restrictions on what the scaling function  $\varphi(t)$  can be. One of the conditions is that there exists *weights*  $h[k]$  such that the scaling function  $\varphi(t)$  (which spans  $V_0$ ) can be expressed as a weighted sum of shifted versions of  $\varphi(2t)$  (which spans  $V_1$ ), i.e. [31]:

$$\varphi(t) = \sum_k h[k] \sqrt{2} \varphi(2t - k), \quad k \in \mathbb{Z} \quad (2.18)$$

<sup>3</sup>The scaling functions are also called father wavelet. The father wavelet acts with the mother wavelet to yield a family of baby wavelets.

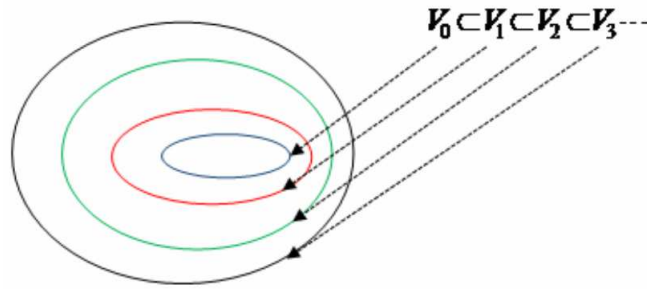


FIGURE 2.4: Spaces Spanned by the Scaling Functions.

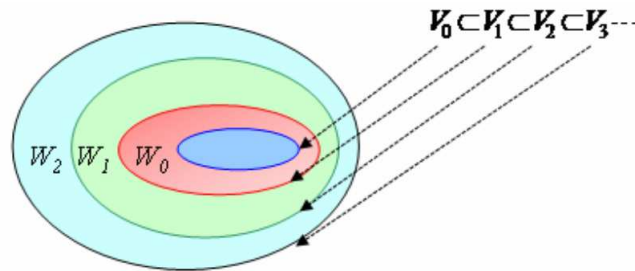


FIGURE 2.5: Spaces Spanned by the Scaling Functions and Wavelets.

where  $h[k]$  denotes the scaling function coefficients. This equation shows that scaling function can be constructed by the sum of its half-length translations.

There are other restrictions on the nature of  $\varphi(t)$  and  $\psi(t)$  which are usually determined by the scaling coefficients  $h[k]$ . We shall delve on them in Chapter 9 where the design of wavelets is discussed in detail.

As mentioned earlier, the wavelets  $\psi(t)$  in MRA are defined as orthogonal bases that span the differences between the spaces spanned by the scaling functions at various scales. Let the subspace spanned by the wavelet be  $W_{j-1}$ , then the function spaces covered by the scaling functions  $V_\alpha$  can be written as:

$$\begin{aligned}
 V_1 &= V_0 \oplus W_0 \\
 V_2 &= V_1 \oplus W_1 = (V_0 \oplus W_0) \oplus W_1 \\
 &\vdots \\
 V_{\alpha+1} &= V_\alpha \oplus W_\alpha = \bigoplus_{l=0}^{\alpha} W_l \quad \forall \alpha \in \mathbb{Z}
 \end{aligned}
 \tag{2.19}$$

Nested vector spaces spanned by the scaling function and wavelet vector spaces are illustrated in fig. 2.5.

It should be noted that the space  $W_0$  spanned by a wavelet is actually a subspace of  $V_1$  ( $W_0 \subset V_1$ ). Therefore there exists a corresponding orthonormal basis of wavelets defined by a weighted sum

of shifted scaling function  $\varphi(2t)$  similar to eq. (2.18),

$$\psi(t) = \sum_k g[k] \sqrt{2} \varphi(2t - k), \quad k \in \mathbb{Z}. \quad (2.20)$$

In eq. 2.20,  $g[k]$  denotes the wavelet function coefficients. Because of the orthogonality condition  $V_0 \perp W_0 \perp W_1 \perp \dots \perp W_\alpha$  the scaling and wavelet coefficients are related to each other by [8, 29]:

$$g[k] = (-1)^k h[L - 1 - k], \quad \text{for } h[k] \text{ of length } L. \quad (2.21)$$

## 2-4 Discrete wavelet transform

For practical applications the continuous wavelet transform is not useful and therefore a discrete version of the wavelet transform is preferred. Assuming an orthogonal transform, the forward discrete wavelet transform (DWT) of a discrete signal or function  $f[n] n = 0, 1, 2, \dots, M - 1$  belonging to  $l^2(\mathbb{Z})$  is defined as <sup>4</sup>:

$$\lambda_{\alpha,\beta} = \langle f[n], \varphi_{\alpha,\beta}[n] \rangle = \frac{1}{\sqrt{M}} \sum_n f[n] \varphi_{\alpha,\beta}[n] = \frac{1}{\sqrt{M}} \sum_n f[n] 2^{\alpha/2} \varphi[2^\alpha n - \beta] \quad (2.22)$$

$$\gamma_{\alpha,\beta} = \langle f[n], \psi_{\alpha,\beta}[n] \rangle = \frac{1}{\sqrt{M}} \sum_n f[n] \psi_{\alpha,\beta}[n] = \frac{1}{\sqrt{M}} \sum_n f[n] 2^{\alpha/2} \psi[2^\alpha n - \beta] \quad (2.23)$$

Here,  $\lambda_{\alpha,\beta}$  and  $\gamma_{\alpha,\beta}$  are the scaling and wavelet transform coefficients and  $\frac{1}{\sqrt{M}}$  is the normalization factor. Usually, the value of  $M$  is limited by the desired resolution  $\alpha$  and is taken to be  $M = 2^\alpha$ .

The inverse transform to approximate  $f[n]$  in terms of the scaling functions  $\varphi_{\alpha,\beta}[n]$  is given as [31]:

$$f[n] = \frac{1}{\sqrt{M}} \left( \sum_{\alpha=-\infty}^{\infty} \sum_{\beta=-\infty}^{\infty} \lambda_{\alpha,\beta} \varphi_{\alpha,\beta}[n] \right) \quad (2.24)$$

<sup>4</sup>For the discrete version the notation of the time unit has been changed from  $t \mapsto n$

This can be rewritten at a desired resolution space  $V_{\alpha_0}$  by a series sum of scaling function of subspace  $\alpha_0$  and wavelet functions of subspace  $\alpha = \alpha_0 \rightarrow \infty$  as follows [31]:

$$f[n] = \frac{1}{\sqrt{M}} \left( \underbrace{\sum_{\beta=-\infty}^{\infty} \lambda_{\alpha_0, \beta} \varphi_{\alpha_0, \beta}[n]}_{V_{\alpha_0}} + \underbrace{\sum_{\alpha=\alpha_0}^{\infty} \sum_{\beta=-\infty}^{\infty} \gamma_{\alpha, \beta} \psi_{\alpha, \beta}[n]}_{\subset W_{\alpha}} \right) \quad (2.25)$$

The parameter  $\alpha_0$  in eq. (2.25) is an integer which sets the coarsest level of approximation of the function  $f[n]$ , the details of the which are filled by its projection onto the wavelet spaces  $W_{\alpha}$ . In terms of the function spaces the resolution  $Nr$  at which  $f[n]$  is approximated can be given as:

$$V_{Nr} = V_{\alpha_0} + \sum_{\alpha=0}^{Nr-1} W_{\alpha} \quad (2.26)$$

## 2-5 Filter bank representation of DWT

One of the breakthroughs of wavelet transform was the possibility of implementing the DWT algorithm using filter banks. Mallat [37, 38, 44] showed that it is possible to perform DWT decomposition and reconstruction using 2-channel filter banks through a hierarchical algorithm known as the pyramidal algorithm. This meant that results of wavelet theory could be developed entirely using filter banks. In the next two sections we shall see how this is done.

### 2-5-1 Analysis filter bank

We start by considering the discrete variant of eq.(2.18) which expresses the scaling functions  $\phi[n]$  as a series sum of shifted versions  $\phi[2n]$  [31],

$$\varphi[n] = \sum_k h[k] \sqrt{2} \varphi[2n - k], \quad k \in \mathbb{Z}, \quad (2.27)$$

Applying the transform  $n \rightarrow 2^{\alpha}n - \beta$  we obtain,

$$\begin{aligned} \varphi[2^{\alpha}n - \beta] &= \sum_k h[k] \sqrt{2} \varphi[2(2^{\alpha}n - \beta) - k] \\ &= \sum_k h[k] \sqrt{2} \varphi[2^{\alpha+1}n - 2\beta - k] \\ &= \sum_{m=2\beta+k} h[m - 2\beta] \sqrt{2} \varphi[2^{\alpha+1}n - m] \end{aligned} \quad (2.28)$$

Similarly, considering the discrete version of eq. (2.20)

$$\psi[n] = \sum_k g[k] \sqrt{2} \varphi[2n - k], \quad k \in \mathbb{Z}, \quad (2.29)$$

and applying the transform  $n \rightarrow 2^\alpha n - \beta$  we obtain,

$$\begin{aligned} \psi[2^\alpha n - \beta] &= \sum_k g[k] \sqrt{2} \varphi[2(2^\alpha n - \beta) - k] \\ &= \sum_k g[k] \sqrt{2} \varphi[2^{\alpha+1} n - 2\beta - k] \\ &= \sum_{m=2\beta+k} g[m - 2\beta] \sqrt{2} \varphi[2^{\alpha+1} n - m] \end{aligned} \quad (2.30)$$

The DWT coefficients at scale  $\alpha$  by coefficients at the higher scale  $\alpha + 1$  can be as follows:

$$\lambda_{\alpha,\beta} = \langle f[n], \varphi_{\alpha,\beta}[n] \rangle = \frac{1}{\sqrt{M}} \sum_n f[n] \varphi_{\alpha,\beta}[n] = \frac{1}{\sqrt{M}} \sum_n f[n] 2^{\alpha/2} \varphi[2^\alpha n - \beta] \quad (2.31)$$

Substituting eq. (2.31) into eq. (2.31) we get,

$$\begin{aligned} \lambda_{\alpha,\beta} &= \frac{1}{\sqrt{M}} \sum_n f[n] 2^{\alpha/2} \sum_{m=2\beta+k} h[m - 2\beta] \sqrt{2} \varphi[2^{\alpha+1} n - m] \\ &= \frac{1}{\sqrt{M}} \sum_{m=2\beta+k} h[m - 2\beta] \sum_n f[n] 2^{\alpha+1/2} \varphi[2^{\alpha+1} n - m] \\ &= \frac{1}{\sqrt{M}} \sum_{m=2\beta+k} h[m - 2\beta] \lambda_{\alpha+1,\beta} \end{aligned} \quad (2.32)$$

Similarly, we find

$$\gamma_{\alpha,\beta} = \langle f[n], \psi_{\alpha,\beta}[n] \rangle = \frac{1}{\sqrt{M}} \sum_n f[n] \psi_{\alpha,\beta}[n] = \frac{1}{\sqrt{M}} \sum_n f[n] 2^{\alpha/2} \psi[2^\alpha n - \beta] \quad (2.33)$$

Substituting eq. (2.31) into eq. (2.33), yields

$$\begin{aligned} \gamma_{\alpha,\beta} &= \frac{1}{\sqrt{M}} \sum_n f[n] 2^{\alpha/2} \sum_{m=2\beta+k} g[m - 2\beta] \sqrt{2} \psi[2^{\alpha+1} n - m] \\ &= \frac{1}{\sqrt{M}} \sum_{m=2\beta+k} g[m - 2\beta] \sum_n f[n] 2^{\alpha+1/2} \psi[2^{\alpha+1} n - m] \\ &= \frac{1}{\sqrt{M}} \sum_{m=2\beta+k} g[m - 2\beta] \gamma_{\alpha+1,\beta} \end{aligned} \quad (2.34)$$

Eq. (2.32) and eq. (2.34) imply that wavelet and scaling DWT coefficients at a certain scale can be calculated by taking a weighted sum of DWT coefficients from higher scales. This can be

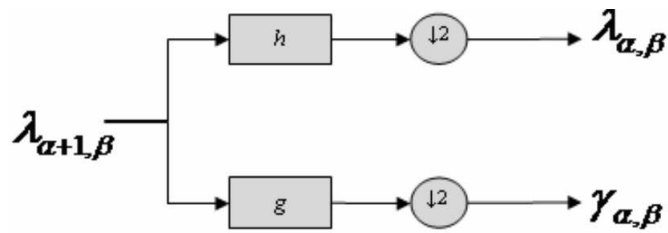


FIGURE 2.6: 2-Channel Analysis Filter Bank [31].

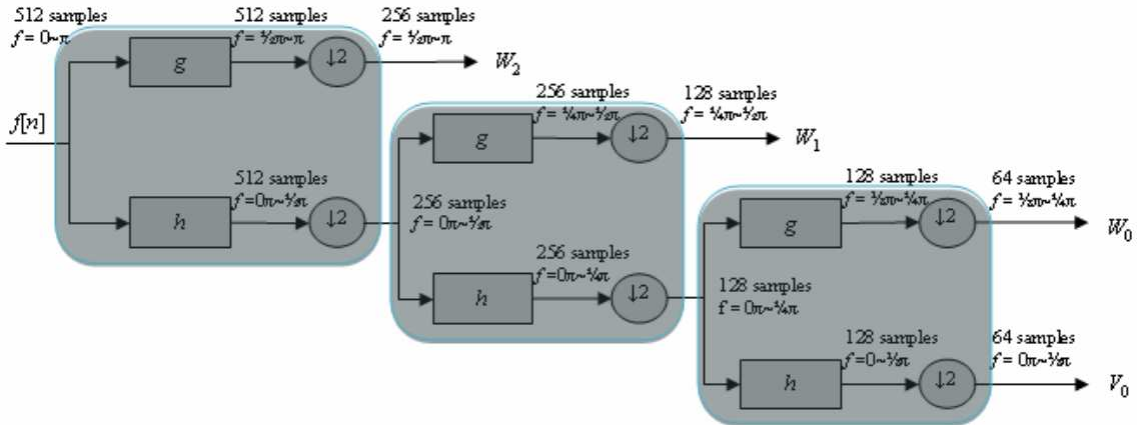


FIGURE 2.7: 3-Stage analysis tree [31].

viewed as convolution between the DWT coefficients at scale  $\alpha + 1$  with wavelet and scaling filter coefficients and subsequently sub-sampling each output with factor-2 to obtain new wavelet and scaling DWT coefficients at scale  $\alpha$ . Therefore, we can implement eqs. (2.27) and (2.29) by a 2-channel filter bank as illustrated in fig. 2.6.

The 2-channel filter bank first splits the input signal in two parts and filters one part with filter  $h$  and the other with filter  $g$ . Both the filtered constituents are then sub-sampled by 2. Each output component will therefore contain half the number of samples and span half of the frequency band compared to the input signal.

The complete representation of the DWT can be obtained by iteration of the 2-channel filter bank and taking repeatedly scaling DWT coefficients  $\lambda$  as input. The number of stages in the iteration process will determine the DWT resolution and therefore the number of channels.

The example of a two band analysis tree with three stages is graphically shown by fig. 2.7. The input signal  $f$  has 512 samples and contains frequencies that lie between 0 and  $\pi$ . The resulting decompositions together will still contain 512 samples and span the same frequency band as the original signal but these will be decomposed in different DWT coefficients.

The sub-band structure of wavelet decomposition in frequency domain for a 3-stage analysis is illustrated in fig. 2.8.

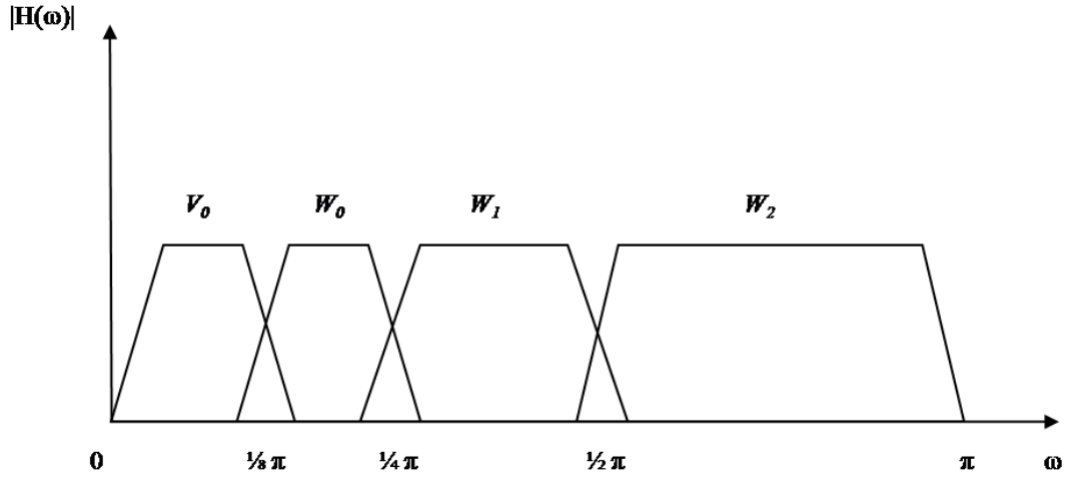


FIGURE 2.8: Frequency bands for the 3-Stage analysis tree [31].

### 2-5-2 Synthesis filter bank

The reconstruction formula is derived by considering a signal in the  $\alpha + 1$  scaling space  $f[n] \in V_{\alpha+1}$  as [31]:

$$f[n] = \frac{1}{\sqrt{M}} \left( \sum_{\beta=-\infty}^{\infty} \lambda_{\alpha+1,\beta} \varphi_{\alpha+1,\beta}[n] \right) = \frac{1}{\sqrt{M}} \left( \sum_{\beta=-\infty}^{\infty} \lambda_{\alpha+1,\beta} \sqrt{2^{\alpha+1}} \psi[2^{\alpha+1}n - \beta] \right). \quad (2.35)$$

This can be expressed in terms of the next scale as [31]:

$$f[n] = \frac{1}{\sqrt{M}} \left( \sum_{\beta} \lambda_{\alpha,\beta} 2^{\alpha/2} \varphi[2^{\alpha}n - \beta] + \sum_{\beta} \gamma_{\alpha,\beta} 2^{\alpha/2} \psi[2^{\alpha}n - \beta] \right). \quad (2.36)$$

Substituting the 2-scale equations eq. (2.27) and eq. (2.29) into eq. 2.36, we get

$$f[n] = \frac{1}{\sqrt{M}} \left( \sum_{\beta} \lambda_{\alpha,\beta} \sum_{m=2\beta+k} h[m - 2\beta] 2^{(\alpha+1)/2} \varphi[2^{\alpha+1}n - m] \right) + \frac{1}{\sqrt{M}} \left( \sum_{\beta} \gamma_{\alpha,\beta} \sum_{m=2\beta+k} g[m - 2\beta] 2^{(\alpha+1)/2} \varphi[2^{\alpha+1}n - m] \right). \quad (2.37)$$

Multiplying both sides of equation eq. (2.37) by  $\varphi[2^{\alpha+1}n - \beta']$  and taking the summation allows us to describe the DWT coefficients at higher scales by those of the lower scale [31]:

$$\lambda_{\alpha+1,\beta} = \sum_m \lambda_{\alpha,\beta} h[\beta - 2m] + \sum_m \gamma_{\alpha,\beta} g[\beta - 2m] \quad (2.38)$$

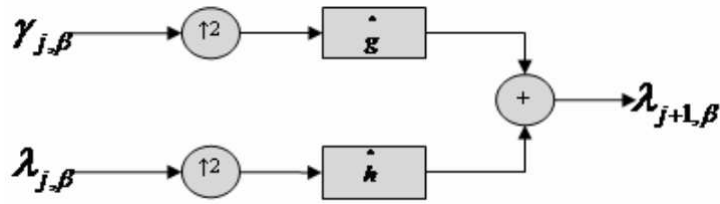


FIGURE 2.9: 2-Channel Synthesis Filter Bank.

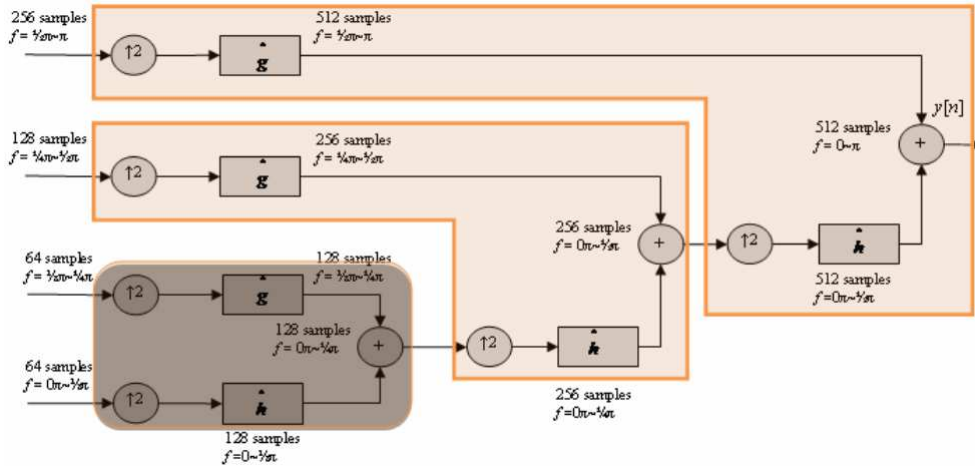


FIGURE 2.10: Synthesis Tree.

The expression eq. (2.38) implies that the DWT coefficients at certain scale level  $\alpha + 1$  can be reconstructed by taking a combination of weighted wavelet and scaling DWT coefficients at previous scale  $\alpha$ .

Introducing, two new variables  $\hat{h}[n]$  and  $\hat{g}[n]$  which are time-reversed versions of  $h[n]$  and  $g[n]$ , i.e.,  $\hat{h}[n] = h[-n]$  and  $\hat{g}[n] = g[-n]$ , eq. (2.38) can be described by the 2-channel synthesis filter bank, illustrated in fig. 2.9.

The 2-channel synthesis filter bank performs operations which are exactly opposite to those of analysis filter bank discussed in the previous section. The wavelet and scaling DWT coefficients are first up-sampled by factor-2 and after that the wavelet function DWT coefficients are filtered with HPF  $\hat{g}$  while scaling function DWT coefficients are filtered with LPF  $\hat{h}$ . The two filtered signals are then added to each other to construct DWT coefficients at higher scale.

The decomposition of a signal in terms of coefficients is called discrete wavelet transform. In order to reconstruct the original signal from coefficients we can apply the inverse wavelet transform, abbreviated IDWT. The IDWT can be efficiently implemented by iterating the 2-channel synthesis filter bank in the same manner like we have done in the previous paragraph for the 2-channel analysis filter bank. The example of 3-stages synthesis tree is illustrated in fig. 2.10.

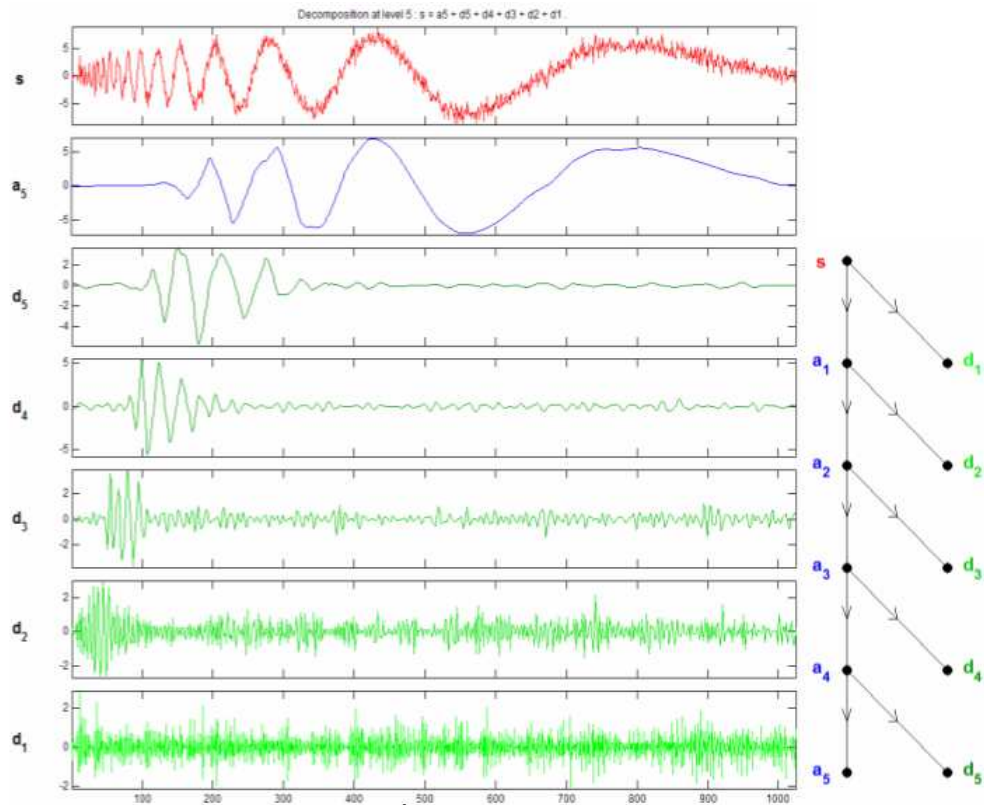


FIGURE 2.11: Discrete Wavelet Transform of the Noisy Doppler (time domain).

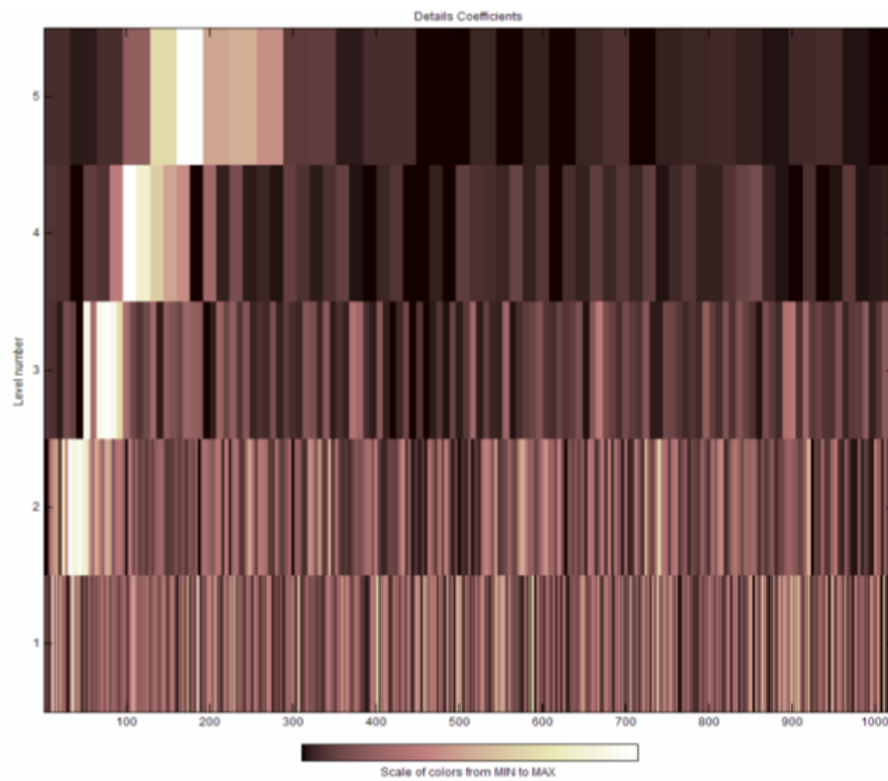


FIGURE 2.12: Discrete Wavelet Transform of the Noisy Doppler (time-scale domain).

If the assumption of orthogonality is valid the reconstructed signal is merely a (over  $\Delta$ ) delayed version of the input signal, i.e.  $x[n] = y[n - \Delta]$ . The filter banks that satisfy this property are called perfect reconstruction filter banks.

Fig. 2.11 depicts the decomposition of a noisy Doppler function into DWT coefficients at different scales. In this figure we can see how the time-varying frequency signal is described by the wavelet transform as a function of scale and translation index. A more common and compact figure of DWT performed on the same signal is shown in fig. 2.12. In this representation the depicted colors contain the scale information.

## 2-6 Wavelet packet transform

The wavelet transform is implemented as a non-uniform filter bank where only the low pass (scaling) branches are iteratively decomposed. The wavelet packet transform is a generalized form of the wavelet transforms where the tree structure used to implement the wavelet algorithm is decomposed on the high pass (wavelet) as well as the low pass filter branches. The original investigation on the topic was carried out by Coifman and Meyer [42, 45]. And it was followed by Wickerhauser [46, 47] who constructed uniform wavelet packet trees and demonstrated its operation for acoustic signal compression. Because the high frequencies are decomposed in the same manner as low frequencies the wavelet packet transform has evenly spaced frequency resolution. Fig. 2.13 shows the frequency bands of a 3-stage wavelet packet tree.

The filter bank structure for wavelet packet transform usually expands to a full binary tree<sup>5</sup>. In order to make clear the distinction between different sets of coefficients we label each wavelet packet  $\xi[n]$  by the level- $l$  which corresponds to the depth of the node in the tree and by the current position  $p$  of the node at a given level. Wavelet packet decomposition recursively splits each parent node in two orthogonal sub-spaces  $W_l^p$  located at the next level [48]

$$W_l^p = W_{l+1}^{2p} \oplus W_{l+1}^{2p+1} \quad (2.39)$$

The subspaces given in eq. (2.39) are those spanned by the basis functions of wavelet packets

$$W_l^p = \overline{\text{span} \{2^{l/2} \xi_l^p[2^l n - k]\}} \quad (2.40)$$

Wavelet packet coefficients  $\xi[n]$  at a certain level are calculated by convolving the wavelet and scaling filter with wavelet packets coefficients from a previous level. This action is performed repeatedly for all wavelet packets until the full binary tree is obtained for the desired depth.

<sup>5</sup>Arbitrary pruning of the full binary tree also lead to a basis for square summable spaces  $l^2(\mathbb{R})$ .

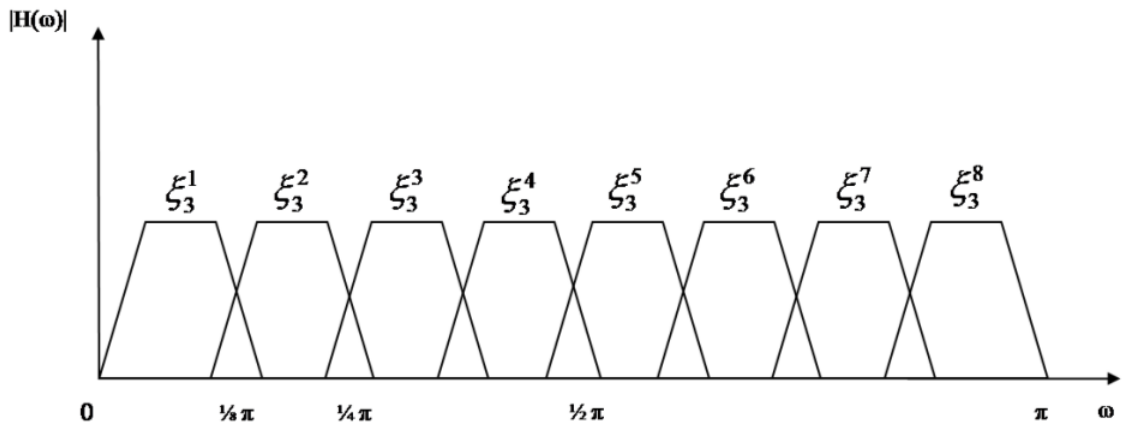


FIGURE 2.13: Frequency Bands for 3-Stage Wavelet Packets Tree.

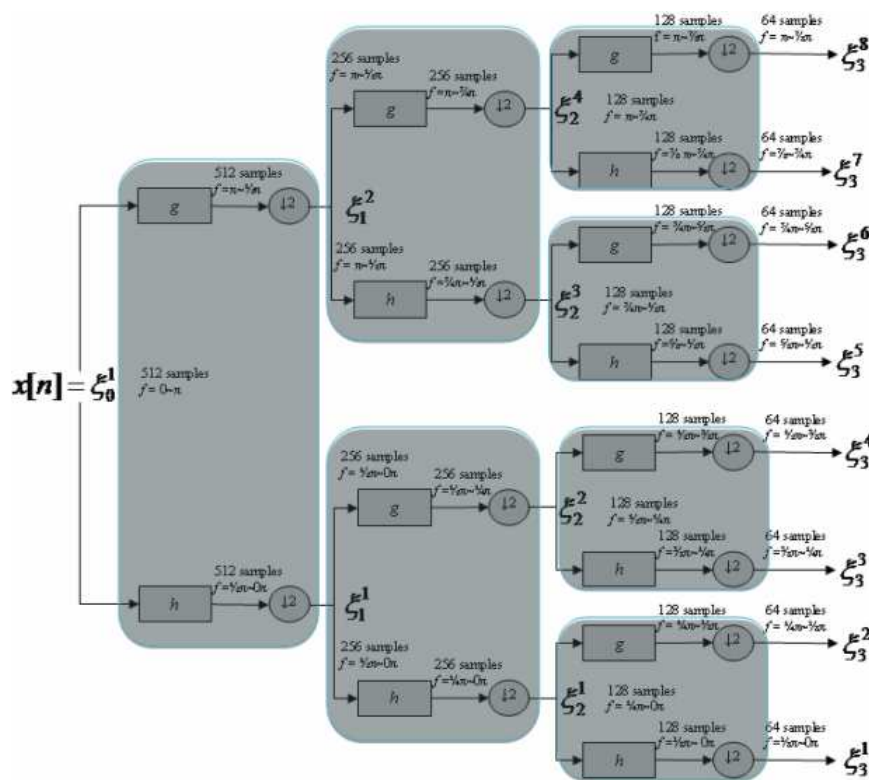


FIGURE 2.14: 3-Stage Wavelet Packet Analysis Tree.

The wavelet packets coefficients  $\xi_{l+1}^{2p+1}[n]$  are generated using the scaling filter and coefficients  $\xi_{l+1}^{2p+1}[n]$  which are created using the wavelet filter [11, 48]

$$\begin{aligned} \xi_{l+1}^{2p}[n] &= \sqrt{2} \sum_k h[k] \xi_l^p[2n - k] \\ \xi_{l+1}^{2p+1}[n] &= \sqrt{2} \sum_k g[k] \xi_l^p[2n - k] \end{aligned} \tag{2.41}$$

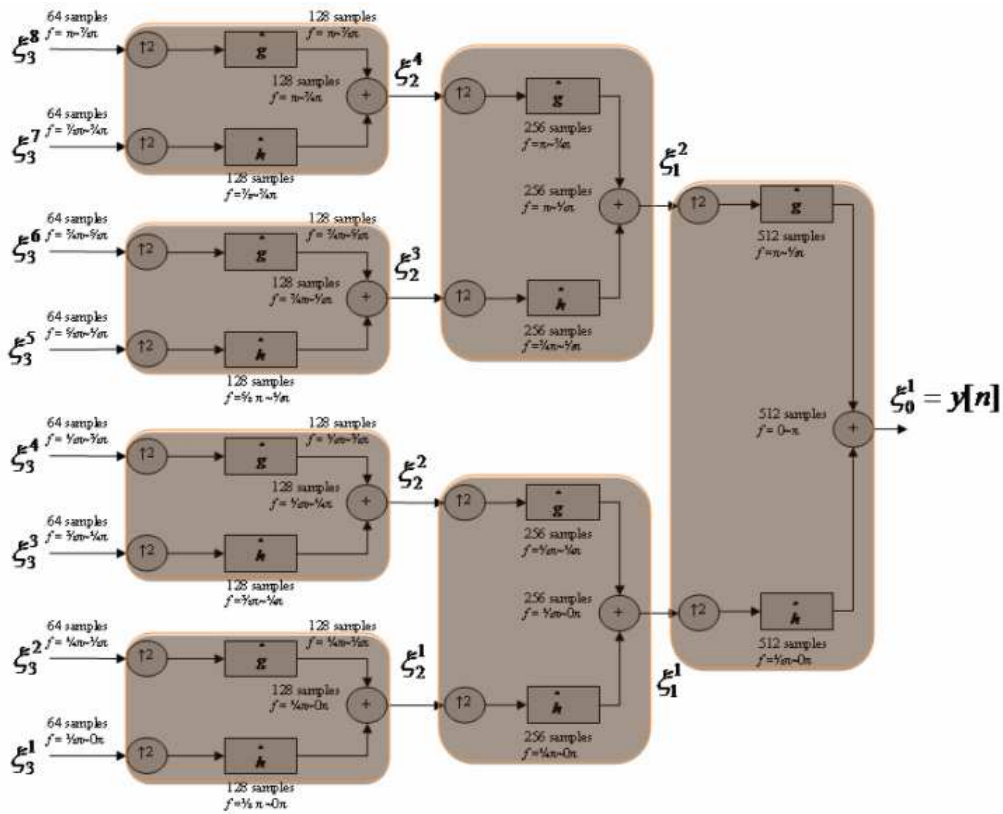


FIGURE 2.15: 3-Stages Wavelet Packets Synthesis Tree.

The expression (2.41) shows the recursive equation for wavelet packets generation. In the regular DWT decomposition for each additional level we need only to perform a single iteration of a 2-channel filter bank while in the wavelet packet transform the number of iterations is exponentially proportional to the number of levels. Therefore, the wavelet packet transform has higher computational complexity when compared to regular DWT. By utilization of the fast filter bank algorithm the wavelet packet transform requires  $O(N \log(N))$  operations, similar to FFT while DWT needs only  $O(N)$  calculations [10].

Fig. 2.14 illustrates the full binary tree for a 3-stages wavelet packet analysis.

The reconstruction of wavelet packets is also performed in an iterative method. For each pair of wavelet packets coefficients at level  $l$  of the tree we can calculate wavelet packets coefficients at the previous level  $l - 1$  by:

$$\xi_l^p[n] = \sum_k h[k] \xi_{l+1}^{2p}[2n - k] + \sum_k g[k] \xi_{l+1}^{2p}[2n - k] \quad (2.42)$$

Fig. 2.15 depicts the 3-stage wavelet packets synthesis tree.

Fig. 2.16 portrays the wavelet packet decomposition of the noisy Doppler function at different scales. The same noisy Doppler signal as used in the DWT example has also been used here.

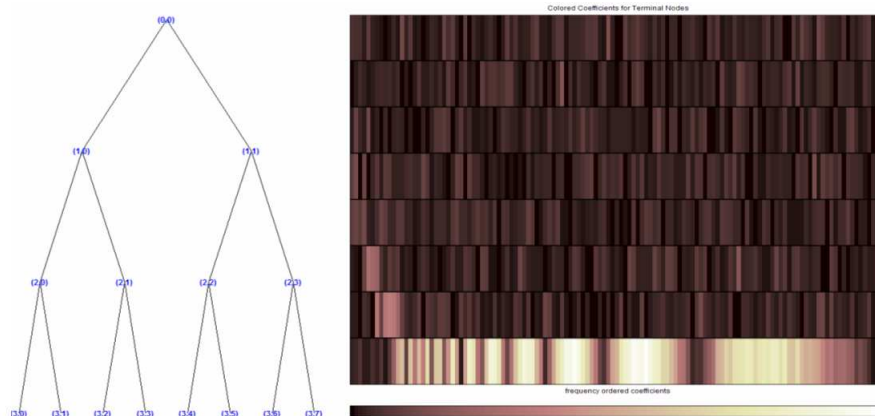


FIGURE 2.16: Discrete Wavelet Packet Transform of the Noisy Doppler. (a) Tree Structure, (b) Wavelet Packet transform in time-scale domain.

## 2-7 Wavelet types

The wavelet transform is a generic tool with infinitely many wavelets. The nature of the wavelet is entirely determined by the filters which characterize it. Each wavelet has certain distinguishing characteristics that make them more suitable for one application than other. Therefore during the design of a system careful considerations of the different wavelet properties should be made according to the system requirements.

### 2-7-1 Wavelet properties

Many considerations go into the design of a wavelet system including properties such as orthogonality, compact support, symmetry, and smoothness. Here we shall discuss a few important ones.

#### i. Compact support

This property ensures that the wavelet has a finite number of non-vanishing coefficients and that the filter banks used to derive the wavelets are of finite length [31]. Compact support is defined by the length of the filter. In order to keep the computational complexity to the minimum usually shorter filters are preferred. However, a longer filter gives more freedom to fine tune other wavelet properties like orthogonality or regularity.

#### ii. Para-unitary Condition

The para-unitary condition is essential for many reasons. Firstly, it is a prerequisite for generating orthonormal wavelets [8, 29]. Second, it automatically ensures perfect reconstruction of

the decomposed signal [29] i.e., the original signal can be reconstructed without amplitude or phase or aliasing distortion, if the filter banks used satisfy the para-unitary condition. A rational transfer function  $A(z)$  is said to be para-unitary when it obeys the relation  $A(\tilde{z})A(z) = 1$ . Here  $A(\tilde{z})$  is the para-conjugate of  $A(z)$  and is given as  $A(\tilde{z}) = A^*(z^{-1})$  where the superscript  $*$  denotes the conjugation of the coefficients. Properties 1 and 2 are necessary and sufficient conditions for the wavelets to be realized. However, they may not always guarantee the generation of regular and well shaped wavelets. Quite often the wavelets can be irregular or even fractal shaped. Therefore to ensure smoothness or regularity of the wavelets the additional property of regularity is important.

### iii. Regularity

This property is a measure of smoothness of the wavelet. The regularity condition requires that the wavelet be locally smooth and concentrated in both the time and frequency domains. It is normally quantified by the number of times a wavelet is continuously differentiable. The simplest regularity condition is the *flatness* constraint which is stated on the low pass filter. A LPF is said to satisfy a  $K$ th order flatness (or  $K$ -regular) if its transfer function  $H(z)$  contains  $K$  zeroes located at the Nyquist frequency ( $z = -1$  or  $\omega = \pi$ ). Parameter  $K$  is called the regularity order and for a filter of length  $L$  it satisfies the relation  $0 \leq K \leq L/2$ .  $K$ -regularity is also an important measure for wavelets because it helps to reduce the number of non-zero coefficients in the high-pass sub-bands and it is one of the easiest ways to determine if a scaling function is fractal.

Another way to determine the regularity of the wavelets is the number of vanishing moments of the wavelet  $\psi(t)$  and scaling functions  $\phi(t)$  [6]. This number is used for the dual vanishing moments to determine the convergence rate of the multi-resolution projections. The  $j$ th moments of the wavelet and scaling functions,  $m_w(j)$  and  $m_s(j)$ , respectively, are defined in continuous time domain as follows [31]:

$$\begin{aligned} m_w(j) &= \int t^j \psi(t) dt \\ m_s(j) &= \int t^j \phi(t) dt \end{aligned} \quad (2.43)$$

Usually the more contribution from the zero wavelet moments of a wavelet, the smoother will be its scaling function. However this is not a tight condition. The smoothness is actually defined by the continuous differentiability of the scaling function. There are two ways in which smoothness can be defined: local by the Hölder measure and global by the Sobolev measure. Different

measures of smoothness are utilized based on the application in hand. In this dissertation we use the  $K$ -regularity as the true measure of smoothness.

#### iv. Symmetry

Symmetrical wavelets have a feature that the transform of the mirror of an image is the same as the mirror of the wavelet transform. None of the orthogonal wavelets except Haar wavelet is symmetric. Although, requiring symmetric wavelets involuntarily means that wavelets are not orthogonal, there are some applications that prefer symmetric wavelets above orthogonal ones. For instance image compression techniques like JPEG2000 uses bi-orthogonal symmetric wavelets. Because by compression of an image we discard one part of the wavelet coefficients containing high detail, the perfect reconstruction has become impossible anyhow. The fulfillment of symmetry property in JPEG2000 on the other hand results in more natural, smooth images.

#### 2-7-2 Popular wavelet families

A wavelet is defined by the choice of low pass filter used, obtained after satisfying the compact support, regularity and para-unitary conditions. For a filter of length  $L$  this is essentially solving  $L$  equations of which  $L/2$  come from the para-unitary constraint and  $K$  from the regularity/flatness constraint. The remaining  $L/2 - K$  conditions offer the freedom to establish a desired wavelet property such as frequency selectivity.

##### a. Daubechies

The Daubechies are a family of compact supported orthonormal wavelets with the highest degree of smoothness. It was derived by Ingrid Daubechies [27] who used all the degrees of freedom  $K$  to generate a wavelet family of maximum regularity for a given filter length  $L$ , or minimum  $L$  for a given regularity [31]. This she did by imposing the maximum number of zero moments to the wavelet function in the vanishing moments' condition.

##### b. Coiflet

Coiflets are a variation of the Daubechies wavelets. They are so named because it was derived by I. Daubechies at the behest of R. Coifman who suggested the construction of an orthonormal wavelet basis with vanishing moment conditions for both wavelet and scaling functions (unlike Daubechies where only the wavelet functions have zero moments). The wavelet function has  $2L$  moments equal to 0 and the scaling function has  $2L - 1$  moments equal to 0.

Name	Compact Support	Orthogonality	Symmetry	K-regularity
Haar	2	Yes	Yes	1
Daubechies	$L$	Yes	No (Far from)	$L/2$
Symlets	$L$	Yes	No (Near from)	$L/2$
Discrete Meyer	102	Yes	No	1
Coiflet	$L$	Yes	No (Near from)	$L/6$
Bi-orthogonal	$(L_1, L_2)$	No	Yes	$\approx (L_1/2, L_2/2)$

TABLE 2.1: Standard Wavelet Specifications.

### c. Symlet

The symlet family of wavelets is another variant of the Daubechies family which are *nearly-symmetrical* (as opposed to being symmetrical). These modifications were also proposed by I. Daubechies and the properties of the two wavelet families are similar.

In Table 2.1 we list some of the most popular wavelets today and give their most important properties.

## 2-8 Summary

In this chapter we presented the basics of the theory of the wavelet transform and explained how the discrete wavelet transform can be efficiently implemented with the Mallat's pyramidal tree algorithm using filter banks. Due to their ease of implementation and the flexibility they provide, wavelets have been applied in diverse fields. Recently, wavelets have been also proposed as a candidate for multi-carrier modulation (MCM). In the next chapter we show how the theory of wavelets and wavelet packets can be applied for MCM.

## Chapter 3

# Wavelet packet modulator

Wavelets, filter banks and multi-resolution analysis which were developed independently in the fields of applied mathematics, signal processing, and computer vision, respectively, have recently converged to form a single theory. In the previous chapter we saw how the theory of wavelets emerged as a natural extension to traditional signal processing tools like Fourier transform. In this chapter we shall see how a multi-carrier communication system can be constructed with wavelets and wavelet packets.

Multi-carrier modulation is a method where the data to be transmitted is divided into several parallel data streams or channels, one for each sub-carrier. Multi-carrier modulation possesses several properties which make it an attractive approach for high speed wireless communication networks. Among these properties is the ability to efficiently access and distribute multiplexed data streams and a reduced susceptibility to impulsive as well as to narrowband channel disturbances.

In existing multi-carrier transmission schemes, such as the popular orthogonal frequency division multiplexing (OFDM), information carrying bits modulate orthogonal trigonometric functions which are then added to obtain a composite signal. These techniques use Fourier transforms and are particularly efficient with regard to bandwidth utilization and simplicity of transceiver design. However, they are not without fault - since the building blocks of OFDM are sine/cosine functions which oscillate to infinity in time, the signals usually have to be truncated resulting in deterioration of performance. Further more the basis functions are static and hence the transmission waveforms cannot be altered according to the demands of the wireless transmission. With an ever increasing demand for high quality wireless services, there is a growing interest towards alternative orthogonal basis functions that can yield better performances in relation to OFDM. It is in this context that that the mathematical precept of wavelets and wavelet packets hold promise.

In this chapter we explain how the theory of wavelets and filter banks can be used to construct a new multi-carrier modulation called the wavelet packet modulator (WPM). The theoretical background presented in this chapter will serve as an important prelude to Chapters 4-9 where we address various issues related to the implementation of WPM. But even before we introduce WPM, we quickly review OFDM and other filter bank based multi-carrier systems. This discussion on alternative MCM techniques will aid in the better understanding of the WPM technique. The contents of the chapter are divided into five sections. Section 3-1 gives an overview of existing modulation techniques currently in use for wireless data transmission. Section 3-2 details the most popular MCM technique, namely, the Orthogonal Frequency Division Multiplexing or OFDM. This discussion on OFDM will be followed by an overview of Filter bank based MCM methods in Section 3-3. Section 3-4 introduces the WPM system implementation. And finally to round off the chapter a summary of the contents is outlined in Section 3-5.

### 3-1 Modulation techniques for wireless communication

In telecommunication systems, modulation is a process where information carrying digital bits are mapped into waveforms (or air waves) so that the message can be physically transmitted. This is done by varying the phase, frequency or amplitude of the waveforms in accordance with the content of the message. While different wireless standards may differ from one another substantially, the air interfaces of all radio platforms operate under one of the three fundamental modulation modes, namely, single-carrier (where the information bits modulate a single waveform or carrier), multi-carrier modulation (where the data is divided into several parallel data streams or channels, one for each sub-carrier) or spread-spectrum (where the signal is transmitted on a bandwidth considerably larger than the frequency content of the original information). Wireless communication systems can hence be viewed as trans-multiplexers characterized by the kind of waveforms they transmit. The properties of the waveform, i.e. the time spread, spectral footprint, shape and the number of carriers, determine the nature of the radio.

#### 3-1-1 Single carrier transmission

In a single carrier system the base band signal modulates the carriers using one of the characteristic frequency, phase, or amplitude [49, 50]. Fig. 3.1 shows the blocks of a typical narrowband, single carrier communication system. At the transmitting end, a source generates an arbitrary stream of data derived from the source alphabet. This stream of data is then linearly modulated by a pulse shaping filter  $S(f)$  and then transmitted to the channel. At the receiver the received signal is demodulated and decoded by a receiving filter  $U(f)$  and after further processing the data is estimated.

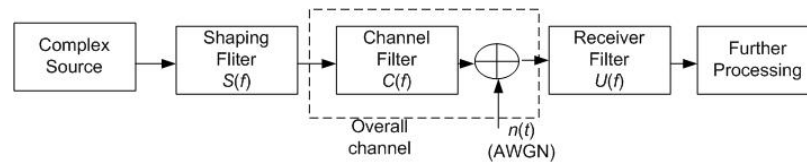


FIGURE 3.1: Baseband equivalent of a narrowband communication system [51].

For digital signals, the information is in the form of bits or collections of bits called symbols, which are modulated onto the carrier. When higher bandwidths (data rates) are used, the duration of one bit or symbol of information becomes smaller. At the same time the system becomes more susceptible to loss of information from impulse noise, signal reflections and other impairments. These impairments can hinder recovery of the transmitted information. In addition, as the bandwidth of the single carrier system is made larger its vulnerability to channel dispersion is also increased. Therefore this method is not preferable in practice.

### 3-1-2 Multi-carrier transmission

In the past decade the rapid progress of telecommunication market has opened niches for new techniques that can accommodate high data rates without loss in performance. In conventional single-carrier communication systems the data is transmitted sequentially and therefore the duration of each symbol is inversely proportional to the data rate  $R_s$ . Higher data rates result in shorter symbol duration. The problem however arises in dispersive channels when the duration of transmitted symbols becomes shorter than the delay introduced by the channel. As a result the received symbols are widely spread in time causing Inter Symbol Interference (ISI). The amount of ISI in a given channel increases with the data rate  $R_s$  limiting the connection speed.

ISI can be significantly reduced by employment of multi-carrier modulation (MCM) technique. MCM subdivides the total bandwidth into  $N$  narrow channels, which are transmitted in parallel. The original data stream at rate  $R_s$  is divided into  $N$  streams each having data rate of  $R_s/N$  and therefore the symbol duration is  $N$  times longer, i.e.  $T_{MC} = NT$ . Fig. 3.2 shows the Time-Frequency footprints of single and multi carrier modulated signals.

Multi-Carrier Modulation (MCM) is the principle of transmitting high data rate by dividing the stream into several parallel bit streams, each of which has a much lower bit rate, and by using these sub-streams to modulate several sub-carriers [49, 50]. Multi-carrier modulation possesses several properties which make it an attractive approach for high speed wireless communication networks. Among these properties is the ability to efficiently access and distribute multiplexed data streams, and a reduced susceptibility to impulsive as well as narrowband channel disturbances.

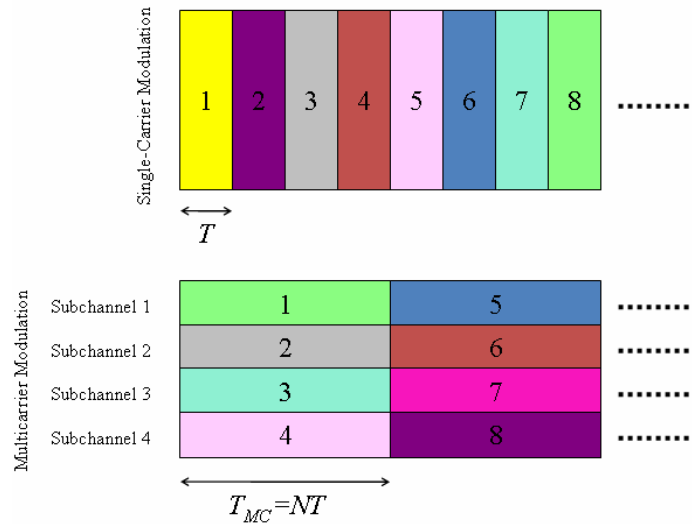


FIGURE 3.2: Single-carrier and multi-carrier Modulation.

Each data symbol in single-carrier systems occupies the entire available bandwidth while an individual data symbol in multi-carrier system only occupies a fraction of the total bandwidth. Therefore, narrow band interference or strong frequency selective attenuation can cause single-carrier transmission to completely fail but in MCM they only affect sub-carriers located at particular frequencies.

### 3-1-3 Frequency division multiplexing

MCM can be implemented using several techniques. The first multi-carrier systems applied frequency division multiplexing (FDM). In FDM the composite multi-carrier signal is obtained by shifting the baseband parallel data streams upwards in frequency by modulating them on different sinusoidal carriers. In order to avoid cross-talk the sub-carriers used in FDM must not overlap. Very often guard bands are inserted between the sub-carriers in order to accommodate for local oscillator imperfections and channel effects like Doppler spread. Fig. 3.3(a) shows the spectrum of composite FDM signal with guard bands.

There is however an alternative approach to transmitting data over a multipath channel. Instead of using carriers with non-overlapping bands, one could partition the spectrum into closely packed sub-bands which overlap. In the next sections we shall see how this is done to optimize utilization of the spectrum, a resource in premium.

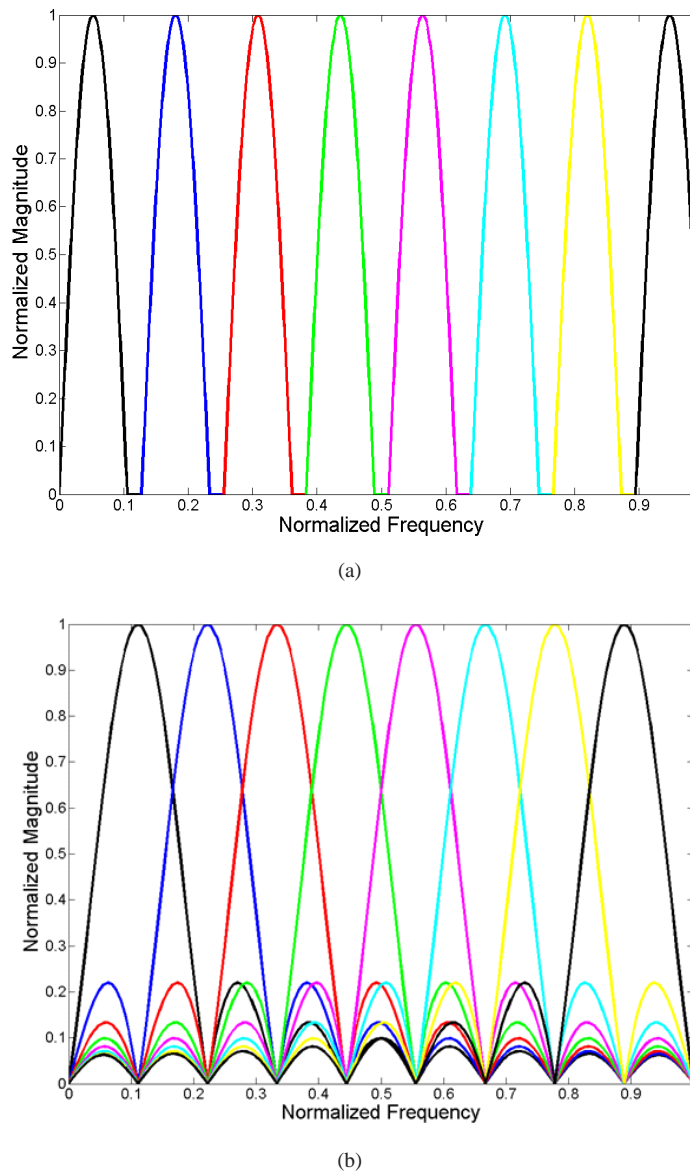


FIGURE 3.3: a) FDM Spectrum (8 sub-carriers with guard bands); (b) OFDM Spectrum (8 sub-carriers).

## 3-2 Orthogonal frequency division multiplexing

Over the years there have been several attempts aiming at optimum utilization of spectral bandwidth through multi-carrier transmission. One of the spectrally efficient multi-carrier methods is Orthogonal Frequency Division Multiplexing (OFDM) [52]. Although the principle of OFDM existed since early sixties the first real life systems appeared only in the 1990s. Today OFDM is the most commonly used multi-carrier modulation technique and is widely adopted across the world. It is in fact the de-facto choice for high-speed data rate transmission in frequency selective fading channels and wireless-Local Area Networks (WLAN). One of the first systems to use OFDM was European Digital Audio Broadcasting (DAB) back in 1995 and in short time

other standards such as Digital Video Broadcasting (DVB), WiFi (IEEE 802.11a/g/j/n), WiMAX (IEEE 802.16), UWB Wireless PAN (IEEE 802.15.3a) and MBWA (IEEE 802.20) followed [49].

The high spectral efficiency of OFDM is due to its orthogonal sub-carriers which allow their spectrum to overlap. Adjacent sub-carriers do not interfere with each other as long as they preserve their orthogonality. Moreover, the frequency guard bands like those used in FDM are no longer necessary. Fig. 3.3(b) illustrates this with the spectrum of OFDM for 8 sub-carriers. The technique has other advantages too - high immunity to multipath delay spread that causes inter-symbol interference (ISI) in wireless channels, immunity to frequency selective fading channels, elegance in implementation through the Fast Fourier Transform (FFT) algorithms and ease of channel equalization.

OFDM transmission system can be efficiently implemented using the Inverse Fast Fourier Transform (IFFT) at the transmitter side and Fast Fourier Transform (FFT) at the receiver side. The Fourier transformation allows us to describe a signal as a linear combination of sinusoids which form an orthogonal basis. These sinusoids in OFDM are referred as sub-carriers and their number is determined by the length of the FFT vector. The orthogonality of sub-carriers over an OFDM symbol period  $T_{MC}$  is achieved by setting the inter-carrier spacing to  $1/T_{MC}$  Hz. Therefore, the frequency of the  $k$ th sub-carrier in  $T$ -spaced OFDM is given by [52]:

$$f_k = \frac{k}{T_{MC}}, \quad k = 0, 1, \dots, N - 1. \quad (3.1)$$

The corresponding  $k$ th sub-carrier at frequency  $f_k$  can therefore be written as [52]:

$$\vartheta_k(t) = e^{j2\pi f_k t} \quad (3.2)$$

An OFDM symbol consists of  $N$  sub-carriers and after being modulated by the OFDM transmitter can be expressed as:

$$S[n] = \sum_{k=0}^{N-1} a_k e^{j2\pi \frac{kn}{N}}, \quad 0 \leq n \leq N - 1 \quad (3.3)$$

In eq. (3.3)  $a_k$  represents the mapped complex data symbols. If we assume an ideal channel and perfect synchronization between OFDM transmitter and receiver, the received sequence  $R[n]$  is identical to the transmitted signal, i.e.  $R[n] = S[n]$ . Under such conditions the demodulated data after FFT for the  $k$ th sub-carrier can be expressed as:

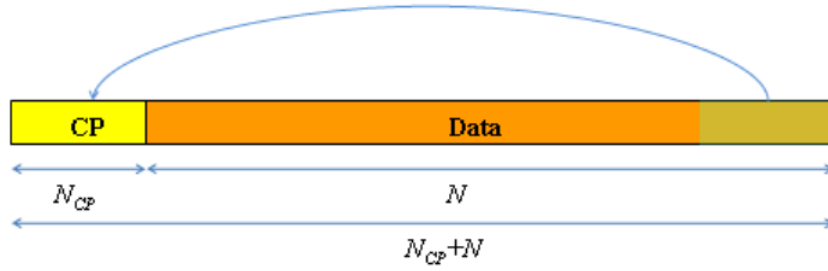


FIGURE 3.4: OFDM Symbol with Cyclic Prefix.

$$\begin{aligned}
 \hat{a}_{k'} &= \frac{1}{N} \sum_{n=0}^{N-1} R[n] e^{-j2\pi \frac{k'n}{N}} \\
 &= \frac{1}{N} \sum_{n=0}^{N-1} \sum_{k=0}^{N-1} a_k e^{j2\pi \frac{kn}{N}} e^{-j2\pi \frac{k'n}{N}} \\
 &= \sum_{k=0}^{N-1} a_k \left( \frac{1}{N} \sum_{n=0}^{N-1} e^{j2\pi \frac{n(k-k')}{N}} \right) \\
 &= \sum_{k=0}^{N-1} a_k \delta[k - k'] = a_k.
 \end{aligned} \tag{3.4}$$

Unfortunately, such an idealistic scenario does not occur in reality and therefore the channel effects and oscillators' imperfections should be taken into consideration during system design. Due to delay spread of the channel, OFDM symbols could overlap one another and perfect reconstruction as described in eq. (3.4) may not be possible. In order to decrease the amount of ISI in dispersive channels guard intervals are inserted between OFDM symbols. Usually in OFDM the cyclic prefix is used as it makes the OFDM signal appear periodic and therefore avoid the discrete time property of the convolution.

The cyclic prefix is a copy of last  $N_{CP}$  samples of OFDM symbols which is appended to the front of each symbol. The effect of the dispersive channels can be efficiently mitigated if the length of a cyclic prefix is set longer than the span of the channel. Fig. 3.4 depicts an OFDM symbol with cyclic prefix. Because the cyclic prefix does not carry any useful information it decreases the spectral efficiency and therefore has to be kept as short as possible. At the receiver side the cyclic prefix is no longer needed and hence discarded before the demodulation process. The OFDM transmitter and receiver block diagrams are illustrated in fig. 3.5(a) and fig. 3.5(b), respectively.

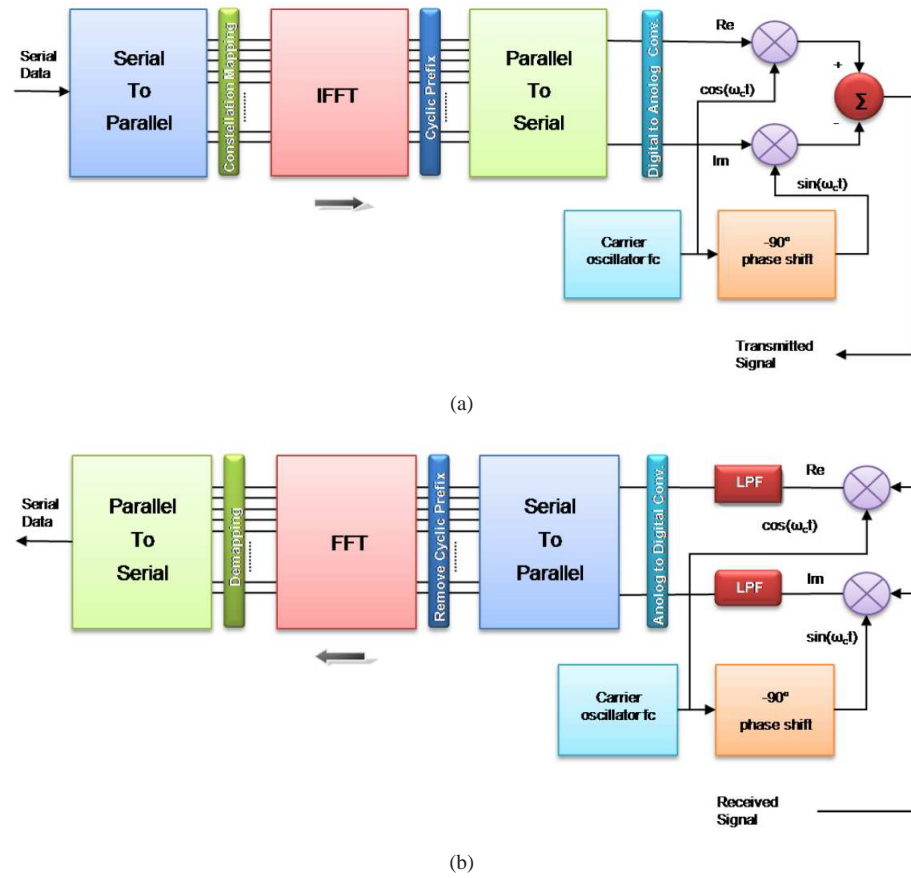


FIGURE 3.5: OFDM Transceiver. (a) Transmitter; (b) Receiver.

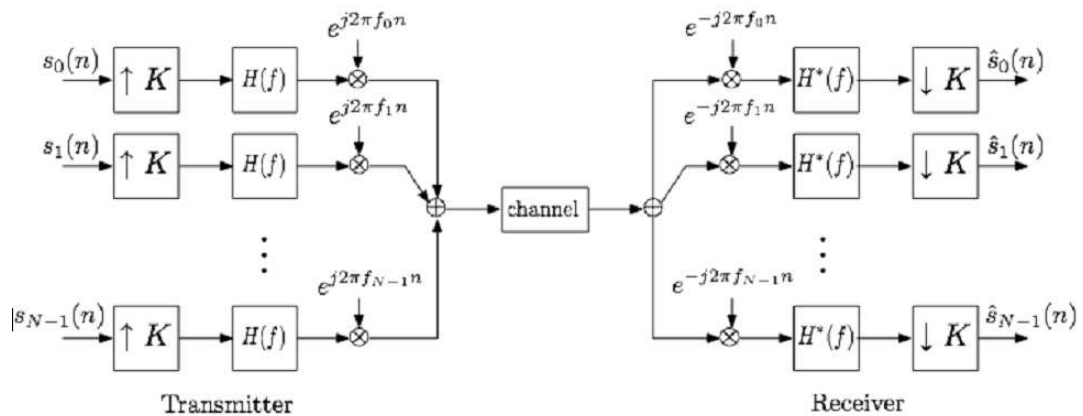


FIGURE 3.6: FMT Transmitter and Receiver [53].

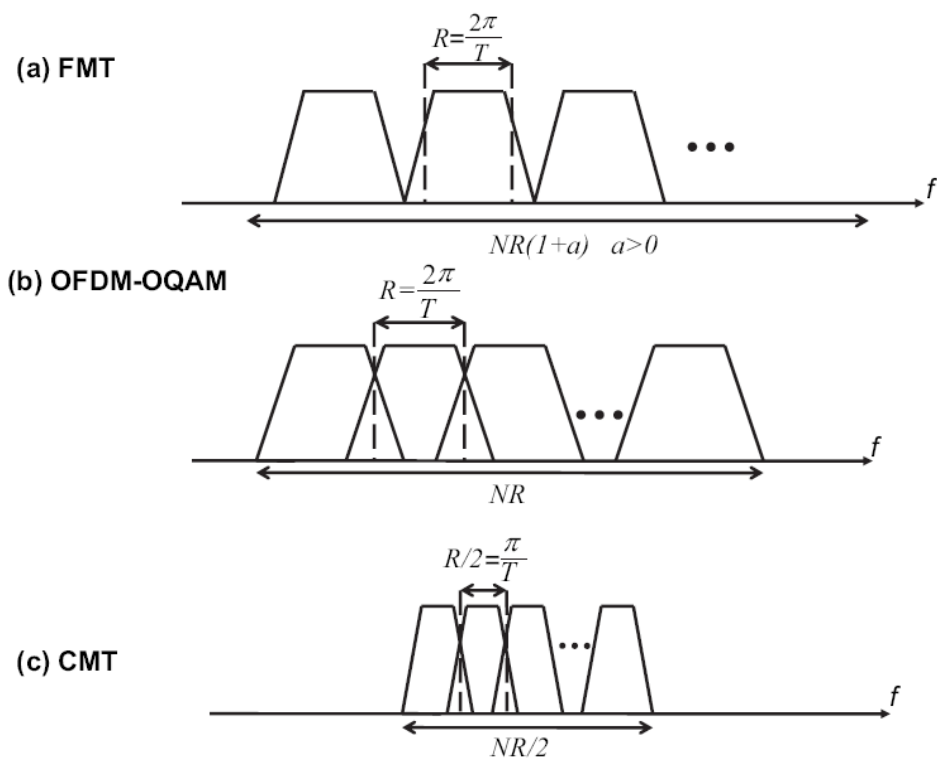


FIGURE 3.7: Sub-carrier signal spectra of (a) FMT, (b) OFDM-OQAM and (c) CMT [53].

### 3-3 Filter bank multi-carrier methods

The characteristics of OFDM carriers follow a sinc-function in the frequency domain as a consequence of using rectangular windows. This causes the sub-carriers to have large side-lobes which spill over into neighboring bands resulting in significant interference. Furthermore, under non-ideal channel conditions the spectral overlap between the sub-channels necessitates the use of cyclic prefix (CP) and frequency offset correction algorithms. Although the CP is an easy solution to mitigate the impairments induced by the channel, it leads to a loss in the data throughput and bandwidth efficiency.

There exist in the literature several alternative multi-carrier techniques to OFDM [53, 54] that better handle this inadequacy of OFDM. We shall discuss a few important ones in the next sub-sections.

#### 3-3-1 Filtered multi-tone (FMT)

In [55, 56] a filter-bank modulation technique called Filtered Multi-tone (FMT) is presented. FMT is similar to Frequency Division Multiplexing (FDM) in the sense that the sub-carriers do not overlap and guard bands are used between carriers to prevent interference. FMT is implemented using filter banks with a single prototype filter  $H(f)$  and its dual  $H^*(f)$ . The prototype filter is usually a Root Nyquist filter [55]. The modulation scheme is usually Quadrature Amplitude Multiplexing (QAM). Fig. 3.6 shows the implementation of the FMT transmitter and the FMT receiver modulator. In the figure,  $N$  denotes the maximum number of  $N$  sub-carriers and  $K$  represents the sampling factor. Usually a choice of  $K > N$  is made for addition of guard bands between the sub-carrier bands. Equalizers are needed after down-sampling at the receiver.

In FMT, orthogonality between sub-channels is ensured by using non-overlapping spectral characteristics as compared with the overlapping sinc-function type spectra employed in OFDM. Since the linear transmission medium does not destroy orthogonality achieved in this manner, cyclic prefixing is not needed. Clearly, the required amount of spectral containment must be achieved with acceptable filtering complexity. In a critically sampled ( $N = K$ ) filter bank, the frequency separation of the pass bands will be  $1/T$  with a total of  $M$  bands. In this way, each of the transmitter pass-band filters will be frequency-shifted versions of the low pass filter as shown in fig. 3.7. An obvious disadvantage of FMT is the inefficient use of bandwidth as the sub-carriers do not overlap.

### 3-3-2 Cosine modulated multi-tone (CMT)

In [57] Boroujeny introduces the Cosine Modulated Multi-tone (CMT) as a capable multi-carrier modulation technique. The CMT uses pulse amplitude modulated (PAM) symbols with vestigial sideband modulation and the sub-carrier bands are maximally overlapped/minimally spaced. Vestigial side-band modulation (illustrated in fig. 3.9) is adopted to maximise bandwidth efficiency. The prototype filters  $H(f)$  and  $H^*(f)$  are selected to be Root-Nyquist filters to aid the demodulation of the data symbols at the receiver. At the receiver equalization is carried out after decimation [57]. Figs. 3.8(a) and 3.8(b) show the blocks of the CMT transmitter and receiver, respectively.

Both FMT and Cosine Modulated Multi-tone (CMT) are filter bank-based modulation techniques [57]. The main difference between the two methods lies in the way the spectral band is used, as shown in fig. 3.7. In FMT, the sub-carrier bands are non-overlapping, thus separation of different sub-carrier signals can be achieved by conventional filtering. On the other hand, in CMT, the sub-carrier bands are allowed to overlap and separation is done through judicious design of the synthesis and analysis filters. It is evident from fig. 3.7 that CMT offers higher bandwidth efficiency than FMT since more sub-carrier bands can be accommodated per unit bandwidth.

The sub-carriers of FMT as well as CMT can be considered to be of narrow bandwidth thereby experiencing a flat fading channel. Hence, the equalization of the channel effects is carried out through a single tap equalizer whose tap weight is the inverse of the channel gain. Training symbols are usually used to initialize the equalizer taps. In CMT the unique nature of the underlying signals allows for blind equalization without training. The procedures are described in greater detail in [57].

### 3-3-3 Offset QAM/staggered multi-tone (SMT)

Another technique suggested is the Staggered Multi-tone (SMT) modulation. The method is also known as Offset QAM and is implemented using poly-phase filter banks [58, 59]. Unlike the FMT, SMT allows overlap of carriers to maximize spectrum utilization. The modulation scheme used is Offset-QAM where the quadrature and in-phase constituents are separated by a time-offset of half the symbol interval. Hence, the name Staggered Multi-tone.

Fig. 3.10 shows the blocks of the OFDM-OQAM transmitter and receiver. In OFDM-OQAM, the sub-carrier bands overlap and are spaced at the symbol rate. Successful signal separation is nevertheless possible thanks to the orthogonality between the sub-carriers which guarantees that the transmitted symbols arrive at the receiver free of inter-symbol (ISI) and inter-carrier interference (ICI). Carrier orthogonality is achieved through time staggering the in-phase and

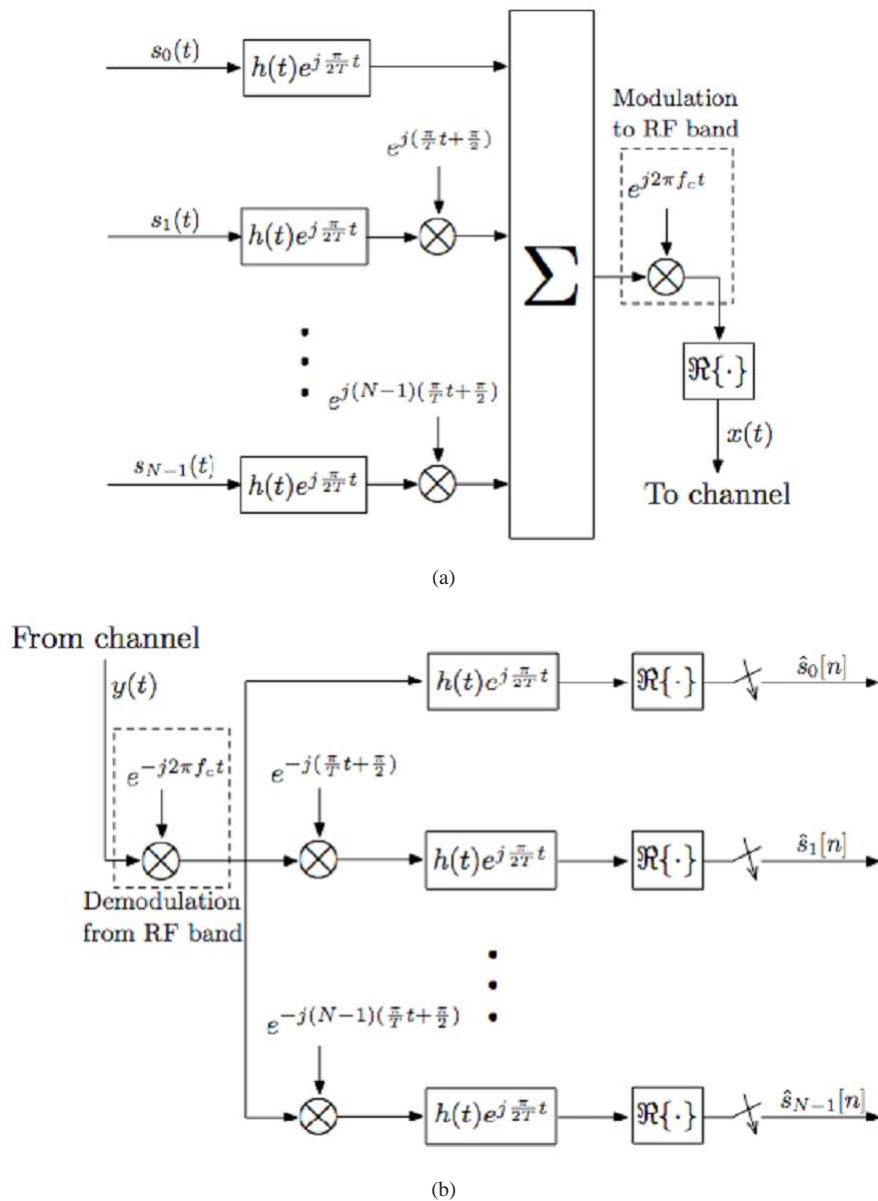


FIGURE 3.8: CMT. (a) Transmitter and (b) Receiver [53].

quadrature components of the sub-carrier symbols and designing proper transmit and receive filters. In OFDM-OQAM, each sub-carrier band is double side-band modulated and carries a sequence of QAM complex valued symbols. Assuming identical symbol duration and number of sub-carriers, the CMT signal occupies half the bandwidth of OFDM-OQAM thereby offering only half the data rate. On the other hand, FMT uses guard bands between adjacent sub-carriers. The width of the guard-bands depends on the specific system implementation. Therefore, for an identical number of carriers and identical symbol timing, FMT requires more bandwidth than OFDM-OQAM and CMT [58].

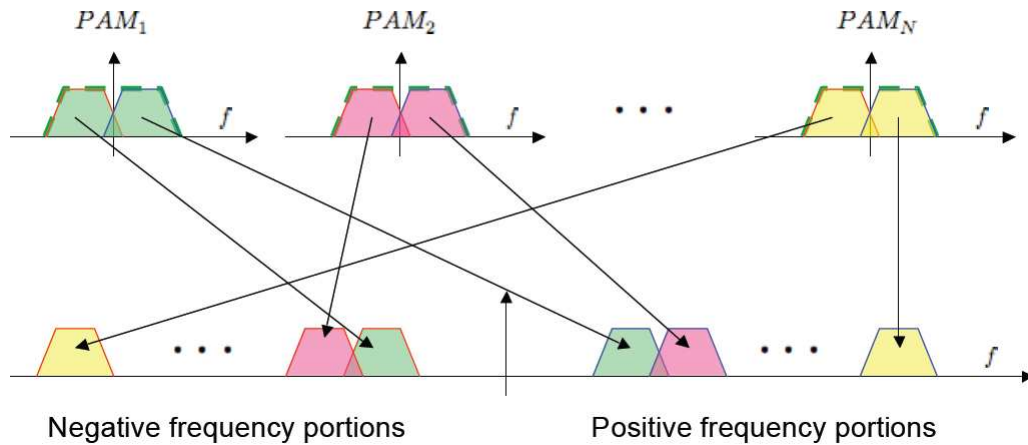


FIGURE 3.9: Illustration of Vestigial Side band Modulation of the CMT carriers [53].

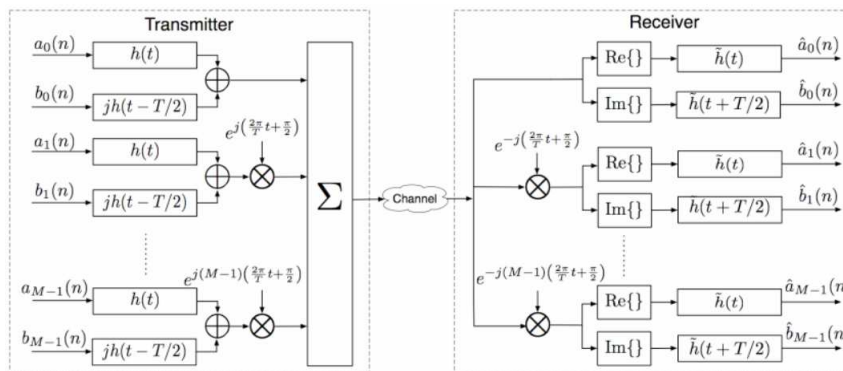


FIGURE 3.10: OFDM-OQAM Transmitter and Receiver [53].

The OFDM-OQAM method is similar to CMT for the case when the sub-carrier bands maximally overlapping (i.e. are minimally spaced), see fig. 3.7. Both OQAM and CMT achieve maximum bandwidth efficiency. Transmit symbols of OFDM-OQAM are offset QAM: in-phase and quadrature components have a time offset of half symbol interval. If the overlaps are limited to adjacent bands and  $H(f)$  and  $H^*(f)$  are a pair of root-Nyquist filters the separation of data symbols at the receiver output is guaranteed. Equalizers are needed after decimators at the receiver.

### 3-4 Wavelet and wavelet packet based multi-carrier modulators

#### 3-4-1 Wavelet packet modulator (WPM)

Recently, the theory of wavelets [12] and wavelet packets [10] has been applied for the design of multi-carrier modulators. The pioneering work on these subjects were carried out by Lindsay [11] who laid out the theoretical foundations to establish the link between wavelet packets and

digital communication. He also showed that the entire WPM transceiver structure can be realized with a pair of conjugate quadrature mirror filters which satisfy a set of constraints. His idea has since then been taken forward by many researchers. The decoding of WPM data with Maximum likelihood estimators has been addressed by Suzuki [13]. The study of an equalization scheme suited for WPM has been conducted by Gracias [14]. In [15, 16] an investigation on the performance of WPM systems in the presence of time offset is performed. In [17] its PAPR performances are analyzed. The advantages of the wavelet transform in terms of the flexibility they offer to customize and shape the characteristics of the waveforms have been demonstrated in [18–21]. Three use-cases where the waveforms are designed and applied to optimize the WPM system performance according to specific system demands are illustrated in [18–20]. In [21], the work of [18, 19] is extended to establish a unifying mathematical framework where the waveforms are designed according to a pre-defined criteria.

WPM is implemented with orthogonal wavelet packet (WP) bases derived from a multi-resolution analysis (MRA). Fundamentally, OFDM and WPM have many similarities as both use orthogonal sub-carriers (which overlap over one-another) to achieve high spectral efficiency. The adjacent sub-carriers do not interfere with each other as long as the orthogonality between sub-carriers is preserved. The difference between OFDM and WPM is in the time-frequency characteristics of the sub-carriers and in the manner in which they are generated. OFDM uses Fourier bases which are trigonometric functions while WPM uses a family of wavelet bases. Different wavelet families result in sub-carriers of distinct nature paving way for adjusting the transmission characteristics of the system. By careful selection of wavelets it is possible in WPM to optimize figures of metrics like bandwidth utilization, sensitivity to synchronization errors, Peak-to-average Power ratio (PAPR), etc.

The starting point to derive the orthogonal wavelet bases is to consider a pair of Quadrature Mirror Filters (QMF) consisting of a half-band low pass filter  $h[n]$  and high pass filter  $g[n]$  of length  $L$  each. These filters share a tight relationship given by [8, 29]:

$$g[L - 1 - n] = (-1)^n h[n] \quad (3.5)$$

Furthermore, they have adjoints or duals which are their complex conjugate time reversed variants [8]:

$$\begin{aligned} h'[n] &= h^*[-n] \\ g'[n] &= g^*[-n] \end{aligned} \quad (3.6)$$

The filter-pair  $h'[n], g'[n]$  are called the synthesis filters and are used to generate the WP carriers for modulation of the data at the transmitter. On the other hand the filter-pair  $h[n], g[n]$ , known as the analysis filters, are used to derive the duals for demodulation of data at the

receiver. Denoting the magnitude responses of these four filters in the frequency domain as  $H(\omega)$ ,  $G(\omega)$ ,  $H'(\omega)$  and  $G'(\omega)$ , the filters satisfy the perfect reconstruction conditions if [8]:

$$\begin{aligned} H^*(\omega + \pi)H'(\omega) + G^*(\omega + \pi)G'(\omega) &= 0 \\ H^*(\omega)H'(\omega) + G^*(\omega)G'(\omega) &= 2 \end{aligned} \quad (3.7)$$

Such filters can be used for various applications from compression of image/speech signals to radio system design. From these QMF filters, the wavelet packet bases  $\xi_l^p$  can be derived recursively through a multi-resolution analysis (MRA) as [31]:

$$\begin{aligned} \xi_{l+1}^{2p}[n] &= \sqrt{2} \sum_k h[k] \xi_l^p[2n - k] \\ \xi_{l+1}^{2p+1}[n] &= \sqrt{2} \sum_k g[k] \xi_l^p[2n - k] \end{aligned} \quad (3.8)$$

In eq. (3.8)  $\xi$  denotes the wavelet packets duals and  $p$  stands for the sub-carrier index at any given tree depth  $l$ . The number of decomposition levels  $l$  of the WP tree determines the maximum number of WPM sub-carriers  $N$  that can be generated and the two are related by the expression  $N \leq 2^l$ .

The WP bases satisfy two orthogonal properties which are crucial for their application to MCM. First, they are orthogonal to themselves for all non-zero integer shifts, i.e. [31]:

$$\langle \xi_l^p[n - j], \xi_l^p[n - k] \rangle = \delta[j - k]; \forall j, k \in \mathbb{Z}. \quad (3.9)$$

Here, the operator  $\langle \cdot \rangle$  represents the inner-product operation. And second, pairs of the WP bases derived out of the same parent are orthogonal to one another for all  $j$  and  $k$  [31]:

$$\langle \xi_l^{2p}[n - j], \xi_l^{2p+1}[n - k] \rangle = 0; \forall j, k \in \mathbb{Z}. \quad (3.10)$$

Eq. (3.8) can be physically realized with a filter bank tree structure obtained by cascading the fundamental  $h[n]$ ,  $g[n]$  filter pair, followed by down-sampling by 2, iteratively as shown under the Discrete Wavelet Packet Transform (DWPT) block in fig. 3.11 [31].

The figure shows a level-2 decomposition scheme which yields up to 4 orthogonal WP bases. The WP duals  $\xi_l^p$  for the transmitter can be obtained by a similar procedure, albeit, with the synthesis filter pairs  $h'[n]$ ,  $g'[n]$ . The processes are referred to as inverse-DWPT (IDWPT) and DWPT at the transmitter and receiver, respectively, analogous to the inverse-FFT (IFFT) and FFT, in OFDM systems.

The WPM transmitter and receiver block diagrams are illustrated in figs. 3.13(a) and 3.13(b), respectively. The WPM modulated signal  $S[n]$  is obtained as a linear combination of the WP

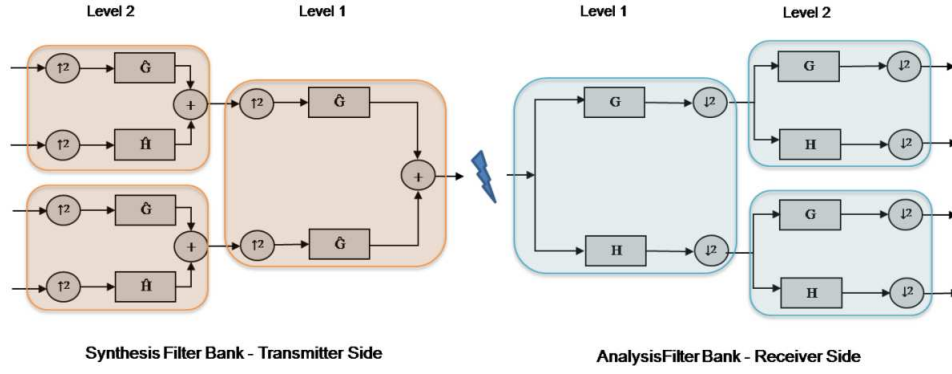


FIGURE 3.11: Wavelet Packed based Transmultiplexer.

duals  $\xi_l^p$  weighted with complex data symbols  $a_{u,k}$ :

$$S[n] = \sum_u \sum_{k=0}^{N-1} a_{u,k} \xi_l^k [n - uN] \quad (3.11)$$

In eq. (3.11)  $k$  denotes the sub-carrier index and  $u$  denotes the WPM symbol index. The constellation symbol modulating  $k$ th sub-carrier in  $u$ th WPM symbol is represented by  $a_{u,k}$ .

At the receiver the data is demodulated with the dual bases. If we assume that the WPM transmitter and receiver are perfectly synchronized and that the channel is ideal, the detected data at the receiver can be given by:

$$\begin{aligned} \hat{a}_{u',k'} &= \sum_n R[n] \xi_l^{k'} [u'N - n] \\ &= \sum_n \sum_u \sum_{k=0}^{N-1} a_{u,k} \xi_l^k [n - uN] \xi_l^{k'} [u'N - n] \\ &= \sum_u \sum_{k=0}^{N-1} a_{u,k} \left( \sum_n \xi_l^k [n - uN] \xi_l^{k'} [u'N - n] \right) \\ &= \sum_u \sum_{k=0}^{N-1} a_{u,k} \delta[u - u'] [k - k'] = a_{u,k} \end{aligned} \quad (3.12)$$

An important property unique to wavelet transform is that the wavelet bases are much longer in length than the duration of a symbol and can overlap in the time domain without losing their orthogonality. The long wavelet bases in WPM allow for better frequency localization of sub-carriers, especially, in relation to OFDM where the rectangular DFT windows result in large side lobes. In fig. 3.12 the spectrum of a WPM system with 8 sub-carriers is depicted. One may

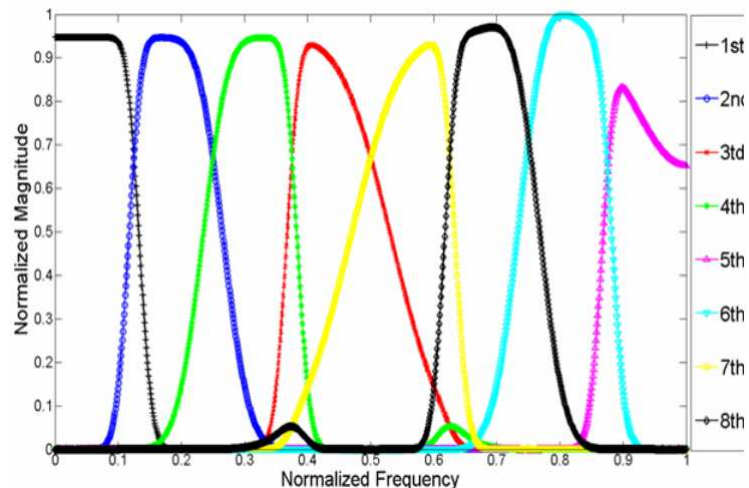


FIGURE 3.12: Spectrum of 8 WPM Orthogonal sub-carriers (for Daubechies filter of Length 20).

observe the relative merits of using WPM over OFDM with regard to frequency selectivity of the sub-carriers from figs. 3.3(b) and 3.12.

An undesirable consequence of time overlap in WPM is that guard bands cannot be used. Although, the addition of a guard interval in OFDM severely decreases spectral efficiency, it is an effective and low complexity method to cope with dispersive channels and time offsets.

### 3-4-2 Variants of wavelet packet modulator

The Wavelet packet modulator can be considered as a generalized form of other multi-carrier modulators based on wavelets. In [12] Negash and Nikookar suggest replacing the conventional Fourier-based complex exponential carriers of a multi-carrier system with orthonormal wavelets. The wavelets are derived from a multistage tree-structured Haar and Daubechies orthonormal QMF bank. An improved performance with respect to reduction of the power of ISI and ICI is reported. This work is extended in [60] by realizing a high-speed digital communication system over a low-voltage power-line. With empirical investigations on a model obtained from measurements of a practical low-voltage powerline communication channel, the authors demonstrate the effectiveness of wavelets for use in OFDM systems, especially with regard to ISI and ICI mitigation. Another real time application of the system is reported in [61] where Wavelet-based OFDM for V-BLAST (vertical Bell laboratories layered space time) [62] is discussed. According to [61] the bit error rate (BER) performance of the wavelet based V-BLAST system is superior to their Fourier-based counterparts. In the conventional systems, the ISI and ICI are reduced by adding a guard interval (GI) using a cyclic prefix (CP) to the head of the OFDM symbol. Adding CP can largely reduce the spectrum efficiency. Wavelet based OFDM schemes do not require CP, thereby enhancing the spectrum efficiency. Moreover, as pilot tones are not

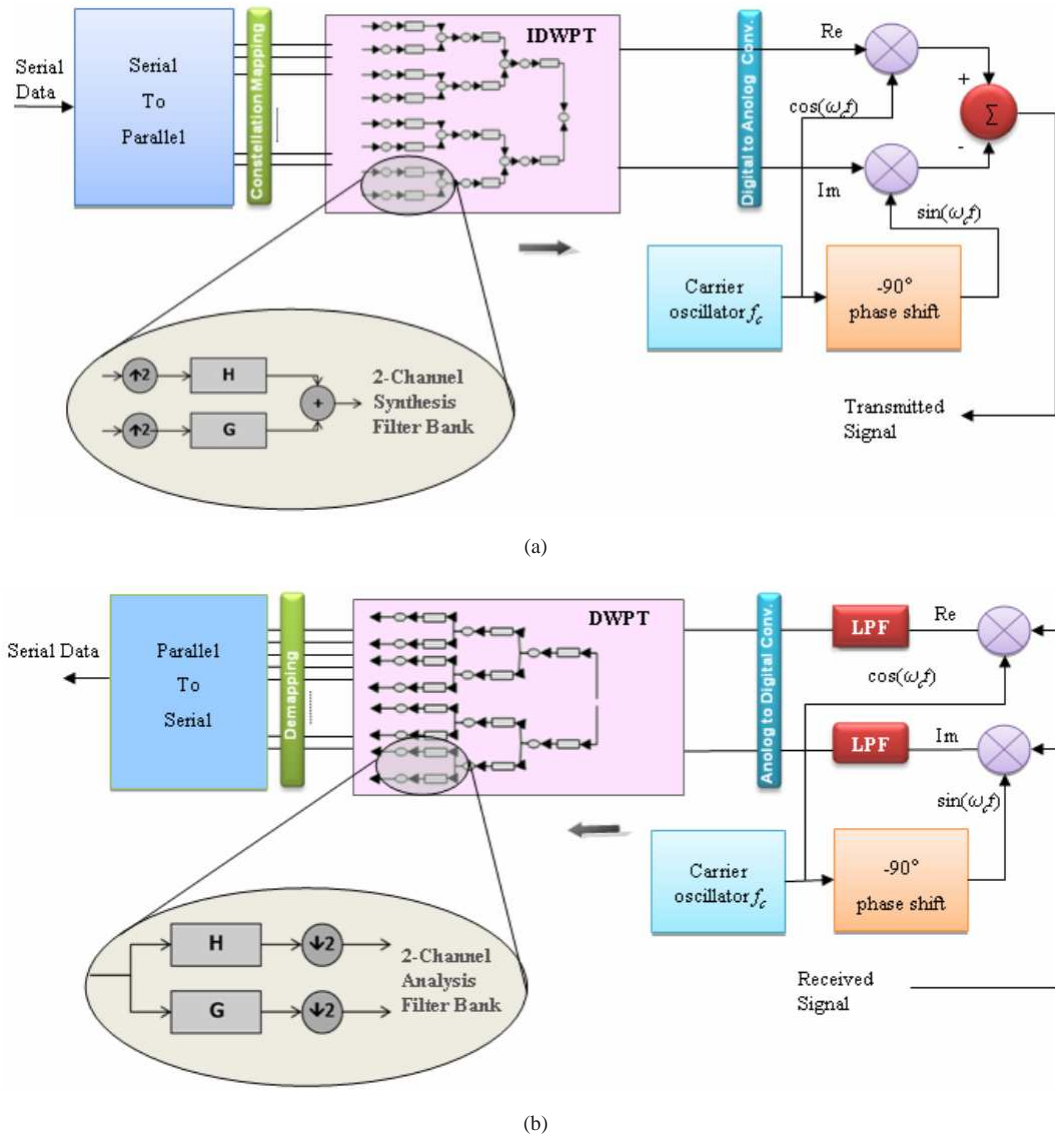


FIGURE 3.13: (a) WPM Transmitter; (b) WPM Receiver.

necessary for the wavelet based OFDM system, they perform better in comparison to existing OFDM systems like 802.11a or HiperLAN, where 4 out of 52 sub-bands are used for pilots. An advanced OFDM modulation scheme called Isotropic Orthogonal Transform Algorithm (IOTA) for future broadband physical layers is proposed in [63]. This system uses isotropic Gaussian functions to generate the carrier waves and gives good spectral efficiency by eliminating the use of a cyclic prefix. In [64] the promise shown by a Haar WOFDM system with Hadamard spreading codes in reducing its peak-to-average power ratio (PAPR) is reported.

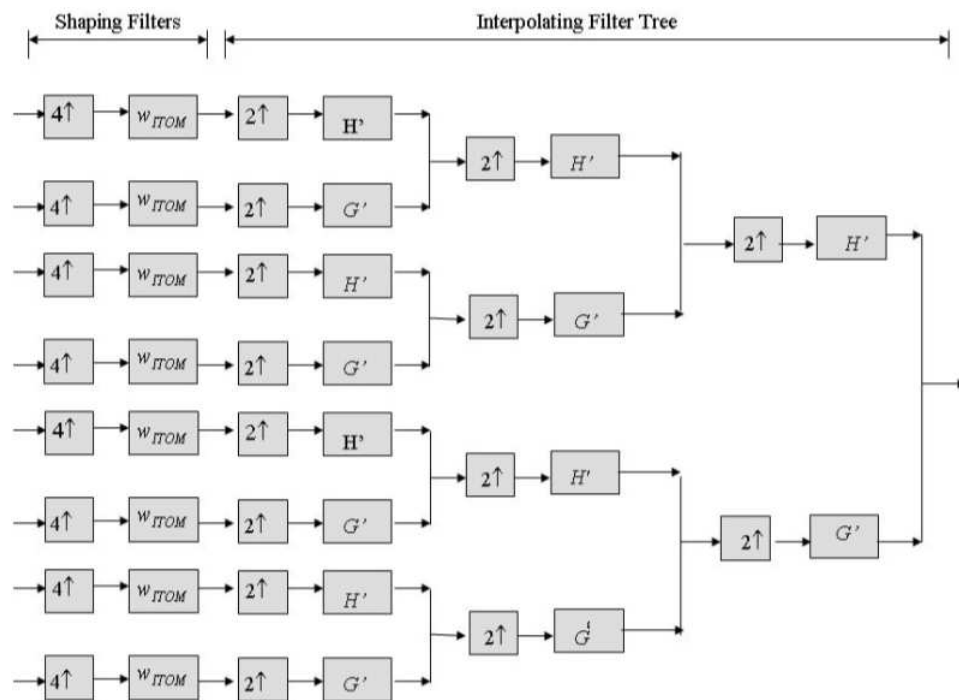


FIGURE 3.14: Modulator of Interpolated Tree Structure (ITOM) [65]. In the figure  $w_{ITOM}$  is the ITOM shaping filters.

### 3-4-3 Interpolated tree orthogonal multiplexing (ITOM)

In the WPM technique the filter banks perform the dual role of shaping the spectrum as well as interpolating in time series. A slight enhancement to this approach would be to separate the two processes and gain greater control over the characteristics of the carriers. This method is called the Interpolated Tree Orthogonal Multiplexing (ITOM) and was introduced by Haris [65]. The procedure is depicted in fig. 3.14. From the figure we can notice that up-sampled shaping filters precede the input ports of the wavelet packet tree structure. Notching over the desired spectral interval is achieved by vacating one or more of the input branches. Figs. 3.15(a) and 3.15(b) illustrate an example of the ITOM mechanism. We may note from figs. 3.15(a) and 3.15(b) as to how well the enabled and disabled carriers fit into the spectral gaps of one-another, illustrating the superiority of the ITOM procedure towards spectrum shaping.

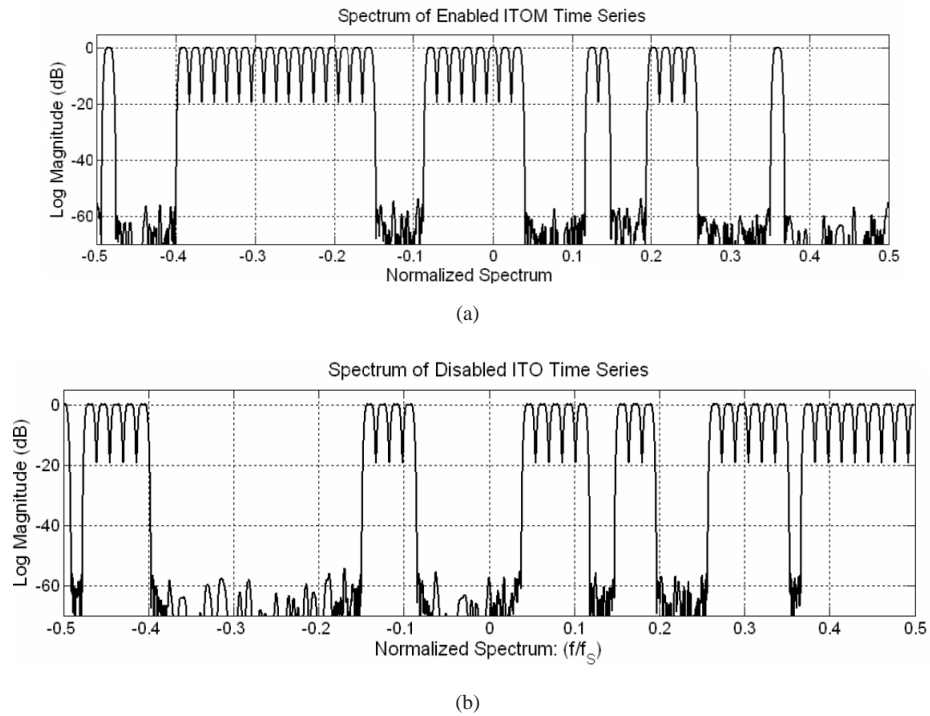


FIGURE 3.15: Illustration of ITOM operation: (a) Spectra of Enabled Spectral Bands of 64-point ITOM; (b) Spectra of Disabled Spectral Bands of 64-point ITOM [65].

### 3-5 Summary

In this chapter we discussed various multi-carrier techniques available for efficient modulation of data. OFDM was presented as the most popular of MCM implementations. Filter bank alternatives to OFDM, like FMT, CMT and SMT, were addressed. The operation of the WPM transceiver, as a wavelet based implementation of orthogonal multi-carrier system, was presented. The WPM is a relatively young multi-carrier transmission technique and very little is known about its operation. In Part-III (includes Chapters 4, 5 and 6) we shall evaluate the WPM system over various performance metrics like:

- sensitivity to loss synchronization (time/frequency/phase),
- peak-to-average power ratio (PAPR) performance and
- influence of channel induced interferences; and mitigation of interference using channel equalization.

## **Part III**

# **Implementation Challenges**

## Chapter 4

# Synchronization errors in wavelet packet modulation

### 4-1 Introduction

The rapid increase in wireless applications and the ensuing lack of free spectrum have prompted engineers to pursue bandwidth efficient multi-carrier techniques. In order to achieve high bandwidth efficiency the sub-carriers have to be closely spaced to each other<sup>1 2</sup>. In this class of multi-carrier systems belong OFDM and WPM [5–7], discussed in Sections 3.2 and 3.5, respectively, of Chapter 3. OFDM and WPM have orthogonal sub-carriers that overlap with one another. The orthogonality property of the transmission bases ensures that the information containing sub-carriers do not interfere. Before the MCM symbol can be demodulated the receiver has to be synchronized properly with the transmitted frame timing, carrier frequency and phase. However, impairments such as frequency offset and/or phase noise, induced by radio front ends or channel conditions, can cause the sub-carriers to lose their mutual orthogonality and impede the transmission of one-another. The rise of interference level due to loss of orthogonality is far more pronounced in multi-carrier transmission than in single carrier systems. This disadvantage of multi-carrier systems places higher demands on the quality of the analog radio components, especially on the choice of oscillators. For OFDM transmission the effects of frequency offset and phase noise are well documented in the literature [5–7, 68–74] and a number of synchronization techniques are reported to estimate and reduce the frequency offset and phase noise effects [75–81]. Similar material for WPM performance does not exist.

---

<sup>1</sup>Portions of this chapter have been published in [66], [15] and [67]. For any material that has been reused, wherever applicable, a written consent has been obtained from the first author.

<sup>2</sup>The author gratefully acknowledges the contributions of Msc student Mr. D. Karamehmedovic for his active co-operation and help with the computer simulations.

Besides frequency and phase misalignment, multi-carrier systems can also suffer from loss of time synchronization. Time synchronization errors occur when the start of the multi-carrier symbol is incorrectly detected. This causes discarding of samples at the beginning or end of the useful symbol and selection of parts of adjacent symbol. Due to loss of time synchronization, disturbances like Inter Symbol Interference (ISI) and Inter Carrier Interference (ICI) occur. The use of cyclic prefix in OFDM can significantly improve the system performance in case of timing errors. However, the use of guard interval is not feasible in WPM systems because the symbols overlap in time. As with the study on the impact of frequency offset and phase noise effects on WPM transmission, the literature on the effects of timing errors on WPM operation is also relatively low in comparison to what is available for OFDM.

In this chapter we address the impact of different synchronization errors on the WPM transmission and compare their performances with that of OFDM. The operation of WPM transceivers, employing different wavelets, is numerically evaluated under different conditions. Analytical expressions for the demodulation of the transmitted WPM data are also derived. Each of the frequency, phase and time errors is treated individually and separately in different sub-sections. The intention of studying the three disturbances separately is in part to gain a better understanding of the individual phenomenon but also to aid ease of analysis. Moreover, the three errors - time, frequency and phase- are caused by disparate processes and the approach to study them separately is a reasonable approximation. First, we present the impact of carrier frequency offsets on WPM/OFDM communication in Section 4.2. This is followed by a discussion on the influence of phase noise in Section 4.3. Lastly, the transmission of WPM/OFDM under a loss of time synchronization error is analyzed in Section 4.4. The chapter ends with a summary in Section 4.5.

## 4-2 Frequency offset in multi-carrier modulation

The orthogonality between sub-carriers is maintained as long as the transmitter and receiver have the same reference frequency. Any offset in the frequency results in loss of orthogonality and the carriers interfere with one-another's transmission. This is due to the reason that during demodulation sampling may not occur at the peaks of the sub-carriers but rather at offset points. Besides the interference, frequency offsets also lead to attenuation and rotation of the sub-carrier phases.

### 4-2-1 Modeling frequency offset errors

An offset in frequency is commonly caused by a misalignment between receiver and transmitter local oscillator frequencies or due to a Doppler shift. The Doppler frequency shift  $f_{dk}$  is proportional to the sub-carrier frequency  $f_k$ , angle of the velocity vector  $\alpha$  and the relative speed between the transmitter and the receiver  $v_r$  and can be expressed as:

$$f_{dk} = \frac{v_r f_k}{c} \cos(\alpha) \quad (4.1)$$

In eq. (4.1)  $c$  denotes the speed of light and it is approximately equal to  $3 \times 10^8$  m/s. The frequency of each sub-carrier can be calculated by taking the sum of main carrier frequency  $f_c$  and baseband sub-carrier frequency  $f_{sc}$  as:

$$f_k = f_c \pm f_{sc} \quad (4.2)$$

Using eqs. (4.1) and (4.2) the relative frequency offset  $\Delta_f$  due to Doppler shift can be expressed as the ratio between the actual frequency offset and sub-carrier spacing, i.e.:

$$\Delta_f = \frac{f_{dk}}{f_c \pm f_{sc}} \cos(\alpha) = \frac{v_r}{c} \cos(\alpha) \quad (4.3)$$

The frequency offset can be modeled at the receiver by multiplying the received signal in the time domain with a complex exponential whose frequency component is equal to frequency offset value. If we denote the transmitted signal by  $S[n]$  and the received signal by  $R[n]$  the relation between the two under the influence of a frequency offset  $\Delta_f$  can be given as:

$$R[n] = S[n]e^{j2\pi\Delta_f n/N + \phi_0} + w[n] \quad (4.4)$$

In eq.(4.4)  $\Delta_f$  denotes the relative frequency offset due to local oscillator mismatch or due to Doppler shift or a combination of both.  $N$  stand for the total number of sub-carriers,  $\phi_0$  is initial phase and  $w$  denotes additive white Gaussian noise (AWGN). Without loss of generality, we consider that  $w[n] = 0$  and  $\phi_0 = 0$ . Hence,  $R[n] = S[n]e^{j2\pi\Delta_f n/N}$ .

### 4-2-2 Frequency offset in OFDM

In OFDM the frequency offset prevents the perfect alignment of FFT bins with the peaks of the sinc pulses i.e. sub-carriers. This is illustrated in fig. 4.1 where the sampling mismatch due to a frequency offset is depicted.

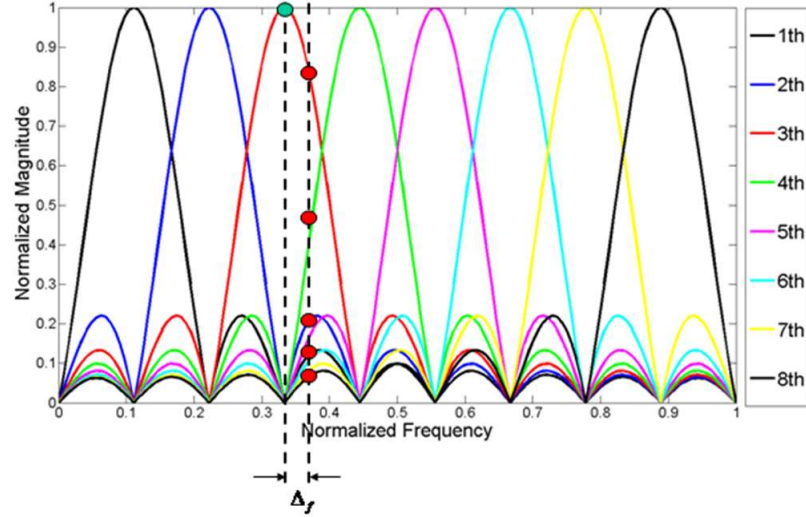


FIGURE 4.1: Illustration of erroneous sampling in OFDM due to Carrier Frequency Offset [82].

The FFT output corresponding to the  $k$ th sub-carrier under frequency offset  $\Delta_f$  can be expressed as:

$$\begin{aligned}
 \hat{a}_{k'} &= \frac{1}{N} \sum_{n=0}^{N-1} R[n] e^{-j2\pi \frac{k'n}{N}} \\
 &= \frac{1}{N} \sum_{k=0}^{N-1} a_k \sum_{n=0}^{N-1} e^{j2\pi \frac{kn}{N}} e^{j2\pi \Delta_f \frac{n}{N}} e^{-j2\pi \frac{k'n}{N}} \\
 &= \frac{1}{N} \sum_{k=0}^{N-1} a_k \sum_{n=0}^{N-1} e^{j2\pi \frac{(k-k'+\Delta_f)n}{N}}
 \end{aligned} \tag{4.5}$$

Using the geometric series properties eq.(4.5) can also be expressed as [74, 76]:

$$\hat{a}_{k'} = \frac{1}{N} \sum_{k=0}^{N-1} a_k \frac{\sin(\pi(k-k'+\Delta_f))}{\sin\left(\frac{\pi(k-k'+\Delta_f)}{N}\right)} e^{j\pi\left(\frac{N-1}{N}\right)(k-k'+\Delta_f)} \tag{4.6}$$

We can split eq.(4.6) into two distinct parts:

$$\begin{aligned}
 \hat{a}_{k'} &= \underbrace{a_{k'} \frac{\sin(\pi\Delta_f)}{N \sin\left(\frac{\pi\Delta_f}{N}\right)} e^{j\pi\left(\frac{N-1}{N}\right)\Delta_f}}_{\text{Useful Signal(Attenuated, PhaseShifted)}} \\
 &+ \underbrace{\frac{1}{N} \sum_{k=0; k \neq k'}^{N-1} a_k \frac{\sin(\pi(k-k'+\Delta_f))}{\sin\left(\frac{\pi(k-k'+\Delta_f)}{N}\right)} e^{j\pi\left(\frac{N-1}{N}\right)(k-k'+\Delta_f)}}_{\text{Intercarrier Interference(ICI)}}
 \end{aligned} \tag{4.7}$$

The first component of eq.(4.7) stands for the useful demodulated signal which has been attenuated and phase shifted due to the frequency offset. Since the attenuation term is independent of the carrier-index all the sub-carriers experience the same degree of attenuation [82]. The second term in eq.(4.7) contains the ICI term which represents the deleterious impact of all other sub-carriers on the decision making of data contained in the carrier of interest. The CFO does not influence the amplitude of the OFDM signal and therefore the total received power is not altered. Furthermore, the total ICI power due to CFO is also not affected by the number of OFDM carriers [82].

### 4-2-3 Frequency offset in WPM

The detected data for the  $k$ th sub-carrier and  $u$ th symbol at the WPM receiver under a loss of frequency synchronization can be expressed as:

$$\begin{aligned}\hat{a}_{u',k'} &= \sum_n R[n] \xi_l^{k'} [u'N - n] = \sum_n \sum_u \sum_{k=0}^{N-1} a_{u,k} \xi_l^k [n - uN] e^{j2\pi\Delta_f(\frac{n}{N})} \xi_l^{k'} [u'N - n] \\ &= \sum_u \sum_{k=0}^{N-1} a_{u,k} \left( \sum_n \xi_l^k [n - uN] e^{j2\pi\Delta_f(\frac{n}{N})} \xi_l^{k'} [u'N - n] \right)\end{aligned}\quad (4.8)$$

Defining the cross-waveform function  $\Omega[\Delta_f]$  as:

$$\Omega_{k,k'}^{u,u'}[\Delta_f] = \sum_n e^{j2\pi\Delta_f(\frac{n}{N})} \xi_l^k [n - uN] \xi_l^{k'} [u'N - n] \quad (4.9)$$

the demodulated information bit of the  $k$ th sub-carrier and  $u$ th WPM symbol corrupted by the interference due to loss of orthogonality can be expressed as:

$$\hat{a}_{u',k'} = \underbrace{a_{u',k'} \Omega_{k',k'}^{u',u'}[\Delta_f]}_{\text{Desired Alphabet}} + \underbrace{\sum_{u;u \neq u'} a_{u,k'} \Omega_{k',k'}^{u,u'}[\Delta_f]}_{\text{ISI}} + \underbrace{\sum_u \sum_{k=0; k \neq k'}^{N-1} a_{u,k} \Omega_{k,k'}^{u,u'}[\Delta_f]}_{\text{Inter Symbol-ICI (IS-ICI)}} \quad (4.10)$$

In eq.(4.10) the first term stands for the attenuated and rotated version of the useful data. The second term gives the ISI due to symbols transmitted on the same sub-channel and the third term denotes the ICI measured over the whole frame.

### 4-2-4 Numerical results for frequency offset errors

In this section we investigate the performance of WPM under frequency offset by means of computer simulations. The WPM transceiver is simulated with different wavelet families and

	<b>WPM</b>	<b>OFDM</b>
Number of sub-carriers	128	128
Number of multi-carrier symbols per Frame	100	100
Modulation	QPSK	QPSK
Channel	AWGN	AWGN
Oversampling factor	1	1
Guard band	-	-
Guard interval	-	-
Carrier frequency $f_c$	0 (base band)	0 (base band)
Frequency offset	$\Delta_f = 5 - 10\%$	$\Delta_f = 5 - 10\%$
Phase noise	-	-
Time offset	-	-

TABLE 4.1: Simulation setup for study of frequency offset effects.

their performances are compared with OFDM. To simplify the analysis, the channel is taken to be additive white Gaussian noise (AWGN). No other distortions except frequency offset is introduced. QPSK is the modulation mode of choice. The number of symbols per frame is set to 100 with each symbol consisting of 128 sub-carriers. Furthermore, the simulated system has no error estimation or correction capabilities nor is guard intervals or guard bands used. Any change from these specifications will be explicitly stated. The parameters of the simulation set-up are summarized in table 4.1.

#### a. Performance under frequency offset error

Fig. 4.2 shows the bit error rate (BER) plots of OFDM and WPM transceivers for a relative frequency offset of 5% from the  $1/T$  spacing. The BER curves for different wavelets and OFDM show similar performance but due to frequency offset they all deviate from the theoretical curve. The biorthogonal wavelet is the exception with a very poor performance compared to the other systems. This is due to the fact that the biorthogonal wavelets do not fulfill the orthogonality condition.

In fig. 4.3 the BER plots is shown for different values of relative frequency offset varying from 0 to 40% for a constant SNR value of 16 dB. We can again see that the performances of majority of the wavelets are very similar to that of OFDM. The biorthogonal wavelet, however, has a poor performance, while Haar wavelet slightly outperforms other wavelets and even OFDM. The results make clear the sensitivity of both WPM and OFDM systems to frequency offset.

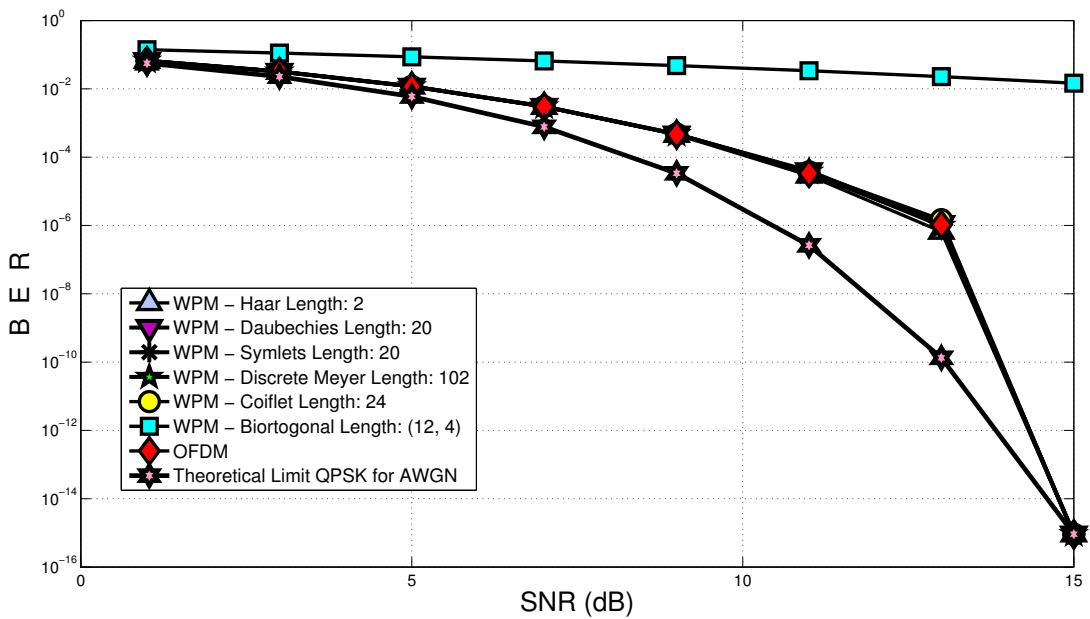


FIGURE 4.2: BER for WPM for different Wavelets and OFDM under a relative frequency offset of 5%.

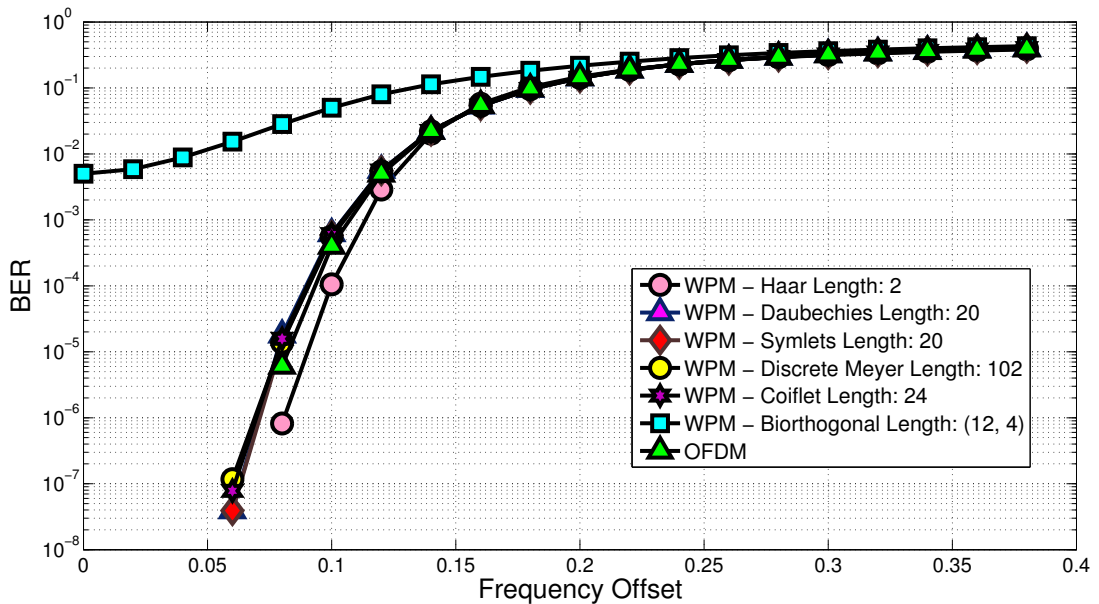


FIGURE 4.3: BER vs. relative frequency offset for WPM and OFDM in an AWGN Channel (SNR = 16 dB).

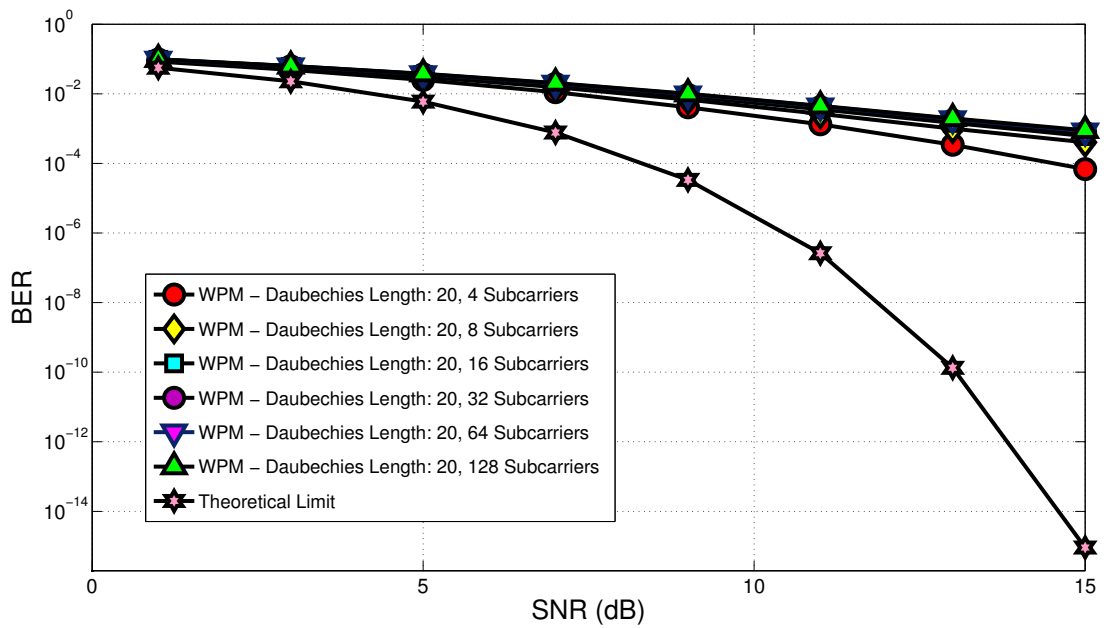


FIGURE 4.4: BER for WPM with different number of sub-carriers. Relative frequency offset = 10%. Wavelet of choice - db10.

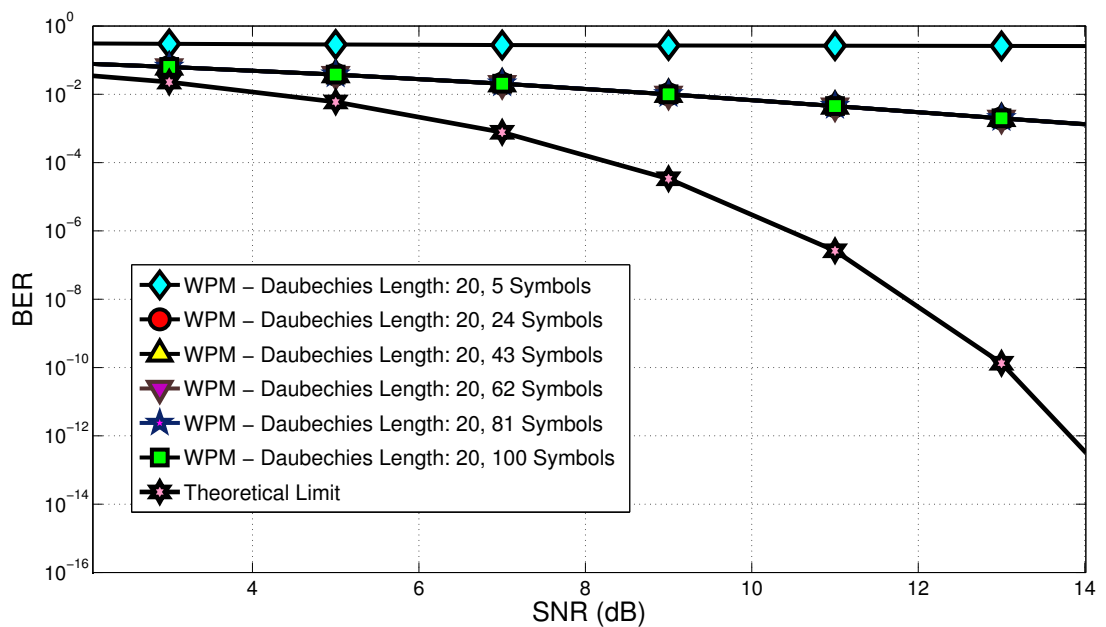


FIGURE 4.5: BER for WPM with different number of multi-carrier symbols/frame. Relative frequency offset - 10%, Wavelet family: Daubechies.

### **b. Influence of number of sub-carriers**

The results of the investigation on the influence of the number of sub-carriers on the WPM system performance under frequency offset are depicted in fig. 4.4. For this set of experiments all the WPM transceivers are simulated with the same wavelet, namely Daubechies-20, but with different number of sub-carriers. Furthermore, the relative frequency offset is set to 10%.

The degradation of WPM performance in the presence of frequency offset is dependent on the number of sub-carriers. This dependency is straightforward when the absolute frequency offset is fixed [5]. As the number of sub-carriers in a given bandwidth increases, the spacing between the sub-carriers decreases and hence the relative frequency offset increases. The results of these studies are plotted in fig. 4.4. For the case considered the relative frequency offset with respect to the inter-carrier spacing is kept constant. The WPM configurations with larger number of sub-carriers are more susceptible to the frequency offset. However, beyond a point this sensitivity saturates and even with increasing number of sub-carriers there is no perceptible differences in performance. For example, we can observe from fig. 4.4 that the performances of WPM with 64 and 128 sub-carriers are almost identical.

### **c. Influence of WPM frame size**

Frequency offset in WPM not only leads to ICI within one symbol but also across the whole frame. Therefore, it is important to see the effect of the frame size in combination with the frequency offset. These results are depicted in fig. 4.5. The plots show that the number of symbols in a frame does not affect the performance of WPM in the presence of frequency offset.

### **d. Influence of wavelet filter length**

The influence of the filter's length in combination with the frequency offset on the BER performance is illustrated in fig. 4.6. This simulation is performed for AWGN channel and a relative frequency offset of 10%. We again choose the Daubechies wavelet but now we alter the number of filter's coefficients and fix the number of sub-carriers to 128. The BER curves shown in fig. 4.6 are all superimposed one over another suggesting that the filter's length and number of wavelets' zero moments have no tangible influence on the system performance operating under a loss of frequency synchronization.

### **e. Constellation plots**

The effect of frequency misalignment between transmitter and receiver on the constellation points is depicted in the fig. 4.7. In order to highlight the effect of frequency offset we assume

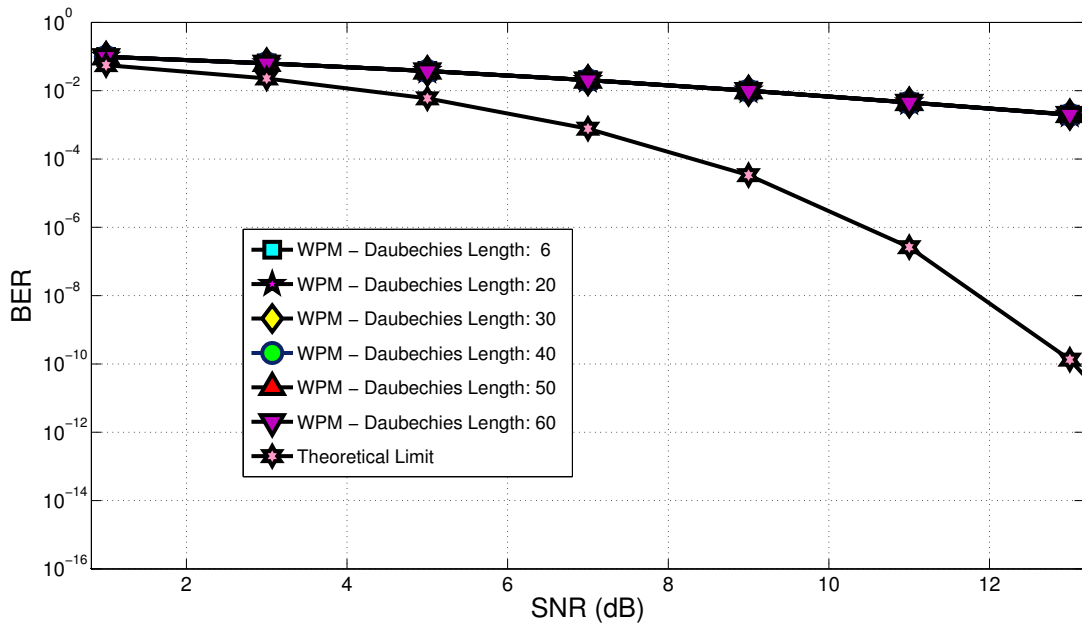


FIGURE 4.6: BER for WPM using Daubechies wavelets of different lengths and relative frequency offset of 10%.

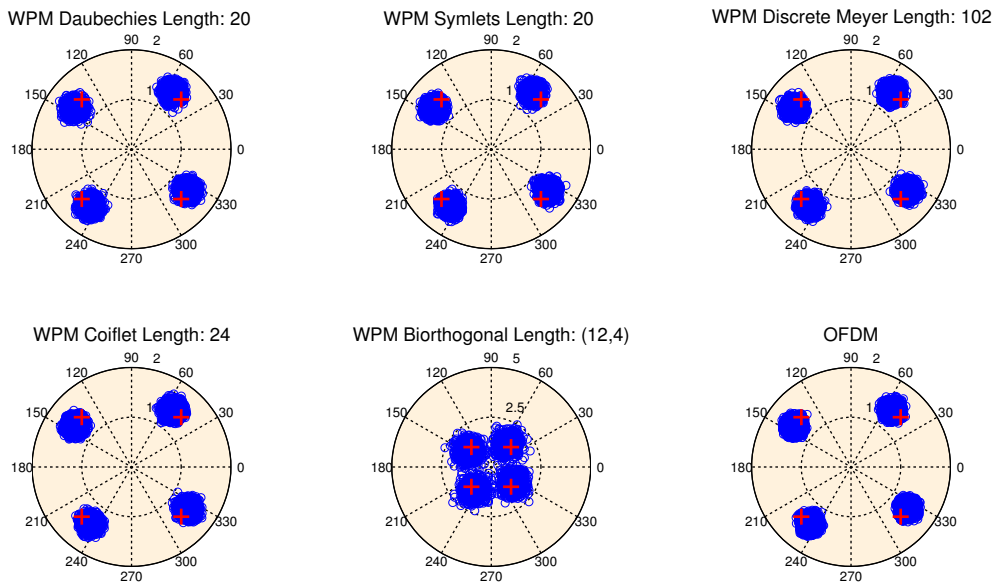


FIGURE 4.7: Constellation points in the presence of a relative frequency offset of 5%.

an ideal channel without any other infarction or noise barring a loss in frequency synchronization (a relative frequency offset of 5% is chosen). The main effect of the frequency offset is the scattering of the constellation points around reference positions due to interference. Other consequences are the anti-clockwise rotation of all constellation points and a marginal attenuation.

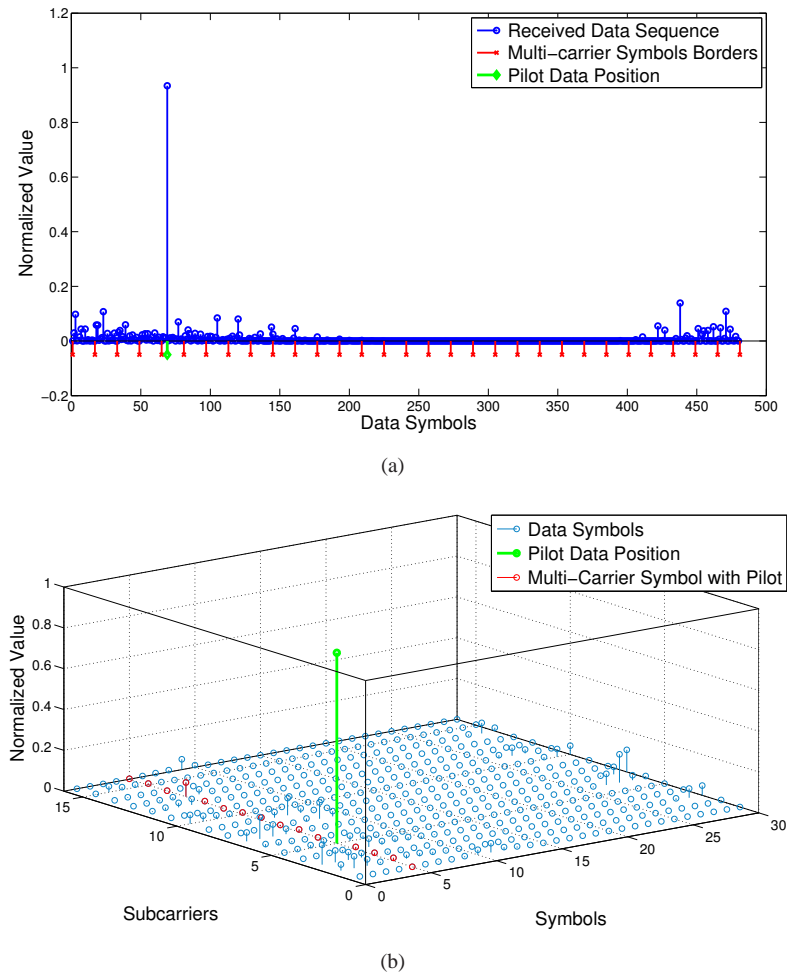


FIGURE 4.8: Spectral energy in a frame of the received WPM signal affected by a frequency offset. (a) 2-D and (b) 3-D. Wavelet used: Daubechies 10.

#### f. Dispersion of sub-carrier energy

The last set of results in this section show the dispersion of the sub-carriers energy due to frequency offset (see figs. 4.8(a) and 4.8(b) for WPM and figs. 4.9(a) and 4.9(b) for OFDM). For clarity of depiction, we have limited the number of sub-carriers to 16 and the frame size to 30 multi-carrier symbols. The channel is assumed to be ideal and all disturbances in the transmission are solely due to the frequency offset. Figs. 4.8(a), 4.8(b), 4.9(a) and 4.9(b) were obtained by transmitting a single non-zero pilot sub-carrier with all other sub-carriers in the frame set to zero.

In an ideal situation without any frequency offset, the only sub-carrier with non-zero value will be the pilot sub-carrier regardless of WPM or OFDM. However, the frequency offset results in loss of orthogonality and sub-carriers begin to interfere with one another. In OFDM the effect of frequency offset is to introduce ICI. This disturbance is confined to within a single multi-carrier

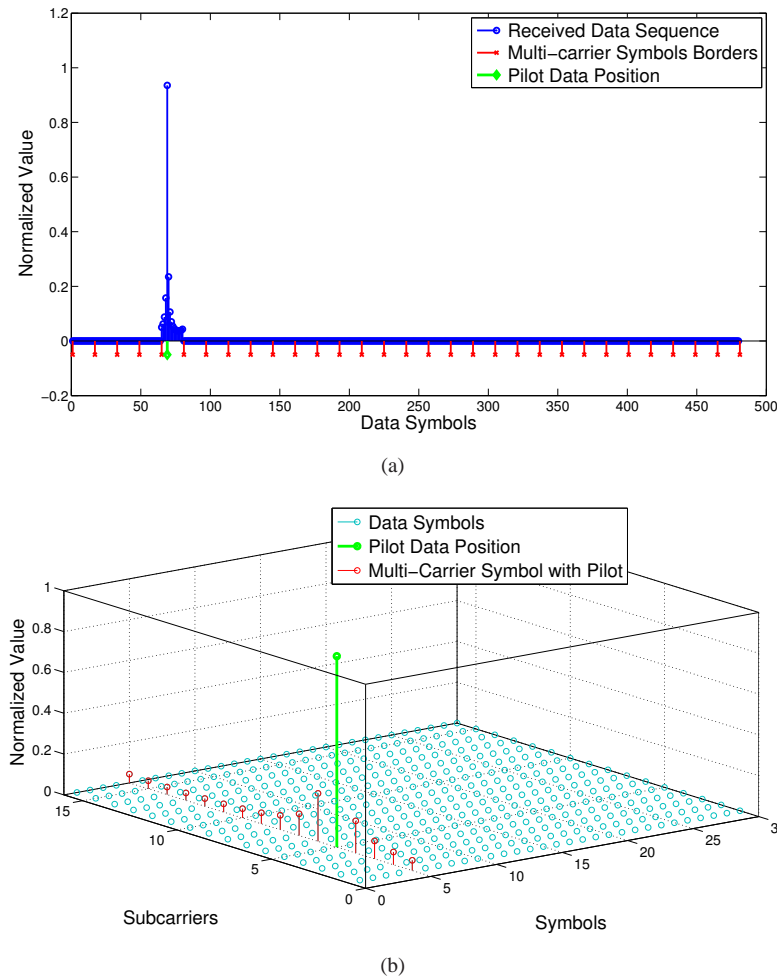


FIGURE 4.9: Spectral energy in a frame of the received OFDM signal affected by a frequency offset. (a) 2-D and (b) 3-D.

symbol and other OFDM symbols are not affected. On the other hand the WPM has overlapping symbols and hence an offset in frequency results in both ICI and inter-symbol-ICI.

In figs. 4.8(a) and 4.8(b) we therefore observe that the energy of the pilot sub-carrier located in the 5th sub-carrier and 5th symbol is spread across the whole frame. This is in agreement with the theoretical derivations carried out in sections 4.2.2 and 4.2.3.

### 4-3 Phase noise in multi-carrier modulation

An ideal local oscillator modulates carriers with a constant amplitude and frequency. However, practical local oscillators suffer from deleterious factors, such as thermal noise [83], which causes the oscillator's central frequency to fluctuate. This uncertainty in the actual frequency or the phase of the signal is referred to as phase noise. Multi-carrier transmission is vulnerable to phase noise since phase noise can cause a loss of orthogonality between the sub-carriers.

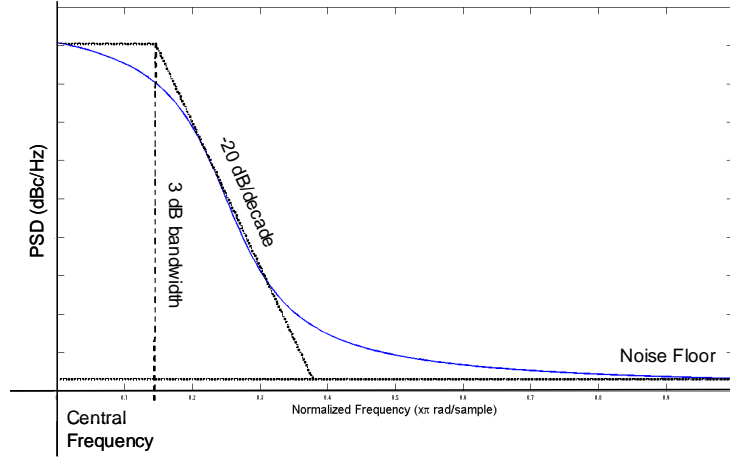


FIGURE 4.10: Single side band PSD of the oscillator.

### 4-3-1 Modeling the phase noise

Phase noise can be represented as a parasitic phase modulation of the oscillator's signal. In the literature there exist many models for the phase noise. Majority of these models are described in terms of the power spectral density (PSD). In the ideal case the PSD of the local oscillator would be a single pulse (delta function) at the central frequency. However, due to imperfections of the oscillator, the PSD of a practical oscillator is distributed over a wider frequency band with highest concentration around oscillator's central frequency. The single side band PSD of free running oscillator can be estimated by the Lorentzian function [84], like the one illustrated in fig. 4.10.

We model the phase noise as a zero mean white Gaussian process  $\phi_w$  with finite variance  $\sigma_w^2$ . The model is based on the work of [69]. The autocorrelation function of the phase noise is given by:

$$R_{\phi_w}[m] = \sigma_w^2 \delta[m] \quad (4.11)$$

The power spectral density of the phase noise can be expressed as:

$$S_{\phi_w}(f) = \sum_{m=-\infty}^{\infty} R_{\phi_w}(m) e^{-j2\pi f m} \quad (4.12)$$

In order to get the desired phase noise bandwidth we perform low pass filtering with filter  $F_\phi$ , in which case the PSD can be given as:

$$S_{\phi_b}(f) = S_{\phi_w}(f) |F_\phi(f)|^2 \quad (4.13)$$

By changing the corner frequency  $f_{c\phi}$  of the filter used we can adjust the phase noise bandwidth. Low values of the corner frequency result in narrow bandwidth for the phase noise while higher values of the corner frequency spread the phase noise.

In the last stage of the model we add phase noise floor to the signal. The phase noise floor is also modeled as a zero mean Gaussian process with finite variance  $\sigma_{wn}^2$ , which is relatively low compared to  $\sigma_w^2$ . The phase noise floor is not correlated so that it spans the whole available bandwidth and has flat PSD.

The total phase noise  $\Delta_\phi$  can now be expressed as a sum of bandwidth limited main noise contribution  $\phi_b$  and phase noise floor  $\phi_{wn}$  as:

$$\Delta_\phi[n] = \phi_b[n] + \phi_{wn}[n] \quad (4.14)$$

Using the phase noise model given above we can write the received signal  $R[n]$  that has been affected by phase noise and AWGN channel as:

$$R[n] = S[n]e^{j\Delta_\phi[n]} + w[n] \quad (4.15)$$

Without loss of generality, we take  $w[n] = 0$ , in which case the received signal can be given as  $R[n] = S[n]e^{j\Delta_\phi[n]}$ .

### 4-3-2 Phase noise in OFDM

The demodulated OFDM data at the receiver's output affected by phase noise can be expressed as:

$$\begin{aligned} \hat{a}_{k'} &= \frac{1}{N} \sum_{n=0}^{N-1} R[n] e^{-j2\pi \frac{k'}{N} n} \\ &= \frac{1}{N} \sum_{k=0}^{N-1} a_k \sum_{n=0}^{N-1} e^{j2\pi \frac{k}{N} n} e^{j\Delta_\phi[n]} e^{-j2\pi \frac{k'}{N} n} \\ &= \frac{1}{N} \sum_{k=0}^{N-1} a_k \sum_{n=0}^{N-1} e^{j\Delta_\phi[n]} e^{j2\pi \frac{[k-k']n}{N}}. \end{aligned} \quad (4.16)$$

To simplify the analysis, the demultiplexed signal can be separated into useful information component and disturbance component. In order to do so we assume that the phase noise is sufficiently small so that it can be approximated as [69]:

$$e^{j\Delta_\phi[n]} \approx 1 + j\Delta_\phi[n]. \quad (4.17)$$

Under this approximation the demodulated OFDM information bit for the  $k$ 'th carrier can be given as:

$$\begin{aligned}
\hat{a}_{k'} &\approx \frac{1}{N} \sum_{k=0}^{N-1} a_k \sum_{n=0}^{N-1} e^{j2\pi \frac{[k-k']n}{N}} + \frac{j}{N} \sum_{k=0}^{N-1} a_k \sum_{n=0}^{N-1} \Delta_\phi[n] e^{j2\pi \frac{[k-k']n}{N}} \\
&\approx a_{k'} + \frac{j}{N} \sum_{k=0}^{N-1} a_k \sum_{n=0}^{N-1} \Delta_\phi[n] e^{j2\pi \frac{[k-k']n}{N}} \\
&= a_{k'} + I_{\Delta_\phi}[k'].
\end{aligned} \tag{4.18}$$

The first component of eq.(4.18) stands for the correctly demodulated symbol while the second term  $I_\phi$  represents the interference caused to each sub-carrier.

The perturbation caused by the phase noise on multi-carrier transmission can be divided into two components:

- Common phase error (CPE) wherein all the information bits contained in a sub-carrier are attenuated and rotated by the same angle.
- Inter-carrier interference (ICI) where the information bits contained in a sub-carrier are corrupted by disturbance from all other sub-carriers.

### 1. Common phase error (CPE) - case when $k' = k$

For this case the disturbance term in eq.(4.18) can be written as:

$$\begin{aligned}
I_{\Delta_\phi}[k'] &= \frac{j}{N} \sum_{k=0}^{N-1} a_k \sum_{n=0}^{N-1} \Delta_\phi[n] \\
&= j\Phi a_{k'}.
\end{aligned} \tag{4.19}$$

The interference component in eq.(4.19) rotates all the constellation points by an angle  $\Phi$ . This angle of rotation  $\Phi$  is common for all sub-carriers and can be defined by the average phase noise given as:

$$\Phi = \frac{1}{N} \sum_{n=0}^{N-1} \phi[n]. \tag{4.20}$$

The common phase error (CPE) is only dependent on low frequencies of the phase noise spectrum up to the frequency of the inter-carrier spacing.

## 2. Inter carrier interference (ICI) - case when $k' \neq k$

For this case the disturbance term in eq.(4.18) can be written as:

$$I_{\Delta_\phi}[k] = \frac{j}{N} \sum_{k=0; k \neq k'}^{N-1} a_k \sum_{n=0}^{N-1} \Delta_\phi[n] e^{j2\pi \frac{(k-k')n}{N}}. \quad (4.21)$$

The error in eq.(4.21) consists of contribution from all other sub-carriers of a OFDM symbol and is known as ICI. The ICI due to phase noise is dependent only on the high frequency phase noise components. In general, the phase noise that causes ICI contains frequencies which are larger than inter-carrier spacing frequency.

### 4-3-3 Phase noise in WPM

As in OFDM, the disturbance caused by phase noise can be divided into two components:

- Common phase error (CPE) wherein all the information bits contained in a sub-carrier are attenuated and rotated by the same angle.
- Inter-Symbol Inter-carrier interference (ICI) where the information bits contained in a sub-carrier are corrupted by disturbance from all other sub-carriers as well as from neighboring symbols.

For ease of representation we first define the cross-waveform function  $\Omega[\Delta_\phi]$  as:

$$\Omega_{k,k'}^{u,u'}[\Delta_\phi] = \sum_n \xi_l^k[n - uN] e^{j\Delta_\phi[n]} \xi_l^{k'}[u'N - n]. \quad (4.22)$$

The detected data at the WPM receiver in presence of the phase noise for the  $k$ th carrier and  $u$ th symbol can be written in terms of the cross-waveform function  $\Omega[\Delta_\phi]$  as:

$$\begin{aligned} \hat{a}_{u',k'} &= \sum_n R[n] \xi_l^{k'}[u'N - n] \\ &= \sum_u \sum_{k=0}^{N-1} a_{u,k} \Omega_{k,k'}^{u,u'}[\Delta_\phi]. \end{aligned} \quad (4.23)$$

Furthermore, assuming that the phase noise is sufficiently small so that it can be approximated as [69]:

$$e^{j\Delta_\phi[n]} \approx 1 + j\Delta_\phi[n], \quad (4.24)$$

Eq.(4.23) can be rewritten as:

$$\begin{aligned}\hat{a}_{u',k'} &\approx \sum_u \sum_{k=0}^{N-1} a_{u,k} \Omega_{k,k'}^{u,u'}[\Delta\phi] + j \sum_u \sum_{k=0}^{N-1} a_{u,k} \Omega_{k,k'}^{u,u'}[\Delta\phi] \\ &\approx \underbrace{a_{u',k'}}_{\text{(Useful Data)}} + \underbrace{I_{\Delta\phi}(u, k)}_{\text{Interference Term}}.\end{aligned}\quad (4.25)$$

The first component in eq.(4.25) stands for the correctly demodulated symbol and the second term represents the disturbances due to the phase offset. Two distinct scenarios arise out of the error term.

### 1. Common phase error (CPE) - case when $k' = k$ and $u' = u$

For this case the disturbance term in eq.(4.25) can be written as:

$$I_{\Delta\phi}(u', k') = j a_{u',k'} \Omega_{k',k'}^{u',u'}[\Delta\phi[n]], \quad (4.26)$$

which describes the rotation of constellation points by an angle which is common for all sub-carriers. The rotation angle is dependent on the average value of phase noise sequence.

### 2. Inter symbol- inter carrier interference (IS-ICI) - case when $k' \neq k$ and/or $u \neq u'$

For this case the disturbance term in (4.25) can be written as:

$$\begin{aligned}I_{\Delta\phi}(u', k') &= j \underbrace{\sum_{k=0; k \neq k'}^{N-1} a_{u',k'} \Omega_{k,k'}^{u',u'}[\Delta\phi[n]]}_{\text{(ICI)}} \\ &\quad + j \underbrace{\sum_{u; u \neq u'} \sum_{k=0}^{N-1} a_{u',k'} \Omega_{k,k'}^{u,u'}[\Delta\phi[n]]}_{\text{(IS-ICI)}}.\end{aligned}\quad (4.27)$$

The first term stands for the inter-carrier interference (ICI) and the second for inter-symbol-inter carrier interference (IS-ICI). The demodulated data hence consists of the estimate of the useful data and the interference terms:

1. common phase error ( $u = u'$  and  $k' = k$ ),
2. inter-carrier interference ( $u = u'$  and  $k' \neq k$ ),

	<b>WPM</b>	<b>OFDM</b>
Number of Sub-carriers	128	128
Number of Multi-carrier Symbols per Frame	100	100
Modulation	QPSK	QPSK
Channel	AWGN	AWGN
Oversampling Factor	1	1
Guard Band	-	-
Guard Interval	-	-
Frequency Offset	-	-
Phase Noise	$\sigma_w^2 = -10$ dBc, $\sigma_{wn}^2 = -20$ dBc, $f_{c\phi} = 0.1$	$\sigma_w^2 = -10$ dBc, $\sigma_{wn}^2 = -20$ dBc, $f_{c\phi} = 0.1$
Time Offset	-	-

TABLE 4.2: Simulation setup for studying the impact of the phase noise.

3. inter-symbol inter-carrier interference ( $u \neq u', k' = k$ . and  $u \neq u', k' \neq k$ ).

Different frequency components of the phase noise have different impacts on the CPE and ICI/IS-ICI terms. If the phase noise bandwidth is concentrated near the central frequency then the CPE term dominates. On the other hand when the phase noise bandwidth is spread the ICI/IS-ICI term takes precedence.

#### 4-3-4 Numerical results for phase noise

The performance degradation associated with phase noise has been evaluated with computer simulations. The simulation setup used is almost identical to that used for the evaluation of performance under frequency offset. More details on the set-up can be found in the Section 4.2.4. An overview of simulation parameters is given in table 4.2.

##### a. Phase noise characteristics

The effect of the phase noise on the WPM and OFDM transmission are illustrated by the PSD plots of the phase noise in figs. 4.11(a) ( narrow-band phase noise) and 4.12(a) (wide-band phase noise). In fig. 4.11(b) the constellation points' diagram of the WPM system operating under a phase noise of relatively low corner frequency is plotted. The dominant effect of such a phase noise is the common phase error which results in the rotation of all constellation points. The constellation points' diagram of the phase noise with relatively high corner frequency is illustrated in the fig. 4.12(b). For this case the interference caused to the sub-carriers is much more acute resulting in more pronounced dispersion of the constellation points.

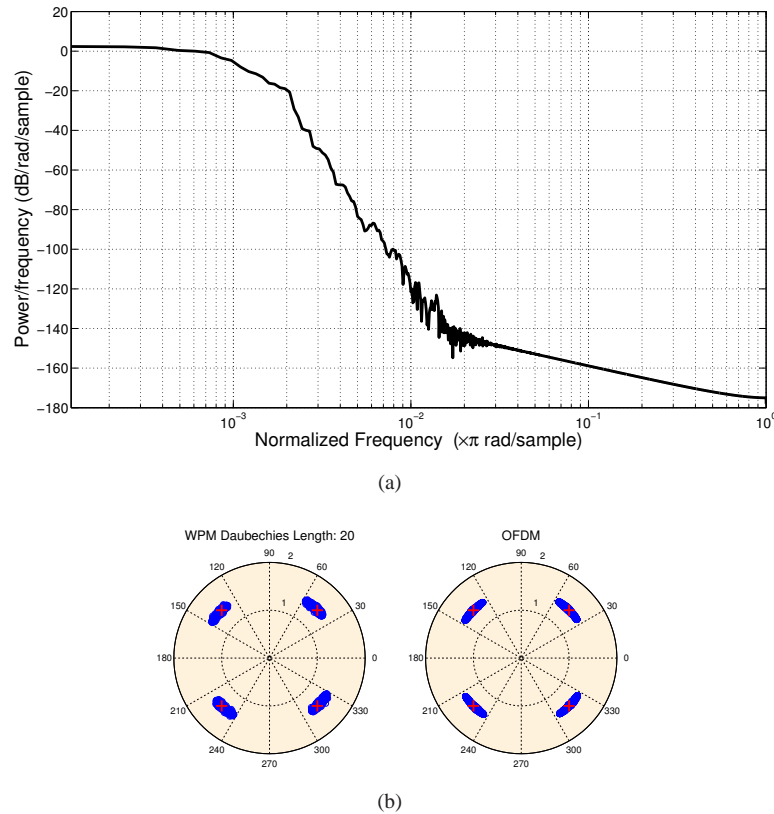


FIGURE 4.11: Phase Noise (Narrow Band); (a): PSD, (b): WPM and OFDM Constellation Points.

It is important to understand the effect of both CPE and ICI/IS-ICI as either of them can limit the performance of the system. In the literature there exists many approaches for the correction of CPE [79, 80]. However, the estimation and correction of the interference (ICI/IS-ICI) is harder to accomplish. Therefore, we limit ourselves here to the study of interference in WPM and OFDM caused by phase noise. In order to conduct this study, we set the phase noise bandwidth to 10% of the total available bandwidth and the variance to -10 dBc (relative to the carrier). For this case the PSD of the phase noise will look similar to the one illustrated in fig. 4.10.

### b. Performance under frequency offset error

Fig. 4.13 shows the bit error rate (BER) of WPM and OFDM in the presence of phase noise. The illustrated behaviors of BER curves are similar to each other with the exception of bi-orthogonal wavelet.

Fig. 4.14 illustrates the effect of the phase noise variance on the BER. This figure is obtained using an AWGN channel with 16 dB SNR while phase noise variance is varied from -10 to 20 dBc with a step-size of 5 dBc. It is natural that the phase noise variance and the performance

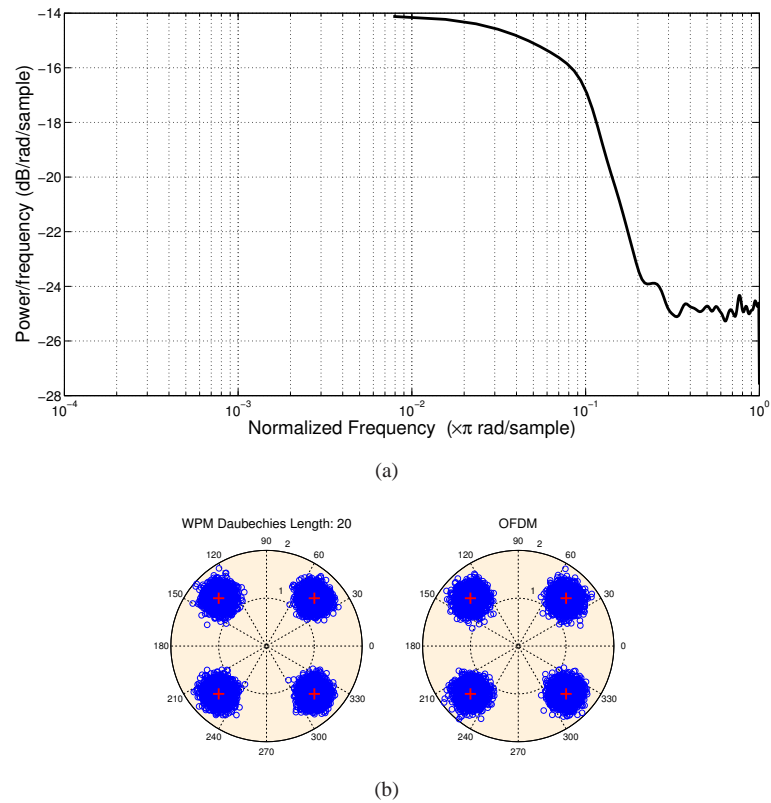


FIGURE 4.12: Phase Noise (Wide Band); (a): PSD, (b): WPM and OFDM Constellation Points.

degradation are closely related. The sensitivity of WPM and OFDM to the variance of the phase noise is confirmed by the plots in fig. 4.14.

### c. Influence of number of sub-carriers and WPM frame size

Figs. 4.15 and 4.16, respectively, show the performance of the WPM under phase noise when the number of sub-carriers and symbols in the frame are altered. The results haven't shown any essential connection between the performance degradation and the number of sub-carriers or the number of symbols per frame.<sup>3</sup>

### d. Influence of wavelet filter length

Fig. 4.17 illustrates the influence of filter's length and the number of zero wavelet moments in combination with the phase noise on the BER. As with the results for frequency offset, there

<sup>3</sup>The results would have been different had the corner-frequency been smaller. This is because the inter-carrier spacing depends on the number of sub-carriers - for low number of sub-carriers the CPE term dominates while for high number of sub-carriers the interference will be the major term [69, 85].

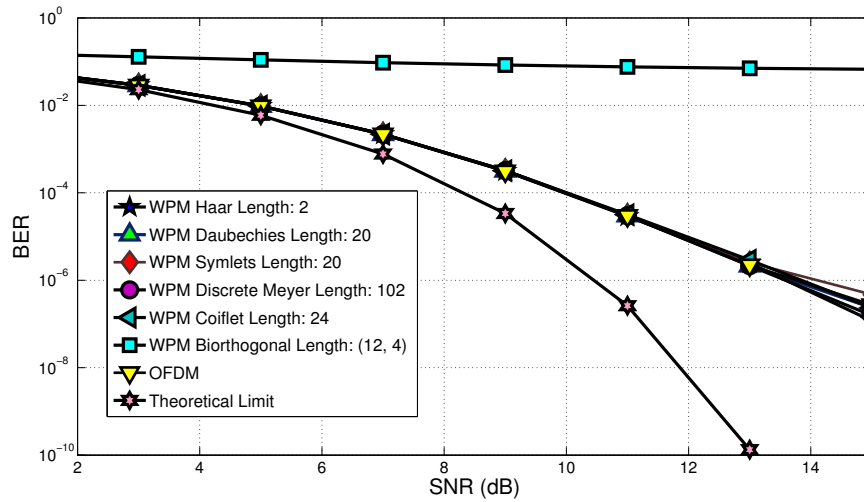


FIGURE 4.13: BER for WPM (with different wavelets) and OFDM under a phase noise of relative bandwidth 10% and variance -10 dBc.

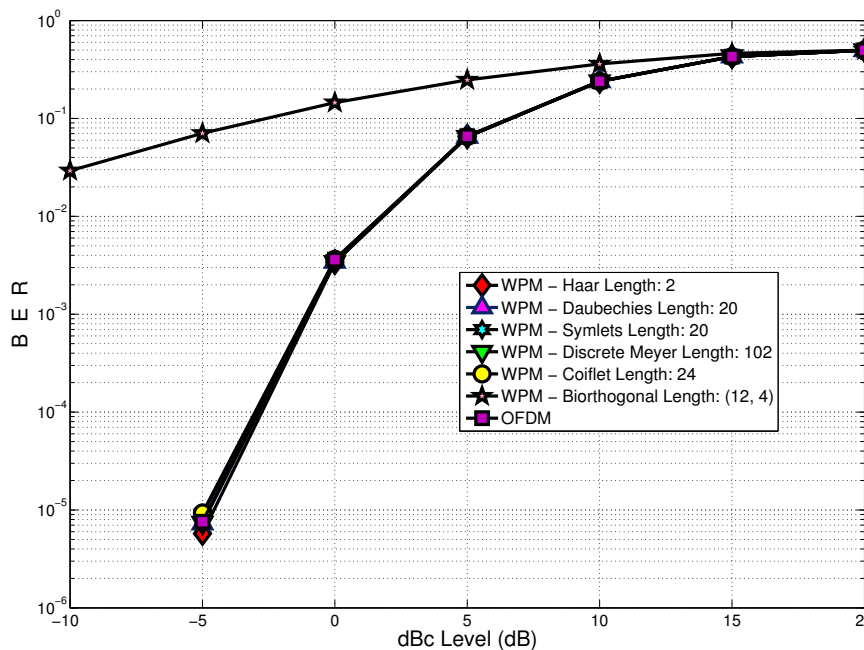


FIGURE 4.14: BER vs. phase noise variance for WPM and OFDM in AWGN Channel (SNR = 16 dB).

are no noticeable influences of the filter’s length and number of wavelets’ zero moments on the system performance when operating under a phase noise.

**e. Constellation plots**

For the completeness of the analysis we show in fig. 4.18 the smearing effect of the phase noise on the constellation points. To highlight the impact of phase noise the channel is assumed to be ideal with no other perturbation (barring phase error).

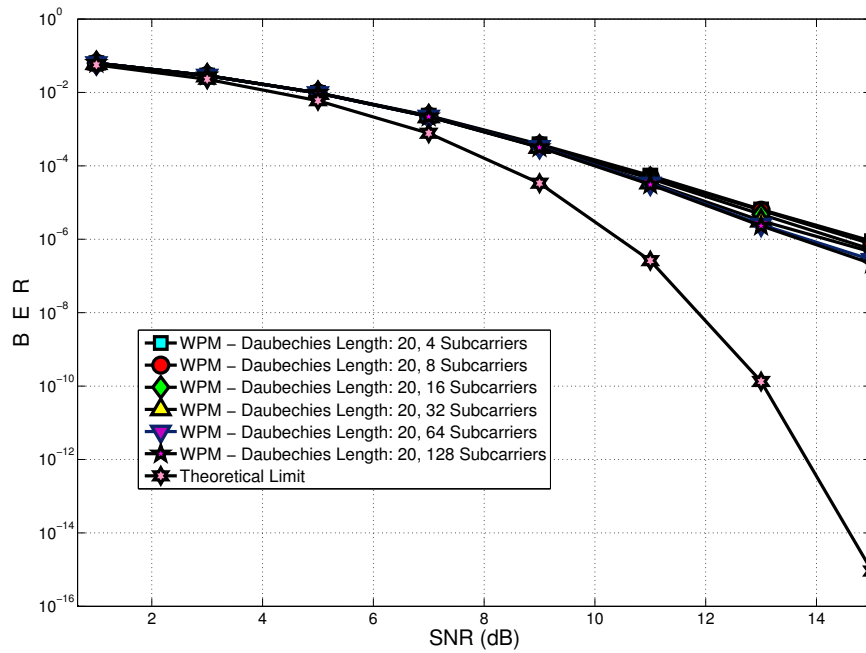


FIGURE 4.15: BER for WPM with phase noise for different number of sub-carriers.

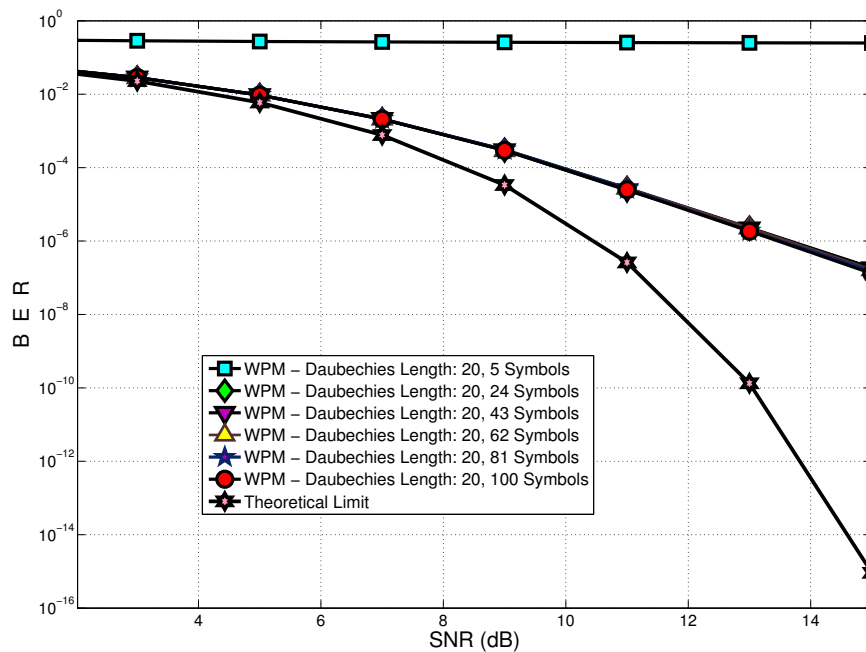


FIGURE 4.16: BER for WPM with phase noise for different number of symbols/frame.

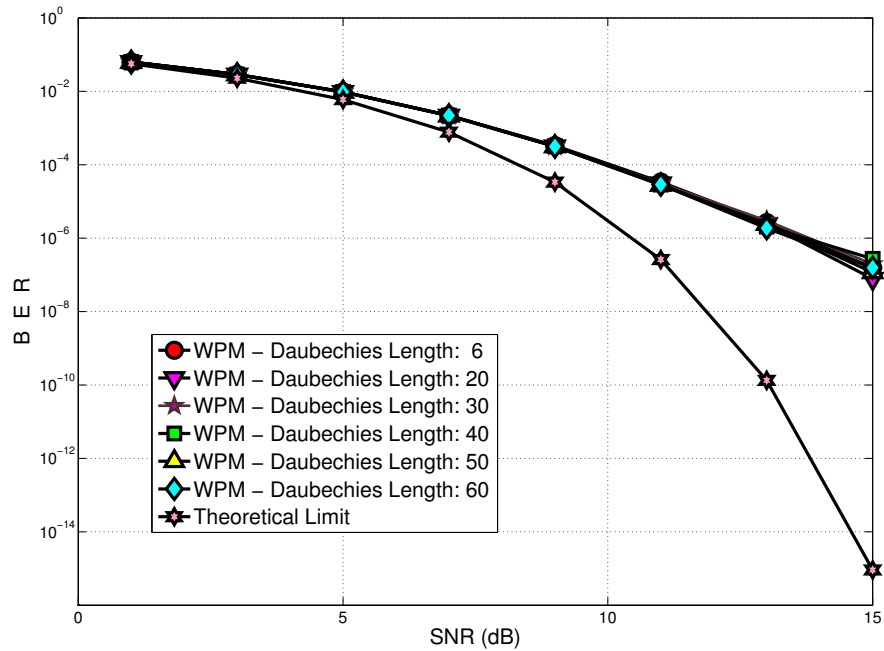


FIGURE 4.17: BER for WPM using Daubechies Wavelets of different lengths, under the influence of Phase Noise.

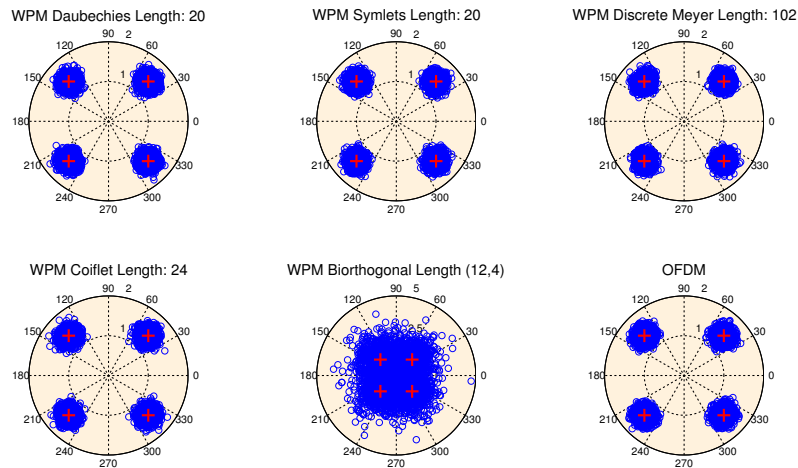
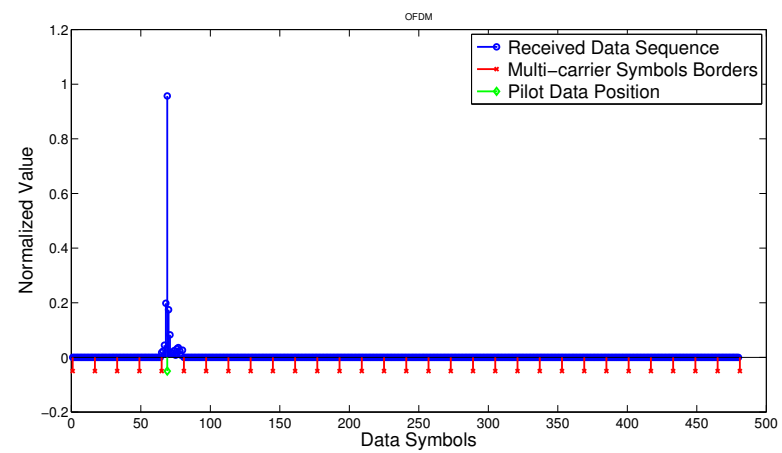
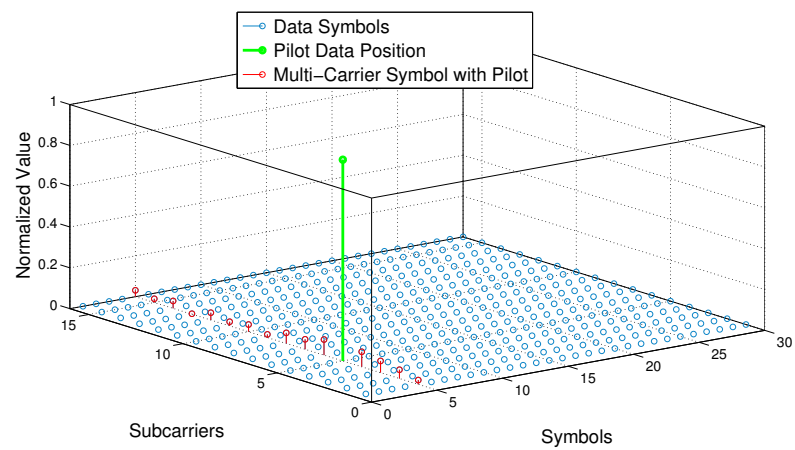


FIGURE 4.18: Constellation points in the presence of phase noise.

The spreading of sub-carrier energy due to phase noise is illustrated in figs. 4.19(a) and 4.19(b) for OFDM and figs. 4.20(a) and 4.20(b) for WPM. Phase noise results in loss of orthogonality and causes the sub-carriers to interfere with one another. In OFDM, interference due to phase noise is limited to within a symbol resulting in an ICI. However, due to the overlap of symbols in WPM, the phase noise causes ICI from other symbols resulting in Inter Symbol-inter carrier interference (IS-ICI). This is illustrated in fig. 4.20(b) where the dispersion of energy of a *pilot* sub-carrier is shown to extend to the entire frame. In the example presented we consider a pilot sub-carrier located at the 5th sub-carrier of the 5th symbol. This dispersion in energy is in agreement with the theoretical derivations carried out in sections 4.3.2 and 4.3.3.

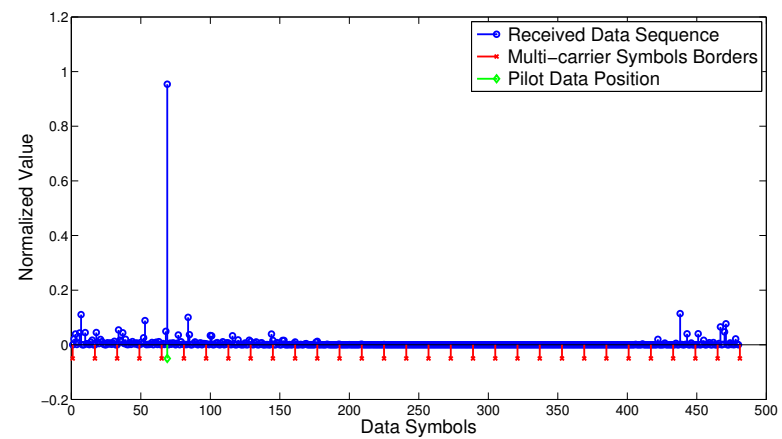


(a)

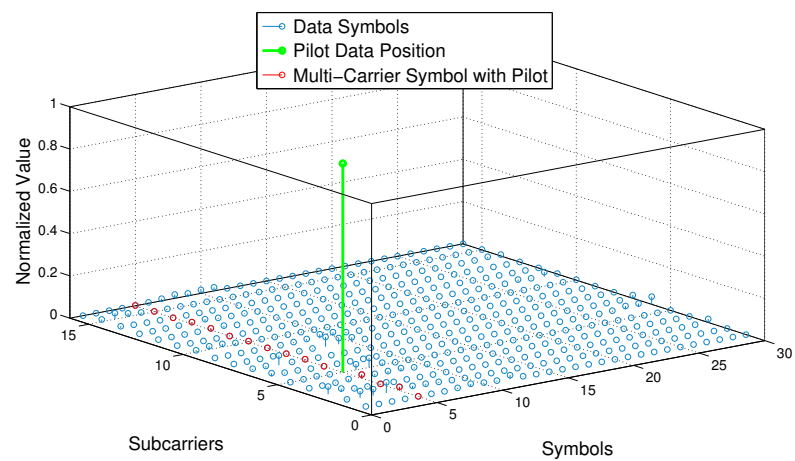


(b)

FIGURE 4.19: Spectral energy in a frame of the received OFDM signal affected by a phase noise. (a) 2D view, (b) 3D View.



(a)



(b)

FIGURE 4.20: Spectral energy in a frame of the received WPM (with Daubechies wavelet) signal affected by a phase noise. (a) 2D view, (b) 3D View.

## 4-4 Performance under loss of time synchronization

Another drawback of multi-carrier transmission is their vulnerability to time synchronization errors which occur when the symbols are not perfectly aligned at the receiver. Because of the time offset, samples outside a symbol get erroneously selected while useful samples at the beginning or at the end of that particular symbol get discarded.

### 4-4-1 Modeling time offset errors

The time synchronization error is modeled by shifting the received data samples by a time offset value  $\Delta_t$ <sup>4</sup> to the left or right, depending on the sign of the  $\Delta_t$  [86]. If we assume that transmitted signal is given by  $S[n]$ , the received signal  $R[n]$  in the presence of time synchronization errors can be expressed as:

$$R[n \pm \Delta_t] = S[n] + w[n] \quad (4.28)$$

Without loss of generality, we assume  $w[n] = 0$ , then,  $R[n \pm \Delta_t] = S[n]$ . Time offset degrades the performances of multi-carrier transceivers by introducing inter-symbol interference (ISI).

WPM and OFDM share many similarities as both are orthogonal multi-carrier systems but with regard to timing error the behaviors are vastly different. The actual length of the WPM symbols is defined by the wavelet used and in general it is significantly longer than the OFDM symbol. In the case of time offset this overlap of the symbols in WPM causes each symbol to interfere with several other symbols while in OFDM the symbols only interfere with their adjacent neighbors. The second important difference between the two transmission schemes is in the use of the guard interval between the symbols. OFDM uses cyclic prefix that significantly improves its performance under loss of time synchronization<sup>5</sup>. On the other hand, the WPM cannot benefit from such a guard interval since many WPM symbols overlap over one another.

### 4-4-2 Time offset in OFDM

The sensitivity of the OFDM to the time synchronization error is reported in [86–88]. A few of the available techniques for OFDM symbol synchronization can be found in [89–93]. The following discussion is based on [86].

Cyclic prefix is an effective and low complexity method to cope with dispersive channels and time synchronization errors in OFDM transceivers. OFDM often employs a cyclic prefix but

<sup>4</sup>The variations in time  $\Delta_t$  is usually modeled as a stochastic process.

<sup>5</sup>However, the use of cyclic prefix is effective only when the time offset induced by the channel does not exceed the length of the cyclic prefix and that the direction of time shift is towards the cyclic prefix.

rarely uses a *postfix*. This means that we have two distinct scenarios under time synchronization errors depending on the direction of the time offset [86]:

- Time synchronization error away from cyclic prefix (to the right).
- Time synchronization error towards cyclic prefix (to the left).

### a. Time offset away from the cyclic prefix

Fig. 4.21(b) illustrates this case by considering a snapshot of the OFDM data consisting of three symbols  $(u - 1, u, u + 1)$ . In this example the FFT window (for data demodulation) is misaligned to the right, i.e. away from the cyclic prefix. Each OFDM symbol consists of  $N$  data samples and an extension of  $N_{CP}$  samples representing the cyclic prefix. The FFT window in the case considered will contain  $N - \Delta_t$  data samples  $((\Delta_t + 1), (\Delta_t + 2), \dots, N)$  of the  $u$ th OFDM symbol, omitting the first  $\Delta_t$  useful samples. Instead  $\Delta_t$  samples  $(1, 2, \dots, \Delta_t)$  of the next  $(u + 1)$ th OFDM symbol will be erroneously selected.

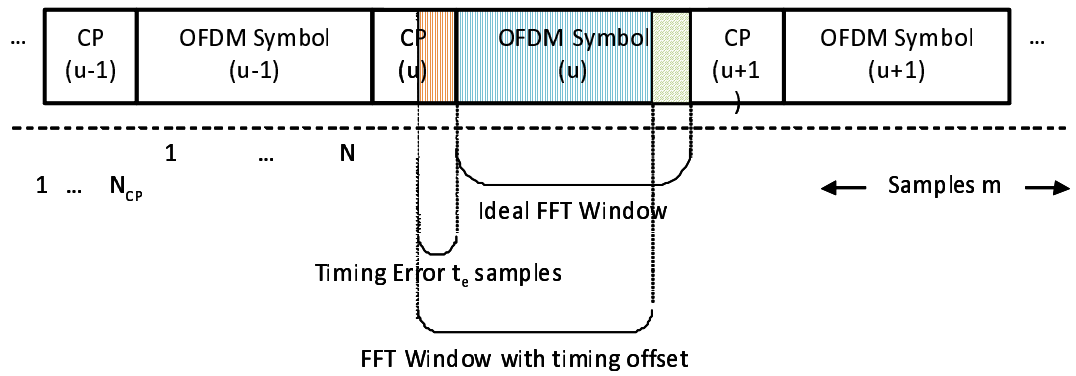
The demodulated OFDM signal after an FFT operation can be given as:

$$\begin{aligned}
 \hat{a}_{u',k'} = & \underbrace{\frac{N - \Delta_t}{N} a_{u',k'} e^{j2\pi \frac{k'}{N} \Delta_t}}_{\text{Useful Data (Attenuated, phase shifted)}} \\
 & + \underbrace{\frac{1}{N} \sum_{n=0}^{N-1-\Delta_t} \sum_{k=0; k \neq k'}^{N-1} a_{u',k} e^{j2\pi \frac{k(n+\Delta_t)}{N}} e^{-j2\pi \frac{k'n}{N}}}_{\text{Inter Carrier Interference}} \\
 & + \underbrace{\frac{1}{N} \sum_{n=N-\Delta_t}^{N-1} \sum_{k=0}^{N-1} a_{u+1,k} e^{j2\pi \frac{k(n-N+\Delta_t)}{N}} e^{-j2\pi \frac{k'n}{N}}}_{\text{Inter Symbol Interference}}. \quad (4.29)
 \end{aligned}$$

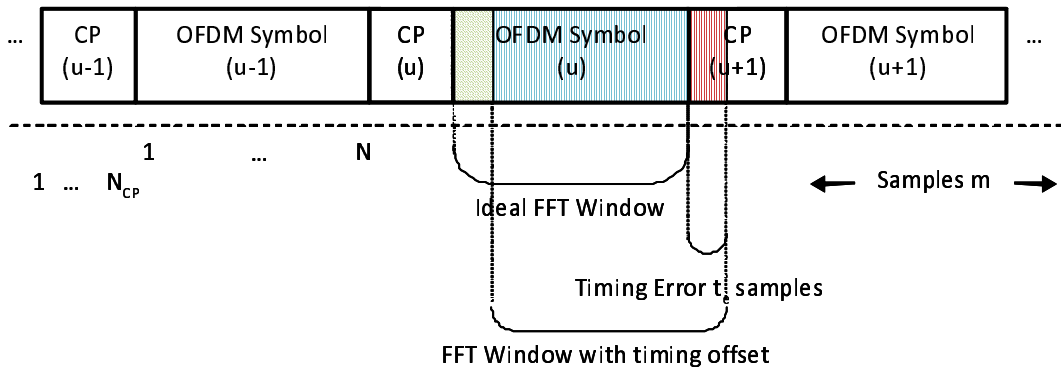
The first component of eq.(4.29) represents the useful signal which is attenuated and phase shifted by a term proportional to the sub-carrier index  $k'$ . The second component of eq.(4.29) gives the ICI and the third component stands for ISI with the next symbol.

### b. Time offset towards the cyclic prefix

Fig. 4.21(a) illustrates the case when the time offset error occurs towards the symbols own cyclic prefix, i.e. to the left. In such a scenario the FFT window consists of the first  $N - \Delta_t$  samples  $(1, 2, \dots, (N - \Delta_t))$  of the considered  $u$ th OFDM symbol and the last  $\Delta_t$  samples of the symbols own cyclic prefix. For convenience we take that  $\Delta_t < N_{CP}$ .



(a)



(b)

FIGURE 4.21: Time offset error in OFDM. (a) Offset towards the cyclic prefix (to the left), (b) Offset away from the cyclic prefix (to the right).

The demodulated OFDM signal affected by time offset in the direction of symbol's own cyclic prefix is given in eq.(4.30), for the case when  $\Delta_t < N_{CP}$ .

$$\hat{a}_{u',k'} = a_{u',k'} e^{-j2\pi \frac{k' \Delta_t}{N}} \tag{4.30}$$

Thanks to the cyclic prefix the orthogonality is preserved and the ISI, ICI terms don't appear. The timing error towards the cyclic prefix therefore results only in a phase shift.

### 4-4-3 Time synchronization error in WPM

The WPM transceivers do not employ guard intervals and therefore the direction of time offset is inconsequential. The demodulation process under time offset error  $\Delta_t$  can be obtained as:

$$\begin{aligned}
 \hat{a}_{u',k'} &= \sum_n R[n] \xi_l^{k'} [u'N - n + \Delta_t] \\
 &= \sum_n \sum_u \sum_{k=0}^{N-1} a_{u,k} \xi_l^k [n - uN] \xi_l^{k'} [u'N - n + \Delta_t] \\
 &= \sum_u \sum_{k=0}^{N-1} a_{u,k} \left( \sum_n \xi_l^k [n - uN] \xi_l^{k'} [u'N - n + \Delta_t] \right). \quad (4.31)
 \end{aligned}$$

For ease of representation we define the cross-waveform function  $\Omega[n]$  as:

$$\Omega_{k,k'}^{u,u'}[\Delta_t] = \sum_n \xi_l^k [n - uN] \xi_l^{k'} [u'N - n + \Delta_t]. \quad (4.32)$$

Eq.(4.32) represents the autocorrelation and the cross-correlation of the WPM sub-carrier  $k$ . When  $k = k'$  the two sub-carriers are time-inversed versions of one another and hence eq.(4.32) gives the autocorrelation sequence of the waveform  $k$ . On the other hand when  $k \neq k'$  the two waveforms correspond to different sub-carriers and in this instance eq.(4.32) represents the cross-correlation between the waveforms  $k$  and  $k'$ .

Using eq.(4.31) and eq.(4.32) we can express the demodulated alphabet for the  $k$ th sub-carrier and  $u$ th WPM symbol corrupted by the interference due to loss of orthogonality as:

$$\hat{a}_{u',k'} = \underbrace{a_{u',k'} \Omega_{k',k'}^{u',u'}[\Delta_t]}_{\text{Desired Alphabet}} + \underbrace{\sum_{u;u \neq u'} a_{u,k'} \Omega_{k',k'}^{u,u'}[\Delta_t]}_{\text{ISI}} + \underbrace{\sum_u \sum_{k=0; k \neq k'}^{N-1} a_{u,k} \Omega_{k,k'}^{u,u'}[\Delta_t]}_{\text{IS-ICI}}. \quad (4.33)$$

In eq.(4.33) the first term stands for the attenuated useful signal. The second term gives the ISI due to symbols transmitted on the same sub-channel and the third term denotes the ICI measured over the whole frame. The received constellation points of WPM under time synchronization errors don't experience linear phase rotation, opposed to OFDM where rotation of constellation points is proportional to the sub-carrier index. The WPM signal in the presence of timing error will however be attenuated and it will suffer from ISI and ICI.

#### 4-4-4 Modulation scheme

The consequence of time-offset in OFDM, regardless of offset direction, is in the introduction of a phase shift <sup>6</sup>. The phase shift is linearly proportional to the sub-carrier index and the value of time offset. The rotation angle  $\Phi_t[k]$  due to timing error is given by, [86]:

$$\Phi_t[k] = \frac{2\pi k \Delta_t}{N}. \quad (4.34)$$

Standard modulation techniques such as coherent (non-differential) Quadrature Phase Shift keying (QPSK) perform poorly under time synchronization errors because the sub-carriers with higher frequency indices experience greater phase shifts. For even a small timing offset (such as  $\Delta_t = 1$ ) the phase rotation experienced by the constellation symbols is in the order of  $0 < \Phi_t[k] < 2$ . The sub-carrier with the highest frequency will therefore experience a phase shift of almost 360 degrees. If this phase shift is not corrected, majority of the detected data would be corrupted even without an ICI or ISI.

The phase rotation due to timing error can be usually reversed by pilot-symbol-aided channel estimation techniques or by the use of differential constellation mapping. In this work we employ differential quadrature phase shift keying (DQPSK) in order to overcome this problem. In the DQPSK scheme the data is modulated on the basis of phase difference between two consecutive constellation symbols thereby ensuring that adjacent sub-carriers experience a phase shift which is independent of the carrier position. The phase rotation of constellation point  $k$  is determined by applying a phase shift of  $\Delta\Phi$  to the previous constellation symbol  $k - 1$ . The difference in phase shift  $\Delta\Phi$  for DQPSK modulation can be given as [86]:

$$\Delta\Phi_b = \frac{2(b-1)\pi}{4}, \quad b \in 1 \dots 4. \quad (4.35)$$

Therefore, the phase difference between two consecutive DQPSK constellation symbols under timing errors becomes [86]:

$$\Delta\phi_{k,k-1} = e^{j\left(\Delta\Phi_b - \frac{2\pi\Delta_t}{N}\right)}. \quad (4.36)$$

Using DQPSK modulation in presence of timing error therefore results in a phase shift that is depending on the value of the time offset but not anymore on the value of sub-carrier index  $k$ . The rotation angle  $\Phi_t[k]$  due to timing error becomes [86]:

$$\Phi_t[k] = \frac{2\pi\Delta_t}{N}, \quad \text{Differential - PSK.} \quad (4.37)$$

---

<sup>6</sup>The discussion presented here is based on [86]

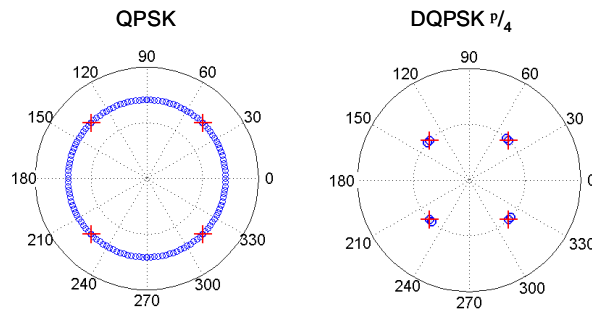


FIGURE 4.22: Constellation plot of received OFDM signal with a timing error of  $\Delta t = 1$ .  
Left: QPSK, Right: DQPSK  $\pi/4$ .

Fig. 4.22 illustrates the rotations of constellation points for received OFDM signal with QPSK and DQPSK modulation modes. We have assumed here an ideal channel and a time offset of  $\Delta t = 1$  samples towards the cyclic prefix.

DQPSK modulation is a simple solution to overcome the problem of phase shift under time synchronization errors. However, DQPSK modulation requires about 2 to 3 dB higher SNR when compared to coherent QPSK to obtain the same BER performance as in the QPSK modulation mode.

#### 4-4-5 Numerical results for time offset

The performances of WPM and OFDM under time synchronization errors are investigated by means of computer simulations. The time offset is modeled as a discrete uniform distribution between -2 and 2 samples, i.e.  $\Delta t \in [-2, -1, 0, 1, 2]$ . The modulation of choice is DQPSK. A cyclic prefix of 16 samples is added to OFDM data while no such guard-interval is used for WPM. Due to the use of cyclic prefix the spectral efficiency of OFDM is decreased by 12.5% while that of WPM remains unchanged. Finally, we oversample the data to magnify the difference in performance between various systems and wavelets. A summary of simulation parameters is given in table 4.3.

##### a. Performance of WPM without time errors

We first evaluate the system performance under ideal conditions. Fig. 4.23 shows the DQPSK constellation points for WPM transmission (various wavelets) in an ideal channel with no time offset. From the plot we may note that perfect estimates of the transmitted data can be obtained at the receiver when the transmitter and receiver ends are in unison.

A timing error results in a loss of time synchronization which causes a loss of orientation of incoming data at the receiver. As a result the data entering the IDFT/IDWT block is misaligned

System parameters	WPM	OFDM
Number of sub-carriers	128	128
Number of multi-carrier symbols per frame	100	100
Modulation	DQPSK	DQPSK
Channel	AWGN	AWGN
Oversampling factor	15	15
Guard band	-	-
Guard interval	-	CP (length: 16)
Frequency offset	-	-
Phase noise	-	-
Time offset	$\Delta_t \in [-2, -1, 0, 1, 2]$ (Uniformly distributed)	$\Delta_t \in [-2, -1, 0, 1, 2]$ (Uniformly distributed)

TABLE 4.3: Simulation setup for evaluation of performance under time synchronization error.

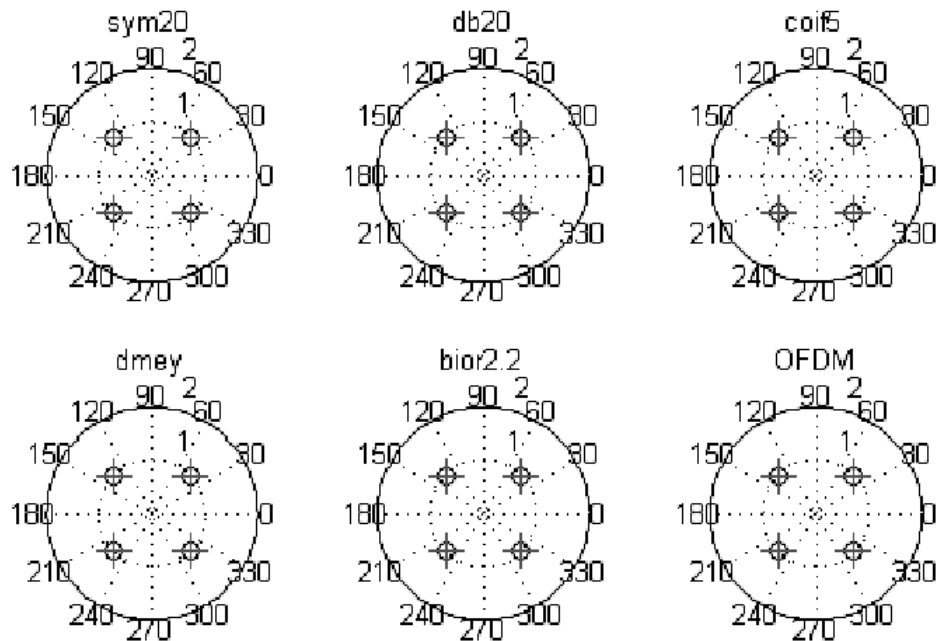


FIGURE 4.23: DQPSK constellation points for WPM setup using various wavelets in an ideal channel with no time offset.

whereby the samples of previous or next OFDM/WPM symbol are selected while valid samples at the beginning or at the end of the symbol in consideration are discarded. We present the impact of time synchronization error in the following sections.

#### b. Performance when time offset is modeled as a discrete uniform distribution

Fig. 4.24 shows the BER curves of OFDM and WPM transceivers over AWGN channel for a uniformly distributed timing offset error  $\Delta_t = 2$  samples. The OFDM system performs much better under time synchronization errors when compared to WPM mainly because of the cyclic

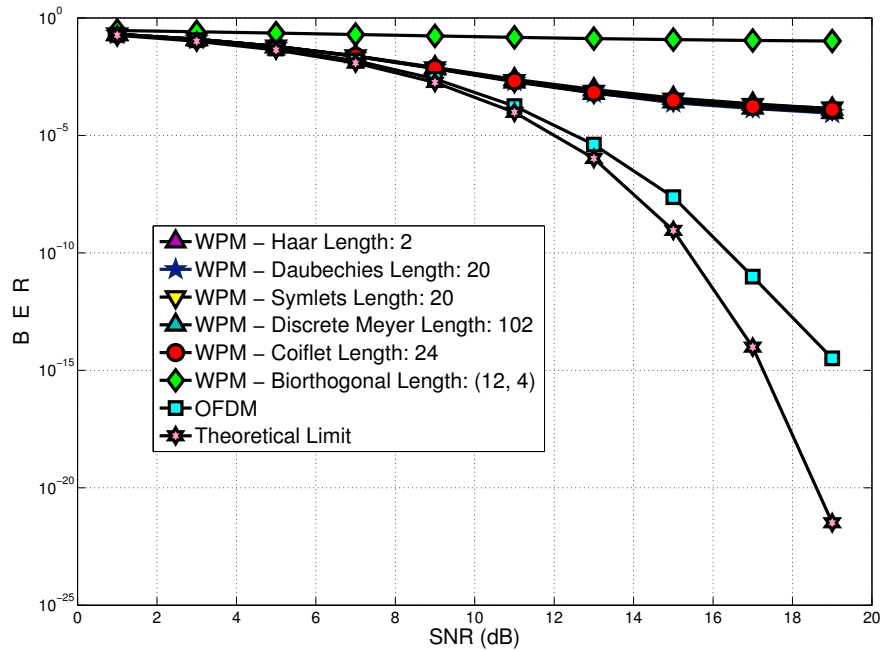


FIGURE 4.24: BER curves for WPM with different wavelets and OFDM under time synchronization errors ( $\Delta_t = 2$ ).

prefix. The WPM cannot benefit from the use of a cyclic prefix and hence performs poorly under time error.

In fig. 4.25 the BER is shown for different time-offsets in the range -15 and 12 samples. The time offset in this simulation is modeled as a one-sided uniform distribution. The time offset is considered to vary between  $\{0, \dots, \Delta_t\}$  to the right and  $\{-\Delta_t, \dots, 0\}$  to the left<sup>7</sup>. The SNR is kept constant at 10dB.

As can be seen in fig. 4.25 the direction of the time offset is inconsequential in WPM transmission. The BER curves of WPM on either side of the time-axis are almost mirror images of one another. However, the situation is different in OFDM where negative values of time offsets (towards the own cyclic prefix) result in much lower BER in comparison to positive time offsets (away from the cyclic prefix). This is due to the use of cyclic prefix which mitigates the deleterious impact of a misalignment of FFT window. However when the time offset exceeds the cyclic prefix the ICI and ISI components reappear.

### c. Influence of number of sub-carriers

Fig. 4.26 shows the performance of the WPM in the presence of time synchronization error when the number of sub-carriers is altered. The plots reveal how with increasing number of WPM sub-carriers the BER decreases. We may recall from the third chapter that the symbol

<sup>7</sup>The values are so chosen to highlight the importance of cyclic prefix in OFDM.

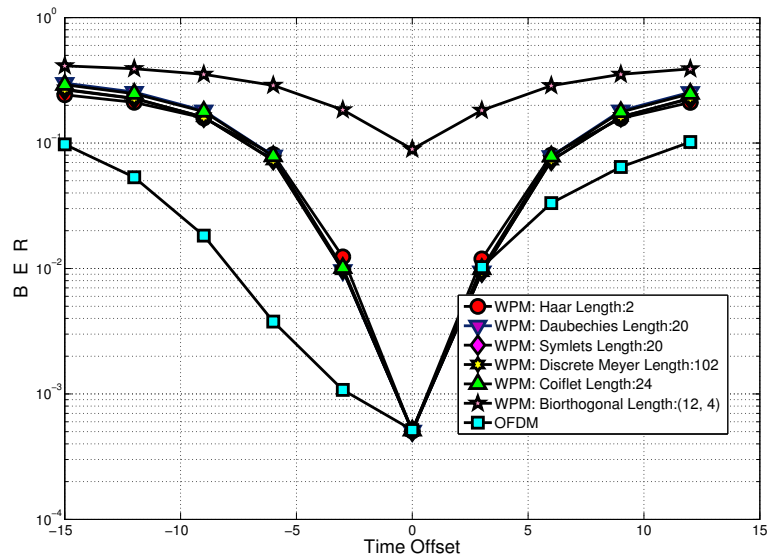


FIGURE 4.25: BER vs. time offset error for WPM and OFDM transmission in an AWGN channel (SNR = 10 dB).

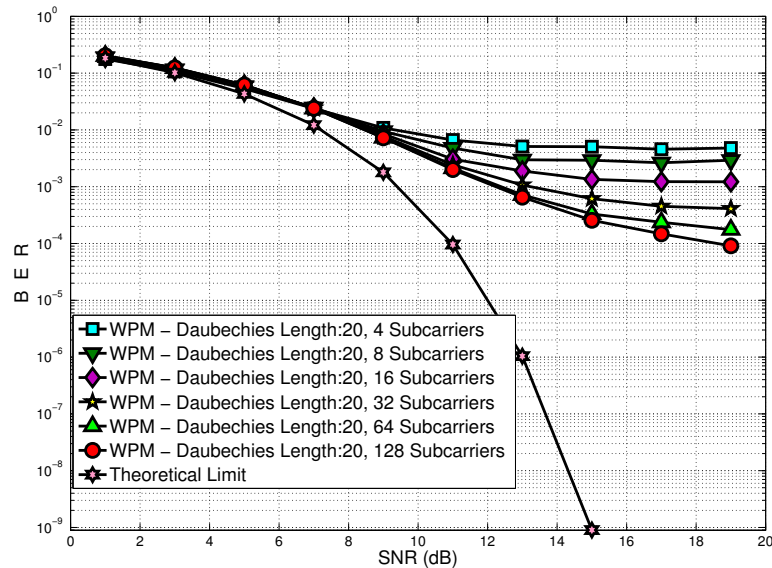


FIGURE 4.26: BER plots for WPM transmission under a loss of time synchronization for different number of sub-carriers,

duration of multi-carrier system is proportional to the number of sub-carrier used. Therefore, the more the number of sub-carriers longer symbol duration and hence smaller relative time offset with respect to multi-carrier symbol length.

**d. Influence of number of symbols/frame**

The simulation results for different number of WPM symbols per frame are depicted in fig. 4.27. The results show that the number of symbols/frame does not influence the BER performance.

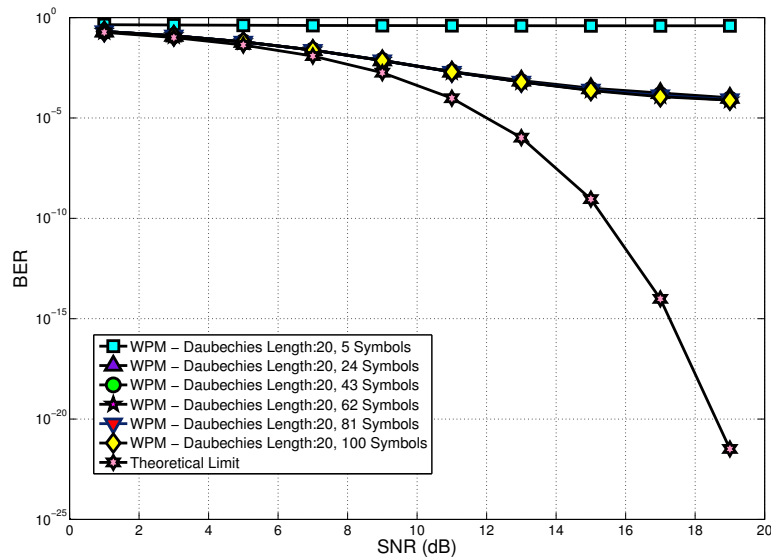


FIGURE 4.27: BER for WPM with timing error for different number of symbols/frame.

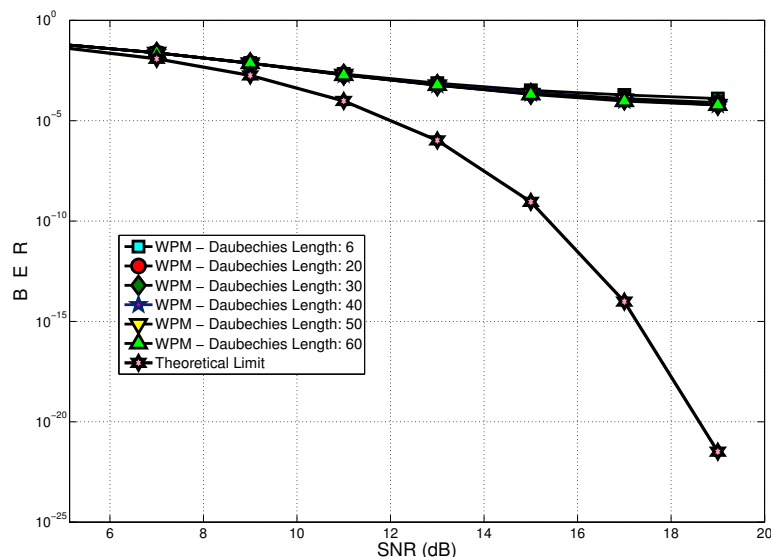


FIGURE 4.28: BER for WPM using Daubechies wavelets of different lengths under a loss of time synchronization.

#### e. Influence of different lengths of wavelet filters

Fig. 4.28 illustrates the influence of filter's length and the number of zero wavelet moments in combination with timing error on the BER. The wavelet family of choice is Daubechies. In the plots the Daubechies filter with 6 coefficients and 3 wavelet zero moments appears to have slightly better BER performance when compared to longer filters of the same family. However, when the length of the filters is increased further the BER curves become closely spaced. Therefore, we can conclude that there is no significant relation between the BER performance under timing errors and the filter's length.

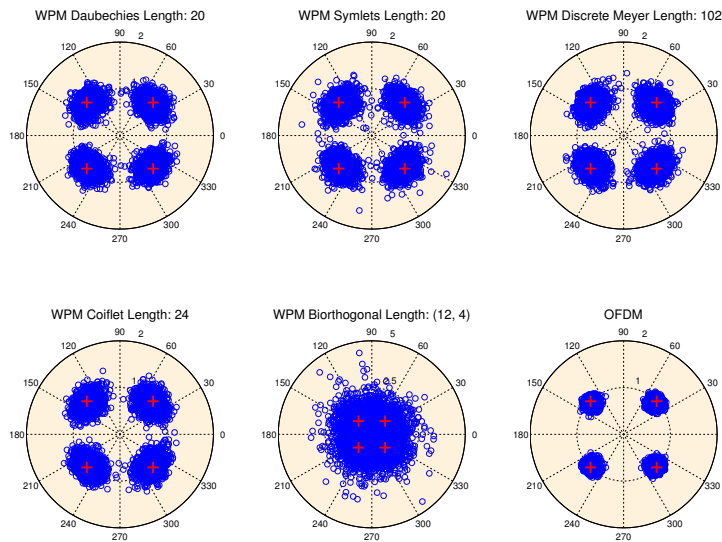


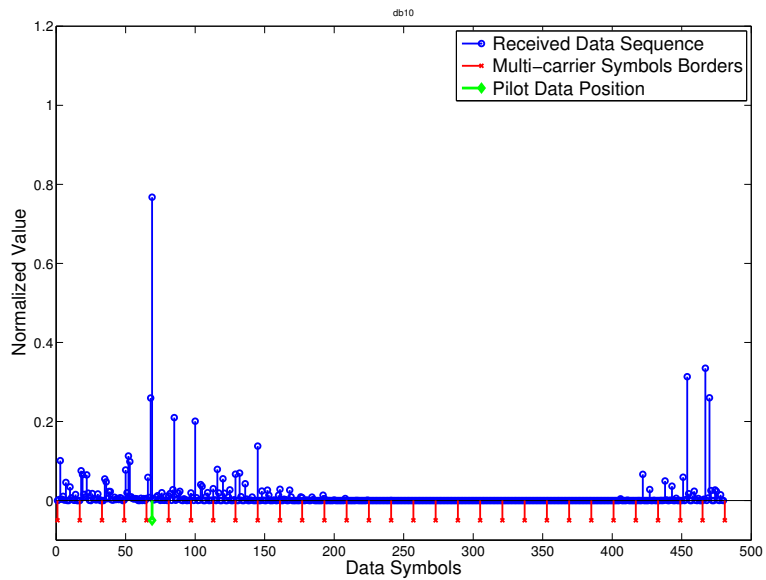
FIGURE 4.29: Constellation points of received signal in the presence of timing error.

### f. Constellation plots

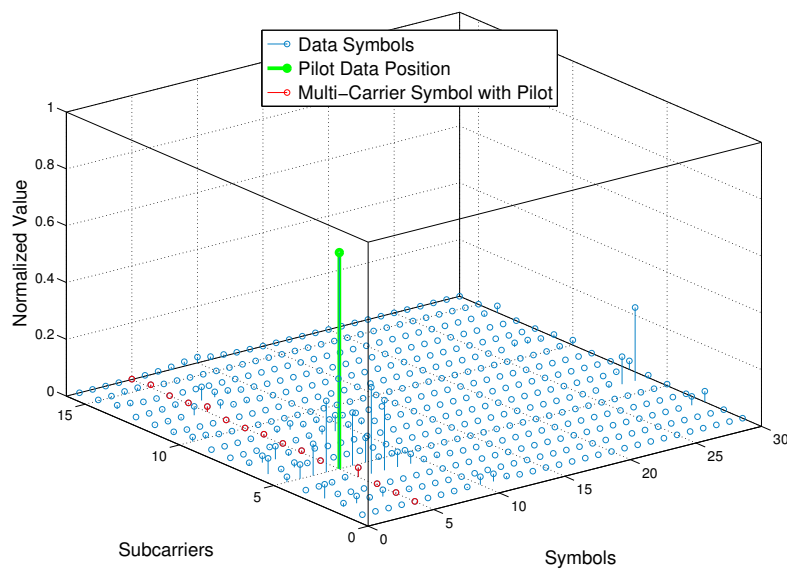
The effect of time synchronization error on the constellation points is depicted in fig. 4.29. In order to highlight the effect of time synchronization error we consider an ideal channel without any noise (apart from the time offset error). The main impact of the time offset is the scattering of the constellation points around the reference modulation points due to interference. OFDM has more concentrated constellation points than any of the WPM system considered.

### g. Dispersion of energy of the sub-carriers

Figs. 4.30(a) and 4.30(b) illustrate the dispersion of sub-carrier energy due to time synchronization error for WPM transmission. The respective plots for OFDM are shown in figs. 4.31(a) and 4.31(b). The timing error in OFDM results in ISI between successive symbols in addition to the ICI. If a cyclic prefix is used the ICI and ISI terms are mitigated for time-errors which occur towards the cyclic prefix (time offset to the left). This is illustrated in figs. 4.30(a) and 4.31(b) where the energy of the pilot symbol disperses into the subsequent symbol (resulting in an ISI) but not into the previous symbol. Furthermore, the energy of pilot sub-carrier also spreads across other sub-carriers within the same symbol (causing ICI). For WPM the dispersion of energy of a single pilot is far more pronounced. The smearing of energy is spread over a large number of symbols with the sub-carriers closest to the pilot sub-carrier affected most (refer figs. 4.30(a) and 4.30(b)).

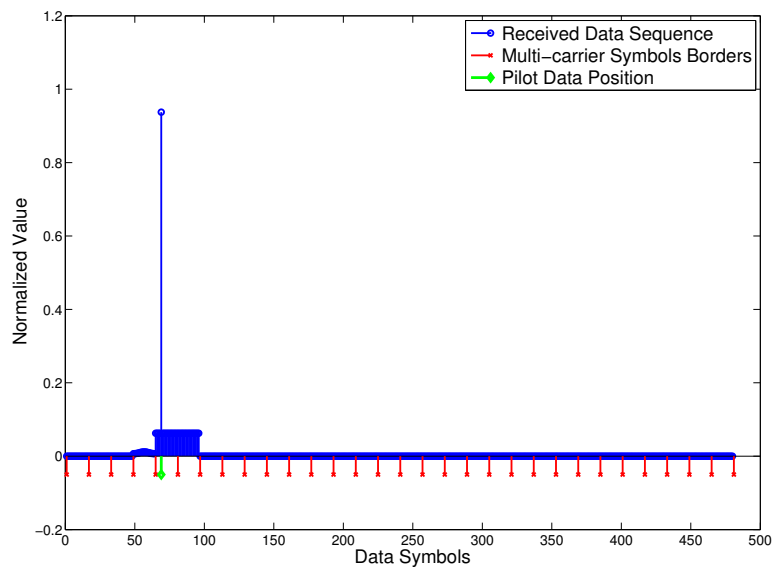


(a)

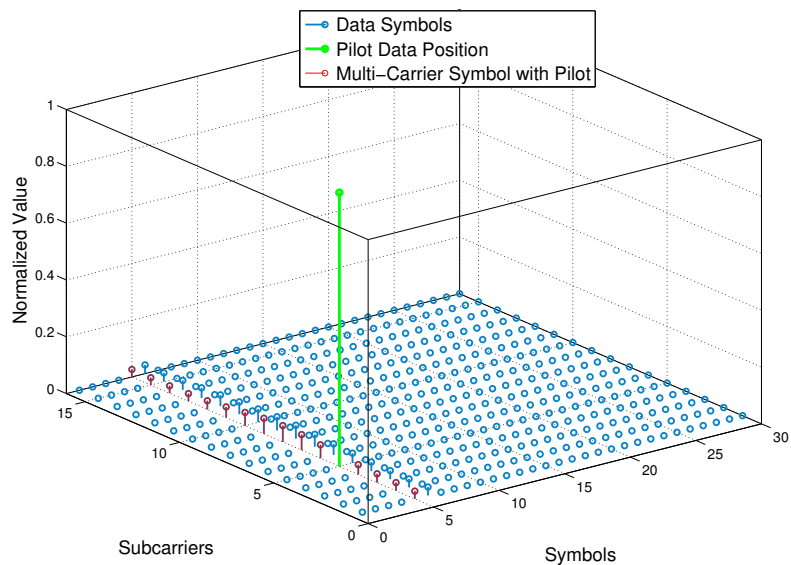


(b)

FIGURE 4.30: Spectral energy in a frame of the received WPM (with Daubechies wavelet) signal affected by timing errors. (a) 2D view, (b) 3D View.



(a)



(b)

FIGURE 4.31: Spectral energy in a frame of the received OFDM signal affected by timing errors. (a) 2D view, (b) 3D View.

## 4-5 Summary

In this chapter we addressed the effects of frequency offset, phase noise and time synchronization error on WPM and OFDM transceivers. The study was conducted using computer simulations. Several well-known families such as Daubechies, Symlets, Discrete Meyer, Coiflet and Bi-orthogonal wavelet were applied and studied. The sensitivity of WPM and OFDM are quite similar in the presence of frequency offset and phase noise. However, the effect of time synchronization loss is far more severe for WPM transmission. The simulations also showed that OFDM has much lower BER under timing errors when compared to WPM. This is largely due to the beneficial use of cyclic prefix in OFDM.

The frequency offset and phase noise lead to a loss of orthogonality between the sub-carriers and cause them to interfere with one-another. In OFDM the disturbances are limited to ICI but in WPM the frequency offset and phase noise cause ICI as well as Inter symbol-ICI.

The effect of time synchronization error was also discussed. Akin to the impact of phase/frequency errors, there are significant differences between the operation of OFDM and WPM in the presence of time errors. Firstly, the ISI in OFDM occurs only between contiguous symbols while in WPM a number of neighboring symbols interfere. Secondly, the timing error in OFDM results in a rotation of constellation symbols proportional to sub-carrier index but in WPM this behavior is absent.

The wavelets used in these computer simulations are standard wavelets that were developed for other applications such as image processing or compression and hence not suitable for modulation of data. In chapter 9 we present the design of new wavelets that minimize the interference due to time-offset errors.

## Chapter 5

# Peak-to-average power ratio performance

### 5-1 Introduction

A major drawback of multi-carrier systems such as the WPM or the classical OFDM is the large variations in their signal envelope <sup>1 2</sup>. Such fluctuations in the signal envelope is due to the inherent nature of these modulation schemes where many independently modulated sub-carriers are combined together to obtain a composite signal. The envelope of the time-domain signal varies with different data symbols and when the sub-carriers add up coherently the peak power of the composite OFDM/WPM signal can be many times larger than the average power. In fact, for  $M$  number of sub-carriers the peak of the signal can be up to  $M$  times the average power if all the sub-carriers are of the same phase. Since practical systems are limited by the maximum operable power, either the WPM/OFDM systems have to function with a large power back-off or risk operating in the non-linear (saturation) regions of the electronic components such as the high power amplifiers (HPA) and the digital-to-analog converters (DAC) in the transceiver chain.

A large back-off would mean that the average signal power has to be kept much lower than the available power so that the amplifier operates in the linear region. On the other hand, functioning in the non-linear regions of the amplifiers can result in distortions such as in-band interference (or inter-modulation distortion) and out-of-band radiation (due to spectral widening of the transmit signal). The in-band interference increases the bit error rate (BER) of the received signal while the out-of-band radiation causes adjacent channel interference (or cross-talk) through

---

<sup>1</sup>Parts of this chapter have been published in [17] and [94]. For any material that has been reused, wherever applicable, a written consent has been obtained from the first author.

<sup>2</sup>The author gratefully acknowledges the contributions of Msc student Ms. Berna Torun for her help with the computer simulations.

spectral spreading. It is therefore important to study the power fluctuations associated with multi-carrier mode transmission and mitigate them.

Typically, the metric peak-to-average power ratio or PAPR is used to characterize the variations in the envelope of the signal. While the quantum of literature available for the study of OFDM and its PAPR performance is significant, the material available for a similar study on WPM is thin. In fact the entire material on the subject can be listed as follows: in [17] a study on the PAPR of WPM signals and its stochastic variations is presented. The study shows that the envelope of the WPM signal is Gaussian and its power distribution Chi-squared. Furthermore, the PAPR performances of the WPM systems for almost all used wavelets are shown to be similar to OFDM. In [95] a multi-pass pruning method to reduce PAPR is proposed. And in [96] a threshold based method to reduce PAPR is suggested. In [97] upper bounds for the maximum PAPR for WPM transmission are derived and based on these results wavelets that minimize PAPR are obtained. A different approach is followed in [98] where the WPM tree structure is adjusted to lower the PAPR.

In this chapter we address the PAPR performance of the WPM systems. We first understand the stochastic nature of the WPM signal, its power variations and its PAPR performance. We then implement two techniques that mitigate PAPR, namely,

- modification of phases of the sub-carriers,
- mathematical optimization of phase selection of sub-carrier through a local search algorithm,

The effectiveness of the proposed algorithms is demonstrated through numerical studies.

The contents of the chapter are organised as follows. We first present a brief overview on the nature of WPM signals in section 5-2. A survey of existing PAPR reduction techniques is presented in section 5-3. The proposed PAPR reduction techniques are then introduced in sections 5-4 and 5-5. In section 5-4 PAPR reduction by modification of sub-carrier phases is presented, while in section 5-5 a mathematical optimization for selection of sub-carrier phases through local search algorithms is explained. The contents of the chapter are summarized in section 5-6.

## 5-2 Distribution of the PAPR

### 5-2-1 OFDM

A multi-carrier signal consists of a number of independently modulated sub-carriers which can result in a large peak-to-average-power ratio when they add coherently. For a system with  $M$

sub-carriers when all the sub-carriers have the same phase the peak power of the transmitted signal can be  $M$  times the average power. The PAPR is one way to measure the variations in the transmitted signal and for critically sampled data  $x[n]$  can be given as:

$$\text{PAPR} = \frac{\max_{0 \leq n \leq M} (|x[n]|^2)}{E(|x[n]|^2)} \quad (5.1)$$

where  $E\{\cdot\}$  is the expectation operator which averages over the ensemble of data samples.

The CDF of the PAPR is one of the most frequently used performance measures for PAPR reduction techniques [52, 99]. From the central limit theorem it follows that for large number of sub-carriers  $M$ , the real and imaginary components of  $x[n]$  follows the Gaussian distribution, each with a zero mean and variance of  $M$  times the variance of one complex sinusoid [52]. The amplitude of the OFDM signal therefore has a Rayleigh distribution and its power distribution becomes a central chi-square distribution with two degrees of freedom and zero mean [52, 100]. The CDF of the power is given as [52]

$$F(z) = \int_0^z \frac{1}{2\sigma^2} e^{-\frac{\mu}{2\sigma^2}} du = 1 - e^{-\frac{z^2}{2\sigma^2}} \quad (5.2)$$

where  $z \geq 0$ . From the power distribution the theoretical CDF for PAPR per OFDM symbol can be derived. Assuming the samples to be mutually uncorrelated (which is true when there is no over sampling) the probability that PAPR is below some threshold level  $z$ , can be written as [52]:

$$\text{Prob}\{\text{PAPR} \leq z\} = [F(z)]^N = \left(1 - e^{-\frac{z^2}{2\sigma^2}}\right)^N \quad (5.3)$$

### 5-2-2 WPM

A WPM signal, like the OFDM signal, is the sum of many information bearing sub-carriers which are statistically independent. The orthogonal sub-carriers are wavelet packet bases derived from a MRA [10] as explained in Chapter 3. The modulated WPM signal  $y[n]$  is obtained as a linear combination of the wavelet packet bases  $\xi_l'^k$  weighted with the complex data symbols  $a_{u,k}$ :

$$y[n] = \sum_u \sum_{k=0}^{M-1} a_{u,k} \xi_l'^k(n - uM) \quad (5.4)$$

#### a. WPM signal characteristics

In fig. 5.1 the CDF curves for the PAPR of the WPM system (theoretical as well as simulated values) for different number of sub-carriers  $M$  are plotted. We can see from the fig. 5.1 that as the number of carriers of the WPM system increases, the simulated and the theoretical (as

represented in equation (5.3)) PAPR curves converge. From about  $M > 128$  carriers the simulated values accurately map the theoretical derivations.

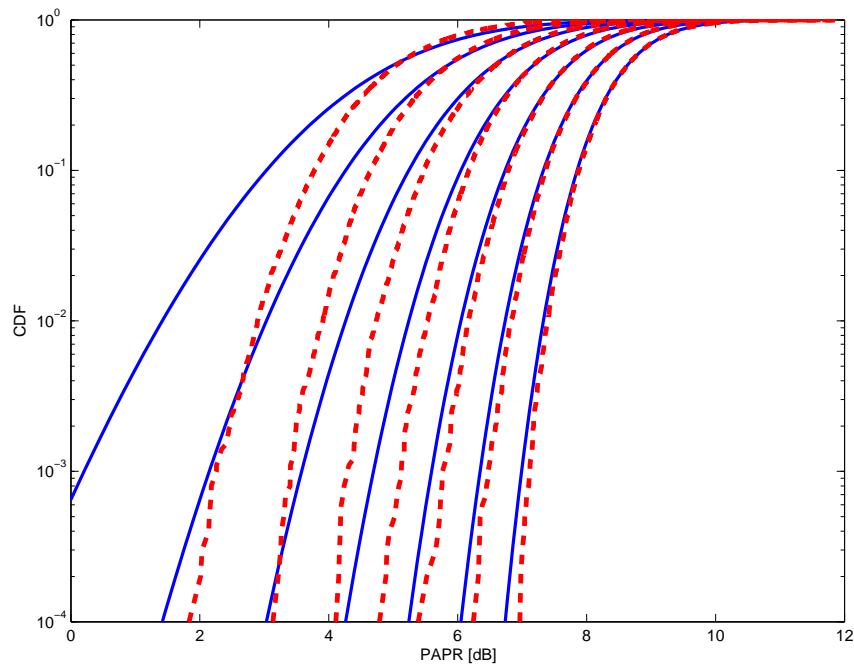


FIGURE 5.1: CDF-distribution of PAPR for different number of sub-carriers. From left to right: 16, 32, 64, 128, 256, 512, 1024 sub-carriers. Dashed lines indicate simulated values while continuous lines represent the theoretical curves. Wavelet of choice is Daubechies-15.

### b. Amplitude distribution

Unlike OFDM which is a complex signal with real and imaginary parts, the WPM signal only has real components. OFDM signal has a Rayleigh distribution and it would be interesting to check the distribution of WPM signal. Fig. 5.2 plots the simulated CDF curves for WPM systems along with Gaussian and Rayleigh distributions. The WPM setup uses Daubechies wavelets with length 15. It is clear from the figure that the patterns of the WPM signal variations follow the Gaussian distribution.

### c. Power distribution

The CLT states that the mean of a sufficiently large number of independent random variables, each with finite mean and variance, will be normally distributed. Based on CLT, when large number of sub-carriers are employed in a WPM system; i.e., large number of levels in the IDWPT, the amplitude of WPM signal follows Gaussian distribution. It is well known from the stochastic theory that the distribution of power of Gaussian signals is Chi-squared. This

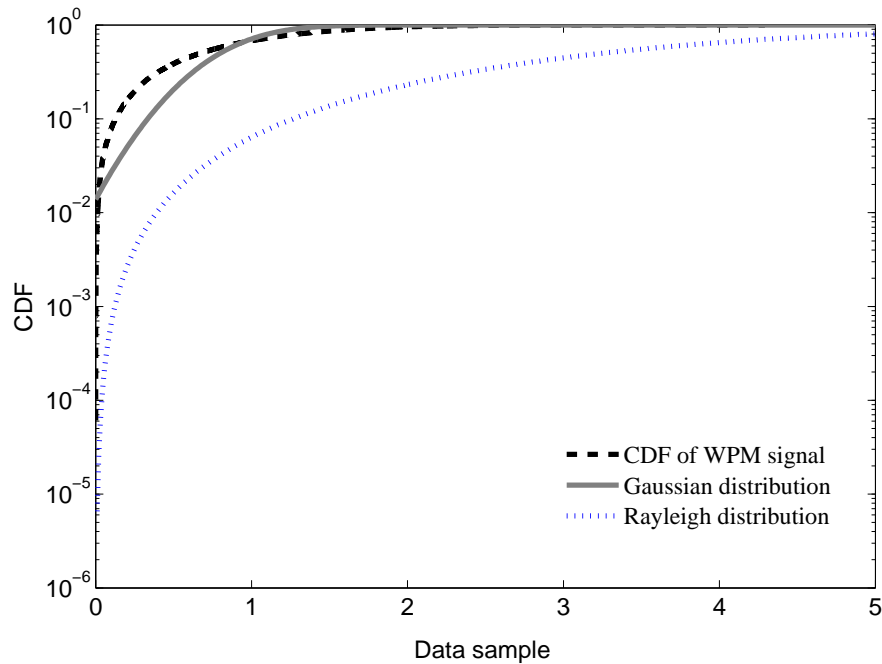


FIGURE 5.2: CDF of WPM signals. The wavelet considered is Daubechies-15. The WPM system is taken to have 128 carriers. Gaussian and Rayleigh signals are also plotted for reference.

TABLE 5.1: Specification of wavelets used.

Name	Orthonormal?	Length
Daubechies	Yes	30
Coiflet	Yes	30
Symlet	Yes	30
Discrete Meyer	Yes	102
Bi-Orthogonal	No	(5,3)

means that the power distribution of WPM signals should also be Chi-squared. This fact is corroborated in fig. 5.3. In fig. 5.3 where the curves for the power distribution of WPM signal are plotted along with Gaussian, Rayleigh and Chi-Square distributions. And in fig. 5.4 the power distributions for WPM signals applying different wavelet families are shown. Almost all the wavelet families have a power distribution which is Chi-squared. The specifications of the wavelets (Daubechies 15, Coiflet 5, Symlet 15 (all of length 30), Discrete Meyer (of length 102) and Bi-Orthogonal 2.2) which are considered are given in table C.1.

#### d. PAPR distribution

Figs. 5.5 and 5.6 show the PAPR performance curves for various wavelet families and various filter lengths, respectively <sup>3</sup>. From fig. 5.5 we can deduce that apart from the bi-orthogonal

<sup>3</sup>There is a fundamental difference in the calculation of PAPR between OFDM and WPM. The PAPR in OFDM is usually calculated per symbol. This is not possible in WPM because WPM symbols overlap in the time-domain and therefore the PAPR has to be calculated per frame.

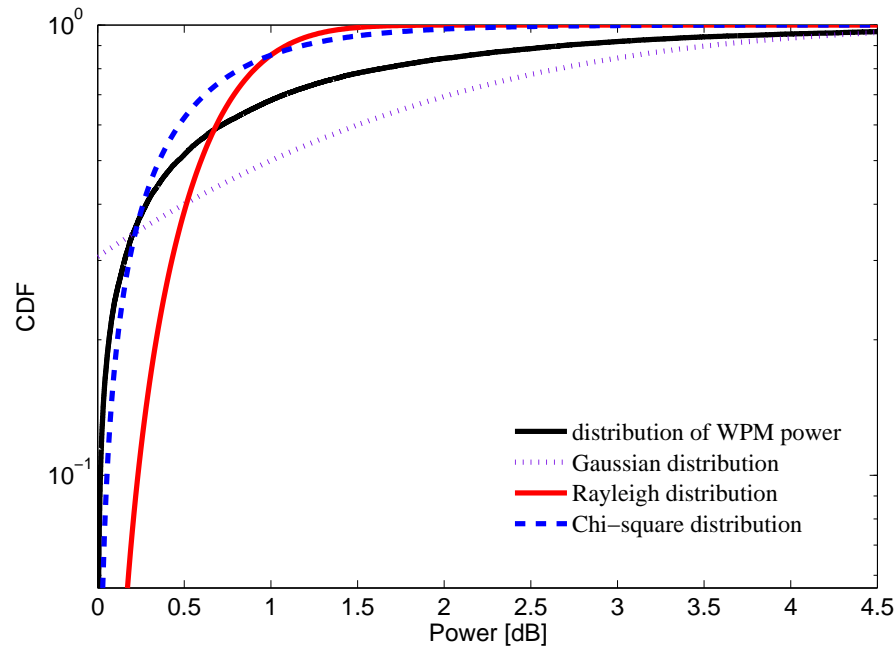


FIGURE 5.3: CDF of power of Gaussian and Wavelet Packet Modulation signals. The wavelet considered is Daubechies-15. The WPM system has 128 carriers.

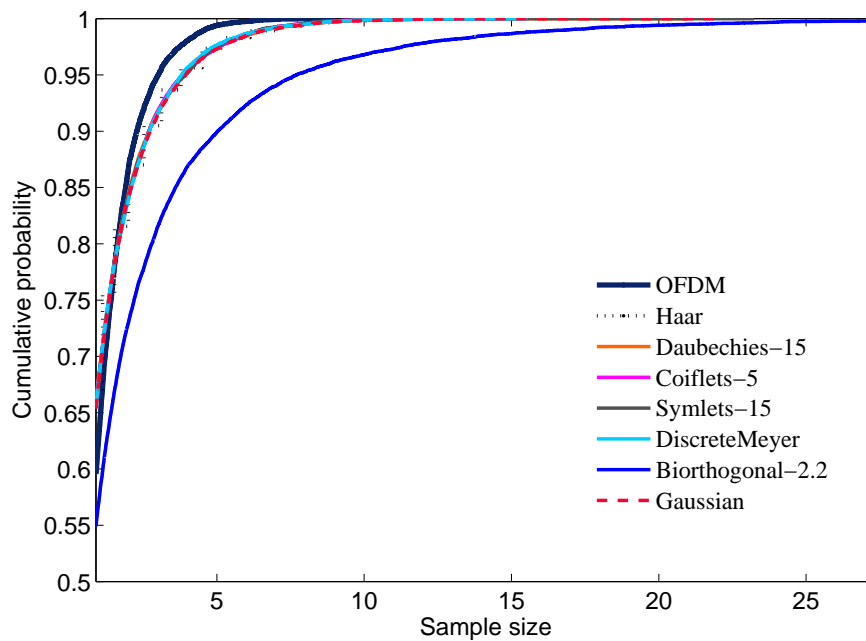


FIGURE 5.4: CDF of power of Wavelet Packet Modulated signals for various families (for 128 carriers).

wavelet, all the other wavelets follow a similar CDF pattern for the PAPR. And from fig. 5.6 it is clear that even with increasing lengths of the wavelet, from Daubechies 2 to Daubechies 45, the PAPR distribution doesn't vary much.

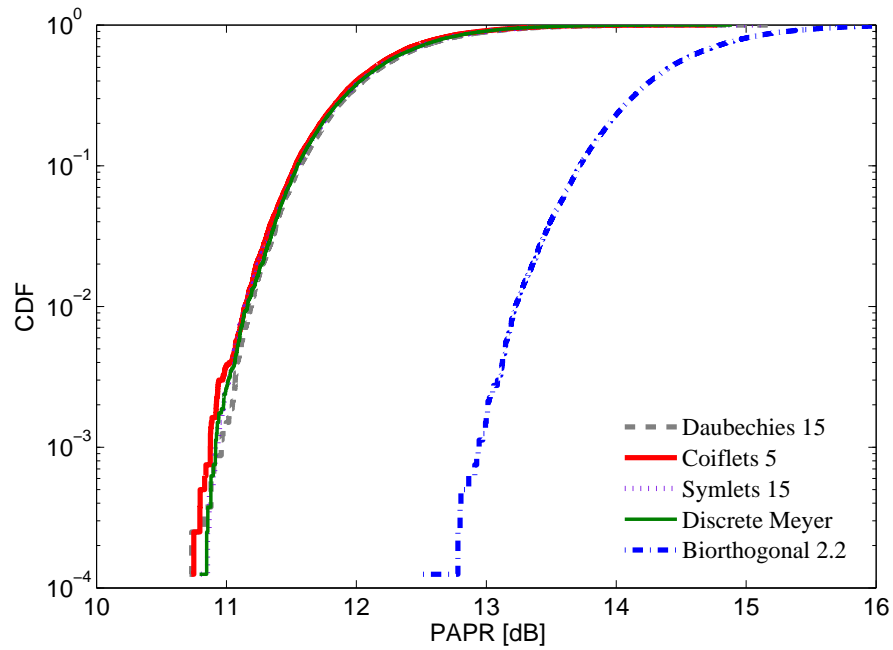


FIGURE 5.5: CDF of PAPR for the WPM system applying several wavelet families. All the configurations are taken to have 128 carriers.

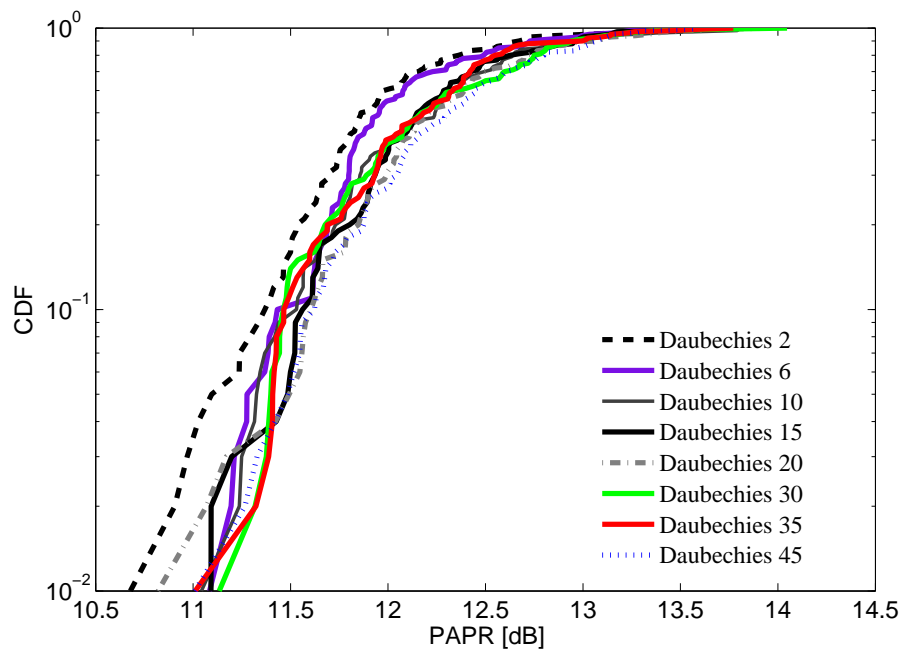


FIGURE 5.6: CDF of PAPR for the WPM system applying different filter lengths of the Daubechies wavelet family. The number of sub-carriers considered is 128.

## 5-3 Techniques to mitigate PAPR

There exists several techniques in the literature for the reduction of PAPR in MCM transmission. These methods can be broadly categorized into signal scrambling and signal distortion techniques.

### 5-3-1 Signal scrambling techniques

Signal scrambling techniques work on the principle of altering the phases of the sub-carriers to decrease the PAPR. Coding can also be used for signal scrambling. A few of the commonly used signal scrambling solutions are block coding [101], selected mapping (SLM) [102], interleaving [103], tone reservation [104] and partial transmit sequences (PTS) [105].

The block coding approach [101] works on the principle that the PAPR can be reduced by not permitting those set of code words that accentuate the peak envelope power of the transmitted signal. In the selected mapping (SLM) method a set of candidate signals is generated representing the same information. Then the signal with the least PAPR is chosen and transmitted [102]. In the interleaving method [103] the data block is partitioned into non-overlapping sub-blocks and then each sub-block is rotated by a statistically independent rotation factor. The rotated data with the lowest peak amplitude is then selected and transmitted. In the tone reservation technique [104] a fraction of the bandwidth is used to synthesize signals of opposite polarity. The synthesized signals are then added to the original signal to minimize the peak of the transmitted signal. Subtraction of peaks reduces the PAPR without altering the transmission capabilities of the OFDM system. A related technique is the partial transmit sequences (PTS) [105] method where a small set of tones are set aside for PAPR reduction. Highly correlated data frames have large PAPR; the PTS thus operates by breaking the correlation patterns in the transmitted data to reduce PAPR.

### 5-3-2 Signal distortion techniques

In the techniques based on signal distortion the high peaks are reduced directly by limiting the signal to within a tolerable upperlimit. Clipping the signal before amplification is a simple method to limit the PAPR. However, clipping may result in large out-of-band (OOB) radiation and in-band distortion. Other practical solutions include peak windowing [106], peak cancellation [107], peak power suppression, weighted multi-carrier transmission [108] and companding [109].

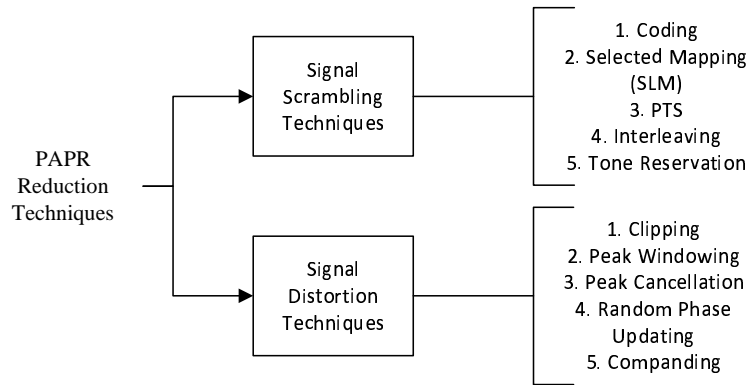


FIGURE 5.7: Classification of commonly known PAPR reduction techniques

In [106] Nee and Wild propound that since large PAPR values occur only infrequently it should be possible to remove the peaks using windowing techniques without affecting the transmission characteristics<sup>4</sup>. A few of the suggested windows include Gaussian, cosine, Kaiser and Hamming windows. The peak cancellation method introduced in [107] suggests subtracting a time-shifted and scaled reference function from the signal to reduce the peak power. Nikookar and Lidsheim [108] propose a phase updating algorithm for the reduction of the OFDM signal. In this algorithm the sub-carrier phases are adjusted based on a stochastic distribution. The phases are then updated till the peak value of the signal is below a predefined threshold. The threshold and the number of iterations for the phase update are altered dynamically. Finally, Wang et.al. [109] propose a simple and effective companding technique to mitigate the PAPR of the OFDM signals. Companding of the signal is done before it is converted into an analog waveform.

Fig. 5.7 shows the classification of various PAPR reduction techniques.

### 5-3-3 Criteria for the selection of best PAPR mitigation strategy

Many factors have to be considered before the right PAPR reduction technique can be chosen<sup>5</sup>. Some of the factors include PAPR reduction capability, distortion induced, power increase in the transmit signal, BER increase at the receiver, loss in data rate, complexity of computation. Many of these requirements are contradictory and cannot be met at the same time.

For example, the amplitude clipping technique removes the signal peaks but results in in-band distortion and out-of-band radiation. Other techniques, like the tone-reservation (TR) method, require additional transmit power because part of the signal power is necessary for the reduction of the carrier peaks. Some techniques may result in a loss of BER at the receiver if the transmit

<sup>4</sup>Usually a small price is paid in the form of self-interference

<sup>5</sup>The discussion is based on [104]

signal power is fixed or equivalently may require large transmit power to maintain the BER after applying the PAPR reduction techniques.

Strategies such as the block coding technique require the data rate to be reduced because some of the information symbols have to be dedicated to controlling PAPR. Methods such as SLM, PTS and interleaving require side-information on the changes made at the transmitter end. This causes a drop in achievable data-rates. Furthermore, if the received side-information is erroneous then the entire data block could be wrongly interpreted. Therefore, the side-information is usually protected with channel coding, further adding to the overhead.

Computational complexity is yet another important consideration in choosing the right PAPR reduction technique. Techniques such as PTS run over many iterations to find a solution. On the other hand, interleaving techniques perform better for large number of interleavers, which however slows down the computation process.

Based on the above discussion, in this work we chose methods based on SLM for mitigation of PAPR in WPM transmission. The SLM is a simple and reliable technique which can be readily applied to WPM to achieve better PAPR performances.

## 5-4 Selected mapping with phase modification

In this section we present the first method to reduce the PAPR of WPM signals. The technique is based on the Selected Mapping (SLM) approach proposed by Bauml [102]. The method works on the principle that the PAPR of a multi-carrier system can be adjusted by varying the phases of the sub-carriers [102]. Different PAPR values for the same information are obtained by altering the phases of the sub-carriers used to modulate the data. The WPM carriers are rotated with a phase-values chosen from an alphabet of finite number of identically spaced phase-shifts. The WPM frame with the least PAPR is then identified and transmitted. The attraction for the method is in its simplicity of implementation and the notable gains it yields with minimal increase in complexity. The disadvantage of the scheme is that side-information on the sub-carrier phases has to be transmitted to the receiver.

### 5-4-1 Description of algorithm

Fig. 5.8 shows the blocks of the proposed WPM system with the PAPR mitigation structure. The bit stream from the information source is first converted to a constellation (QPSK/BPSK) stream and then replicated to obtain a finite number of copies, say  $L_{SLM}$ . Each of the replicated set is then serial-to-parallel (S/P) converted and then phase-shifted by a random phase sequence.

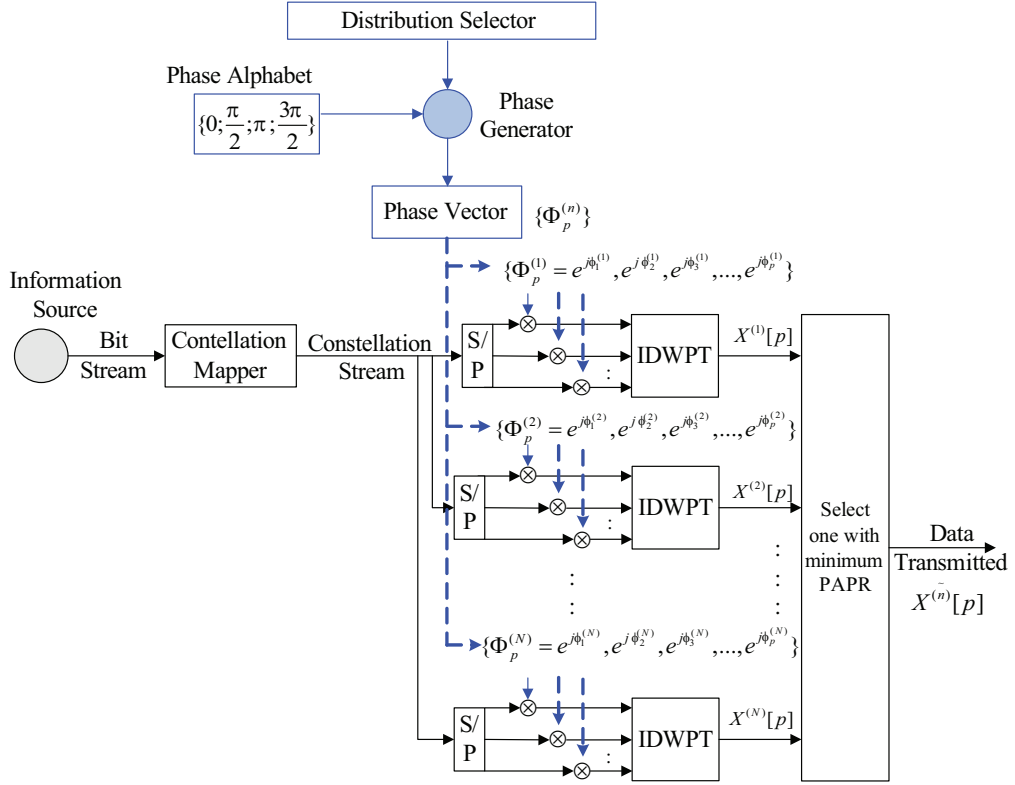


FIGURE 5.8: WPM Transmitter Block diagram with the SLM based PAPR reduction technique

The phase sequences are generated by a phase generator which chooses between different phase alphabets  $\phi$ , their distribution and creates a phase vector  $\Phi_p^{(n)}$ . Here  $n (= 1, 2, 3, \dots, L_{SLM})$  stands for the index of the frame and  $p (= 1, 2, 3, \dots, M_{SLM})$  denotes the sub-carrier index. The phase vector thus contains  $L_{SLM}$  rows each with  $M_{SLM}$  columns. Denoting the information bearing WPM frame by the notation  $\mathbf{X}[p]$ , the  $L_{SLM}$  different WPM frames  $\mathbf{X}^{(n)}[p]$  obtained by sub-carrier wise multiplication with the phase-vector  $\Phi_p^{(n)}$  can be given as:

$$\mathbf{X}^{(n)}[p] = \mathbf{X}[p] \times \Phi_p^{(n)} = \mathbf{X}[p] \times e^{j\phi_p^{(n)}} \quad (5.5)$$

The phase-shifted information bearing streams are then transformed by an IDWPT operation and the PAPR of the transformed composite signal is calculated. Amongst the set of  $L_{SLM}$  PAPR values, the frame with the least value is selected and transmitted. Defining the candidate time domain WPM frame as  $x = \text{IDWPT}(\mathbf{X}^{(n)}[p])$ , the index of this frame can be given as:

$$\hat{n} = \underset{1 \leq n \leq L_{SLM}}{\text{argmin}} (\text{PAPR}(x^{(n)})) \quad (5.6)$$

In order to ensure that the transmitter and receiver operate harmoniously, the chosen index of the frame  $\hat{l}$  is sent to the receiver as a side-information. Typically for a size  $L_{SLM}$  vector, the

number of bits required to send  $\hat{l}$  will be  $\log_2(L_{SLM})$ . However, to prevent corruption of this precious message, more bits may be used to encapsulate this message by channel coding.

The algorithm to calculate and select the minimum PAPR for WPM is summarized in algorithm 1.

---

**Algorithm 1** SLM Pseudocode

---

- 1: Obtain the source message.
  - 2: Replicate it a finite number of times, say  $L_{SLM}$ .
  - 3: Generate phase sequences from the chosen phase alphabet (e.g.  $\phi \in (0, \pi/2, \pi, 3\pi/2)$ ).
  - 4: Multiply frame sequences element/carrier-wise by  $M_{SLM}$ -length phase sequences. Here  $M_{SLM}$  is also the number of WPM carriers.
  - 5: Do the IDWPT transform for each resulted frame sequence for each replicated copy of the data.
  - 6: Calculate the PAPR per frame of the signal for each replicated copy of the data and find the PAPR.
  - 7: List all the PAPR values; select the minimum PAPR and transmit.
  - 8: Send as side information the index of the frame with minimum PAPR,  $\hat{l}$  to recover the data in the receiver.
- 

### 5-4-2 Numerical results

In this section we present results of the studies and evaluate the performance of WPM system with the PAPR reduction technique. The investigations are carried out using computer simulations and the performance metric of choice is the CCDF. The WPM system is realized using a filter bank structure with 7 levels of decomposition (128 sub-carriers). The modulation scheme used is QPSK. The phase alphabet is taken to be  $\phi \in (0, \pi/2, \pi, 3\pi/2)$  which is randomly chosen while generating the phase vector. The wavelet of choice is Daubechies 5 (denoted db5) which is of length 10. These simulation parameters will be used through out the experiments unless stated otherwise. To properly evaluate the improvements due to the PAPR reduction technique, a reference PAPR-CCDF curve obtained for db5 wavelet for the case without PAPR reduction (i.e. no phase modification) will also be provided.

#### a. Performance of the PAPR mitigation technique

In the first set of results we verify the impact of the PAPR reduction technique. Fig. 5.9 shows the CCDF curves for the variation of PAPR under the PAPR reduction technique for different number of replications,  $L_{SLM}$ . A reference curve with no PAPR reduction is also included. It is evident from the plots that the improvements are significant and bring in up to 3dB reduction in PAPR in comparison to the case when no PAPR reduction technique is used.

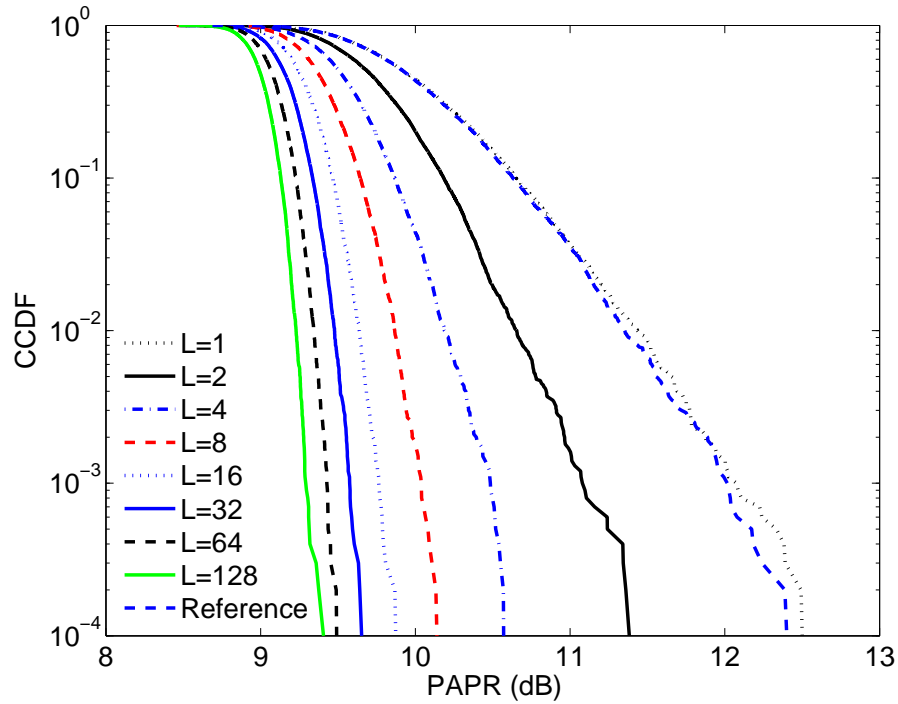


FIGURE 5.9: CCDF of the PAPR of the WPM signal for different values of  $L_{SLM}$ . The wavelet considered is Daubechies 5 (length 10). A reference curve with no PAPR reduction is also plotted.

### b. Influence of phase-sequence distribution

To gauge the impact of the distribution of the phase sequences we now consider different stochastic distributions. The distributions considered are random sequences, Golay sequences [110, 111] and Hadamard sequences. The number and length of all the sequences are taken to be equal. The phase alphabet is taken to be  $\phi \in (0, \pi/2, \pi, 3\pi/2)$  and the value of  $L_{SLM}$  is fixed at 8. Fig. 5.10 shows the respective plots and it can be deduced from the figures that though all the distributions yield notable improvements, there is no perceivable differences in their performances.

These results are important because the similarity in the performances when using pseudo-random and random sequences indicates that the receiver only has to know the key used at the transmitter to generate the pseudo-random phase sequences (instead of the entire phase sequence). This aids in significant reduction of the side information.

### c. Impact of phase alphabet

We now evaluate the impact of the phase alphabet on the PAPR reduction mechanism. The results are plotted in fig. 5.11 where a range of cardinalities for the phases are considered. The

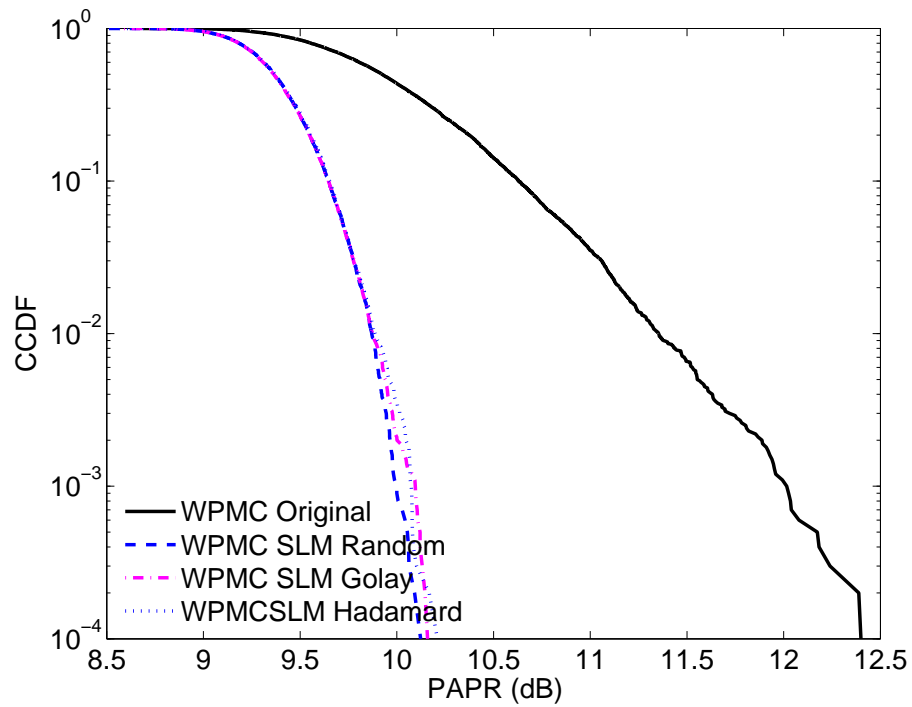


FIGURE 5.10: Complementary cumulative distribution function (CCDF) of the PAPR of WPM for different distributions of the phase sequences. The wavelet considered is Daubechies 5 (length 10).

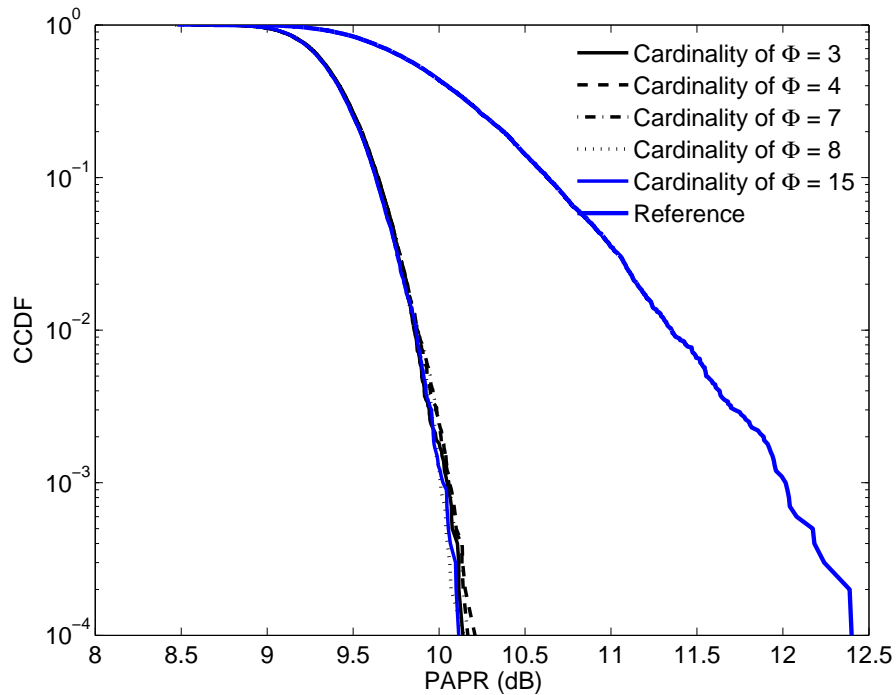


FIGURE 5.11: CCDF of the PAPR of WPM using the PAPR reduction technique for different phase sequences. The wavelet considered is Daubechies 5 (length 10).

results show that the choice of the phase alphabet does not affect the performance of the PAPR reduction technique.

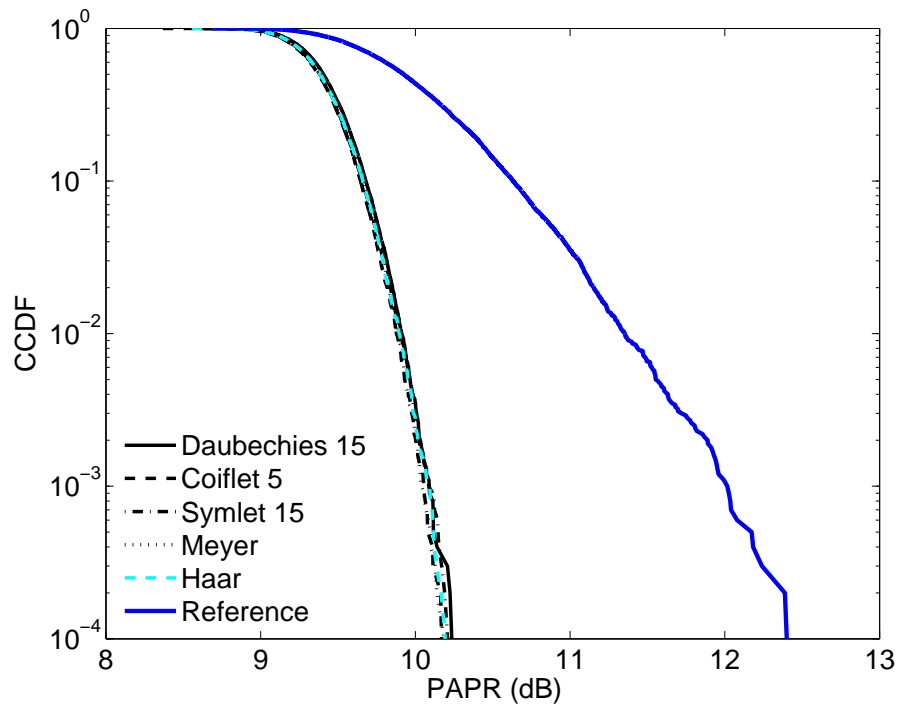


FIGURE 5.12: CCDF of the PAPR for several wavelets.

#### d. Impact of wavelet families

We now analyze the conduct of the PAPR reduction technique for different wavelet families and for different filter lengths. In these set of experiments the value of  $L_{SLM}$  is taken to be 8. The various wavelet families considered are Daubechies 15, Coiflet 5, Symlet 15 (all of length 30), Meyer (of length 102) and Haar. Figs. 5.12 and 5.13 show the PAPR performance curves for various wavelet families and various filter lengths, respectively. From fig. 5.12 we can deduce that all the wavelets follow a similar CCDF pattern for their PAPR performances. And from fig. 5.13 it is clear that even with increasing lengths of the wavelet filter, from Daubechies 2 to Daubechies 35, the PAPR distribution is limited to a variation of about 0.8 dB. In all instances the proposed technique reduces the PAPR between 1.5 and 2.5dB.

#### e. Influence of the PAPR reduction technique on the BER performance

We finally plot the BER performances of the WPM system (fig. 5.14). The curves plotted are for the cases when the phase sequences are generated randomly and pseudo-randomly. For the case with random phase change two figures are plotted. In the first case (denoted Case-1) the receiver has complete and perfect knowledge of the random phases used at the transmitter. In the second scenario (marked Case-2) the receiver operates with no knowledge of the phases used at the transmitter. For the scenarios when phases with Golay and Hadamard distributions are used, the transmitter and receiver only share the keys of the pseudo-random polynomial. As

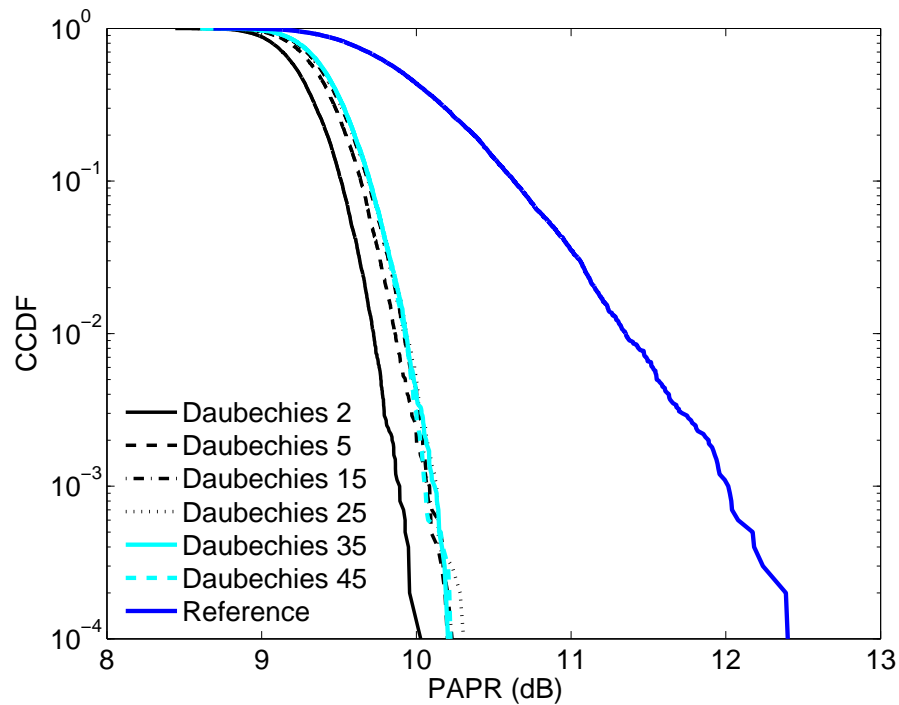


FIGURE 5.13: CCDF of the PAPR for the WPM system with different filter lengths of the Daubechies wavelet family.

a reference the BER plot for the case with no PAPR reduction technique is also plotted. The results show the importance of having complete knowledge on the phase sequences. Even a slight mismatch in the phase information at the receiver deteriorates the system performance. Since a perfect replication of randomly generated phases is not possible at the receiver, the application of pseudo-random generators can be considered. This is supported by the results plotted in fig. 5.10 where the PAPR reduction due to pseudo-random codes is shown to be as good as that of random phase generators and in fig. 5.14 where the BER curves show that using PAPR reduction mechanism with pseudo-random phase generators does not result in any loss in performance.

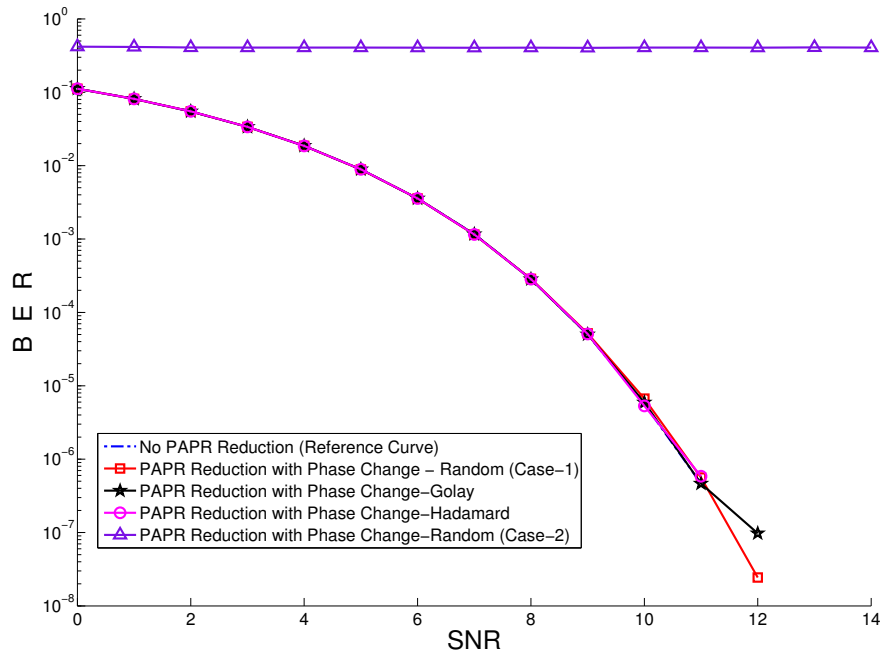


FIGURE 5.14: BER vs. SNR (dB) for the cases with and without PAPR reduction (phase modification) and for various distributions of the phase. For the case with random phase change two figures are plotted. In the first case (denoted Case-1) the receiver has complete and perfect knowledge of the random phases used at the transmitter. In the second scenario (marked Case-2) the receiver operates with no knowledge of the phases used at the transmitter. For the scenarios when phases with Golay and Hadamard distributions are used, the transmitter and receiver only share the keys of the pseudo-random polynomial.

## 5-5 Hill climbing optimization heuristics for minimization of PAPR in WPM transmission

In the SLM method a whole set of candidate signals representing the same information are generated. Then the most favorable signal as regards to minimum PAPR is chosen and transmitted. Instead of an arbitrary selection of the sub-carrier phases, it is also possible to find the optimum set of phase values that result in the lowest possible PAPR at all instances. This can be determined by a local search around a selected set of phase-shift in an  $M$ -dimensional space (for  $M$  number of sub-carriers). Local search is a meta-heuristic where the most suitable solution amongst a number of candidate solutions is determined such that a target or objective function is maximized (or minimized) [112]. Such local search algorithms move in the search space until a solution considered satisfactory<sup>6</sup> is obtained within a bounded period. In this section we present a method to optimize selection of sub-carrier phases to minimize the PAPR of the transmitted WPM signal. A mathematical optimization tool known as the hill climbing algorithm is applied to obtain the optimal set of phase adjustments which guarantee a low PAPR.

<sup>6</sup>The local search heuristic only guarantees a local minima and not a global optimum solution.

### 5-5-1 PAPR reduction as an optimization problem

A multi-carrier modulated signal is the sum of many information bearing sub-carriers which are statistically independent. For a reasonably large number (about 64 or more) of sub-carriers the distribution of these symbols in the time-domain is Gaussian. Hence, the signals may occasionally exhibit high fluctuations or spikes in the transmitted power. The objective of the optimization problem is therefore to minimize such fluctuations in the power (characterized by the metric PAPR) of the studied signal by adjusting the phases of the sub-carriers.

Formally, the problem can be mathematically stated as,

$$\min_{\phi_i} J(\phi) = \frac{\max_n(|y[n]|^2)}{\mathbf{E}(|y[n]|^2)} \quad (5.7)$$

subject to

$$0 \leq \phi_i \leq 2\pi.$$

Here  $J(\phi)$  denotes the objective function,  $\phi_i$  gives the phases of the sub-carriers  $i = 1, 2, \dots, M$  and  $y[n] = \text{IDWPT}(X_i e^{j\phi_i})$  with  $X_i$  representing the complex symbols after constellation mapping on the  $i^{\text{th}}$  sub-carrier.

The phase sequences  $\phi_i$  are determined by this optimization process. The phase-shifted information bearing streams are then transformed by an IDWPT operation and the objective value, which is the PAPR of the transformed composite signal, is calculated.

### 5-5-2 Hill climbing algorithm

We use a local search algorithm called the hill climbing algorithm to improve the selection of the phases. Hill climbing is a mathematical optimization technique which belongs to the family of local search algorithms. A local search algorithm starts with a candidate solution and then iteratively searches for better solutions in the neighborhood. When the algorithm cannot improve the solution any further, it terminates. Ideally, at the point of termination the obtained solution should be as close as possible to the optimum solution. However, like all local search algorithms, the hill climbing technique does not guarantee the best solution <sup>7</sup>.

An advantage of employing the hill climbing technique is that the method does not require the target functions to be differentiable. This is particularly useful for WPM systems because the wavelet signals cannot be readily expressed mathematically and hence mathematical operations like partial differentiation and integration can prove unwieldy.

<sup>7</sup>Since the intention here is to minimize PAPR (and not necessarily find the lowest possible PAPR) the hill climbing algorithm is suitable for the problem in hand.

The hill climbing algorithm maximizes (or minimizes) the objective function  $J(\phi)$  through an iterative process. In each iteration, the algorithm alters a single element <sup>8</sup> in  $\phi$  and determines whether the change improves the value of  $J(\phi)$ . Any change that improves  $J(\phi)$  is retained. The process continues until no change can be found to improve it further. This solution of  $J(\phi)$  is then said to be *locally optimal*. The elements of  $\phi$  can take both continuous and discrete values.

Different variants of the hill climbing method employ different processes of selection to identify the sample points  $\phi$ . Some chose the new points randomly; others try all possible values and select the one which best maximizes (or minimizes) the target function. In any event, if the newly selected point produces a solution better than the previous one, it is retained. However, if there are no further improvements to be had another point in the search space is chosen. The algorithm stops when the desired solution has been obtained or when the stipulated run-time of the algorithm has lapsed.

In the discrete vector spaces, the combinatorial problem may be visualized as a graph with the vertices of the graph denoting different states of  $\phi$ . Hill climbing traverses the vertices, always locally, increasing (or decreasing) the objective function. An appropriate step size is determined and the states of  $\phi$  are either incremented or reduced by the value of  $\phi$  leading to a gradient descent if the target function is to be minimized or to a gradient ascent if it is to be maximized. More details on the hill climbing algorithm can be found in [112–114].

The block diagram of the proposed scheme is presented in fig. 5.15.

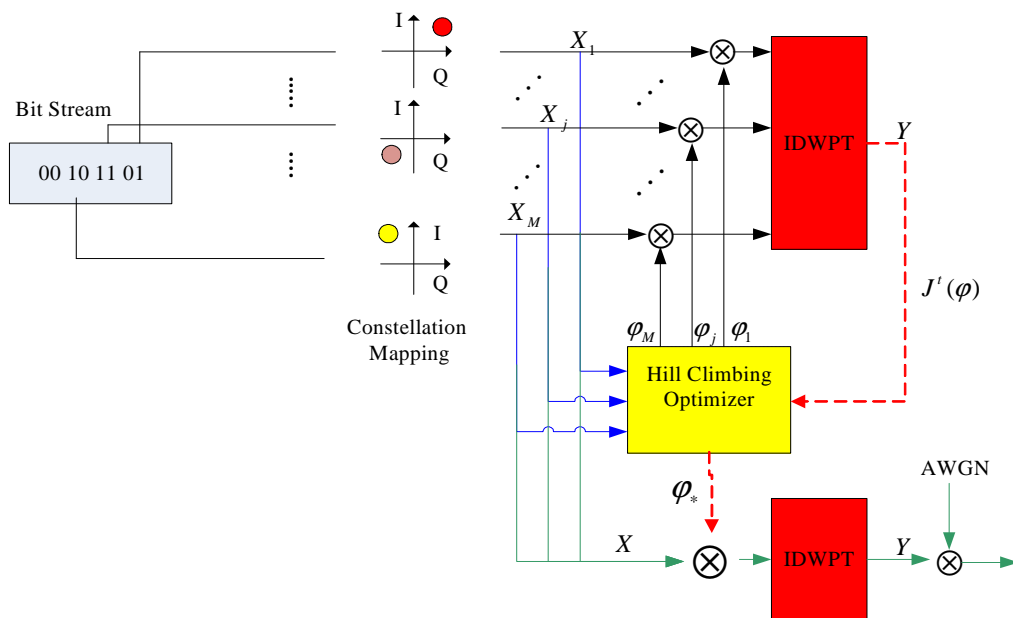


FIGURE 5.15: Block diagram of the hill climbing based PAPR reduction method.

In the next section, we show how the hill climbing search algorithm can be used to optimize the SLM algorithm presented in section 5-4 and reduce the PAPR in WPM transmission.

<sup>8</sup>This is in contrast to the gradient descent method where all the elements of the target function are adjusted.

### 5-5-3 Mitigation of PAPR for WPM systems with hill climbing algorithm

For a WPM system with  $M$  sub-carriers (refer fig. 5.15) the search space is a  $M$ -dimensional phase vector where the phases can take values between 0 and  $2\pi$ . The initial candidate solution is a vector  $\phi$  of randomly selected phases where  $0 \leq \phi_j \leq 2\pi$ ,  $j = 1, 2, \dots, M$ . The WPM sub-carriers are phase-modified with the  $M$ -length phase sequence. The IDWPT transform for the obtained frame sequence is then obtained and the PAPR of the signal is calculated.

The hill climbing method starts with a random  $M$ -dimensional phase vector  $\phi$  and calculates the PAPR (which is the objective function) of the modulated frame. A step size for the phase increments or decrements is then chosen. Each element of the phase vector is then modified iteratively by adding or subtracting it by the step size to obtain a new phase vector that produces a different PAPR value. When this method cannot improve the PAPR anymore, the algorithm terminates.

The hill climbing technique is presented in algorithm 2. Initially, an equal step size  $s_j$  is set for all the elements of  $j = 1, 2, \dots, M$ . The step size  $s_j$  determines by how much the  $j^{\text{th}}$  dimension of the phase vector is to be updated. At each epoch  $t$  one of the phases, say  $\phi_k$ , is updated by  $\phi_k^{(t+1)} = \phi_k^{(t)} + s_k$ . The WPM sub-carriers are phase shifted by the new value  $\phi^{(t+1)}$  and the PAPR of the signal is calculated. It must be noted that during a particular epoch all other phase values  $\phi_{j,j \neq k}$  are kept unchanged<sup>9</sup>. If the objective function,  $J(\phi^{(t+1)})$  decreases, i.e.,  $J(\phi^{(t+1)}) < J(\phi^{(t)})$ , then  $\phi_k^{(t+1)}$  becomes  $\phi_k^{(t+1)} = \phi_k^{(t)} + s_k$ . On the other hand, if the value of the objective function increases,  $J(\phi^{(t+1)}) > J(\phi^{(t)})$ , then  $\phi_k^{(t+1)}$  becomes  $\phi_k^{(t+1)} = \phi_k^{(t)} - s_k$ . If there is no change in the objective function value, then  $s_k$  is set to zero.

$$\phi_k^{(t+1)} = \begin{cases} \phi_k^{(t)} + s_k & \text{if } J(\phi^{(t+1)}) < J(\phi^{(t)}) \\ \phi_k^{(t)} - s_k & \text{if } J(\phi^{(t+1)}) > J(\phi^{(t)}) \\ \phi_k^{(t)} & \text{if } J(\phi^{(t+1)}) = J(\phi^{(t)}). \end{cases} \quad (5.8)$$

At each epoch the algorithm aims to minimize the PAPR. To aid fast convergence of the algorithm to the minima the step size is decreased exponentially. Whenever there is a change in the direction of the optimization in two consecutive epochs, for example,

$$J(\phi^{(t-1)}) < J(\phi^{(t)}) \text{ and } J(\phi^{(t)}) > J(\phi^{(t+1)}),$$

or,

$$J(\phi^{(t-1)}) > J(\phi^{(t)}) \text{ and } J(\phi^{(t)}) < J(\phi^{(t+1)}),$$

<sup>9</sup>This follows the fundamental principle of the hill climbing technique where only one element is altered at any given instance

the step size of the corresponding dimension is halved. Furthermore, if the step size becomes lower than a certain predefined threshold (a very small value) it implies that the solution cannot be improved any further with changes in that dimension. In such a case the step size is set to zero. If  $s_j = 0, \forall j$ , then the algorithm terminates. When the algorithm stops, a near-optimal phase vector  $\phi_*$  that produces a frame with a minimized PAPR is obtained.

---

**Algorithm 2** Hill climbing based PAPR reduction algorithm
 

---

**Require:**  $\mathbf{X}$  { $\mathbf{X}$  are the symbols on each sub-carrier}

- 1:  $stepsize = 0.1$  {how much the phases can be updated at each epoch}
  - 2:  $maxepochs = 1000$  {maximum number of epochs (iterations)}
  - 3:  $\phi_i = rand(0, 2\pi)$  where  $i = 1, \dots, M$  {initially selected phase vector for each sub-carrier}
  
  - 4:  $s_i = stepsize$  where  $i = 1, \dots, M$  {phase change for local search}
  - 5:  $d_i = 1$  where  $i = 1, \dots, M$  {direction of optimization 1:decreased  $J(p)$  0:increased  $J(p)$ }
  - 6: Generate  $\mathbf{Y} = IDWPT(\mathbf{X}e^{j\phi})$  {Modulate the new frame}
  - 7:  $J(\phi^{(1)}) = PAPR(\mathbf{Y})$  {Calculate the PAPR and BER (objective value,  $J(\phi)$ )}
  - 8: **for**  $t = 1$  to  $maxepochs$  **do**
  - 9:   **for**  $i = 1$  to  $M$  **do**
  - 10:      $q = \phi^{(t)}$
  - 11:      $q_i = q_i + s_i$
  - 12:     Generate  $\mathbf{Y} = IDWPT(\mathbf{X}e^{jq})$
  - 13:      $J(\phi^{(t+1)}) = PAPR(\mathbf{Y})$
  - 14:     **if**  $J(\phi^{(t+1)}) < J(\phi^{(t)})$  **then**
  - 15:          $\phi_i^{(t+1)} = \phi_i^{(t)} + s_i$
  - 16:          $d_i^{t+1} = 1$
  - 17:     **else**
  - 18:         **if**  $J(\phi^{(t+1)}) > J(\phi^{(t)})$  **then**
  - 19:              $\phi_i^{(t+1)} = \phi_i^{(t)} - s_i$
  - 20:              $d_i^{t+1} = -1$
  - 21:         **else**
  - 22:              $s_i = 0$
  - 23:              $d_i^{t+1} = 0$
  - 24:         **end if**
  - 25:     **end if**
  - 26:     **if**  $d^t + d^{t+1} = 0$  **then**
  - 27:          $s_i = s_i/2$  {Fluctuations close to minima, decrease the step size}
  - 28:     **end if**
  - 29:   **end for**
  - 30:    $\phi_* = \phi^{(t+1)}$
  - 31:   Generated  $\mathbf{Y} = IDWPT(\mathbf{X}e^{j\phi_*})$
  - 32:    $J(\phi_*) = PAPR(\mathbf{Y})$
  - 33:   **if**  $\sum_{i=1}^M s_i = 0$  **then**
  - 34:     Break;
  - 35:   **end if**
  - 36: **end for**
-

TABLE 5.2: Parameters used in the simulations

Parameter	Value
Number of SLM replicas $N_{SLM}$	4
Dimension $M$	16
Step size $s_j$	0.1
Maximum number of epochs	100

#### 5-5-4 Numerical results

In this section we present results of the studies and evaluate the performance of WPM system with the proposed hill climbing based PAPR mitigation scheme. The WPM system is realized using a filter bank structure with 4 levels of decomposition (16 carriers) and the wavelet of choice is Daubechies 5 (denoted db5) which is of length 10. The modulation scheme used is Quadratic Phase Shift Keying (QPSK). The figure-of-merit used is the complementary cumulative distribution function (CCDF). These simulation parameters will be used through out the experiments unless stated otherwise.

##### a. Performance of the algorithm to reduce PAPR

We first evaluate the impact of the PAPR reduction technique. In fig. 5.16 the results of the proposed hill climbing technique are plotted along with that of the SLM technique. The parameters used for the hill climbing are tabulated in table 5.2. For the SLM technique the phases are chosen from a phase alphabet of  $\phi \in (0, \pi/2, \pi, 3\pi/2)$ . As a reference the case with no PAPR reduction is also plotted.

##### b. Convergence of the algorithm

The starting point of the search algorithm and the choice of the step size play an important role on the convergence of the algorithm to a minima. If a large step size is selected then the algorithm could overlook potential solutions in the search space. On the other hand, if the step size is small then the required number of epochs to converge to a minima could be high.

In order to avert long execution times the maximum number of epochs in the proposed algorithm is bounded. Furthermore, the convergence of the algorithm to a minima is facilitated by exponential updates to the step size. The phenomenon is illustrated in fig. 5.17 where the initial phase vector is marked with *start* and the minima to which the algorithm converges to is marked *stop*. In the example considered the algorithm 2 converges to a minima in around 2000 epochs. The results of the PAPR reduction algorithm to different step sizes are plotted in fig. 5.18.

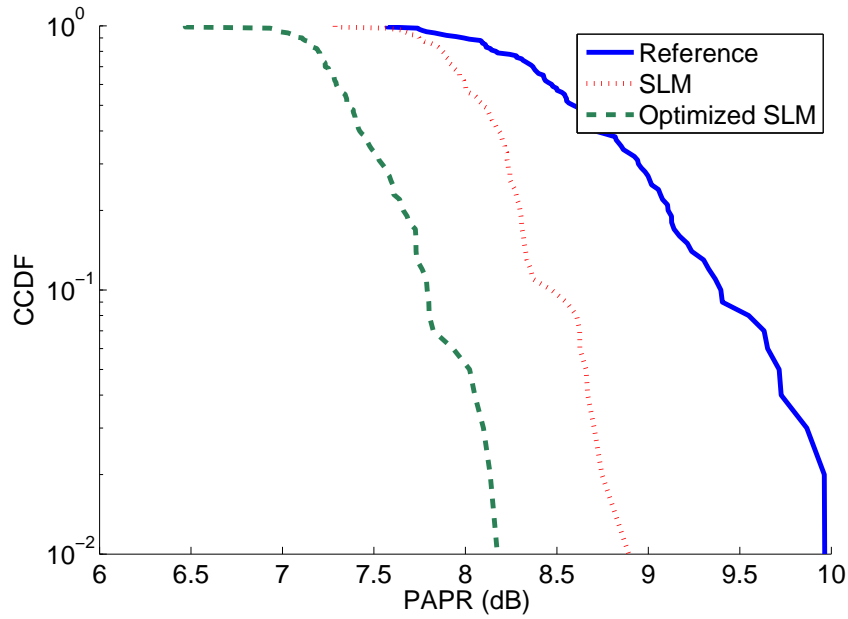


FIGURE 5.16: Performance of PAPR mitigation strategy with hill climbing optimization. The WPM system is realized using a filter bank structure with 4 levels of decomposition and QPSK modulation scheme. As reference the results of the standard SLM approach as well as case that without any PAPR reduction are plotted. For SLM, the number of phase-shifted replicas of the original frame,  $N_{SLM} = 4$ .

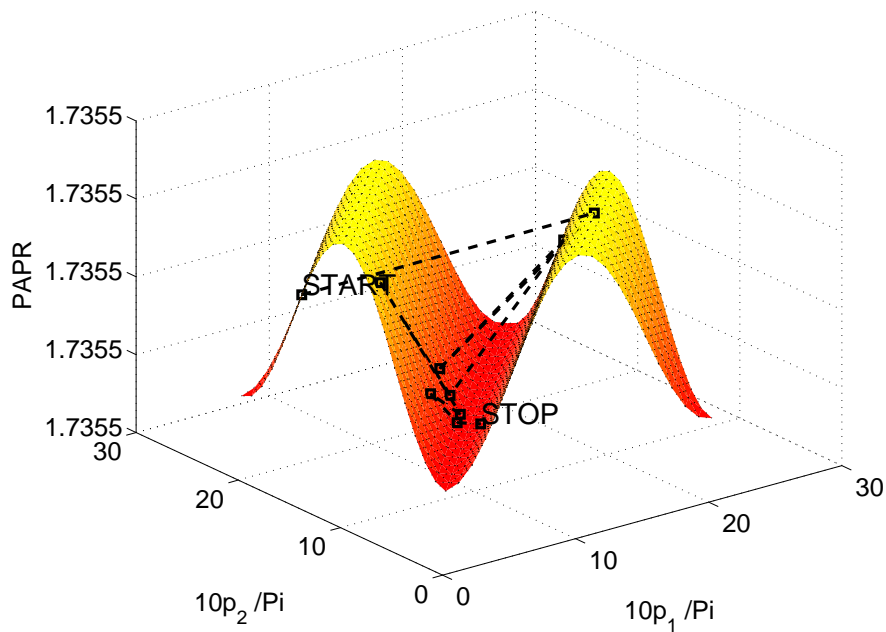


FIGURE 5.17: Demonstration of the impact of the initially selected step size where  $s_j = 0.01$ ,  $\forall j$  on the PAPR reduction technique. The wavelet considered is Daubechies 15 (length 30). For the case considered algorithm 2 converges to a minima in about 2000 epochs.

### c. Impact of the wavelet family

We now evaluate the performance of the PAPR reduction technique for different wavelet families. In fig. 5.19, the impact of the selected wavelet family on the performance of the PAPR

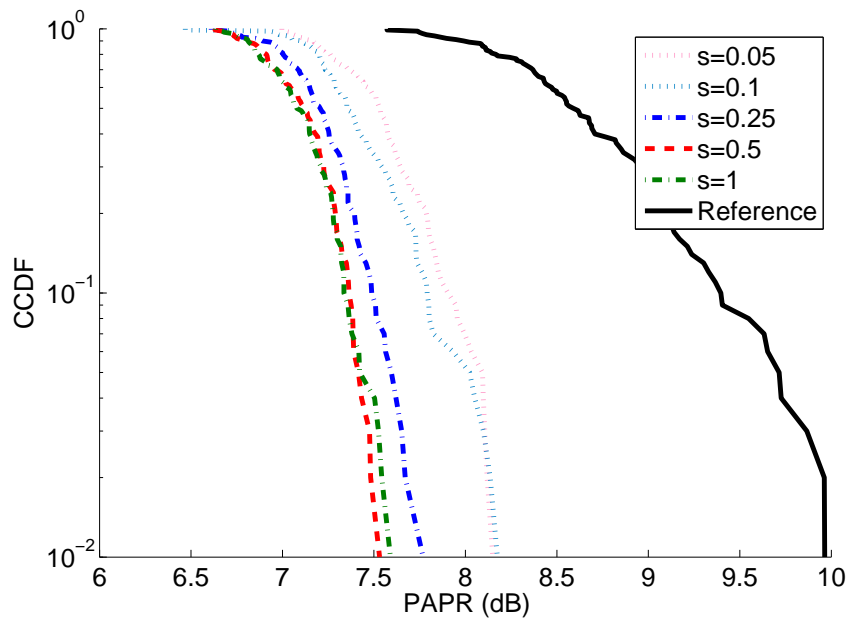


FIGURE 5.18: Impact of the step size  $s_i$  on the PAPR reduction technique.

reduction is presented. Daubechies 5 (of length 10), Coiflet 5, Symlet 15 (both of length 30), Meyer (of length 102) and Haar wavelets are compared. An improvement in the PAPR performance can be observed for all the wavelet families. For a CCDF value of about  $10^{-2}$ , the PAPR gained with the mitigation technique is about 2dB when compared to the case where no optimization technique is applied.

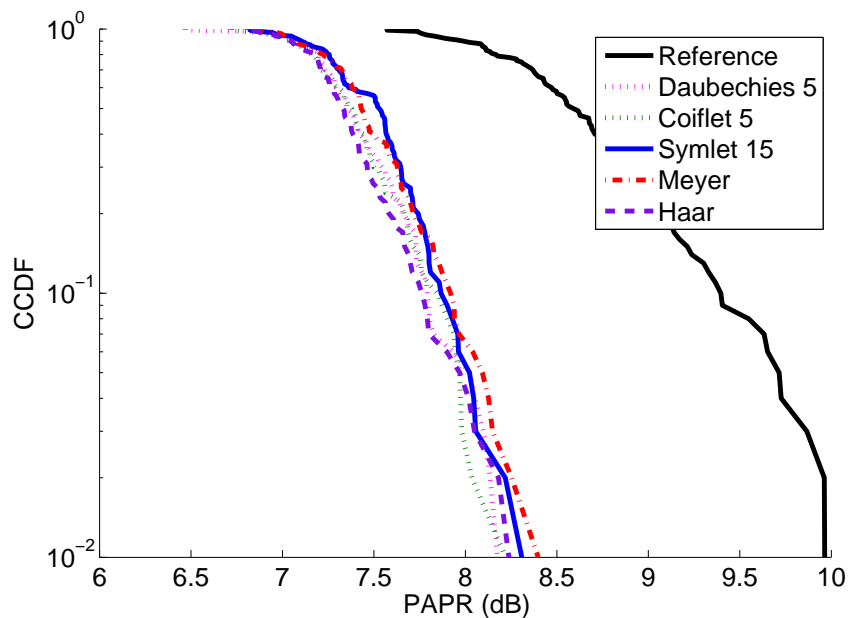


FIGURE 5.19: CCDF of the PAPR of WPM using hill Climbing based optimization method for different wavelet families. The WPM system is realized using a filter bank structure with 4 levels of decomposition and QPSK modulation scheme.

In fig. 5.20 the performance of the PAPR reduction technique for different wavelet filter lengths is shown. Though the differences in the performances are not much, one may note that with increasing lengths of the wavelet filters the PAPR values also increase.

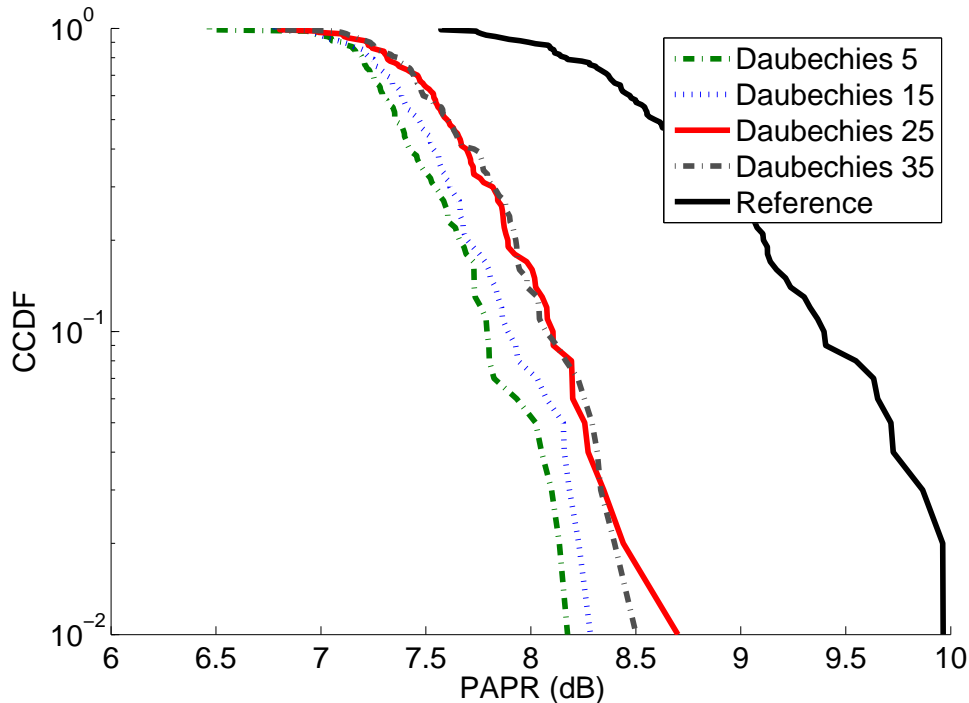


FIGURE 5.20: CCDF of the PAPR of WPM using hill Climbing based optimization method with different filter lengths of the Daubechies wavelet family.

A two-dimensional demonstration ( $M = 2$ ), of this technique is presented in fig. 5.21 for five different wavelet families. In the figure the axes  $p_1$  and  $p_1$  indicate the selected phases for the two sub-carrier ( $M = 2$ ) expressed in discrete values in the range 0 to  $2\pi$ . In the figure, the phase vector selected at the commencement of the algorithm is marked with *start* and the near-optimal phase vector obtained at the end of the search algorithm is denoted as *stop*.

#### d. Computational complexity of the algorithm

The computational complexity of a hill climbing algorithm is  $O(TK)$  where  $T$  is the number of iterations and  $K$  is the average number of neighbor solutions. The value of  $K$  depends on the number of sub-carriers  $M$  and can be given as  $K = 2M$ <sup>10</sup>. Consequently, the complexity of the hill climbing algorithm is  $O(TM)$ . When calculating the complexity of the overall implementation, the computations necessary to execute the IDWPT must also be taken into account. The IDWPT complexity can be derived to be  $O(M \log_2 M)$  [10] and therefore, the overall complexity of the algorithm can be given as  $O(TM^2 \log_2 M)$ .

<sup>10</sup>For each sub-carrier a phase value can either be increased or decreased by a step size

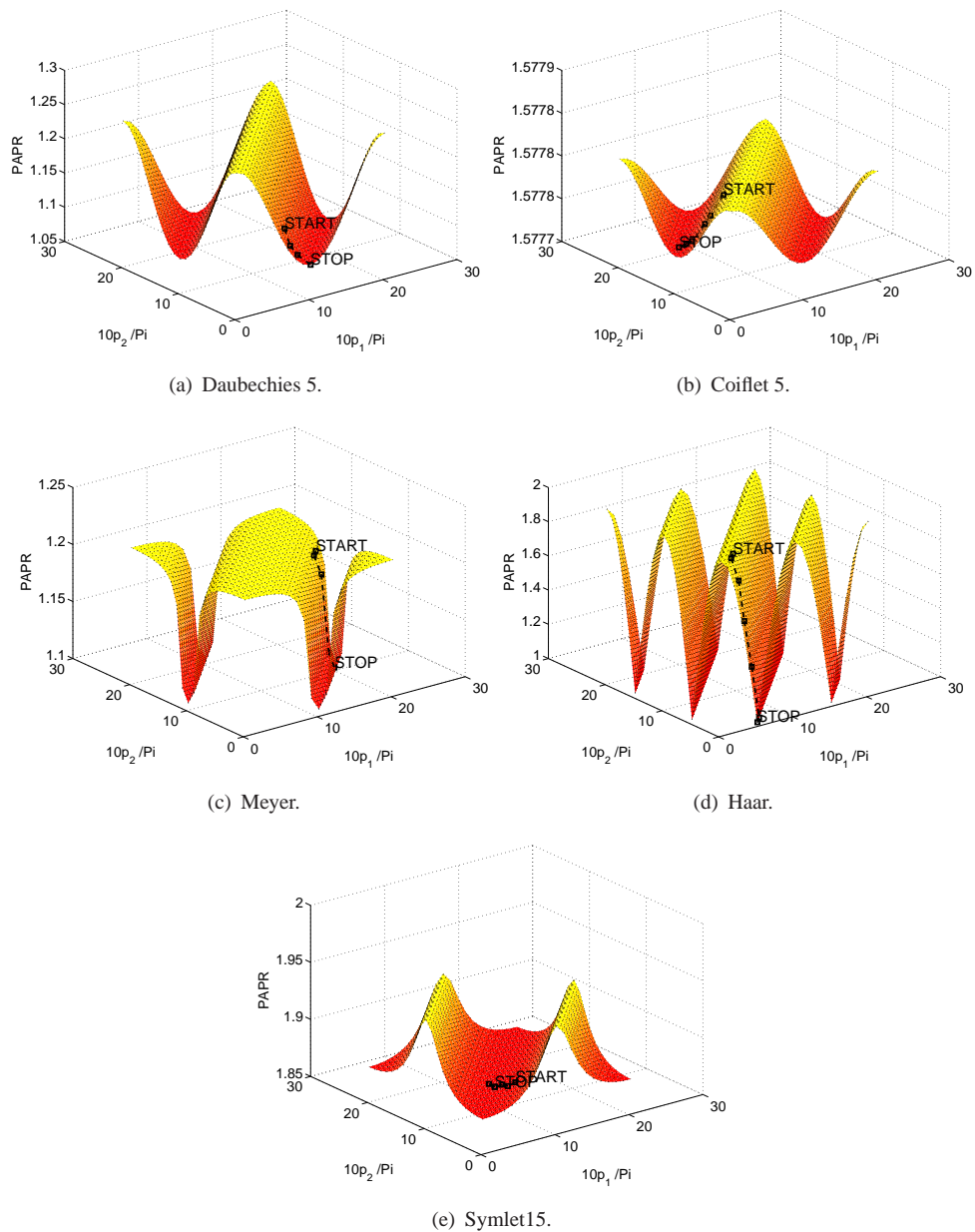


FIGURE 5.21: Demonstration of Algorithm 2 for various wavelet families.

## 5-6 Summary

In this chapter we presented a study on the PAPR performance of the WPM system. Furthermore, two strategies to mitigate the PAPR in WPM transmission were proposed.

- Selected mapping (SLM) with phase modification: The method exploited the fact that by altering the phase of the WPM sub-carriers one can alter the PAPR of the transmitted signal. By altering the phases of the sub-carriers that modulate the information, WPM frames with different PAPRs can be obtained for the same information sequence. By

selecting the frame with the least PAPR the WPM system can be prevented from operating in the saturation region of the electronic circuitry in the transceiver chain.

- Optimization of phase selection: The SLM technique was enhanced by proposing a mathematical heuristic to optimize the selection of phases to reduce PAPR. To do so, the objective of minimizing the PAPR is posed as a mathematical optimization problem and solved using a local-search algorithm known as the hill climbing heuristic. The main benefit of using the hill climbing technique for WPM systems is that the method does not require the target functions to be differentiable. This is critical because the wavelet signals cannot be readily expressed as mathematical functions and hence operations like partial differentiation or integration are not easy.

The operation of the proposed methods were demonstrated and verified through numerical computations. Comparing the two techniques, the hill climbing optimizer outperforms SLM based phase modification or scrambling based techniques. The large side information requirement of this optimization technique reduces the applicability of this technique. To reduce the side-information two strategies may be employed (a) quantization of phases to a finite number and (b) bundling of sub-carriers into groups where all the sub-carriers within a group undergo the same phase shift [108].

## **Part IV**

# **Demonstration of Advantages**

## Chapter 6

# Wavelet packet spectrum estimation

In this chapter, we investigate the application of wavelet packet transform (WPT) for spectral estimation and analysis<sup>1 2</sup>. The main attraction for the method is the trade-offs it offers in terms of satisfying various figure-of-merits such as high frequency resolution, good side-lobe suppression and low variations in the estimated power spectral density (PSD). The performance of the system is evaluated through computer simulations. The results of the experiments show that the wavelet based approach offers great flexibility and adaptability apart from its performances which are comparable and at times even better than Fourier based estimates.

In addition to this, a couple of optimizations which lead to significant performance gains by correcting edge-artifacts in standard wavelet packet transforms are presented.

The rest of the chapter is organized as follows. The fundamentals of conventional spectrum estimation techniques like Periodogram, Corellogram, Welch and Blackman-Tukey are provided in Section 6.1. In Section 6.2 these spectrum estimation techniques are interpreted as a filter bank analysis problem. Two new techniques, namely, Multi taper spectrum estimation (MTSE) and Filter bank spectrum estimation (FBSE) are also presented in this section as a class of filter bank estimators. We then introduce the wavelet packet spectrum estimator (WPSE) in Section 6.3 as an advancement to the existing approaches. The WPSE is realized with a tree structure consisting of para-unitary filters. In Section 6.4 a couple of optimizations which improve WPSE performance is explained. Section 6.5 presents the simulation setup and the results of the study. A comparative analysis of WPSE with existing methods is provided in Section 6.6. The chapter ends with a summary in Section 6.7.

---

<sup>1</sup>Parts of this chapter have been published in [115] and [116]. For any material that has been reused, wherever applicable, a written consent has been obtained from the first author.

<sup>2</sup>The author gratefully acknowledges the contributions of Msc student Mr. D .D. Ariananda for his active cooperation and help with the computer simulations.

## 6-1 Introduction

Spectral Analysis is the process of determining the distribution in frequency of the power of a finite length signal from a finite set of measurements [117]. Metrics like variance and bias of measurement as well as complexity of method are important considerations when choosing the right spectrum analysis tool. Variance is the variations or fluctuations in the measurement which occur due to the fact that an infinite number of PSD values are estimated from a finite sample set [117]. On the other hand, a bias can be due to 2 factors - smearing (or smudging) and leakage (or spillage) [117]. Both these problems arise due to the limitations in the band-pass filter, principally, with regard to their main and side lobes [117]. The effect of the main lobe is to smear the estimate resulting in reduced frequency resolution. Side lobes on the other hand contribute to transferring power from the desired to the undesirable bands causing leakages [117]. The criterion for the optimum band-pass filters - narrow main lobes with low side lobes - is conflicting and hence cannot be met simultaneously. Naturally, compromises have to be made with regard to the choice of the band-pass filter. The best approach hence would be the one which offers a trade-off between a desirable main-lobe and a tolerable side-lobe.

Consider<sup>3</sup>, a discrete time signal  $x[n]$  consisting of  $N_s$  random data samples and of finite energy and zero mean i.e.  $E\{x[n]\} = 0$ . Here  $E\{\cdot\}$  is the expectation operator which averages over the ensemble of data samples. Defining the correlation function  $R_{xx}[k]$  as:

$$R_{xx}[k] = E\{x^*[n-k]x[n]\}, 0 \leq k \leq N_s - 1, \quad (6.1)$$

there are two ways in which the power spectral density of the signal can be calculated. In the first method, known as the direct method (or frequency domain approach), the PSD  $S_{xx}^{\text{Dir}}(\omega)$  is estimated directly from the signal  $x[n]$  as [117, 118],

$$S_{xx}^{\text{Dir}}(\omega) = \lim_{N_s \rightarrow \infty} E \left\{ \frac{1}{N_s} \left| \sum_{n=0}^{N_s-1} x[n] e^{-j\omega n} \right|^2 \right\}. \quad (6.2)$$

In the second approach, referred as the indirect method (or time domain approach), the auto-correlation function  $R_{xx}[k]$  of the signal being estimated is considered and from this autocorrelation value, the power spectrum density  $S_{xx}^{\text{inDir}}(\omega)$  is found by applying the Discrete Fourier Transform [117, 118], i.e.,

$$S_{xx}^{\text{inDir}}(\omega) = \sum_{k=-\infty}^{\infty} R_{xx}[k] e^{(-j\omega k)} \quad (6.3)$$

---

<sup>3</sup>The discussion is based on [117] and has been summarized here for ready reference

### 6-1-1 Periodogram

The most commonly known spectrum estimator is the periodogram, which is based on the direct method of spectrum estimation as presented in eq.(6.2). Since the signal to be estimated is usually of finite length  $N_s$ , the expectation and limit operation in eq.(6.2) can be omitted to obtain the reformulated PSD estimate  $\widehat{S}_{xx}^p(\omega)$  as [117]:

$$\widehat{S}_{xx}^p(\omega) = \frac{1}{N_s} \left| \sum_{n=0}^{N_s-1} x[n]e^{-j\omega n} \right|^2. \quad (6.4)$$

### 6-1-2 Correlogram

The correlogram uses the autocorrelation function of the input signal  $R_{xx}[k]$  to compute the PSD. The PSD is obtained from the DFT of  $R_{xx}[k]$ , i.e., [117]:

$$\widehat{S}_{xx}^c(e^{j\omega}) = \sum_{k=-\infty}^{\infty} R_{xx}[k] \exp(-j\omega k) \quad (6.5)$$

There are two possible ways to compute the covariance function  $R_{xx}[k]$ , namely, the standard biased and the standard unbiased estimation [118]. The standard unbiased estimate is expressed as [117]:

$$\widehat{R}_{xx}[k] = \frac{1}{N-k} \sum_{n=k}^{N-1} x^*[n-k]x[n], 0 \leq k \leq N-1, \quad (6.6)$$

and the standard biased estimate is given as [117]:

$$\widehat{R}_{xx}[k] = \frac{1}{N} \sum_{n=k}^{N-1} x^*[n-k]x[n], 0 \leq k \leq N-1. \quad (6.7)$$

In eqs.(6.6) and (6.7)  $\widehat{R}_{xx}[k]$  denotes the approximate of the autocorrelation function  $R_{(xx)}[k]$ . Amongst the two approaches, the biased approach is usually preferred. The is so because for large lags in the unbiased approach  $k$  the factor  $(N-k)$  will be small leading to erratic values of the  $R_{xx}[k]$ . Moreover, the value of  $\widehat{R}_{xx}[k]$  is guaranteed to be positive semi-definite [117].

### 6-1-3 Other techniques

The main deficiency of the techniques presented above is the use of rectangular window to truncate the input data samples to finite length. This windowing introduces a discontinuity between the original signal and the aliased version produced by a DFT transformation. In the frequency domain, the rectangular window results in a Dirichlet Kernel which is described by

the width of the main lobe and the level of side lobe [119]. The width of the main lobe is related to the frequency resolution of the power spectra, and the level of side lobe is related to the ratio between maximum and minimum spectral power that is distinguishable by the estimator. The rectangular window compromises the frequency resolution resulting in leakage and a biased estimate. For  $N_s$  number of data samples, the spectral resolution limit of Periodogram is  $1/N_s$ . That is, the periodogram cannot resolve those details of the signal which are separated by less than  $1/N_s$  cycles per sampling interval [117].

Another problem with the periodogram is that the estimates are coarse with low precision and large variance. Moreover, this variance does not improve with more data. The only way to reduce the variance of the periodogram is to average the PSD estimates. This can be done by computing several (shorter) periodograms and use these to compute averages of each PSD estimate. This method is known as Bartlett method. Conversely, the periodogram coefficients can also be weighted by windows. This is what happens in the Blackman-Tukey method. Bartlett method and Blackman-Tukey method can be combined together so that one computes an average of several windowed periodograms. This is the Welch method.

The choice of segment size and the number of segments determine the frequency resolution and the variance that the methods presented above can offer. Apart from these two parameters, the choice of window also has an important role to play. The window function determines the dynamic spectrum range of the estimator as well as the attainable spectral resolution. The window functions can thus be used as a lever to control the resolution and the range of the estimator. Some of the popular windows used are the Triangular, Blackman, Hamming, Kaiser and Hann window functions.

An important point to note is that almost all these window functions have smaller weights for data samples located around the edges. Therefore, in the final computation of the PSD all the data samples are not equally represented. In order to mitigate this effect the data segments are allowed to overlap. In [118], Porat suggests a 50 percent segment overlap. For this case, all data samples have equal representation since samples located near the edges of a particular segment will be located at the center of the adjacent segments.

## 6-2 Spectrum estimation as a filter bank analysis problem

In this section we explain how traditional spectrum estimators can be interpreted as a filter bank analysis problem. Since the proposed wavelet packet based spectrum estimator (WPSE) is entirely based on filter bank theory such a discussion will greatly aid in its understanding. The discussion is based on an analysis provided in [117].

### 6-2-1 Filter bank interpretation of spectrum analysis

As mentioned before, spectrum estimation is about finding the power spectrum density (PSD) of a finite sample set  $x[n]$ ,  $n = 1, 2, \dots, N$  for the frequency band  $|\omega| \leq \pi$ . Usually the Fourier transform is used to obtain a Periodogram estimate. Let us first consider eq.(6.4) as a function of frequency (instead of the angular frequency) [117]:

$$\widehat{S}_{xx}^p(e^{j2\pi f}) = \frac{1}{N_s} \left| \sum_{n=1}^{N_s} x[n] e^{-j2\pi f n} \right|^2. \quad (6.8)$$

For any given frequency  $f_i$ , eq.(6.8) can be rewritten as [117]:

$$\widehat{S}_{xx}^p(e^{j2\pi f_i}) = \frac{1}{N_s} \left| \sum_{n=1}^{N_s} x[n] e^{-j2\pi f_i n} \right|^2 = \frac{1}{N_s} \left| \sum_{n=1}^{N_s} x[n] e^{j2\pi f_i (N_s - n)} \right|^2 \quad (6.9)$$

The second operation in eq.(6.9) is possible since  $|e^{j2\pi f_i N_s}| = 1$ . By introducing a new variable  $k = N - n$ , we can rewrite eq.(6.9) as [117]:

$$\widehat{S}_{xx}^p(e^{j2\pi f_i}) = \frac{1}{N_s} \left| \sum_{k=0}^{N_s-1} x[N_s - k] e^{j2\pi f_i k} \right|^2 = \left| \sum_{k=0}^{N_s-1} h_i[k] x[N_s - k] \right|^2, \quad (6.10)$$

where,

$$h_i[k] = \begin{cases} w[k] e^{j2\pi f_i k} & \text{for } k = 0, 1, 2, \dots, N_s - 1 \\ 0 & \text{otherwise} \end{cases} \quad (6.11)$$

and window function  $w[k] = 1/\sqrt{N_s}$ .

If  $h_0[k]$  ( $= w[k]$ ) is taken to be a prototype FIR low-pass filter, then  $h_{i;i \neq 0}[k]$ s will constitute a bank of band-pass filters centered at frequencies  $f_i$  and obtained by modulating the prototype filter  $h_0[k]$ . The spectrum analysis problem posed in eq.(6.8) can be perceived as passing  $N_s$  samples of the studied signal through a filter bank with impulse responses  $h_i[k]$  as illustrated in fig. 6.1. For the classic periodogram, the function  $w[k]$  is a rectangular window with  $w[k] = 1/\sqrt{N_s}$ .

The frequency response  $H_i(\omega)$  of the filter  $h_i[k]$ , which is,

$$H_i(\omega) = \sum_{k=0}^{\infty} h_i[k] e^{-j\omega k} \quad (6.12)$$

can be easily derived to be [117]:

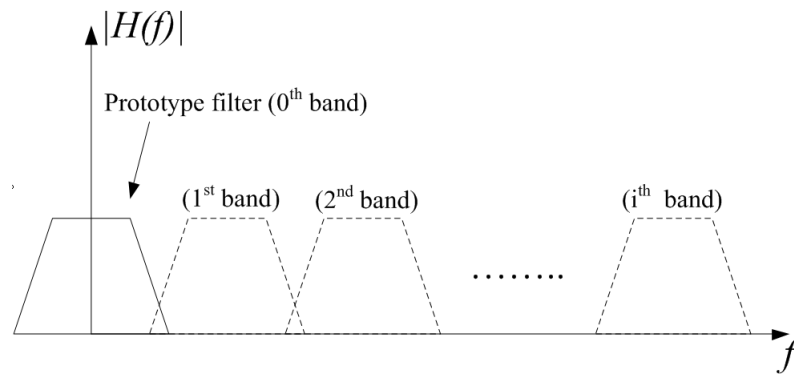


FIGURE 6.1: Illustration of the filter bank concept [120].

$$\begin{aligned}
 H_i(\omega) &= \frac{1}{\sqrt{N_s}} \sum_{k=0}^{N-1} e^{j(\omega_i - \omega)k} = \frac{1}{\sqrt{N_s}} \frac{e^{j(\omega_i - \omega)N_s} - 1}{e^{j(\omega_i - \omega)} - 1} \\
 &= \frac{\sin[N_s(\omega_i - \omega)/2]}{\sqrt{N_s} \sin[(\omega_i - \omega)/2]} \exp \left[ j \left( \frac{N_s - 1}{2} \right) (\omega_i - \omega) \right]. \quad (6.13)
 \end{aligned}$$

It is clear that the frequency response of the periodogram with the rectangular window  $w[k] = 1/\sqrt{N_s}$  as prototype filter will have large side lobes leading to large leakages. In order to obtain a prototype filter with smaller side lobes, the rectangular window is replaced with a window function that tapers smoothly on both sides. Examples of popular window functions are Hanning, Kaiser and Blackman [118].

### 6-2-2 Multi-taper spectral estimator (MTSE)

A more intuitive approach would be to employ the Multi-taper spectrum estimator (MTSE) suggested by Thomson [118, 121]. In this method multiple orthogonal prototype filters are used for each band. The outputs of each filter are then averaged to obtain the estimate. Since the filters are orthogonal to each other the outputs are uncorrelated and the estimates have low variance. To improve the accuracy of the estimates a mini-max algorithm is employed to ensure that the filters have maximum energy in the bands (with minimal side-lobe) of interest. The orthogonal basis vectors used in MTSE are slepian functions (prolate spherical sequences). The MTSE uses multiple orthogonal prototype filters to improve the variance and reduce the side-lobe and leakage. Fig. 6.2 illustrates the magnitude response of the first seven MTSE prolate filters of length 128 [120]. In this figure, only the even numbered filters are shown for the sake of clarity.

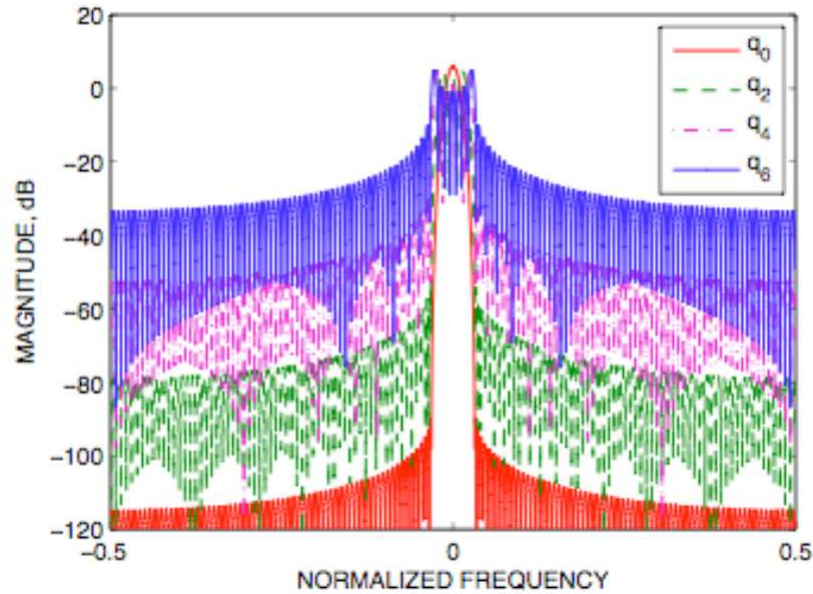


FIGURE 6.2: Magnitude responses of the first seven prolate filters of length 128. For clarity, only the even numbered filters are shown. The odd numbered filters have responses that fall in between the presented ones [120].

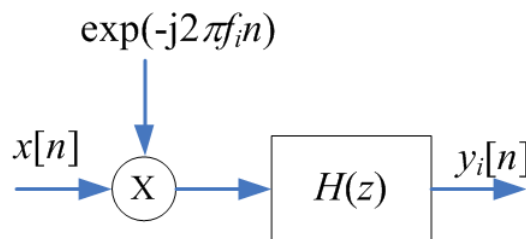


FIGURE 6.3: Demodulation of the  $i$ th sub-carrier of the received signal before it is processed by the root-Nyquist filter [120].

### 6-2-3 Filter bank spectral estimator (FBSE)

An example of a spectrum estimator which is completely based on filter banks is the Filter bank spectrum estimator (FBSE) proposed by Farhang-Boroujeny [120]. While in Thomson's MTSE, the estimate at a frequency point  $f_i$  is obtained by averaging the output of multiple prototype filters, FBSE simplifies MTSE by employing only one prototype filter in the zeroth band as shown in fig. 6.3.

FBSE is implemented with a pair of matched root Nyquist-filter. A filter with transfer function  $H(z)$  is said to satisfy the Nyquist criterion if [122]:

$$\sum_{k=0}^{O_S-1} P(z e^{-j2\pi f k}) = O_S \quad (6.14)$$

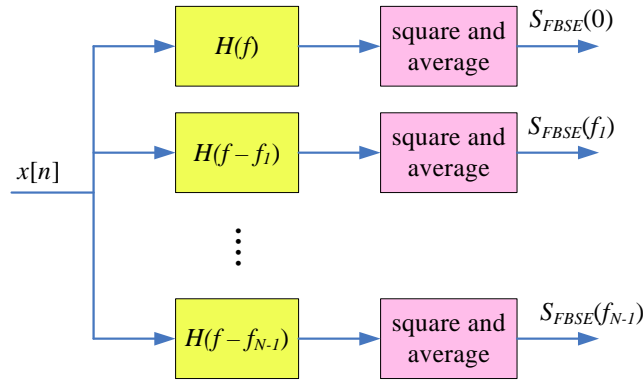


FIGURE 6.4: Illustration of Filter Bank Spectral Estimator (FBSE) proposed by Farhang-Boroujeny [120].  $S_{FBSE}(f_i)$  is the FBSE estimate at  $i$ -th frequency sub-band [53].

In eq.(6.14),  $P(z)$  is the product filter  $P(z) = H(z)H(z^{-1})$  and  $O_S$  is an integer called the over sampling factor [122]. In multi-carrier communication, such filters are useful to design a pair of matched transmit and received filters whose cascade is a Nyquist pulse shape. When  $|z| = 1$ , then  $P(z) = H(z)H(z^{-1}) = |H(z)|^2$ .  $P(z)$  is called a Nyquist filter and  $|H(z)| = P(z)^{1/2}$  a root-Nyquist filter.

Fig. 6.4 shows the FBSE implementation. In the figure  $H(f)$  is the prototype filter, which is root-Nyquist filter while the rest of the filters are modulated versions of  $H(f)$ . The frequency response of the prototype filter  $H(f)$  and its modulated versions are shown in fig. 6.5. The output power of each filter is a measure of the estimated power over the corresponding sub-band. Hence, the power spectral density (PSD) estimate of  $i$ -th sub band of the filter bank is represented as [120]:

$$\hat{S}\left(\frac{i}{N}\right) = \text{avg} \left[ |y_i[n]|^2 \right] \quad (6.15)$$

In eq.(6.15), the operator  $\text{avg}\{\cdot\}$  stands for time averaging while  $y_i[n]$  is the output signal of the  $i$ -th sub-band filter. The basic idea of FBSE is to assume that filter bank-based multi-carrier communication technique is used as the communication system of choice. The same filter bank can then be used for spectrum estimation. In this filter bank architecture, it is presumed that the filters at the receiver and transmitter side are a pair of matched root-Nyquist filters  $H(z)$  as shown in fig. 6.3 [122]. At the receiver end, the received signal is down-converted to baseband, low-pass filtered, and decimated [120] before it is finally forwarded to the root-Nyquist filter for data demodulation and spectrum estimation.

Comparing MTSE and FBSE, the later is usually better when the PSD is calculated for a large number of samples. On the other hand, when the available data samples are limited, then MTSE is preferable. Another important advantage of FBSE underlined in [120] is the possibility of

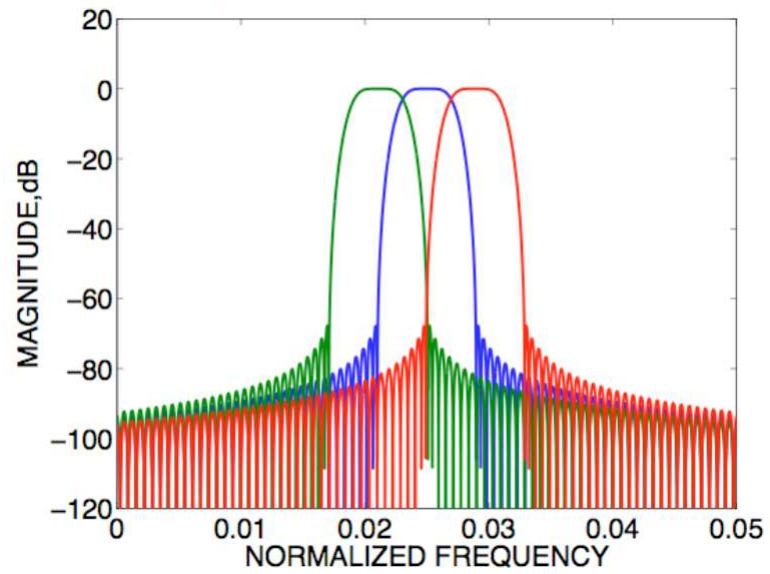


FIGURE 6.5: Optimally designed Root Nyquist Filter by Farhang-Boroujeny in [122] as prototype filter for FBSE.

applying FBSE as a multi-carrier modulator. This is possible due to the fact that the filter-bank in the receiver module can be used both for spectrum estimation and as well as for signal demodulation. More information on this topic is available in [120].

### 6-3 Wavelet packet spectrum estimator (WPSE)

In this section, we describe the proposed spectrum estimation approach based on discrete wavelet packet transform in greater detail. The motivation for using WP filters is manifold. First, the orthogonality of the filters ensures that the filtered outputs are not correlated and hence the bias in the estimates is reduced. Next, the DWPT, which is a lapped transform, allows the WP filters to overlap in time. This means that the WP filters can be of longer lengths with sharper transitions and localized frequency bands. Third, since all the WP filters are obtained by cascading low-pass filters, the variances in the estimates are inherently lower. Furthermore, the tree structure of WPSE can be adjusted to fine tune the frequency resolution, variance and bias in the estimates. For example, greater the levels of decomposition, more the number of sub-bands (or estimate points) and hence better the frequency resolution. Lastly, the wavelet families can be carefully chosen so as to improve the accuracy of the estimates.

#### 6-3-1 Wavelet packet representation

It is well known from the theory of wavelets that compactly supported wavelet can be derived from perfect reconstruction filter banks [8, 29, 31]. Two channel filter banks split the given signal into coarse (low-frequency) and detail (high-frequency) components. The high- and low-pass filters remove the lower- and upper-half frequency components, respectively. As a result, the output signal spans only half of the frequency band spanned by the input signal. However, the time scale of the signal remains unchanged. To retain the same number of samples, the filter outputs are down-sampled by a factor of 2. Therefore, one step decomposition process consisting of half band filtering and down sampling reduces the time resolution by a half and reduces the frequency band spanned by the signal by half as well. The scheme is then iterated successively on both the coarse and detailed versions until the desired degree of resolution to form a cascaded tree structure. The cascaded two channel filter banks structure recursively decomposes the signal being estimated and maps the signal components into the frequency domain. This process may be likened to passing the received signal into a bank of filters where the output point of each filter is a wavelet packet node. The output of each wavelet packet node corresponds to a particular frequency band. In fig. 6.6, a level-4 decomposition procedure generating 16 wavelet packet coefficients is illustrated. Fig. 6.6 also depicts the relationship between the order of wavelet packet node number and its frequency ordering for a 4-level decomposition. There are 16 nodes in the lowest level shown in fig. 6.6 corresponding to 16 frequency bands. These 16 frequency bands span the normalized frequency range  $[0, \pi]$  or  $[0\text{Hz}, 0.5f_s\text{Hz}]$ , where  $f_s$  Hz is the sampling frequency.

The decomposition of the signal into different frequency bands with different resolutions is possible. The resolution of the estimate can be adjusted by increasing or decreasing the number

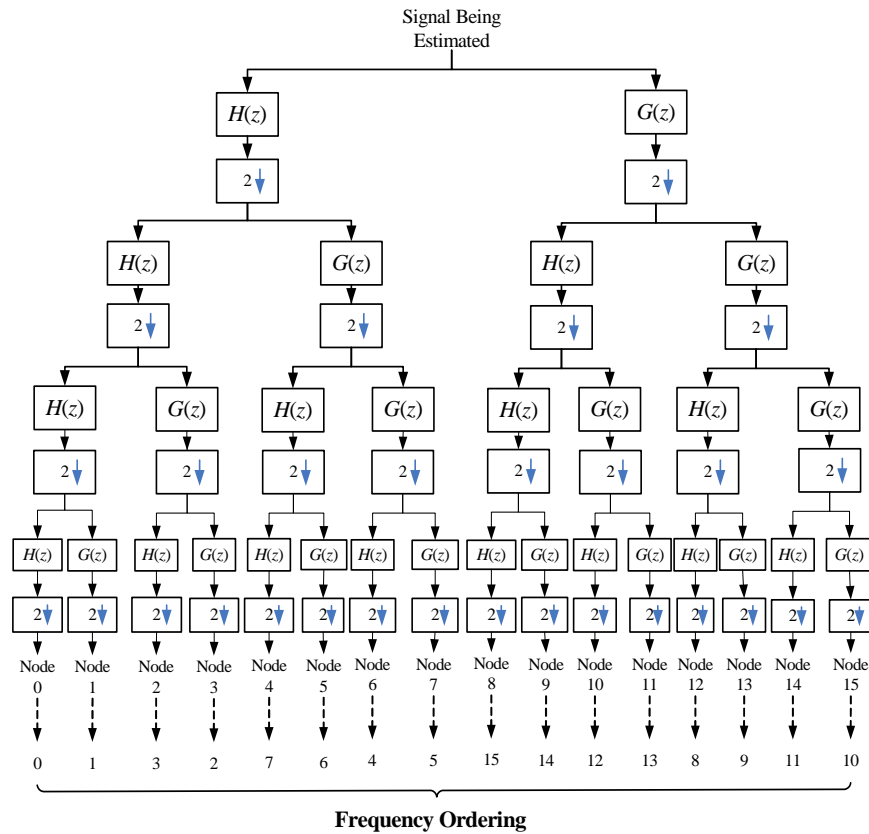


FIGURE 6.6: Wavelet packet tree for four levels wavelet packet decomposition. Here  $H(z)$  and  $G(z)$  denote the low- and high-pass decomposition filters, respectively.  $\downarrow$  represent decimation by 2. It should be noted that the coefficients of the wavelet packet transform are not ordered by increasing order of frequency. Gray code conversion is required to obtain the correct frequency order.

of decomposition levels. The greater the degree of decomposition, the better the frequency resolution is. The number of successions is usually limited by the desired level of frequency resolution and available computational power. An added advantage is that the output at every level can be chosen according to the desired frequency resolution.

### 6-3-2 Frequency ordering of wavelet packet coefficients

It is of utmost importance to identify the bands spanned by the wavelet packet coefficients and their relative frequency ordering. The coefficients of the wavelet packet transform are not naturally ordered by increasing order of frequency. Instead, they are numbered on the basis of a sequential binary gray code value [123].

To understand the working of the wavelet packet transform, consider the example shown in figs. 6.7 and 6.8 where the decomposition of a signal spanning 0 – 8 Hz is considered for

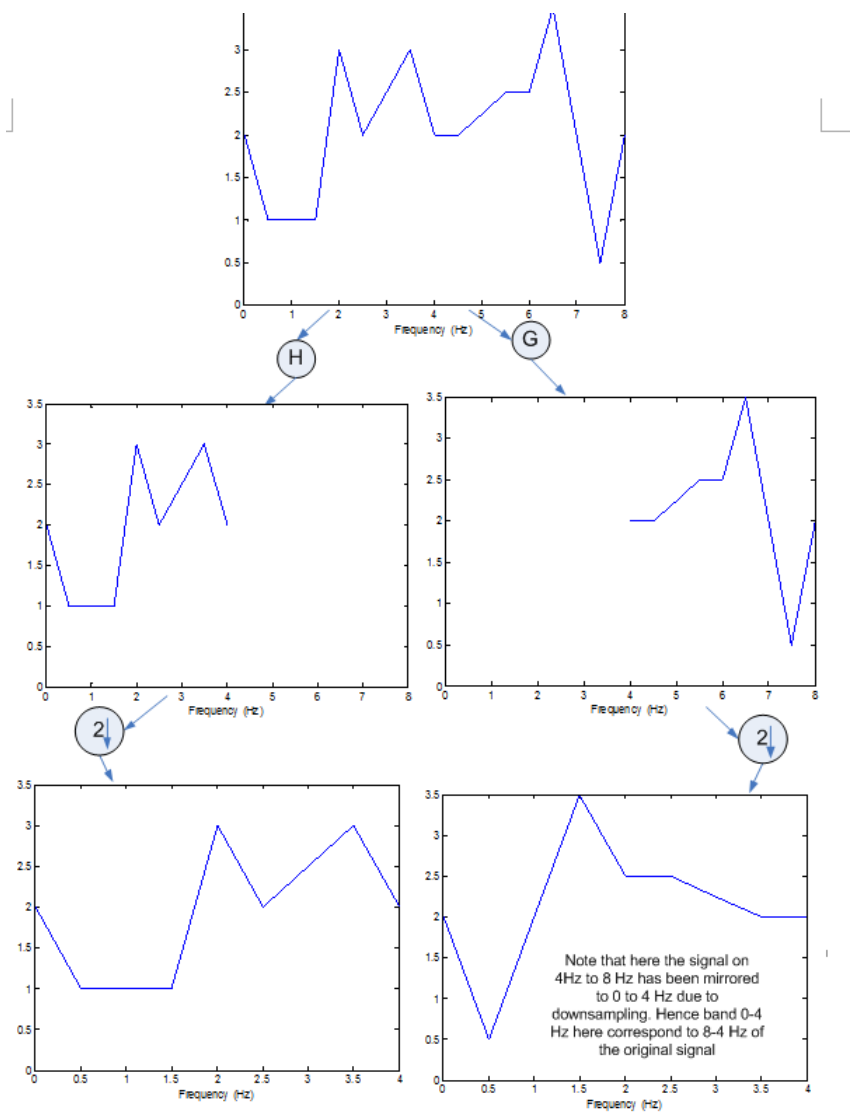


FIGURE 6.7: Level 1 Decomposition: Mirroring of high-pass components due to down-sampling. In the figure,  $2 \downarrow$  denotes down sampling by 2 [123].

up to two levels<sup>4</sup>. The output of a decomposition process is the result of the scaling (the low-pass filter) and the wavelet function (the high-pass filter) followed by down sampling. Down sampling generates two new filter results with half the number of elements in the time domain. In addition to this, it also results in mirroring of the high-pass components in the frequency domain. This swaps the low and high-pass components in a subsequent decomposition as exemplified in the figures.

<sup>4</sup>The discussion presented here is based on [123]

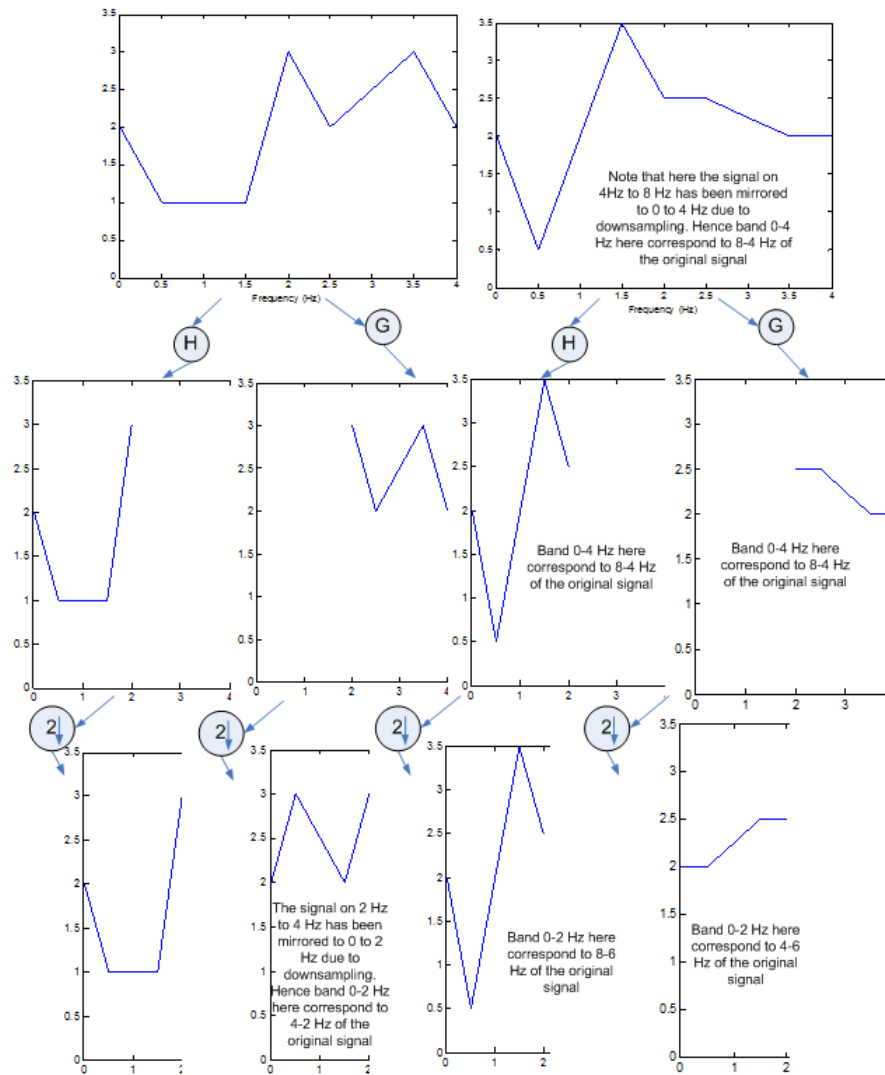


FIGURE 6.8: Level 2 Decomposition (continued from previous figure): The 2-levels wavelet packet decomposition is applied. Due to down sampling all the high frequency parts are mirrored. The low and high-frequency parts are swapped in a subsequent transform. In the figure,  $2 \downarrow$  denotes down-sampling by 2. Note that the output of the 1st wavelet packet node correspond to 0-2Hz, 2nd wavelet packet node correspond to 2-4Hz, 3rd and 4th node correspond to 6-8Hz and 4-6Hz respectively [123].

### 6-3-3 Re-ordering of wavelet packet coefficients

#### A. Gray to binary code conversion

When the wavelet packet algorithm is recursively applied the resultant wavelet packet coefficients obtained follow the Gray code sequence [123]. The binary to Gray code conversion formula is given as [123]:

$$GC(b_i) = (b_i + b_{i+1}) \text{ mod } 2. \tag{6.16}$$

Here,  $n$  is the decimal number  $n$  with a binary representation of the form of  $b_4b_3b_2b_1$  ( $b_1$  is the least significant bit and  $b_4$  the most significant bit).

Instead of the usual Gray Code Permutation, we here present an alternative algorithm to convert the sequence from Gray to binary. This method is computationally simpler and does not involve any binary to decimal conversion (or vice versa). If the wavelet packet nodes are in sequence (from the smallest number to the largest), the algorithm for obtaining the frequency band order can be stated as follows:

- Initialize a vector **alpha** with elements 0 and 1 (**alpha** = [0 1])
- Define the required level of wavelet packet decomposition  $L$
- For  $j = 2$  to  $L - 1$  do
  - **beta** = **alpha** + **2j**;
  - Flip the element of **beta**
  - Append **beta** at the end of **alpha**

### 6-3-4 Wavelet packet based spectrum estimation as a filter bank analysis problem

The WPSE can be considered as a natural extension to MTSE. The WPSE also uses different orthogonal filters as prototype filters. Akin to MTSE and periodogram, the WPSE estimates are the outputs of a bank of filter having a pass-band around that point. However, instead of Slepian sequences the WPSE filters are derived by cascading wavelet packet decomposition filters. However, in contrast to MTSE, these filters are realized by cascading several analysis low-pass and/or high-pass filters, which are derived from single prototype according to two scale equations and quadrature mirroring. The impulse response of these cascaded filters, called the wavelet packet duals, can be represented as:

$$\Omega_i[k] = \xi_l^i[k] = \beta[k] * \beta[2k] * \dots * \beta[2^{l-2}k] * \beta[2^{l-1}k] \quad (6.17)$$

where  $0 \leq i \leq 2^l - 1$  and  $\beta[k]$  are the branch filters given as:

$$\beta[k] = \begin{cases} h[k], & \text{for low - pass branch} \\ g[k], & \text{for high - pass branch} \end{cases} \quad (6.18)$$

Fig. 6.10 presents the proposed wavelet packet based spectrum estimator as a filter bank. In this figure the decomposition level is 3 which results in 8 estimation points. The eight cumulative filters divide the normalized frequency range  $[0, \pi]$  into 8 equal sub-bands. Higher the levels of

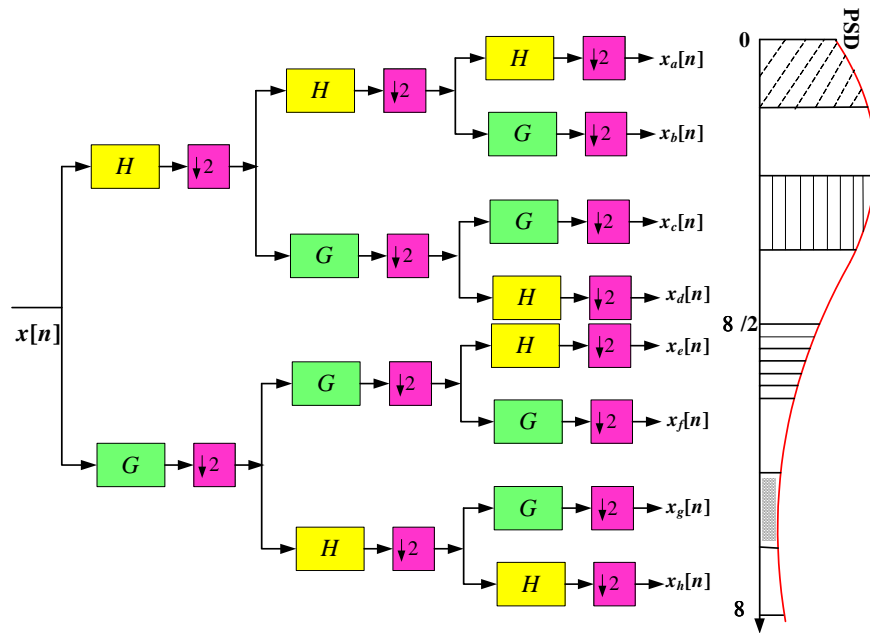


FIGURE 6.9: Wavelet packet decomposition of a signal. Here  $H$  and  $G$  denote the frequency responses of the low- and high-pass decomposition filters, respectively. The down-arrows  $\downarrow$  represents decimation by 2. The  $x_i$ 's denote the wavelet packet coefficients. Besides the decomposition, the Power Spectral Density (PSD) of the decomposed signal components in successive octave bands normalized to the Nyquist frequency is shown. The order of filter in each level is modified in order to match frequency ordering from 0 to  $\pi$ .

decomposition more the number of sub-bands (or estimate points) and thus greater the degree of frequency resolution.

**B. Modified wavelet packet tree structure**

A more convenient approach is to avoid this Gray to binary conversion altogether by modifying the WPSE tree structure [123]. Fig. 6.9 illustrates the modified structure of the wavelet packet tree (3-level of decomposition) in order to match the frequency ordering. We can note the difference of this structure with the first 3 level of the tree shown in fig. 6.6, especially the order of analysis low-pass filter  $H$  and high-pass filter  $G$  in each level.

**6-3-5 Wavelet packet transform and energy conservation**

The relationship between the amplitude of the signal and wavelet coefficients has to be established to develop the wavelet packet spectrum estimator. The Parseval relation proves that the Fourier transform is a lossless unitary transform. Likewise, we need to assert if the wavelet

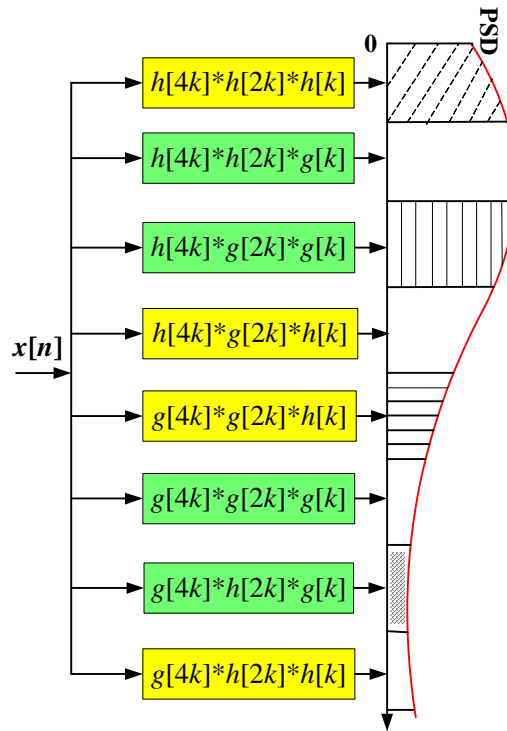


FIGURE 6.10: Wavelet packet based spectrum estimation concept from the point of view of filter bank paradigm. Here 3-level decomposition is employed resulting in 8 virtual filters splitting the normalized frequency band  $[0, \pi]$  into eight sub-bands corresponding to eight estimate points.

packet transforms preserves energy too. In order to ascertain this relation, we start by representing a function  $f(x)$  in Hilbert Space as the linear combination of the basis functions  $\varphi_i(x)$ :

$$f(x) = \sum_i \alpha_i \varphi_i(x) \quad (6.19)$$

Here  $\alpha_i$  can be obtained from the inner-product of the basis functions  $\varphi_i(x)$  and the studied signal  $f(x)$ :

$$\alpha_i = \langle \varphi_i(x), f(x) \rangle \quad (6.20)$$

The norm of the function can be computed from the transform coefficients:

$$\|f(x)\| = \sum_i |\alpha_i|^2 = \sum_i |\langle \varphi_i(x), f(x) \rangle|^2 \quad (6.21)$$

By assuming that a function  $g(x)$  has transform coefficients  $\beta_i$ , we can derive the generalized Parseval equation by taking the inner product between two functions  $f(x)$  and  $g(x)$  in Hilbert Space:

$$\langle f(x), g(x) \rangle = \sum_i \bar{\alpha}_i \beta_i = \sum_i \langle f(x), \varphi_i(x) \rangle \langle \varphi_i(x), g(x) \rangle \quad (6.22)$$

Here,  $\overline{\alpha_i}$  denotes the complex conjugate version of  $\alpha_i$ . According to Todorovska and Hao [124], the Parseval relation for Discrete Orthogonal Wavelet Transform and its inverse is obtained by substitution on generalized Parseval Equation in the above expression. The forward and inverse discrete wavelet transforms for the discrete signal  $x[n]$  can be represented as follows [124]:

$$x[n] = \sum_{k=1}^{N/2^J} c(J, k) \varphi_{J,k}[n] + \left( \sum_{j=1}^J \sum_{k=1}^{N/2^j} d(j, k) \psi_{j,k}[n] \right) \quad (6.23)$$

$$\begin{aligned} c(J, k) &= \langle \varphi_{J,k}[n], x[n] \rangle \quad \text{and} \\ d(j, k) &= \langle \psi_{j,k}[n], x[n] \rangle \end{aligned} \quad (6.24)$$

In eqs.(6.23) and (6.24),  $J$  is the decomposition level and  $N$  is the total number of samples. These expressions are known as the synthesis and analysis equations, respectively. The first component in eq.(6.24) is the coarse part of signal  $x[n]$ , which is represented as a linear combination of the scaling function  $\varphi_{J,k}[n]$ . On the other hand, the second part of eq.(6.24) is the detail version of  $x[n]$ , which is represented as a linear combination of wavelet functions  $\psi_{j,k}[n]$ . If we consider another signal,  $y[n]$  with  $d^{(i)}(j, k)$  and  $c^{(i)}(J, k)$  as its wavelet packet coefficients, the Parseval relation for  $y[n]$  and  $x[n]$  can be described as:

$$\langle x[n], y[n] \rangle = \sum_{n=-\infty}^{\infty} x[n]y[n] = \left( \sum_{j=1}^J \sum_{k=1}^{N/2^j} d^{(i)}(j, k) d(j, k) \right) + \left( \sum_{k=1}^{N/2^J} c^{(i)}(J, k) c(J, k) \right) \quad (6.25)$$

Taking  $x[n] = y[n]$ , the Parseval relation in terms of the norm of  $y[n]$  can be given as [124]:

$$\|y[n]\|^2 = \sum_{n=-\infty}^{\infty} |y[n]|^2 = \left( \sum_{j=1}^J \sum_{k=1}^{N/2^j} |d(j, k)|^2 \right) + \sum_{k=1}^{N/2^J} |c(J, k)|^2 \quad (6.26)$$

This clearly shows that the wavelet transform is a lossless transform and there is no loss of energy when we transform the time-domain data to the wavelet domain. This feature is a fundamental reason why a spectrum estimator based on wavelets can be built. Parseval's relation holds well for both conventional discrete wavelet transform and wavelet packet decomposition.

### 6-3-6 Calculating power spectrum density from wavelet packet coefficients

Since the Wavelet packet transform obeys the Parseval relationship, we can obtain the wavelet based spectrum estimates. Considering that the wavelet packet nodes span the frequency band

$[0 \ 0.5f_s]$ , where  $f_s$  is the sampling frequency, and that the levels of wavelet packet decomposition is  $n$  there will be  $2^n$  wavelet packet nodes. This decomposition will divide the band  $[0 \ 0.5f_s]$  into  $2^n$  equal bands.

The power spectrum density estimate  $\widehat{S}_{xx}^{WPM}(f_k)$  of the frequency band spanned by the  $k$ th WP can be calculated from the energy  $\Phi(f_k)$  detected in the  $k$ th band as follows:

$$\widehat{S}_{xx}^{WPM}(f_k) = \frac{\Phi(f_k)}{N_s f_k} (\text{watt}/(\text{radian}/\text{sample})); \text{ where } 1 \leq k \leq 2^C. \quad (6.27)$$

Here  $N_s$  connotes the number of input samples. With these steps the WP indices can be mapped to their respective frequency bins and an accurate estimation of the radio spectrum can be performed.

## 6-4 Optimizations to wavelet packet implementation

We now present the Enhanced WPSE (E-WPSE) which fine tunes the operation of WPSE by bringing in a couple of improvisations. These optimizations correct artifacts which inherently occur in WPSE and lead to significant gains.

### 6-4-1 Enhanced WPSE to mitigate edge artifacts

Before presenting the details of the E-WPSE, it will be useful to take a closer look at the standard implementation of the Wavelet Packet algorithm again. Supposing that the input signal  $x[n]$  is of length  $N_s$  (with  $N_s$  taken to be even for convenience) and if we take the length of the filters  $h$  and  $g$  to be  $L$ , then the down-sampled sub-band signals  $x_h[n]$  and  $x_g[n]$  (connoting low- and high-pass branch outputs, respectively) will each be of length  $(L + N_s)/2$ . However, if the length of the samples before and after the wavelet packet operation is to be kept constant then the lengths of sub-band signals  $x_h[n]$  and  $x_g[n]$  have to be  $N_s/2$  (see fig. 6.11). To do so the standard wavelet packet implementations drop the  $L/2$  sub-band samples near the edges which exceed the length  $N_s/2$ . Naturally, this abrupt truncation of the data samples results in aberrations like ringing around the edges and produces spurious high frequency components leading to inaccurate estimation.

In order to correct this artifact we avoid the excessive length by adding the last  $L/2$  samples of each sub-band signal to the first  $L/2$  samples (see fig. 6.12). This periodic extension is similar to the use of cyclic prefix in OFDM and is a most convenient fix to the problem of edge based artifacts and ringing. We call the new method Enhanced WPSE or E-WPSE.

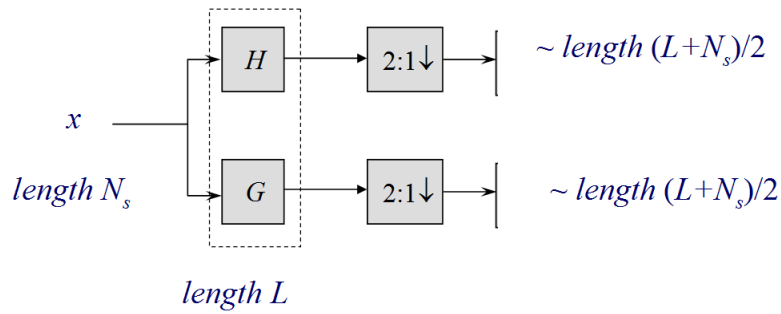


FIGURE 6.11: Two-channel filter bank implementation: convolution operation and increased sample lengths.

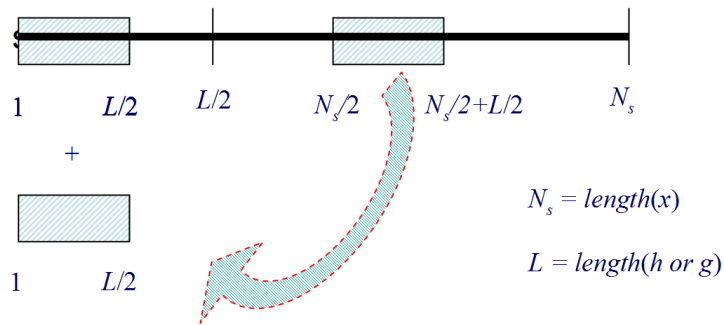


FIGURE 6.12: Two-channel filter bank implementation: periodic extension to fix edge-based artifacts.

### 6-4-2 Enhanced WPSE with padding

A requirement in the implementation of E-WPSE is that the number of samples at each level of the WP tree is even. This means that for a level- $C$  decomposition the number of data samples considered must be a multiple of  $2^C$ . If this is not the case, then the input samples should be padded with additional bits to make the data length a multiple of  $2^C$ . The padding can be done in two ways. In the first method, the additional bits are added to the input data before the decomposition process. In this regard three approaches are considered, namely, zero padding (ZP), cyclic prefix (CP) padding and symmetric padding (SP). Assuming  $N$ -length samples for  $N < \alpha \cdot 2^C$  where  $\alpha$  is the smallest integer leading to a multiple of  $2^C$ , the zero padding is performed by appending  $\alpha \cdot 2^C - N$  zeros at the end of the received samples. When cyclic prefix is used, the last  $\alpha \cdot 2^C - N$  samples of the received sequences  $x[n]$  are copied and prefixed to the original sequences. The data sequence can be given as:

$$x[N - (\alpha \cdot 2^C - N - 1)] \dots x[N - 1] x[N] x[0] x[1] \dots x[N - 1] x[N].$$

In symmetric padding, the last  $\alpha \cdot 2^C - N$  samples of the received sequences  $x[n]$  are copied and then flipped before they are suffixed to the data samples. The order of the sequences can be given as:

$$x[0] x[1] \dots x[N - 1] x[N] x[N] x[N - 1] \dots x[N - (\alpha \cdot 2^C - N - 1)].$$

In the second scheme of padding, instead of adding all the extra bits before the decomposition process, a single bit is added only to those decomposition stages where the number of samples is odd. For example, a sequence  $x[n]$  having 38400 samples passed into the wavelet packet tree with 11-level of decomposition will not require one-bit pad during the decomposition process up to level-9. However, at level-10 and level-11, one bit pad will be required. In this work, the additional bit used is a zero bit.

## 6-5 Experiment scenarios, sources and their characteristics

In order to investigate the performance of the wavelet packet based spectrum estimation technique, four different types of sources are considered, namely, partial-band, single-tone, multi-tones and swept-tone. The test sources are so chosen that they shed different insights into the operation of the spectrum estimation tool. The partial-band source (see fig. 6.13-A) has its energy spread over a continuous range of frequencies and occupies the normalized frequency band from  $0.25\pi$  to  $0.75\pi$ . The partial band source is implemented as a OFDM system with the number of carriers adjusted according to the bandwidth considered for the study. The single tone source (see fig. 6.13-B) has all of its energy at one frequency and is in the middle of the frequency range spanned by the WPSE, namely at  $0.5\pi$ . The multi-tones source (see fig. 6.13-C) consists of seven equi-spaced single tones located from  $0.125\pi$  to  $0.875\pi$ .

Finally, a swept tone source (refer fig. 6.14) is introduced to measure how well the estimation schemes perform when there are temporal variations in the bands occupied by the data source. The swept tone source is a chirp signal in which the frequency increases ('up-chirp') with time. After a sweep of incremental chirps the signal winds back to the original frequency to start with the next sweep cycle.

Table 7.2 summarizes the description of sources used in the experiment.

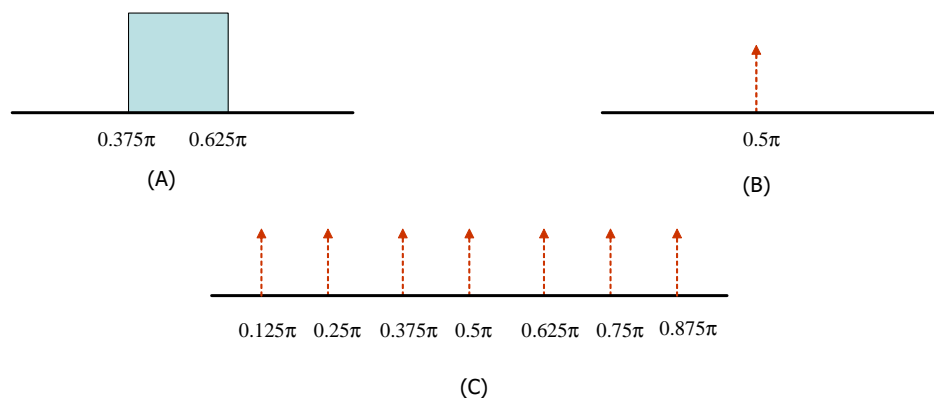


FIGURE 6.13: Sources and their characteristics. The sources considered are: (A) Partial Band, (B) Single-tone and (C) Multiple Tone.

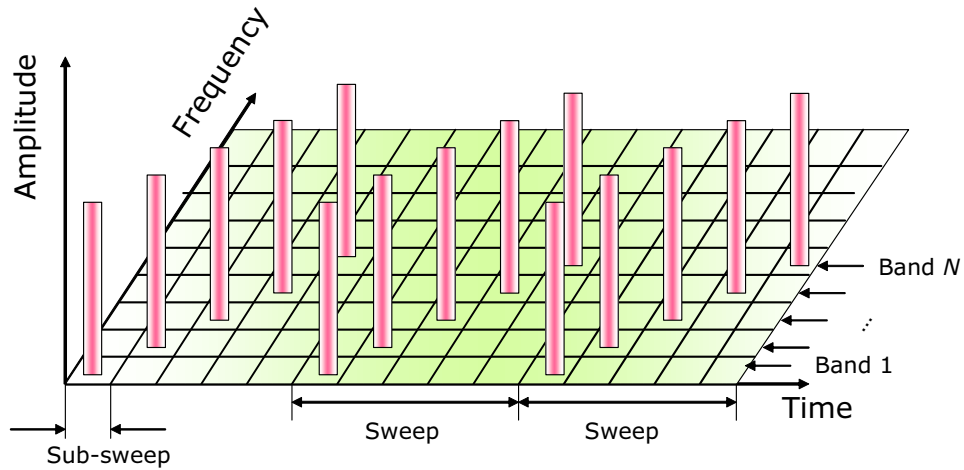


FIGURE 6.14: Swept Tone Source.

Type of sources	Description
Partial band	Consists of a partial band source occupying the normalized frequency range $[0.375, 0.625\pi]$ . (See fig. 6.13-A)
Single tone	A single tone at normalized frequency $0.5\pi$ . (See fig. 6.13-B)
Multi-tone	Consists of 7 single tones occupying the normalized frequencies occurring at $0.125\pi, 0.25\pi, 0.375\pi, 0.5\pi, 0.625\pi, 0.75\pi$ and $0.875\pi$ . (See fig. 6.13-C)
Swept tone	Consists of a source which occupies different frequency bands at different time instances. A total of 20 sweeps (each of 640 samples) covering the frequency band of $[0.2\pi, 0.8\pi]$ is considered. (See fig. 6.14)

TABLE 6.1: Description of test sources.

For the WPSE, a level-7 decomposition tree is considered. Several wavelet families are investigated namely Daubechies families, Coiflet, Symlet, Discrete Meyer, Biorthogonal and Reverse Biorthogonal. The WPSE results are compared with existing techniques such as Welch, Periodogram estimates, periodogram with windowing (Hann, Hamming and Blackman) and MTSE. In Welch, the input samples are divided into smaller segments and the periodogram for each segment is computed.

The number of data samples considered in the experiments is 12800. The Welch estimate is obtained by dividing the received samples into 399 segments of 64 samples each. Consecutive segments of the samples overlap with one-another by 50%. Before the averaging of data samples a Hamming window is applied on each segment. To gauge the swept tone source, 20 sweeps (each of 640 unit samples) are considered. The sweep spans the normalized frequency band

$[0.2\pi, 0.8\pi]$ . In order to present the effect of highly time-varying frequency on spectrum estimation, the estimate for five portions of a single sweep is displayed. The estimation technique depicts the first 128 unit samples of a single sweep followed by the next 128 unit samples of the same sweep and so on until the fifth 128 unit samples of the same sweep.

## 6-6 Results and analysis

In this section we present the results of our study on using WPSE to estimate different kinds of data sources.

### 6-6-1 Partial band source estimation

In the estimation of partial band sources the performance of the candidate techniques are gauged using four performance metrics, namely,

- side lobe suppression,
- variance of the estimated PSD in pass-band ,
- variance of the estimated PSD stop band,
- and transition between pass-band and stop-band (transition band).

The best system is one which yields good side lobe suppression, low stop/pass-band variance and a narrow transition band. Indeed all these desirable properties may not be realized at the same instance and one may have to trade-off between the desirables to select the best system.

#### A. Comparison with Welch and Periodogram estimators

We first compare the performance of the WPSE with Welch and Periodogram techniques. Fig. 6.15 depicts the estimates of a partial band source with Periodogram, Welch and WPSE estimators (employing Daubechies wavelets). For the sake of clarity only two decomposition levels are presented. The number of data samples considered in the experiment is 12800.

From the plots we may notice that the Periodogram estimates have a good resolution but have large variances in the pass-band. The Welch estimator divides the data samples into smaller segments, calculates the local periodogram of each segment and then averages them to arrive at the final estimate. Hence, the variances in the PSD estimates are low; however, the averaging of the estimates results in loss of information on sharp transitions in the studied signal. Of interest

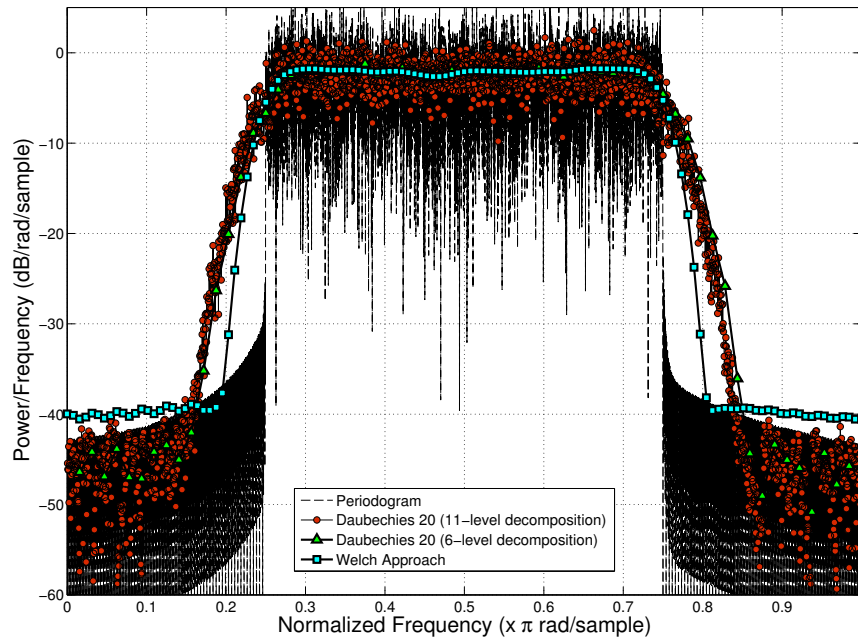


FIGURE 6.15: PSD estimates of the partial band source with Periodogram, Welch and WPSE (Daubechies 20 wavelet) estimators. The number of data samples considered is 12800. In the Welch estimator the data samples are windowed (Hamming) into smaller segments of 64 samples each with an overlap of 50%.

is the WP approach where one may increase or decrease the decomposition levels to achieve the desired variance versus frequency resolution trade-off.

When the performance of the WPSE is compared to Fourier-based periodogram, the transition band of the periodogram output is sharper. However, on account of the variance of the estimated PSD the WPSE performs significantly better than the periodogram. This is crucial in radio transmission where large variances in the estimate could lead to erroneous judgements on the presence/absence of sources. Hence, in the metric of variance of estimated PSD, it can be said that orthogonal wavelet based estimate is preferable in comparison to the periodogram for partial band source estimation.

Comparing WPSE and Welch, the Welch technique performs marginally better. The averaging of estimates in the Welch plays an important role in ensuring that the PSD has a small variance even when maintaining sharp transition bands. However, it may be noted that the transition band guaranteed by Welch is only fractionally better than that found in WPSE using the Discrete Meyer wavelet<sup>5</sup>. This implies that there is scope for further improvement in WPSE performance when the length of the wavelet filter is increased.

In the metric of stop band suppression, the level of estimated power in the unoccupied bands for Welch is higher than that of WPSE or periodogram. This is a direct consequence of the data partitioning carried out in Welch which results in lower number of samples available for

<sup>5</sup>Length of Discrete Meyer filter length is 102

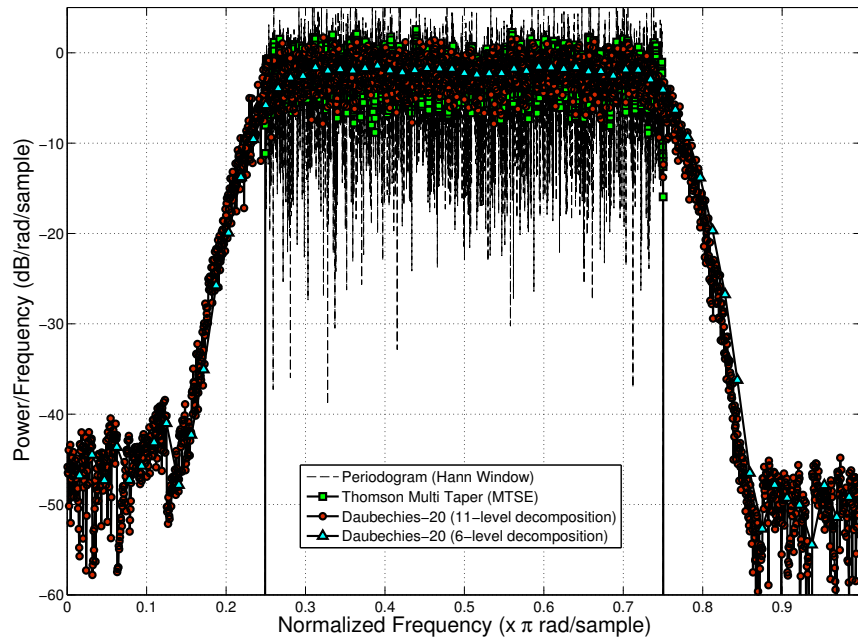


FIGURE 6.16: PSD estimates of partial band source according to two different decomposition level of frequency selective wavelet based approach, Thomson's MTSE and Periodogram using Hann window. The number of samples in this experiment is 12800.

estimation. Consequently, the Welch introduces a wider main lobe in its window kernel and causes more leakage than the periodogram. The WPSE offers better rejection than both Welch and periodogram in the unoccupied frequency bands and also decays fast in the stop band.

### B. Comparison with windowed Periodogram and MTSE methods

Applying the window to the periodogram (plots presented in figs. 6.16 and 6.17) reduces the side lobes and hence leakage into the stop bands. However, it does not solve the problem of large variances in the pass band. In fact, all the windowed-periodogram outputs have variances much larger than WPSE. Lastly, the MTSE offers excellent frequency resolution but they too suffer from large variances.

### C. Impact of wavelet families

In this set of experiments the influence of wavelet families on the performance of WPSE is evaluated. Several well-known wavelet families including Daubechies-15, Coiflet-5, Symlet-15, Discrete Meyer, Biorthogonal-3.9, Reverse and Biorthogonal 3.9 are investigated. Daubechies-15, Coiflet-5 and Symlet-15 have a filter length of 30. On the other hand, Discrete Meyer has filter length of 102 while both Biorthogonal3.9 and Reverse Biorthogonal 3.9 have filter length of 20.

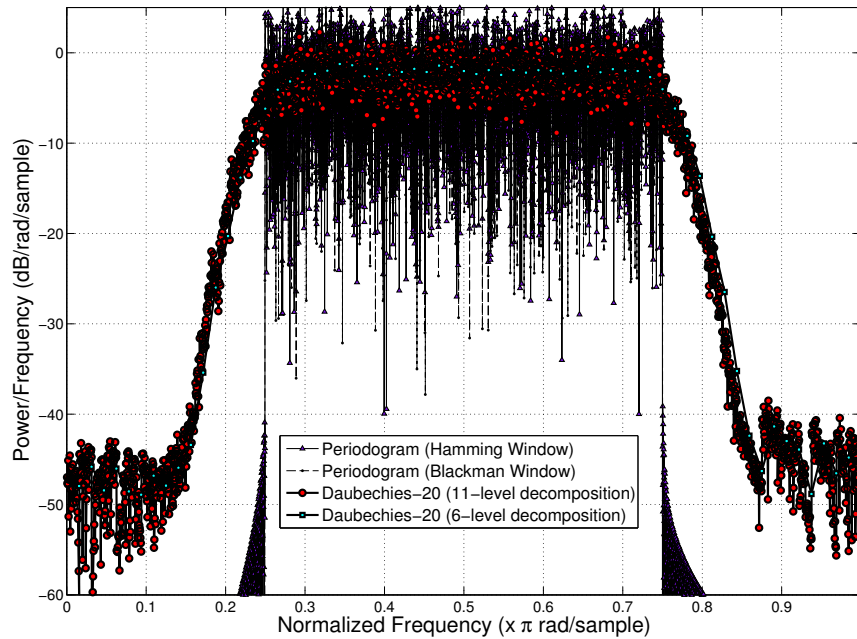


FIGURE 6.17: PSD estimates of partial band source according to different decomposition level of frequency selective wavelet based approach together with Periodogram using Hamming and Blackman window. The number of samples in this experiment is 12800.

Figs. 6.18 and 6.19 depict the performances of various wavelet families for WPSE. Welch and periodogram results have also been provided as reference. The figures show that Discrete Meyer wavelet has the best performance amongst all wavelet families. However, it should be noted that the length of the Discrete Meyer filter is 102 and thus exacts a higher cost of implementation. It may also be noted that the performance of non-orthogonal wavelet families (Biorthogonal 3.9 and its reverse counter part) is very bad and hence unsuitable for WPSE applications.

#### D. Impact of wavelet lengths

Fig. 6.20 illustrates the effect of filter length on the performance of the WPSE. In this case, the Daubechies family is selected for the experiment. It should be noted that the length of the filter is twice the index of the wavelet. For example, Daubechies-4 has filter length of 8. It should also be noted that Haar is actually Daubechies-1 and has a filter length of 2. From the figure, it is evident that the longer the filter length, the smaller the transition band. Longer filter length also corresponds to a better suppression of power in the unoccupied bands. However, a higher price is paid for the implementation.

#### E. Impact of decomposition levels

In fig. 6.21, WPSE estimates at four different decomposition levels, namely level-5, level-7, level-9 and level-11, are displayed. Of interest is the change in the variance and resolution of

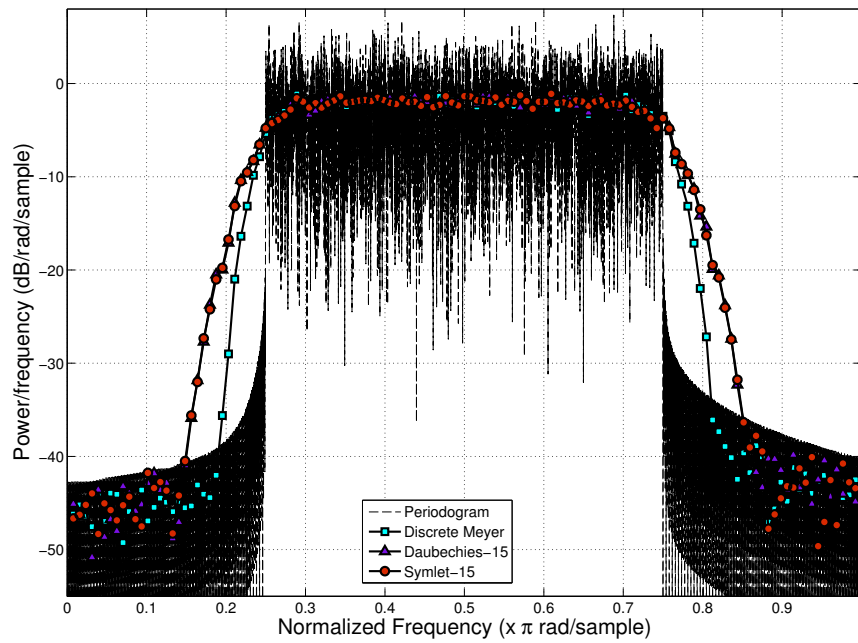


FIGURE 6.18: Periodogram and wavelet based estimates (Daubechies 15, Symlet 15, Frequency Selective (Length =30), Discrete Meyer) for partial band source.

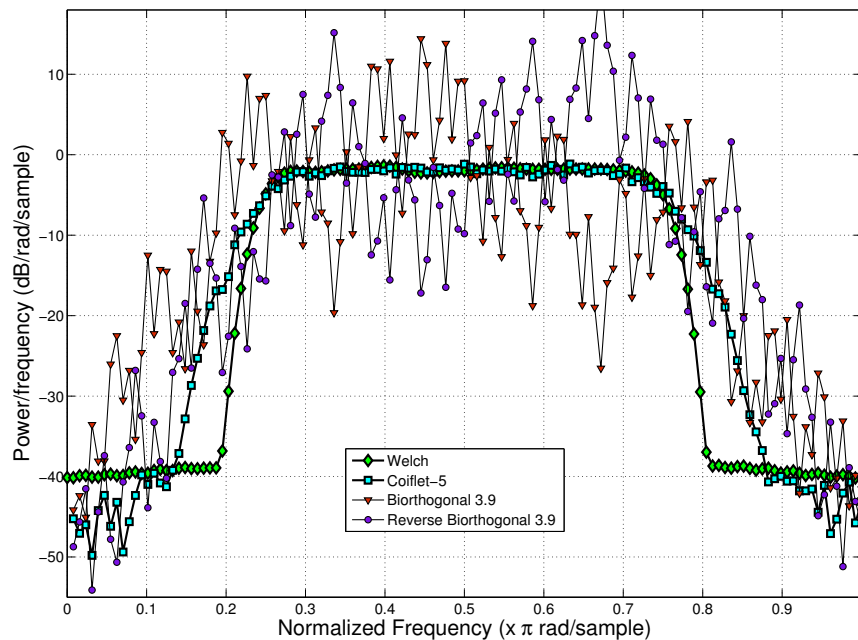


FIGURE 6.19: Welch and wavelet based estimates (Coiflet-5, biorthogonal 3.9, and reverse biorthogonal 3.9) for partial band source. The number of samples in this experiment is 12800. The overlap percentage and the length of each segment employed in Welch is 50% and 64 samples, respectively. Hamming window is used in the Welch estimation. A level-7 decomposition tree is used for WPSE.

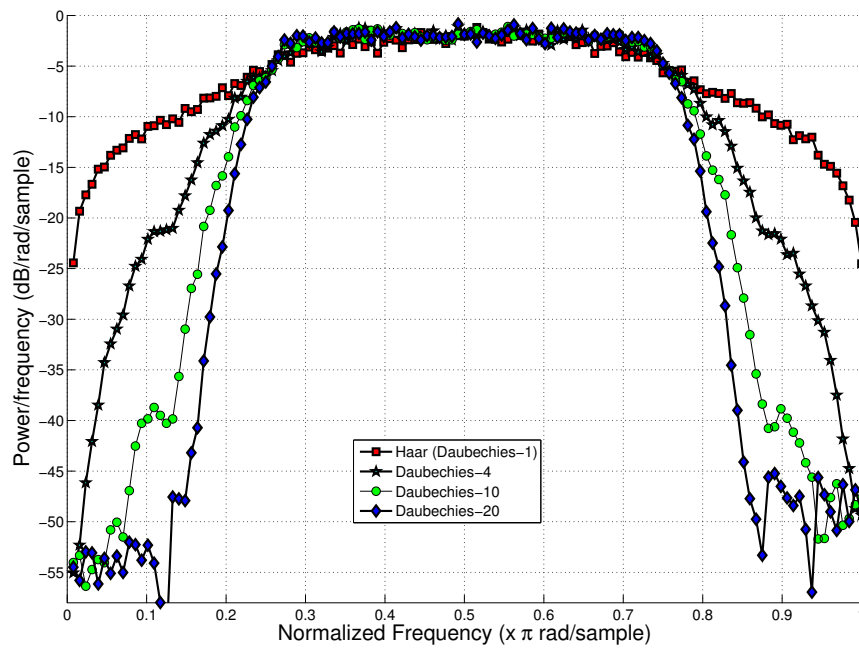


FIGURE 6.20: Wavelet based estimates for partial band source using Daubechies family with different filter length. A level-7 decomposition tree is used for WPSE. The number of samples in this experiment is 12800.

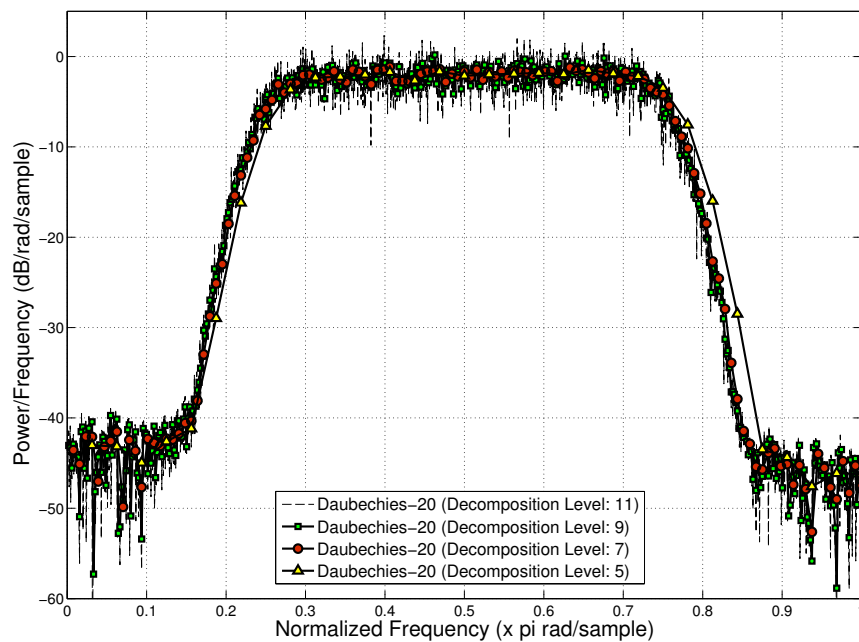


FIGURE 6.21: PSD estimates of partial band source according to various decomposition level of Frequency Selective Wavelet of length 30. The number of samples in this experiment is 12800.

Estimation Tech- nique	Side-lobe suppression	Variance in pass-band	Transition band	Variance in stop band
Welch	$\approx$	-	$\approx$	-
Periodogram	-	++	-	++
Periodogram with Window	-	++	-	++
MTSE	-	+	-	+

TABLE 6.2: Comparison of WPSE performance with other techniques for estimation of a partial-band source. The notations +, - and  $\approx$  indicate whether the WP approach performs favorably, negatively or similar, respectively, in comparison to the other method.

the estimated PSD with increasing/decreasing number of decomposition levels. With a decrease in the depth of signal decomposition, the variance of the estimated PSD is reduced. This is to be expected because for lower number of data decompositions, wider bands are spanned by the wavelet packet nodes. On the other hand, the total energy contained in a single wavelet packet node would be averaged over larger frequency band resulting in smaller variances in the estimates.

Table 6.2 summarizes the performance comparison of the WPSE with other techniques for the estimation of a partial-band source. The notations +, - and  $\approx$  indicate whether the WP approach performs favorably, negatively or similar, respectively, in comparison to the other method.

### 6-6-2 Single-tone source estimation

With regard to the estimation of single tone source, the performance metrics used are:

- variance of the estimated power spectrum density (PSD),
- mean power in stop band,
- frequency resolution, and
- leakage suppression or power rejection in the unoccupied band (side-lobe suppression).

The number of samples in these experiments is 12800 while the configuration of Welch method used here is the same as in the case of partial band source. The same wavelet families as employed for the study of partial band sources are also employed here.

#### A. Comparison with Welch and Periodogram methods

Fig. 6.22 shows the Periodogram, Welch and WPSE estimates for the single tone source. From the figure, it can be noted that the variance of the WPSE estimates are far lower than that of

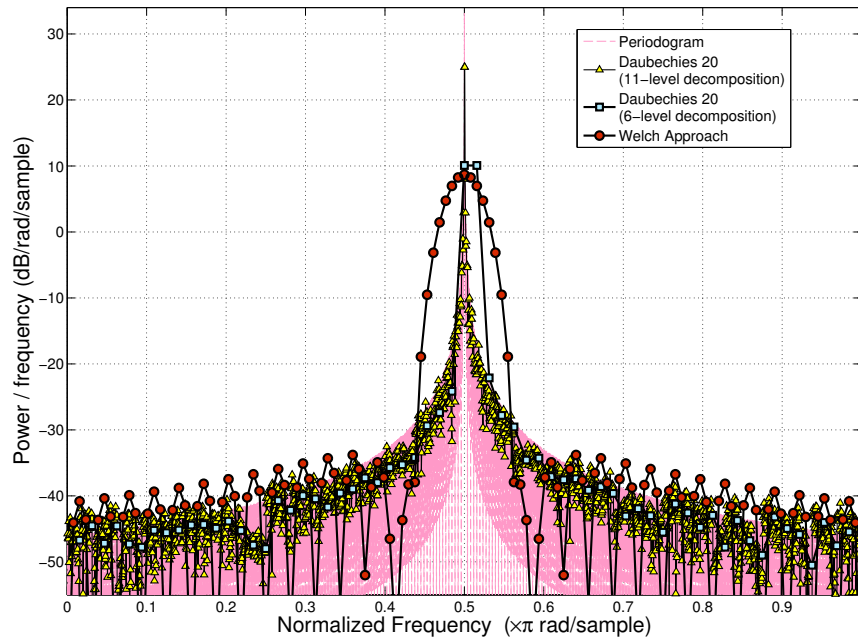


FIGURE 6.22: PSD estimation of single tone source with WPSE, Periodogram and Welch methods. The number of samples considered in this experiment is 12800. The overlap percentage and the length of each segment employed in Welch is 50% and 64 samples, respectively. Hamming window is used in the Welch estimation.

Periodogram. The plots also show that the resolution offered by WPSE is better than that of Welch. The averaging of estimates in Welch, which results in lower variance of partial band estimates, is also the reason for the poor frequency resolution in the estimation of single tone source <sup>6</sup>. On the other hand the periodogram estimates offer a very good frequency resolution and side lobe suppression which are comparable to the wavelet based estimates. However, the variances in the periodogram estimates remain high.

The results of these studies also exemplify the fact that the wavelet based estimates have characteristics in between that of periodogram (excellent frequency resolution but large stop band variance) and Welch (low stop band variance but poor frequency resolution). The WPSE can be made to operate between the strengths of the Welch (low variance) and periodogram (excellent resolution) estimations without compromising too much on either of these metrics by merely increasing/decreasing the levels of decomposition.

## B. Comparison with windowed-Periodogram and MTSE techniques

Figs. 6.23 and 6.24 show the impact of windowing on the reduction of side lobe level of the Periodogram estimates. Periodogram with Hann, Hamming and Blackman windows offer better marginally better frequency resolution than WPSE. The MTSE also offers a good frequency resolution and side lobe rejection.

<sup>6</sup>Averaging results in smearing of peaks and transitions of the studied data

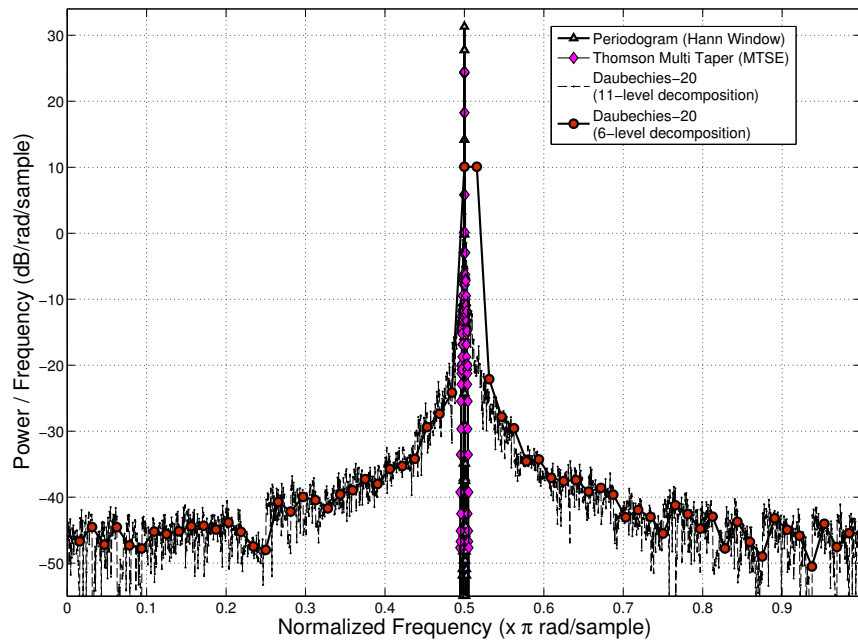


FIGURE 6.23: PSD estimation of single tone source with WPSE, Thomson's MTSE and Periodogram using Hann window. The number of data samples considered is 12800.

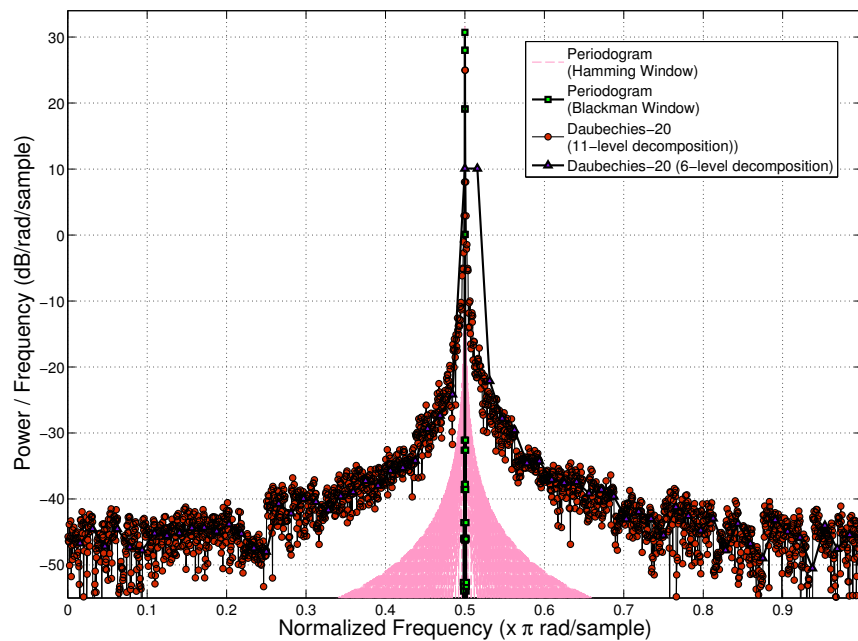


FIGURE 6.24: PSD estimation of single tone source with WPSE, Periodogram with Hamming window and Blackman window. The number of samples considered is 12800.

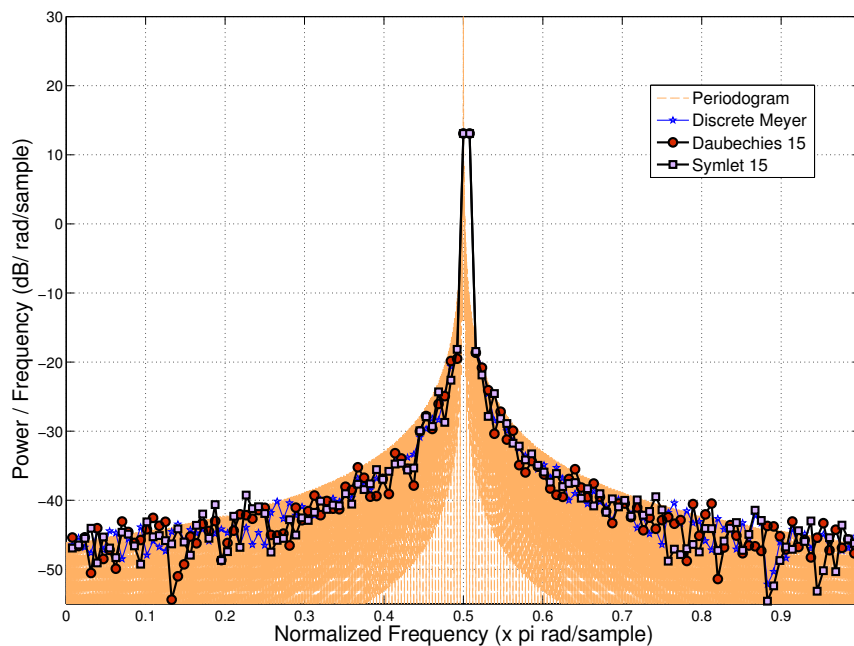


FIGURE 6.25: Periodogram and WPSE (Daubechies 15, Symlet 15, Discrete Meyer) for single tone source. The number of samples in this experiment is 12800. A level-7 decomposition tree is used for WPSE.

### C. Impact of wavelet families

Figs. 6.25 and 6.26 depict the WPSE estimates with various wavelet families for the estimation of single tone source. Welch and periodogram estimates have also been provided to serve as a reference. As expected, the Discrete Meyer wavelet, having longer filter length, performs better than other wavelet families. However, in terms of frequency resolution, all orthogonal wavelet based estimates perform similarly. The performance of biorthogonal wavelets is poor making them unsuitable candidates.

### D. Influence of filter length

Fig. 6.27 illustrates the effect of filter length on the performance of the wavelet based estimates. There is no clear correlation between the length of filter and the frequency resolution of the WPSE. However, on account of the variance of estimate in the stop band, a clearer pattern emerges - the longer the decomposition filters the smaller the variance of the power in the stop band.

### E. Influence of decomposition level

Fig. 6.28 shows the plots for the single tone source estimation with WPSE at different decomposition levels. The results show that WPSE structures of higher decomposition levels lead to

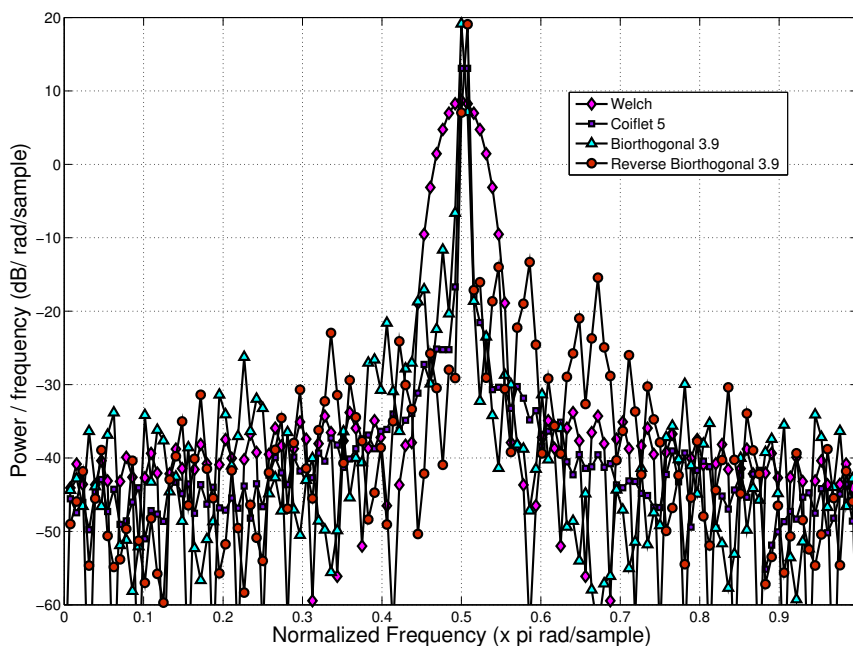


FIGURE 6.26: Welch and wavelet based estimates (Coiflet-5, biorthogonal 3.9, and reverse biorthogonal 3.9) for single tone source. The number of samples in this experiment is 12800. The overlap percentage and the length of each segment employed in Welch is 50% and 64 samples, respectively. Hamming window is used in the Welch estimation. A level-7 decomposition tree is used for WPSE.

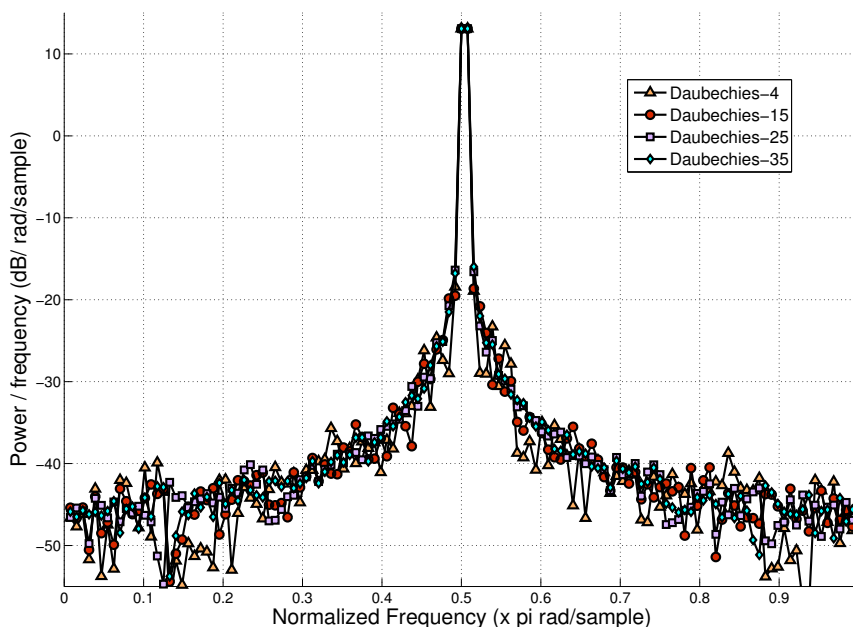


FIGURE 6.27: Wavelet based estimates for single tone source using Daubechies family with different filter length. A level-7 decomposition tree is used for WPSE. The number of samples considered is 12800.

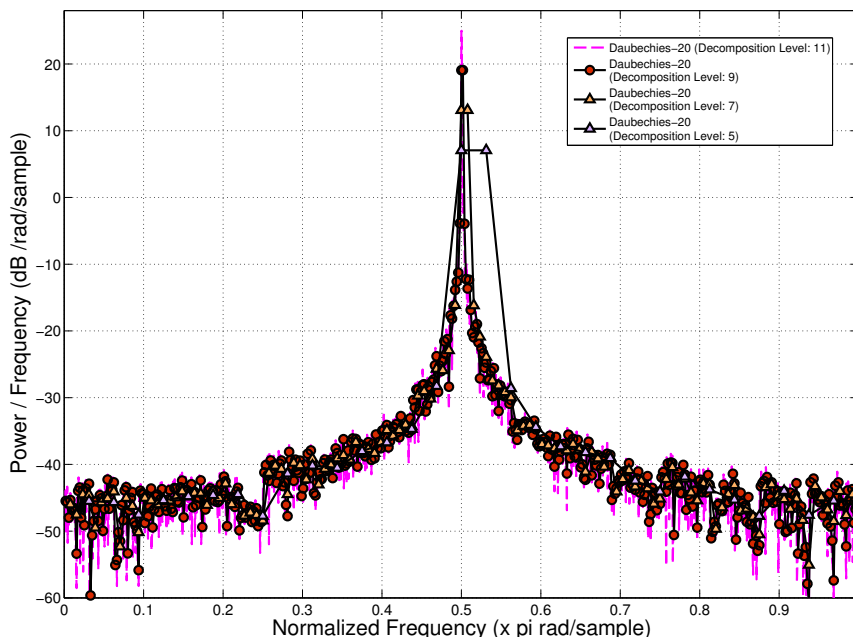


FIGURE 6.28: PSD estimates of single tone source according to various decomposition level of frequency selective wavelet. The number of samples in this experiment is 12800.

Estimation Technique	Tech-nique	Mean Power in stop-band	Variance in stop-band	Frequency resolution	Side lobe
Welch		+	≈	++	+
Periodogram		≈	++	≈	≈
Periodogram with Window		-	++	≈	-
MTSE		-	+	≈	-

TABLE 6.3: Comparison of WPSE performance with other techniques for estimation of a single-tone source. The notations +, - and ≈ indicate whether the WP approach performs favorably, negatively or similar in comparison to the other method.

better frequency resolution. However, as the decomposition level is increased (from 5 to 11 in the example shown), the variances of the estimates increase as well. The wavelet based estimates tend to approach periodogram estimate for higher order decomposition levels and the Welch based estimate for lower orders.

Table 6.3 summarizes the performance comparison of the WPSE with other techniques for the estimation of a single-tone source. The notations +, - and ≈ indicate whether the WP approach performs favorably, negatively or similar in comparison to the other method.

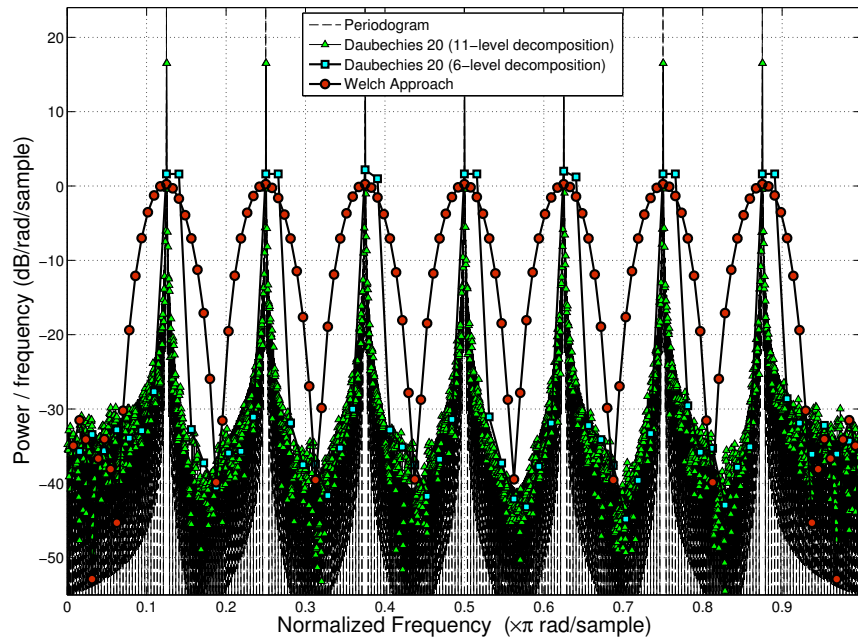


FIGURE 6.29: PSD estimates of multi-tone source for different decomposition level of Daubechies-20 together with Periodogram and Welch Estimate. The number of samples considered is 12800. The overlap percentage and the length of each segment employed in Welch is 50% and 64 samples, respectively. Hamming window is used in the Welch estimation.

### 6-6-3 Multi-Tone Source Estimation

#### A. Comparison with Welch and Periodogram methods

Fig. 6.29 illustrates the Periodogram, Welch and WPSE results for the estimation of multi-tones sources. The number of samples in these experiments is 12800 while the configuration of Welch method used here is the same as in the case of partial band and single tone source. The performance comparison of the candidate techniques follow trends similar to the estimation of single tone sources. The performance of orthogonal WPSE is better than that of Welch for frequency resolution and stop band power suppression. The periodogram has better frequency resolution compared to WPSE but the variances in the estimates are large.

#### B. Comparison with windowed-Periodogram and MTSE techniques

Outcomes similar to single tone estimation occur when the WPSE estimation of multi-tone sources are compared with that of windowed periodogram and MTSE (refer figs. 6.30 and 6.31). Increasing the level of decomposition improves the frequency resolution of wavelet based estimates to the extent that the results are compared with the frequency resolution offered by windowed periodogram and MTSE. Both the MTSE and the windowed periodogram outperform WPSE for power rejection in the unoccupied bands.

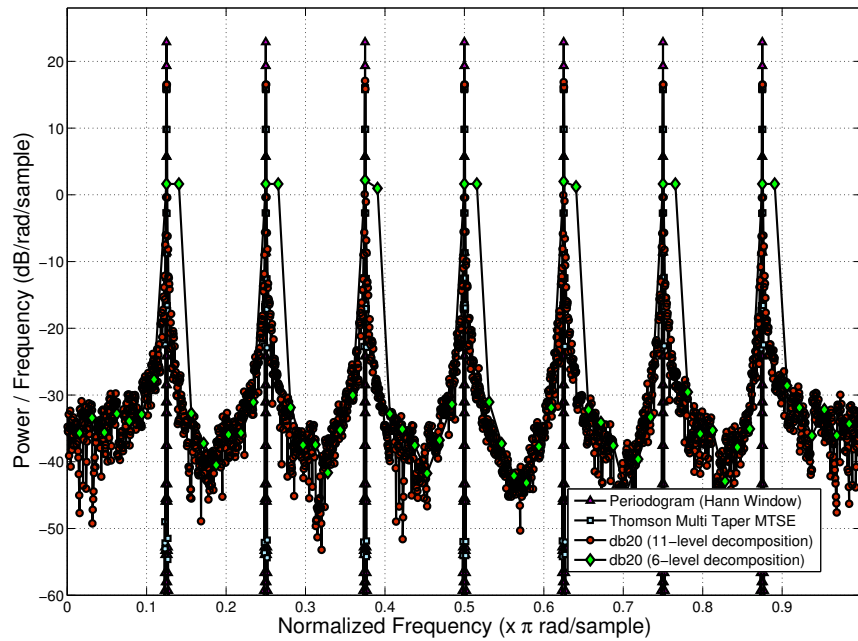


FIGURE 6.30: PSD estimates of multi-tones source according to different decomposition level of Daubechies-20 together with Thomson's MTSE and Periodogram using Hann window. The number of samples in this experiment is 12800.

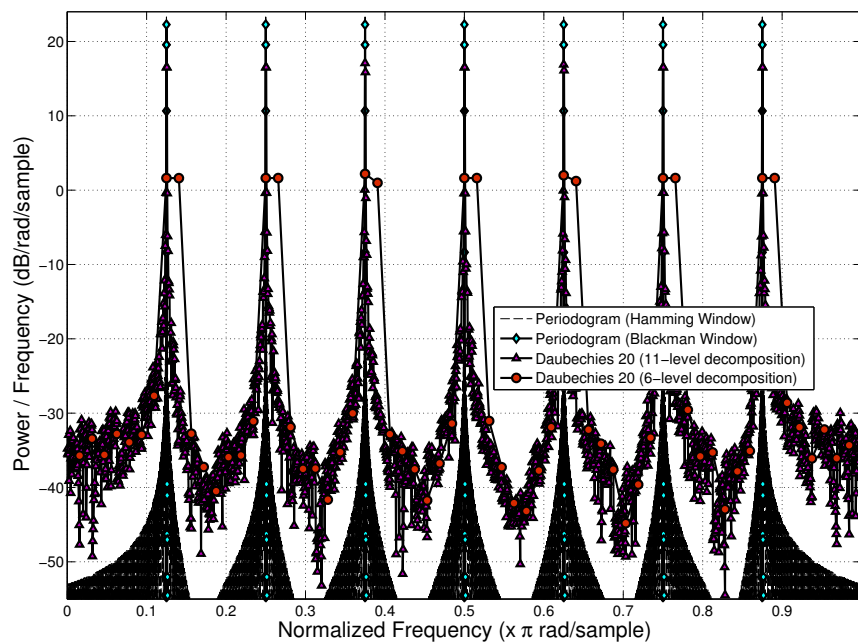


FIGURE 6.31: PSD estimates of multi-tones source according to different decomposition level of Daubechies-20 together with Periodogram using Hamming window and Blackman window. The number of samples in this experiment is 12800.

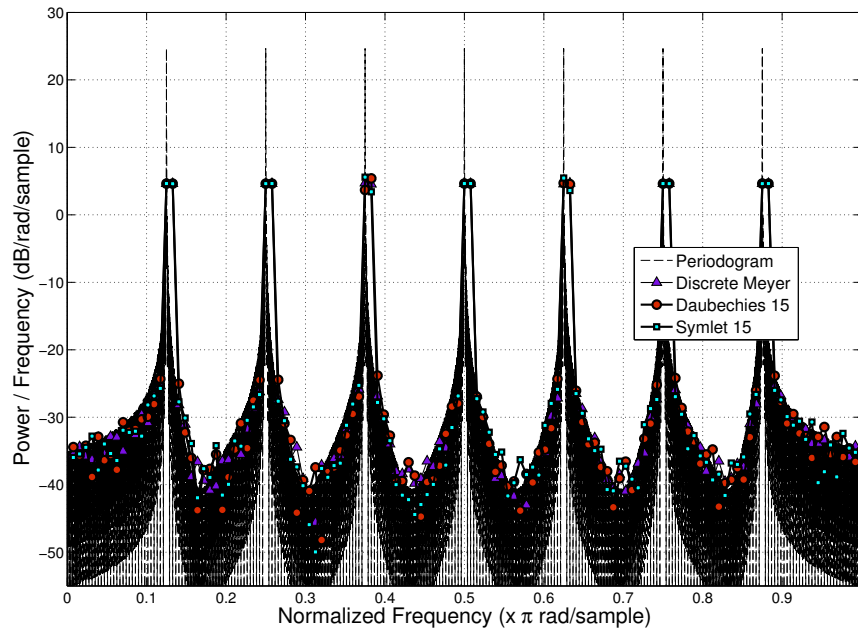


FIGURE 6.32: Wavelet based estimate for multi tones source (Daubechies 15, Symlet 15 and Discrete Meyer).

### C. Impact of wavelet families

Figs. 6.32 and 6.33 show the WPSE for a multiple tone source with various wavelet families. As in the estimation of the single tone source, the performance of biorthogonal wavelet based estimate is far worse than the orthogonal wavelet based estimate. Apart from this, there are no other palpable differences in the performances of the orthogonal wavelet based estimates in terms of frequency resolution.

### E. Impact of decomposition levels

Fig. 6.34 shows the effect of the decomposition level on the wavelet based PSD estimates. The results are similar to single tone source, namely the higher the wavelet packet decomposition level, the more similar the estimates to the periodogram estimates. On the other hand, lowering the decomposition level makes the WPSE performance similar to that of the Welch technique.

#### 6-6-4 Swept-tone source estimation

The motivation for studying swept tone sources is to understand the ability of the candidate techniques to gauge signals that vary with time. Such an analysis will be particularly useful for testing the applicability of WPSE for Cognitive Radios where the characteristics of the signals studied can vary with time.

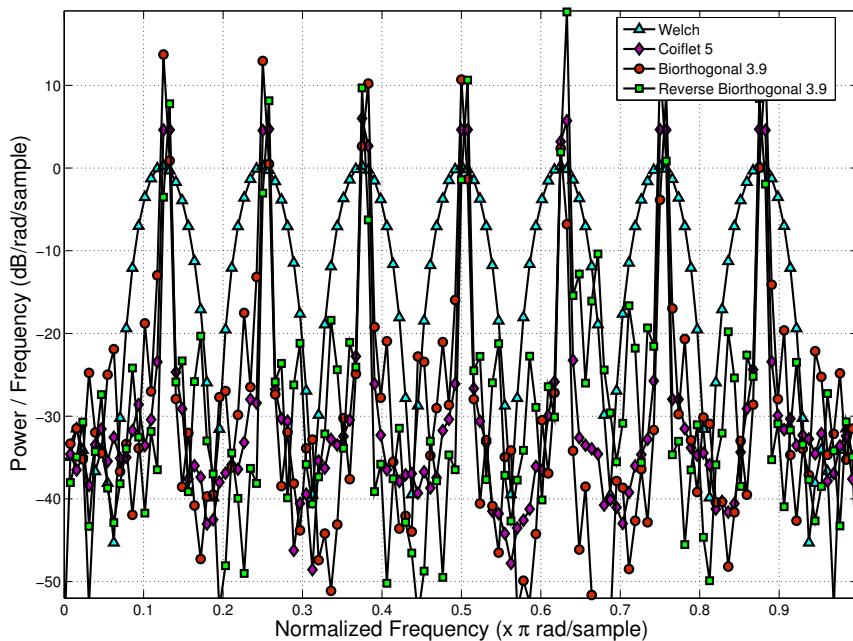


FIGURE 6.33: Wavelet based estimate for multi-tone source (Coiflet 5 Biorthogonal 3.9, Reverse Biorthogonal 3.9).

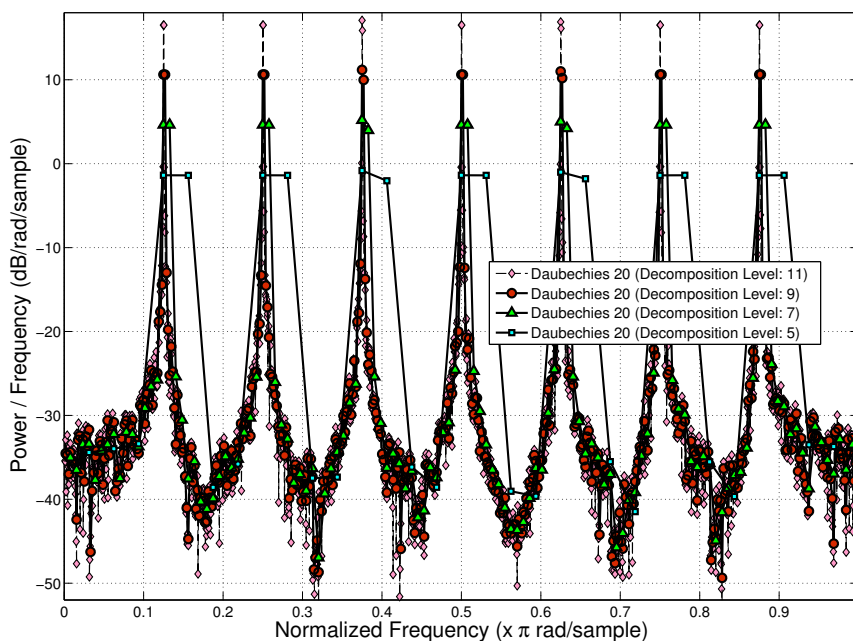


FIGURE 6.34: PSD estimates of multi-tones source according to various decomposition level of Daubechies-20. The number of samples in this experiment is 12800.

Twenty sweeps are conducted to estimate the swept tone source. We do not investigate the spectral estimate of the entire 20 sweeps in a single attempt because the results would be no different from the estimation of partial band sources. Instead, we investigate the snapshot of a portion of single sweep. Five snapshots are taken on a single sweep with each snapshot corresponding to 20% of the total sweep period. Each sweep spans from the lowest frequency range ( $0.1f_s$  or  $0.2\pi$ ) to the highest ( $0.4f_s$  or  $0.8\pi$ ). The first snapshot corresponds to the left most lobe while the fifth snapshot corresponds to the right most lobe.

Figs. 6.35, 6.36, 6.37 and 6.38 show the periodogram, Welch as well as WPSE estimates (using different wavelets) for the swept tone source. None of the WPSE configuration surpasses the performance of the Welch method. The Welch technique demonstrates good side lobe suppression, small variance and a resolution that matches with that of orthogonal wavelet based estimates. On the other hand, the performance of orthogonal wavelet based estimates is quite comparable with the periodogram in terms of side lobe or stop band power suppression with the added advantage of smaller variance.

Comparing the performance of different wavelets, it can be observed from fig. 6.38 that the performance of bi-orthogonal wavelet is far worse than its orthogonal counterparts. Among the orthogonal wavelets, Discrete Meyer wavelets perform better than other wavelets, especially, with respect to the minimization of pass-band variance. However, for other metrics like transition-band and stop-band power suppression, there are no clear performance differences.

Fig. 6.39 depicts the effect of filter length on the performance of the WPSE for the estimation of swept-tone source. For clarity of expression only two Daubechies wavelets are depicted in the figure. It can be inferred from the plots that estimation with wavelet-filters of longer lengths (say Daubechies 20) is better both in terms of the variance and stop-band power suppression. However, the frequency resolution of the estimates are identical even with increased filter lengths (compare Daubechies-4 results with Daubechies-20).

Fig. 6.40 illustrates the differences in the performance of the WPSE for the estimation of swept tone sources for different levels of signal decomposition. We can observe from the plots that with increasing number of decomposition levels, the frequency resolution increases. However, this is also accompanied by large variations in the estimates.

Fig. 6.41 shows a 3-dimensional plot of the estimation for 2 sweeps of the swept-tone source.

### 6-6-5 Estimation with limited number of samples

It will be interesting to see how the performances of the candidate techniques compare when the numbers of data samples available for estimation are limited. Such a study will be particularly useful when the span time available for radio analysis is limited (e.g. as in the case of cognitive

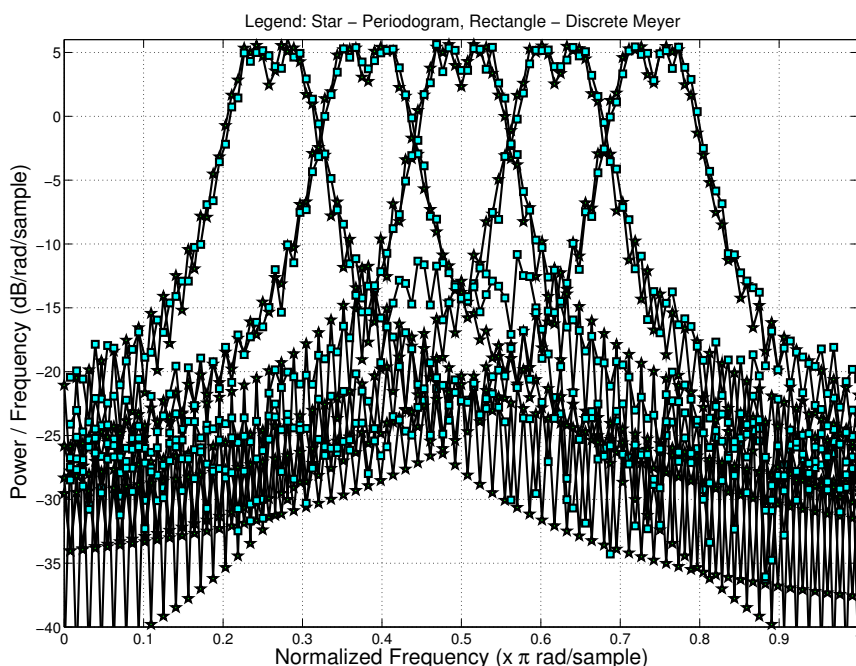


FIGURE 6.35: Periodogram and wavelet based estimate (Daubechies 15 and Discrete Meyer) for a single sweep of swept tone source. Five portions of single sweep is captured (the most left lobe is the first 20% of the sweep, the most right lobe is the fifth 20% of the sweep).

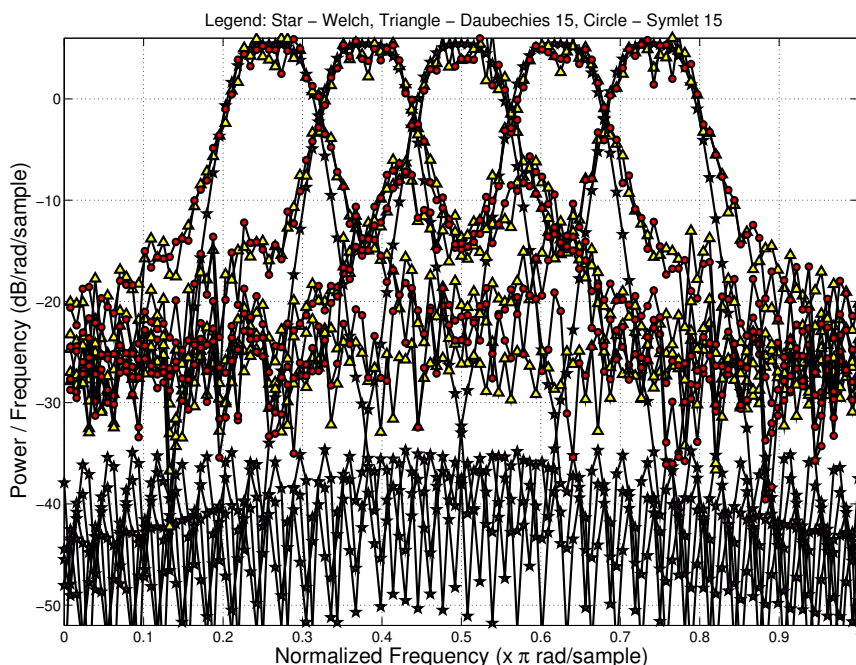


FIGURE 6.36: Welch and wavelet based estimates (Symlet 15 and Frequency Selective (Length = 30)) for a single sweep of swept tone source. Five portions of single sweep are captured (the most left lobe is the first 20% of the sweep, the most right lobe is the fifth 20% of the sweep).

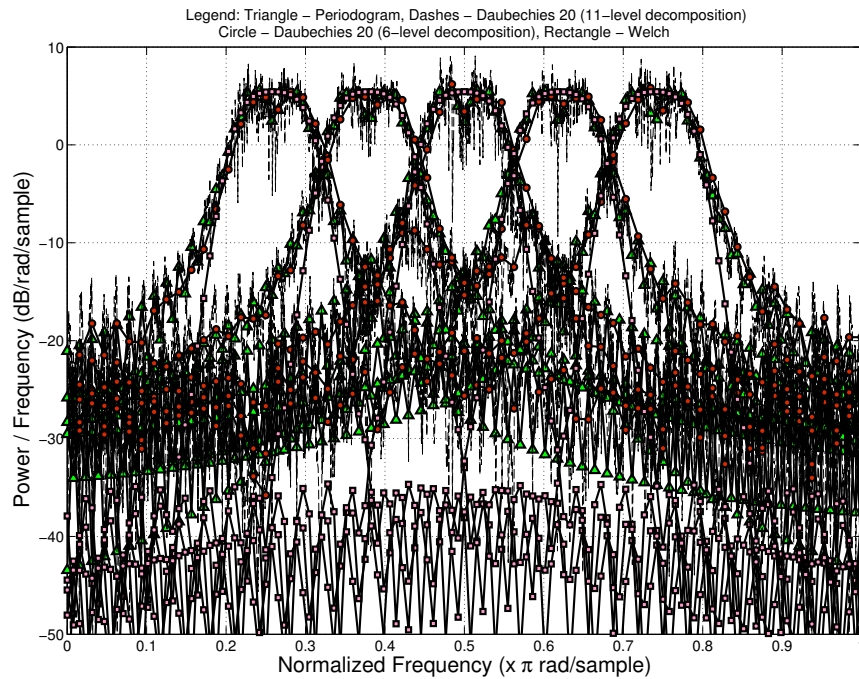


FIGURE 6.37: Periodogram, Welch, Daubechies-15 and Discrete Meyer based estimates for a single sweep of swept tones source. 5 portions are captured (most left lobe is the first 20% and most right lobe is the fifth 20% of the sweep).

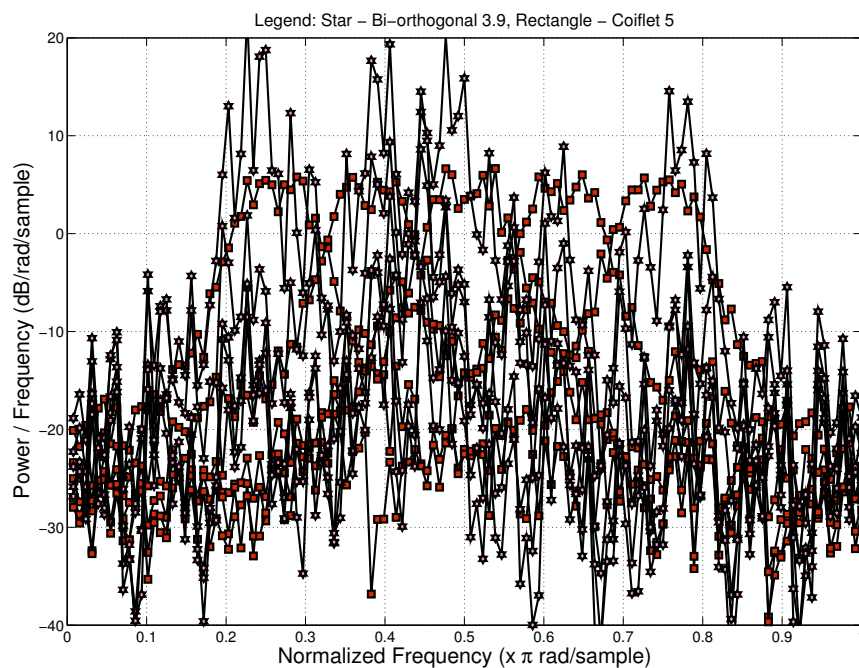


FIGURE 6.38: Wavelet based estimate for a single sweep of swept tone source (Coiflet 5 and Biorthogonal 3.9). Five portions of single sweep is captured (the most left lobe is the first 20% of the sweep, the most right lobe is the fifth 20% of the sweep).

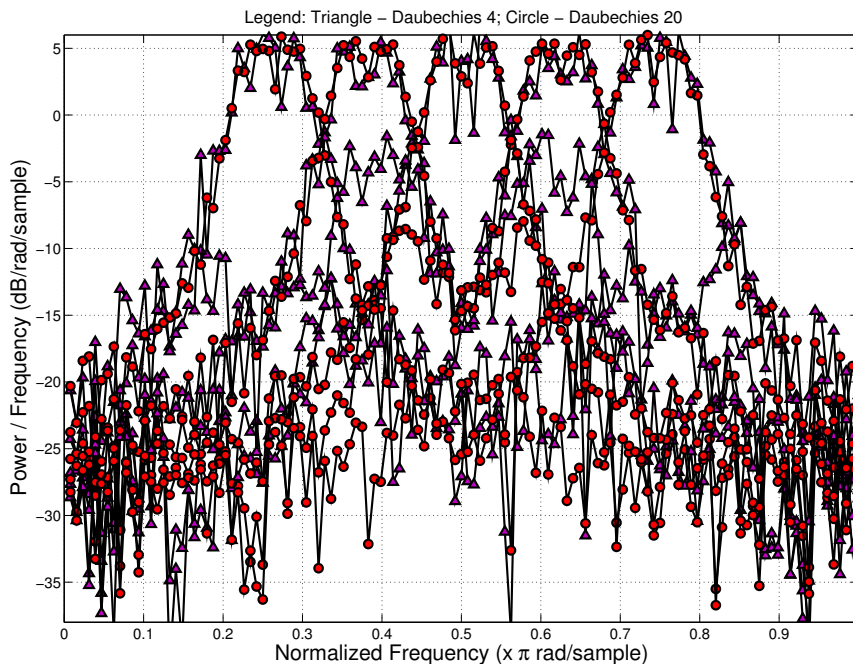


FIGURE 6.39: Wavelet based estimate for a single sweep of swept tone source (using Daubechies family with different filter length). Five portions of single sweep are captured (the most left lobe is the first 20% of the sweep, the most right lobe is the fifth 20% of the sweep).

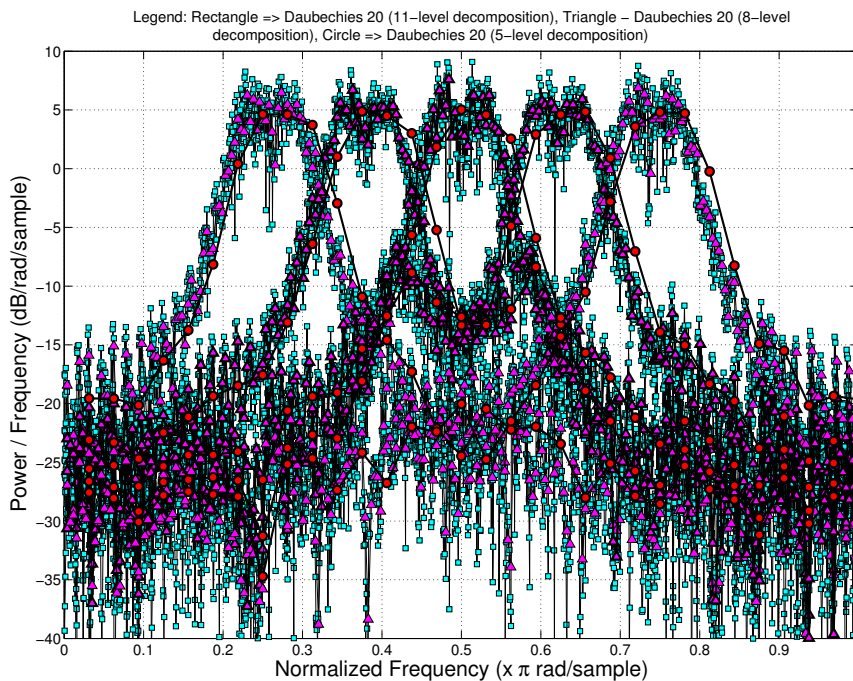


FIGURE 6.40: Wavelet based estimate for a single sweep of swept tone source using Daubechies family at different levels of decomposition. Five portions of single sweep are captured (the most left lobe is the first 20% of the sweep, the most right lobe is the fifth 20% of the sweep).

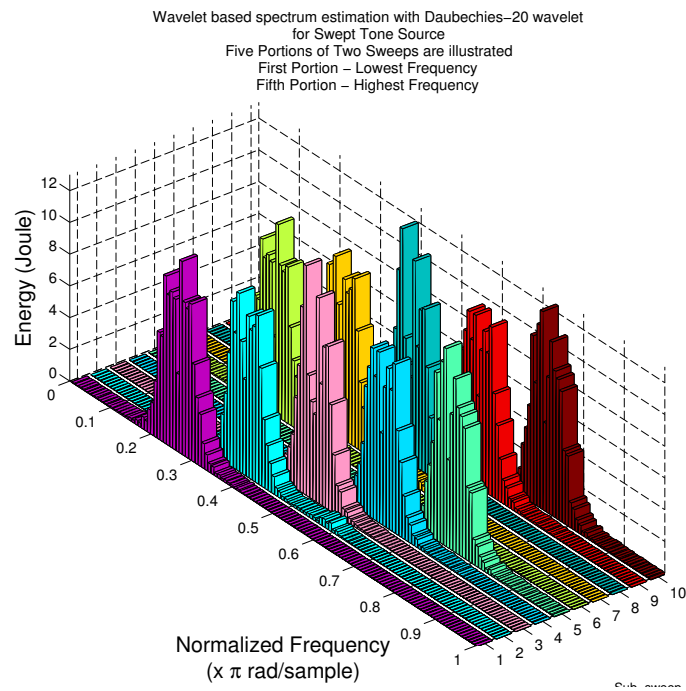


FIGURE 6.41: Three dimensional plot of energy of spectrum estimates using frequency selective wavelet (2 sweeps, each of 640 samples).

radio applications). The number of samples used in the experiments is 384. Apart from WPSE, the other estimators used are welch and periodogram. The parameters of Welch used here are exactly the same as the ones used in the previous set of experiments, i.e. a Hanning window of window size is 64 with 50% overlap.

### A. Partial band

Figs. 6.42 and 6.43 depict the PSD plots of WPSE along with the periodogram and Welch estimates for small number of samples. One may observe from the figures that the performances of all the techniques deteriorates when the number of samples are reduced. Comparing Welch and WPSE, both perform similarly in the metric of stop-band rejection. This is on expected lines because the number of samples in each segment for both cases is the same, namely 64. However, the variations in the Welch output is larger when the number of samples is reduced because the estimates are now averaged over 11 segments (instead of 399, as before). The periodogram estimates for small number of samples also leaks more into the unoccupied bands when compared with the earlier case with 12800 samples. This is also to be expected since the size of the window in the case of 384 samples is much smaller leading to more leakage.

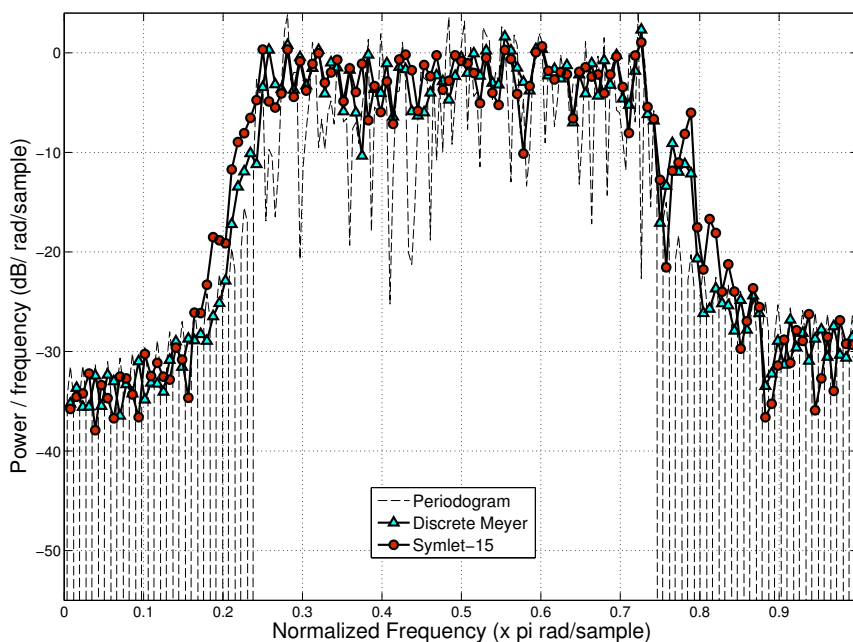


FIGURE 6.42: Periodogram and WPSE (Symlet 15, and Discrete Meyer) estimation of a partial band source. The number of samples considered is 384. A level-7 decomposition tree is used for WPSE.

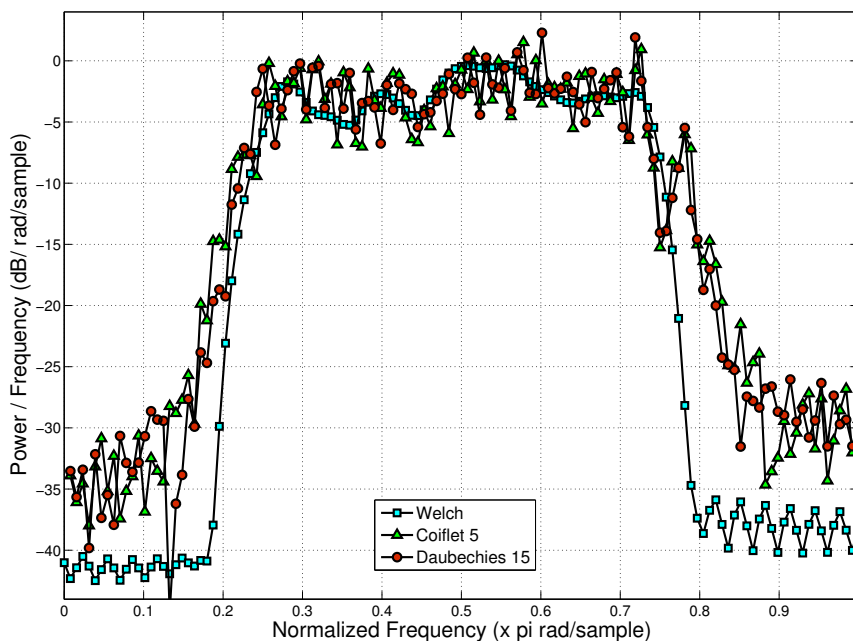


FIGURE 6.43: Welch and WPSE (Coiflet-5, Daubechies-15) estimation of a partial band source. The number of samples considered is 384. The overlap percentage and the length of each segment employed in Welch is 50% and 64 samples, respectively. Hamming window is used for Welch estimation. A level-7 decomposition tree is used for WPSE.

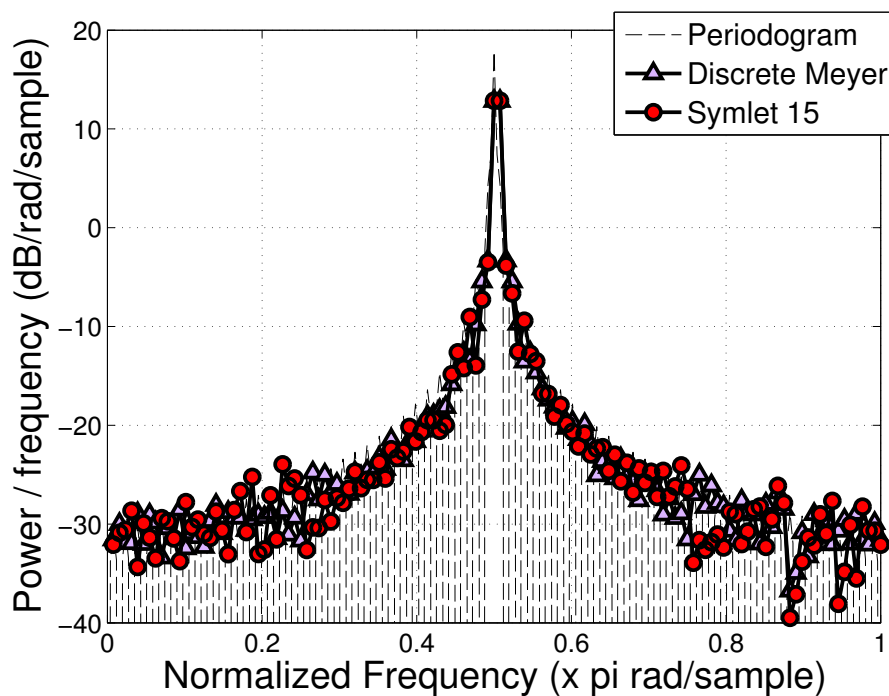


FIGURE 6.44: Periodogram and WPSE (Symlet 15, and Discrete Meyer) estimation of single tone source. The number of samples in this experiment is 384. A level-7 decomposition tree is used for WPSE.

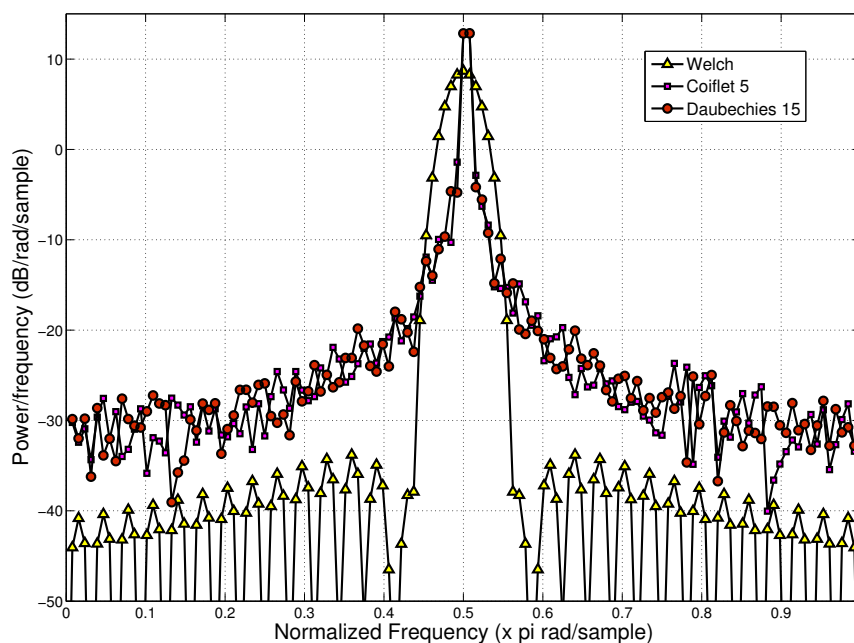


FIGURE 6.45: Welch and WPSE (Coiflet-5, Daubechies-15) estimation of single tone source. The number of samples in this experiment is 384. The overlap percentage and the length of each segment employed in Welch is 50% and 64 samples, respectively. Hamming window is used for Welch estimation. A level-7 decomposition tree is used for WPSE.

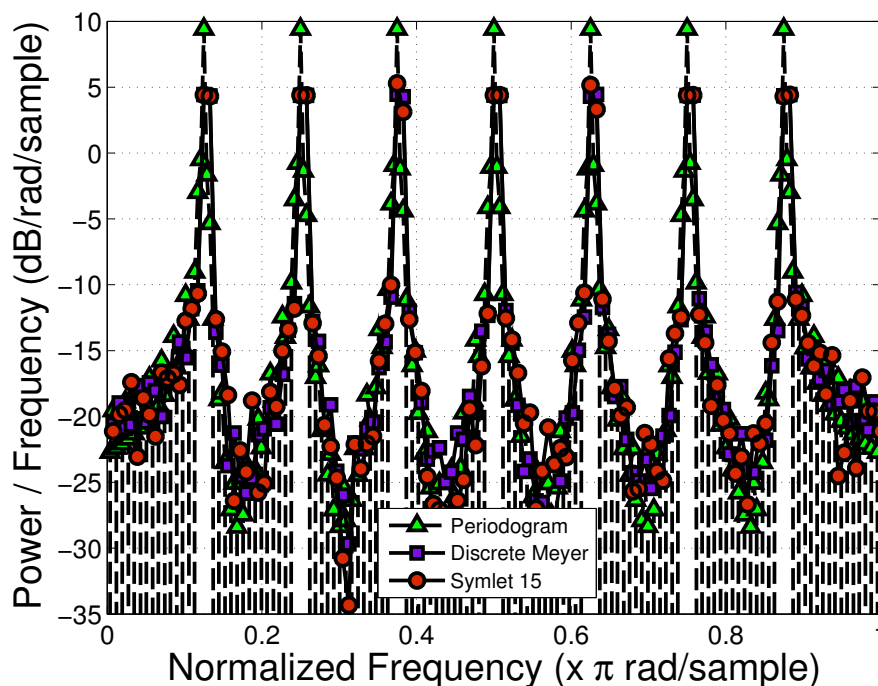


FIGURE 6.46: Periodogram and WPSE (Symlet 15, and Discrete Meyer) estimation of a multi-tone source. The number of samples in this experiment is 384. A level-7 decomposition tree is used for WPSE.

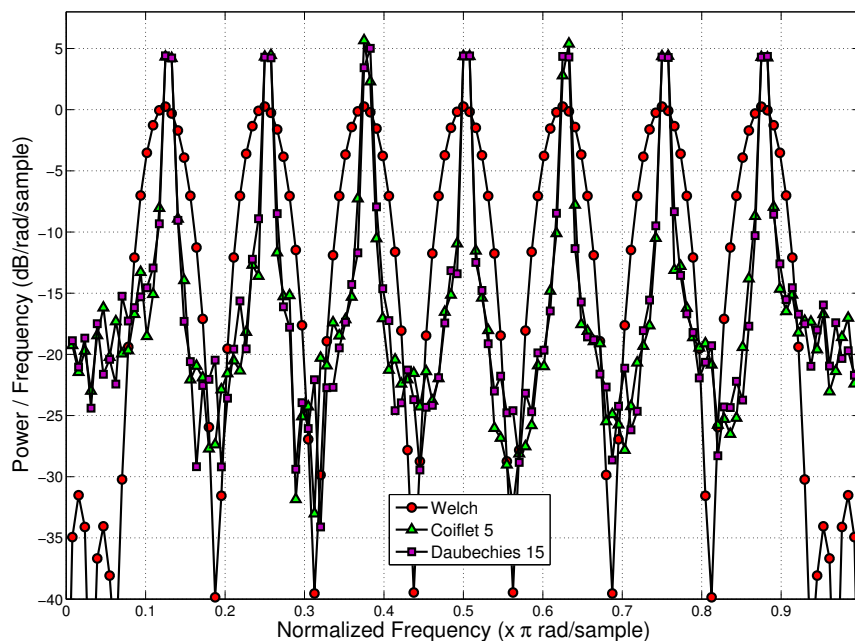


FIGURE 6.47: Welch and WPSE (Coiflet-5, Daubechies-15) estimation of a multi-tones source. The number of samples in this experiment is 384. The overlap percentage and the length of each segment employed in Welch is 50% and 64 samples, respectively. Hamming window is used in the Welch estimation. A level-7 decomposition tree is used for WPSE.

## B. Single tone

The plots for the estimation of a single tone source with 384 data samples are provided in figs. 6.44 and 6.45. From the plots we may observe that the resolution of the estimates is not affected by a reduction in the number of data samples. However, the periodogram and WPSE estimates have a poorer frequency resolution and leak into the neighboring bands with a decreased number of data samples. The Welch estimates, on the other hand, have the same side-lobe level as before because the window size of the data segments remains 64 even with the reduced sample set.

## C. Multi-Tone

Figs. 6.46 and 6.47 compare WPSE performance with Welch and Periodogram methods for the estimation of multi-tone sources when the number of samples is low. For the case considered, there seems to be no tangible differences in the performances of the Welch estimator. On the other hand, both periodogram and WPSE estimates suffer from higher side lobes with a decrease in the number of data samples.

### 6-6-6 Enhanced wavelet packet spectrum estimator (E-WPSE)

We now present results of the evaluation of the Enhanced-Wavelet Packet Spectrum Estimator (E-WPSE) introduced in Section 7.5.

#### A. Estimation of partial band source

We first evaluate the performance of E-WPSE for the estimation of a partial band source. Figs. 6.48, 6.49, 6.50 and 6.51 show the estimation of a partial band source with various techniques. The results are provided in four different figures for ease and clarity of depiction. The figure of merit used to evaluate the various estimation techniques are:

- side lobe suppression,
- variance of the estimated PSD in pass-band and stop-band, and
- transition between pass-band and stop-band (transition band).

The best estimator is the one which has a sharp transition band, good side-lobe suppression and Out-Of-Band (OOB) energy reduction, and low stop/pass-band variance. All these metrics may

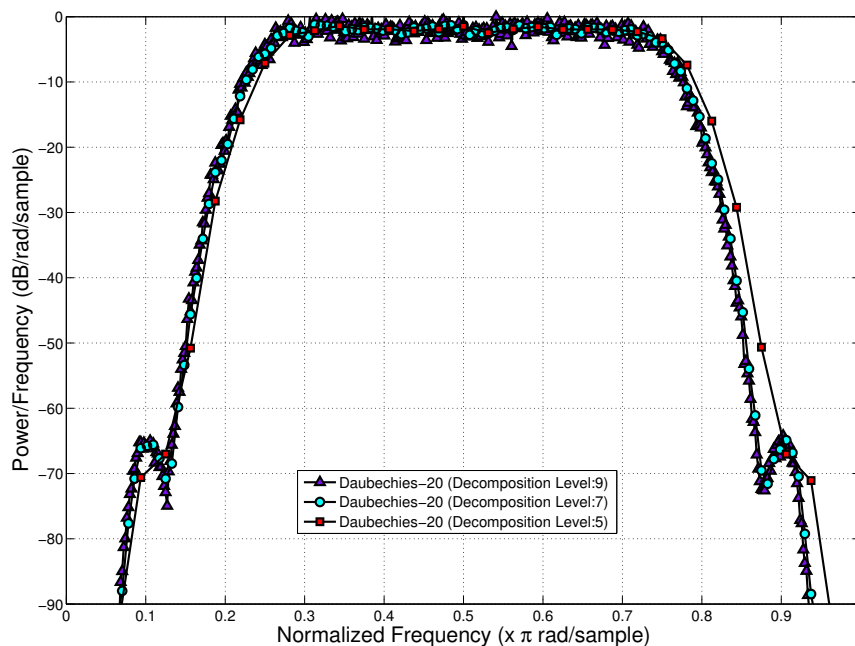


FIGURE 6.48: Estimation of a partial-band source with E-WPSE at various WP decomposition levels. The wavelet used is Daubechies-20.

not be realized at the same instance and the desired features have to be traded to select the best system.

In fig. 6.48, the wavelet based PSD estimates are displayed at 3 different decomposition levels to understand the influence of the iteration level on WPSE performance. The wavelet used is Daubechies-20.

In the next three figures (figs. 6.49, 6.50 and 6.51) the E-WPSE results are compared with other approaches.

### A.1. Comparison with Welch and periodogram techniques

The Periodogram has a sharp transition band but has a large variance in the pass-band (see fig. 6.49). The Welch averages the estimates and hence the variances are low; this also results in a poor transition band. Of interest are the WP approaches, WPSE and E-WPSE, which have significantly lower variance in comparison to the Periodogram. With regard to sidelobe levels and OOB, the performances of the Welch and WPSE approaches match. E-WPSE on the other hand comfortably outperforms both the Welch and the WPSE by a significant margin (up to 60 dB gains in OOB reduction).

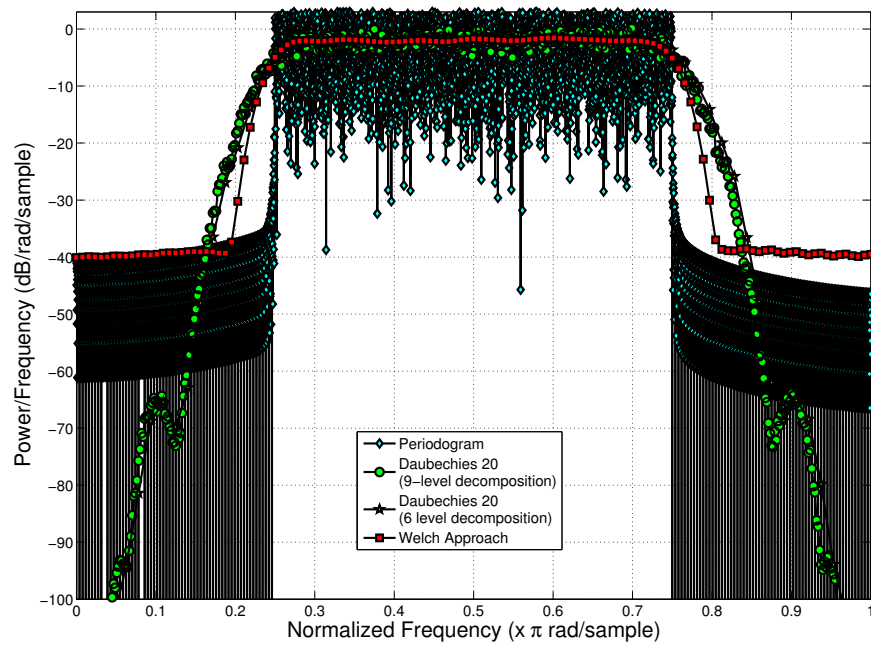


FIGURE 6.49: Comparison in performance of the estimation of a partial-band source between E-WPSE, WPSE, periodogram and Welch methods. The wavelet used is Daubechies-20.

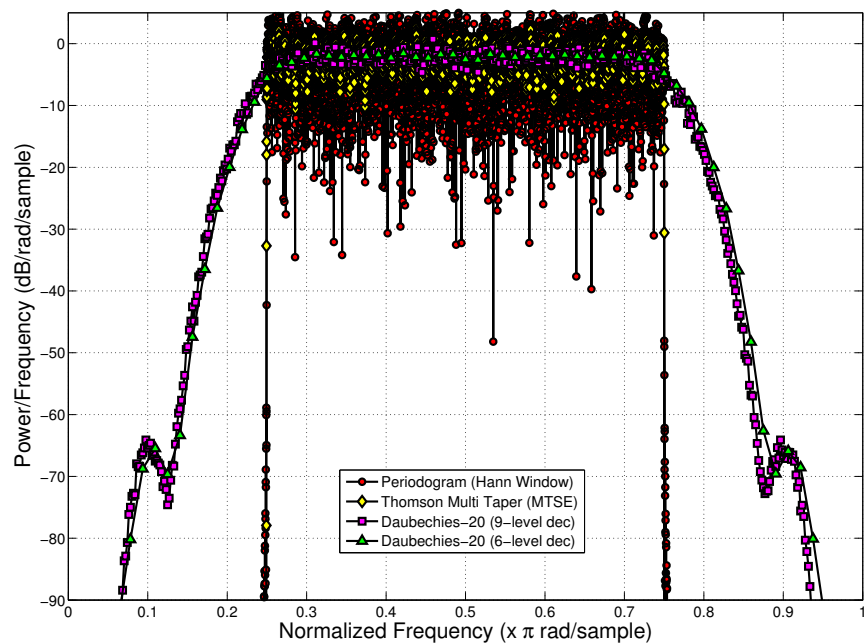


FIGURE 6.50: Comparison in performance of the estimation of a partial-band source between E-WPSE, MTSE, periodogram with Hann window and Welch methods. The wavelet used is Daubechies-20.

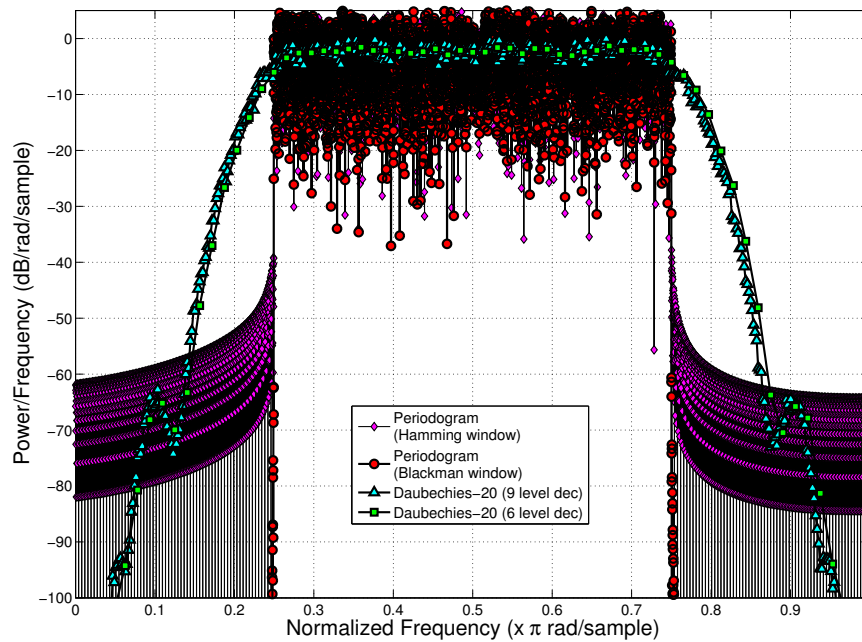


FIGURE 6.51: Comparison in performance of the estimation of a partial-band source between E-WPSE, WPSE, Periodogram (with Hamming and Blackman window) methods. The wavelet used is Daubechies-20.

## A.2. Comparison with Windowed periodogram and MTSE

Applying the window to the periodogram (see figs. 6.50 and 6.51) reduces the side lobes in the estimates but it does not solve the problem of large variances. All the results with windowed-periodogram have variances much larger than the WPSE estimates. Lastly, the MTSE estimates have good frequency resolution but they too suffer from significant variance.

## A.3. Influence of decomposition levels

One may increase or decrease the decomposition levels of the WPSE/E-WPSE systems to achieve the desired variance of the estimated PSD. With a decrease in the depth of data decomposition the variance is marginally improved though it is also accompanied by a small decrease in frequency resolution. This effect is illustrated in fig. 6.48 where the estimates for different levels of decomposition are depicted.

Table 6.4 summarizes the performance comparison of the E-WPSE with other techniques. The notations +, - and  $\approx$  indicate whether the WP approach performs favorably, negatively or similar in comparison to the other method. It is clear from the PSD curves and the table that the E-WPSE compares favorably with existing approaches in almost all the performance measures.

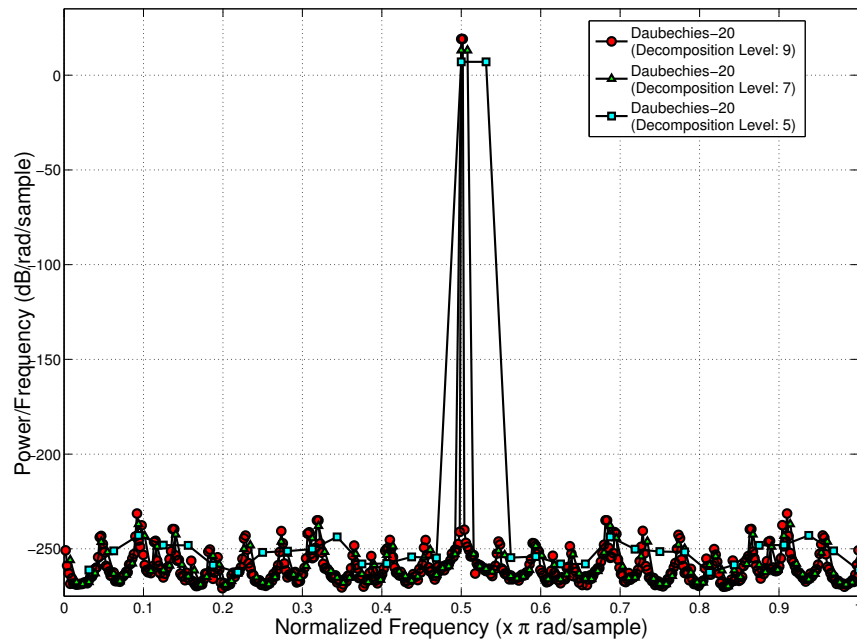


FIGURE 6.52: E-WPSE estimation of a single tone source at different decomposition levels. Wavelet applied is Daubechies-20.

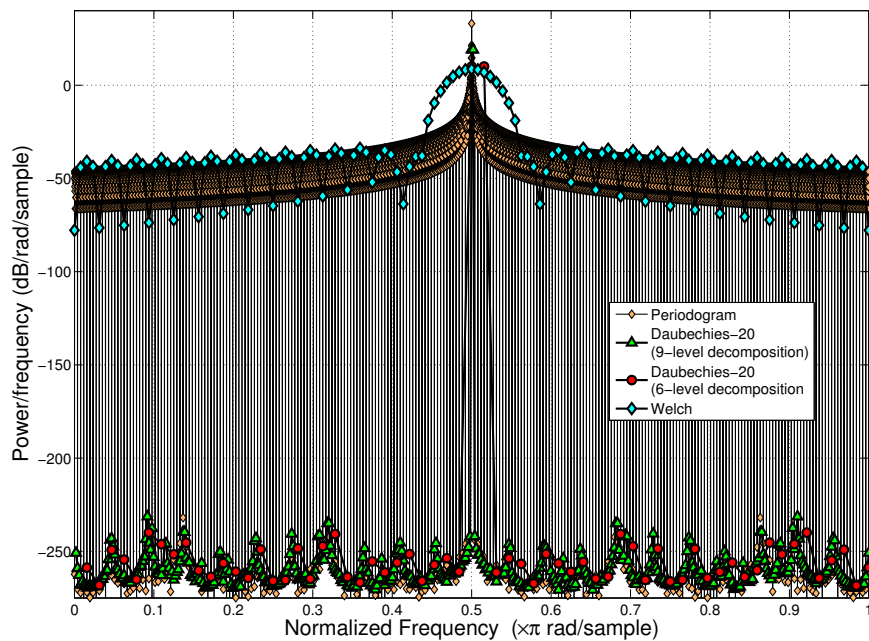


FIGURE 6.53: E-WPSE estimation of a single tone source and its comparison with Periodogram and Welch results. Wavelet applied is Daubechies-20.

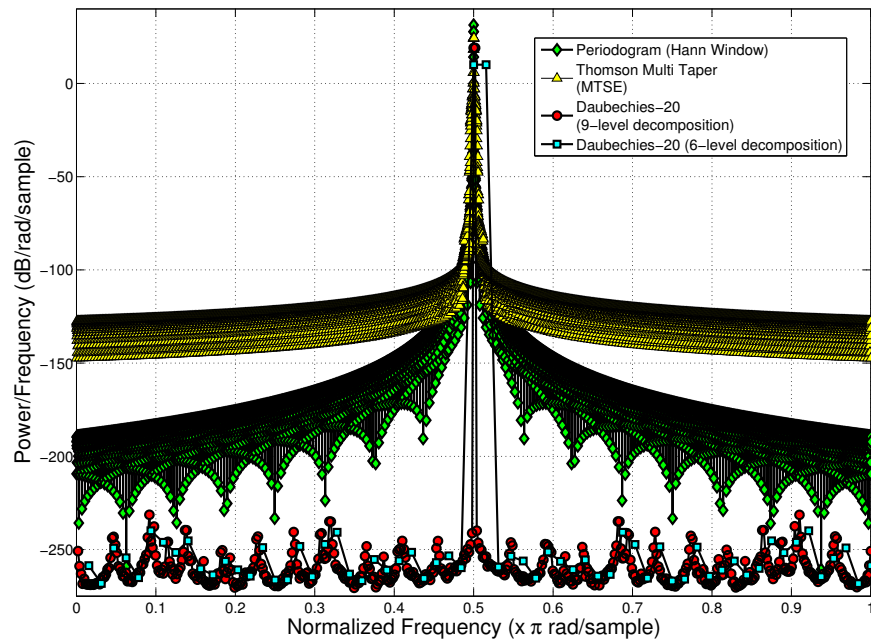


FIGURE 6.54: E-WPSE estimation of a single tone source and its comparison with Thomson's MTSE and Periodogram with Hann window. Wavelet applied is Daubechies-20.

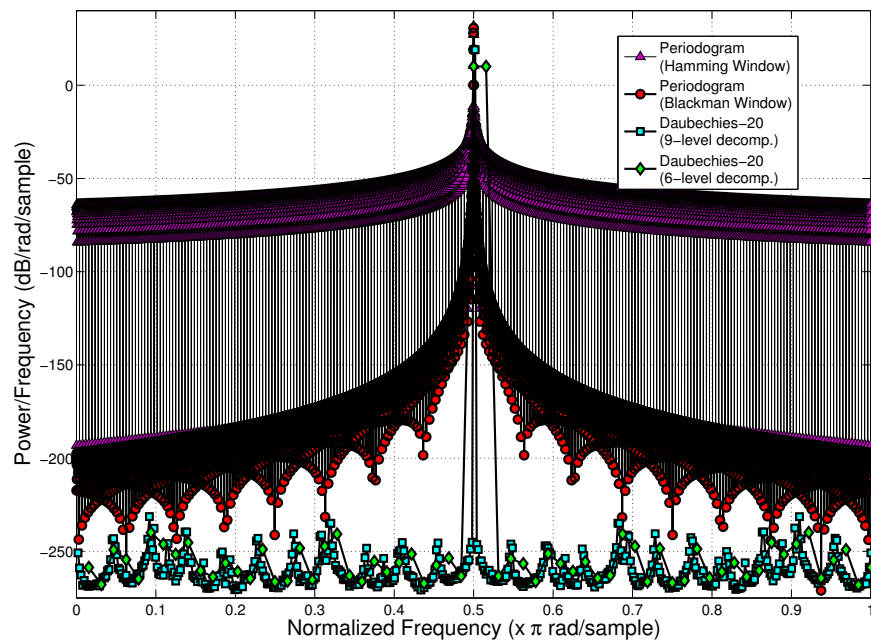


FIGURE 6.55: E-WPSE estimation of a single tone source and its comparison with Periodogram (using Hamming and Blackman windows). Wavelet applied is Daubechies-20.

Estimation Tech- nique	Side-lobe suppression	Variance in pass-band	Transition band	Variance in stop band
Welch	+++	$\approx$	++	$\approx$
Periodogram	++	+++	-	++
Periodogram with Window	$\approx$	++	$\approx$	++
MTSE	-	+	-	+

TABLE 6.4: Comparison of E-WPSE performance with other techniques for estimation of a partial-band source. The notations +, - and  $\approx$  indicate whether the WP approach performs favorably, negatively or similar in comparison to the other method.

## B. Single tone source

For the evaluation of single-tone source estimation, the performance metrics used are:

- mean power in stop band,
- variance in stop band,
- frequency resolution, and
- side lobe suppression.

Figs. 6.52, 6.53, 6.54 and 6.55 show the PSD estimates for single tone source. The results of this experiment make it clear that for the evaluation of single tone sources, the E-WPSE is an excellent choice.

### B.1. Comparison with Welch and periodogram methods

The Welch estimator windows the data, calculates the estimates of the windowed segments and then averages them to obtain the final estimate. Hence, it smears the details in the data causing poor frequency resolution (see fig. 6.53). On the other hand, the periodogram output suffers from large variations making it difficult to distinguish the actual output from spurious noise.

### B.2. Comparison with Windowed periodogram and MTSE techniques

MTSE offers good resolution but has large sidelobes (see fig. 6.54). The windowed periodogram reduces the sidelobes but at the same time smudges the estimates (see figs. 6.54 and 6.55). Amongst all the methods the E-WPSE offers the best resolution with exceedingly low side lobes (almost -250 dB).

Estimation Tech- nique	Mean power in stop-band	Stop-band variance	Frequency resolution	Side-lobe suppression
Welch	+++	++	++++	+++
Periodogram	++	++	≈	+++
Periodogram with Window	++	++	+	+++
MTSE	++	+	≈	+++

TABLE 6.5: Comparison of E-WPSE performance with other techniques for estimation of a single tone source. The notations +, - and  $\approx$  indicate whether the WP approach performs favorably, negatively or similar in comparison to the other method.

### B.3. Influence of decomposition levels

As in the case of partial band estimation, higher WP decompositions lead to better frequency resolution (refer fig. 6.52).

Table 6.5 summarizes the comparison of the wavelet packet approach with other approaches for single tone estimation.

#### 6-6-7 Impact of padding on E-WPSE estimation

As mentioned earlier, the implementation of E-WPSE requires the number of received samples to be multiples of  $2^C$  where  $C$  is the number of WP decomposition levels. When this is not the case, extra bits have to be added either in the form of cyclic prefix or zero padding or symmetrical padding.

Fig. 6.56 illustrates the impact of padding schemes on the E-WPSE performance for the estimation of a partial-band source. In this example the number of samples considered is 6400. Since this is a multiple of 128 ( $=2^7$ ), no padding is required for a level-7 decomposition. However, when the level is increased to 9, padding is necessary to make the number of samples a multiple of 512 ( $=2^9$ ). Fig. 6.56 shows that all forms of padding (CP/ZP/SP) lead to a loss in performance with the OOB level around -40 dB.

However, when a single zero bit is added only in stages where the number of input samples is odd, the results are encouraging. In fact this approach is found to maintain the excellent OOB energy levels that E-WPSE offers. For a level-9 decomposition, a single zero bit padding is necessary only at the 9th decomposition stage since it is only here that the number of samples is odd.

The impact of padding schemes on the E-WPSE estimates for Multi-tones source is illustrated in fig. 6.57. The pattern that emerges from the results is very similar to that of partial-band source estimation - ZP/SP/CP diminishes E-WPSE performance while single bit addition preserves it.

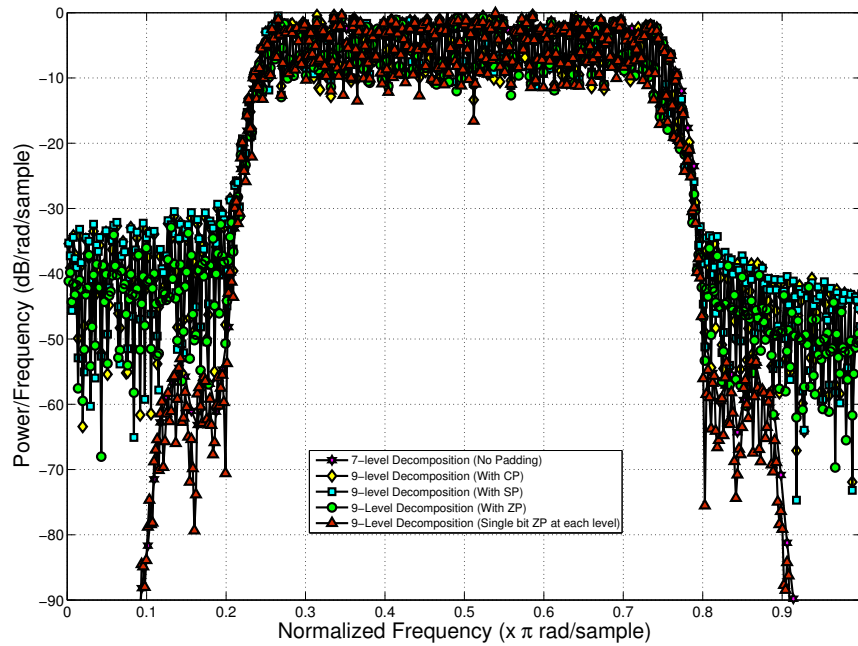


FIGURE 6.56: Evaluation of impact of padding on E-WPSE estimation of partial band source. No padding is required for level- WP tree, for level-9 tree Zero Padding (ZP), Cyclic Prefix (CP) and Symmetric padding (SP) performed before decomposition process and single zero bit added at those stages when the number of samples is odd.

Comparing the two methods of padding, it is clear that adding an additional zero-bit only in those stages where the input is odd is more profitable than adding the extra bits in a single attempt before the estimation process versus. This is because the second approach preserves the benefits offered by E-WPSE. This difference in performance can be intuitively answered. First, the impact of padding is only experienced in those decomposition stages where the extra bit is added (and not by all levels as is the case in the first approach). Second, at any given level, the padding process is spread over different wavelet packet inputs minimizing the influence of the appended samples.

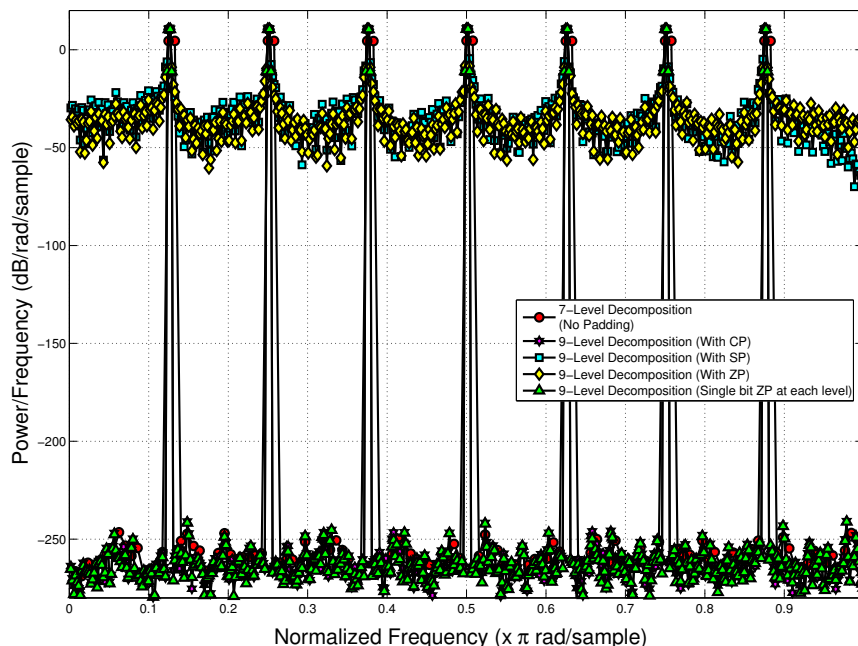


FIGURE 6.57: Evaluation of impact of padding on E-WPSE estimation of multi-tone source. No padding is required for level- WP tree, for level-9 tree Zero Padding (ZP), Cyclic Prefix (CP) and Symmetric padding (SP) performed before decomposition process and single zero bit added at those stages when the number of samples is odd.

## 6-7 Summary

In this chapter, the application of the wavelet packet transform for spectrum estimation was proposed and investigated. Four classes of sources with different features and characteristics were used to gauge the operation of the developmental system and the results were compared with that of well-known periodogram, windowed-periodogram, Welch and MTSE methods. The performance metrics used were variance and frequency resolution of the estimated PSD as well as side-lobe level in the unoccupied band. We also investigated the impact of decomposition level on the wavelet-based estimates. The studies showed that the proposed estimator operated well for all types of sources and its performances were comparable or at times even better than existing techniques.

## Chapter 7

# A wavelet packet transceiver for spectral analysis and dynamic spectrum access

A reconfigurable wavelet packet transceiver for spectral analysis and dynamic spectrum access is presented <sup>1</sup>. The transceiver consists of a Wavelet Packet Spectral Estimator (WPSE) and a Wavelet Packet Multi-carrier Modulator (WPM) both of which are implemented using filter banks. The WPSE estimates the radio environment and identifies spectrum holes and occupied bands. This information is then used to shape the time-frequency characteristics of the WPM transmission waveform in a way that the occupied bands are evaded. This is done by vacating those sub-carriers which lie in and around the occupied bands. The WPM sub-carriers are orthogonal wavelet packet (WP) bases derived from a fundamental 2-channel para-unitary filter pair which is uniformly iterated to form a tree structure. The WPSE uses the same filter bank structure as used for WPM data modulation and hence doesn't add to the implementation costs. Through computer simulations the operation of the proposed system is demonstrated. The performances are also compared with two other candidate systems based on Fast Fourier Transform (FFT) and Orthogonal Frequency Division Multiplexing (OFDM). The studies show that WPSE/WPM, in comparison to FFT/OFDM, offers better bit-error-rate (BER) performance and bandwidth efficiency. This is facilitated by the excellent time-frequency localization of wavelet filters which results in better estimation of spectrum and spectral confinement of the transmission waveform.

---

<sup>1</sup>Parts of this chapter have been published in [125], [126] and [127].

## 7-1 Introduction

Advances in wireless technologies have led to a host of new and innovative wireless applications and services. With each passing day there is demand for more wireless services even when the popularity of existing applications is on the rise. As a result the demand for valuable resources such as transmission spectrum has far exceeded their availability. Meanwhile, studies commissioned by international agencies, such as the Federal Communications Commission (FCC) in the United States, show that large portion of licensed frequency bands remain unused for most of the time and that the congestion of the spectrum is more due to the inadequacies of the access techniques than due to non-availability of spectrum [128, 129]. This has sparked a debate in the telecommunications circles on the need to revamp existing spectrum regulatory policies and introduce newer approaches. One such initiative is the idea of Cognitive Radio, a new paradigm that promises opportunistic utilization of unused spectrum and efficient spectrum management. In [129] Haykin defines Cognitive Radio as “an intelligent wireless communication system that is cognizant of its environment, learns from it and adapts its internal states to statistical variations in the incoming Radio-frequency (RF) stimuli by making changes in certain operating parameters in real time with objectives of highly reliable communications whenever and wherever needed, and efficient utilization of the radio spectrum.”

Modulation schemes, transmission bandwidth, transmit power, channel coding, and carrier frequency are examples of radio/PHY layer parameters that can be adjusted to facilitate realization of cognitive radio. The modulation scheme is chosen in such a way that the data is transmitted reliably using the least possible spectrum; in another words the modulation method must be spectrally efficient. Spectral efficiency is influenced by the noise and propagation condition. The latter varies with time due to environmental change, hence the modulation scheme should be able to adapt to the channel propagation variation. It should also support multi-node communication considering that several nodes can exist in a Cognitive Radio network.

Recently an innovative strategy for efficient access and utilization of spectrum, called Spectrum Pooling, has been proposed [130]. Spectrum pooling is a spectrum management principle where licensed (primary) users put their unused spectrum into a pool from which secondary users can rent spectrum. In spectrum pooling public access to the spectrum is provided without sacrificing the transmission quality of the actual license users by overlaying new radios on existing ones. Spectral utilization is optimized by allowing rental (i.e., unlicensed) users to transmit and receive data over portions of spectra where the primary users (i.e., licensees) are inactive. This is done in a way that the rental users (RUs) do not hinder the licensed user (LU) transmission. In such a setting LUs are ordinary mobile terminals and their associated base stations. They thus do not possess much intelligence. The RUs, on the other hand, should be capable of sensing the radio environment and optimally utilize the available resource. At the same time, the RUs should relinquish control of the resources once the LU begins transmission.

To implement such radios, multi-carrier Modulation (MCM) techniques like OFDM have been recommended as suitable physical layer candidates [130]. The characteristics of the transmission waveform can be readily shaped to occupy the time-frequency gaps of the LU system by merely activating and vacating the sub-carriers. In addition to this the FFT module used for modulation of information bits can also be used for spectral analysis.

Unfortunately, OFDM for CR is not without problems. A number of short-comings of OFDM in its application in CR have been noted in [85] and [131]. The problems arise from the fact that the filters that characterize the OFDM sub-carriers have large side lobes causing significant out-of-band (OOB) energy leakage and interference to neighboring communication systems. While techniques like windowing have been suggested to overcome this problem, they are ineffective as they reduce the bandwidth efficiency further.

In this backdrop, we introduce the wavelet packet modulator (WPM) [10, 11] as an alternative multi-carrier technique for CR applications. The motivation for pursuing WPM is in the promise of better confinement of spectra and lower out-of-band energy spillage. This ability is due to the fact that WPM symbols overlap in time resulting in greater localization in frequency. The signal energy can hence be better confined without leaking into neighboring bands. Furthermore, as in FFT/OFDM, the WPM receiver structure used for data demodulation can also be used for spectrum analysis to detect occupied/free bands at virtually no additional cost.

The rest of the chapter is organized as follows. In Section 7.2, a short review of existing multi-carrier methods for CR is provided. Section 7.3 explains the WPM transceiver and the spectrum analyzer based on wavelet packets. In Section 7.4 the experimental setup considered for the simulation studies is detailed. The results of the experiments are analyzed and discussed in Section 7.5. A summary of the study is provided in Section 7.6.

## 7-2 Multi-carrier methods for Cognitive Radio

### 7-2-1 FFT based OFDM

OFDM is a natural PHY layer candidate for CR systems given its advantages such as ease of implementation, flexibility and elegance in operation <sup>2</sup>. The short-coming of the OFDM is primarily due to the large side-lobes of the filters that characterize the sub-carrier. The power spectrum of a OFDM transmit signal  $S_{xx}^{OFDM}(f)$  can be given as [53]:

$$S_{xx}^{OFDM}(f) = \frac{1}{N_{FFT}} \left| \sum_{m=0}^{N_{FFT}} \sqrt{P_m} A_m \int_{-(1+\alpha)\frac{T_u}{2}}^{(1+\alpha)\frac{T_u}{2}} w(t) e^{-j2\pi(f-f_m)t} dt \right|^2. \quad (7.1)$$

<sup>2</sup>The discussion presented here is based on [53]

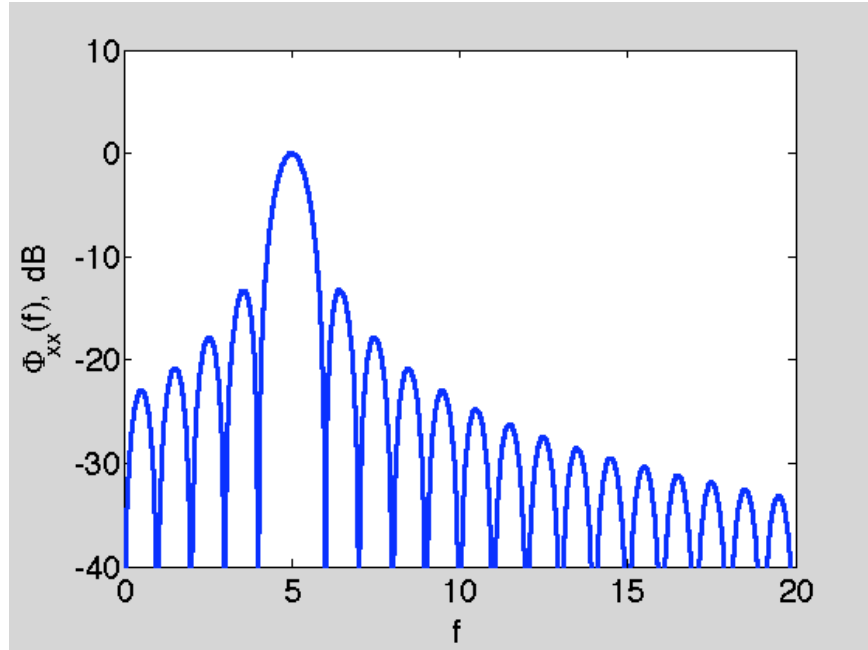


FIGURE 7.1: Power Spectrum Density of OFDM Carrier [53].

Here  $T_u$  is the total symbol duration (includes cyclic prefix),  $w(t)$  is the window function used to shape the signal,  $\alpha$  is the roll-off factor of the window,  $A_m$  is the QAM/PSK mapped information which modulates the sub-carrier  $f_m$  with an allocated power of  $\mathbb{P}_m$ . The power spectrum of individual carriers  $S_{x_m x_m}^{OFDM}(f)$  depends on the window function  $w(t)$  used to shape the sub-carriers through the following relation [53]:

$$S_{x_m x_m}^{OFDM}(f) = A_m |W(f - f_m)|^2 \quad (7.2)$$

Here  $W(f)$  is the transfer function of the window function  $w(t)$ . For conventional OFDM the window is a rectangular function. For this case, the power spectrum of each carrier  $S_{x_m x_m}^{OFDM}(f)$  becomes [53]:

$$S_{x_m x_m}^{OFDM}(f) = A_m |\text{sinc}((f - f_m)T_u)|^2 \quad (7.3)$$

where,

$$\text{sinc}(x) = \frac{\sin(\pi x)}{\pi x} \quad (7.4)$$

Since  $S_{x_m x_m}^{OFDM}(f)$  varies as  $(\text{sinc}(f))^2$  it introduces large side lobes. In fact the first side lobe for rectangular window occurs at  $-13\text{dB}$  (refer Fig. 7.1).

To alleviate this problem windows that taper gently are used (refer Fig. 7.2). A commonly used window is the raised-cosine function, which is defined as [85]:

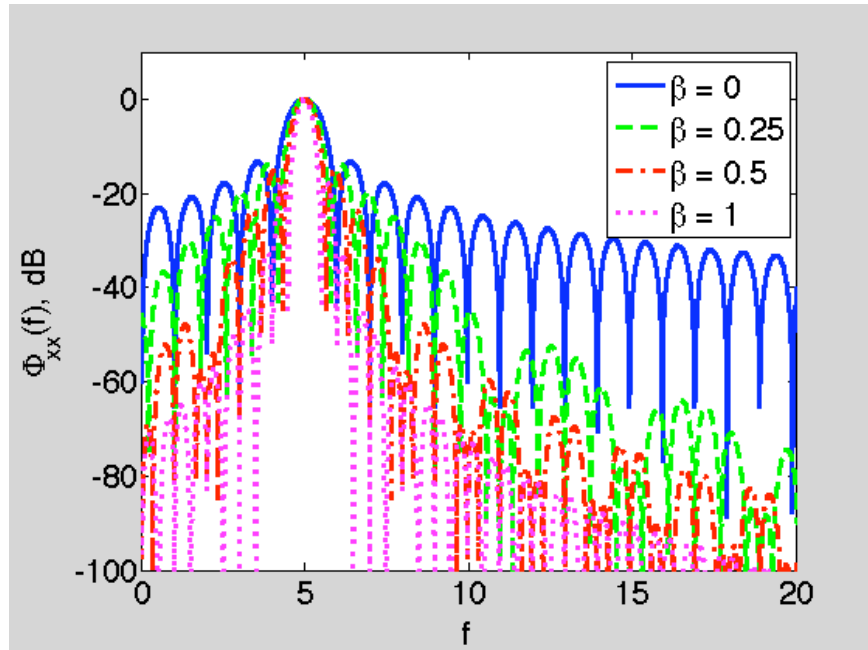


FIGURE 7.2: Power Spectrum Density of OFDM Carrier with different windows [53].

$$w_{rc}(t) = \begin{cases} \frac{1}{2T_u} \left\{ 1 + \cos \left[ \frac{\pi}{\alpha T_u} \left( |t| - \frac{T_u(1-\alpha)}{2} \right) \right] \right\} & \text{for } 0 \leq |t| \leq \frac{T_u(1-\alpha)}{2}, \\ \frac{1}{2T_u} \left\{ 1 + \cos \left[ \frac{\pi}{\alpha T_u} \left( |t| - \frac{T_u(1-\alpha)}{2} \right) \right] \right\} & \text{for } \frac{T_u(1-\alpha)}{2} \leq |t| \leq \frac{T_u(1+\alpha)}{2}, \\ 0 & \text{Otherwise.} \end{cases} \quad (7.5)$$

While windows like the raised-cosine function significantly reduce the side lobes, they also increase the symbol duration by a factor of  $(1 + \alpha)$  hence reducing the bandwidth efficiency. Therefore, for dynamic spectrum access applications OFDM imparts significant overhead to the transmission of useful information.

### 7-2-2 Filter bank multi-carrier methods

There exist in literature several alternative multi-carrier techniques to OFDM for CR applications [131]. In [55] a filter-bank modulation technique called Filtered Multi-tone (FMT) is presented. FMT is similar to Frequency Division Multiplexing (FDM) in the sense that the sub-carriers do not overlap and guard bands are used between carriers to prevent interference. FMT is implemented using filter banks with a single prototype filter and its dual. The prototype filter is usually a Root Nyquist filter [55]. The inadequacy of this method is in its inefficient use of bandwidth as the sub-carriers do not overlap.

Another technique suggested is the Staggered Multi-tone (SMT) modulation. The method is also known as Offset QAM and is implemented using poly-phase filter banks [58]. Unlike FMT,

the method SMT allows overlap of carriers to maximize spectrum utilization. The modulation scheme used is Offset-QAM where the Quadrature and In-phase components are separated by a time-offset of half the symbol interval. Hence the name Staggered Multi-tone.

In [57] Boroujeny presents the Cosine Modulated Multi-tone (CMT) method as a capable multi-carrier modulation technique for CR applications. CMT is similar to FMT except that it allows overlap of adjacent bands [57]. Maximization of bandwidth is achieved by using vestigial side-band modulation.

We shall see in the next section that the WPSE/WPM method presented in this chapter is also suitable for DSA.

In the WPM technique the filter banks perform the dual role of shaping the spectrum as well as interpolating in time series. In [65] the two processes are separated to have a greater control over the characteristics of the carriers. This method, called the Interpolated Tree Orthogonal Multiplexing (ITOM), was introduced in [65] by Fred Harris. In ITOM, shaping of the transmission waveform spectra is performed external to the wavelet packet tree structure. Notching over the desired spectral interval is achieved by vacating one or more of the input branches.

### 7-3 Wavelet packet transceiver for spectral analysis and dynamic spectrum access

The main elements of the proposed CR system are the WPSE spectral analyzer, WPM transceiver and the spectrum vector manipulator. Fig. 7.3 depicts the blocks of the proposed system. The two main tasks of the proposed system are -

- spectrum analysis of radio environment to gather data on spectrum holes and occupied bands, and
- adaptive data transmission on idle bands through wavelet packet modulation.

At the transmitting end, an incoming high-rate serial data stream is split into  $N_{WPM}$  lower-rate parallel streams. The data in each parallel branch is then up-sampled by  $N_{WPM}$  and used to modulate  $N_{WPM}$  sub-carriers. Meanwhile, the WPSE evaluates the channel and performs a radio scene analysis to estimate LU frequency bands and detect spectrum holes. Based on the spectrum estimates, the cognitive modules dynamically de-activate those sub-channels of the WPM system that lie in and around the spectrum of the LU. The idea is to dynamically sculpt the transmission signal in a way it has no or very little time-frequency components competing with the LU. This way the CR can seamlessly co-exist with the LU. The sub-carriers are then modulated and scaled to the desired energy level to obtain the WPM transmission signal.

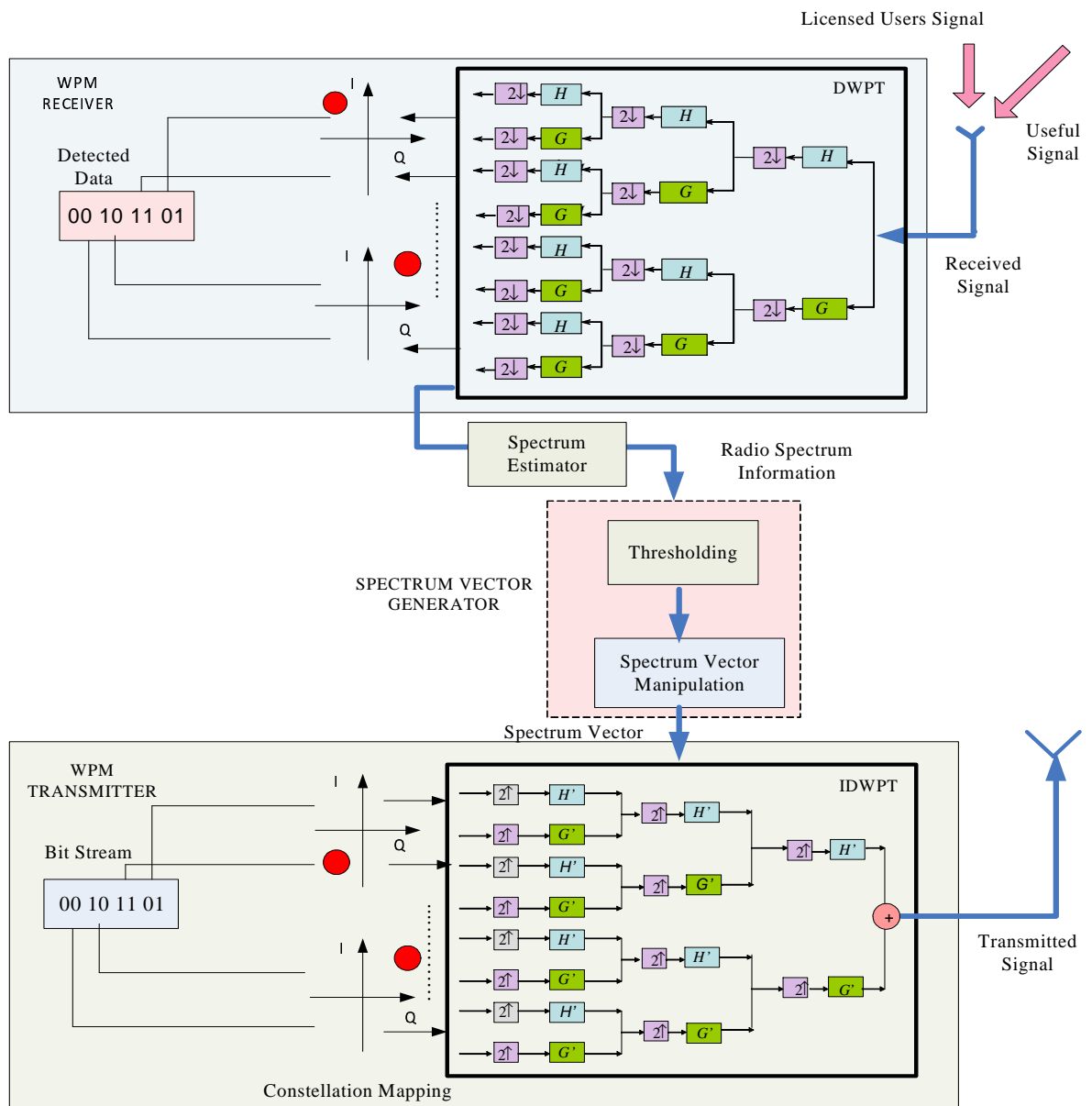


FIGURE 7.3: The proposed WPSE/WPM-based transceiver. The transmitter side contains the inverse discrete wavelet packet transformer (IDWPT) used to develop multi-carrier modulated signals. The receiver side consists of the discrete wavelet packet transformer (DWPT) used for spectrum estimation and multi-carrier data demodulation. IDWPT and DWPT are realized using filter bank analysis.  $H'$  and  $G'$  are the low and high pass synthesis filters whereas  $H$  and  $G$  are the low and high pass analysis filters. Down and Up arrows refer to down and up-sampling, respectively.

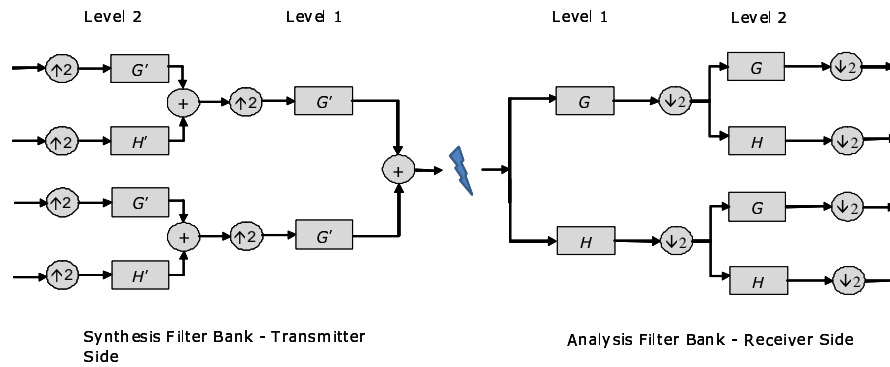


FIGURE 7.4: Wavelet Packed based Transmultiplexer.

### 7-3-1 Wavelet packet multi-carrier modulation (WPM)

WPM is implemented with orthogonal wavelet packet bases derived from a multi-resolution analysis (MRA) [7]. The procedure uses a pair of Quadrature Mirror Filters (QMF) which consists of a half-band high and low pass filter duo (represented by their impulse responses  $h[n]$  and  $g[n]$ ). Furthermore, they also have adjoints or duals  $\{h'[n], g'[n]\}$  which are their complex conjugate time-inversed versions.

The pair  $\{h'[n], g'[n]\}$  is called the analysis filter-pair and is used to generate the wavelet packet carriers for modulation of data at the transmitter end. On the other hand the combination  $\{h[n], g[n]\}$  is called the synthesis filter-pair and is used to derive the wavelet packet carrier duals for demodulation of data at the receiver end. The processes are referred to as inverse discrete wavelet packet transformation (IDWPT) at the transmitter and discrete wavelet packet transformation (DWPT) at the receiver, analogous to the inverse discrete Fourier Transform (IDFT) and the DFT, respectively, in OFDM systems [10]. Such systems are used for applications as varied as compression techniques in image/speech processing to transceiver design in communication theory.

### 7-3-2 Wavelet packet spectrum estimator (WPSE)

Spectrum sensing is an important functionality of Cognitive Radio (CR). Accuracy and speed of estimation are the key indicators to select the appropriate spectrum sensing technique. Conventional spectrum estimation techniques which are based on Fourier Transform (FT) suffer from familiar problems such as low frequency resolution, high variance of estimated power spectrum and high side lobes/leakages. Methods such as multi-taper spectrum estimation successfully alleviate these deficiencies but exact a high price in terms of complexity.

In this backdrop we present the WPSE as a promising spectral analysis tool. While the DWPT structure can be used for spectrum analysis the frequency information is not readily available.

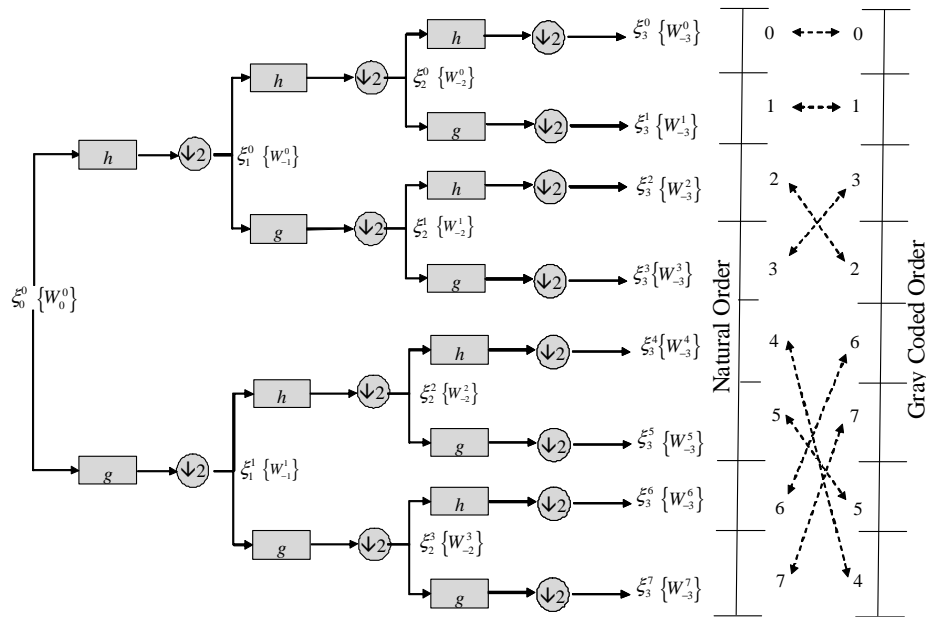


FIGURE 7.5: Wavelet Packet decomposition and ordering of the decomposed components in gray code order.

This is because the DWPT output is in the wavelet (time-scale) domain and has to be mapped into appropriate frequency bins. Furthermore, the wavelet packets are ordered as a binary Gray code sequence and not by increasing order of frequencies. This can be explained as follows - the output of any 2-channel analysis is the result of low/high-pass filtering followed by decimation by 2. Decimation generates two new filter outputs with half the number of elements and causes a form of aliasing called *band-shuffling* where the high-pass components are mirrored [11]. When the WP algorithm is applied recursively, the frequency ordering of the resultant WPs follows the Gray code order [123]. Fig. 7.5 illustrates this. The first step in the translation is therefore a Gray to Binary code conversion to re-order the WP indices. After this the PSD of the studied signal is obtained for each frequency bin from the energy contained in each wavelet packet node (details in Chapter-6).

### 7-3-3 Identification of spectrum holes and waveform shaping

The information on the radio environment obtained from the spectrum analysis is then processed to identify spectrum holes and occupied bands. This is carried on a sub-band-by-sub-band basis where the power contained in each WP sub-band is independently compared to a predetermined threshold. When the threshold exceeds the power of a sub-band the licensed user is declared to be present and if it is less than the threshold, the band is considered to be vacant and available for use. This information is used to shape the WPM spectrum.

The information about estimated PSD is passed to the carrier de-activation block containing a threshold and spectrum vector manipulation block (see Fig. 7.3). The threshold block decides

whether a particular band is occupied or not based on a defined threshold. When the power in a certain band is below the threshold value, the band is declared being ON (usable). The band is declared OFF (unusable) when the detected power is above the threshold. The threshold block produces a spectrum vector containing binary values 1 and 0 corresponding to the ON and OFF status, respectively.

Due to spectral spill-over it is also possible that the frequency bands adjacent to the band of consideration have a power above the threshold. Therefore, on such occasions it is necessary to de-activate carriers adjacent to the band of interest. For this purpose, the spectrum vector manipulation block is added to customize the spectrum vector. This block is also used to modify the format of the spectrum vector if the decomposition level in the receiver is different from the reconstruction level in the transmitter.

The spectrum vector determines whether a particular sub-carrier should be turned on or not. It is fed to the Inverse Discrete Wavelet Packet Transform (IDWPT) block in the transmitter where the requisite carriers are chosen. Based on the spectrum vector, the CR transmitter dynamically vacates the sub-carriers of the WPM system lying in and around the occupied frequency band. This is analogous to shaping the spectrum of the CR signal so that time-frequency components competing with LU are eliminated.

## 7-4 Simulation setup

### 7-4-1 System parameters

In this work a WPM based CR system with 128 equally spaced carriers obtained from a uniform level-7 decomposition of QMF is considered. The same tree structure is also used for spectrum analysis. Quadrature Phase Shift Keying (QPSK) is used as the modulation scheme while the choice of wavelet is a family of Frequency Selective filter banks [132]. These wavelets have narrow transition bands and are characterized by the parameters regularity index (K-regularity)  $K_r$ , length of filter  $L_f$  and transition band  $B_t$ . In this work, these parameters are taken to be  $K_r = 19$ ,  $L_f = 50$  and  $B_t = 0.2\pi$ . We shall explain these classes of filters in more detail in Chapter 8. The LU is taken to be a partial band source whose bandwidth is an integer multiple of the WPM sub-channel band. Table 7.1 summarizes the simulation parameters.

### 7-4-2 Comparison with Periodogram/Welch-OFDM systems

To evaluate the operation of the WPSE/WPM system the performances are compared with two OFDM configurations employing Periodogram and Welch modules, respectively, for spectrum

System parameters	WPM based CR	OFDM based CR
Number of sub-carriers	128 (7-level uniform WP decomposition)	128
Licensed user/interference source	OFDM based system of different bands	OFDM based system of different bands
Sub-carrier spacing of licensed user/interfering source $\Delta_f^{LU}$	Sub-carrier spacing $\Delta_f^{WPM-CR}$ equal to that of the LU, i.e. $\Delta_f^{WPM-CR} \approx \Delta_f^{LU}$	Sub-carrier spacing equal $\Delta_f^{OFDM-CR}$ to of the LU, i.e. $\Delta_f^{OFDM-CR} \approx \Delta_f^{LU}$
Number of multi-carrier symbols per Frame	100	100
Modulation	QPSK	QPSK
Channel	AWGN	AWGN
Oversampling Factor	1	1
Channel/source coding	None	None
Guard Band	None	None
Filter characteristics	Maximally frequency selective $L_f = 50, K_r = 19, B_t = 0.2$	Not Applicable
Time/Phase/Frequency Offset	0	0
Active Source	-2.1 dB	-2.1 dB
Threshold to determine presence/absence of source	-7dB	-7dB

TABLE 7.1: Simulation parameters.

estimation. In the Welch method the estimate is obtained by dividing the samples into 400 overlapping segments (50% overlap, Hamming window) each of 64 samples. Then a periodogram of each segment is calculated and averaged to obtain the true estimate. Fig. 7.6 shows the blocks of the Periodogram (or Welch) - OFDM based CR transceiver.

The Periodogram/Welch estimator analyses the radio environment and passes on information on the frequency content of the received signals to the threshold block. The threshold operation is performed on every sub-band and decision on occupied/free bands is encoded in a spectrum vector containing ones and zeros. This vector is then used to activate/vacate the OFDM carriers to shape the spectrum of the transmitted signal.

### 7-4-3 Sources and their characteristics

In order to investigate the performance of the WPSE/WPM system four different types of sources are considered, namely, partial-band, single-tone, multi-tones and swept-tone. The partial-band

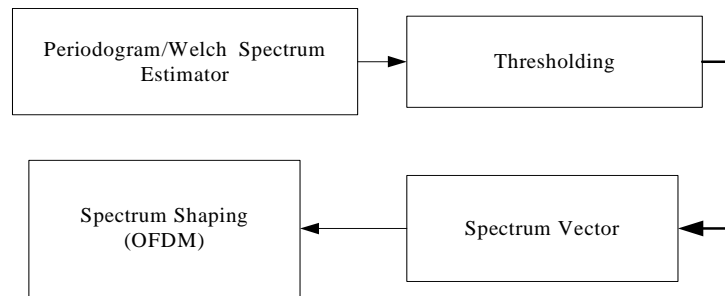


FIGURE 7.6: CR Transceiver based on Periodogram Family Spectrum Estimator and OFDM.

source has its energy spread over a continuous range of frequencies. In this work we have considered four different kinds of partial band sources, namely, single-band, triple-band, quadruple-band and quintuple-band, as presented in Fig. 7.7-A, Fig. 7.7-B, Fig. 7.7-C and Fig. 7.7-D, respectively. The single tone source (refer Figure Fig. 7.7-E) has all of its energy at one frequency and is taken to be in the middle of the range (at  $0.5\pi$ ) spanned by the WPSE. The multi-tones source (refer Fig. 7.7-F) consists of seven single tone sources located at normalized frequency from  $0.125\pi$  to  $0.875\pi$  and they are equally spaced.

Finally, a swept tone source (refer Chapter 6, fig. 6.14) is used to test how well the candidate schemes perform when there are temporal variations in the occupied frequency. The swept-tone source is a chirp signal in which the frequency increases (*up-chirp*) with time. After a sweep of incremental chirps the signal winds back to the original frequency to start with the next sweep cycle.

The test sources are so chosen that they shed different insights into the operation of the candidate systems.

#### 7-4-4 Experiment scenarios

The experiments are divided into two broad categories. In the first set the LU is taken to occupy fixed bands of contiguous frequencies. The evaluation of the test sources - four kinds of partial-band, single-tone, multi-tone and swept-tone - come under this category. In the second set the normalized frequency range  $[0, \pi]$  is divided into 128 equal bands (or frequency bins) and the LU is randomly activated and de-activated over a finite set of bins. The LU characteristics in the two experiments are listed in tables 7.2 and 7.3, respectively. An active source is taken to operate at  $-2.1\text{dB}$  level. In experiment 1 the threshold to evaluate the presence/absence of the LU is set to  $-7\text{dB}$ . This threshold was found after a series of empirical evaluations. In experiment 2, this threshold is varied between  $-3\text{dB}$  and  $-7\text{dB}$ .

Partial-band LUs are modeled using an OFDM setup. OFDM is the most popular technology for wide-band digital communication. Hence, the LU is modeled on OFDM in spite of the fact

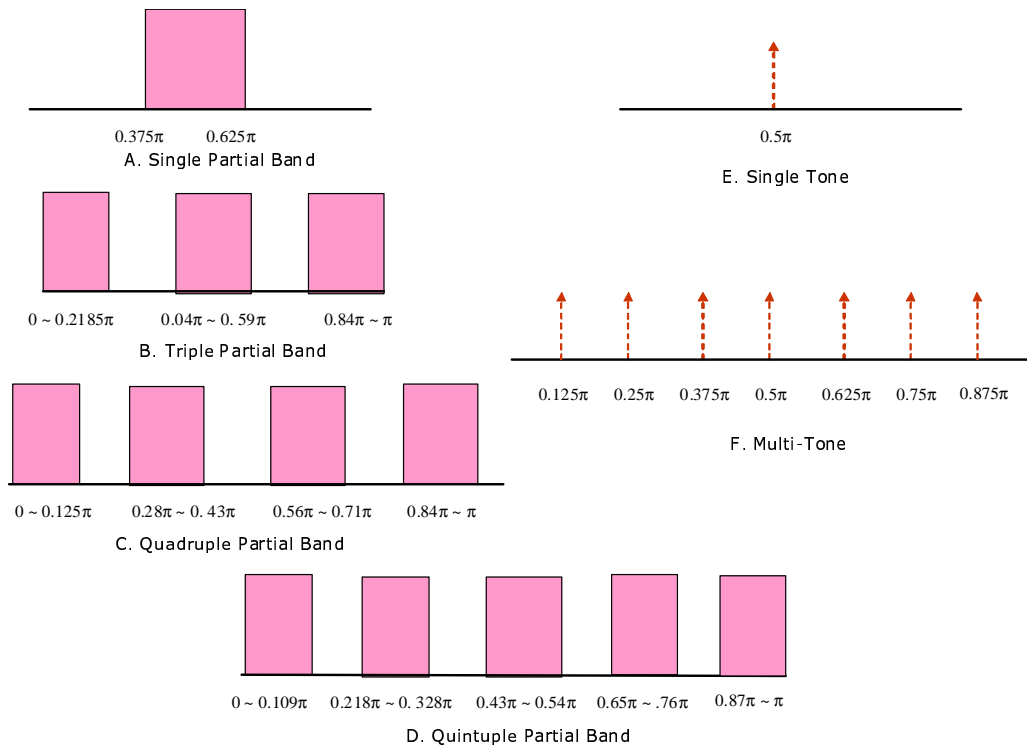


FIGURE 7.7: Sources and their characteristics. The sources considered are: (A) Partial band, (B) Triple partial band, (C) Quadruple partial band, (D) Quintuple partial band, (E) Single-tone and (F) Multiple tone.

that OFDM has poor spectral confinement properties. The bandwidth of the LU is adjusted by activating and vacating the requisite number of its sub-carriers. The sub-carrier spacing of each LU carrier  $\Delta_f^{LU}$  is taken to be the same as that of the WPM based CR  $\Delta_f^{WPM-CR}$  as well as that of the OFDM based CR  $\Delta_f^{OFDM-CR}$  candidates.

The WPSE-WPM operation is also compared with Periodogram-OFDM and Welch-OFDM configurations. All three systems operate under the same conditions.

Since the focus of this work is on the demonstration of WPM/WPSE as a PHY layer candidate for dynamic spectrum access, we have made the practical assumption that both the transmitter and receiver are at all times aware of the details of the active/vacated carriers. Alternatively, the systems could also operate under a collective spectrum pooling regime [130].

## 7-5 Results and analysis

### 7-5-1 Characteristics of OFDM and WPM sub-channels

Before presenting the results we first revisit the point on WPM being a lapped transform and its attendant benefits. The waveforms used in WPM are longer than the transform duration of

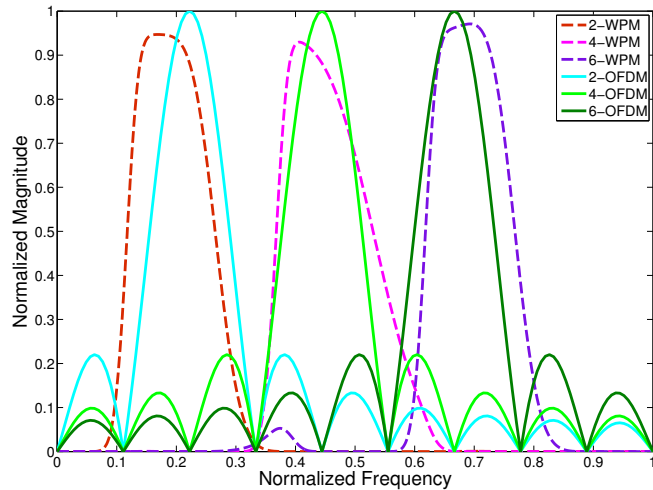


FIGURE 7.8: Spectrum of WPM and OFDM sub-carriers. For ease of depiction the 2nd, 4th and 6th sub-carriers alone of a 8-carriers system are shown.

one symbol and the symbols overlap in time. For a filter of length  $L_f$  the overall symbol length  $L_{sym}$  with  $N_{WPM}$  carriers can be shown to be [10]:

$$L_{sym} = (L_f - 1)(N_{WPM} - 1) + 1 \quad (7.6)$$

Longer waveforms allow for better frequency localization of the sub-carriers. This is illustrated in fig. 7.8, where the spectrum of the carriers of WPM and OFDM are plotted. For clarity of depiction only the 2nd, 4th and 6th sub-carriers of an 8-carrier system have been shown. Clearly the side lobes of the WPM sub-carriers are much lower than that of the OFDM system.

### 7-5-2 Comparison of efficiency of spectrum estimators

The first task of the Cognitive radios is to evaluate the spectrum to identify the LU characteristics. Table 7.4 lists the number of LU carriers that actually coincide with the CR versus the number of carrier removals recommended by various estimation techniques. Three different kinds of LU characteristics are considered, namely, partial band, triple partial band and quintuple partial band. It is clear from the tabulated values that the WPSE method is the most efficient in identifying the right number of CR carriers that coincide with the LU for all cases. The Periodogram estimator also gives good estimates. However, the Welch estimator suggests a larger number of CR sub-carriers operating in LU-bands than is actually the case (False alarm).

Type of sources	Description
Partial band	Consists of a partial band source occupying the normalized frequency range $[0.375, 0.625\pi]$ . (See Fig. 7.7-A)
Triple Partial band	Consists of a 3 Partial Band LU occupying the normalized frequency ranges $[0, 0.2188\pi]$ , $[0.4063\pi, 0.5938\pi]$ and $[0.8125\pi, \pi]$ , respectively. (See Fig. 7.7-B)
Quadruple Partial Band	Consists of a 4 Partial Band LU occupying the normalized frequency ranges $[0, 0.125\pi]$ , $[0.2813\pi, 0.4375\pi]$ , $[0.5625\pi, 0.7188\pi]$ and $[0.8438\pi, \pi]$ , respectively. (See Fig. 7.7-C)
Quintuple Partial Band	Consists of a 5 Partial Band LU occupying normalized frequency: $[0, 0.1094\pi]$ , $[0.2188\pi, 0.3281\pi]$ , $[0.4375\pi, 0.5469\pi]$ , $[0.6563\pi, 0.7656\pi]$ , $[0.875\pi, \pi]$ . (See Fig. 7.7-D)
Single tone	A single tone at normalized frequency $0.5\pi$ . (See Fig. 7.7-E)
Multi-tone	Consists of 7 single tones occupying the normalized frequencies occurring at $0.125\pi$ , $0.25\pi$ , $0.375\pi$ , $0.5\pi$ , $0.625\pi$ , $0.75\pi$ and $0.875\pi$ . (See Fig. 7.7-F)
Swept tone	Consists of a source which occupies different frequency bands at different time instances. A total of 20 sweeps (each of 640 samples) covering the frequency band of $[0.2\pi, 0.8\pi]$ is considered. (See Chapter 6, Fig. 6.14)

TABLE 7.2: Description of Licensed Users used in experiment 1.

Types of scenario	Description
Scenario A	64 sources are randomly activated and de-activated over 128 frequency bins and each source occupies 2 frequency bins.
Scenario B	32 sources are randomly activated and de-activated over 128 frequency bins and each source occupies 4 frequency bins.
Scenario C	16 sources are randomly activated and de-activated over 128 frequency bins and each source occupies 8 frequency bins.

TABLE 7.3: Description of the licensed users used in experiment 2.

Source types	Number of LU carriers co-inciding with CR	Recommended number of CR carrier removals		
		Periodogram	Welch	WPSE
Partial Band	32	33	36	32
Triple	76	77	84	76
Quadruple	76	79	87	76
Quintuple	72	76	83	72

TABLE 7.4: Actual number of LU carriers versus the number of carrier removals recommended by various estimation techniques.

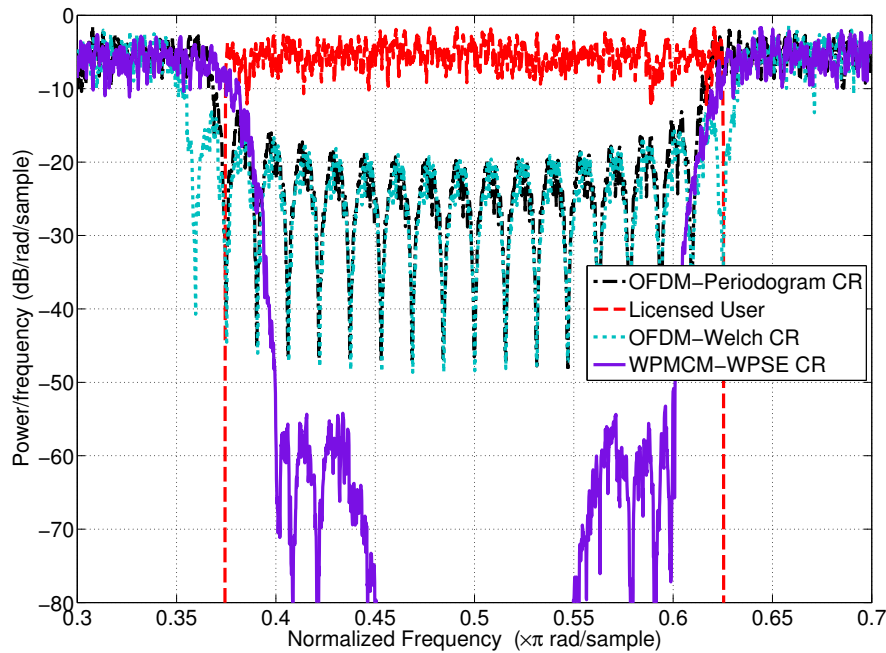
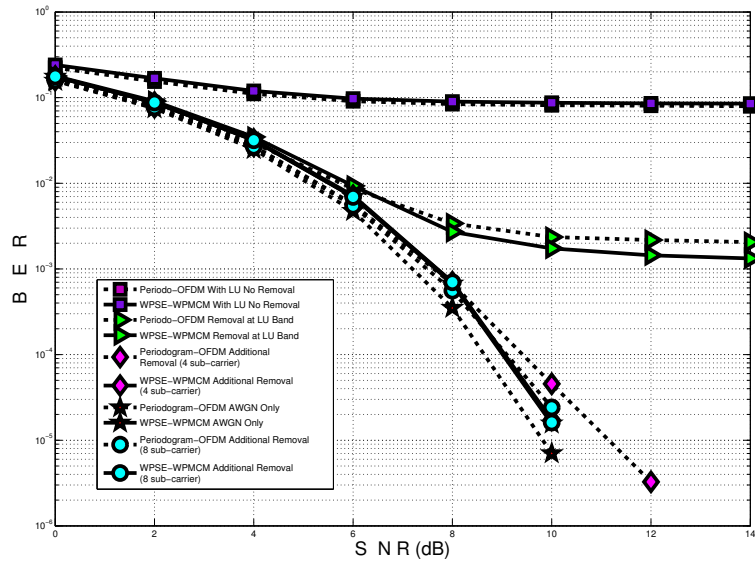


FIGURE 7.9: Plots of spectrum adaptation (Partial Band LU case) based on Periodogram/OFDM CR, Welch/OFDM CR and WPSE/WPM CR. Only those carriers corresponding to frequency bands with LU energy above the threshold are de-activated.

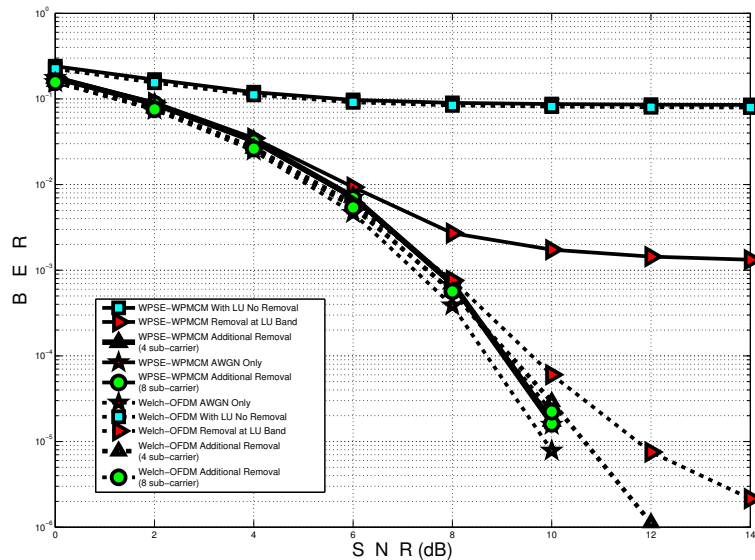
### 7-5-3 Evaluation of different sources

#### A. Partial band source

Fig. 7.9 shows the Power Spectral Density (PSD) plots of the enabled bands of the three CR configurations considered, namely, Periodogram/OFDM, Welch/OFDM and WPSE/WPM. The CR carriers coinciding with LU bands have been de-activated. The figure also shows the spectrum of the partial band LU. The plots clearly demonstrate the advantages of the proposed WPSE/WPM based CR system, in relation to the OFDM systems, in offering sharper spectrum shaping, better out-of-band (OOB) energy rejection and significantly lower interference to the LU. In fact the results show that the OOB rejection in WPSE/WPM is at least 40dB greater than that in the OFDM based systems.



(a)



(b)

FIGURE 7.10: BER Performance of WPSE-WPM based CR system for Partial Band LU case. (a) Comparison with Periodogram-OFDM based CR system, (b) Comparison with Welch-OFDM based CR system.

In fig. 7.10(a), the BERs of the WPSE/WPM CR system and Periodogram/OFDM CR system are compared. In fig. 7.10(b) the BERs of the WPSE/WPM CR system and Welch/OFDM CR system are shown. The plots show that the WPSE/WPM system better the performances of the Periodogram/OFDM system. When additional carriers abutting the sides of the LU (like an adaptive guard band) are removed the interference energy is reduced even further. As more and more carriers adjacent to LU are vacated, the performance of the WPSE/WPM CR system converges faster than the Periodogram/OFDM CR system towards the theoretical limit (no interference case). There is therefore a trade-off between the desirable rejection of interference

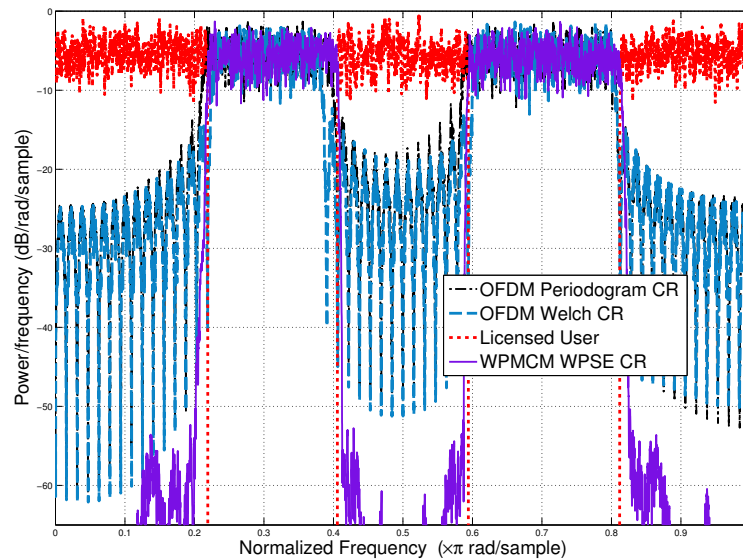


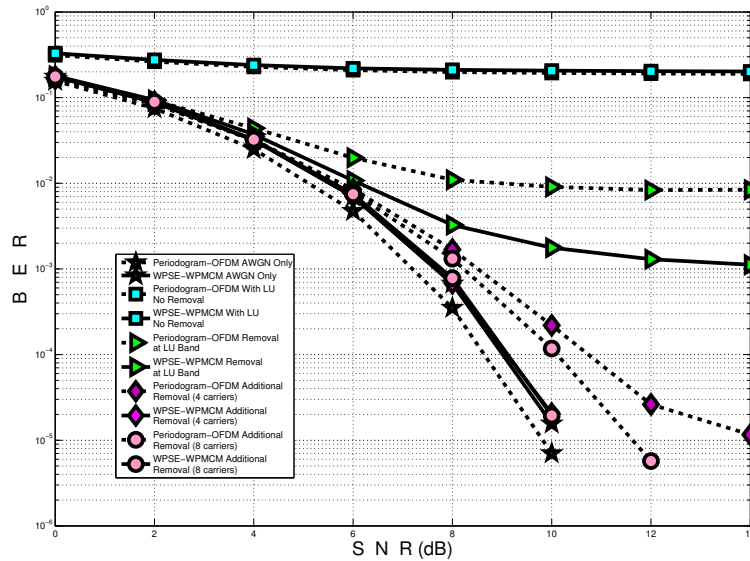
FIGURE 7.11: Plots of spectrum adaptation (Triple-Partial Band LU case) based on Periodogram/OFDM CR, Welch/OFDM CR and WPSE/WPM CR. Only those carriers corresponding to frequency bands with LU energy above the threshold are de-activated.

and bandwidth utilization. When more number of carriers are removed to reduce OOB energy, the bandwidth (and hence the throughput) is sacrificed. The best technique is therefore the one which gives good BER and OOB reduction for the lowest number of carrier removals possible. Clearly the results point towards WPSE/WPM.

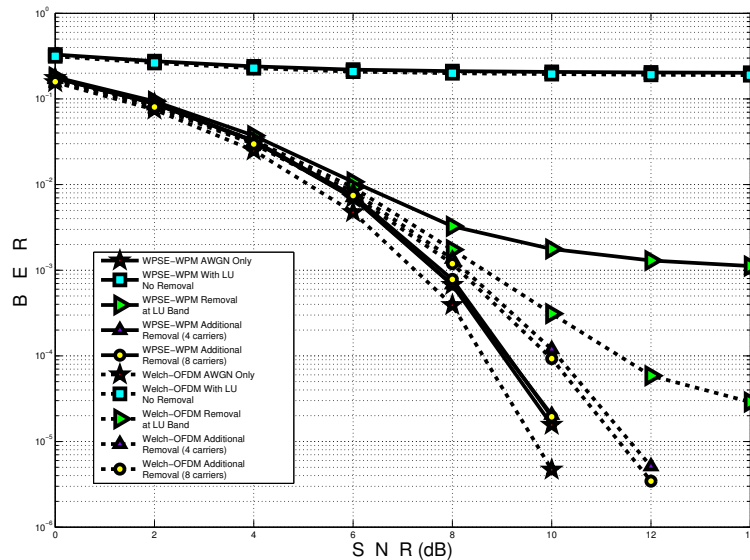
Three other LU cases, with triple, quadruple and quintuple partial band features, are investigated next. The PSD plot for the triple band LU are shown in fig. 7.11 while the BER curves are depicted in figs. 7.12(a) and 7.12(b). The corresponding PSD plots for the quadruple partial band LU are available in fig. 7.13 while the respective BER plots are provided in figs. 7.14(a) and 7.14(b). The plots for Quintuple sources are available in figs. 7.15, 7.16(a) and 7.16(b). The trends in the results are similar to that seen in the evaluation of the Partial Band LU. In comparison to OFDM, the WPM signal rejects OOB energy much better with lower interference to the LU (see figs. 7.11, 7.13 and 7.15). In fact the OOB power is at about -55 dB which is 40dB lower than in Periodogram (or Welch)/OFDM systems. Furthermore, the BER performances are also good (see figs. 7.12(a), 7.12(b), 7.14(a), 7.14(b), 7.16(a) and 7.16(b)).

### Carrier removal and reduction of interference

We now present results on the interference caused by candidate CR systems on the LU and the impact of removing carriers in-and-around the CR bands. An interference is caused because the sub-carriers of the multi-carrier based CR system spills into neighboring bands resulting in out-of-Band energy. One method suggested to minimize the interference is to remove carriers of CR adjacent to the LU [130].



(a)



(b)

FIGURE 7.12: BER Performance of WPSE-WPM based CR system for Triple-Partial Band LU case. (a) Comparison with Periodogram-OFDM based CR system, (b) Comparison with Welch-OFDM based CR system.

Figs. 7.17, 7.18, 7.19 and 7.20 depict the plots for the interference caused by the candidate CR systems for the four partial band LUs considered in this work. The figures also show as to how the removal of different number of carriers in and around the LU alleviates the problem of mutual interference. More the number of carriers removed, lower the interference. However, a price is paid in the form of inefficient spectral utilization. It is therefore important that only the right number of sub-carriers is removed.

Comparing the different candidate CR systems, it is clear from the results that the WPSE/WPM

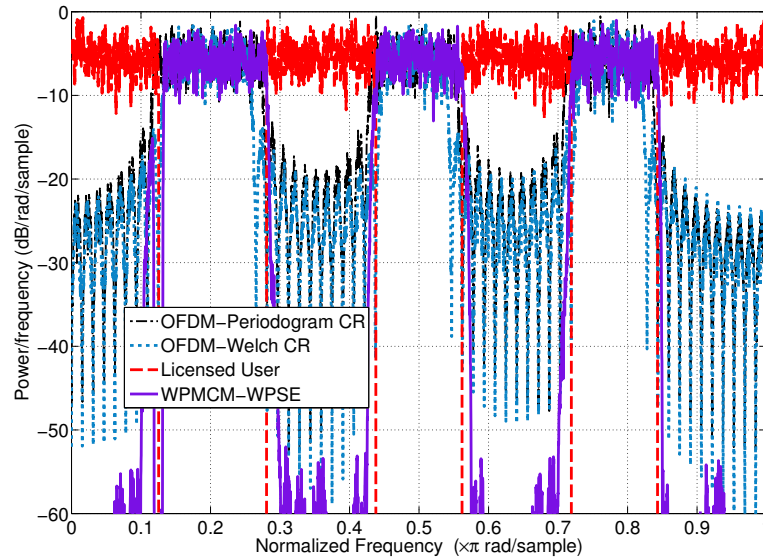


FIGURE 7.13: Plots of spectrum adaptation (Quadruple-Partial Band LU case) based on Periodogram/OFDM CR, Welch/OFDM CR and WPSE/WPM CR. Only those carriers corresponding to frequency bands with LU energy above the threshold are de-activated.

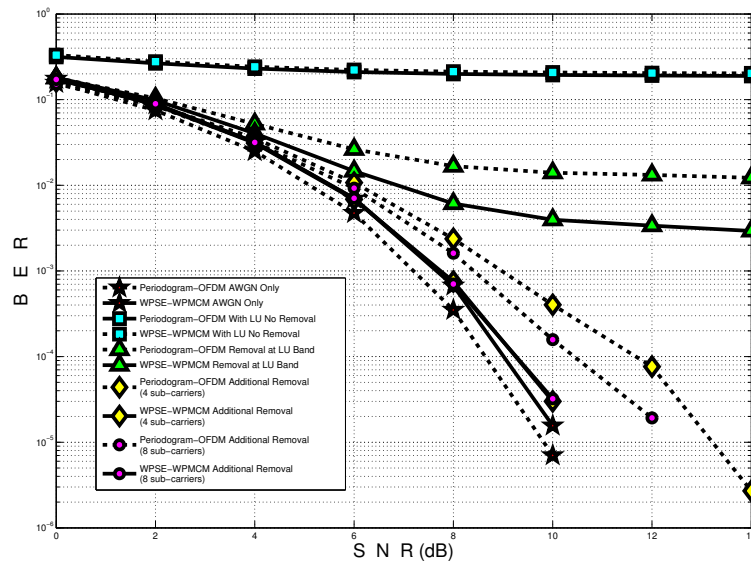
based system comfortably outperforms the other two systems - Periodogram/OFDM and Welch/OFDM in guarantying better interference suppression. In fact, for the partial band case the WPSE/WPM system ensures up to 45 dB lower interference than the other two systems. Furthermore, the interference values with carrier removals taper much faster in WPSE/WPM than in Periodogram/OFDM or Welch WPSE. These results are consistent for all four LU sources.

## B. Multi-tone source

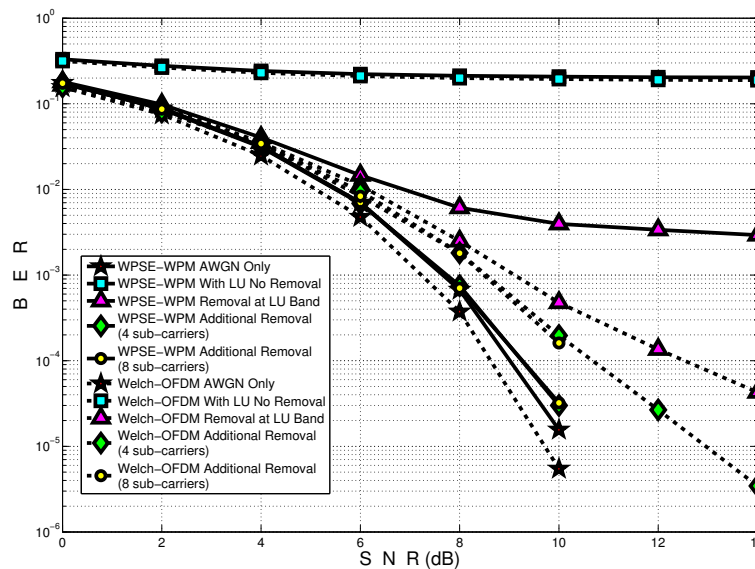
Fig. 7.21 shows the WPSE estimates of the multi-tone LU and the spectrum shaped CR. In the figure only those CR carriers that coincide with LU are de-activated. The figure shows how well the adapted CR's signal operates in the nulls of the LU signal. This is so even when no additional carriers apart from those that coincide with the LU bands are de-activated. The corresponding BER performance curves are plotted in fig. 7.22. The PSD and BER curves clearly show the advantages of spectrum shaping. Interestingly, unlike the case of the partial band source, it is enough to vacate only those CR carriers (totaling 14) that co-exist with the LU to obtain good performances. This implies that no additional carriers adjacent to the LU operating band have to be de-activated.

## C. Single-tone source

Fig. 7.23 depicts the wavelet packet based estimate of a single tone LU along with the spectrum adapted CR. The results obtained are similar to those of the multi-tone LU. In fig. 7.24 the



(a)



(b)

FIGURE 7.14: BER Performance of WPSE-WPM based CR system for Quadruple-Partial Band LU case. (a) Comparison with Periodogram-OFDM based CR system, (b) Comparison with Welch-OFDM based CR system.

BER performance of various CR configurations are shown. From figs. 7.23 and . 7.24, it can be deduced that the wavelet-based spectrum shaping approach performs well for single tone sources. Indeed unlike the partial band case there is no need for de-activation of additional carriers.

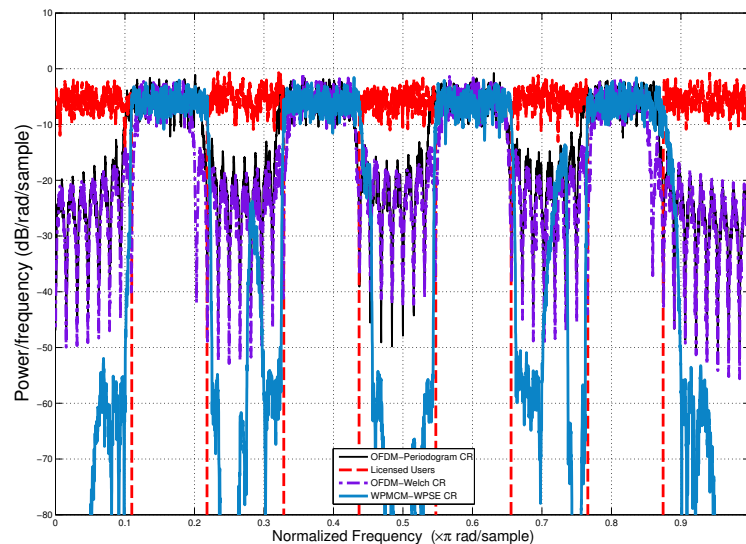


FIGURE 7.15: Plots of spectrum adaptation (Quintuple-Partial Band LU case) based on Periodogram/OFDM CR, Welch/OFDM CR and WPSE/WPM CR. Only those carriers corresponding to frequency bands with LU energy above the threshold are de-activated.

#### D. Swept-tone source

We now present results for the study with swept tone LU. In the experimental setup considered each sweep spans five chirps (or frequency increments). To estimate the swept tone LU, 20 sweeps in the normalized frequency band  $0.2\pi - 0.8\pi$  are considered. Each sweep consists of 640 data samples resulting in a total of 12800 samples for 20 sweeps. The spectrum estimation module takes a snapshot (or sub-sweep) containing 128 samples corresponding to 20% of a single sweep. Hence, five snapshots of a single sweep are available. Based on each 128-samples snapshot, spectrum vector generator has to determine the carriers to be turned off so that the WPM signal can be adapted accordingly.

Fig. 7.25(a) depicts the LU and CR PSD curve. In this figure, only the PSD of the fourth and the fifth sub-sweeps of LU signal are displayed together with the corresponding adapted CR PSD. It should also be noted that only the carriers that coincide with LU are de-activated in this figure. If the interference between the LU and CR signals needs to be reduced, it is possible to additionally de-activate the carriers adjacent to the band occupied by LU. Fig. 7.25(b) illustrates the effect of de-activation of four additional carriers that are adjacent to the LU band. And in fig. 7.26 the BER performance of WPM based CR system is plotted.

#### 7-5-4 Evaluation of efficiency of spectral utilization

We now present the results of the second set of experiments. In these experiments the bands occupied by the LU varies with time. Fig. 7.27 shows a snapshot of the LU characteristics over three different time periods. The details of the sources are provided in Table 7.1. The aim of

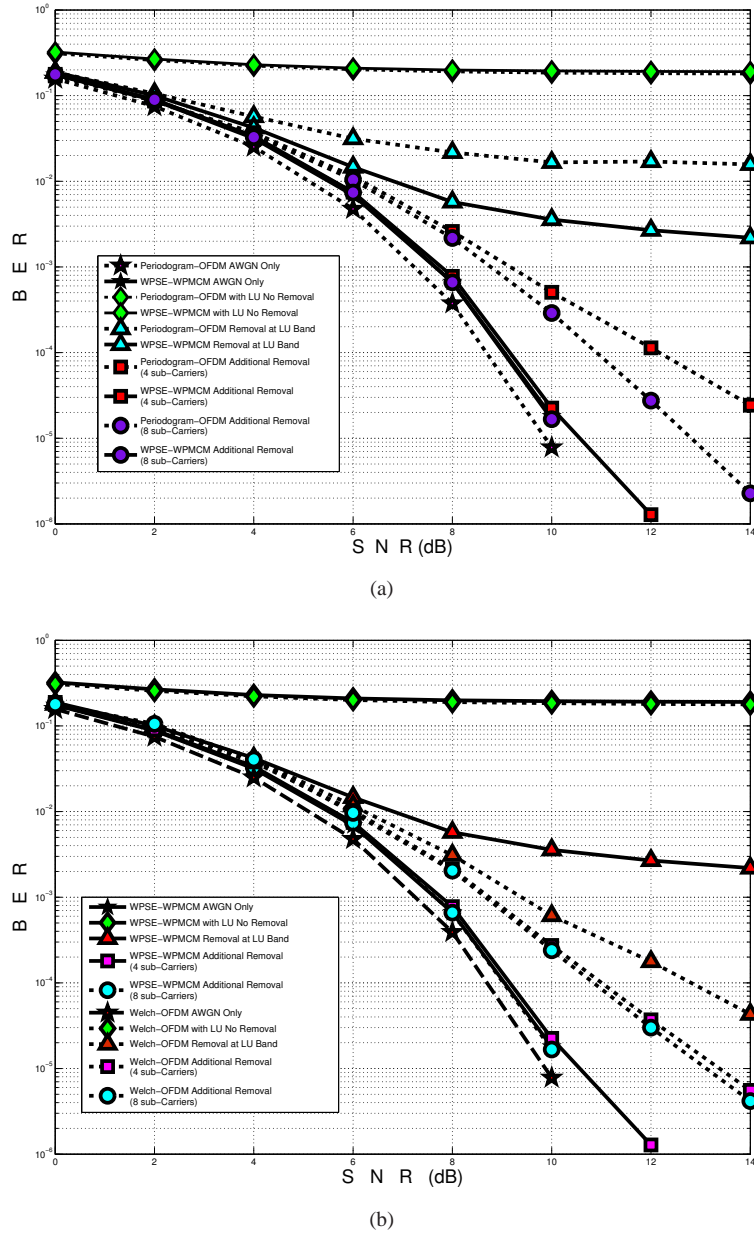


FIGURE 7.16: BER Performance of WPSE-WPM based CR system for Quintuple-Partial Band LU case. (a) Comparison with Periodogram-OFDM based CR system, (b) Comparison with Welch-OFDM based CR system.

these experiments is to compare and contrast as to how accurately the various CR configurations map the LU characteristics and how efficiently the spectrum is utilized. The figure-of-merit considered is the redundancy factor  $\eta_{\text{red}}$  which is defined as the difference between the number of CR carriers removed  $\eta_{\text{removed}}$  and those which actually coincide with the LU  $\eta_{\text{coincide}}$ ,

$$\eta_{\text{red}} = n_{\text{removed}} - n_{\text{coincide}} \quad (7.7)$$

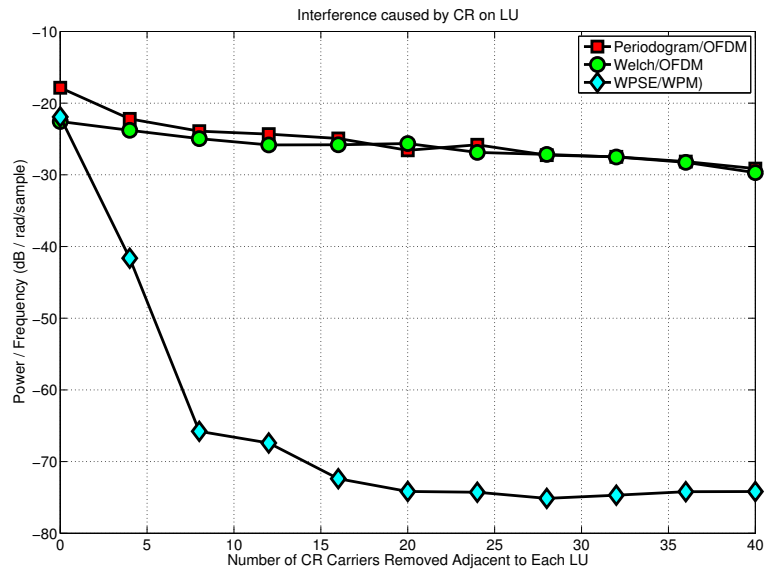


FIGURE 7.17: Interference caused by the CR on the LU (Partial Band source).

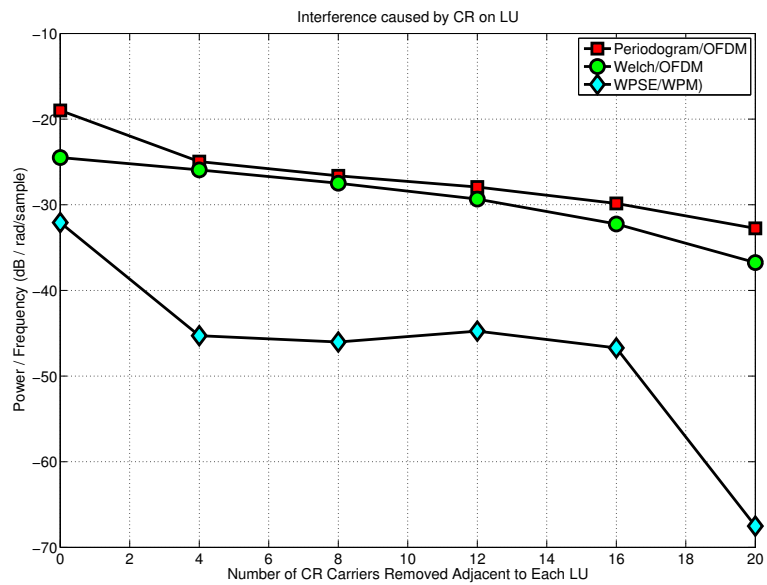


FIGURE 7.18: Interference caused by the CR on the LU (Triple-Partial Band source).

A positive value of  $\eta_{red}$  indicates that more carriers are removed than essential and hence the spectrum is not efficiently utilized. On the other, a negative  $\eta_{red}$  implies that a lower number of carriers than necessary have been removed, hence the chances of interfering with LU transmission is high. Therefore, the best method is the one which yields a redundancy factor  $\eta_{red}$  close to zero i.e. only the necessary carriers are removed.

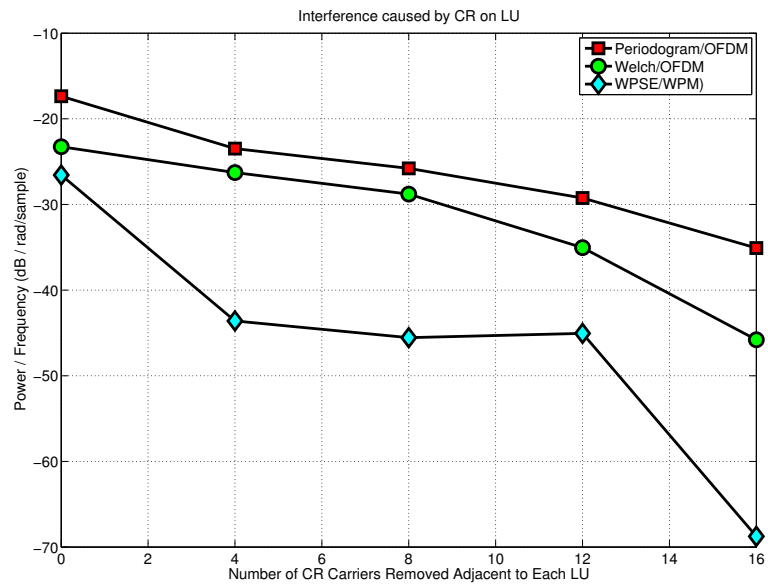


FIGURE 7.19: Interference caused by the CR on the LU (Quadruple-Partial Band source).

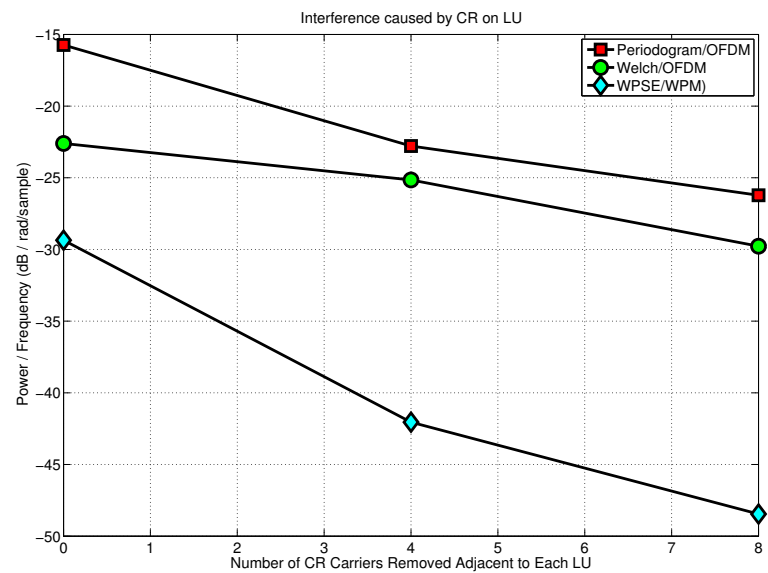


FIGURE 7.20: Interference caused by the CR on the LU (Quintuple-Partial Band source).

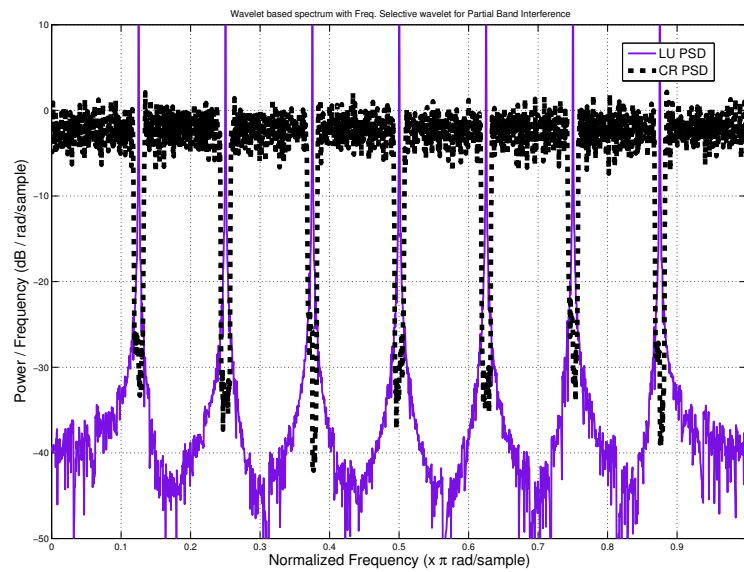


FIGURE 7.21: Spectrum adaptation of WPSE/WPM system co-existing with a multi-tone LU. Only those carriers that correspond to the frequency bands of the LU are de-activated (14 carriers). The wavelet decomposition filters used here have a length of 50, a K-regularity index of 7 and a transition band of  $0.2\pi$ . A 11-level WP decomposition tree is used for spectrum estimation.

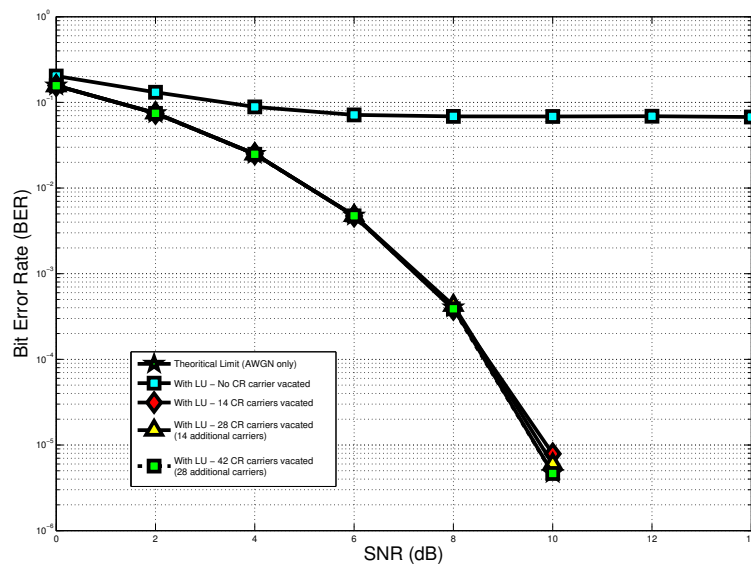


FIGURE 7.22: Performance of wavelet packet-based CR co-existing with a multi-tone licensed user. The wavelet decomposition filters used here have a length of 50, a K-regularity index of 7 and a transition band of  $0.2\pi$ . A 11-level WP decomposition tree is used for spectrum estimation.

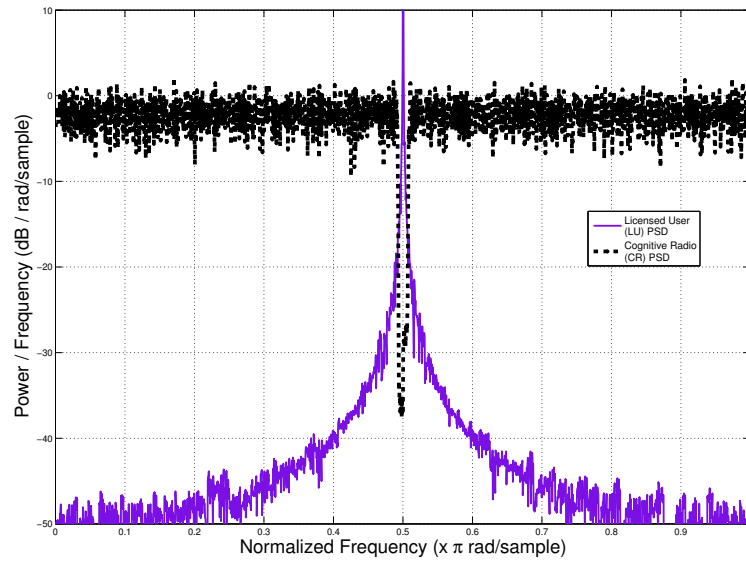


FIGURE 7.23: Spectrum adaptation of WPSE/WPM system co-existing with a single-tone LU. Only those carriers that correspond to the frequency bands of the LU are de-activated (14 carriers). The wavelet decomposition filters used here have a length of 50, a K-regularity index of 7 and a transition band of  $0.2\pi$ . A 11-level WP decomposition tree is used for spectrum estimation.

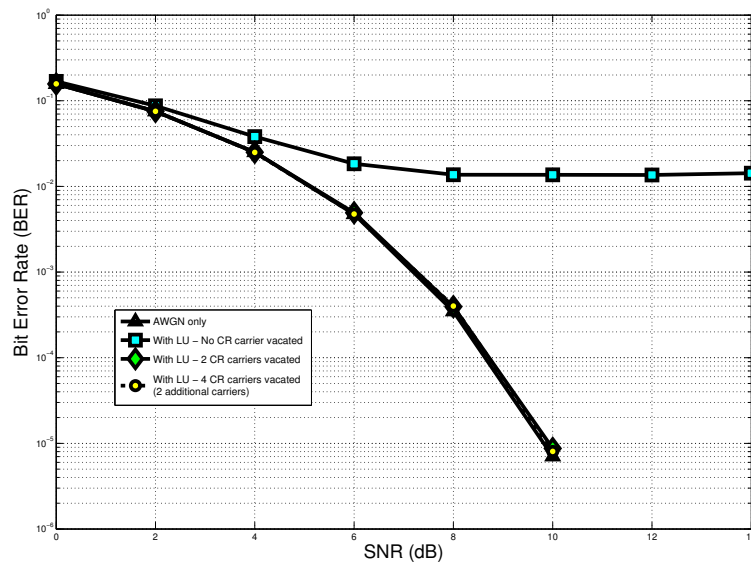
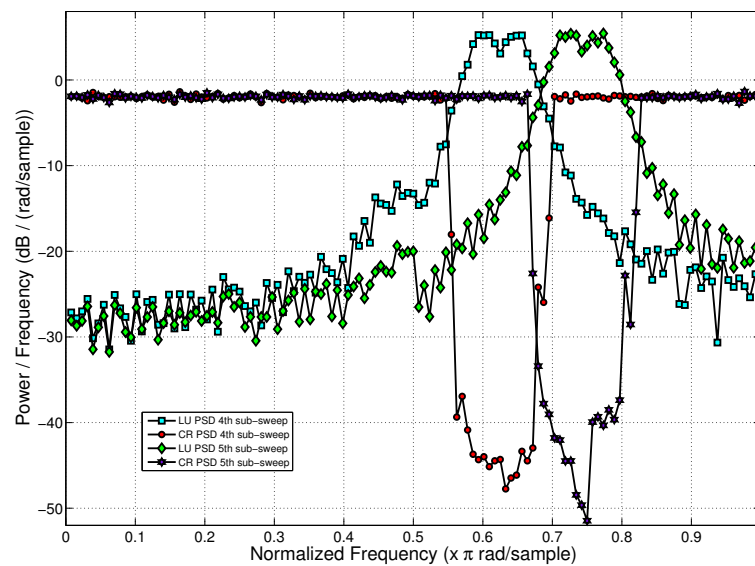
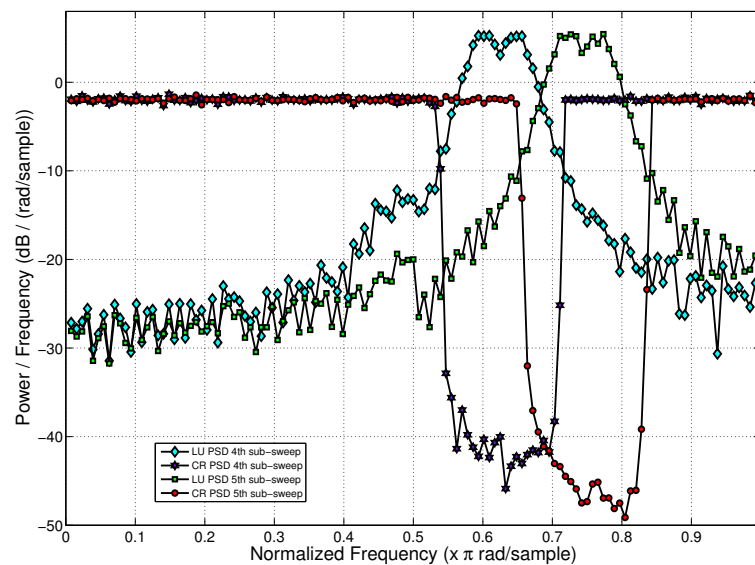


FIGURE 7.24: Performance of wavelet packet-based CR co-existing with a single-tone licensed user. The wavelet decomposition filters used here have a length of 50, a K-regularity index of 7 and a transition band of  $0.2\pi$ . A 11-level WP decomposition tree is used for spectrum estimation.



(a)



(b)

FIGURE 7.25: PSD of adapted CR source for a swept tone LU with sub-sweep size of 128 samples. In this case, every single sweep contains 5 sub-sweeps and only the 4th and 5th sub-sweeps are displayed. The wavelet decomposition filters used here have length of 50, K-regularity index of 7 and transition band of  $0.2\pi$ . The 7-level wavelet decomposition is used in spectrum estimation module. (a) Only carriers correspond to the bands with energy above threshold are de-activated. (b) Two bands in the left and two bands in the right side of bands having energy above threshold are also de-activated.

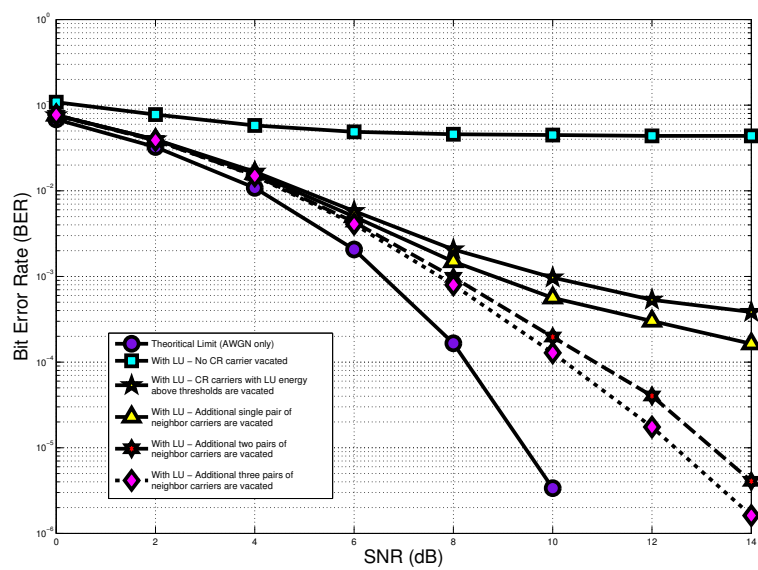


FIGURE 7.26: Performance of wavelet based spectrum estimation and spectrum adaptation in WPMCM CR system for swept tone LU case with sub-sweep size of 128 samples. The wavelet decomposition filters used here have length of 50, K-regularity index of 7 and transition band of  $0.2\pi$ . The 7-level wavelet decomposition is used in spectrum estimation module.

Table 7.5 shows the redundancy in the de-activated carriers for the three CR systems for the case when the normalized frequency range  $[0, \pi]$  is split into 128 equal frequency bins and 64 LU sources (each occupying 2 adjacent frequency bins) are randomly activated or vacated. Three thresholds -3, -5 and -7dB are considered. From the table entries it is clear that the Welch/OFDM pair de-activates more carriers than needed while the Periodogram/OFDM combination de-activates less than needed. For example, when the threshold level is set to -7dB, the Welch/OFDM system de-activates around 35 sub-carriers more than needed. As a result, this

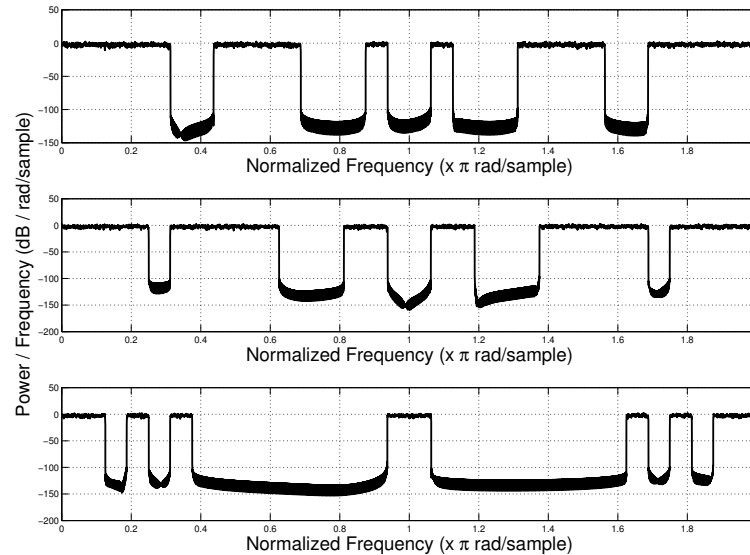


FIGURE 7.27: PSD of the LU over three different frame periods.

Types of CR Systems	Threshold	BER (at SNR = 8dB)	Redundancy in Average Numbers of De-activated Carriers
Periodogram-OFDM	-3 dB	0.1588	-52.2488
Periodogram-OFDM	-5 dB	0.0445	-0.5491
Periodogram-OFDM	-7 dB	0.0574	0.0000
Welch-OFDM	-3 dB	0.1616	-44.7847
Welch-OFDM	-5 dB	0.0955	0.5300
Welch-OFDM	-7 dB	0.0056	34.9094
WPSE-WPM	-3 dB	0.0779	-17.6369
WPSE-WPM	-5 dB	0.0259	-0.1428
WPSE-WPM	-7 dB	0.0167	2.4944

TABLE 7.5: Illustration of redundancy in number of vacated carriers for the three CR systems (Periodogram-OFDM, Welch-OFDM, and WPSE-WPMCM) in the presence of randomly activated 64 LU signals occupying 128 frequency bins in the normalized frequency range  $[0, \pi]$ . Each source occupies 2 frequency bins. A positive value for the redundancy factor implies that the CR system has vacated more sub-carriers than needed (false alarm) and a negative value indicates that the CR system has vacated a lower number of sub-carriers than necessary (miss-detection).

Types of CR Systems	Threshold	BER (at SNR = 8dB)	Redundancy in Average Numbers of de-activated carriers
Periodogram-OFDM	-3 dB	0.1476	-51.9472
Periodogram-OFDM	-5 dB	0.0233	-0.4981
Periodogram-OFDM	-7 dB	0.0224	0.0000
Welch-OFDM	-3 dB	0.0871	-28.5088
Welch-OFDM	-5 dB	0.0321	0.2359
Welch-OFDM	-7 dB	0.0020	24.0451
WPSE-WPM	-3 dB	0.0823	-15.8528
WPSE-WPM	-5 dB	0.0224	-0.1506
WPSE-WPM	-7 dB	0.0193	2.4891

TABLE 7.6: Illustration of redundancy in number of vacated carriers for the three CR systems (Periodogram-OFDM, Welch-OFDM, and WPSE-WPMCM) in the presence of randomly activated 32 LU signals occupying 128 frequency bins in the normalized frequency range  $[0, \pi]$ . Each source occupies 4 frequency bins. A positive value for the redundancy factor means that the CR system has vacated more sub-carriers than needed (false alarm) and a negative value means that the CR system has vacated a lower number of sub-carriers than necessary (miss-detection).

Types of CR Systems	Threshold	BER(at SNR = 8dB)	Redundancy in Average numbers of de-activated carriers
Periodogram-OFDM	-3 dB	0.1533	-51.8838
Periodogram-OFDM	-5 dB	0.0242	-0.4988
Periodogram-OFDM	-7 dB	0.0169	0.0000
Welch-OFDM	-3 dB	0.0524	-12.6600
Welch-OFDM	-5 dB	0.0075	0.1881
Welch-OFDM	-7 dB	0.0012	9.0328
WPSE-WPMCM	-3 dB	0.0632	-13.6359
WPSE-WPMCM	-5 dB	0.0189	-0.1334
WPSE-WPMCM	-7 dB	0.0098	2.4288

TABLE 7.7: Illustration of redundancy in number of vacated carriers for the three CR systems (Periodogram-OFDM, Welch-OFDM, and WPSE-WPMCM) in the presence of randomly activated 16 LU signals occupying 128 frequency bins in the normalized frequency range  $[0, \pi]$ . Each source occupies 8 frequency bins. A positive value for the redundancy factor means that the CR system has vacated more sub-carriers than needed (false alarm) and a negative value means that the CR system has vacated a lower number of sub-carriers than necessary (miss-detection).

system wastes bandwidth which is precious. On the other hand, the Periodogram/OFDM combination de-activates about 50 carriers (case when threshold is set to  $-3\text{dB}$ ) less than necessary. This indicates that this method does not shape the CR spectra adequately. The WPSE/WPM pair performs efficiently for all the scenarios with the redundancy factor being close to zero with a low BER.

Another important observation one can make is the impact of the threshold value used to evaluate the presence or absence of a LU. When the threshold is set to a low value (say  $-7\text{dB}$ ), more number of carriers is removed than necessary. This may reduce the mutual interference between the CR and LU and hence improve the BER. But also has the negative effect of poorer spectral utilization. On the other hand, when the threshold is set to a high value (say  $-3\text{dB}$ ), lower number of carriers are removed than required. This means that the mutual interference between the LU and CR is not completely eliminated.

In table 7.6 the case when 32 sources (each occupying 4 frequency bins) are randomly activated and de-activated are listed. And in table 7.7 the case where 16 sources (each occupying 8 frequency bins) are randomly activated and de-activated is illustrated. The pattern in these results also follows the one described earlier and the WPSE/WPM emerges as the best choice.

## 7-6 Summary

In this chapter, a wavelet packet based CR transceiver with spectrum estimation capabilities was presented. The sub-carriers are orthogonal wavelet packet bases derived from a tree structure consisting of fundamental para-unitary 2-channel filter pairs. The WPSE uses the same filter bank structure as used for the data modulation and hence is implemented at no additional cost. The co-existence of the CR station with LU is enabled by dynamically activating or vacating the CR sub-carriers to occupy the time-frequency gaps of the LU. The main advantage of using wavelet packets for CR is in its property of allowing the symbols to overlap in time without losing its orthogonality. This results in greater localization of the wavelet packet carriers in frequency. This implies that the transmitted signal can be better shaped and confined without leaking into neighboring bands.

Through simulation studies the benefits of the proposed system were demonstrated. The performances were also compared with existing systems based on FFT and OFDM. The studies showed that the proposed WPM method offered better BER performance and bandwidth efficiency at a lower interference to the licensees. This is illustrated by the high out-of-band energy rejection which is at least  $40\text{dB}$  more than that in OFDM systems. Furthermore, the method accurately shaped the CR characteristics with only the right number of carriers removed (very

less redundancy) paving the way for excellent spectrum utilization and a good throughput at an acceptable BER.

It is worth pointing out that the complexity in the implementation of the WPM system has been shown to be comparable with that of OFDM [10]. A. Jamin in [10] shows that the WPM implementation costs is of the same order as that of OFDM and can even be lower for medium to large size transforms and wavelet filters of moderate length. In addition this, we furthered the work in [13] by investigating the application of WPM based multi-carrier modulation to a multi-antenna cognitive radio system employing the vertical Bell-labs layered space-time (V-BLAST) receiver architecture.

## Chapter 8

# A unified framework to design orthonormal wavelet bases

### 8-1 Introduction

In the previous chapters we evaluated the WPM system performance under metrics like operation under loss of time/frequency/phase synchronization (chapter 4)) and PAPR (chapter 5)<sup>1 2</sup>. We also presented two applications of the WPM structure for spectrum estimation (chapter 6) and as a wide-band multi-carrier modulation technology for dynamic spectrum access (DSA) (chapter 7). In this chapter we advance the state- of-the-art in WPM to design wavelet bases for use in communication formats. The possibility of adapting the characteristics of the WPM transmission is pursued with two examples where families of wavelets which are i) maximally frequency selective and ii) have the lowest cross correlation energy, respectively, are developed. To this end a generic, unified framework that facilitates the design of new wavelet bases that cater to a requirement is established. Suitable optimizations are introduced when and where necessary to make the problem tractable. Numerical solvers are used to obtain the solution.

An important point to note is that by design of wavelet bases we essentially mean the design of filters used to obtain the wavelets. This is because the WPM system is realized with a tree structure made of cascaded half-band low/high-pass filter pairs. As we shall see later in the chapter, this is both an advantage and a disadvantage. The advantage being that the design process is reduced to that of deriving Finite Impulse Response (FIR) filters; hence standard,

---

<sup>1</sup>This chapter is an extended version of the publication [21]. Parts of it also appeared in [18] and [20]. Wherever applicable, for any material that has been reused from a publication where this author is the second author, a written consent and approval has been obtained from the first author.

<sup>2</sup>The author gratefully acknowledges the contributions of Msc student Mr. D. Karamehmedovic for his active co-operation and help with the computer simulations.

well established methods can be employed; the disadvantage is that the relationship between the filters and the wavelet bases is sometimes not straightforward or explicit.

The rest of the chapter is organized as follows. Section 8.2 outlines the basics of the design process. The design process is exemplified with two examples in Section 8.3 and Section 8.4. In Section 8.3 the design of maximally frequency selective wavelet is considered while Section 8.4 will delve on the filters with low cross correlation errors. In each of these sections the design process is formulated as an optimization problem. The numerical results and their analysis is also presented in the respective sections. A summary of the material in the chapter is provided in Section 8.5.

## 8-2 Criterion for design of wavelets

### 8-2-1 Design procedure

The attributes of the WPM system greatly depend on the set of transmission bases utilized which in turn is determined by the filters used. This means that by adapting the filters one can adapt the WPM characteristics to satisfy a system specification. Choosing the right filter though is a delicate task. The filters have to satisfy a number of constraints and cannot be arbitrarily chosen. Besides the design objectives there are other budgets which have to be considered in order to guarantee that the designed wavelet is valid. The design procedure consists of 3 major steps, namely:

1. Formulation of the design problem, i.e. stating the design objectives and constraints mandated by wavelet theory.
2. Application of suitable optimizations and transformations to make the problem tractable.
3. Utilization of numerical solvers to obtain the required filter coefficients.

At the end of the design procedure a low-pass FIR filter  $h[n]$ , satisfying the design and wavelet constraints, is obtained. From this filter the other three filters  $h[n]$ ,  $h'[n]$  and  $g'[n]$ , are derived through the QMF relation (see Chapter 3). In the following sections we will elaborate on each of these processes.

### 8-2-2 Filter bank implementation of WPM

First, a quick recap of the wavelet and WPM theory. It is well known that compactly supported orthonormal wavelets can be obtained from a tree structure constructed by successively iterating

discrete two-channel para-unitary filter banks [8, 27]. Time and frequency limited orthonormal wavelet packet bases  $\xi(t)$  can be derived by recursively iterating discrete half-band high  $g[n]$  and low-pass  $h[n]$  filters, as <sup>3</sup>:

$$\begin{aligned}\xi_{l+1}^{2p}(t) &= \sqrt{2} \sum_m h[m] \xi_l^p(t - 2m) \\ \xi_{l+1}^{2p+1}(t) &= \sqrt{2} \sum_m g[m] \xi_l^p(t - 2m)\end{aligned}\quad (8.1)$$

In eq.(8.1) the subscript  $l$  denotes the level in the tree structure and superscript  $p$  indicates the waveform index. The number of bases  $p$  generated is determined by the number of iterations  $l$  of the two-channel filter bank. eq.(8.1), known as the *2-scale equation*, can be interpreted as follows - a basis function belonging to a certain sub-space of lower resolution can be obtained from shifted versions of the bases belonging to a sub-space of higher resolution; and the weights  $h$  and  $g$  used in the transformation are low- and high-pass in nature.

The filters  $h$  and  $g$  form a quadrature mirror pair and are also known as the analysis filters. These filters have duals/adjoints known as synthesis filters which are also a pair of half-band low-  $h'$  and high-pass filters  $g'$ . All these four filters share a tight relation and hence it is enough if the specifications of one of these filters are available. The wavelet packet sub-carriers (used at the transmitter end) are generated from the synthesis filters. The wavelet packet duals (used at the receiver end) are obtained from the analysis filters. The entire WPM transceiver structure can thus be realized by this set of two QMF pairs. Hence, the design process can also be confined to the construction of one of the filters, usually the low-pass analysis filter  $h$ . A thorough analysis on the topic can be found in chapters 2 and 3.

### 8-2-3 Important wavelet properties

The wavelet tool can be a double edged sword - on the one hand there is scope for customization and adaptation; on the other hand there are no clear guidelines to choose the best wavelet from for a given application. In order to ease the selection process design constraints such as orthogonality, compact support and smoothness are imposed. We had outlined these properties in chapter 2; here we shall discuss them in more detail.

<sup>3</sup>The expressions are considered in continuous time-domain to convenience derivations

### A. Wavelet existence and compact support

This constraint is necessary to ensure that the wavelet has finite non-zero coefficient and thus the impulse response of the wavelet decomposition filter is finite as well. This property can be derived by simply integrating both sides of the two-scale equation [133]: <sup>4</sup>:

$$\begin{aligned}
 \int_{-\infty}^{\infty} \xi(t) dt &= \sqrt{2} \int_{-\infty}^{\infty} \sum_n h[n] \xi(2t - n) dt \\
 \int_{-\infty}^{\infty} \xi(t) dt &= \sqrt{2} \sum_n h[n] \int_{-\infty}^{\infty} \xi(2t - n) dt \\
 \int_{-\infty}^{\infty} \xi(t) dt &= \sqrt{2} \sum_n h[n] \int_{-\infty}^{\infty} 0.5 \xi(2t - n) d(2t - n)
 \end{aligned} \tag{8.2}$$

Substituting  $u = 2t - n$ , eq.(8.2) can be rewritten as:

$$\begin{aligned}
 \int_{-\infty}^{\infty} \xi(t) dt &= \frac{1}{\sqrt{2}} \sum_n h[n] \int_{-\infty}^{\infty} \xi(u) du \\
 \frac{\int_{-\infty}^{\infty} \xi(t) dt}{\int_{-\infty}^{\infty} \xi(u) du} &= \frac{1}{\sqrt{2}} \sum_n h[n]
 \end{aligned} \tag{8.3}$$

Finally we obtain the compactly supported wavelet constraint as:

$$\sum_n h[n] = \sqrt{2}. \tag{8.4}$$

It should be noted that the derivation that is given above is only possible if the scaling function is absolutely integrable and the integration of the scaling function is non-zero. Due to this fact, eq.(8.4) is also recognized as the wavelet existence constraint.

### B. Para-unitary condition

The para-unitary or the orthogonality condition is essential for many reasons. First, it is a prerequisite for generating orthonormal wavelets [8, 27]. Second, it automatically ensures perfect reconstruction of the decomposed signal i.e., the original signal can be reconstructed without amplitude or phase or aliasing distortion. To satisfy the para-unitary constraint the scaling filter

<sup>4</sup>The subscripts denoting the decomposition level  $l$  and the waveform index  $p$  have been dropped for convenience.

coefficients have to be orthogonal at even shifts [8, 27]. The constraint can be derived using the orthonormality property of the scaling function and its shifted version as follows:

$$\int_{-\infty}^{\infty} \xi(t)\xi(t-k)dt = \delta(k) \quad (8.5)$$

Substituting the two-scale equation eq.(8.1) in eq.(8.5) we get:

$$\begin{aligned} \int_{-\infty}^{\infty} \sum_n h[n] \xi(2t-n)\sqrt{2} \sum_m h[m] \xi(2(t-k)-m)\sqrt{2}dt &= \delta[k], \\ 2 \sum_n h[n] \sum_m h[m] \int_{-\infty}^{\infty} \xi(2t-n)\xi(2(t-k)-m)dt &= \delta[k], \\ 2 \sum_n h[n] \sum_m h[m] \int_{-\infty}^{\infty} 0.5\xi(2t-n)\xi(2(t-k)-m)d(2t) &= \delta[k]. \end{aligned} \quad (8.6)$$

Or,

$$\sum_n h[n]h[n-2k] = \delta[k], \text{ for } k = 0, 1, \dots, (L/2) - 1. \quad (8.7)$$

Eq.(8.7) is called the double-shift orthogonality relation of the wavelets. In eq.(8.7),  $L$  represents the length of the low-pass filter. For a filter of length  $L$  the orthogonality condition eq.(8.7) imposes  $L/2$  non-linear constraints on  $h[n]$ .

### C. Flatness/K-Regularity

This property is a rough measure of the smoothness of the wavelet. The regularity condition is needed to ensure that the wavelet is smooth in both the time- and frequency-domains [29]. It is normally quantified by the number of times a wavelet is continuously differentiable. The simplest regularity condition is the *flatness* constraint which is stated on the low-pass filter (LPF). A LPF is said to satisfy  $K$ th order flatness if its transfer function  $H(\omega)$  contains  $K$  zeros located at the Nyquist frequency ( $\omega = \pi$ ). For any function  $Q(\omega)$  with no poles or zeros at ( $\omega = \pi$ ) this can be written as:

$$H(\omega) = \left( \frac{1 + e^{j\omega}}{2} \right)^K Q(\omega), \quad (8.8)$$

with  $Q(\pi) \neq 0$ .

In eq.(8.8),  $Q(\omega)$  is a factor of  $H(\omega)$  that does not have any single zero at  $\omega = \pi$ . Having  $K$  number of zeros at  $\omega = \pi$  also implies that  $H(\omega)$  is  $K$ -times differentiable and its derivatives

are zero when they are evaluated at  $\omega = \pi$ . Considering that

$$H(\omega) = \sum_n h[n] \exp(-j\omega n), \quad (8.9)$$

the  $k$ th order derivative of  $H(\omega)$  would be

$$H^{(k)}(\omega) = \sum_n h[n] (-jn)^k \exp(-j\omega n). \quad (8.10)$$

The evaluation of eq.(8.10) at  $\omega = \pi$  would result in,

$$\begin{aligned} \sum_n h[n] (-jn)^k \exp(-j\pi n) &= H^{(k)}(\pi), \\ \sum_n h[n] (-j)^k (n)^k (e^{-j\pi})^n &= 0, \\ \sum_n h[n] (-1)^n (n)^k &= 0. \end{aligned} \quad (8.11)$$

Therefore, the K-regularity constraint in terms of the low-pass filter coefficients can be given as:

$$\sum_n h[n] (n)^k (-1)^n = 0, \text{ for } k = 0, 1, 2, \dots, K - 1. \quad (8.12)$$

#### 8-2-4 Degrees of freedom to design

Eqs.(8.4), (8.7) and (8.12) are necessary and sufficient conditions for the set to form an orthonormal basis and have to be imposed for all wavelet design procedures. For a filter of length  $L$  the design process is about obtaining  $L$  unknown filter variables from  $L$  equations. Of these  $L$  equations, one is required to satisfy the wavelet existence condition,  $L/2$  come from the para-unitary constraint,  $K - 1$  from the regularity constraint and the remaining  $L/2 - K$  conditions offer the possibility for establishing the design objective. The larger the value of  $L/2 - K$ , more the degree of freedom for design and greater is the loss in regularity. There is therefore a trade-off to be made. The  $L/2 - K$  degrees of freedom that remain after satisfying the wavelet existence, orthogonality and K-regularity condition can be used to design a scaling filter with the desired property (see fig. 8.1). In Sections 9.3 and 9.4 we illustrate this with two examples.

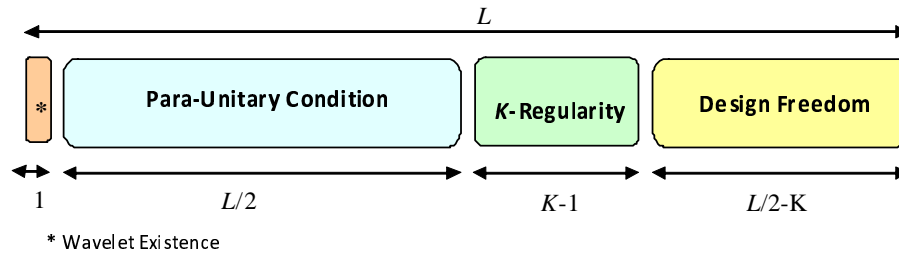


FIGURE 8.1: Wavelet conditions and degrees of freedom for design.

### 8-3 Example 1 - Maximally frequency selective wavelets

As the first example we consider the design of filters which are maximally frequency selective. Frequency selectivity is a useful property for many applications especially, in the fields of Cognitive radio, for dynamic spectrum access and LTE-advanced<sup>5</sup>, where the spectrum of a transmission signal has to be accurately shaped to match a frequency mask with low leakages to the neighboring bands. We shall see in Section 9.3.5 that the frequency selective filters yield wavelet bases with a well confined spectral footprint. Such bases are ideal for applications such as wavelet packet based spectrum estimation (WPSE) presented in chapter 6 and for spectrum shaping presented in chapter 7.

To obtain the frequency selective filters the design parameters are stated in the frequency-domain in terms of the desired magnitude response  $|H(\omega)|^2$  of the LPF (see fig. 8.2). In the figure  $\omega_p$  and  $\omega_s$ , denote pass- and stop-band frequencies, respectively.  $[0, \omega_p]$  is the pass-band,  $[\omega_s, \pi]$  is the stop-band and  $[\omega_p, \omega_s]$  is the transition band  $B_t$ .  $\Delta_b$  denotes the maximum ripple that can

<sup>5</sup>In Long Term Evolution advanced (LTE-advanced) the spectrum can be allocated over non-contiguous frequency bands. This possibility necessitates that the frequency bands are well confined without any side lobes or spill-over.

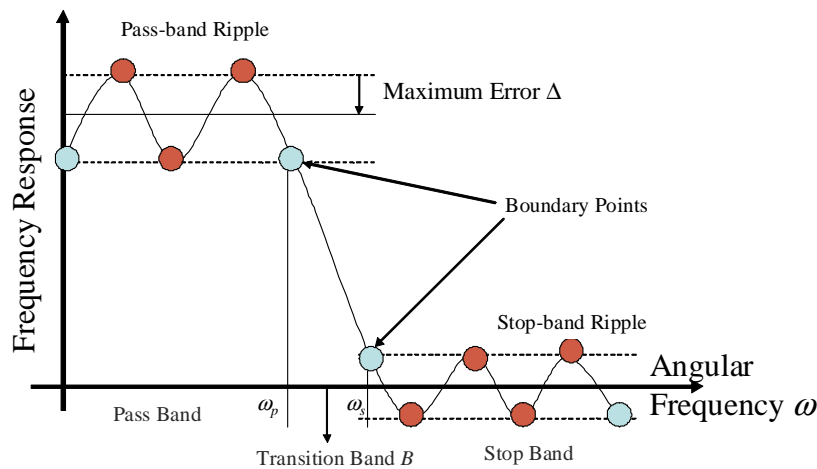


FIGURE 8.2: Plot of magnitude response  $|H(\cdot)|^2$  of the designed filter.

be tolerated and the stop-band constraint can be stated as

$$0 \leq |H(\omega)|^2 \leq \Delta_b \text{ for } \omega \in [\omega_s, \pi], \quad (8.13)$$

where,

$$|H(\omega)|^2 = \sum_n \sum_m h[n]h[m]e^{-j\omega(n-m)}. \quad (8.14)$$

In terms of the impulse response, eq.(8.14) can be expressed as:

$$0 \leq \sum_n \sum_m h[n]h[m]e^{-j\omega(n-m)} \leq \Delta_b \text{ for } \omega \in [\omega_s, \pi]. \quad (8.15)$$

### 8-3-1 Formulating the design problem

This procedure was originally proposed by Parks and McClellan [134] for the design of FIR filters. However, it has to be adapted to accommodate the constraints (see Section 9.2.4) mandated by the wavelet theory [132]. The design goal is to generate filters with the desired transition band  $B_t$  and minimum error  $\Delta_b$  while satisfying the wavelet constraints. For a given transition band  $B_t$ , this optimization problem can be formally stated as:

*Problem 1: Minimize  $B_t$  subject to the wavelet constraints eqs.(8.4),(8.7), (8.12) and the filter constraint eq.(8.15).*

i.e.,

MINIMIZE:  $\Delta_b$

SUBJECT TO:

$$\begin{aligned} \sum_n h[n] &= \sqrt{2}, \\ \sum_n h[n]h[n-2k] &= \delta(k) \text{ for } k = 0, 1, \dots, (L/2) - 1, \\ \sum_n h[n](n)^k(-1)^n &= 0 \text{ for } k = 0, 1, 2, \dots, K - 1, \\ 0 \leq |H(\omega)|^2 &\leq \Delta_b \text{ for } \omega \in [\omega_s, \pi]. \end{aligned} \quad (8.16)$$

for fixed values of  $B_t$ ,  $L$  and  $K$ .

It should be noted that we define the stop-band constraint only within the range of  $\omega \in [\omega_s, \pi]$  due to the inherent anti-symmetry property of  $(|H(\omega)|^2 - 1)$  about  $\omega = \pi/2$  (see fig. 8.2) [132].

The stop band constraint can thus be simplified as:

$$\begin{aligned}
 |H(\omega)|^2 &= H(e^{j\omega})H(e^{-j\omega}) \\
 &= \left( \sum_n h[n]e^{-j\omega n} \right) \left( \sum_m h[m]e^{j\omega m} \right) \\
 &= \sum_n \sum_m h[n]h[m]e^{-j\omega(n-m)}.
 \end{aligned} \tag{8.17}$$

Hence, the stop-band constraint can be written as:

$$0 \leq \sum_n \sum_m h[n]h[m]e^{-j\omega(n-m)} \leq \Delta_b \quad \forall \omega \in [\omega_s, \pi] \tag{8.18}$$

From eqs.(8.7) and (8.18), it is clear that both the double-shift orthogonality and the stop-band constraints are non-linear and non-convex. Therefore, the optimization problem can only be solved by general purpose solvers which do not guarantee a global solution. Furthermore, when the number of constraints increases these general purpose algorithms often fail to provide a valid solution. In order to overcome this difficulty, some authors have suggested multiple starting point techniques or branch-and-bound method [135].

In this work the objective function and the constraints are solved using convex optimization and semi-definite programs [136–142]<sup>6</sup>. In the following sections we convert the design constraints into a convex form and obtain the solution with the aid of convex optimization tools [143–145].

### 8-3-2 Transformation of problem from non-convex to convex

Fortunately, it is possible to transform the non-convex/non-linear equations into a linear/convex problem by reformulating the constraints in terms of the autocorrelation sequence  $r_h[k]$  [146–149]:

$$r_h[k] = \sum_{m \in \mathbb{Z}} h[m]h[m+k] \tag{8.19}$$

Taking into account the inherent symmetry of the autocorrelation sequence it can be defined more precisely as:

$$r_h[l] = \sum_{n=0}^{L-l-1} h[n]h[n+l] \quad \text{for } l \geq 0 \tag{8.20}$$

In eq.(8.20),  $L$  is the length of the FIR filter and the autocorrelation function is symmetric about  $l = 0$ , i.e:

$$r_h[-l] = r_h[l] \tag{8.21}$$

<sup>6</sup>In Appendix A1 we have briefly discussed convex optimization and semi-definite programming.

We derive the four constraints eqs.(8.4), (8.7), (8.12) and (8.18) in terms of  $r_h[l]$  in the following sections.

### A. Compact support or admissibility constraint

The compact support constraint in eq.(8.4) can be rewritten as:

$$\begin{aligned} \sum_{n=0}^{L-1} h[n] &= \sqrt{2}, \text{ or} \\ \sum_{n=0}^{L-1} h[n] \sum_{m=0}^{L-1} h[m] &= 2. \end{aligned} \quad (8.22)$$

Taking  $m = n + l$ , we have:

$$\sum_{n=0}^{L-1} \sum_{l=-n}^{L-n-1} h[n] h[n+l] = 2 \quad (8.23)$$

Reversing the order of the summation and considering the fact that the impulse response of filter  $h[n]$  has non-zero values only at  $0 \leq n \leq L - 1$ , we obtain:

$$\sum_{l=-(L-1)}^{L-1} \sum_{n=0}^{L-l-1} h[n] h[n+l] = 2 \quad (8.24)$$

The compact support constraint in eq.(8.4) can then be rewritten as:

$$\sum_{l=-(L-1)}^{L-1} r_h[l] = 2 \quad (8.25)$$

Taking into consideration the double shift orthonormality property (see eq. (8.7)) and the fact that the autocorrelation sequence is symmetric, we can simplify eq.(8.25) further as:

$$r_h[0] + 2 \sum_{l=1}^{L-1} r_h[l] = 2 \quad (8.26)$$

$$\sum_{l=1}^{L-1} r_h[l] = \frac{1}{2} \quad (8.27)$$

Eq.(8.27) is the compactly supported wavelet constraint stated in terms of the autocorrelation sequence  $r_h[l]$ .

### B. Double shift orthogonality constraint

The double shift orthogonality constraint presented in eq.(8.7), can be expressed in terms of the autocorrelation sequence  $r_h[l]$  as follows:

$$\sum_m h[m]h[m+2k] = r_h[2k] = \delta[k] \quad (8.28)$$

It should be noted that eq.(8.28) is obtained by applying  $n - 2k = m$  on eq.(8.7). Hence the final double-shift orthogonality constraint in terms of the autocorrelation sequence  $r_h[l]$  is:

$$r_h[2k] = \delta[k] = \begin{cases} 1, & \text{if } k = 0 \\ 0, & \text{otherwise.} \end{cases} \quad (8.29)$$

Here  $k = 0, 1, \dots, \lfloor \frac{L-1}{2} \rfloor$ .

We again make use of the symmetry property to simplify it. In contrast to eq.(8.7) which was non-convex, eq.(8.29) consists of linear equalities and is convex.

### C. K-Regularity constraint

The regularity constraint can be reformulated in terms of the autocorrelation sequence  $r_h[l]$  by considering the square of the absolute value of eq.(8.8) i.e.:

$$|H(\omega)|^2 = \left( \frac{1 + e^{-j\omega}}{2} \right)^K \left( \frac{1 + e^{j\omega}}{2} \right)^K |Q(\omega)|^2 \quad (8.30)$$

Requiring the transfer function  $H(\omega)$  to have  $K$  zeros at the Nyquist frequency ( $\omega = \pi$ ) is equivalent to requiring  $|H(\omega)|^2$  to have  $2K$  zeros at  $\omega = \pi$ . Taking into account the fact that  $|H(\omega)|^2$  is the Fourier transform of the autocorrelation sequence of  $r_h[l]$ , we can represent the  $2k$ th order derivative of  $|H(\omega)|^2$  as follows:

$$\left( |H(\omega)|^2 \right)^{(2k)} = \sum_l r_h[l] (-jl)^{2k} \exp(-j\omega l) \quad (8.31)$$

The evaluation of eq.(8.31) at  $\omega = \pi$  would yield:

$$\begin{aligned} \sum_l r_h[l] (-jl)^{2k} \exp(-j\pi l) &= \left( |H(\pi)|^2 \right)^{(2k)}, \\ \sum_l r_h[l] (-j)^{2k} (l)^{2k} (e^{-j\pi})^l &= 0, \text{ and} \\ \sum_l r_h[l] (l)^{2k} (-1)^l &= 0. \end{aligned} \quad (8.32)$$

Now, for a filter of length  $L$ , the filter index  $l$  varies as  $-(L-1) \leq l \leq (L-1)$ ; therefore eq.(8.32) becomes:

$$\sum_{l=-L+1}^{L-1} (-1)^l (l)^{2k} r_h[l] = 0, \text{ for } k = 0, 1, \dots, K-1. \quad (8.33)$$

In eq.(8.33),  $K$  represents the desirable regularity index of the wavelet. Making use of the symmetry property of the autocorrelation sequence  $r_h[l]$  and taking into consideration that it has a zero value for  $l = 0$ , eq.(8.33) can be further simplified as:

$$\sum_{l=1}^{L-1} (-1)^l (l)^{2k} r_h[l] = 0, \text{ for } k = 0, 1, \dots, K-1. \quad (8.34)$$

#### D. Stop-band constraint

Defining  $n = m + k$ , eq.(8.18) can be expressed as:

$$|H(\omega)|^2 = \sum_m \sum_k h[m]h[m+k]e^{-j\omega k} = \sum_k r_h[k]e^{-j\omega k} \quad (8.35)$$

Therefore, the stop-band constraint becomes:

$$0 \leq \sum_k r_h[k]e^{-j\omega k} \leq \Delta_b \text{ for } \omega \in [\omega_s, \pi] \quad (8.36)$$

The autocorrelation sequence  $r_h[k]$  is symmetric about  $k = 0$ , (i.e,  $r_h[l] = r_h[-l]$ ) [132]. Hence, eq.(8.36) can be modified as,

$$\begin{aligned} |H(\omega)|^2 &= r_h[0] + \sum_l r_h[l] \left( e^{-j\omega l} + e^{j\omega l} \right) \\ &= r_h[0] + 2 \sum_l r_h[l] \cos(\omega l), \end{aligned} \quad (8.37)$$

for  $l = 1, 2, \dots, L-1$  and  $\omega \in [\omega_s, \pi]$ .

Consequently, the stop-band constraint in eq.(8.36) can be written as,

$$0 \leq r_h[0] + 2 \sum_l r_h[l] \cos(\omega l) \leq \Delta_b, \quad (8.38)$$

for  $l = 1, 2, \dots, L-1$  and  $\omega \in [\omega_s, \pi]$ .

### E. Spectral factorization and discretization on stop band constraint

The reformulated optimization problem consists of the objective function and the design constraints expressed in terms of the autocorrelation sequence  $r_h[l]$  and therefore the optimal solution will also be in the autocorrelation domain. Since our interests lie in the filter coefficients  $h[n]$ , we have to obtain  $h[n]$  from  $r_h[l]$ . There are no unique solutions to the filter coefficient that can be obtained for a given  $r_h[l]$ . We borrow the spectral factorization algorithm proposed in [146] to obtain unique filters which satisfy the minimum-phase property [147]. The spectral factorization of an autocorrelation sequence  $r_h[l]$  can be performed as long as the logarithm function of its Fourier transform  $R_h(\omega)$  remains in  $\mathbb{R}$ <sup>7</sup>. To ensure this, the following additional constraint is enforced:

$$R_h(\omega) = |H(\omega)|^2 \geq 0, \text{ for } \omega \in [0, \pi]. \quad (8.39)$$

Using eq.(8.38), the time domain representation of eq.(8.39) can be given as,

$$r_h[0] + 2 \sum_l r_h[l] \cos(\omega l) \geq 0 \text{ for } l = 1, 2, \dots, L-1 \text{ and } \omega \in [0, \pi]. \quad (8.40)$$

Since we have an infinite number of inequalities in eq.(8.40), we discretize it in the interval  $\omega \in [0, \pi]$ . This is necessary in order to make the optimization problem practically solvable. One such approach is proposed in [146] where the continuous variable  $\omega$  is replaced with the discrete variable  $\omega_i = i\pi/d$ , defined on the finite set  $i = [0, \dots, d]$ . A typical value of  $d$  suggested in [146] is  $15n$ . As a result, the constraint required for successful spectral factorization after applying the discretization process becomes:

$$r_h[0] + 2 \sum_{l=1}^{L-1} r_h[l] \cos(i\pi l/d) \geq 0 \text{ for } i = 0, 1, \dots, d. \quad (8.41)$$

For simplicity of expression, heron, we refer to eq.(8.41) as the spectral factorization constraint. As with the spectral factorization constraints, the number of stop-band constraints defined in eq.(8.38) is also infinite. Hence, the stop-band constraints also have to be discretized to make the problem practically solvable. After the discretization, the stop-band constraints in eq.(8.38) can be rewritten as:

$$0 \leq r_h[0] + 2 \sum_{l=1}^{L-1} r_h[l] \cos(i\pi l/d) \leq \Delta_b \text{ for } i = \left\lceil \frac{\omega_s}{\pi} \right\rceil * d, \dots, d. \quad (8.42)$$

The optimization problem in terms of the autocorrelation sequence  $r_h[l]$  can thus be summarized as:

MINIMIZE:  $\Delta_b$

<sup>7</sup>See Appendix A2 for more details on the Kolmogorov spectral factorization algorithm.

SUBJECT TO:

$$\begin{aligned}
& \sum_{l=1}^{L-1} r_h[l] = \frac{1}{2} \\
r_h[2k] = \delta[k] &= \begin{cases} 1, & \text{if } k = 0, \\ 0, & \text{otherwise} \end{cases}, \text{ where } k = 0, 1, \dots, \lfloor \frac{L-1}{2} \rfloor \\
& \sum_{l=1}^{L-1} (-1)^l (l)^{2k} r_h[l] = 0 \text{ for } k = 0, 1, \dots, K-1, \\
0 \leq r_h[0] + 2 \sum_{l=1}^{L-1} r_h[l] \cos(i\pi l/d) &\leq \Delta_b \text{ for } i = \lceil \frac{\omega_s}{\pi} \rceil * d, \dots, d, \\
r_h[0] + 2 \sum_{l=1}^{L-1} r_h[l] \cos(i\pi l/d) &\geq 0 \text{ for } i = 0, 1, \dots, d.
\end{aligned} \tag{8.43}$$

### 8-3-3 Reformulation of optimization criterion in the $Q(\omega)$ function domain

The optimization problem stated above is both convex and linear. Therefore, in principle any linear or convex programming tool can be used to solve this optimization problem. However, a numerical problem may arise for long filters (when the value of  $L$  and  $K$  are large) when the regularity constraint in eq(8.28) becomes ill-conditioned [132, 145]. In order to alleviate this the optimization problem is expressed in terms of the  $Q(\omega)$  function, which is defined as:

$$\begin{aligned}
|H(\omega)|^2 &= \left( \frac{1 + e^{-j\omega}}{2} \right)^K \left( \frac{1 + e^{j\omega}}{2} \right)^K |Q(\omega)|^2 \\
&= \left( \frac{(1 + e^{j\omega})(1 + e^{-j\omega})}{4} \right)^K |Q(\omega)|^2 \\
&= \left( \frac{(1 + \cos(\omega))}{2} \right)^K |Q(\omega)|^2.
\end{aligned} \tag{8.44}$$

The time-domain representation of eq.(8.44) can be shown to be [145]:

$$r_h[l] = 2^{-2K} \sum_{n=-K}^K \binom{2K}{n+K} r_q[l-n], \text{ for } l = 0, 1, \dots, L-1. \tag{8.45}$$

Here,  $r_q[l]$  is also an autocorrelation sequence. As with  $r_h[l]$ , the symmetry property also holds good for  $r_q[l]$ . The constraints now are redefined in terms of the autocorrelation sequence  $r_q[l]$ .

### A. Compact support

The property of compact support for wavelets is stated in terms of the autocorrelation sequence  $r_q[l]$  by combining eqs.(8.4) and (8.44) and taking  $\omega = 0$ . It can be noticed that:

$$\sum_n h[n] = H(\omega)|_{\omega=0} = \sum_n h[n] \exp(-j\omega n) \Big|_{\omega=0} = \sqrt{2} \quad (8.46)$$

$$|H(\omega)|^2 \Big|_{\omega=0} = 2 \quad (8.47)$$

By substituting eq.(8.44) into eq.(8.47) we obtain:

$$\left\{ \left( \frac{1 + e^{-j\omega}}{2} \right)^K \left( \frac{1 + e^{j\omega}}{2} \right)^K |Q(\omega)|^2 \right\} \Big|_{\omega=0} = 2 \quad (8.48)$$

$$|Q(\omega)|^2 \Big|_{\omega=0} = 2 \quad (8.49)$$

$$\left\{ r_q[0] + 2 \sum_{l=1}^{L_q-1} r_q[l] \cos(\omega l) \right\} \Big|_{\omega=0} = 2 \quad (8.50)$$

We finally come up with the compactly supported wavelet constraint in term of autocorrelation sequence  $r_q[l]$  as follows:

$$r_q[0] + 2 \sum_{l=1}^{L_q-1} r_q[l] = 2. \quad (8.51)$$

### B. Double shift orthogonality

Based on eqs.(8.29) and (8.46), the double shift orthogonality constraint in term of autocorrelation sequence  $r_q[l]$  can be represented as:

$$r_h[2l] = 2^{-2K} \sum_{n=-K}^K \binom{2K}{n+K} r_q[2l-n] = \delta[l] \text{ for } l = 0, 1, \dots, \lfloor \frac{L-1}{2} \rfloor.$$

$$\text{Or, } \sum_{n=-K}^K \binom{2K}{n+K} r_q[2l-n] = 2^{2K} \delta[l]. \quad (8.52)$$

Eq.(8.52) defines the double shift orthogonality constraint in terms of the autocorrelation sequence  $r_q[l]$ .

### C. Spectral factorization

The easiest way to reformulate the spectral factorization constraint in terms of the autocorrelation sequence  $r_q[l]$  is by combining eqs. (8.39) and (8.44) as follows:

$$|H(\omega)|^2 \geq 0 \text{ for } \omega \in [0, \pi] \quad (8.53)$$

$$\left(\frac{1 + \cos(\omega)}{2}\right)^K |Q(\omega)|^2 \geq 0 \text{ for } \omega \in [0, \pi]. \quad (8.54)$$

Since the factor  $1 + \cos(\omega)$  above is always positive, we can rephrase it as:

$$|Q(\omega)|^2 \geq 0 \text{ for } \omega \in [0, \pi] \quad (8.55)$$

Discretizing it in the interval  $\omega \in [0, \pi]$ , the spectral factorization constraint in term of autocorrelation sequence  $r_q[l]$  can be written as:

$$r_q[0] + 2 \sum_{l=1}^{L_q-1} r_q[l] \cos(i\pi l/d) \geq 0 \text{ for } i = 0, 1, \dots, d. \quad (8.56)$$

It is clear from eq.(8.8) that since  $Q(\omega)$  has  $K$  zeros less than  $H(\omega)$ , the length of the filter  $q[n]$  will be  $L_q = L - K$ .

### D. Stop band constraint

As with the spectral factorization constraints, the stop-band constraint in terms of the autocorrelation sequence  $r_q[l]$  is obtained by combining eqs.(8.17), (8.18) and (8.44) as follows:

$$0 \leq |H(\omega)|^2 \leq \Delta_b \text{ for } \omega \in [\omega_s, \pi] \quad (8.57)$$

$$0 \leq \left(\frac{1 + \cos(\omega)}{2}\right)^K |Q(\omega)|^2 \leq \Delta_b \text{ for } \omega \in [\omega_s, \pi] \quad (8.58)$$

Discretizing it in the interval  $\omega \in [\omega_s, \pi]$  the stop-band constraint can be expressed in terms of the autocorrelation sequence  $r_q[l]$  as:

$$0 \leq \left(\frac{1 + \cos(i\pi/d)}{2}\right)^K \left( r_q[0] + 2 \sum_{l=1}^{L_q-1} r_q[l] \cos(i\pi l/d) \right) \leq \Delta_b, \quad (8.59)$$

for  $i = \lceil \frac{\omega_s}{\pi} \rceil * d, \dots, d$  and  $L_q = L - K$ .

It is clear from eq.(8.59) that when the optimization problem is expressed in terms of the autocorrelation sequence  $r_q[l]$ , the necessity for  $|H(\omega)|^2$  to have  $2K$  zeros at  $\omega = \pi$  has been

imposed implicitly. Therefore, the regularity constraints are not explicitly expressed when the optimization problem is conducted in the  $Q(\omega)$  domain.

The spectral factorization constraints stated in eqs.(8.54) and (8.56) will be automatically fulfilled if the stop-band constraint stated in eq.(8.59) is satisfied. In fact the stop band constraint eq.(8.59) is more stringent than the spectral factorization constraint eq.(8.56).

In summary, the optimization problem in terms of the autocorrelation sequence  $r_q[l]$  can be stated as:

MINIMIZE:  $\Delta_b$

SUBJECT TO:

$$\begin{aligned}
 r_q[0] + 2 \sum_{l=1}^{L_q-1} r_q[l] &= 2, \\
 \sum_{n=-K}^K \binom{2K}{n+K} r_q[2l-n] &= 2^{2K} \delta[l], \text{ for } l = 0, 1, \dots, \lfloor \frac{L-1}{2} \rfloor, \\
 0 \leq \left( \frac{1 + \cos(i\pi/d)}{2} \right)^K \left( r_q[0] + 2 \sum_{l=1}^{L_q-1} r_q[l] \cos(i\pi l/d) \right) &\leq \Delta, \\
 \text{for } i = \left\lceil \frac{\omega_s}{\pi} \right\rceil * d, \dots, d \text{ and } L_q = L - K. &
 \end{aligned} \tag{8.60}$$

Once we find the optimal autocorrelation sequence  $r_q[l]$ , the spectral factorization is employed in order to derive the optimal sequence  $q[l]$  from  $r_q[l]$ . Finally, the optimal wavelet low-pass filter coefficients are computed using the time-domain equivalent of eq.(8.8) [145]:

$$h[l] = 2^{-K} \sum_{k=0}^K \binom{K}{k} q[l-k]. \tag{8.61}$$

### 8-3-4 Solving the convex optimization problem

Since the optimization problem posed above is linear it is also convex. Therefore, any linear or convex optimization tool can be used to solve this problem. We used SeDuMi [150], a generic Semi-Definite Programming (SDP) solver, to solve the optimization problem. SeDuMi stands for Self-Dual Minimization as it implements a self-dual embedding technique for optimization over self-dual homogeneous cones [150]. It comes as an additional Matlab® package and can

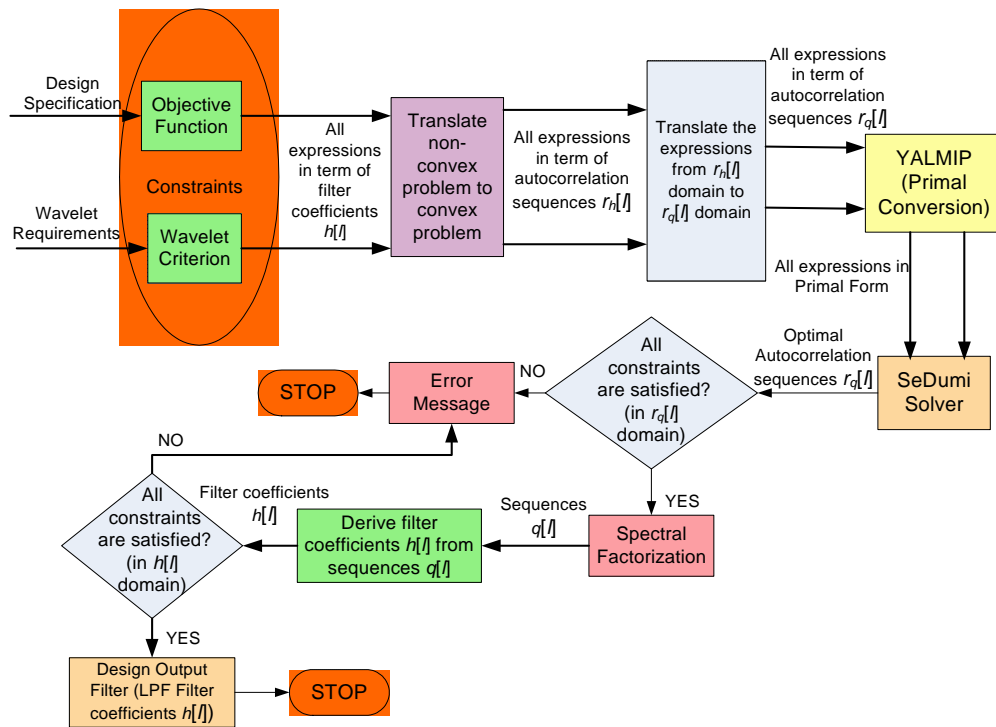


FIGURE 8.3: Flow chart of the optimum wavelet design process for wavelet packet based spectrum estimation.

be used for linear, quadratic and semi-definite programming. Normally it requires a problem to be described in a primal standard form but with modeling languages like YALMIP (short for Yet Another LMI Parser) the optimization problems can be directly expressed in a user-friendly higher level language [151]. Thus YALMIP allows the user to concentrate on the high-level modeling without having to worry about low-level details. We have developed a filter optimization program that incorporates most of the available optimization routines for Matlab© and which relies on YALMIP to translate the problem into the standard form.

The blocks of the filter design program are elucidated in fig. 8.3. The design process consists of both analytical and numerical modules. In the analytical part, the non-convex problem is converted into a convex one, followed by a transformation of the expression from autocorrelation  $r_h[l]$  domain into autocorrelation  $r_q[l]$  domain. In the numerical part the convex problem is solved and the solution is obtained in terms of  $r_q[n]$ . After that, another analytical process is initiated to derive optimum low-pass filter coefficients  $h[n]$  from the sequences  $q[n]$ , which is obtained by applying spectral factorization on  $r_q[l]$ . We use the spectral factorization algorithm proposed in [146]. From the autocorrelation sequence, this spectral factorization algorithm derives filter coefficients with length  $L$  having a minimum phase property<sup>8</sup>. At the end of the design process the filter coefficients of the analysis LPF will be generated. From the analysis LPF  $h[n]$ , the HPF  $g[n]$  and the synthesis filters, LPF  $h'[n]$  and HPF  $g'[n]$ , can be obtained

<sup>8</sup>We chose filters having minimum phase because they guarantee stability

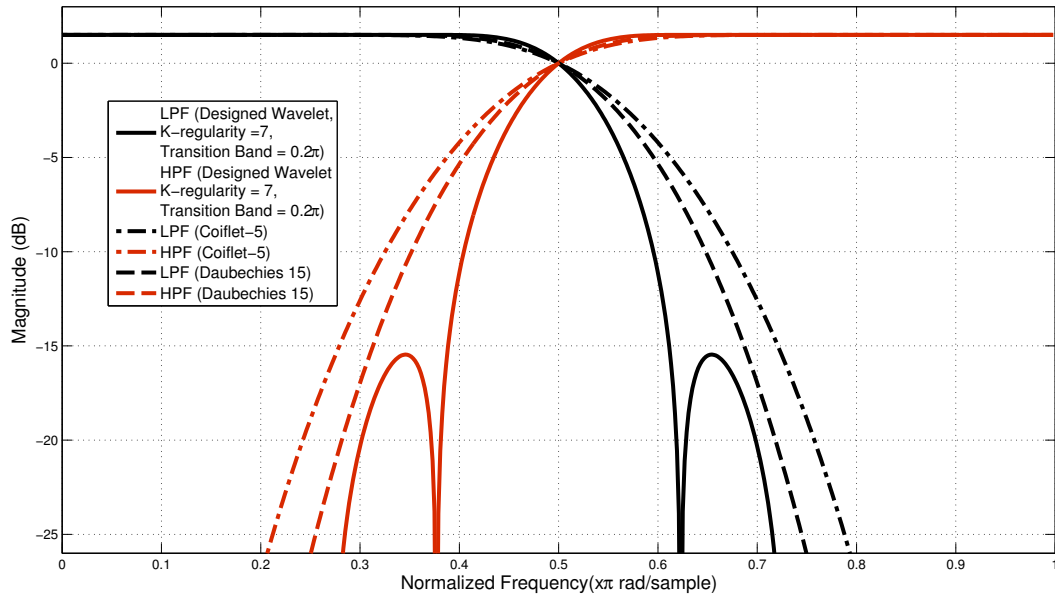


FIGURE 8.4: Frequency response of Daubechies-15, Coiflet-5 and the designed wavelet low-pass (LPF) and high-pass (HPF) filter with  $L=30$ ,  $K=7$ ,  $B_t=0.2\pi$ .

through the QMF equations. And from these set of filters the WPM carriers and their duals can be derived using the 2-scale eq.(8.1).

### 8-3-5 Results and analysis

In this section we present a few results to demonstrate the design procedure. The main variables of the design process are the length and regularity order of the filter. Regularity has to be equal to or larger than 1 to ensure that the wavelet existence constraint is satisfied and it may not exceed  $L/2$ . If the selected value for regularity is close to the upper limit, the degrees of freedom available for the optimization of the objective function will be lowered. On the other hand, imposing a small regularity can result in highly irregular wavelets.

#### A. Frequency and impulse responses of the newly designed filter

We consider two wavelets with filter lengths  $L = 30$  and  $L = 40$ . It is certainly possible to design filters of other lengths too. In the first example, shown in fig. 8.4, the frequency response of the designed wavelet filters is compared with Daubechies and Coiflet wavelet filters. For fairness of comparison all of these wavelet filters have a length of 30. A K-regularity index of 7 and transition band ( $B_t$ ) of  $0.2\pi$  is enforced on the designed wavelet filters. From fig. 8.4, it is evident that the filters obtained from the design have better frequency selectivity, with sharper transition between the pass- and stop-bands, than their Daubechies and Coiflet counterparts. A small price however is paid in terms of the ripples introduced in the side lobe. Fig. 8.5 presents

Index	Low-Pass Filter	High-Pass Filter	Index	Low-Pass Filter	High-Pass Filter
1	0.0000	-0.0201	16	-0.0611	-0.0074
2	-0.0000	0.1437	17	0.0206	-0.0395
3	0.0001	-0.4279	18	0.0892	-0.0017
4	0.0002	0.6521	19	-0.0357	0.0223
5	-0.0006	-0.4454	20	-0.1296	0.0055
6	0.0001	-0.0789	21	0.0469	-0.0097
7	0.0024	0.3037	22	0.1943	-0.0049
8	-0.0026	-0.0350	23	-0.0350	0.0026
9	-0.0049	-0.1943	24	-0.3037	0.0024
10	0.0097	0.0469	25	-0.0789	-0.0001
11	0.0055	0.1296	26	0.4454	-0.0006
12	-0.0223	-0.0357	27	0.6521	-0.0002
13	-0.0017	-0.0892	28	0.4279	0.0001
14	0.0395	0.0206	29	0.1437	0.0000
15	-0.0074	0.0611	30	0.0201	0.0000

TABLE 8.1: Optimal filter coefficients for filter length  $L = 30$ ,  $K$ -regularity=7, Transition Band= $0.2\pi$ .

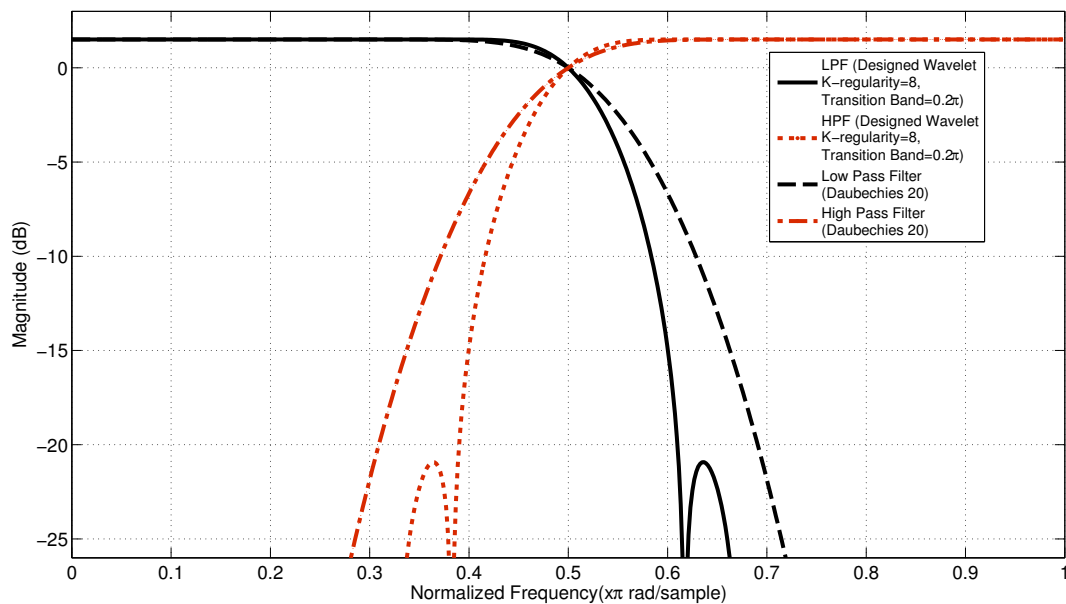


FIGURE 8.5: Frequency response of Daubechies-20 and the designed wavelet low-pass (LPF) and high-pass (HPF) filter with  $L = 40$ ,  $K = 8$ ,  $B_t = 0.2\pi$ .

similar comparison for  $L = 40$ . In this example, only the maximally frequency selective wavelet and Daubechies-20 filters are considered.

Figs. 8.6 and 8.7 depict the impulse responses of the high and low-pass filters of the optimally designed wavelets for  $L = 30$ ,  $K = 7$ ,  $B_t = 0.2\pi$  and  $L = 40$ ,  $K = 8$ ,  $B_t = 0.2\pi$ , respectively. The coefficients of the designed wavelet filter for  $L = 30$ ,  $K = 7$ ,  $B_t = 0.2\pi$  and  $L = 40$ ,  $K = 8$ ,  $B_t = 0.2\pi$  are presented in tables 8.1 and 8.2, respectively.

Index	Low-Pass Filter	High-Pass Filter	Index	Low-Pass Filter	High-Pass Filter
1	0.0000	-0.0071	21	-0.0404	-0.0018
2	0.0000	0.0630	22	0.0035	0.0261
3	0.0000	-0.2416	23	0.0586	0.0047
4	0.0000	0.5128	24	-0.0110	-0.0154
5	0.0001	-0.6110	25	-0.0818	-0.0053
6	-0.0000	0.2958	26	0.0194	0.0077
7	-0.0001	0.1849	27	0.1122	0.0044
8	0.0004	-0.2882	28	-0.0249	-0.0030
9	0.0001	-0.0275	29	-0.1538	-0.0028
10	-0.0013	0.2128	30	0.0179	0.0006
11	0.0006	-0.0179	31	0.2128	0.0013
12	0.0028	-0.1538	32	0.0275	0.0001
13	-0.0030	0.0249	33	-0.2882	-0.0004
14	-0.0044	0.1122	34	-0.1849	-0.0001
15	0.0077	-0.0194	35	0.2958	0.0000
16	0.0053	-0.0818	36	0.6110	0.0001
17	-0.0154	0.0110	37	0.5128	-0.0000
18	-0.0047	0.0586	38	0.2416	0.0000
19	0.0261	-0.0035	39	0.0630	-0.0000
20	0.0018	-0.0404	40	0.0071	0.0000

TABLE 8.2: Optimal filter coefficients for filter length  $L = 40$ , K-regularity=8, Transition Band= $0.2\pi$ .

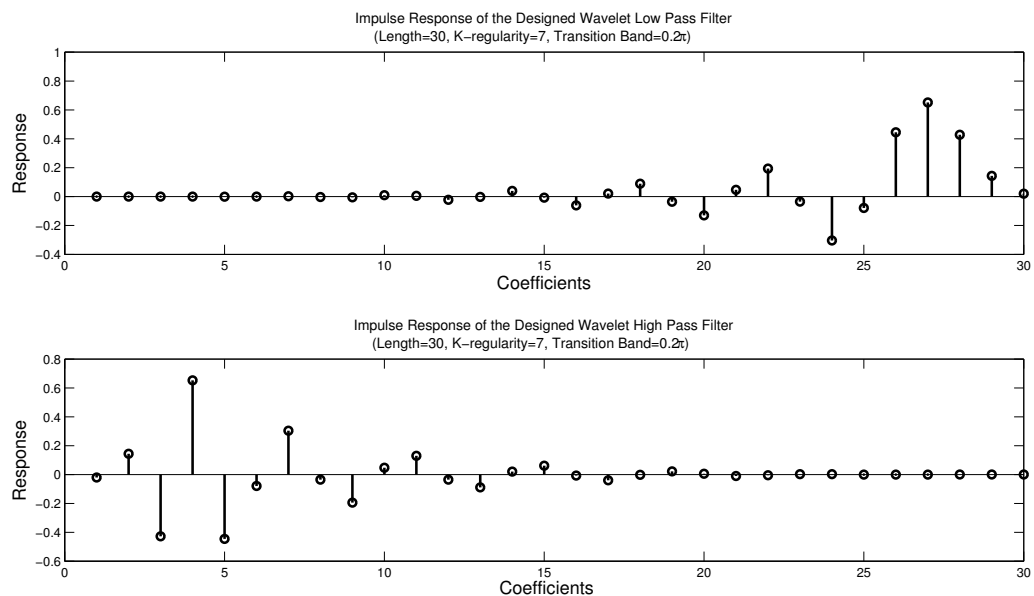


FIGURE 8.6: Impulse response of the designed optimal wavelet filter with length  $L = 30$ , K-regularity  $K = 7$ , overall transition band  $B_t = 0.2\pi$ .

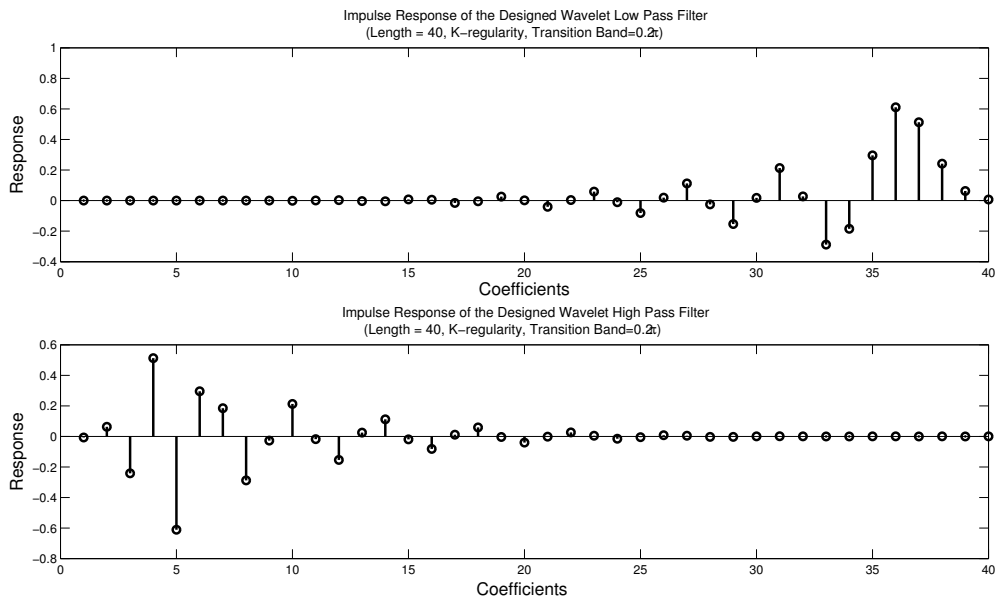


FIGURE 8.7: Impulse response of the designed optimal wavelet filter with length  $L = 40$ ,  $K$ -regularity = 8, overall transition band  $B_t = 0.2\pi$ .

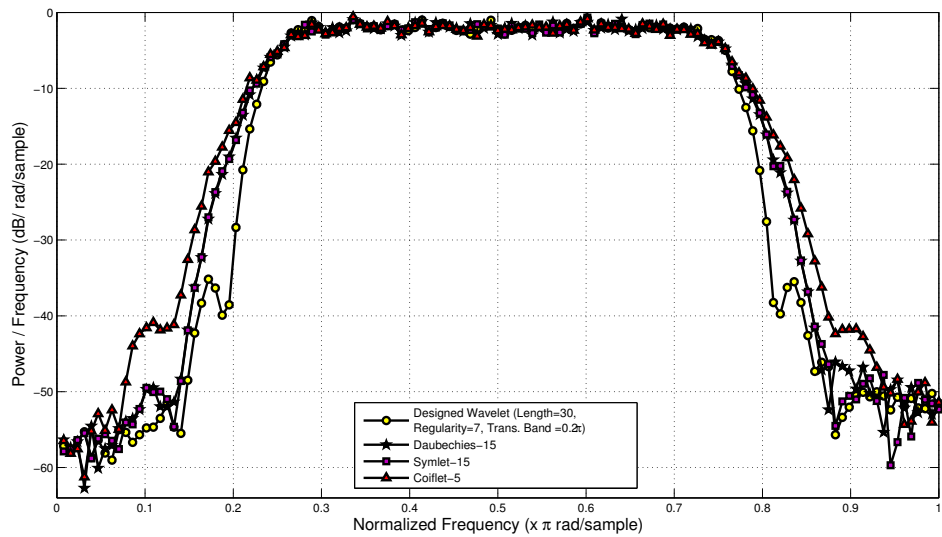


FIGURE 8.8: Estimates of a partial band source with Coiflet-5, Daubechies-15, Symlet-15 and the designed optimal wavelet filter with length  $L=30$ ,  $K$ -regularity = 7, overall transition band  $B_t = 0.2\pi$ . The wavelet decomposition level used here is 7. The number of samples in this experiment is 12800.

Type of source	Description
Partial band	Frequency occupied: $[0.25\pi, 0.75\pi]$
Single tone	Frequency occupied: $0.5\pi$
Multi-band	Consist of 3 active bands occupying normalized frequency bands $[0.08\pi, 0.19\pi]$ , $[0.47\pi, 0.58\pi]$ , and $[0.86\pi, 0.97\pi]$ , respectively.

TABLE 8.3: Description of three types of sources used in the experiments.

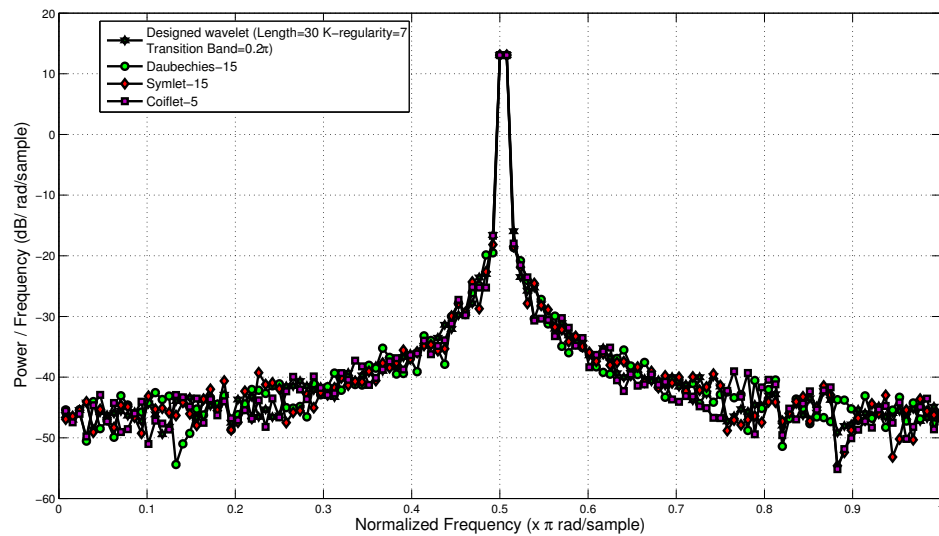


FIGURE 8.9: Estimates of single-tone source based on Coiflet-5, Daubechies-15, Symlet-15 and the designed optimal wavelet filter with length  $L=30$ ,  $K$ -regularity = 7, overall transition band  $B_t = 0.2\pi$ . The wavelet decomposition level used here is 7. The number of samples in this experiment is 12800.

## B. Evaluation of spectrum estimator performance

We now examine the performance of the wavelet packet based spectrum estimator or WPSE (presented in Chapter 7) with the newly designed wavelet. For this purpose, three types of sources are considered, namely, partial-band, single-tone and multi-band. The partial-band source has its energy spread over a continuous range of frequencies and it occupies the normalized frequency band from  $0.25\pi$  to  $0.75\pi$ . The single-tone source has all of its energy at one frequency and is in the middle of the range spanned by the wavelet based spectrum estimation at  $0.5\pi$ . The third source has a multi-band characteristic with three active bands occupying the normalized frequency bands of  $0.08\pi$ - $0.19\pi$ ,  $0.47\pi$ - $0.58\pi$  and  $0.86\pi$ - $0.97\pi$ , respectively. The details of all the sources are provided in table 8.3.

- Partial-band source

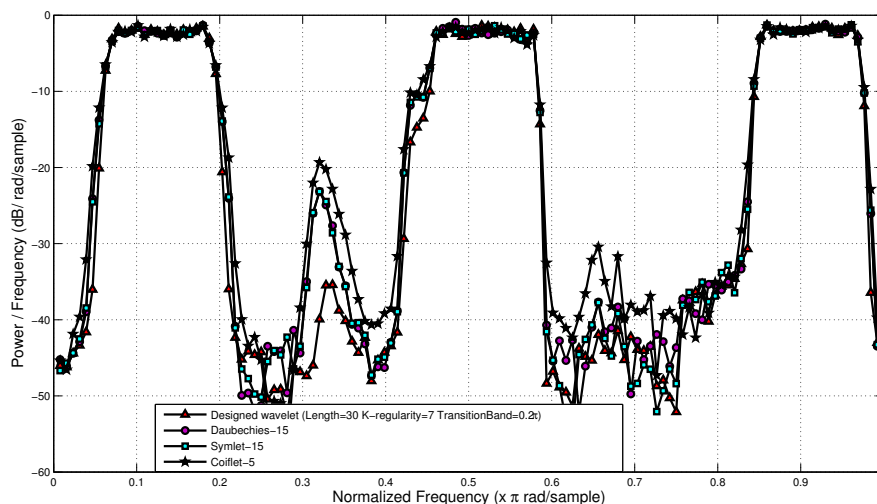


FIGURE 8.10: Spectrum shaping with WPM carriers based on the wavelets: Coiflet-5, Daubechies-15, Symlet-15 and the designed optimal wavelet filter with length  $L = 30$ ,  $K$ -regularity = 7, transition band  $B_t = 0.2\pi$ .

Fig. 8.8 presents how the spectrum estimation of a partial-band source with the newly designed wavelet compares with those based on the standard wavelet family. Here, the number of samples is set to 12800. The specifications for the optimal wavelet are  $L$  (length) = 30,  $K$  (regularity index) = 7 and  $B_t$  (transition bandwidth) =  $0.2\pi$ . It is clear from the figure that the newly designed wavelet outperforms Daubechies, Coiflet and Symlet wavelets of the same length. The improvements are with regard to frequency selectivity and the sharp transition between occupied band and unoccupied band.

- Single-tone source

For the estimation of the single-tone source, as illustrated by the plots in fig. 8.9, the difference in performances of the designed wavelet and the standard ones is not tangible. The frequency resolution of the single tone source is influenced more by the levels of decomposition than by frequency selectivity of the filter used. Hence, there is no perceivable differences in the performances of various wavelets.

- Multiple-Bands source

The benefit of frequency selective filters is that the WPM carriers derived from them have narrow and well-confined spectral footprints. Moreover, they also aid in better estimation of signals. Fig. 8.10 illustrates this characteristic where the frequency selective wavelets are shown to efficiently carve the bands between the desirable and undesired footprints while all other wavelets have residual infringing components. This feature is useful in applications such as Cognitive Radio and LTE-advanced where the transmission signal characteristics have to be shaped to accurately map a frequency mask.

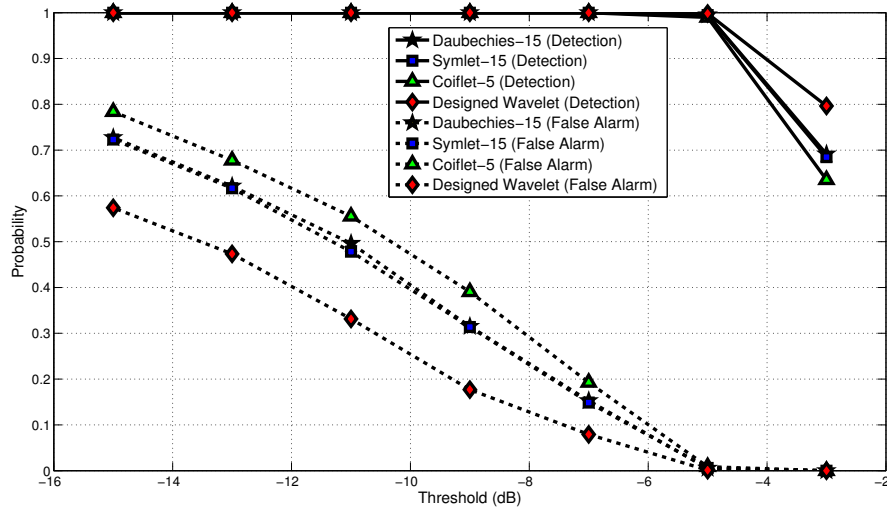


FIGURE 8.11: Detection and false alarm probability of the spectrum estimation based on various wavelet families. The length of the wavelet filter is 30, the wavelet decomposition level is 7 and the sample space is of size 12800. The K-Regularity of the designed wavelets is 7 with a normalized transition band  $B_t$  of  $0.2\pi$ .

### C. Evaluation of the receiver operating characteristics (ROC)

The receiver operating characteristic (ROC) is used as the second figure-of-merit to gauge the performance of the spectrum estimator. To obtain the probability of detection ( $P_d$ ) and false alarm ( $P_{fa}$ ), we divide the normalized frequency range  $[0, \pi]$  into 128 equal bands (or frequency bins). Each bin is occupied by one source meaning that overall there are 128 sources. These 128 sources are randomly activated/de-activated and the  $P_d$  and  $P_{fa}$  are calculated for each threshold for a sample space of 100 experiments. An active source operates around -2.1 dB power and the threshold is varied between -3dB to -15dB. The number of samples used to estimate is 12800. Fig. 8.11 depicts the  $P_d$  and  $P_{fa}$  as a function of threshold level; the plots clearly underline the superiority of the newly designed wavelet in relation to other wavelet families of the same filter length. The frequency selectivity inherent in the proposed wavelet has allowed the spectrum estimator to have better  $P_d$  and  $P_{fa}$  for all thresholds in comparison to Daubechies, Symlet and Coiflet based estimators. The ROC depicted in fig. 8.12 further endorses the benefits and superiority of the estimator based on the designed wavelet.

### D. Other studies - filter characteristics and their influence

We now study the impact of altering the filter design parameters on the ROC. The plots in fig. 8.13 show the impact of filter length on the ROC. The results show that for a given regularity order, the longer the filters, the better the  $P_d$  and  $P_{fa}$  of the estimates. This is to be expected because filters which are longer offer more degrees of freedom to minimize the pass-band and stop-band ripple. Likewise, for a given filter length, a lower K-regularity index results

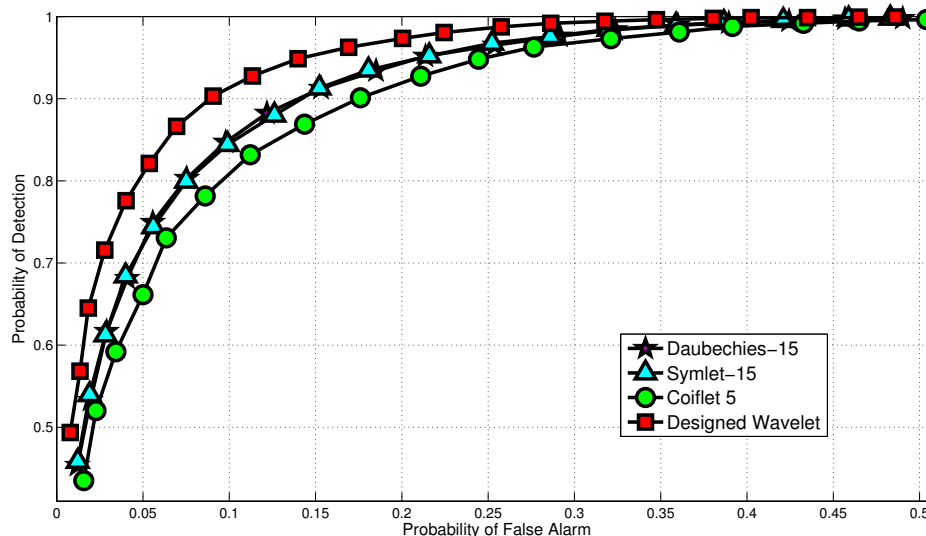


FIGURE 8.12: Receiver operating characteristic of spectrum estimation based on various wavelet families. In this scenario, the length of wavelet decomposition filter is 30, the wavelet decomposition level is 7 and the sample space is of size 384. The K-Regularity of the designed wavelets with SDP is 7 with a normalized transition band of  $0.2\pi$ .

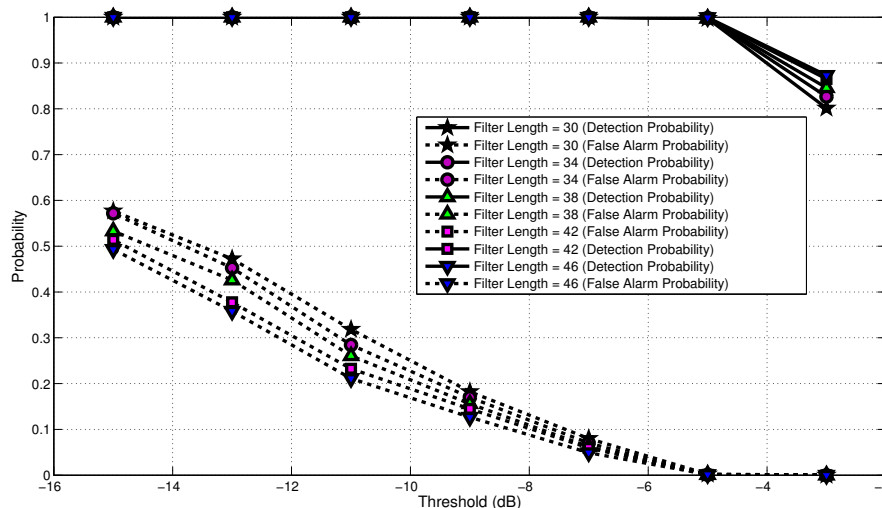


FIGURE 8.13: Detection and false alarm probability of the spectrum estimation based on the newly designed wavelet with variations on filter lengths. In this scenario, the wavelet decomposition level is 7 and the sample space is of size 12800. The K-Regularity of the designed wavelets with Semi-Definite Programming is 7 with a transition band of  $0.2\pi$ .

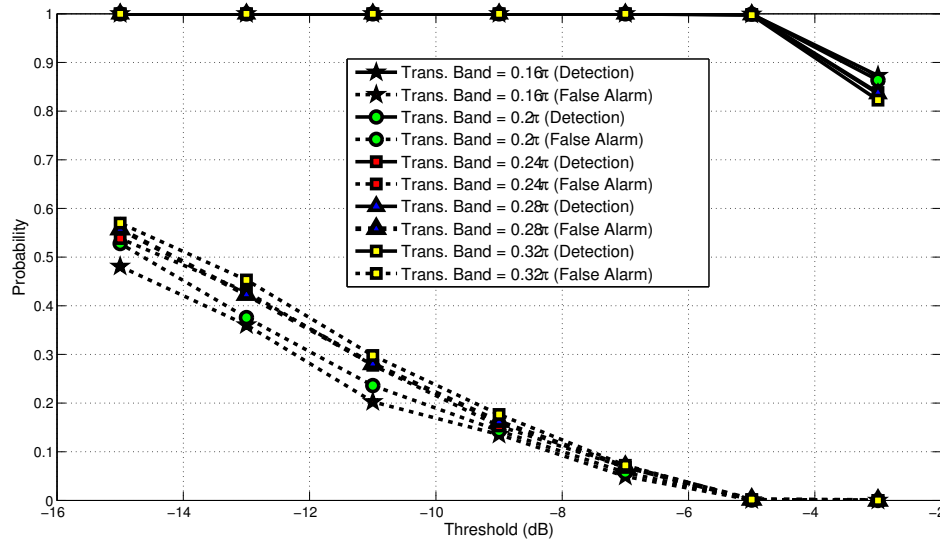


FIGURE 8.14: Detection and false alarm probability of the spectrum estimation based on newly designed wavelet with variations on transition band. In this scenario, the length of wavelet decomposition filter is 40, the wavelet decomposition level is 7 and the sample space is of size 12800. The K-Regularity of the designed wavelets with Semi-Definite Programming is 6.

in a greater degree of freedom available to minimize the pass/stop-band ripple yielding better performance results.

Fig. 8.14 exemplifies the influence of transition band variation on the detection and false alarm probability. The result further exemplifies the importance of frequency selectivity on the quality of the estimates. Here, configurations with narrower transition bands offer lower false alarm and higher detection probability.

## 8-4 Example 2 - Wavelets with low cross correlation error

As a second example we design filters with low cross-correlation energy between the low- and high-pass filters with the objective of minimizing the interference due to timing errors in WPM transmission. In Chapter 4 we found out that multi-carrier systems are highly sensitive to loss of time synchronization. A loss in time synchrony results in samples outside a WPM symbol getting erroneously selected, while useful samples at the beginning or at the end of the symbol getting discarded. It also introduces ISI and ICI causing a performance degradation.

We also observed that though WPM and OFDM share many similarities as orthogonal multi-carrier systems, they are significantly different in their responses to loss of time synchronization. This difference is a result from the fact that the WPM symbols overlap with each other and they are longer than the OFDM symbol<sup>9</sup>. Under a loss in time synchronization, the overlap of the symbols in WPM causes each symbol to interfere with several other symbols while in OFDM

<sup>9</sup>The length of the symbol and the degree of overlap is determined by the length of wavelet filter used.

each symbol interferes only with its neighbors. The second difference is in the usage of guard intervals. OFDM benefits from the cyclic prefix which significantly improves its performance under timing errors. WPM cannot use guard intervals because of the symbol overlap.

Fortunately, WPM offers the possibility of adjusting the properties of the waveforms in a way that the errors due to loss of synchronization can be minimized. In this section we present a method to design a new family of wavelet filters which minimize the energy of the timing error interference

### 8-4-1 Time offset errors in WPM

The time synchronization error is modeled by shifting the received data samples  $R[n]$  by a time offset  $\Delta_t$  to the left or right as:

$$R[n \pm \Delta_t] = S[n] + w[n]. \quad (8.62)$$

Here,  $S[n]$  denotes the transmitted signal and  $w[n]$  the Gaussian noise.

Recalling, from Chapter 3, that in ideal conditions when the WPM transmitter and receiver are perfectly synchronized and the channel is benign, the estimation of the data contained in the  $u$ th symbol and  $k$ th sub-carrier  $\hat{a}_{u',k'}$  is the same as the transmitted data  $a_{u,k}$ <sup>10</sup>. However, errors are introduced in the demodulation decision making process under time offset errors  $\Delta_t$  as elucidated below:

$$\begin{aligned} \hat{a}_{u',k'} &= \sum_n R[n] \xi_l^{k'}[(u'N - n + \Delta_t)] \\ &= \sum_n \sum_u \sum_{k=0}^{N-1} a_{u,k} \xi_l^k[n - uN] \xi_l^{k'}[u'N - n + \Delta_t] \\ &= \sum_u \sum_{k=0}^{N-1} a_{u,k} \left( \sum_n \xi_l^k[n - uN] \xi_l^{k'}[u'N - n + \Delta_t] \right). \end{aligned} \quad (8.63)$$

Defining the cross waveform function  $\Omega(\Delta_t)$  as:

$$\Omega_{k,k'}^{u,u'}[\Delta_t] = \sum_n \xi_l^k[n - uN] \xi_l^{k'}[u'N - n + \Delta_t], \quad (8.64)$$

<sup>10</sup>To distinguish the receiver and transmitter end parameters, apostrophes are used in the receiver-end symbol  $u'$  and carrier  $k'$  index.

the demodulated data corrupted by the interference due to loss of orthogonality at the receiver for the  $k$ th sub-carrier and  $u$ th symbol can be expressed as:

$$\hat{a}_{u',k'} = \underbrace{a_{u',k'} \Omega_{k',k'}^{u',u'}[\Delta_t]}_{\text{Desired Alphabet}} + \underbrace{\sum_{u; u \neq u'} a_{u,k'} \Omega_{k',k'}^{u,u'}[\Delta_t]}_{\text{ISI}} + \underbrace{\sum_u \sum_{k=0; k \neq k'}^{N-1} a_{u,k} \Omega_{k,k'}^{u,u'}[\Delta_t]}_{\text{IS-ICI}} + \underbrace{w_{u',k'}}_{\text{Gaussian Noise}}. \quad (8.65)$$

In eq.(8.65) the first term stands for the attenuated useful signal, the second term denotes ICI, the third term gives ISI and the last term stands for Gaussian noise.

## 8-4-2 Formulation of the design problem

### A. Design criterion

The information contained in the sub-carriers can be correctly decoded if the waveforms used have large distances between one another. In WPM this is achieved through the orthogonality of the generated waveforms. In disturbance-free environments the cross-correlations of WPM waveforms equals zero and perfect reconstruction is possible despite the time and frequency overlap. However, the timing error  $\Delta_t$  leads to the loss of orthogonality between the waveforms and consequently they begin to interfere one with another leading to ICI and ISI, stated as:

$$\Omega_{k,k'; k \neq k'}^{u,u'}[\Delta_t] = \sum_n \xi_l^k(n - uN) \xi_l^{k'}(u'N - n + \Delta_t). \quad (8.66)$$

The design objective is therefore to generate wavelet bases  $\xi$  and their duals  $\xi'$  that minimize interference energy in the presence of a timing error, i.e.,

MINIMIZE:

$$\sum_{u,k; k \neq k'} \left| \Omega_{k,k'}^{u,u'}[\Delta_t] \right|^2 \text{ with respect to } \{ \xi, \xi' \}. \quad (8.67)$$

### B. Wavelet-domain to filter bank-domain

The waveforms in WPM are created by the multi-level tree structure filter bank. Using Parseval's theorem of energy conservation it can be easily proved that the total energy at each level is equal regardless of the tree's depth. Therefore, minimizing the interfering energy at the roots of the tree will automatically lead to a decrease of total interfering energy at the higher tree branches. Furthermore, the two-channel filter banks through the 2-scale equation are related, albeit explicitly, to the WPM waveforms. Therefore the design process can be converted into a tractable filter design problem. We should hence be able to minimize the deleterious effects of

time synchronization errors in WPM by minimizing the following cross-correlation function:

$$\sum_{\Delta_t} |r_{hg}[\Delta_t]|^2 = \sum_n |h[n]g[n - \Delta_t]|^2 = \sum_n |h[n]((-1)^n h[L - n + \Delta_t])|^2 \quad (8.68)$$

The design problem of minimizing the interference energy due to timing offset can now be formally stated as an optimization problem satisfying the objective function eq.(8.68) and constraints eqs.(8.4), (8.7) and (8.12), i.e.,

MINIMIZE:

$$\sum_{\Delta_t} |r_{hg}[\Delta_t]|^2 \text{ with respect to } h[n] \quad (8.69)$$

SUBJECT TO:

$$\begin{aligned} \sum_n h[n] &= \sqrt{2} \\ \sum_n h[n]h[n - 2k] &= \delta[k], \text{ for } k = 0, 1, \dots, (L/2) - 1 \\ \sum_n h[n] (n)^k (-1)^n &= 0, \text{ for } k = 0, 1, 2, \dots, K - 1. \end{aligned} \quad (8.70)$$

As in the first example, the majority of constraints in eq.(8.70) are non-linear and non-convex. As before, we shall move to the auto-correlation domain ( $r_h[k] = \sum_{m \in \mathbb{Z}} h[m]h[m + k]$ ) to simplify the problem.

### 8-4-3 Transformation of the mathematical constraints from a non-convex problem to a convex/linear one

The admissibility, para-unitary and K-regularity conditions are readily available in the auto-correlation domain (eqs.(8.27), (8.29) and (8.34), respectively). The spectral factorization condition eq.(8.42) can also be reused. Therefore, we only have to derive the objective function. We know that,

$$r_h[n] = \begin{cases} \sum_{m=0}^{L-n-1} h[m]h[m+n], & n \geq 0 \\ r_h(-n), & n < 0 \end{cases} \quad (8.71)$$

and that,

$$\begin{aligned} r_g[n] &= \sum_{m=0}^{L-n-1} g[m]g[m+n] \quad \text{where } n \geq 0 \\ &= \sum_{m=0}^{L-n-1} ((-1)^m h[L - m])((-1)^{m+n} h[L - (m + n)]) = (-1)^n r_h[n]. \end{aligned} \quad (8.72)$$

Applying the corollary <sup>11</sup>: “The sum of squares of a cross-correlation between two functions equals the inner product of the autocorrelation sequences of these two functions.”, and considering the double shift orthogonality property,

$$r_h[2x] = \delta[x] = \begin{cases} 1, & \text{for } x = 0 \\ 0, & \text{otherwise,} \end{cases} \quad \text{where } x = 0, 1, \dots, \lfloor \frac{L-1}{2} \rfloor, \quad (8.73)$$

the cross-correlation function  $r_{hg}[n]$  can be rewritten in terms of  $r_h[n]$  as follows:

$$\begin{aligned} \sum_{n=0}^{L-1} |r_{hg}[n]|^2 &= \sum_{n=0}^{L-1} r_h[n] r_g[n] \\ &= \sum_{n=0}^{L-1} r_h[n] ((-1)^n r_h[n]) \\ &= \underbrace{\sum_{x=0}^{(L/2-1)} (r_h[2x+1])^2}_{\text{Odd numbered values}} - \underbrace{\sum_{x=0}^{(L/2-1)} (r_h[2x])^2}_{\text{Even numbered values}} \\ &= \sum_{n=0}^{(L/2-1)} (r_h[2n+1])^2 - 1. \end{aligned} \quad (8.74)$$

The new optimization problem can therefore be stated as,

MINIMIZE:

$$\sum_{n=0}^{(L/2-1)} (r_h[2n+1])^2, \quad (8.75)$$

subject to the wavelet constraints eqs.(8.27), (8.29) and (8.34), the spectral factorization criterion eq.(8.42) and the design constraint eq.(8.74).

Or,

MINIMIZE:

$$\sum_{n=0}^{(L/2-1)} (r_h[2n+1])^2, \quad (8.76)$$

---

<sup>11</sup>Proved in Appendix A4

0.1198	0.4982	0.6609	0.2032
-0.0291	0.1594	-0.1449	-0.3016
0.2063	0.2059	0.16541	-0.0566
0.0712	-0.0095	-0.0083	0.0091
-0.0049	-0.0007	0.0015	-0.0003

TABLE 8.4: Optimal Filter Coefficients.

SUBJECT TO:

$$\begin{aligned}
\sum_{n=1}^{L-1} r_h[n] &= \frac{1}{2} \\
r_h[2k] &= \delta(k) = \begin{cases} 1, & \text{for } k = 0 \\ 0, & \text{otherwise} \end{cases} \quad \text{where } k = 0, 1, \dots, \left\lfloor \frac{L-1}{2} \right\rfloor \\
\sum_{n=1}^{L-1} (-1)^n (l)^{2k} r_h[n] &= 0 \text{ for } k = 0, 1, \dots, K-1 \\
r_h[0] + 2 \sum_{n=1}^{L-1} r_h[n] \cos(i\pi l/d) &\geq 0 \text{ for } i = 0, 1, \dots, d.
\end{aligned} \tag{8.77}$$

The equations are now convex and can be solved using the setup presented in Section 9.3.4 and illustrated by fig. 8.3 .

#### 8-4-4 Results and analysis

In this section we present a few results to demonstrate the design procedure. As before, the main variables of the design process are the length and regularity order of the filter.

##### A. Frequency and impulse responses of the designed filter

In this example we have set the length of the filter to 20 though it is also possible to design filters of other lengths. The order of regularity chosen is 5, which is a compromise between optimization space and wavelet regularity. The impulse response of the designed optimal filter is illustrated in fig. 8.15 and numerical values of filter coefficients are given in table 8.4. Although the optimal filter is designed in the autocorrelation domain, the minimum-phase time-domain coefficients obtained through spectral factorization satisfy all constraints mandated by the design process. The wavelet and scaling function of the newly designed optimal filter are illustrated in fig. 8.16, respectively. The frequency response is shown in fig. 8.17. Table 8.5 shows the specifications of the various filters used in the thesis along with the values of the corresponding objective functions. Clearly, the newly designed wavelet has the lowest interference energy.

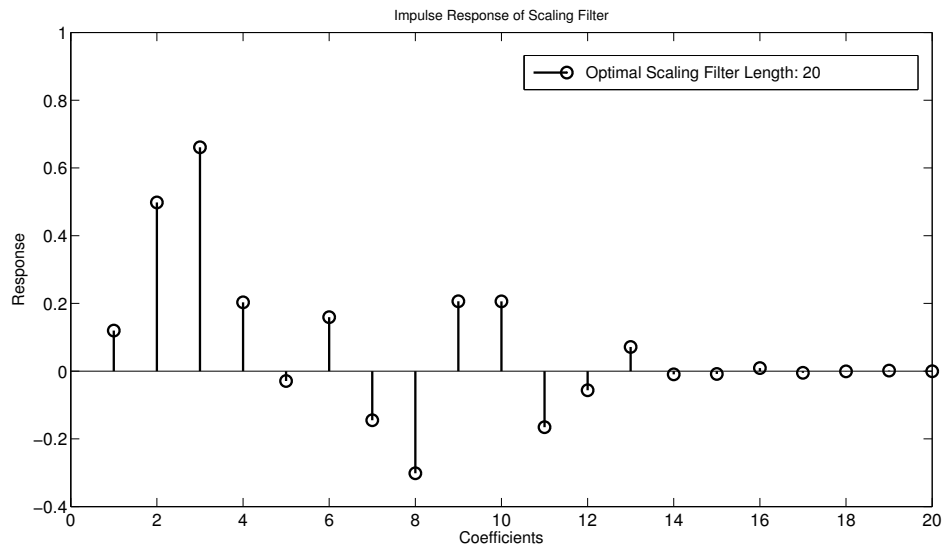


FIGURE 8.15: Impulse response of the optimal LPF with 20 coefficients.

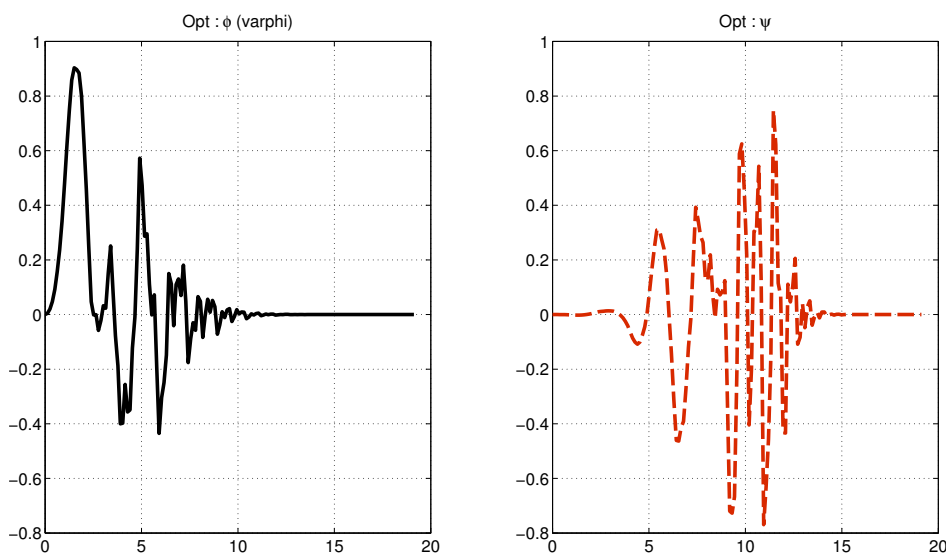


FIGURE 8.16: Optimal Filter; (a) Scaling Function, (b) Wavelet Function.

Name	Length	K-Regularity	$\sum_{n=0}^{L/2} (r_h[2n + 1])^2$
Haar	2	1	-
Daubechies	20	10	0.41955
Symlets	20	10	0.41955
Discrete Meyer	102	1	0.45722
Coiflet	24	4	0.41343
Optimal	20	5	0.36814

TABLE 8.5: Wavelet specifications and objective function.

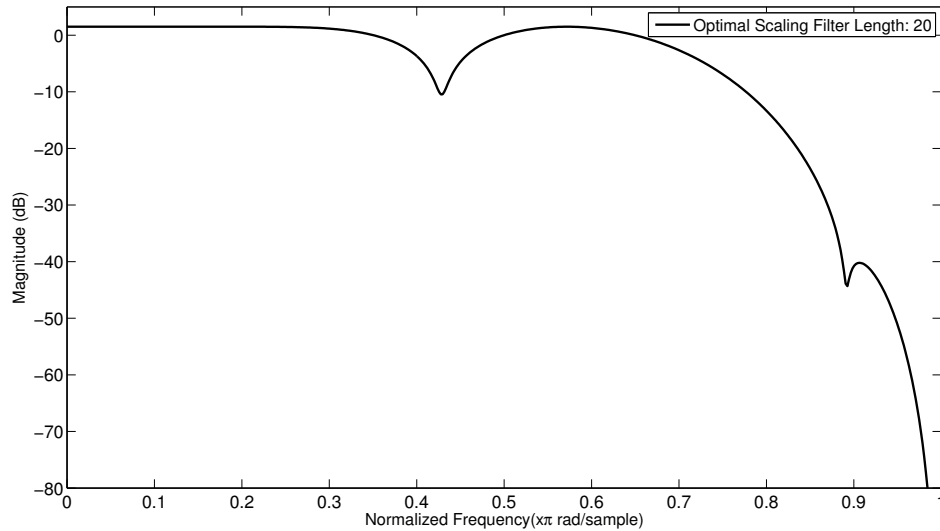


FIGURE 8.17: Frequency Response (in dB) of the designed filter.

Parameters	WPM	OFDM
Number of Sub-carriers	128	128
Number of Multi-carrier symbols per frame	100	100
Modulation	DQPSK	DQPSK
Channel	AWGN	AWGN
Oversampling Factor	15	15
Guard Band	-	-
Guard Interval	-	-
Frequency Offset	-	-
Phase Noise	-	-
Time Offset	$t = 2$	$t = 2$

TABLE 8.6: Simulation setup for study on time synchronization error.

### B. Evaluation of the designed filter under a loss of time synchronization

The performance of the designed wavelet is compared and contrasted with several known wavelets by means of computer simulations. We have designed a communication system with DQPSK modulation and 128 orthogonal sub-carriers, corresponding to a wavelet packet tree of 7 stages. Guard intervals are not used and no error estimation or correction capabilities are implemented. To simplify the analysis, perfect frequency and phase synchronization are assumed. The time offset  $\Delta_t$  is modeled as discrete uniform distribution between -2 and 2 samples, i.e.  $\Delta_t \in [-2, -1, 0, 1, 2]$ . In order to highlight the difference in performances between various wavelets, an oversampling factor of 15 is applied. The details are tabulated in Table 8.6.

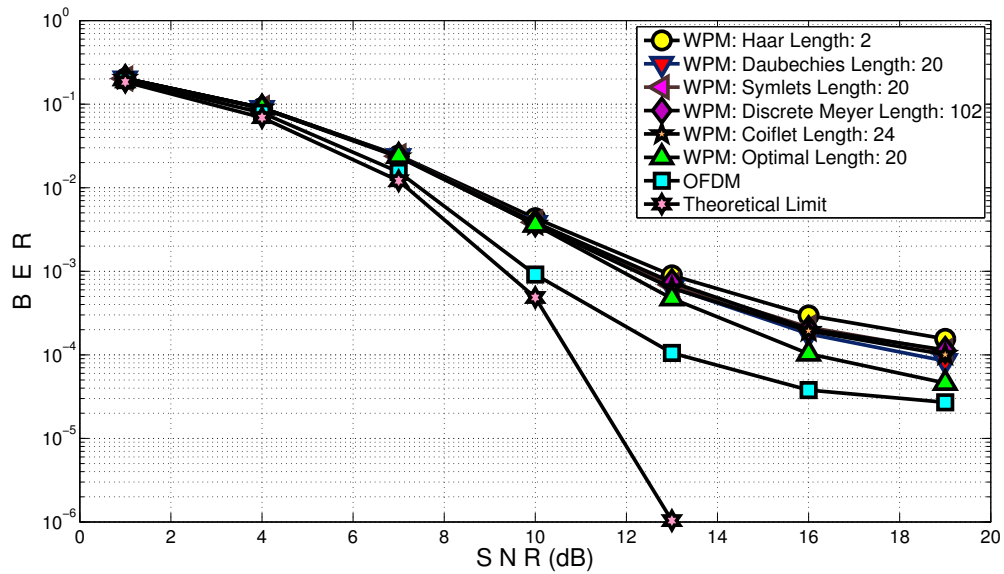


FIGURE 8.18: BER Performance of Different Wavelets and OFDM under Time Synchronization Errors.

Wavelet	Haar	Daubechies	Symlets	Discrete Meyer	Coiflet
Improvement	5.03 dB	2.17 dB	3.25 dB	3.25 dB	2.98 dB

TABLE 8.7: Performance improvement of designed optimal wavelet over standard Wavelets in the presence of time errors (measured at BER of  $10^{-4}$ ).

Fig. 8.18 shows the Bit Error Rate (BER) performances of the WPM system with different kinds of wavelets and OFDM. The channel is taken to be an AWGN channel and the transmitter-receiver ends operate under a loss of time-synchronization.

The plots in fig. 8.18 reveal that the designed optimal wavelet has better BER performance in the presence of timing errors when compared to performances of commonly known wavelets. However, OFDM tolerates a loss of time synchrony better than WPM. This is due to fact that under time synchronization errors the ISI in OFDM arises only between two adjacent symbols while in WPM several symbols interfere with each other. Table 8.7 shows the relative gains in the SNR performance of the designed optimal wavelet over standard wavelets in the presence of timing errors. The values have been calculated for a bit-error-rate (BER) of  $10^{-4}$ .

BER and Mean Square Error (MSE) calculated for different values of time offset are shown in figs. 8.19 and 8.20, respectively. Because the direction of timing error is inconsequential for WPM systems the time offset  $\Delta_t$  is considered to follow a uniform distribution 1 and 5 samples. The results presented corroborate the gains brought in by the newly designed wavelets.

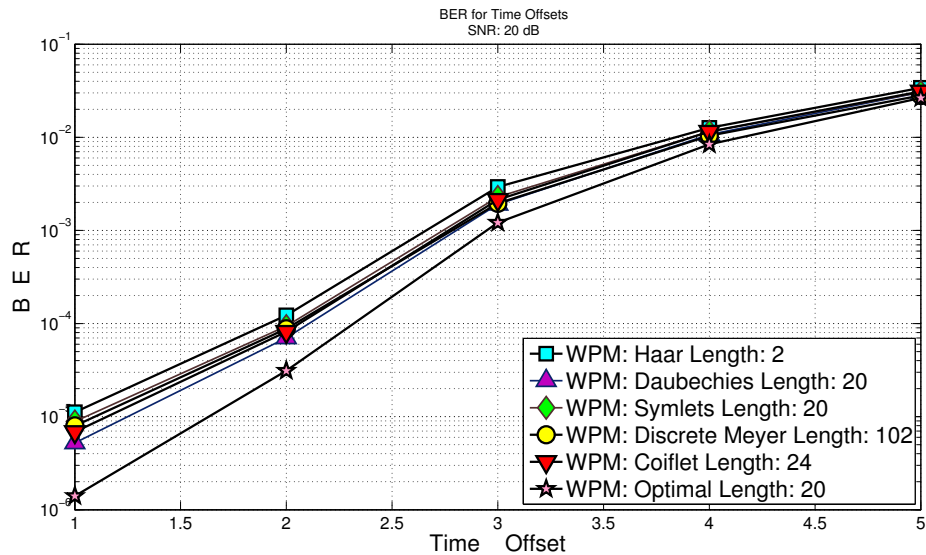


FIGURE 8.19: BER vs. Time Offset for WPM in any AWGN channel (SNR = 20dB).

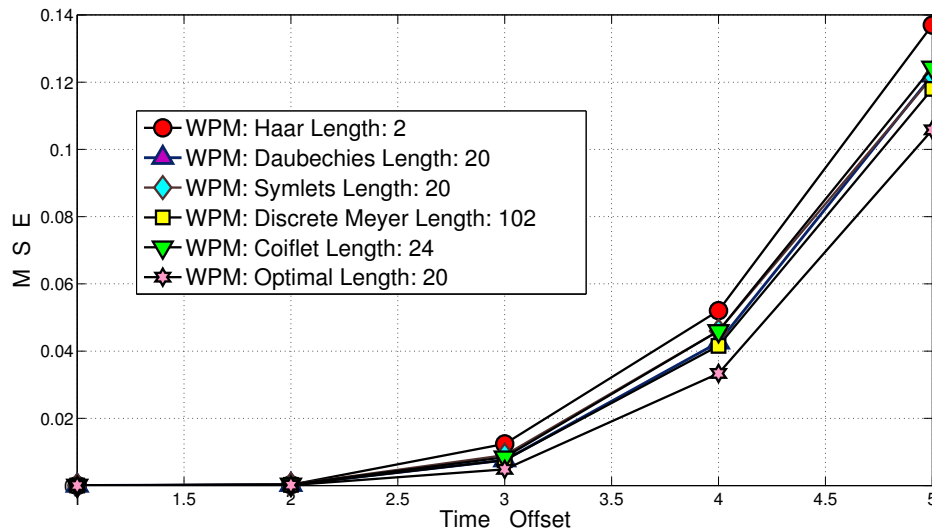


FIGURE 8.20: MSE vs. Time Offset for WPM in an AWGN channel (SNR = 20dB).

### C. Dispersion of sub-carrier energy

In figs. 8.21 (2-D plots) and 8.22 (3-D plots) the diffusion of sub-carriers energy to adjacent regions due to time synchronization error are portrayed. For clarity of depiction we have limited the number of sub-carriers to 16 and the WPM frame size to 30 multi-carrier symbols. From a total of 480 sub-carriers in each frame, one pilot sub-carrier is set to a non-zero value while the remaining 479 sub-carriers are made zero. In order to accentuate the effect of a timing error the channel is taken to be ideal. It can be seen from the figures that the amplitudes of interfering sub-carriers is reduced by employing the newly designed filter (denoted as 'optimal filter' in the graphs).

Wavelet	Haar	Daubechies	Symlets	D-Meyer	Coiflet	Designed
<b>Interference Variance (<math>10^{-5}</math>)</b>	5.1088	3.0751	3.0721	3.1651	3.0639	2.8775
<b>Max. Interference to Signal Amplitude</b>	14.14 %	8.36 %	7.97 %	6.66 %	8.25 %	4.51 %

TABLE 8.8: Interference Variance and Maximum (Max.) Interference Amplitude Ratio.

In table 8.8 the values of interference variance and maximal interference amplitude ratio in relation to signal amplitude are given. These values are obtained for a single pilot sub-carrier under a constant time-offset.

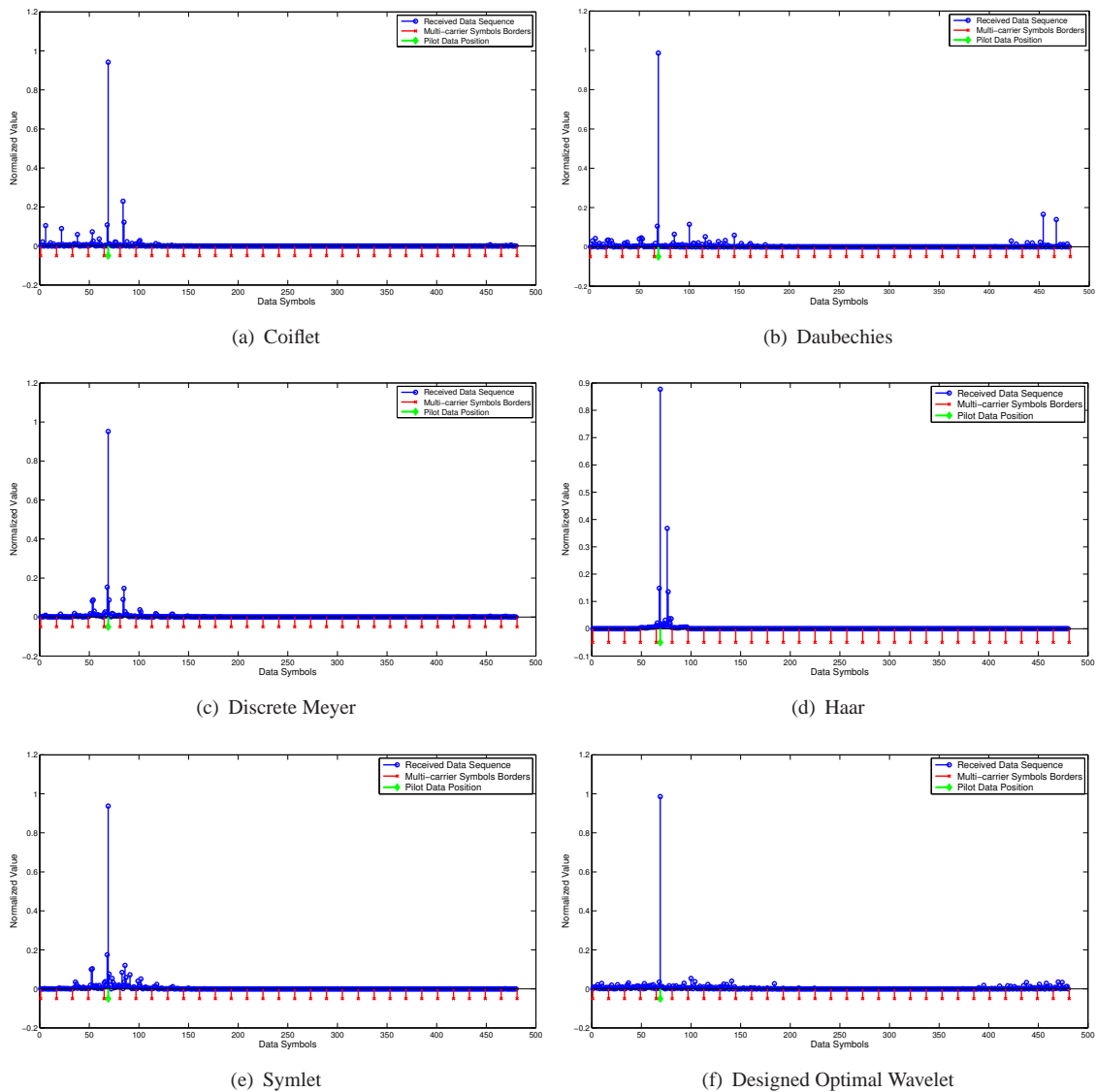


FIGURE 8.21: Received Spectral Energy (2-dimension) in a frame in the presence of a timing error.

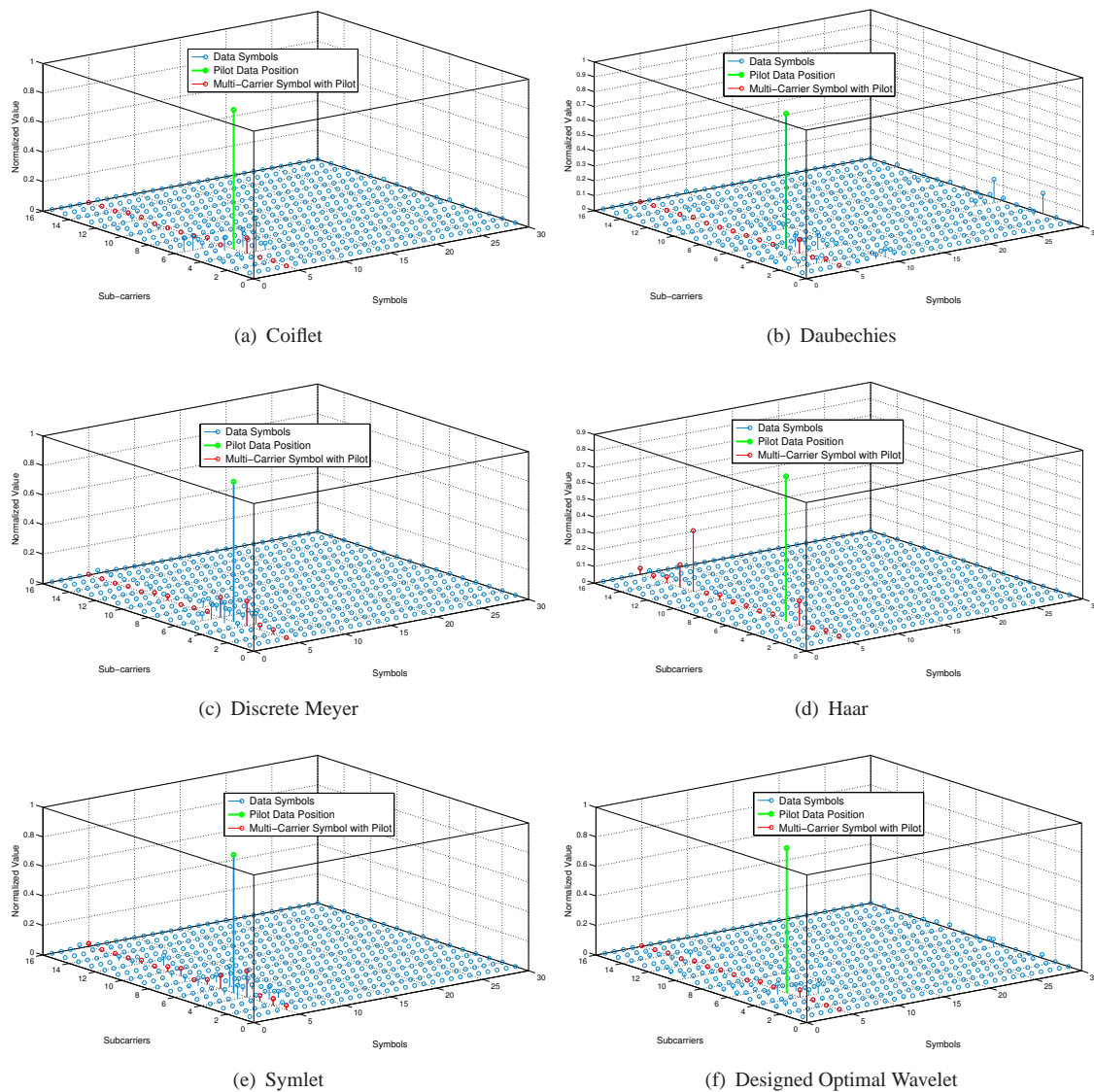


FIGURE 8.22: Received Spectral Energy (3-dimension) in a frame in the presence of a timing error.

### 8-5 Summary

Wavelet Packet Modulation has recently emerged as a strong candidate for multi-carrier transmission because of its offer of enormous adaptability and flexibility to system designers. In this chapter, we presented a methodology to design new wavelets according to a given design specification. The design process was described as an optimization problem that accommodated the design objectives and additional constraints necessary to ensure wavelet existence and orthonormality. In order to obtain the global minimum, the original non-convex constraints and objective function were translated into the autocorrelation domain. Using the new formulation,

the design problem was expressed as a convex optimization problem and efficiently solved using semi-definite programming techniques. Two case studies - (a) where the cross-correlation between the filters was lowest, and (b) where the filters were maximally frequency selective - were used to demonstrate the design mechanism. The simulation results revealed that the newly designed wavelet satisfied all the design objectives and outperformed standard wavelets.

The wavelet design framework presented in this chapter can easily be applied for other design criteria (say reduction of PAPR or ISI or ICI) by merely altering the objective function. However, to be able to do so, the desirable properties of the wavelet bases must be translated into realizable objective functions. This can at times be challenging because the relationship between wavelet functions and filters is implicit and not direct. Another area of future research is to establish weights to evaluate the various trade-offs between the desirable (and at times contradictory) goals.

## **Part V**

# **Conclusion**

## Chapter 9

# Conclusions and future research topics

### 9-1 Introduction

The convergence of information, multimedia and wireless communications has raised the vision of ubiquitous and pervasive communication - communication anywhere, anytime and anything. However, each of the incumbent wireless systems operate with different technologies, standards, interfaces, hardware (processors, Radio Frequency (RF) front end, antennas), software (drivers, firmware), network subscriptions, frequency bands and identities. In fact state-of-the-art multi-radios only share the display and keyboard!

The consequence is that users have to constantly switch between different devices, modes and networks impoverishing their experience. Therefore, there is an emergent need for a generic, universal radio that integrates different standards and air interfaces. The challenge is to seize on the right technical strategy to provide a common telecommunications medium that connects devices and thereby people.

Digital communication systems can be viewed as trans-multiplexers characterized by the transmission waveforms. The time-frequency properties of the pulse shaping filter, i.e. the time spread and frequency footprint, determine the type of communication system (TDMA, FDMA, CDMA, OFDM, UWB, MC-CDMA etc). Different radios have different transmission characteristics which are greatly altered by the nature of the waveforms used. Transmission waveforms can thus be considered as the *genes* of the radios - the fundamental unit of change. By altering the time-frequency characteristics of the waveforms, wireless systems which optimize resources and system performance can be envisaged. In order to integrate different radios we propose the realization of a flexible and generic wavelet packet based Multi-Carrier Modulation (WPM) Radio that can emulate different use-cases. Wavelets and wavelet transforms are used as the technology of choice because their characteristics can be widely customized to fulfill the requirements of intelligent wireless communication systems.

A generic wavelet based MCM radio will be a natural replacement for multi-tone schemes like OFDM. It can also generate single carrier schemes since they are just a special case of multi-carrier signals. A variant of UWB systems called multi-band OFDM (MB-OFDM) already exist where the wide band OFDM operates at different frequency bands at different instances. Multi band-WPM can be an extension to MB-OFDM and can be applied for UWB transmission. Multiple access communication is also possible with wavelets. With their offer of greater flexibility in designing signature waveforms, and their inherent orthogonality property, they can play a vital role in the design of waveforms and receivers for multiple access systems.

The possibility of applying wavelet theory for the design of flexible and generic radios capable of handling multiple radios has been explored in the framework of this thesis work. The results of these studies have been recorded in various publications and reports. This thesis work was dedicated to the demonstration of the Wavelet Packet Modulator (WPM) as a wide-band multi-carrier technology alternative to the well known OFDM. Additionally, the application of WPM to a multi-antenna/MIMO architecture is investigated in [152]. In [153], a method to shape Ultra wide-band (UWB) signals using the wavelet packet transform is presented. Bit error rate (BER) and outage probability performance of the proposed system in the presence of competing sources is analyzed and suitable strategies to mitigate the impact of interference presented. And in [154], a novel receiver design that utilizes the time and frequency localization properties of Wavelet transform is proposed for a wavelet-based single carrier system.

It is important to underline here that the all the communication modes explained above employ the same signal processing architecture and hence they can be combined into a single radio unit.

The advantages of wavelet transform in terms of the flexibility they offer to customize and shape the characteristics of the waveforms have been demonstrated in [155–158]. Two use-cases where the waveforms are designed and applied to optimize the system performance according to specific system demands are illustrated in [155, 156]. In [157], the efforts of [155, 156] is extended to establish a unifying mathematical framework where the waveforms can be designed according to any engineering requirement. And in [158] search heuristics ,based on a genetic/neural code, are used to solve numerical problems associated with wavelet design. Finally, the ability of wavelet radios to opportunistically exploit radio resources is illustrated in [159] where a WPM based scheme for cognitive radio systems is addressed. In this proposal, the transmission waveform of WPM is sculpted to make use of the unoccupied time-frequency gaps of the licensed users.

In this thesis the operation of the novel Wavelet Packet Modulator was successfully evaluated. The importance of the study lies in the fact that very little literature exists in this field. The main contribution of the work is in the mathematical modeling of the WPM system in MATLAB© and numerical analysis of its performance. The challenges involved in the practical implementation

of the system were listed and studied. The functioning of the proposed WPM system under various performance metrics was studied. Some of the figures of merit evaluated include:

- PAPR performance,
- sensitivity to loss of synchronization (time/frequency/phase),
- robustness to channel vagaries,
- operation under interfering sources.

Suitable interventions that addressed issues like PAPR, channel equalization were devised, implemented and tested. The proposed system was successfully applied and verified for two practical applications namely, spectrum estimation and dynamic spectrum access. The adaptable features of the system were demonstrated in the form of wavelet design suited to the system specification.

Numerical results and comparative studies with FFT/OFDM-based systems validated the efficacy of the algorithms deployed. The results of the study made it clear that WPM based radios can be a viable alternative to existing technologies.

## 9-2 Summary of chapters and key conclusions

The key inferences and conclusions of the study are summarized chapter-wise in the following sections.

### A. Study of WPM performance under loss of Synchronization (Chapter – 4)

In this chapter we evaluated the effects of loss of synchronization between the transmitter and receiver, due to frequency offset or phase noise or timing error, on WPM transmission. The performances were also compared with OFDM. The key inferences and notable contributions of the study can be summarized as follows:

- Orthogonal multiplexing schemes like WPM and OFDM are vulnerable to loss of synchronization in time, frequency or phase.
- **Effect of frequency offset** – The effect of frequency offset is to cause the sub-carriers to lose their mutual orthogonality which results in mutual interference. In OFDM, the performance degradation is limited to the interference amongst the sub-carriers (referred as Inter-carrier Interference (ICI)) within one OFDM symbol duration. However, in WPM

the sub-carriers from multiple symbols interfere with each other causing Inter Symbol-Inter Carrier Interference or IS-ICI. This dissimilarity in the interference behavior is due to the manner in which the sub-carriers in wavelet and Fourier based systems are created. The signals generated by OFDM overlap only in frequency domain while WPM generated signals overlap in both frequency and time domain.

- **Impact of phase noise** – Depending on the bandwidth of the phase noise two scenarios can emerge in the presence of phase noise:
  - i. if the phase noise bandwidth is small compared to inter-carrier spacing the dominant effect is a constant rotation of constellation symbols.
  - ii. if the phase noise bandwidth is greater than the inter-carrier spacing the rotational behavior is less pronounced but instead the interference dominates.
- As with the effect of frequency offset, the interference due to phase noise corrupts the OFDM signal only with ICI while in WPM signals are corrupted with IS-ICI.
- **Impact of loss of time synchronization** – OFDM benefits from the use of the cyclic prefix to greatly reduce the errors due to loss of time synchronization. WPM cannot benefit from such constructions due to the time overlap of the symbols. Nevertheless, the cyclic prefix in OFDM fails to prevent interference from occurring if the offset value is larger than the size of the prefix or when the offset is in the direction opposite to the symbol's own prefix. When parts of the neighboring symbols are erroneously selected at the OFDM or WPM receiver windows, the demodulated data is afflicted by ISI and ICI. In OFDM, ISI arises only due to neighboring multi-carrier symbols, while in WPM more symbols, in addition to the contiguous ones, contribute to the generation of ISI.
- To understand the impact of loss of synchronization, analytical expressions were derived. To corroborate the theoretical findings, a computer simulation platform was set-up and the performances of OFDM and WPM systems were examined in the presence of carrier frequency offset, phase noise or time synchronization errors. Several well-known wavelets such as Daubechies, Symlets, discrete Meyer, Coiflets and bi-orthogonal wavelets were applied and studied.

From the study it can be concluded that the performance degradation of WPM and OFDM affected by carrier frequency offset and phase noise are comparable. However, WPM is far more severe to time offset than OFDM, thereby, necessitating a strong and robust synchronization algorithm to recover loss of time synchronization.

## B. PAPR performance studies (Chapter – 5)

In this chapter, a study on the effect of PAPR on the Wavelet Packet Modulator was presented. The summary of the study and key novelties are enlisted below:

- The statistical distribution of WPM signals and its power variations were studied. The envelope of the WPM signal and its power were found to follow the Gaussian and Chi-squared distribution, respectively.
- The effect of PAPR on the Wavelet Packet Modulator (WPM) scheme was then evaluated. Various WPM configurations, with different wavelet families, pulse shapes and lengths, were considered. OFDM was also included as reference. Almost all the wavelets performed similarly with regard to their PAPR performances. Moreover, the WPM operations were comparable with that of OFDM.
- To alleviate the PAPR impact on WPM transmission, 2 techniques were employed:
  - i. First, a selected mapping (SLM) approach with phase modification technique to reduce the PAPR in the Wavelet Packet Modulation system was studied. By creating replicas of the original message by randomly altering the phases of the sub-carriers that modulate the information, different WPM frames with different PAPR values could be obtained. Then, the WPM frame with the least PAPR should be transmitted. The attraction for this method is its simplicity and elegance of implementation.
  - ii. Next, we extended the selected mapping technique by optimizing the selection of phase offset of the sub-carriers. The technique employed a heuristic algorithm known as the Hill Climbing optimization which is based on neural networks.

From the studies it was found that the stochastic nature of the WPM signal as well as its PAPR performance are similar to that of the OFDM. Furthermore, the PAPR mitigation strategies devised for one system can be used for the other with minor adjustments.

## C. Wavelet packet spectrum estimator(WPSE) (Chapter – 6)

In this chapter, we investigated the application of wavelet packet transform (WPT) for spectral estimation and signal analysis. The main contributions of the study are:

- **Wavelet packet spectrum estimator (WPSE)** – Implementation of wavelet packet based spectrum estimator on a simulation platform.

- Evaluation of the performances of the proposed WPSE and its comparison with traditional techniques like Periodogram, Welch, Windowed periodogram and MTSE. To gauge the performance of the estimator, different test sources with variegated characteristics were utilized. The figures of merit employed were - out of band (OOB) energy rejection, variance of the estimates and frequency resolution.
- **Enhanced wavelet packet spectrum estimator (E-WPSE)** –Optimization of WPSE performance through mitigation of edge based artifacts that occur in standard WPSE.

The key inferences on the study of WPSE may be summarized as follows:

- i. The wavelet transform is a unitary transform which conserves energy,
- ii. Since the mathematical precept of wavelets is tightly coupled to the filter bank theory, the WPSE can be formulated as a filter bank analysis problem,
- iii. An effectual spectrum estimator based on the theory of wavelets can be built by exploiting the filter bank structure of wavelet packet decomposition,
- iv. The decomposition level of the wavelet packet tree can be tuned to adjust the performance of the wavelet-based estimates with respect to variance of the estimated PSD and frequency resolution.
- v. Based on the level of decomposition, the WPSE performance ranges between that of Welch and periodogram.
- vi. The wavelet packet based approach gives all wavelet coefficients at all decomposition levels. The presence of all of these coefficients allows for obtaining multiple estimates from different level of the tree with different degree of variance and frequency resolution, in one snapshot and one operation. This feature can be exploited to construct an adaptable and re-configurable spectrum estimation mechanism. This feature of WPSE can be of enormous advantage in a dynamic and variegating environment.

The results of the experiments showed that the WPSE offered great flexibility and adaptability apart from its performances which are comparable and at times even better than Fourier based estimates. The studies also showed that the E-WPSE system offered excellent OOB rejection, small variance of the estimates, and good frequency resolution making it a very competitive technique. In comparison to existing estimators the E-WPSE gave significant performance gains especially with an out-of-band rejection of up to 60dB for partial band and about 200 dB for multi-tone sources.

#### D. WPSE/WPM for Dynamic Spectrum Access (Chapter – 7)

In this chapter we presented a Wavelet Packet spectrum estimator (WPSE), Wavelet Packet Modulator (WPM) combination as a multi-carrier solution for dynamic spectrum access solution. The key contributions of the study can be enlisted, as:

- A wavelet packet transceiver that combined the wavelet packet-based spectrum estimator (WPSE) with a Multi-carrier modulator was established.
- The WPSE unit used the same filter bank structure as used for WPM transmission. Hence spectrum analysis was possible at virtually no additional cost.
- The proposed WPSE/WPM system was tested for *dynamic spectrum access use cases*. Typical applications for such systems include Cognitive radio and LTE-advanced.
- The system was evaluated for various scenarios and use cases. The performances were compared and contrasted with two other candidate systems based on FFT/Periodogram.

From the numerical studies, the performance of the WPSE/WPM transceiver was found to be excellent in terms of BER performance, rejection of out-of-band energy and interference to neighboring sources. Comparing with the performance of OFDM/FFT based configurations, the studies showed that WPSE/WPM performed better in regard to estimation of spectrum and confinement of transmitted waveform spectra. This in turn contributed to better bit-error rate (BER) performance and bandwidth efficiency.

#### E. Design of Wavelets (Chapter – 8)

In this chapter we presented a general, unified approach to design and develop orthogonal wavelet packet bases according to a requirement. The important inferences and original contributions of the study are detailed below:

- We advanced the state-of-the-art in WPM to design wavelet bases for use in communication formats. This is necessitated by the fact that the wavelets currently in use are not custom-built for multi-carrier systems.
- To do so we established a generic, unified framework that facilitates the design of new wavelet bases that cater to a requirement.
- The possibility of adapting the characteristics of the WPM transmission is illustrated with two examples where families of wavelets which are maximally frequency selective or have the lowest cross correlation energy, are developed.

- The design of wavelet filters is subject to multiple constraints. Besides the primary goal (for e.g. derivation of wavelets with high frequency selectivity) there are other constraints mandated by the wavelet theory that have to be fulfilled. These *budgets* of the filter-design process were expressed as a convex optimization problem. The *global* solutions for the design problem were obtained using a mathematical numerical solver known as semi definite programming (SDP). The solution-filters were then tested for conformance with design goals.

Some of the conclusions from the design of the two candidate wavelet-filters can be stated thus:

1. Design of Maximally Frequency Selective Wavelets:

- WPSE results with the newly designed filters yielded more accurate results than ones based on standard wavelets such as Coiflets, Symlets and Daubechies.
- The WPM carrier using the new wavelets guaranteed sharper transition bands and better time-frequency localization than commonly known wavelets.

2. Design of wavelets with low cross correlation energy:

- To address the high sensitivity of WPM to a time offset, we designed a new wavelet filter which reduces the timing error interference.
- Studies on the WPM operation showed that the newly designed optimum filter ensured better performance on loss of time synchronization when compared to standard wavelets such as Daubechies, Symlets, discrete Meyer, Coiflets, etc.

The results of these studies affirmed the promise that a WPM system hold in devising flexible communication systems whose characteristics can be tailored according to the engineering requirements.

### 9-3 Future research topics

In this section we present a few ideas to enhance this PhD work. The content is divided into three sections (refer fig. 9.1), namely,

1. **Enhancements to this PhD**, where suggestions to improve the study conducted during this dissertation are presented.
2. **Related Studies**, where activities which are related to this dissertation (but not treated in this work) are listed.

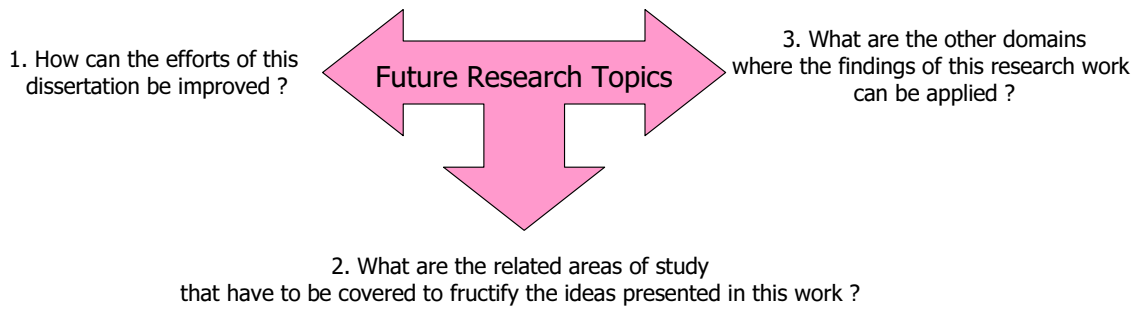


FIGURE 9.1: Future research topics

3. **Beyond this work**, where other domains and fields where the research findings of the areas can be readily applied and translated, are enlisted.

### 9-3-1 Enhancements to this PhD

#### A. Study of WPM performance under loss of Synchronization

- In this thesis the vulnerability of WPM to time synchronization errors was addressed. However, in the implementation all the sub-carriers were taken to experience the same time or frequency offset. This model can be extended with different sub-carriers undergoing different offsets.
- Furthermore, a robust synchronization algorithm to detect and correct large time offsets can be implemented.

#### B. PAPR performance studies

- Study those cases where the data is correlated (e.g. transmission of a picture or audio information); important is its impact on the PAPR performance or on the mitigation techniques.
- Explore the possibility of data clipping as a PAPR mitigation technique and the utilization of wavelet de-noising methods at the receiver to retrieve data.
- Conduct PAPR studies with more sophisticated power amplifier models.
- Explore the possibility of designing new wavelets for PAPR reduction.
- Study the impact of over-sampling on the PAPR performance of WPM.
- Exploit the tree structure of WPM to come out with the best tree formation that guarantees minimum PAPR. Unlike OFDM which divides the communication channel into orthogonal sub-channels of equal bandwidths, WPM uses an arbitrary time-frequency plane tiling

to create orthogonal sub-channels of different bandwidths and symbol rates. When transmitting the same data in WPM, alternative tree representations can be used resulting in different sub-channel spacing in time and frequency which are not necessarily uniform. This feature of WPM can be utilized for the reduction of PAPR. In particular, each of the alternative (pruned) trees could result in a different value for PAPR, and an algorithm to choose the optimum tree structure can be devised such that the structure achieves the minimum PAPR.

- Analyze the complexity in which the cost of implementing the reduction technique along with the loss in data-rate, is considered.

### C. Wavelet packet spectrum estimator (WPSE)

- Explore the possibility of applying compressed sampling for Wavelet Packet based spectrum estimation.
- Expand edge-mitigation studies to include more sophisticated approaches (including windowing techniques) to reduce artifacts in WPSE filter bank implementation.
- Study of dual tone sources to understand the resolution abilities of WPSE.
- Derive analytical expressions for WPSE variance and bias.
- Explore the possibility of applying windows to the WPSE method to tackle spurious spectral growth (also known as spectral carving).
- Utilize co-operative spectrum sensing with focus on diversity exploitation to improve the WPSE probability of errors/estimation. This can also be useful in avoiding shadowing and hidden node problems.
- Analyze the ability of WPSE for a sparse representation of the radio environment (frequency information) with a lower number of coefficients. This helps in a co-operative spectrum sensing scenario where a lower amount of information sharing means indirectly leads to a lesser clogging of the bandwidth.
- Investigate the properties of WPSE to guarantee good time resolution. This property can be useful in scenarios where the time information is vital (e.g. estimation of swept tone sources, discussed in Chapters 7 and 8 of this dissertation).
- Optimize dynamic spectrum utilization: In [160] Z. Tian and G.B. Giannakis propose a wavelet-based wide-band spectrum sensing approach for dynamic spectrum management. In their approach, the signal spectrum over a wide frequency band is decomposed into elementary building blocks of non-overlapping sub-bands that are well characterized by local

irregularities in frequency. Then the entire wide-band is modeled as a sequence of consecutive frequency sub-bands, where the power spectral characteristic is smooth within each sub-band but exhibit a discontinuous change between adjacent sub-bands. Information on the locations and intensities of spectrum holes and occupied bands is derived by considering the irregularities in PSD. The main attraction of using wavelets in this application is in the ability of wavelets to analyze singularities and irregular structures which can be used to characterize the local regularity and edges of signals. Hence, the method is also called Edge detection. The method of Z.Tian and G.B. Giannakis can be enhanced further by designing new wavelets that are best suited for the application instead of using generalized wavelets.

#### **D. WPSE-WPM for dynamic spectrum access**

- The WPSE/WPM system was evaluated for various dynamic spectrum access use cases. Future research can include more scenarios, especially, the cases where the nature of the licensed user (LU) varies frequently or when the data available to gauge the LU characteristics is limited.
- More extensive evaluation of the system performance under different channel conditions are still needed.

#### **E. Design of wavelets**

- The unique features offered by wavelets to tailor and customize new filters were explored in this thesis in order to make WPM transmission less sensitive to time synchronization errors or reduce spectral spillage into neighboring bands. The innovative wavelet filter design template can also be used for other design goals by merely altering the objective function and other design *budgets*. For instance, wavelet filters which can decrease frequency offset and phase noise sensitivity, reduce Peak-to-Average Power Ratio (PAPR) or increase spectral efficiency could be designed. However, to be able to do so, the desirable properties of the wavelet bases must be translated into realizable objective functions. This can at times be challenging because the relationship between wavelet functions and filters is implicit and not direct.
- Another area of research is to establish weights to gauge the trade-offs on offer between various desirable (and at times contradictory) goals.
- An added advantage of using the wavelet theory for Multi-carrier modulation is in the possibility of improving transmission security. Because newly designed wavelets are unique

in nature, the transmitted signal can only be decoded by the WPM receiver which is acquainted with filter coefficients used by the WPM transmitter.

## F. Channel equalization

- The studies in this thesis were confined to channels that were time-invariant. Therefore a natural extension to the work will be to consider channels that vary with time and/or are frequency dispersive.
- The equalizer in this thesis focused on the removal of ISI. Devising an equalizer which handles both the Inter-symbol interference and Inter-carrier interference can be a fruitful area of further research.
- A blind equalizer in which the transmitted signal is inferred from the received signal making use only of the transmitted signal statistics (without availability of channel information.), can be a productive area of future research.
- Information on channel modeling and representation of the channel using wavelet packets can be used to customize the transceiver tree structure based on the channel condition and further simplify the equalization process.

### 9-3-2 Related studies

One of the prime motives for pursuing wavelet based systems is in the flexibility and adaptability that they offer. This capability can be readily exploited to provide better services to users and enrich their experience. In order to realize these capabilities many technological challenges have to be overcome. Apart from that there are other related subjects that have to be addressed. Foremost amongst them is an understanding of how an engineering requirement translates to a particular system specification. To successfully map this relation, a careful and thorough study on the following areas must be conducted:

- i. impact of waveform characteristics on various performance metrics,
- ii. the trade-offs in performance characteristics with regard to the design of waveforms. For e.g. research questions such as *do the waveforms that yield the best PAPR performance affect the BER performance?* and *What about its performance with respect to ISI/ICI reduction?* have to be addressed,
- iii. a thorough analysis on the complexity issues,

- iv. mapping of the complexity analysis and trade-off issues in an *easy-to-understand-and-to-present* manner such that the user can make effective choices based on his needs and necessities. For example, if the user desires low battery power consumption he should be able to operate with a single radio with sufficient features for gainful communication. On the other hand, he should also be made aware of the consequences of his choice and how it may affect the quality of service (such as lower speed, lower bandwidth, throughput etc.).

Other topics which have to be covered for the practical implementation of WPM, include,

- i. ensuring backward compatibility with existing technologies and systems,
- ii. making the system generic and flexible so that it can be easily scaled,
- iii. establishing suitable mechanisms to analyze the radio environment and utilize them effectively in radio reconfiguration schemes,
- iv. demonstration of the system capabilities through a proof of concept (POC),
- v. development of software tools to adequately test and verify the system,
- vi. standardization of the technology to ensure compatibility across different development platforms.

### 9-3-3 Beyond this work

Apart from the suggested improvements cataloged above, there are other areas of wireless system design where the wavelet packet architecture can be readily applied. Here we discuss a few of them:

#### A. Wavelet-Based modeling of time-variant wireless channels

Currently available wireless channel models are based on statistical impulse response models derived from empirical results. While these models perform adequately for time-invariant channels, they fail to accurately map time-varying channels. The wavelet transform is a way of decomposing a signal of interest into a set of basis waveforms, called wavelets, which thus provide a way to analyze the signal by examining the coefficients (or weights) of wavelets. Due to their inherent joint time-frequency localization property and their ability to accurately characterize the time-varying nature of the estimation problem, the wavelets offer various advantages for channel modeling. Some of them are: accurate characterization of time-varying as well as frequency selective multi-path fading channels, fast convergence of estimating the channel, representation of the channel with a fewer number of coefficients, small output error, and clear interpretation of modeling error.

## B. Multiple access communication

Wavelets and wavelet packets possess unique properties that make them attractive for use in multiple access communications. With their offer of greater flexibility in designing signature waveforms, and their inherent orthogonality property, they can play a vital role in the design of waveforms and receivers for multiple access systems. Further, wavelets can facilitate the design of user signature waveforms for code division multiple access (CDMA) communication systems. By randomly clipping the wavelet construction tree, a complete and orthonormal basis is generated. This basis eventually spawns spreading codes that are orthogonal to one another. Moreover, they display greater capacity to suppress multiple access interferences. The design and construction of orthogonal signatures for use in a spread signature CDMA system is discussed in [5]. According to [161] wavelets allow for simpler equalization and detection of CDMA signals at the receiver.

Multi-carrier CDMA or MC-CDMA is a data transmission technique that combines Multi-carrier modulation (MCM) and CDMA. It is a spread spectrum technology, where the spreading is performed in the frequency domain, unlike CDMA, where the spreading is done in the time domain. By combining the best of MCM and CDMA, MC-CDMA promises high speed, large bandwidth, better frequency diversity to combat frequency-selective fading and good performance in severe multi-path conditions. MC-CDMA has thus emerged as a strong candidate for future wireless systems. In comparison to the conventional Fourier-based MC-CDMA systems, introducing wavelets to MC-CDMA yields the following advantages:

- i. They provide three levels of orthogonality, namely,
  - between the sub-carriers,
  - between the wavelets and scaling functions, and
  - between the spreading sequences.

Therefore in comparison to conventional MC-CDMA systems, they offer new dimensions to combat multipath fading, ICI and interference or jamming signal by providing

- ii. They provide flexibility in choosing the spacing between the sub-carrier frequencies.
- iii. They offer a wide choice of wavelet families to choose from.

## C. Wavelet radio for green communication

Recent studies have shown that the energy costs account for as much as half of a mobile service provider's annual operating expenses. Therefore making the communication equipment more efficient in relation to its power consumption not only has implications with regard to

environmental pollution, it also makes economic sense. The theme of Green Communications is to design energy-efficient communication techniques and protocols which optimally utilize available resources and minimize power consumption. Wavelet-based technologies offer a lot of tools for research and development of Green communication devices. The methodologies can be classified into two broad categories:

i. Customization of waveforms

- While there is no explicit relationship between power optimization and waveforms, the nature and characteristics of the waveform can be altered to suit a set of requirements which can indirectly contribute to a more efficient system resulting in lower requirements of power and energy. These criterion could typically be:
  - minimization of ISI, ICI or PAPR,
  - greater tolerance and robustness to time/frequency/phase offset errors
  - robustness towards interference from competing sources
  - possibilities for opportunistic communication (e.g. Cognitive Radio) where unused resources can be cleverly utilized.
- It is important to note that every performance metric that is influenced by the characteristics of the transmission waveform can be mapped into a design constraint and exploited to yield efficient systems.

ii. Customization of tree structure

- The wavelet-based systems are realized from a tree structure obtained by cascading a fundamental Quadrature Mirror Filter (QMF) pair of low and high pass filters. The construction of this tree structure can be adjusted to come out with an optimum tree structure that caters to various requirements. The requirements could typically be:
  - Identification and isolation of the *atoms* of interference in both time and frequency domains.
  - Flexibility with time-frequency tiling of the carriers leading to multi-rate systems which can transmit with different rates in different bands. This feature can be exploited in scenarios where the channel characteristics are not uniform.
- It can be proved that the complexity of Wavelet systems is by and large simpler than OFDM systems. A lower complexity also means lower power requirements in the execution of the signal processing algorithms. The implementation of Wavelet systems can be simplified even further if fast-wavelet transforms are employed.
- In addition to these advantages, the promise of an integrated and universal wavelet-based radio can also immensely help in the optimization of the system performance. By integrating multiple radios the wavelet-based systems do away with the need for

multiple firmwares, software, drivers etc and reduce power consumption and improve battery life.

#### **D. Wavelet based multiple-input multiple-output communications (MIMO)**

OFDM-MIMO (Multiple-Input Multiple-Output) combination has been successfully applied to enhance the throughput and range of wireless networks without the ensuant increase in bandwidth or power requirements. Since OFDM and WPM share many properties, as both are orthogonal multi-carrier techniques, there is potential for a WPM systems to be used in a multi-antenna MIMO setup.

### **9-4 Concluding remarks**

In a recent article in The Communication magazine, Steve Weinstein [162], a pioneer in the development of OFDM traces back the journey of OFDM right from its inception in 1966 when Chang [163] published the first paper on multi-carrier modulation, to the development of the first proof of concept by Bell Labs in 1985 [164] and its first major consumer deployment as ADSL in 1993 and finally its standardization as IEEE 802.11a in 1999. In his concluding remarks he advocates wavelet-based systems as true successors of OFDM, especially, for the development of futuristic low power *Green Radios* which are intelligent and adaptable.

The research and investigation, on the utilization of wavelet technology for smart resource aware radio systems, as presented in this thesis, can be considered as a fruitful attempt at tackling the various technical questions that will shorten the development time from conception to practical realization of wavelet radios . Furthermore in an era when bold predictions as the *PHY Layer is Dead* [165] are made, the work on wavelet-based radios can increase the capacities of the wireless link and open new vistas for gainful research on radio design.

# Appendix A

## Design of Wavelets

### A-1 Semi-definite programming

Semi-definite Programming (SDP) is a sub-field of convex optimization, which can efficiently exploit interior point methods to find an optimal solution [136, 137]. The main advantages of convex optimization methods are that they always achieve global minimum without being trapped in the local minima, and that they can determine explicitly the feasibility of a given set of constraints. SDP algorithms can be used to solve linear, quadratic and semi-definite problems, which all are part of convex optimization problems.

The optimization problems in SDP can be described as minimization of an objective linear function over the intersection of the semi-definite cone with an affine space. This cone is shaped by constraints that form a set of positive symmetric semi-definite matrices, called Linear Matrix Inequality (LMI) constraint [138]. LMI gives boundaries of feasible region in which SDP solver tries to find an optimal solution for the objective function. This region is generally non-smooth and non-linear but it has to be convex in order to be solvable by SDP [138–142].

A set  $C$  is said to be convex if the line segment between any two arbitrary selected points in  $C$  also lies in  $C$ . In case of points  $X_1$  and  $X_2$  we can show the convexity by:

$$\Gamma X_1 + (1 - \Gamma)X_2 \in C \text{ for } X_1, X_2 \in C \text{ and } 0 \leq \Gamma \leq 1. \quad (\text{A.1})$$

The example of convex and non-convex set is illustrated by fig. A.1. For each two points in pentagon the line segment lies in the defined set and therefore blue figure (left) is convex. The red figure (right) is obviously not convex since two points  $X_1$  and  $X_2$  are within the set but the line which connects them is partially not contained in the set.

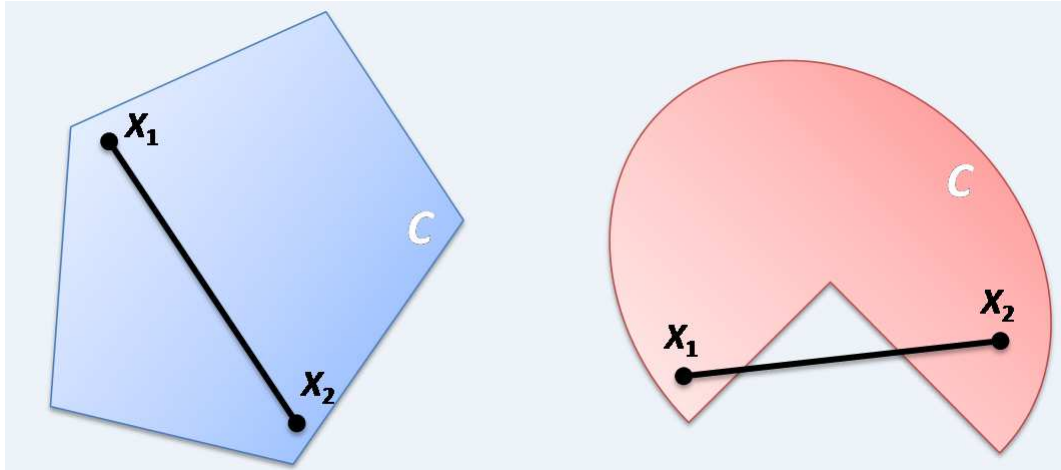


FIGURE A.1: Convexity. Left: Convex Set, Right: Non-Convex Set.

## A-2 Spectral factorization

The Kolmogorov spectral factorization method is based on construction of the minimum phase spectral factor  $SF_{mp}(z)$  from the autocorrelation function. The power series expansion of  $SF_{mp}(z)$  is given by:

We can decompose  $\log SF_{mp}(z)$  into real and imaginary parts as:

$$\log SF_{mp}(z) = \mu(z) + j\eta(z) \quad (\text{A.2})$$

Here,  $\mu(\omega)$  and  $\nu(\omega)$  are Hilbert transform pairs. For  $z = e^{j\omega}$  we have:

$$\begin{aligned} \mu(\omega) &= \log |SF_{mp}(e^{j\omega})| \\ &= \frac{1}{2} \log R_h(\omega) \\ &= \sum_{n=0}^{\infty} d_n \cos n\omega, \eta(\omega) \\ &= - \sum_{n=0}^{\infty} d_n \sin \omega n. \end{aligned} \quad (\text{A.3})$$

In eq.(8.39)  $R_h(\omega)$  denotes the Fourier transform of autocorrelation sequence. We can find the coefficients  $d_n$  by:

$$d_n = \frac{1}{2\pi} \int_0^{2\pi} \frac{1}{2} \log R_h(\omega) e^{-jn\omega} d\omega \quad (\text{A.4})$$

### A-3 Sum of squares of cross-correlation function

The sum of squares of cross-correlation magnitude is related to the autocorrelation sequences of low pass filter  $H$  and high pass filter  $G$  according to the following equation:

$$\begin{aligned} \sum_{n=0}^{L-1} |r_{hg}[n]|^2 &= \sum_{n=0}^{L-1} r_h[n] ((-1)^n r_h[n]) \\ &= r_h[n] \cdot r_g[n]. \end{aligned} \quad (\text{A.5})$$

**Proof:**

$$\begin{aligned} \sum_n |r_{hg}(n)|^2 &= \sum_n \left( \sum_p h[p+n]g[p] \right)^2 \\ &= \sum_n \sum_m \sum_p h[p+n]g[p]h[m+n]g[m] \\ &= \sum_m \sum_p g[p]g[m] \sum_n^L h[p+n]h[m+n] \\ &= \sum_m \sum_p g[p]g[m] \sum_{n=m-p} h[m]h[2m-p] \\ &= \sum_m \sum_p r_h[m-p]g[p]g[m] \\ &= \sum_p \sum_{n=m-p} r_h[n]g[p]g[n+p] \\ &= \sum_n r_h[n]r_g[n] \\ &= r_h[n] \cdot r_g[n]. \end{aligned} \quad (\text{A.6})$$

### A-4 Partitioning of energy

The sum of squares of the time series elements  $x$  is given by:

$$\|x\|^2 = \sum_{t=0}^{N-1} x(t)^2 \quad (\text{A.7})$$

Energy is preserved at any level  $1 \leq l \leq J$  of the transform as given by eq.(A.8), where  $\zeta$  denotes WPT coefficients.

$$\|x\|^2 = \sum_{p=0}^{2^l-1} \|\zeta_l^p\|^2 \quad (\text{A.8})$$

**Proof:**

Let us first define equivalent sequence filter  $v$ , built from the combination of filters  $h[n]$ ,  $g[n]$  and down-sampling as:

$$v_{l,p,n} = \sum_{i=0}^{L-1} v_{p,i} v_{l-1, \lfloor p/2 \rfloor, n-2^{l-1}i} \quad (\text{A.9})$$

where,

$$\begin{aligned} v_{1,0,n} &= h[n] \\ v_{1,1,n} &= g[n]. \end{aligned} \quad (\text{A.10})$$

The discrete Fourier transform (DFT) of  $x$  is given by:

$$X(k) = \sum_{t=0}^{N-1} x(t) e^{-j2\pi \frac{k}{N} t} \quad (\text{A.11})$$

Similarly follows the DFT of the filter  $v$ :

$$\Upsilon_{l,p,k} = \prod_{m=0}^{l-1} M_{l,p,m,2^m k \bmod N} \quad (\text{A.12})$$

where

$$\begin{aligned} M_{0,2^m i \bmod N} &\equiv H_{2^m i \bmod N} \\ M_{1,2^m i \bmod N} &\equiv G_{2^m i \bmod N} \\ \tilde{H}_i &= \sum_{n=0}^{N-1} h(n) e^{-j2\pi \frac{n}{N} k} \\ \tilde{G}_i &= \sum_{n=0}^{N-1} g(n) e^{-j2\pi \frac{n}{N} k} \end{aligned} \quad (\text{A.13})$$

Parseval's theorem states that the sum of squares of a sequence with length  $N$  is equal to the sum of the moduli squared of its DFT divided by  $N$ . Now the WPT coefficients are given by the convolution of time-domain filter sequence with elements  $x$ , which in frequency-domain can be expressed as:

$$\begin{aligned}
 \sum_{p=0}^{2^l-1} \|\zeta_l^p\|^2 &= \sum_{p=0}^{2^l-1} \frac{1}{N} \sum_{k=0}^{N-1} |X(k)|^2 |\Upsilon_{l,p,k}|^2 \\
 &= \frac{1}{N} \sum_{k=0}^{N-1} |X(k)|^2 \sum_{n=0}^{2^l-1} |\Upsilon_{l,p,k}|^2 \\
 &= \frac{1}{N} \sum_{k=0}^{N-1} |X(k)|^2 \sum_{n=0}^{2^l-1} \left| \prod_{m=0}^{l-1} M_{l,p,m,2^m k \bmod N} \right|^2 \\
 &= \frac{1}{N} \sum_{k=0}^{N-1} |X(k)|^2 \prod_{m=0}^{l-1} \left[ \left| \tilde{H}_{2^m k \bmod N} \right|^2 + \left| \tilde{G}_{2^m k \bmod N} \right|^2 \right] \quad (\text{A.14})
 \end{aligned}$$

The wavelet and scaling filter are chosen in such way that their frequency responses are mirror images of each other with respect to frequency of  $\pi/2$ . Therefore, we get for the normalized wavelets:

$$\left| \tilde{H}(\omega) \right|^2 + \left| \tilde{G}(\omega) \right|^2 = 1 \quad (\text{A.15})$$

Equation eq.(A.14) can hence be written as:

$$\sum_{n=0}^{2^l-1} \|\zeta_l^p\|^2 = \frac{1}{N} \sum_{k=0}^{N-1} |X(k)|^2 \prod_{m=0}^{l-1} I(m) = \sum_{t=0}^{N-1} x(t)^2 = \|x\|^2 \quad (\text{A.16})$$

## Appendix B

# Graphical User Interface

During the course of this project a graphical user interface (GUI) was developed to facilitate the computer modeling and simulation of various WPM configurations. The GUI is based on Matlab. Two GUIs were developed - one to test WPM operation and the other to design wavelets.

### B-1 GUI for WPM testing

Fig. B.1 shows the screenshot of the interface used for running the WPM simulations. The interface can also be used for simulating OFDM. It has provisions to test different wavelet families like Daubechies, Symlets, Coiflet and Discrete Meyer. Wavelet families of different filter lengths can also be evaluated. Other parameters that can be adjusted are: the number of carriers of WPM/OFDM systems, the number of symbols per frame, the length of the cyclic prefix in OFDM, channel conditions, infarctions such as frequency/ phase or time offset errors, amongst others. Different kind of outputs in the form of Bit-error rate curves, scatter plots, 2D/3D energy plots can be obtained with the interface.

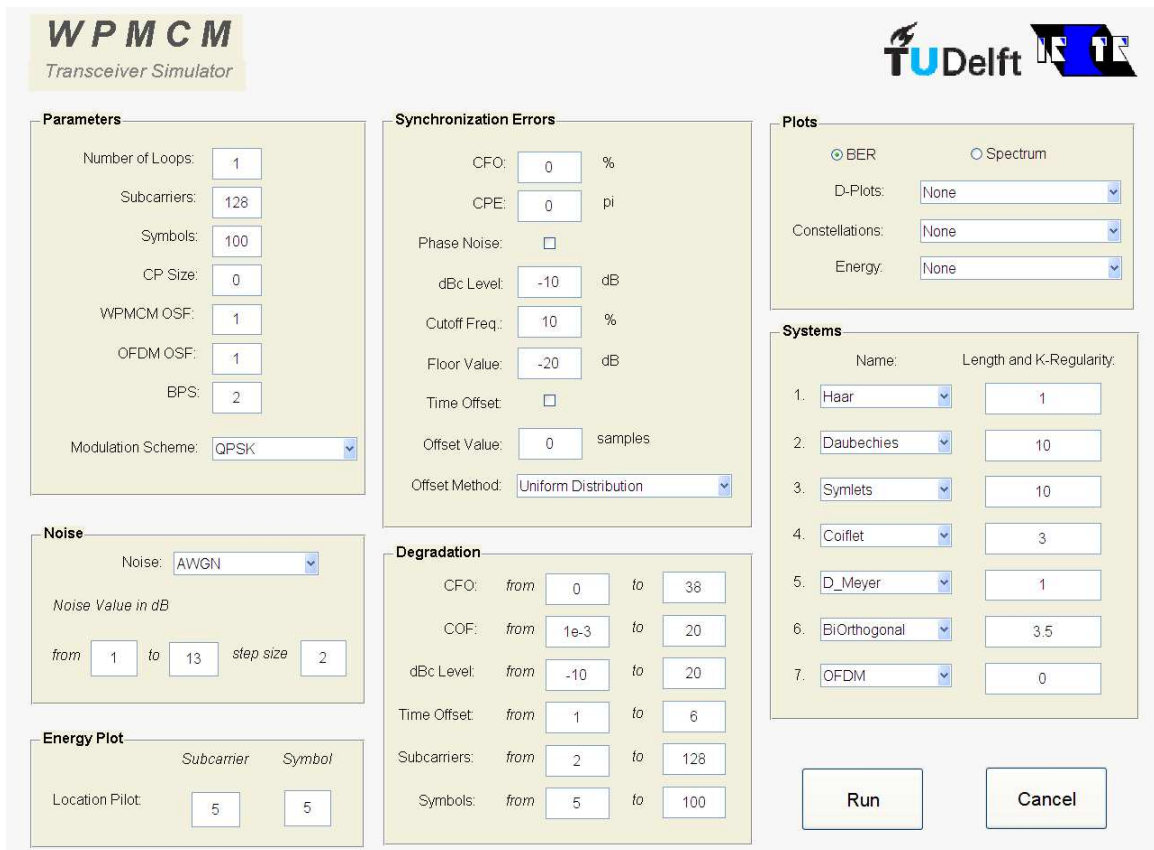


FIGURE B.1: Wavelet Packet Filter Design Program

## B-2 GUI for wavelet design

The screenshot of the wavelet filter design interface is shown in fig. B.2. The interface allows the entry of wavelet parameters like the filter length, the desired regularity (or flatness) and the order of differentiability. Apart from these mandatory conditions, other budgets may also be specified.

The program uses Semi Definite Programming (SDP) to design optimized filters according to the user specifications. To ensure smooth operation of the programs at least two additional Matlab packages are needed, namely: - Yalmip, [online available at <http://control.ee.ethz.ch/~joloef/wiki/pmwiki.php>] - SeDuMi, [online available at <http://sedumi.mcmaster.ca>]

### B-2-1 Details of the filter design program

The desired length of the filter, regularity and the minimal number of times that the scaling function is continuously differentiable are mandatory fields. The field *Filter Length* must always be an even number because of the double shift orthogonality constraint. *K-Regularity* has to be smaller or equal to the half of the *Filter Length* but it should be always greater than 1 in order for

the filter coefficients to satisfy the wavelet existence constraint. *Differentiability*, if applicable, has to be smaller than half of the *K-Regularity*. The field *Objective Function* is used to set a scalar expression which has to be minimized. The field *Additional Constraint* can be used to set an extra constraint or an extra set of the constraints.

Three optimization methods are used for design of new filters:

- Optimal Convex
- Optimal Convex 2
- Optimal Non-Convex.

Optimal Convex is the most stable of the three methods and works on the autocorrelation sequence of filter  $Q(\omega)$  (refer Chapter 9). It has built-in additional continuous differentiability constraint, opposed to other two methods which don't support it.

Optimal Convex 2 method works well only for short filters. For large filter lengths this method becomes unstable. Optimal Convex 2 works on autocorrelation sequence of the filter  $H$ .

The optimal non-convex method works directly on filter coefficients with non-convex constraints and therefore does not use SDP optimization algorithms. The disadvantage of this method is that the results are usually local minimum. Furthermore, for large filter lengths this method runs into numerical problems.

The interface generates output such as:

- Filter Impulse Response,
- Filter Frequency Response,
- Wavelet and Scaling Function,
- Wavelet Packet Plot,
- Wavelet Packet Spectrum.

The interface has inbuilt diagnostics to test the validity of data entered. It also verifies if the results of the optimization algorithm satisfy the conditions mandated.

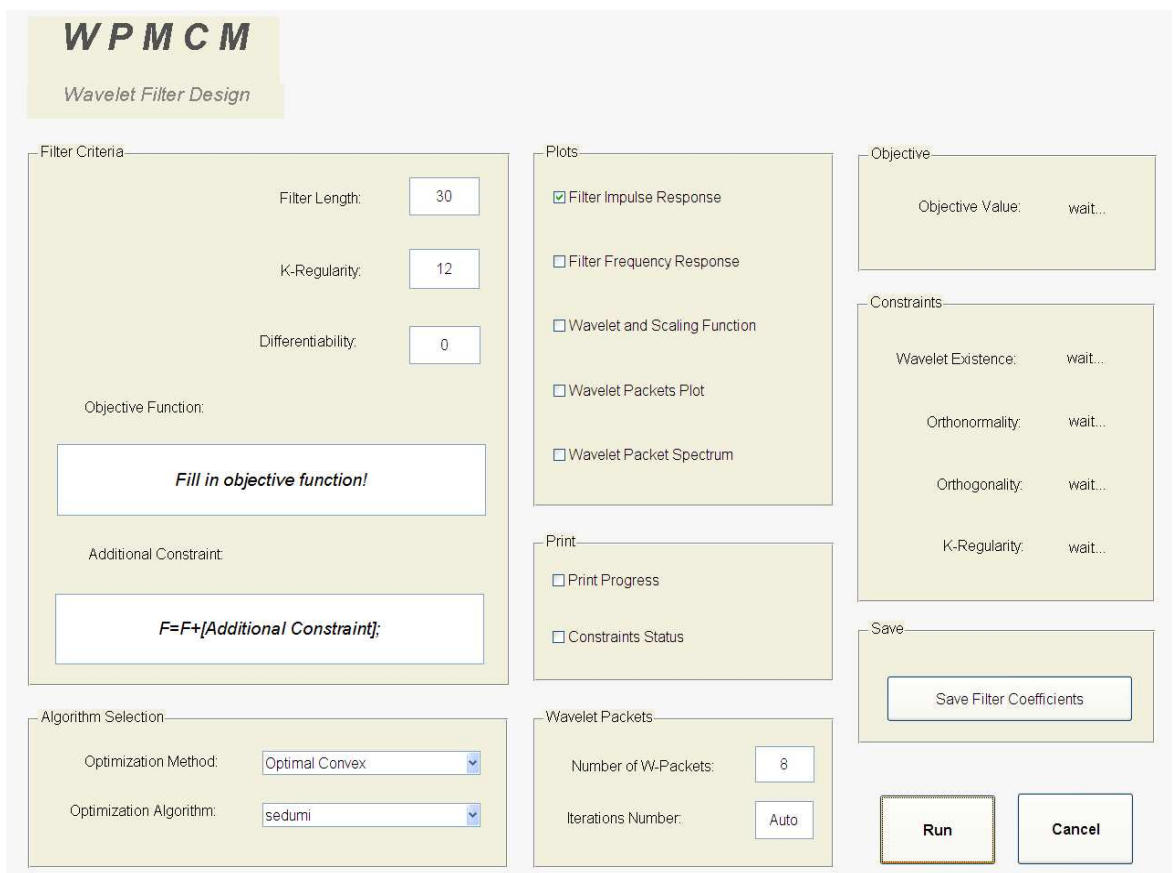


FIGURE B.2: Wavelet Packet Filter Design Program

## Appendix C

# Channel Equalization in WPM by minimization of peak-distortion

### C-1 Introduction

A radio communication link can corrupt transmission of information between a sender and a receiver<sup>1 2</sup>. Frequency-selective or dispersive channels can lead to a loss of orthogonality between the signals of a multi-carrier system causing disturbances such as the Inter-symbol interference (ISI) and Inter-carrier Interference (ICI). Channel equalization is a simple technique to counteract the deleterious effects of the wireless channel. Channel equalization for WPM systems is unique because the WPM symbols overlap in time. Hence, both inter-symbol interference (ISI) and inter-symbol inter-carrier interference (IS-ICI) occur and have to be factored in the design of the equalizer. In this chapter we present a basic time-domain equalizer for the compensation of channel induced distortions on the WPM transmission.

While there exists many techniques for equalization of OFDM channels, the extant body of research for WPM systems is limited to the work of Gracias [14] and Jamin [10]. In [14] a channel equalization method for a generic WPM structure is presented. The method works by exploiting the fact that for sufficiently narrow band sequences, a channel can be modeled as an attenuation and delay. Thus, equalization is reduced to a problem of determining the delay introduced by the channel for each of the wavelet packet sub-carriers. To accurately determine the delay experienced by each sub-carrier, a minimum square variance algorithm is proposed. The algorithm is shown to perform well, analytically and through simulation studies, for a simple delay-channel.

---

<sup>1</sup>The contents of this chapter have been published in [166]. For any material borrowed from [166] a written consent has been obtained from the first author.

<sup>2</sup>The author gratefully acknowledges the contributions of Msc student Mr. Anurag Bajpai for his help with the computer simulations.

In [10] a distributed equalizer architecture which exploits the tree structure of WPM is suggested. Since the WPM transceiver is organized as a set of filter-pair structures, the signal can be accessed at different rates at each stage of the WPM tree structure and equalized independently. The equalizer is modeled as a lattice structure with the series elements countering the ISI and the shunt elements handling the ICI. The method can be considered as a class of post-detection equalizer and has been demonstrated to work for time-invariant channels.

The disadvantage of both the methods presented above is their high order of complexity and the difficulty in scaling them to systems with large number of sub-carriers (say 64 or 128). In this backdrop we present a simple and efficient equalizer for WPM systems. The equalizer applies the principle of peak-distortion criterion where the maximum inter-symbol interference induced by the channel is minimized. The operation of the proposed algorithm is demonstrated through numerical simulations. Investigations to understand the impact of the wavelet family, length of the wavelet filters, and the number of equalizer taps on the performance of the equalizer are carried out.

The rest of the chapter is organized as follows - section C-2 describes the proposed equalization technique. The details of the simulation environment and important test parameters are provided in section C-3. The numerical results of the study are presented and discussed in section C-4. Finally, the chapter concludes with a summary of important inferences in section C-5.

## C-2 Equalization by minimization of the peak-distortion

Consider that a data sequence of length  $N$ ,  $x[n] = [x_0 x_1 x_2 \dots x_{N-1}]$ , is transmitted into the radio channel <sup>3</sup>. Assuming that the channel has a memory of  $L_c$  with coefficients  $c[n] = [c_0 c_1 c_2 \dots c_{L_c-1}]$ , the received signal  $y[n]$  can be given as,

$$y[n] = x[n] * c[n] + \eta[n]. \quad (\text{C.1})$$

Here  $*$  stands for the convolution operator and  $\eta[n]$  represents the Additive White Gaussian Noise (AWGN).

The multi-path effects of the wireless channel introduces Inter Symbol Interference (ISI) and distorts the transmission of information. Hence, an equalizer is necessary at the receiver to remove ISI and obtain an uncorrupted signal. In C.1 the WPM receiver with the equalizer is shown. The equalization is carried out in the time-domain before the demodulation of data.

---

<sup>3</sup>The discussion presented in this section is based on [50], chapter-10.

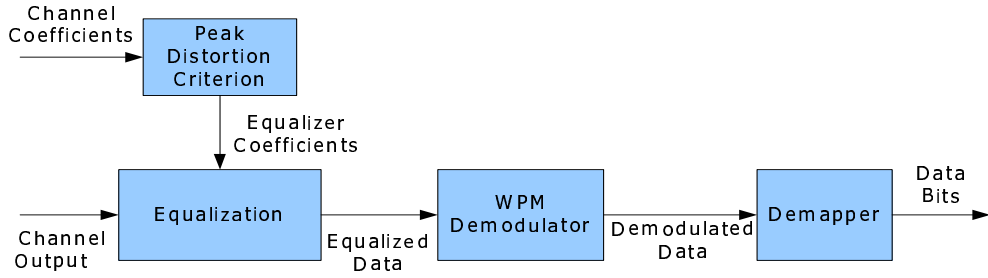


FIGURE C.1: Blocks of the peak-distortion equalizer.

In order to design an efficient equalizer to remove (or minimize) the channel distortion, we use a performance metric called the peak-distortion criterion [50, 167]. Peak-distortion may be defined as the worst case ISI at the output of an equalizer [50]. Representing the impulse response of the channel with  $c_n$  and that of the equalizer with  $e_n$ , we can define a single equivalent filter  $q_n$  as the convolution between  $c_n$  and  $e_n$ , as,

$$q_n = \sum_{j=-\infty}^{\infty} e_j c_{n-j}. \tag{C.2}$$

Under these circumstances, two scenarios can be defined to understand the nature of the equalization process,

- a. when the equalizer has infinite number of taps, and
- b. when the equalizer has a finite number of taps.

### C-2-1 Equalizer with Infinite Taps

With an equalizer of infinite taps, the output at the  $k$ th sampling instance can be expressed as [50]:

$$\hat{I}_k = q_0 I_k + \sum_{n \neq k} I_n q_{k-n} + \sum_{j=-\infty}^{\infty} e_j \eta_{k-j}. \tag{C.3}$$

In (C.3) the first term represents the desired symbol scaled by a factor  $q_0$ , the second term is the ISI and the third term is AWGN. The peak value of this distortion  $\Omega(e)$ , is given by [50]:

$$\Omega(e) = \sum_{n=-\infty, n \neq 0}^{\infty} |q_n| = \sum_{n=-\infty, n \neq 0}^{\infty} \left| \sum_{j=-\infty}^{\infty} e_j c_{n-j} \right|$$

Indeed,  $\Omega(e)$  is a function of the equalizer tap weights. For an equalizer with infinite taps, it is possible to select the tap weights such that  $\Omega(e) = 0$ , i.e., the ISI can be completely eliminated.

Under these circumstances, the tap weights can be determined as,

$$q_n = \sum_{j=-\infty}^{\infty} e_j c_{n-j} = \begin{cases} 1, & n = 0 \\ 0, & n \neq 0 \end{cases} \quad (\text{C.4})$$

In the frequency domain (C.4) can be written as:

$$Q(f) = E(f)C(f) = 1 \quad (\text{C.5})$$

or,

$$E(f) = \frac{1}{C(f)} \quad (\text{C.6})$$

From (C.6) it can be inferred that in order to completely eliminate the ISI, the equalizer should be an inverse of the channel filter. For this reason the peak-distortion criterion is also referred to as zero-forcing equalization.

### C-2-2 Equalizer with Finite Taps

Thus far, we have considered an equalizer of infinite length. Let us now consider an equalizer of finite length, say,  $2M+1$ . Since  $e_j = 0$  for  $|j| > M$ , the convolution of  $c_n$  with  $e_n$  is zero outside the range  $-M \leq n \leq M + L - 1$ . That is,  $q_n = 0$  for  $n < -M$  and  $n > M + L - 1$ , where  $L$  is the channel length. With  $q_0$  normalized to unity, the peak-distortion becomes

$$\Omega(e) = \sum_{n=-M, n \neq 0}^{M+L-1} |q_n| = \sum_{n=-M, n \neq 0}^{M+L-1} \left| \sum_j e_j c_{n-j} \right|. \quad (\text{C.7})$$

Although the equalizer has  $2M + 1$  adjustable parameters, there are  $2M + L$  non-zero values in  $q_n$ . Therefore, it is impossible to completely eliminate the ISI and there will always remain residual interference even when the optimum coefficients are used.

The peak-distortion criterion given in (C.7) has been shown to be a convex function of the equalizer coefficients [50]. The general solution of the peak-distortion criterion can be obtained by the method of steepest descent. The minimum value of the peak-distortion  $\Omega(e)$  can be obtained by selecting the equalizer coefficients to force  $q_n = 0$  for  $1 \leq |n| \leq M$  and  $q_0 = 1$ . It can be given as [50]:

$$\Omega_0 = \frac{1}{|c_0|} \sum_{n=1}^L |c_n| \quad (\text{C.8})$$

In [50] the value of  $\Omega_0$  has been shown to be less than unity which means that the ISI is not severe .

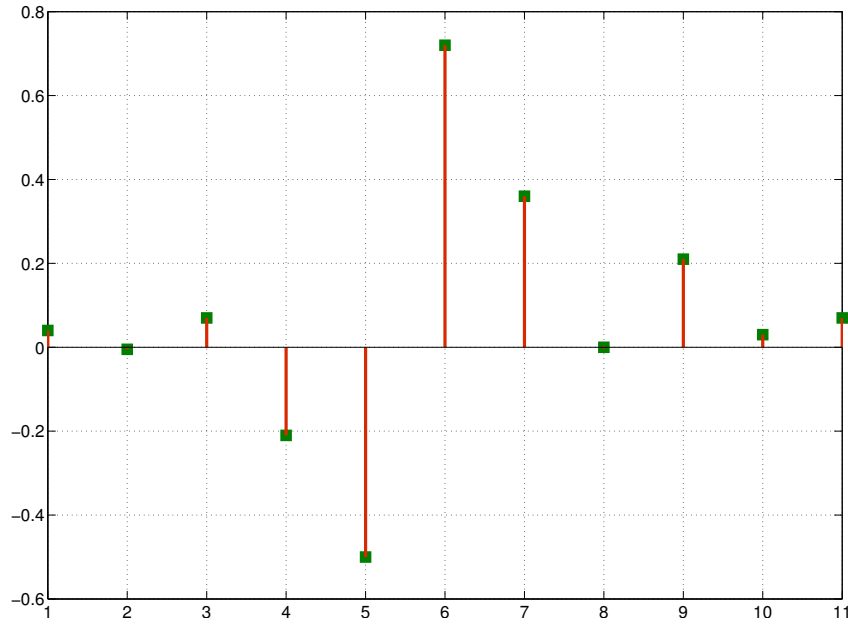


FIGURE C.2: Impulse Response-11 tap Channel

### C-3 Simulation Setup

In this section we evaluate the performance of WPM system with the proposed channel equalizer and present results of the studies. The investigations were carried out with computer simulations. The performance metric of choice is the Bit error rate performance (BER). The WPM system is realized using a filter bank structure with 7 levels of decomposition (128 carriers). The modulation scheme used is Quadratic Phase Shift Keying (QPSK). The wavelet of choice is Daubechies 20 (denoted db20) which is of length 40. These simulation parameters will be used through out the experiments unless stated otherwise.

Two channels were considered for the experiments. The first one is a benevolent channel proposed by Proakis [50] whose impulse response is given by:

$$h_{chn1} = [0.04, -0.005, 0.07, -0.21, -0.5, 0.72, 0.36, 0, 0.21, 0.03, 0.07]. \quad (\text{C.9})$$

The channel has a memory of 11-taps and does not have any high order frequency selectivity or nulls. The discrete time channel characteristics of this channel is plotted in Fig. C.2 and the amplitude response of this channel is depicted in Fig. C.3.

The second channel considered is a 15 tap channel, with high order of frequency selectivity. This channel is proposed by European Telecommunications Standards Institute (ETSI) for Digital Video Broadcasting [168]. The discrete time channel characteristics of this channel is plotted in Fig. C.4 and the amplitude response of this channel is depicted in Fig. C.5.

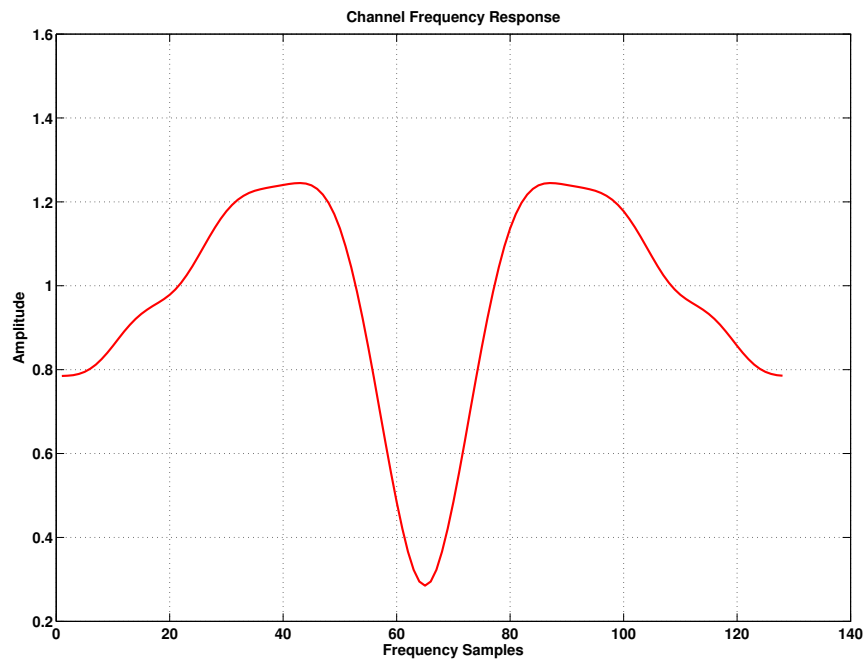


FIGURE C.3: Channel Frequency Response-11 tap Channel

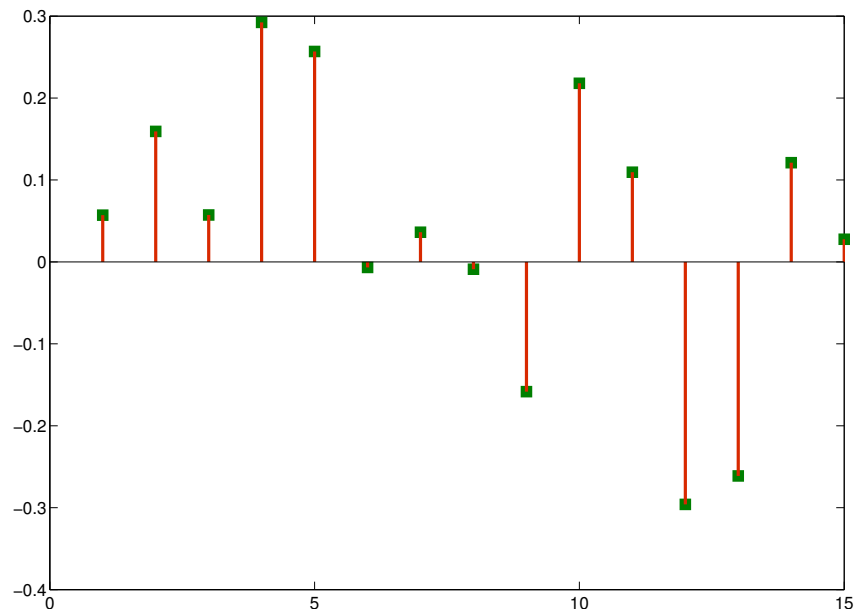


FIGURE C.4: Impulse Response-15 tap Channel

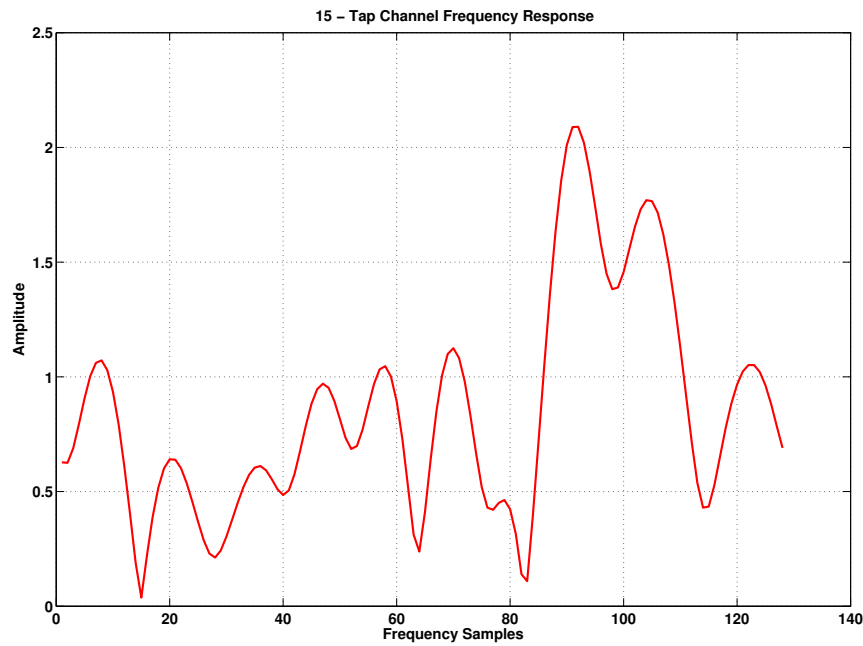


FIGURE C.5: Channel Frequency Response-15tap Channel

## C-4 Simulation Results

### C-4-1 Performance under Channel Condition-1

The BER performance of the WPM system under Channel-1 with the proposed equalizer is shown in Fig. C.6 where the notable improvements brought about by the equalizer can be observed. The number of taps of the equalizer used in this experiment is 15. The corresponding constellation diagram for the received and equalized data at a SNR of 21dB are shown in Fig. C.7. We can observe from Fig. C.7 the improvements brought about by the equalizer in reducing the dispersion of received data.

A further investigation was carried out to verify the impact of the equalizer taps on the system performance. Fig. C.8 depicts the BER curves of the WPM system operating with an equalizer of different number of taps. Barring the case with an equalizer of 5 taps, the performance of the system for other scenarios is good and comparable. In order to minimize the complexity, for the channel under consideration, an equalizer of 12 taps would be adequate.

In Fig. C.9 a comparison of the BER performance of the WPM system with different wavelets under the same channel conditions and a 15-tap ZF equalizer, is made. It can be seen from the plots that there are no tangible differences in the performances of the WPM system operating with different wavelets. The only exception is the bi-orthogonal wavelet, Bior3.5, which performs worst because the sub-carriers generated by this wavelet are not orthogonal.

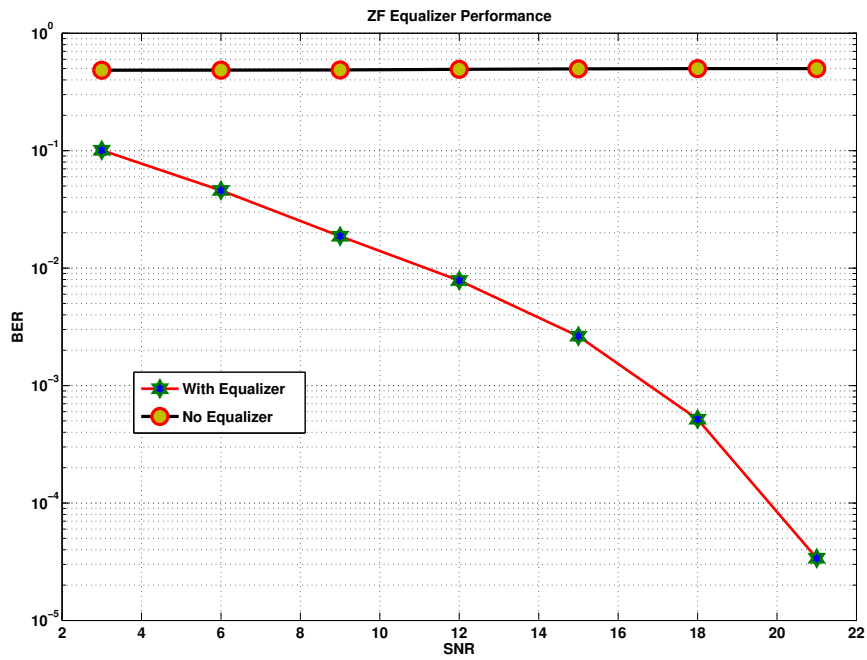


FIGURE C.6: Performance of ZF Equalizer for Channel-1

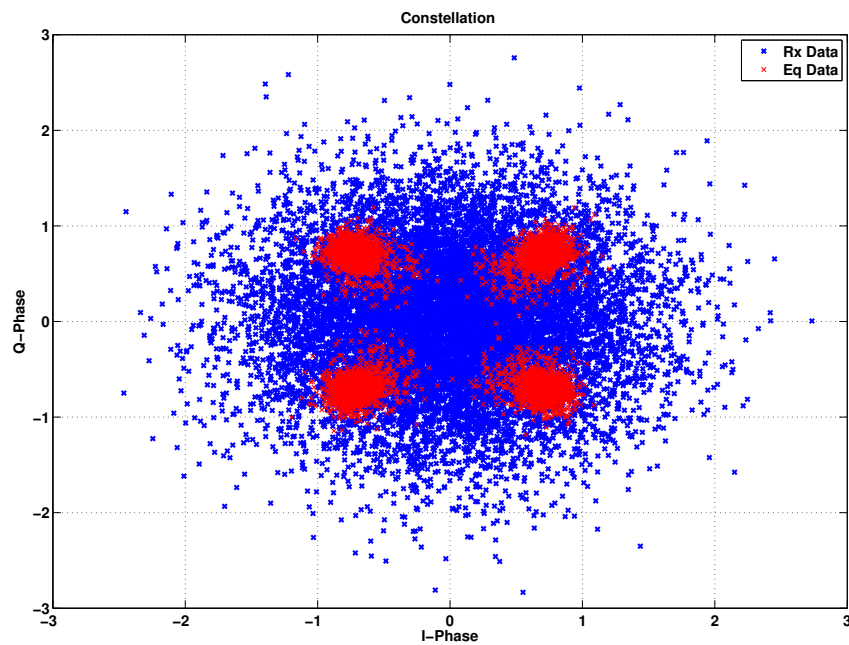


FIGURE C.7: Constellation of the received and equalized data

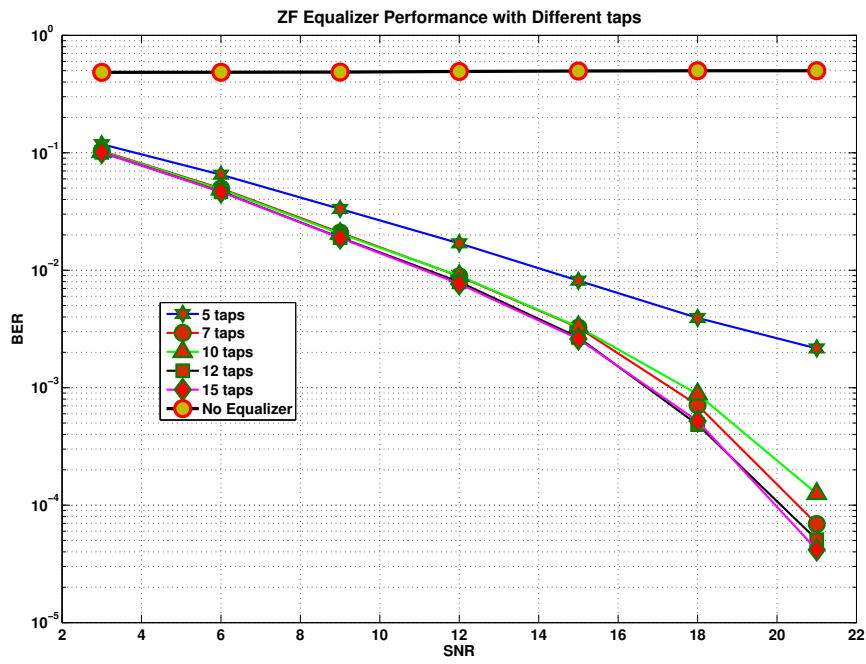


FIGURE C.8: ZF Equalizer performance with different taps for a 11 tap Channel

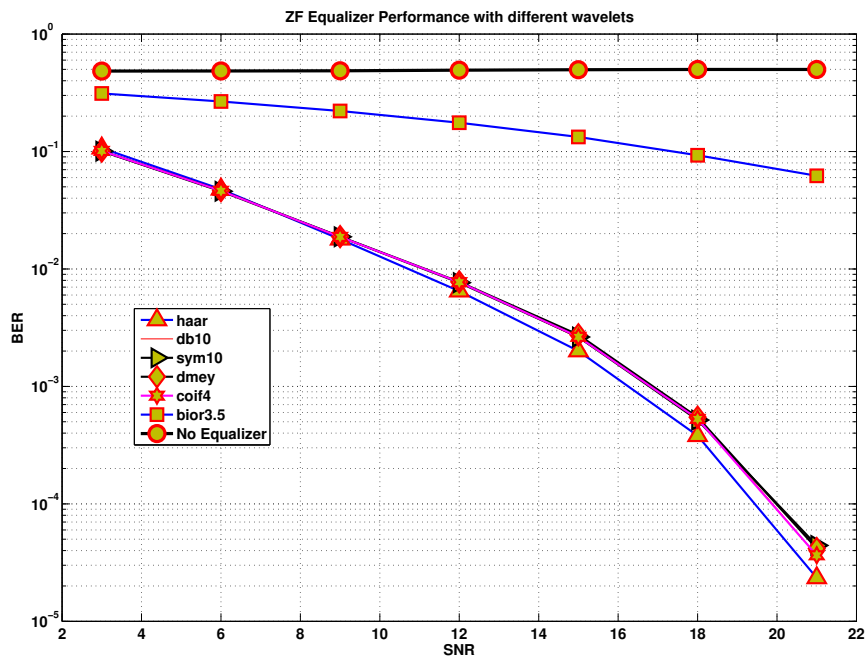


FIGURE C.9: ZF Equalizer with different Wavelets

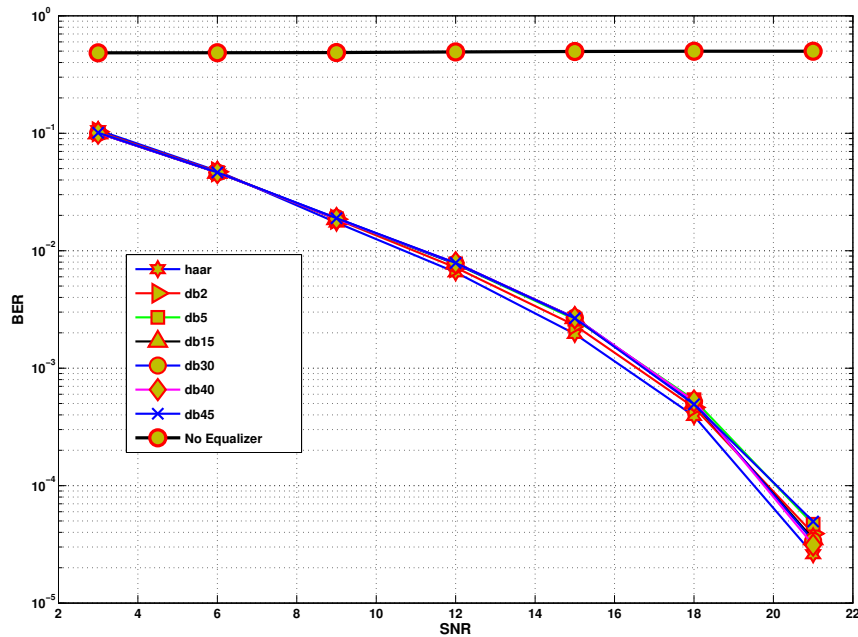


FIGURE C.10: Wavelets of Daubechies Family

In Fig. C.10 the BER plots for the WPM system with the Daubechies family of wavelets of different lengths is plotted. The number of taps of the equalizer is fixed at 15. We can observe from the plots that there is no perceivable difference in the performances of the system.

We now compare the operation of the WPM and OFDM systems under channel-1 conditions. The number of OFDM sub-carriers considered is 128 and the length of the cyclic prefix (CP) is taken to be 32. The comparison was made for two kinds of equalizer at the OFDM receiver: the first where a frequency domain equalizer is used, and second when a time domain equalizer is applied. It can be seen from Fig. C.11 that when comparing WPM and OFDM systems, OFDM with frequency domain equalization outperforms WPM. But with equalization in the time domain the performances of WPM and OFDM are comparable.

#### C-4-2 Performance under Channel Condition-2

The BER performance of the WPM system under Channel-2 for a 200 tap equalizer is shown in Fig. C.14. The constellation diagram for the received and the equalized signal at a SNR of 21dB is shown in Fig. C.13. The improvements brought about by the equalizer in improving the BER performance as well as in mitigating the diffusion of received data can be observed from Figures C.14 and C.13, respectively.

Equalizers of other lengths can also be employed to mitigate the effect of ISI on the WPM system performance. In Fig. C.14 a comparison of equalizers with different lengths is shown below. It can be deduced from the plots that with increasing tap lengths of the equalizer the

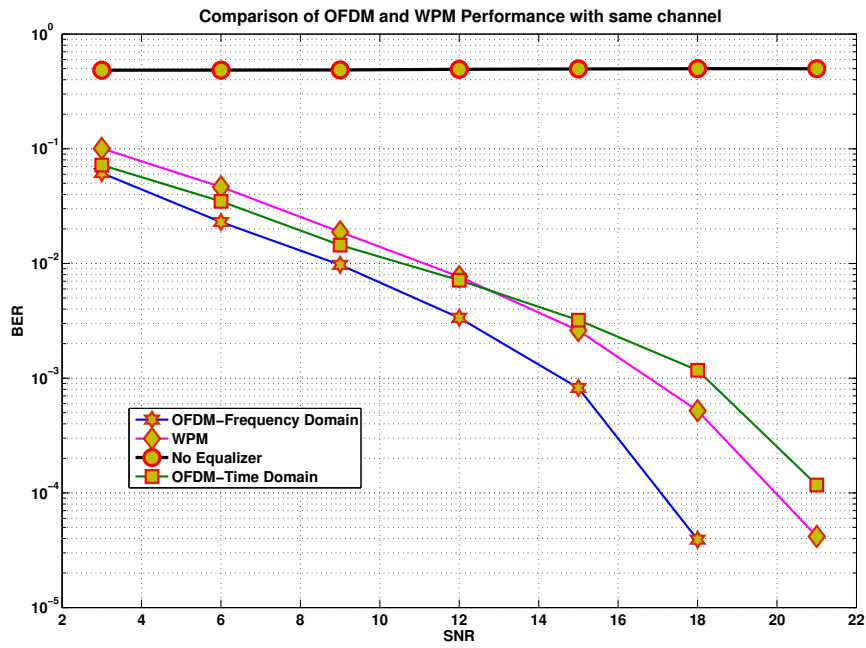


FIGURE C.11: WPM versus OFDM

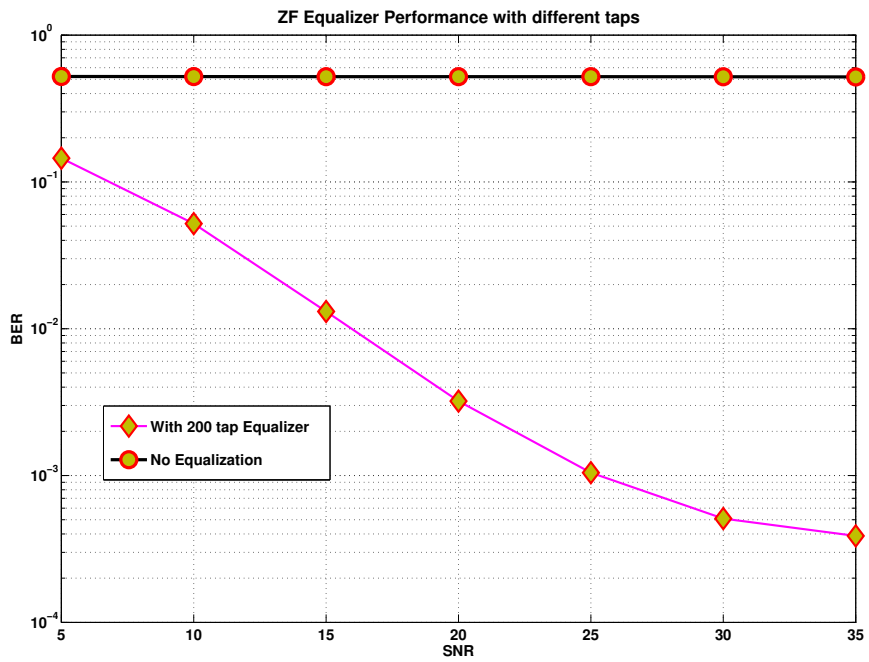


FIGURE C.12: ZF Equalizer performance for a 15 tap Channel

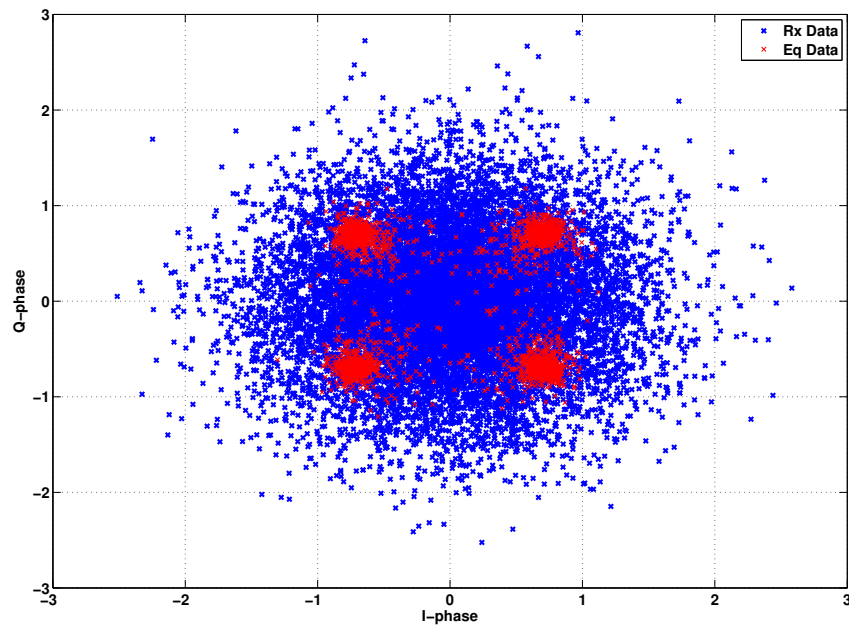


FIGURE C.13: Constellation of the received and equalized data

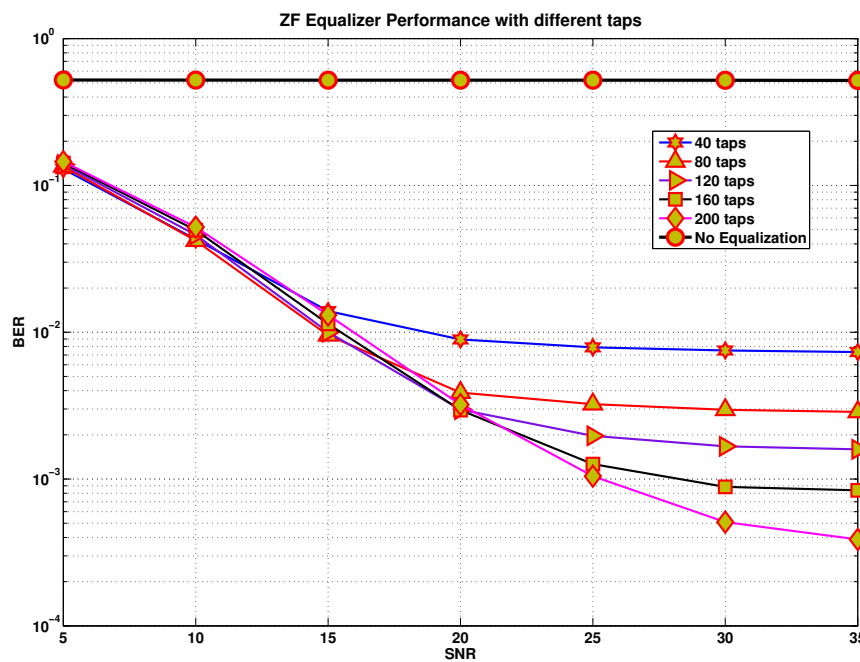


FIGURE C.14: ZF Equalizer performance with different taps for a 15 tap Channel

BER performance improves. However, this improvement is at the price of increased system complexity. Thus, there is a trade-off on offer between the complexity of the equalizer and the performance gains it can yield.

In Fig. C.15 a comparison of different wavelets for the same channel conditions and with a 200-tap ZF equalizer is made. The wavelets used for the study are tabulated in Table C.1. It can be seen that shorter the length of the waveform, better the performance of the wavelet. This is

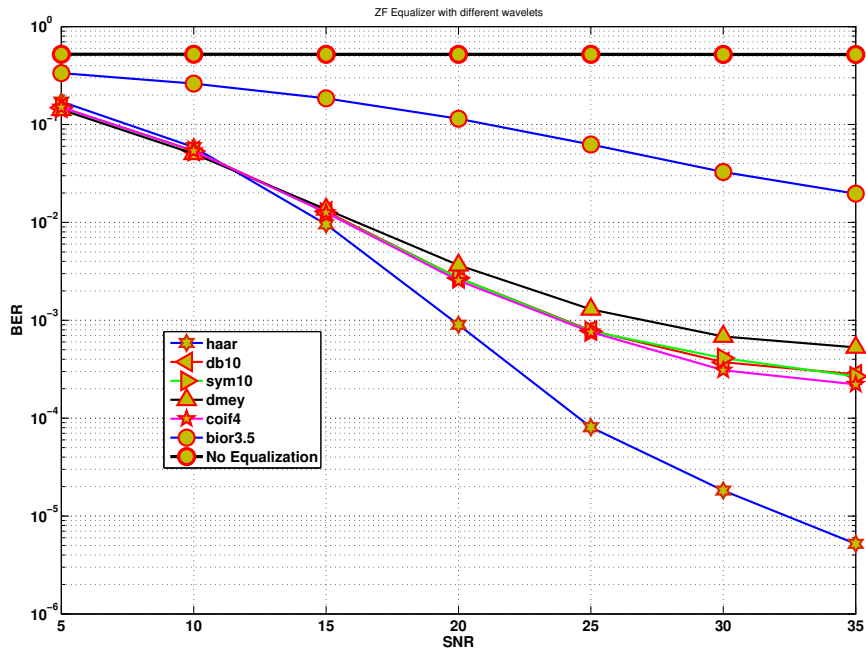


FIGURE C.15: ZF Equalizer with different wavelets

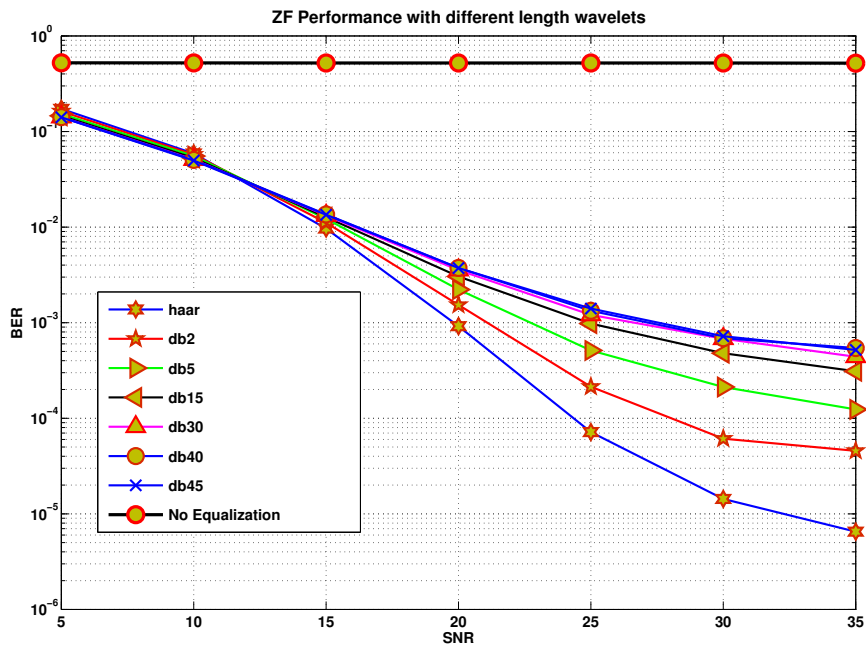


FIGURE C.16: ZF Equalizer Daubechies family of different lengths

TABLE C.1: Wavelet Specifications.

Name	Short form	Orthonormal?	Length
Haar	Haar	Yes	2
Daubechies	db10	Yes	20
symlet	sym10	Yes	20
Coiflet	coif4	Yes	24
Discrete Meyer	dmey	Yes	102
Bi-Orthogonal	bior3.5	No	(5,3)

because the WPM system employs the Discrete wavelet packet transform (DWPT) which is a lapped transform i.e. the symbols overlap in time. This means the waveforms used in WPM are longer than the transform duration of one symbol. For a filter of length  $L_f$  the overall symbol length  $L_{sym}$  with WPM  $N$  carriers can be shown to be [10]:

$$L_{sym} = (L_f - 1)(N_{WPM} - 1) + 1 \quad (\text{C.10})$$

Therefore, when the length of the wavelet filter is longer, more number of WPM symbols overlap resulting in higher ISI. To better corroborate this, the effect of the length of the wavelet on the WPM performance operating under Channel-2 conditions have been plotted in Fig. C.16. Although the wavelets belong to same family, the ones which are longer cause greater ISI leading to poorer BER performance.<sup>4</sup>

A comparison of WPM and OFDM system performances under Channel-2 is shown in Fig. C.17. It can be seen that the performance of WPM and OFDM is comparable when frequency domain equalization is used in OFDM. But with a time-domain equalizer the performance of OFDM is poorer than WPM.<sup>5</sup>

### C-4-3 Eye Diagrams

In communication theory, eye patterns (diagrams) are widely used as a qualitative performance indicator of a system [167]. The information in digital communications is stored in pulses of one or zero and when these two pulses are superimposed on each other several times, a pattern similar to the human eye emerges.<sup>6</sup> The center of the pattern is the point at which the signal clock samples the signal. Since the signal is digital in nature, it must be completely high or low at the sampling point. Hence, an *open* eye indicates that the signal is fully high or low at the sample moment. On the other hand, if a signal trace crosses through the eye, then the eye is partially *closed* causing an ambiguity in decision making leading to data errors. Horizontal

<sup>4</sup>Since channel-1 was not severe and could be easily equalized, the length of the wavelet did not have significant impact on the WPM system performance.

<sup>5</sup>Unlike the frequency domain equalizer, the time-domain equalizer for OFDM system does not benefit from the property of circular convolution.

<sup>6</sup>The pulse is not a sharp rectangle and has a finite rise and fall time.

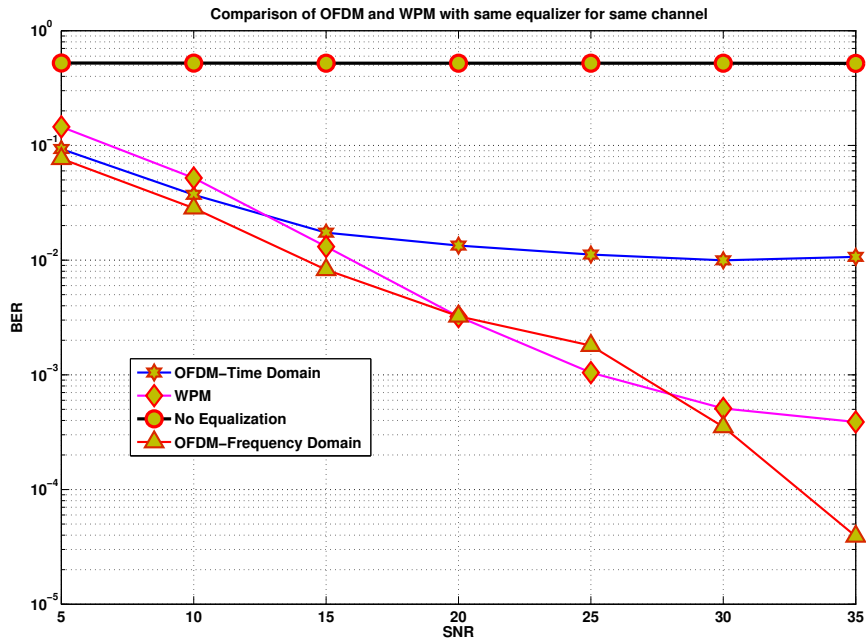


FIGURE C.17: OFDM versus WPM

opening of the eye signifies the jitters or timing errors and vertical opening of the eye determines the noise margin, i.e. difference between the logic High and logic low [167]. Eye diagrams can also be used to check for ISI in a digital communication system [167]. It provides an excellent way to estimate the amount of ISI and the ability of the equalizer to mitigate it. We now show the eye diagram of the data at different stages of the transceiver chain. In Fig. C.18 the QPSK modulated data at the transmitter is shown. Since there is no ISI the eye is completely open. The information bits are modulated by the WPM and then transmitted to the radio channel to be received by the WPM receiver. Figure C.19 shows the eye diagram of the data received at the receiver. The received data has inherent overlap due to the WPM modulation as well as ISI induced by the channel; therefore the eye is *closed*. The received data is then equalized and demodulated by the WPM demodulator. In Fig. C.20 the eye pattern at the output of the equalizer is shown. It is observable from the eye diagram that the equalizer has mitigated the ISI considerably.<sup>7</sup>

<sup>7</sup>Even after equalization of data there exists a residual ISI. This is because the equalizer is of finite length and does not neutralize all of the channel induced artifacts. However, the amount of remnant ISI is tolerable and the BER performance does not suffer much.

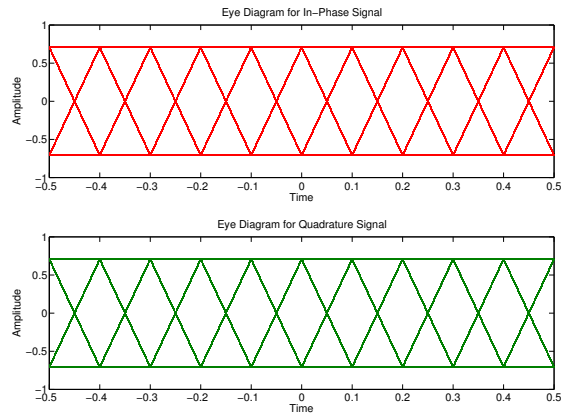


FIGURE C.18: Eye diagram of QPSK modulated data at the transmitter

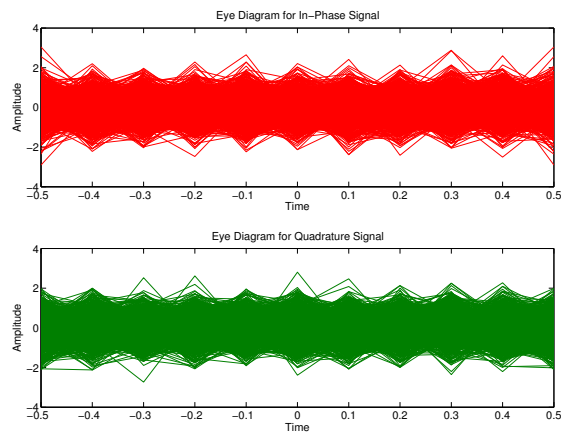


FIGURE C.19: Eye diagram of the Received Data

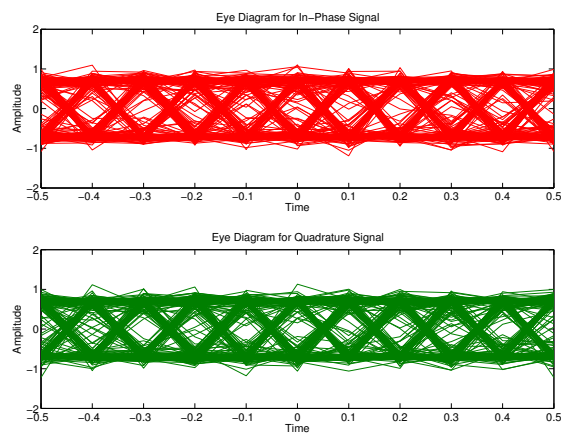


FIGURE C.20: Eye diagram of the QPSK Symbols after equalization at the receiver

## C-5 Conclusion

In this chapter we presented a time-domain equalizer for the mitigation of channel artifacts on the Wavelet Packet Modulator. The equalizer operated on the principle of nullifying the maximum inter-symbol interference induced by the channel. Various realistic channels conditions with different memories and characteristics were applied. Furthermore, investigations to understand the impact of:

- the wavelet family,
- length of the wavelet filters, and
- the number of taps of the equalizer,

on the performance of the equalizer were evaluated. The operation of the WPM system were also compared to the orthogonal frequency division multiplexing. For most channel conditions the equalizer performed adequately yielding significant performance improvements. Results of the simulation studies illustrated notable enhancement in Bit Error Rate (BER) performance for the scenarios considered. The studies of this worked were confined to channels that were time-invariant. Furthermore, the equalizer focused entirely on the removal of ISI (and not ICI).

# Bibliography

- [1] D. C. R. W. Brodersen, A. Wolisz and S. M. Mishra, “CORVUS: A Cognitive Radio Approach for Usage of Virtual Unlicensed Spectrum,” *Berkeley Wireless Research Center (BWRC)*, 2004.
- [2] “News@cisco. cisco visual networking index forecast predicts continued mobile data traffic surge.” 2010. [Online]. Available: [http://newsroom.cisco.com/dlls/2010/prod\\_020910b.html](http://newsroom.cisco.com/dlls/2010/prod_020910b.html)
- [3] “News@cisco. global mobile traffic growth.” 2010. [Online]. Available: [http://www.flickr.com/photos/cisco\\_pics/4333710126/sizes/z/in/photostream](http://www.flickr.com/photos/cisco_pics/4333710126/sizes/z/in/photostream).
- [4] “Fiber to the home (ftth) council, salisbury. advantages of fiber to the home.” 2010. [Online]. Available: [http://www.salisburync.gov/ftth/fiber\\_advantages.pdf](http://www.salisburync.gov/ftth/fiber_advantages.pdf)
- [5] G.Wornell, “Emerging applications of multirate signal processing and wavelets in digital communications,” *Proc. of IEEE*, vol. 84, no. 22, pp. 586 – 603, April 1996.
- [6] M. Lakshmanan and H. Nikookar, “A review of wavelets for digital wireless communication,” *Wireless Personal Communications*, vol. 37, no. 3, pp. 387–420, 2006.
- [7] A. Lindsey, “Wavelet packet modulation for orthogonally multiplexed communication,” *IEEE Transactions on Signal Processing*, vol. 45, no. 5, pp. 1336 – 1339, May 1997.
- [8] P. Vaidyanathan, *Multirate systems and filter banks*. Upper Saddle River, New Jersey: Prentice Hall, 1993.
- [9] L. Ramac and P. Varshney, “A wavelet domain diversity method for transmission of images over wireless channels,” in *IEEE Journal on Selected Areas in Communications*, vol. 18, no. 6, June 2000.
- [10] A. Jamin and P. Mahonen, “Wavelet packet modulation for wireless communications,” *Wireless Communications and Mobile Computing Journal*, vol. 5, no. 2, pp. 123 – 137, Mar. 2005.
- [11] A. Lindsay, “Wavelet packet modulation for orthogonally transmultiplexed communications,” *IEEE Transactions on Signal Processing*, vol. 45.

- [12] B. Negash and H. Nikookar, "Wavelet-based multicarrier transmission over multipath wireless channels," *IEE Electronics Letters*, vol. 36, no. 21.
- [13] N. Suzuki, M. Fujimoto, T. Shibata, N. Itoh, and K. Nishikawa, "Maximum likelihood decoding for wavelet packet modulation," in *IEEE Vehicular Technology Conference (VTC)*, 1999.
- [14] S. Gracias and V. U. Reddy, "Wavelet packet based channel equalization," *Springer*, vol. 21, no. 1, pp. 75–89, 1996.
- [15] M.K.Lakshmanan and H. Nikookar, "Comparison of Sensitivity of OFDM and Wavelet Packet Modulation to Time Synchronization Error," in *Proc. of the IEEE 17th International Symposium on Personal, Indoor and Mobile Radio Communications, (PIMRC)*, Cannes, France, September 2008.
- [16] D. Karamehmedovic, M. K. Lakshmanan, and H. Nikookar, "Performance degradation study of Wavelet Packed based Multi-carrier Modulation under Time Synchronization Errors," in *WPMC*, Lapland, Finland, September 2008.
- [17] B.Torun, M. Lakshmanan, and H. Nikookar, "On the analysis of peak-to-average power ratio of wavelet packet modulation," in *Proc. of European Wireless Technology Conference*, Roma, Italy, 29 Sept. – 1 Oct. 2009, pp. 1 – 4.
- [18] D. Karamehmedovic, M. K. Lakshmanan, and H. Nikookar, "Optimal Wavelet Design for Multicarrier Modulation with Time Synchronization Error," in *52nd Global Communications Conference (GLOBECOM)*, Hawaii, USA, November 2009.
- [19] M. Lakshmanan and H. Nikookar, "Construction of Optimal Bases for Wavelet Packet Modulation under Phase Offset Errors," in *3rd European Wireless Technology Conference*, Paris, France, September 2010.
- [20] D.D.Ariananda, M.K.Lakshmanan, and H.Nikookar, "Design of Best Wavelet Packet Bases for Spectrum Estimation," in *20th Memorial Symposium of Personal, Indoor and Mobile Radio Communications (PIMRC)*, Tokyo, Japan, September 2009.
- [21] M. Lakshmanan, H. Nikookar, D. Karamehmedovic, and D. D. Ariananda, "A Unified Framework to Design Orthonormal Wavelets Packet Bases for Multi-Carrier Modulation," in *Proc. IEEE International Conference on Communications (ICC)*, Cape town, South Africa, May 2010.
- [22] H.Nikookar and M.K.Lakshmanan, "Wavelet Radio: Smart, Adaptive and Reconfigurable Radio Systems Based on Wavelets," Munich/Germany, Oct. 2007.
- [23] ———, "Wavelets for Wireless Communication," Jaipur/India, Dec. 2007.

- [24] —, “Wavelet based Multicarrier Communication Techniques for Cognitive Radios,” Aalborg/Denmark, 2009.
- [25] —, “An Introduction to Wavelets for Cognitive Radio,” Sendai/Japan, Sep. 2009.
- [26] G.Jovanovic-Dolecek, *Multirate Systems: Design and Applications*. Hershey PA: IDEA Group Publishing, 2002.
- [27] I. Daubechies, *Ten Lectures on Wavelets*. Philadelphia: SIAM, 1992.
- [28] G. Strang and T. Nguyen, *Wavelets and Filter Banks*. Wellesley-Cambridge Press, 1996.
- [29] M. Vetterli and J. Kovacevic, *Wavelets and Subband Coding*. Englewood Cliffs, New Jersey: Prentice Hall PTR, 1995.
- [30] B.Burke, *The World According to Wavelets: The Story of a Mathematical Technique in the Making*. Upper Saddle River, New Jersey: A K Peters, May 1998.
- [31] C.S.Burns, R.A.Gopinath, and H.Guo, *Introduction to Wavelets and Wavlet Transform, a Primer*. Prentice Hall, 1998.
- [32] A. Grossmann and J. Morlet, “Decomposition of hardy functions into square integrable wavelets of constant shape,” *SIAM J. Math.*, vol. 15, pp. 723 – 736, 1984.
- [33] Y. Meyer, *Principe d incertitude, bases hilbertiennes et algebres d operateurs*. Bourbaki seminar, 1985-86, no. 662.
- [34] J. A.Cohen, “Wavelets: The mathematical background,” in *Proc. IEEE*, vol. 84, no. 4, pp. 514 – 522, April 1996.
- [35] G. Kaiser, *A Friendly Guide to Wavelets*. Boston: Bitkhäuser, 1994.
- [36] A.Akansu, “Wavelet and subband transforms: Fundamentals and communication applications frequency,” *IEEE Communications Magazine*, vol. 35, no. 22, pp. 104 – 115, December 1997.
- [37] S.G.Mallat, “A theory for multiresolution signal decomposition: The wavelet representation,” *IEEE Transaction on Pattern Recognition and Machine Intelligence*, vol. 11, pp. 674 – 693, July 1989.
- [38] —, “Multiresolution approximation and wavelet orthonormal bases of  $l_2$ ,” *Transactions of the American Mathematical Society*, vol. 315, pp. 69 – 87, July 1989.
- [39] M.Weeks, *Digital Signal Processing using MATLAB and Wavelets*. Hingham: Infinity Science Press LLC, 2007.

- [40] “Wikipedia. short time fourier transform.” 2010. [Online]. Available: <http://en.wikipedia.org/wiki/STFT>
- [41] “Wikipedia. continuous wavelet transform.” 2010. [Online]. Available: [http://en.wikipedia.org/wiki/Continuous\\_wavelet\\_transform](http://en.wikipedia.org/wiki/Continuous_wavelet_transform)
- [42] Y. Meyer, *Ondelletes function splines, et analysys graduees*. Lectures given at the Mathematics Department, University of Torino, 1986.
- [43] I. Daubechies, “Orthonormal bases of compactly supported wavelets, ii. variations on a theme,” *SIAM J. Math. Anal.*, vol. 24 (2), pp. 499 – 519, 1993.
- [44] S. Mallat, “A theory for multiresolution signal decomposition: the wavelet representation,” *Pattern Analysis and Machine Intelligence, IEEE Transactions on*, vol. 11, no. 7, pp. 674 –693, jul 1989.
- [45] R. Coifman and Y. Meyer, “Orthonormal wave packet bases,” *preprint, Numerical Algorithms Research Group, Yale University*, 1989.
- [46] R. Coifman, Y. Meyer, and V. Wickethauser, “Adapted waveform analysis, wavelet packets and applications,” *preprint, Numerical Algorithms Research Group, Yale University*, 1992.
- [47] M. Wickerhauser, *Adapted Wavelet Analysis from Theory to Software*. Wellesley, MA: A.K. Peters, 1994.
- [48] A. Lindsey, *Generalized Orthogonally Multiplexed Communication via Wavelet Packet Basis*. Ph.D. dissertation, Faculty of the Russ College of Engineering and Technology, Ohio University, 1995.
- [49] H. Nikookar, *Advanced Topics in Digital Wireless Communications*. IRCTR-Delft University of Technology, 2004.
- [50] J. G. Proakis, *Digital Communications, Fourth Edition*. McGraw-Hill, New York, 2000.
- [51] N. Erdol, F. Bao, and Z. Chen, “Wavelet modulation: a prototype for digital communication systems,” in *In IEEE Southcon Conference*, 1995, pp. 168–171.
- [52] R. Van Nee and R. Prasad, *OFDM for wireless multimedia communications*. Artech House, Inc. Norwood, MA, USA, 2000.
- [53] B. Farhang-Boroujeny, “Signal Processing Techniques for Spectrum Sensing and Communications in Cognitive Radios.” [Online]. Available: [www.crowncom.org/2007/t2.pdf](http://www.crowncom.org/2007/t2.pdf)
- [54] P. Amini, R. Kempter, and B. Farhang-Boroujeny, “A comparison of alternative filterbank multicarrier methods for cognitive radio systems,” in *Proceeding of the SDR 06 Technical Conference and Product Exposition*, 2006.

- [55] G. Cherubini, E. Eleftheriou, and S. Olcer, "Filtered multitone modulation for vdsl," in *in Proc. IEEE Globecom*, 14-17 November 1999, pp. 1139–1144.
- [56] P. Amini, R. Kempter, R. Chen, L. Lin, and B. Farhang-Boroujeny, "Filter bank multitone: A physical layer candidate for cognitive radios," in *SDR Forum Technical Conference*, Hyatt Regency, Orange County, California, 14-17 November 2005.
- [57] B. Farhang-Boroujeny, "Multicarrier modulation with blind detection capability using cosine modulated filter banks," *IEEE Transactions on Communications*, vol. 51, no. 12, pp. 2057 – 2070, December 2003.
- [58] B. Saltzberg, "Performance of an efficient parallel data transmission system," *IEEE Transactions on Communications Technology*, vol. 15, no. 6, pp. 805 – 811, December 1967.
- [59] B. Hirosaki, "An orthogonally multiplexed qam system using the discrete fourier transform," *IEEE Transactions on Communications*, vol. 29, no. 7, July 1981.
- [60] Y. Zhang and S. Cheng, "A novel multicarrier signal transmission system over multipath channel of low-voltage power line," in *IEEE Transactions on Power Delivery*, 2004.
- [61] Z. Rafique, N. Gohar, and M. Mughal, "Performance comparison of OFDM and WOFDM based V-BLAST wireless systems," in *IEICE Transactions on Communications*, 2005.
- [62] P. W. Wolniansky, G. J. Foschini, G. D. Golden, and R. A. Valenzuela, "V- BLAST: An architecture for realizing very high data rates over the rich- scattering wireless channel," in *Proc. ISSSE-98*, Pisa, Italy, September 1998.
- [63] D. Lacroix, J. Javaudin, and N. Goudard, "IOTA, an advanced OFDM Modulation for future broadband physical layers," in *7th Wireless World Research Forum (WWRF) meeting*.
- [64] K. Anwar, A. Priantoro, M. Saito, T. Hara, M. Okada, and H. Yamamoto, "On the PAPR reduction for wavelet based transmultiplexer," in *IEEE International Symposium on Communications and Information Technology, 2004. ISCIT 2004*, 2004, pp. 812–815.
- [65] F. Harris and E. Kjeldsen, "A Novel Interpolated Tree Orthogonal Multiplexing (ITOM) Scheme with Compact Time-Frequency Localization: an Introduction and Comparison to Wavelet Filter Banks and Polyphase Filter Banks," in *Proceedings of Software Defined Radio Technical Conference and Product Exposition*, Orlando, USA, November 2006.
- [66] M. Lakshmanan, D. Karamehmedovic, and H. Nikookar, "An Investigation on the Sensitivity of Wavelet Packet Modulation to Time Synchronization Error," *Wireless Personal Communications*, 2010.

- [67] D. Karamehmedovic, M. Lakshmanan, and H. Nikookar, "Performance of WPMCM and OFDM in the Presence of Carrier Frequency Offset and Phase Noise," *Journal of Communications*, 2008.
- [68] T. Pollet, M. Bladel, and M. Moeneclaey, "BER sensitivity of OFDM systems to carrier frequency offset and Wiener phase noise," *IEEE Transaction on Communications*, vol. 43, pp. 191 – 193, April 1995.
- [69] A.G. Armada, "Understanding the effect of phase noise in OFDM," *IEEE Transaction on Broadcasting*, vol. 47, no. 2, pp. 153 – 159, June 2001.
- [70] H. Nikookar and R. Prasad, "On the Sensitivity of Multi-carrier Transmission over Multipath Channels to Phase Noise and Frequency Offset," in *Proc. 7th IEEE International Symposium Personal, Indoor Mobile Radio Communication (PIMRC)*.
- [71] T.C.W. Schenk, R. der Hofstad, and E.R. Fledderus, "Distribution of the ICI term in phase noise impaired OFDM systems," *IEEE Transaction on Wireless Communications*, vol. 6, no. 4, pp. 1488 – 1500, April 2007.
- [72] H. Steendam and M. Moeneclaey, "Sensitivity of orthogonal frequency division multiplexed systems to carrier and clock synchronization errors," *Elsevier Signal Processing*, pp. 1217 – 1229, November 1997.
- [73] L. Tomba, "On the effect of Wiener phase noise in OFDM systems," *IEEE Transaction on Communications*, vol. 46, no. 5, May 1998.
- [74] K. Sathanathan and C. Tellambura, "Probability of error calculation of OFDM system with frequency offset," *IEEE Transaction on Communications*, vol. 49, no. 11, pp. 1884 – 1888, November 2001.
- [75] H. Nikookar and B.G. Negash, "Frequency Offset Sensitivity Reduction of Multi-carrier Transmission by Waveshaping," in *Proc. IEEE International Conference on Personal Wireless Communications (ICPWC '2000)*, December 2000, pp. 444–448.
- [76] J. Armstrong, "Analysis of new and existing methods of reducing intercarrier interference due to frequency offset in OFDM," *IEEE Transaction on Communications*, vol. 47, no. 3, pp. 365 – 369, March 1999.
- [77] P.H. Moose, "A technique for orthogonal frequency division multiplexing frequency offset correction," *IEEE Transaction on Communications*, vol. 42, no. 10, pp. 2908 – 2914, October 1994.
- [78] A.G. Armada and M. Calvo, "Phase noise and sub-carrier spacing effects on the performance of an OFDM communication system," *IEEE Communication Letters*, vol. 2, no. 1, pp. 1 – 13, January 1998.

- [79] Y.C.Lion and K.C.Chen, "Estimation of Wiener Phase Noise by the Autocorrelation of the ICI Weighting Function in OFDM System," in *in Proc. 16th IEEE International Symposium on Personal, Indoor and Mobile Radio Communications (PIMRC)*, 2005, pp. 725–729.
- [80] P.Robertson and S.Kaiser, "Analysis of the Effects of the Phase Noise in Orthogonal-Frequency Division Multiplexed (OFDM) Systems," in *in Proc. IEEE International Conference on Communications (ICC)*, vol. 3, June 1995, pp. 1652 – 1657.
- [81] V.S.Abhayawardhana and I.J.Wassell, "Common Phase Error Correction with Feedback for OFDM in Wireless Communication," in *in Proc. IEEE Globecom*, vol. 1, November 2002, pp. 651 – 655.
- [82] A.B.Narasimhamurthy, M. Banavar, and C. Tepedelenliouglu, *OFDM Systems for Wireless Communications*. Morgan and Claypool Publishers, 2010.
- [83] T.Schenk, *RF Imperfections in High-rate Wireless Systems*. Springer, 2008.
- [84] A.Demir, A.Mehrotra, and J.Roychowdhury, "Phase noise in oscillators: a unifying theory and numerical methods for characterization," *IEEE Transactions on Circuits and Systems*, pp. 655 – 674, May 2000.
- [85] R.Corvaja and S.Pupolin, "Phase Noise Limits in OFDM Systems," in *in Proc. International Wireless Personal Multimedia Communications Symposium (WPMC '03)*, October 2003, pp. 19 – 22.
- [86] C.R.N.Athaudage, "BER Sensitivity of OFDM Systems to Time Synchronization Error," in *in Proc. IEEE International Conference on Communication Systems (ICCS 2002)*, vol. 1, November 2002, pp. 42 – 46.
- [87] Y.Mostofi and D.C.Cox, "Mathematical analysis of the impact of timing synchronization errors on the performance of an ofdm system," *IEEE Transaction on Communications*, vol. 54, no. 2, pp. 1 – 13, February 2002.
- [88] D.Liu, Y.Tang, D.Sang, and S.Li, "Impact of the Timing Error on BER Performance of TDD Pre-equalized OFDM System," in *in Proc. IEEE International Conference on Personal Wireless Communications (ICPWC S2000)*, vol. 1, September 2004, pp. 714 – 718.
- [89] D.Lee and K.Cheun, "Coarse symbol synchronization algorithms for ofdm systems in multipath channels," *IEEE Communication Letters*, vol. 6, no. 10, pp. 446 – 448, October 2002.

- [90] M.Sandell, J.J.Beekm, and P.O.Brjesson, "Timing and Frequency Synchronization in OFDM Systems using the Cyclic Prefix," in *International Symposium on Synchronization*, vol. 1, September 1995, pp. 16 – 19.
- [91] M.Tanda, "Blind symbol-timing and frequency-offset estimation in ofdm systems with real data symbols," *IEEE Transactions on Communications*, vol. 52, no. 10, pp. 1609 – 1612, October 2004.
- [92] A.J.Coulson, "Maximum likelihood synchronization for ofdm using a pilot symbol: algorithms," *IEEE Journal on Selected Areas in Communications*, vol. 19, no. 12, pp. 2486 – 2494, December 2001.
- [93] B. Yang, K.B.Letaief, R.S.Cheng, and Z.Cao, "Timing recovery for ofdm transmission," *IEEE Journal on Selected Areas in Communications*, vol. 18, no. 11, pp. 2278 – 2291, November 2000.
- [94] B.Torun, M. Lakshmanan, and H. Nikookar, "Peak-to-average power ratio reduction of wavelet packet modulation by adaptive phase selection," *PIMRC, Sept., Istanbul, Turkey*, 2010.
- [95] M. Baro and J. Ilow, "Improved papr reduction for wavelet packet modulation using multi-pass tree pruning," in *Proc. of the IEEE 18th International Symposium on Personal, Indoor and Mobile Radio Communications, PIMRC*, Athens, Greece, 3-7 Sept. 2007, pp. 1 – 5.
- [96] H. Zhang, D. Yudo, and F. Zhao, "Research of PAPR reduction method in multicarrier modulation system," in *Proc. of the International Conference on Communications, Circuits and Systems*, vol. 1, HongKong, China, 27-30 May 2005, pp. 91 – 94.
- [97] N. Le, S. Muruganathan, and A. Sesay, "Peak-to-average power ratio reduction for wavelet packet modulation schemes via basis function design," in *Proc. of the IEEE 68th Vehicular Technology Conference, VTC 2008-Fall*, Calgary, BC, Canada, 21-24 Sept. 2008, pp. 1 – 5.
- [98] V. Kumbasar and O. Kucur, *Digital Signal Processing*. Elsevier, Nov. 2008, vol. 18, no. 6, ch. Better wavelet packet tree structures for PAPR reduction in WOFDM systems, pp. 885 – 891.
- [99] S. Litsyn, *Peak power control in multicarrier communications*. Cambridge Univ Pr, 2007.
- [100] M. Gautier, C. Lereau, M. Arndt, and J. Lienard, "Papr analysis in wavelet packet modulation," in *Communications, Control and Signal Processing, 2008. ISCCSP 2008. 3rd International Symposium on*, St Julians, Portugal, 12-14 Mar. 2008, pp. 799 – 803.

- [101] A. Jones, T. Wilkinson, and S. Barton, "Block coding scheme for reduction of peak to mean envelope power ratio of multicarrier transmission schemes," *Electronics Letters*, vol. 30, p. 2098, 1994.
- [102] R. Bauml, R. Fischer, and J. Huber, "Reducing the peak-to-average power ratio of multicarrier modulation by selected mapping," *Electronics Letters*, vol. 32, pp. 2056 – 2057, 1996.
- [103] A. Jayalath and C. Tellambura, "The use of interleaving to reduce the peak-to-average power ratio of an ofdm signal," in *Global Telecommunications Conference, 2000. GLOBECOM '00. IEEE*, vol. 1, 2000, pp. 82 –86 vol.1.
- [104] J. Tellado, *Multicarrier modulation with low PAR: applications to DSL and wireless*. Springer Netherlands, 2000.
- [105] S. Muller and J. Huber, "OFDM with reduced peak-to-average power ratio by optimum combination of partial transmit sequences," *Electronics letters*, vol. 33, no. 5, 1997.
- [106] R. van Nee and A. de Wild, "Reducing the peak-to-average power ratio of ofdm," in *Proc. of the 48th IEEE Vehicular Technology Conference, VTC 98*, vol. 3, 18-21 1998, pp. 2072 –2076 vol.3.
- [107] T. May and H. Rohling, "Reducing the peak-to-average power ratio in OFDM radio transmission systems," *Proc. of IEEE Vehicular Technology Conference, VTC 98*, pp. 2774–2778, 1998.
- [108] H. Nikookar and K. Lidsheim, "Random phase updating algorithm for OFDM transmission with low PAPR," *IEEE Transactions on Broadcasting*, vol. 48, no. 2, pp. 123–128, 2002.
- [109] X. Wang, T. Tjhung, and C. Ng, "Reduction of peak-to-average power ratio of OFDM systems using a companding technique," *IEEE Transactions on Broadcasting*, vol. 45, no. 3, 1999.
- [110] J. Davis and J. Jedwab, "Peak-to-mean power control and error correction for ofdm transmission using golay sequences and reed-muller codes," *Electronics Letters*, vol. 33, no. 4, pp. 267 –268, Feb. 1997.
- [111] ———, "Peak-to-mean power control in OFDM, Golay complementary sequences, and Reed–Muller codes," *IEEE Transactions on Information Theory*, vol. 45, no. 7, p. 2397, 1999.
- [112] S. J. Russell and P. Norvig, *Artificial Intelligence: A Modern Approach*, 2nd ed. Upper Saddle River, New Jersey: Prentice Hall, 2003.

- [113] W. Press, S. Teukolsky, W. Vetterling, and B. Flannery, *Numerical recipes in Fortran; the art of scientific computing*. New York, NY, USA: Cambridge University Press New York, NY, USA, 1993.
- [114] Z. Michalewicz and D. Fogel, *How to solve it: modern heuristics*. Springer-Verlag New York Inc, 2004.
- [115] M.K.Lakshmanan, D.D.Ariananda, and H.Nikookar, "A Study on the Performance of Wavelet Packets for Spectral Analysis," in *International Conference on Signal Processing and Communications (SPCOM 2010)*, Indian Institute of Science (IISc), Bangalore, India, July 2010.
- [116] D.D.Ariananda, M.K.Lakshmanan, and H.Nikookar, "A Study on the Application of Wavelet Packet Transforms to Cognitive Radio Spectrum Estimation," in *4th International Conference on Cognitive Radio Oriented Wireless Networks and Communications (CROWNCOM)*, Hannover, Germany, June 2009.
- [117] P. Stoica and R. Moses, *Introduction to Spectral Analysis*. Upper Saddle River, NJ: Prentice Hall Inc, 1997.
- [118] J. G. Proakis and D. Manolakis, *Digital Signal Processing: Principles, Algorithms and Applications, Fourth Edition*. Prentice Hall Inc, Upper Saddle River, NJ, 2007.
- [119] B. Porat, *A Course in Digital Signal Processing*. John Wiley and Sons, Inc., 1996.
- [120] B. Farhang-Boroujeny, "Filter banks spectrum sensing for cognitive radios," *IEEE Transaction on Signal Processing*, vol. 56, pp. 1801 – 1811, May 2008.
- [121] D. J. Thomson, "Spectrum estimation and harmonic analysis," *Proceeding of IEEE*, vol. 70, no. 9, September 1982.
- [122] B. Farhang-Boroujeny, "A square-root nyquist (m) filter design for digital communication systems," *IEEE Transaction on Signal Processing*, vol. 56, pp. 2127 – 2132, May 2008.
- [123] A. Jensen and A. la Cour-Harbo, *Ripples in Mathematics: The Discrete Wavelet Transform*. Springer, Germany, 2001.
- [124] M. I. Todorovska and T. Y. Hao, *Information granulation and dimensionality reduction of seismic vibration monitoring data using orthonormal discrete wavelet transform for possible application to data mining*. Dept. of Civil Eng., U. Southern California: Research Report CE 03-02, 2003.
- [125] M.K.Lakshmanan, D.D.Ariananda, and H.Nikookar, "A Reconfigurable Wavelet Packet Filter Bank Transceiver for Spectral Analysis and Dynamic Spectrum Access," in *Fifth IEEE International Symposium on New Frontiers in Dynamic Spectrum Access Networks 2011 (DySPAN 2011)*, Aachen, Germany, May 2011.

- [126] M.K.Lakshmanan and H.Nikookar, "Optimum Wavelet Packet Construction for Multicarrier-based Cognitive Radio System," in *The 10th International Symposium on Wireless Personal Multimedia Communications (WPMC)*, Jaipur, India, December 2007.
- [127] M. Lakshmanan, I. Budiarto, and H. Nikookar, "Maximally frequency selective wavelet packets based multi-carrier modulation scheme for cognitive radio systems," in *Proc. of the IEEE Global Telecommunications Conference, GLOBECOM*, Washington DC, USA, 26-30 Nov 2007, pp. 4185 – 4189.
- [128] J. Mitola III, *Cognitive Radio: An Integrated Agent Architecture for Software Defined Radio*. Doctoral Dissertation, May 2000.
- [129] S. Haykin, "Cognitive radio: Brain empowered wireless communications," in *IEEE Journal On Selected Areas In Communications*, vol. 23, no. 2, pp. 201 – 220, February 2005.
- [130] T. Weiss and F. Jondral, "Spectrum pooling: An innovative strategy for the enhancement of spectrum efficiency," *IEEE Communication Magazine*, March 2004.
- [131] B. Farhang-Boroujeny and R. Kempter, "Multicarrier communication techniques for spectrum sensing and communication in cognitive radios," *IEEE Communication Magazine*, April 2008.
- [132] O. Rioul and P. Duhamel, "A remez exchange algorithm for orthonormal wavelets," *IEEE Trans. Circuits Systems - II*, vol. 41, no. 8, pp. 550 – 560, August 1994.
- [133] W. J. Phillips, "Wavelet and filter banks course notes," 2003. [Online]. Available: <http://www.engmath.dal.ca/courses/engm6610/notes/notes.html>
- [134] T. W. Parks and J. H. McClellan, "Chebyshev approximation for nonrecursive digital filters with linear phase," *IEEE Transaction on Circuit Theory*, vol. 19, no. 2, pp. 189 – 194, March 1972.
- [135] E.L.Lawler and D.E.Wood, "Branch-and-bound methods: A survey," *JSTOR Operations Research*, vol. 14, no. 4, pp. 699 – 719, August 1966.
- [136] E.Alizadeh, "Interior point methods in semidefinite programming with applications to combinatorial optimization," *SIAM Journal of Optimization*, vol. 5, pp. 13 – 51, August 1995.
- [137] Y. Ye, *Interior Point Algorithms: Theory and Analysis*. Wiley, New York, 1997.
- [138] S.Boyd, L. Ghaoui, E.Feron, and V.Balkrishnan, "Linear matrix inequalities in system and control theory," *SIAM Study in Applied Mathematics*, vol. 15, June 1994.
- [139] S.Boyd and L.Vandenberghe, *Convex Optimization*. Cambridge University Press, 2004.

- [140] L.Vandenberghe and S.Boyd, "Semidefinite programming," *SIAM review*, vol. 38, no. 1, March 1998.
- [141] H.Wolkowicz, R.Saigal, and L.Vandenberghe, *Handbook of Semidefinite Programming*. Kluwer Academic Publisher, 2000.
- [142] R.Hettich and K.O.Kortanek, "Semidefinite programming: Theory, methods and applications," *SIAM Review*, vol. 35, no. 3, pp. 380 – 429, September 1993.
- [143] A.Karmakar, A.Kumar, and R.K.Patney, "Design of an optimal two-channel orthogonal filterbank using semidefinite programming," *IEEE Signal Processing Letters*, vol. 14, no. 10, pp. 692 – 694, October 2007.
- [144] J.Wu and K.M.Wong, "Wavelet packet division multiplexing and wavelet packed design under timing error effects," *IEEE Transaction on Signal Processing*, vol. 45, no. 12, pp. 2877 – 2890, December 1997.
- [145] J.K.Zhang, T.N.Davidson, and K.M.Wong, "Efficient design of orthonormal wavlet bases for signal representation," *IEEE Transactions on Signal Processing*, vol. 52, no. 7, July 1999.
- [146] S.P.Wu, S.Boyd, and L.Vandenberghe, "Fir filter design via semidefinite programming and spectral factorization," in *Proceeding IEEE Concerence on Decision and Control*, pp. 271 – 279, 1996.
- [147] B.Alkire and L.Vandenberghe, "Convex optimization problems involving finite autocorrelation sequences," *Mathematical Programming, Series A93*, pp. 331 – 359, 2002.
- [148] K. T.N.Davidson, L.Zhi-Quan, "Orthogonal Pulse Shape Design via Semidefinite Programming," in *IEEE International Conference on Acoustics, Speech and Signal Processing (ICASSP '99)*, vol. 5, March 1999, pp. 2651 – 2654.
- [149] T.N.Davidson, L.Zhi-Quan, and J.F.Sturm, "Linear matrix inequality formulation of spectral mask constraints with applications to fir filter design," *IEEE Transaction on Communications*, vol. 50, no. 11, pp. 2702 – 2715, November 1999.
- [150] J. Sturm, "Using sedumi 1.02, a matlab toolbox for optimization over symmetric cones," *Optimization Methods and Software*, vol. 11 – 12, 1999. [Online]. Available: <http://sedumi.mcmaster.ca/>
- [151] J.Löfberg, "A toolbox for modeling and optimization in matlab," 2004. [Online]. Available: <http://control.ee.ethz.ch/~joloef/wiki/pmwiki.php>
- [152] M.K.Lakshmanan, I. Budiarjo, and H.Nikookar, "Wavelet Packet Multi-carrier Modulation MIMO Based Cognitive Radio Systems with VBLAST Receiver Architecture," in

- IEEE Wireless Communications and Networking Conference (WCNC)*, Las Vegas, USA, March-April 2008.
- [153] M.K.Lakshmanan and H.Nikookar, "Mitigation of Interference from Wideband IEEE 802.11a Source on UWB Wireless Communication using Frequency Selective Wavelet Packets," in *International Waveform Diversity and Design (WDD) Conference*, Pisa, Italy, June 2007.
- [154] —, "Best Bases Selection for Wavelet Domain Communication Systems," in *International Waveform Diversity and Design (WDD) Conference*, Orlando, USA, January 2009.
- [155] D. Karamehmedovic, M.K.Lakshmanan, and H.Nikookar, "Optimal Wavelet Design for Multicarrier Modulation with Time Synchronization Error," in *52nd Global Communications Conference (GLOBECOM)*, Hawaii, USA, November 2009.
- [156] D.D.Ariananda, M.K.Lakshmanan, and H.Nikookar, "Design of Best Wavelet Packet Bases for Spectrum Estimation," in *20th Memorial Symposium of Personal, Indoor and Mobile Radio Communications (PIMRC)*, Tokyo, Japan, September 2009.
- [157] M. Lakshmanan, H. Nikookar, D. Karamehmedovic, and D. D. Ariananda, "A Unified Framework to Design Orthonormal Wavelets Packet Bases for Multi-Carrier Modulation," in *Proc. IEEE International Conference on Communications (ICC)*, Cape town, South Africa, May 2010.
- [158] M. Lakshmanan, B.Torun, and H. Nikookar, "Hill Climbing Optimization Heuristics for Minimization of Peak-to-Average Power Ratio in Wavelet Packet Modulator," in *submitted to the 54th Global Communications Conference (GLOBECOM)*, USA, November 2011.
- [159] M.K.Lakshmanan and H.Nikookar, "Construction of optimum wavelet packets for multi-carrier based spectrum pooling systems," in *Special Issue Wireless Personal Communications*, vol. 54, June 2010.
- [160] Z. Tian and G. B. Giannakis, "A Wavelet Approach to Wideband Spectrum Sensing for Cognitive Radios," in *Proceeding of International Conference on Cognitive Radio Oriented Wireless Networks and Communications*, Greece, 8 – 10 June 2006.
- [161] H. Zhang and H. Fan, "Wavelet Packet Waveforms for Multicarrier CDMA Communication," in *Proc. International Conf. on Acoust. Speech, Signal Proc.*, Orlando, FL, May 2002.
- [162] S. Weinstein, "Introduction to the history of ofdm," in *IEEE Communications Magazine*, vol. 47, no. 11, November 2009.

- [163] R. W. Chang, "High-speed multichannel data transmission with bandlimited orthogonal signals," in *Bell Sys. Tech. J.*, vol. 45, December 1966, pp. 1775 – 96.
- [164] "A brief history of ofdm," 2010. [Online]. Available: [http://www.wimax.com/commentary/wimax\\_weekly/sidebar-1-1-a-brief-history-of-ofdm](http://www.wimax.com/commentary/wimax_weekly/sidebar-1-1-a-brief-history-of-ofdm)
- [165] "Panel discussions at ieee 69th vehicular technology conference (vtc-spring)," April 2009. [Online]. Available: <http://www.ieeevtc.org/vtc2009spring/panels.php#Panel02>
- [166] A. Bajpai, M. K. Lakshmanan, and H. Nikookar, "Channel Equalization in Wavelet Packet Modulation by Minimization of Peak Distortion," in *22nd IEEE International Symposium on Personal Indoor and Mobile Radio Communications (PIMRC)*, Toronto, Canada, September 2011.
- [167] R. Gitlin, J. Hayes, and S. Weinstein, *Data communications principles*. Springer, 1992.
- [168] *Digital Video Broadcasting (DVB); Framing structure, channel coding and modulation for digital terrestrial television*. European Standard (Telecommunications series), Nov. 2004, vol. 1.5.1.

# Summary

## **Reconfigurable and Adaptive Wireless Communication Systems based on Wavelet Packet Modulators**

Wavelet Packet Modulation (WPM) is a multi-carrier transmission technique that uses orthogonal wavelet packet bases to combine a collection of information bits into a single composite signal. This system can be considered as a viable alternative, for wide-band communication, to the popular Orthogonal Frequency Division Multiplexing (OFDM) system. The main advantage of WPM is that the transmission characteristics of the system can be adapted according to the radio environment to maximize resource utilization.

The WPM is a system under development and has not been studied extensively. In this research work the operation of a WPM radio is successfully evaluated. The thesis primarily focuses on the question of how efficient and robust wireless radios can be designed with the aid of wavelet theory. To do so the challenges involved in the practical implementation of the system are evaluated and understood. Suitable mechanisms that address communication theory figure-of-merits such as Peak-to-average power ratio (PAPR), loss of time/phase/frequency synchronization, channel equalization are devised and tested.

Furthermore, the advantages of the WPM system for wireless transmission are demonstrated in three scenarios, namely,

1. Wavelet packets for spectrum estimation.
2. Wavelet packets for dynamic spectrum access.
3. Design of new wavelets based on system requirements.

The efficacy of the proposed algorithms is validated using computer simulations and numerical analysis. The results of the research show that the WPM is an effective addition to existing wireless transmission modes.

*Madan Kumar Lakshmanan*

# Samenvatting

## **Reconfigurable and Adaptive Wireless Communication Systems based on Wavelet Packet Modulators**

Wavelet Packet Modulation (WPM) is een multi-dragger transmissie techniek die gebruik maakt van een orthogonale wavelet pakket bases om een verzameling van parallelle signalen te combineren in een enkel composiet signaal.

Dit systeem kan worden beschouwd als een levensvatbaar alternatief, als een brede band transmissie techniek, voor het populaire Orthogonal Frequency Division Multiplexing (OFDM) systeem. Het grote voordeel van WPM is dat de transmissie-eigenschappen van het systeem kunnen worden aangepast aan de radio-omgeving om benutting van resources te maximaliseren.

De WPM is een systeem in ontwikkeling en is nog niet uitgebreid bestudeerd. In dit onderzoek is het werk van de werking van het nieuwe Wavelet Packet Modulator (WPM) radio is met succes geëvalueerd. Het proefschrift richt zich primair op de vraag hoe efficiënte en robuuste draadloze radio's kunnen worden ontworpen met behulp van wavelet theorie.

Om dit te doen zijn de uitdagingen van een praktische implementatie van het systeem geëvalueerd en in kaart gebracht. Geschikte mechanismen die gaan over communicatie theorie figuur-of-verdiensten, zoals Piek-tot-gemiddeld vermogen ratio (PAPR), verlies van tijd / fase / frequentie-synchronisatie, kanaal egalisatie zijn bedacht en getest.

Bovendien zijn de voordelen van het WPM-systeem voor draadloze transmissie aangetoond in drie scenario's, namelijk:

1. Wavelet packets voor spectrum schatting.
2. Wavelet packets voor dynamische toegang tot het spectrum.
3. Ontwerp van nieuwe golven op basis van systeem eisen.

De effectiviteit van de voorgestelde algoritmen zijn gevalideerd met behulp van computersimulaties en numerieke analyse. De resultaten van het onderzoek tonen aan dat WPM een krachtige aanvulling op de bestaande draadloze transmissie modi kan worden.

*Madan Kumar Lakshmanan*

# Curriculum Vitae

**Madan Kumar Lakshmanan** received the B.E. (with distinction) in electrical engineering from the University of Madras, Chennai, India, in 2000. In the same year he joined the Indian software firm, Polaris Software Labs Ltd., where he developed applications for Tele-communications. At Polaris, he was awarded the "On The Spot Of Excellence Award" for his efforts. In 2003, he moved to the Indian Institute of Technology, Madras (IIT-M), India, to lead a team of junior researchers to develop and establish a wireless communications network for rural connectivity. In 2004, he was granted the Royal Dutch/Shell Chevning scholarship to pursue a Masters program in Telecommunications at the Delft University of Technology (TU Delft). He completed his Masters (CUM LAUDE) in 2006 and continued with his PhD studies at the International Research Center for Telecommunications Transmission and Radar (IRCTR) of TU Delft where he is currently conducting radio/physical layer studies on applying the mathematical precept of Wavelet transform for adaptive and re-configurable wireless Radios. He received the BEST STUDENT PAPER award at the 10th International Symposium on Wireless Personal Multimedia Communications (WPMC-2007) held in Jaipur, India, December 2007. He won the NETEL-COM AWARD 2010 conferred by the Netelcom group, suppliers of professional telecommunication equipment in the Netherlands, for his scientific contributions as a PhD student in the field of telecommunications.